KAUNAS UNIVERSITY OF TECHNOLOGY

DOVYDAS BLAŽEVIČIUS

SYNTHESIS AND APPLICATION OF NEW CARBAZOLE- AND PHENOXAZINE-BASED COMPOUNDS FOR ORGANIC LIGHT EMITTING DIODES

Doctoral dissertation
Natural Sciences, Chemistry (N 003)

2024, Kaunas

KAUNO TECHNOLOGIJOS UNIVERSITETAS

DOVYDAS BLAŽEVIČIUS

NAUJŲ KARBAZOLO ARBA FENOKSAZINO DARINIŲ SINTEZĖ IR NAUDOJIMAS ORGANINIUOSE ŠVIESOS DIODUOSE

Daktaro disertacija
Gamtos mokslai, chemija (N 003)

2024, Kaunas

Disertacija rengta 2020–2024 metais Kauno technologijos universiteto Cheminės technologijos fakultete Polimerų chemijos ir technologijos katedroje. Mokslinius tyrimus rėmė Lietuvos mokslo taryba.

Mokslinis vadovas:
prof. dr. Saulius GRIGALEVIČIUS (Kauno technologijos universitetas, gamtos mokslai, chemija, N 003).

Mokslinė konsultantė:
vyresn. m. d. dr. Gintarė KRUČAITĖ (Kauno technologijos universitetas, technologijos mokslai, medžiagų inžinerija, T 008).

Redagavo: anglų kalbos redaktorius dr. Armandas Rumšas (leidykla „Technologija"), lietuvių kalbos redaktorė Rita Malikėnienė (leidykla „Technologija").

Chemijos mokslo krypties disertacijos gynimo taryba:
prof. dr. Vytautas GETAUTIS (Kauno technologijos universitetas, gamtos mokslai, chemija, N 003) – **pirmininkas**;
vyresn. m. d. dr. Marytė DAŠKEVIČIENĖ (Kauno technologijos universitetas, gamtos mokslai, chemija, N 003);
vyr. m. d. dr. Marius FRANCKEVIČIUS (Valstybinis mokslinių tyrimų institutas Fizinių ir technologijos mokslų centras, Vilnius, gamtos mokslai, fizika, N 002);
doc. dr. Rasa KERUCKIENĖ (Kauno technologijos universitetas, gamtos mokslai, chemija, N 003);
doc. dr. Jolanta ROUSSEAU (Artua universitetas, Prancūzija, gamtos mokslai, chemija, N 003).

Disertacija bus ginama viešame Chemijos mokslo krypties disertacijos gynimo tarybos posėdyje 2024 m. rugsėjo 30 d. 15 val. Kauno technologijos universiteto Rektorato salėje.

Adresas: K. Donelaičio g. 73–402, LT-44249 Kaunas, Lietuva.
Tel. (+370) 608 28 527; el. paštas doktorantura@ktu.lt

Disertacija išsiųsta 2024 m. rugpjūčio 30 d.
Su disertacija galima susipažinti interneto svetainėje http://ktu.edu ir Kauno technologijos universiteto bibliotekoje (Gedimino g. 50, LT-44239 Kaunas, Lietuva).

TABLE OF CONTENTS

LIST OF TABLES

LIST OF FIGURES

LIST OF SCHEMES

LIST OF ABBREVIATIONS

3DPA-DiKTa – 3,7,11-tris(diphenylamino)quinolino[3,2,1-de]acridine-5,9-dione;

4CzIPN – 1,2,3,5-tetrakis(carbazol-9-yl)-4,6-dicyanobenzene;

4CzPN – 3,4,5,6-tetra(9H-carbazol-9-yl)phthalonitrile;

4CzTPN-Me – 2,3,5,6-tetrakis(3,6-dimethylcarbazol-9-yl)-1,4-dicyanobenzene;

4TCzBN - 2,3,5,6-tetrakis(3,6-di-tert-butyl-9H-carbazol-9-yl)benzonitrile;

ΔE_{ST} – difference between singlet and triplet excited state energy levels;

ACRDSO2 – 2-(4-(9,9-dimethylacridin-10(9H)-yl)phenyl)thianthrene 5,5,10,10-tetraoxide;

B3PymPm – 4,6-bis(3,5-di(pyridin-3-yl)phenyl)-2-methylpyrimidine;

B3PyPB – 1,3-bis(3,5-dipyrid-3-ylphenyl)benzene;

Bphen – bathophenanthroline;

CBP – 4,4′-bis(N-carbazolyl)-1,1′-biphenyl;

CE – current efficiency;

CIE – International Commission on Illumination;

CT – colour temperature;

CV – cyclic voltammetry;

CzPhPy – 4,6-bis(3-(9H-carbazol-9-yl)phenyl)pyrimidine;

D-A – donor-acceptor;

DACT-II – 9-(4-(4,6-diphenyl-1,3,5-triazin-2-yl)phenyl)-N3,N3,N6,N6-tetraphenyl-9H-carbazole-3,6-diamine;

D-A-D – donor-acceptor-donor;

DMAC-BP – bis(4-(9,9-dimethylacridin-10(9H)-yl)phenyl)methanone;

DMAC-TRZ – 10-(4-(4,6-Diphenyl-1,3,5-triazin-2-yl)phenyl)-9,9-dimethyl-9,10-dihydroacridine;

DMSO – dimethyl sulfoxide;

DPA-Ph-AQ – 2,6-bis(4-(diphenylamino)phenyl)anthracene-9,10-dione;

DSC – differential scanning calorimetry;

E_B – the photo-retinitis or blue light hazard weighted radiation;

E_g – electronic/optical bandgap energy;

EL – electroluminescence;

EML – emissive layer;

E_S – singlet state energy;

E_T – triplet state energy;

ETL – electron transport layer;

EQE – external quantum efficiency;

Fir6 – bis(2,4-difluorophenylpyridinato)-tetrakis(1-pyrazolyl)borate iridium(III);

FIrpic – bis[2-(4,6-difluorophenyl)pyridinato-C2,N](picolinato)iridium;

HAT-CN – 1,4,5,8,9,11-hexaazatriphenylenehexacarbonitrile;

HOMO – highest occupied molecular orbital;

HTL – hole transport layer;

Ir(2-phq)$_3$ – tris(2-phenylquinoline)iridium(III);

Ir(bt)$_2$(acac) – bis(2-phenylbenzothiazolato)(acetylacetonate)iridium(III);

Ir(MDQ)$_2$acac – bis(2-methyldibenzo[f,h]quinoxaline)(acetylacetonate) iridium(III);

Ir(piq)$_2$acac – bis(1-phenylisoquinoline)(acetylacetonate)iridium(III);

Ir(piq)$_3$ – tris(1-phenylisoquinoline)iridium(III);

Ir(ppy)$_2$acac – bis[2-(2-pyridinyl-N)phenyl-C](acetylacetonato)iridium(III);

Ir(ppy)$_2$(bpmp) – [2-(4-methyl-5-phenyl-2-pyridinyl-κN)phenyl-κC]bis[2-(2-pyridinyl-κN)phenyl-κC]iridium;

Ir(ppy)$_3$ – tris[2-phenylpyridine]iridium(III);

IRF – instrument response function;

IQE – internal quantum efficiency;

Liq – 8-quinolinolato lithium;

L$_{max}$ – maximum luminance;

LTPL – low-temperature photoluminescence;

LUMO – lowest unoccupied molecular orbital;

mCBP – 3,3′-di(9H-carbazol-9-yl)-1,1′-biphenyl;

mCP – 1,3-bis(N-carbazolyl)benzene;

MPE – maximum permissible exposure limit;

MS – mass spectrometry;

MSS – melatonin suppression sensitivity;

NMR – nuclear magnetic resonance;

NPB – N,N′-di(1-naphthyl)-N,N′-diphenyl-(1,1′-biphenyl)-4,4′-diamine;

OBA-O – 10-(4-[1,4]benzoxaborino[2,3,4-kl]phenoxaborin-6-ylphenyl)-10H-phenoxazine;

oCBP – 2,2′-di(9H-carbazol-9-yl)-1,1′-biphenyl;

OLED – organic light-emitting diode;

PCzTrz – 9-(4-(4,6-diphenyl-1,3,5-triazin-2-yl)phenyl)-3,6-diphenyl-9H-carbazole;

PE – power efficiency;

PEDOT:PSS – poly(3,4-ethylenedioxythiophene)-poly(styrenesulfonate);

PhOLED – phosphorescent organic light-emitting diode;

PL – photoluminescence;

PLQY – photoluminescence quantum yield;

PO-01 – bis(4-phenylthieno[3,2-c]pyridinato-N,C2')(acetylacetonate) iridium(III);

PO-T2T – 2,4,6-tris[3-(diphenylphosphinyl)phenyl]-1,3,5-triazine;

PPF – dibenzo[b,d]furan-2,8-diylbis(diphenylphosphine oxide);

PPT – 2,8-bis(diphenyl-phosphoryl)-dibenzo[b,d]thiophene;

PVK – poly(9-vinylcarbazole);

PXZ-DPS – 10,10'-(4,4'-sulfonylbis(4,1-phenylene))bis(10H-phenoxazine);

RISC – reverse intersystem crossing;

SDPS-4PhCz – 3,3',6,6'-tetrakis(9-phenyl-9H-carbazol-3-yl)-spiro-diphenylsulfone;

S$_{LC}$(480) – the melatonin suppression spectrum per lux for a reference blue light;

S$_{LC}$(λ) – the melatonin suppression spectrum per lux for a given polychromatic light;

SPPO13 – 2,7-bis(diphenylphosphoryl)-9,9'-spirobifluorene;

TADF – thermally activated delayed fluorescence;

TAPC – 1,1-bis[(di-4-tolylamino)phenyl]cyclohexane;

tBuCzDBA – 9,10-bis(4-(3,6-ditertbutyl-9H-carbazol-9-yl)-2,6-dimethyl-phenyl)-9,10-diboraanthracene;

TBAHS – tetrabutylammonium hydrogensulfate;

14

TCTA – tris(4-carbazoyl-9-ylphenyl)amine;

T_{cr} – crystallization temperature;

TCz-Trz – 2,4,6-tris(2-(9H-carbazol-9-yl)phenyl)-1,3,5-triazine;

T_d – decomposition temperature;

TFB – poly(9,9-dioctylfluorene-alt-N-(4-sec-butylphenyl)-diphenylamine);

T_g – glass transition temperature;

TGA – thermo-gravimetric analysis;

THF – tetrahydrofuran;

T_m – melting temperature;

TmPyPB – 1,3,5-tris(3-pyridyl-3-phenyl)benzene;

TPBi – 2,2',2"-(1,3,5-benzinetriyl)-tris(1-phenyl-1-H-benzimidazole);

TRPL – time-resolved photoluminescence;

TSPO1 – diphenyl[4-(triphenylsilyl)phenyl]phosphine oxide;

TXO-PhCz – 2-(9-phenyl-9H-carbazol-3-yl)-10,10-dioxide-9H-thioxanthen-9-one;

V_{ON} – turn-on voltage.

1. INTRODUCTION

Since Thomas A. Edison patented the incandescent light bulb in 1880, the pursuit of more efficient, adaptable, and visually pleasing lighting solutions has been a driving force behind ongoing innovation. Factors such as the population growth, urbanization, industrialization, and the widespread adoption of electrical appliances and technologies have led to a significant increase in the global electricity consumption. According to data from the *International Energy Agency*, global electricity usage has been rising steadily, averaging by around 2% annually over the past decade, and now already reaching an estimated 25,000 terawatt-hours [1], with approximately 19% dedicated solely to artificial lighting [2]. Concerns over limited energy sources, the environmental impact, and the escalating energy consumption and prices [3] have underscored the need for energy-efficient lighting solutions for various applications, including displays and illumination appliances. *Organic Light Emitting Diodes* (OLEDs) have emerged as a promising alternative, following pioneering research by C. W. Tang in 1986 [4], OLEDs have been fascinating researchers, engineers, and consumers with their impressive capabilities, propelling them from a mere laboratory curiosity to a multi-billion-dollar business endeavour [5]. OLEDs utilizing organic compounds that emit light when exposed to an electric current offer numerous advantages over the traditional light sources, such as incandescent or fluorescent bulbs, including higher brightness, wide-angle visibility, energy efficiency, the contrast ratio, thinness, and flexibility. Moreover, OLEDs can be deposited onto devices using cost-effective wet processes such as spin-coating or ink-jet printing, potentially reducing the greenhouse gas emissions and the overall environmental impact.

Over the past decade, not only the research community, but also various industries have been dedicating their resources for the development of high-performance, long-lifetime OLED devices. Despite incredible achievements, like external quantum efficiencies (EQE) surpassing 30% [6–8], and power efficiencies (PE) exceeding 100 lm/W [9–11], there are still challenges to overcome. Maintaining high efficiency alongside prolonged lifetimes for deep-blue OLEDs remains difficult [12]. The presence of noble metals in phosphorescent materials poses future cost and environmental concerns [13,14]. Substantial efficiency roll-off at high luminance is another issue. This roll-off is due to factors like concentration quenching, triplet-triplet annihilation, and singlet-triplet annihilation. These problems are exacerbated by the long exciton lifetimes characteristic of phosphorescent OLEDs (PhOLEDs) [15–18] and thermally activated delayed fluorescence (TADF) OLEDs [19–21]. To counter some of the presently outlined problems, host-guest systems are commonly utilized to disperse emitters into host matrices. The design and synthesis of new OLED materials for the application as hosts and emitters remain crucial for the continued advancement of this technology.

The aim of this work is to design, synthesize, and investigate novel carbazole- and phenoxazine-based materials, and to apply them as hosts or emitters in the emissive layers of organic light-emitting diodes

Tasks through which the aim of the dissertation could be achieved:

1. To synthesize and investigate low molecular weight compounds containing pyridinyl-carbazole and oxetane fragments, and to test these materials as hosts for phosphorescent organic light emitting devices.

2. To synthesize and characterize low molecular weight derivatives based on carbazole or phenoxazine, incorporating a central oxetane fragment, to test these materials as hosts in phosphorescent organic light-emitting diodes.

3. To develop an environmentally friendly candlelight organic light-emitting diode with a low corelated colour temperature by utilizing a newly synthesized phenoxazine-based host material.

4. To review the latest progress of the published derivatives based on benzophenone. To explore their application(s) in OLED devices, both as host materials and emitters, and to identify opportunities presented by benzophenone-based compounds in advancing the OLED technology.

5. To design, synthesize, and investigate bicarbazole-diphenyl sulfone-based twisted donor-acceptor-donor derivatives as bifunctional materials for the application as deep-blue emitters and host materials for green OLEDs.

6. To synthesize and characterize a series of twisted donor-acceptor-donor derivatives, integrating bicarbazole as the electron donor and benzophenone as the electron acceptor, to apply materials as blue emitters in OLEDs.

7. To synthesize and investigate donor-acceptor derivatives which would combine bicarbazole as the electron donor with benzophenone as the electron acceptor, and would utilize these compounds as blue emitters in OLEDs.

Scientific novelty of the work:

OLED technologies have typically been categorized into three generations: the 1st generation utilizes fluorescent emitters, followed by the 2nd generation employing phosphorescent emitters, while the 3rd generation OLEDs utilize materials with the TADF effect. In the first-generation fluorescent OLEDs, upon electrical excitation, only 25% internal quantum efficiency (IQE) could be achieved utilizing by only singlet emissive excitons [22,23]. In contrast, phosphorescent and TADF emitters have the capability to achieve IQE rates of up to 100% by utilizing triplet excitons through the utilization of the intersystem singlet to triplet crossing [24,25], while TADF emitters convert triplet excitons into emissive singlet excitons through reverse intersystem crossing [26–32]. However, as the emission peaks shift towards the deep-blue region, the nonradiative transition rate of phosphorescent emitters' d-orbitals tends to increase [23,33–35], and, in order to solve this problem, small-molecule fluorescent materials are being redeveloped due to their high colour purity and low costs [36]. For phosphorescent and TADF emitters, to avoid concentration quenching, triplet-triplet, and singlet-triplet annihilation mechanisms, the host–guest systems are commonly employed to distribute emitting molecules into host matrices. Herein, materials published in articles of this dissertation directly contribute to solving the problems outlined above, and to add value to all three OLED generations – derivatives are used as deep-blue and blue fluorescent emitters or host materials specifically tailored to phosphorescent or TADF emitters.

The first article pertaining to this thesis focuses on the synthesis, investigation, and application of pyridinyl carbazole fragments containing oxetane derivatives as hosts for the development of blue and green PhOLEDs. The most efficient blue device demonstrated an impressive external quantum efficiency of 10.3%. Similarly, the most efficient green PhOLED displayed an EQE of 9.4% at a luminance level of 1000 cd/m², as required for lighting applications.

The second publication simplified the structures described in the first article, by utilizing a one-step synthetic procedure to produce phenoxazine or carbazole substituted oxetanes as the host materials for yellow PhOLEDs. The simpler structure did not decrease the efficiency, and the most effective device in this study achieved an EQE of 10.9%.

The third paper utilized an already proven host material which had been synthesized in the course of researching for the second publication. A phenoxazine-based derivative was employed as the host for a mix of orange-red and yellow phosphorescent emitters to obtain omni-friendly low-colour-temperature candlelight OLEDs. The resulting device outperformed commercial lighting sources in terms of melatonin suppression sensitivity and reached a record-breaking maximum permissible exposure limit of 57700s. The new device achieved a maximum EQE of 10.2%, which was significantly higher than that of the commercial host material 4,4′-bis(*N*-carbazolyl)-1,1′-biphenyl (CBP) using device.

After a fourth publication, which was a review of benzophenone-based derivatives for OLEDs, novel materials for the subsequent publications were designed.

The fifth paper was produced with the objective to utilize a carbazole fragment differently than in the first two publications. This time, carbazole in a form of bicarbazole was used as an electron donor in combination with a diphenyl sulfone electron acceptor to produce new bifunctional compounds. A maximum EQE of 4.0% was achieved when new materials were being used as deep blue emitters, thereby approaching the theoretical efficiency limit of fluorescent devices. When utilized as hosts for a green phosphorescent iridium-based emitter, the same materials also achieved a maximum PE of 45 lm/W. Moreover, new materials were employed as hosts with a TADF green emitter, yielding a maximum EQE of 11%.

The sixth publication also included the utilization of bicarbazole, but this time it was combined with a benzophenone electron acceptor in a series of twisted derivatives involving the D-A-D type configuration. These novel compounds were applied as blue emitters in OLEDs, and a remarkable EQE of 5.3% was achieved, closely aligning with the theoretical limit observed in the first-generation devices.

The seventh paper delved into simplifying the materials investigated in the sixth publication into a twisted D-A architecture, by utilizing bicarbazole and benzophenone as the main building blocks. All the materials of the new series of compounds were assessed as potential blue emitters in solution-processed devices. The most promising OLED described in the publication achieved a peak EQE of 2.7%.

Contribution of the author:

The author has researched and reviewed benzophenone-based materials described in Chapter 2.4, has designed, and synthesized all the organic compounds

described in Sections 2.1–2.3 and 2.5–2.7. The author has analysed the results of thermal, photophysical and electrochemical measurements of the newly synthesized derivatives as well as the electroluminescent characteristics of the newly formed devices. Also, the author systematically used the obtained information in the preparation of the manuscripts. Dr. Gintarė Kručaitė and Dr. Daiva Tavgenienė, both representing the Department of Polymer Chemistry and Technology, Kaunas University of Technology (KTU), advised and assisted with the purification, and identification of new compounds. *Thermogravimetric analysis* (TGA) and *differential scanning calorimetry* (DSC) were performed by Dr. Eigirdas Skuodis (Department of Polymer Chemistry and Technology, KTU). Dr. Ernestas Zaleckas (Institute of Agricultural Engineering and Safety, Vytautas Magnus University, Kaunas, Lithuania), Dr. Simona Sutkuvienė (Department of Biochemistry, Vytautas Magnus University) and Prof. Jwo-Huei Jou (Department of Materials Science and Engineering, National Tsing Hua University (NTHU)) advised on the preparation and editing of the manuscripts. Dr. Iram Siddiqui, Dr. Mangey Ram Nagar, Dr. Prakalp Gautam, Dr. Shahnawaz Shahnawaz, Dr. Sujith Sudheendran Swayamprabha, Dr. Ming-Ruei Jiang, Dr. Rohit Ashok Kumar Yadav, Abhijeet Choudhury and Jin-Tin Lin, all representing the Department of Materials Science and Engineering of NTHU, measured various photophysical, electrochemical and electroluminescent characteristics of the new materials, fabricated and characterized the OLED devices. Also, Dr. Iram Siddiqui, Dr. Prakalp Gautam and Dr. Shahnawaz Shahnawaz prepared some drafts of the manuscripts. Dr. Krishan Kumar (School of Chemical Sciences, Indian Institute of Technology – Mandi) and Dr. Subrata Banik (Department of Chemistry, School of Chemical and Biotechnology, SASTRA Deemed University) performed DFT calculations and analysed the obtained data. Prof. Saulius Grigalevičius (Department of Polymer Chemistry and Technology, KTU) advised on the design and the synthetic paths of novel electroactive derivatives as well as on the preparation of manuscripts.

Scientific publications on the topic of the dissertation:

All the co-authors and publishers have been properly informed, and have explicitly allowed to use the following publications in this dissertation:

1. **Blazevicius, Dovydas**; Tavgeniene, Daiva; Sutkuviene, Simona; Zaleckas, Ernestas; Jiang, Ming-Ruei; Swayamprabha, Sujith Sudheendran; Yadav, Rohit Ashok Kumar; Jou, Jwo-Huei; Grigalevicius, Saulius. Pyridinyl-carbazole fragments containing host materials for efficient green and blue phosphorescent OLEDs // *Molecules*. Basel: MDPI. ISSN 1420-3049. 2021, Vol. 26, iss. 15, art. No. 4615, p. 1–10. DOI: 10.3390/molecules26154615 [IF: 4.927; Q2].

2. **Blazevicius, Dovydas**; Krucaite, Gintare; Shahnawaz, Shahnawaz; Swayamprabha, Sujith Sudheendran; Zaleckas, Ernestas; Jou, Jwo-Huei; Grigalevicius, Saulius. Easily synthesized and cheap carbazole- or phenoxazine-based hosts for efficient yellow phosphorescent OLEDs // *Optical Materials*. Amsterdam: Elsevier. ISSN 0925-3467. eISSN 1873-1252. 2021, Vol. 118, art. No. 111251, p. 1–6. DOI: 10.1016/j.optmat.2021.111251 [IF: 3.754; Q2].

3. Shahnawaz, Shahnawaz; Siddiqui, Iram; Nagar, Mangey Ram; Choudhury, Abhijeet; Lin, Jin-Tin; **Blazevicius, Dovydas**; Krucaite, Gintare; Grigalevicius, Saulius; Jou, Jwo-Huei. Highly efficient candlelight organic light-emitting diode with a very low color temperature // *Molecules*. Basel: MDPI. ISSN 1420-3049. 2021, Vol. 26, iss. 24, art. No. 7558, p. 1–17. DOI: 10.3390/molecules26247558 [IF: 4.927; Q2].

4. **Blazevicius, Dovydas**; Grigalevicius, Saulius. A review of benzophenone-based derivatives for organic light-emitting diodes // *Nanomaterials*. Basel: MDPI. ISSN 2079-4991. 2024, Vol. 14, iss. 4, art. No. 356, p. 1–35. DOI: 10.3390/nano14040356 [IF: 5.300; Q1].

5. Gautam, Prakalp; Shahnawaz, Shahnawaz.; Siddiqui, Iram; **Blazevicius, Dovydas**; Krucaite, Gintare; Tavgeniene, Daiva; Jou, Jwo-Huei; Grigalevicius, Saulius. Bifunctional bicarbazole-benzophenone-based twisted donor–acceptor–donor derivatives for deep-blue and green OLEDs // *Nanomaterials*. Basel: MDPI. ISSN 2079-4991. 2023, vol. 13, iss. 8, art. No. 1408, p. 1–8. DOI: 10.3390/nano13081408 [IF: 5.300; Q1].

6. **Blazevicius, Dovydas**; Siddiqui, Iram; Gautam, Prakalp; Krucaite, Gintare; Tavgeniene, Daiva; Nagar, Mangey Ram; Kumar, Krishan; Banik, Subrata; Jou, Jwo-Huei; Grigalevicius, Saulius. Bicarbazole-benzophenone-based twisted donor-acceptor-donor derivatives as blue emitters for highly efficient fluorescent organic light-emitting diodes // *Nanomaterials*. Basel: MDPI. ISSN 2079-4991. 2024, Vol. 14, iss. 2, art. No. 146, p. 1–14. DOI: 10.3390/nano14020146 [IF: 5.300; Q1].

7. Siddiqui, Iram; Gautam, Prakalp; **Blazevicius, Dovydas**; Jayakumar, Jayachandran; Lenka, Sushanta; Tavgeniene, Daiva; Zaleckas, Ernestas; Grigalevicius, Saulius; Jou, Jwo-Huei. Bicarbazolebenzophenone based twisted donor-acceptor derivatives as potential blue TADF emitters for OLEDs // *Molecules*. Basel: MDPI. ISSN 1420-3049. 2024, Vol. 29, iss. 7, art. No. 1672, p. 1–17. DOI: 10.3390/molecules29071672 [IF: 4.600; Q2].

2. CONCISE LITERATURE REVIEW

2.1. Organic Light-Emitting Diode

Electroluminescence is the phenomenon where a material emits light when the electric current passes through it, representing the direct conversion of electrical energy into luminous energy. One of the initial discoveries of this phenomenon was observed in single crystals of anthracene following experiments published in 1965 [37]. However, it took more than two decades for this process to be incorporated into electroluminescent devices, until the work published by C. W. Tang and S. A. VanSlyke in 1986 [4], as previously mentioned. The earliest OLED devices had a simple structure consisting of a single organic layer sandwiched between a cathode and an anode, as illustrated in Figure 1 (a). Soon after the creation of the first device, researchers realized the importance of selecting the appropriate electrodes with the suitable properties for the hole or electron injection with the objective to reduce the driving voltages in devices [38], and, not long after that, in 1988, C. Adachi with colleagues presented a three-layer structure of OLED which also utilized the organic

hole transport (HTL) and electron transport layers (ETL) [39]. Following this milestone, OLEDs began to incorporate even more layers, evolving towards the architecture seen in the modern times, as depicted in Figure 1 (b), with this structure sometimes including additional electron and/or hole blocking layers, more than one charge transport layers stacked on top of each other, etc.

Over the years, a very high number of materials have been used for the formation of OLED layers. For the substrate, amorphous or polycrystalline silicon is usually used. The anode material should meet certain standards, such as good chemical stability, low electrical resistivity, and high work function [40]. Indium-tin oxide (ITO) emerged as the optimal and most popular choice for such applications. The cathodes within these devices are tasked with electron generation and are predominantly made from aluminium for experimental objectives, although they can also be composed of an array of metals or alloys. This includes materials such as magnesium, silver, or combinations thereof [41,42].
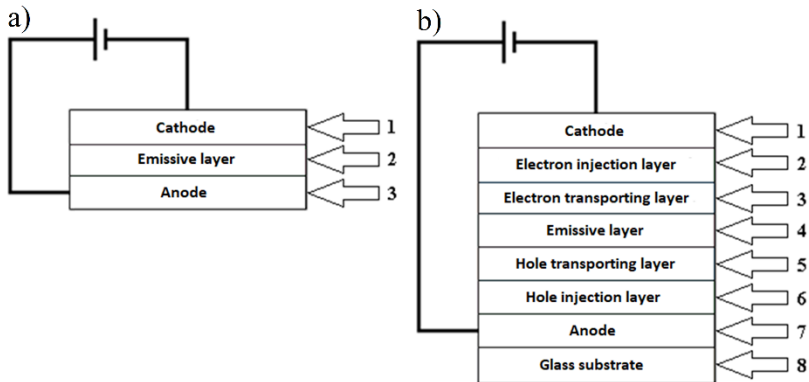
Figure 1. Schematic structure of simple (a) and modern (b) OLEDs

When subjected to electric current, electrodes produce charge carriers – specifically, electrons and holes – which migrate towards each other. Their conjunction gives rise to excitons within the emissive layer (EML), which, upon recombination, emit light. However, a significant challenge in this process is the presence of high energy barriers between the layers. To mitigate this issue, additional charge transport layers must be introduced between the electrodes and the emissive layer to reduce the energy barrier.

For instance, in order to minimize the energy barrier between the anode and the emissive layer, the appropriate materials for hole injection and/or transport are employed [43]. These materials necessitate specific characteristics, including an optimal HOMO level to ensure the minimal energy barriers for hole injection from the anode into the emissive layer, and a suitable LUMO level to minimize the electron migration from the emissive layer to the hole transport layer, a high hole mobility, and the ability to form thin and morphologically stable films [44–46]. These characteristics are commonly found in several well-known commercial compounds, depicted in Figure 2. These hole transporting/injecting materials include 1,4,5,8,9,11-hexaazatriphenylenehexacarbonitrile (HAT-CN), 1,1-bis[(di-4-

tolylamino)phenyl]cyclohexane (TAPC), 1,3-bis(*N*-carbazolyl)benzene (mCP), poly(9,9-dioctylfluorene-alt-*N*-(4-sec-butylphenyl)-diphenylamine) (TFB), N,N′-di(1-naphthyl)-*N*,*N*′-diphenyl-(1,1′-biphenyl)-4,4′-diamine (NPB), tris(4-carbazoyl-9-ylphenyl)amine (TCTA), *N*,*N*′-bis(naphthalen-1-yl)-N,N′-bis(phenyl)-2,2′-dimethylbenzidine (α-NPD), poly(9-vinylcarbazole) (PVK), and poly(3,4-ethylenedioxythiophene)-poly(styrenesulfonate) (PEDOT:PSS), which typically feature electron-donating components such as diphenylamine, naphthylamine, and carbazole, owing to their high charge carrier mobility and a low ionization potential.
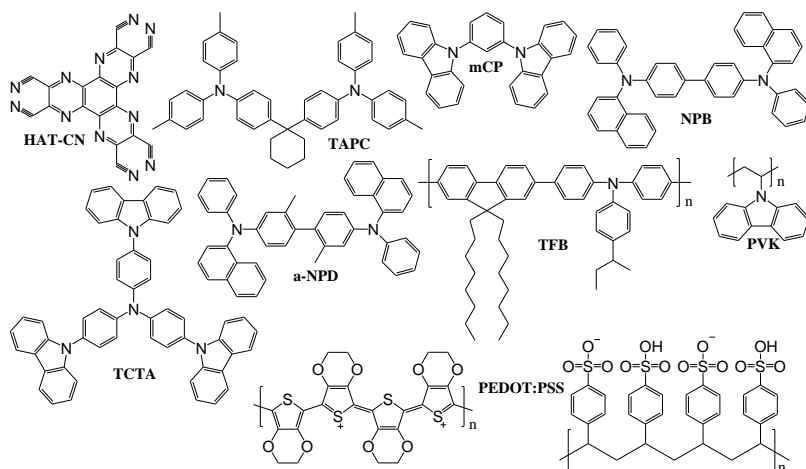
Figure 2. Commercial materials used for hole transport/injection layers

The same principle also applies to electrons necessitating additional OLED layers for the electron transport and/or injection to minimize the energy barrier. Typically, electron mobility in organic materials is lower than hole mobility. An ideal electron transporting material should not only exhibit high electron mobility and morphological stability, but also possess suitable HOMO and LUMO levels for effective electron transport from the cathode to the emissive layer while isolating holes and excitons within the emissive layer. Numerous studies have explored the incorporation of electron-withdrawing groups, such as pyridine, pyrimidine, triazine, and phosphine oxide, to enhance the electron-transport capabilities of the materials [47–51]. These fragments are prevalent in widely-used commercial electron transport materials depicted in Figure 3.
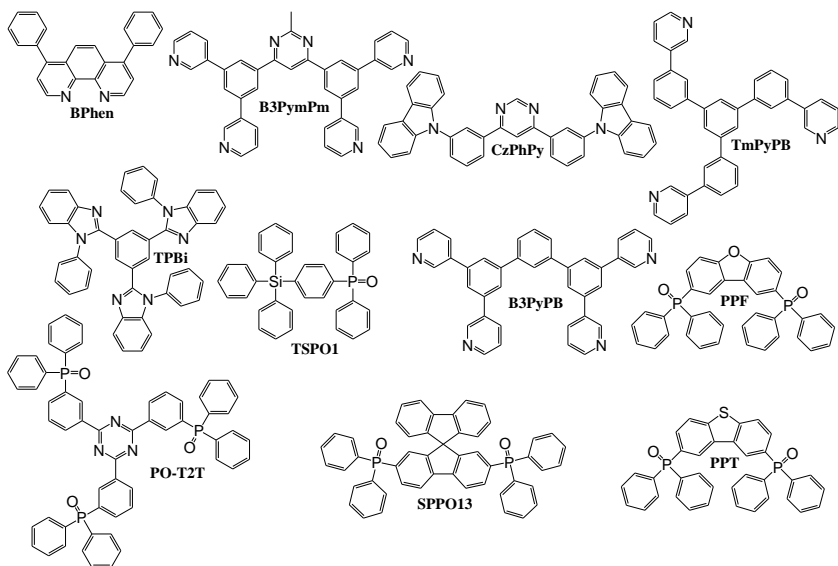
Figure 3. Commercial materials used for electron transport/hole blocking layers

Commercial electron transport materials include bathophenanthroline (Bphen), 4,6-bis(3,5-di(pyridin-3-yl)phenyl)-2-methylpyrimidine (B3PymPm), 4,6-bis(3-(9H-carbazol-9-yl)phenyl)pyrimidine (CzPhPy), 1,3,5-tris(3-pyridyl-3-phenyl)benzene (TmPyPB), 2,2',2''-(1,3,5-benzinetriyl)-tris(1-phenyl-1-H-benzimidazole) (TPBi), 2,4,6-tris[3-(diphenylphosphinyl)phenyl]-1,3,5-triazine (PO-T2T), 1,3-bis(3,5-dipyrid-3-ylphenyl)benzene (B3PyPB), dibenzo[b,d]furan-2,8-diylbis(diphenylphosphine oxide) (PPF), 2,8-bis(diphenyl-phosphoryl)-dibenzo[b,d]thiophene (PPT), diphenyl[4-(triphenylsilyl)phenyl]phosphine oxide (TSPO1) and 2,7-bis(diphenylphosphoryl)-9,9'-spirobifluorene (SPPO13). Between the cathode and the electron-transporting layer, additional measures are often taken to reduce the energy barrier for the electron transport even further. Electron injection layers are commonly employed for this purpose, traditionally composed of inorganic materials such as LiF, Cs2CO3, CsF, MoO3, Rb2CO3, Ca, or, occasionally, organic compounds like 8-quinolinolato lithium (Liq). The incorporation of these materials has been shown to enhance the overall efficiency of OLEDs, and further improvements can be attained by optimizing the thicknesses of these layers [52].

The final layer yet to be discussed is the emissive layer (EML), which serves as the source of light emission in OLEDs. All the objectives of this dissertation are closely related to the layer that is predominantly composed of organic molecules and which exhibits electroluminescence when charge carriers from the adjacent layers generate excitons which recombine within the EML. The composition and structure of the EML dictate the colours and the luminance levels emitted by OLED displays, thereby influencing their visual performance. As mentioned above, OLEDs are commonly categorized into three generations based on their mechanisms of light generation and the components of the emissive layer. The first generation employs fluorescent emitters, followed by the second generation utilizing phosphorescent

emitters (PhOLED), while the third generation relies on materials exhibiting the thermally activated delayed fluorescence (TADF) effect.

2.2. Fluorescent OLEDs

Initially, OLEDs exclusively employed fluorescent materials; hence, they are commonly referred to as 1st generation OLEDs, and their fundamental operational concept is depicted in Figure 4.
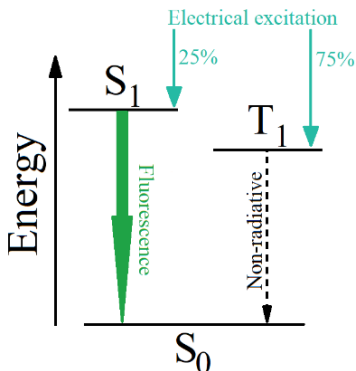
Figure 4. Basic working principle of fluorescent OLEDs

Fluorescent substances, when electrically stimulated, can only exploit singlet excitons for light emission, as triplet excitons undergo non-radiative recombination. Considering spin statistics, merely 25% of all excitons are effectively utilized for light emission, thereby yielding a maximum internal quantum efficiency (IQE) of 25%. When factoring in an average light outcoupling the efficiency of 20%, the theoretical maximum external quantum efficiency (EQE) amounts to around 5% [53].

Despite these relatively modest efficiency figures and their comparative disadvantage against the newer OLED generations, the persistent challenge of poor stability in blue phosphorescent OLEDs remains a significant limitation. As previously mentioned, the nonradiative transition rate of phosphorescent materials tends to increase as the emission approaches the deep-blue region with the CIEy coordinate lower than 0.1, posing difficulties in achieving a high efficiency [33,34,54,55]. Deep-blue emitters would not only decrease the necessity for a large number of pixels dedicated to the blue emission, but would also lower the overall cost of the device; therefore, the development of high-efficiency and stable deep-blue fluorophores is crucial for this objective. To address this issue, there is ongoing redevelopment of small-molecule fluorescent materials due to their advantages in the colour purity, stability, and cost-effectiveness [35].

Therefore, it is increasingly important to use new versatile organic materials to make highly efficient deep-blue OLEDs with simpler designs for big commercial projects. To surpass the 25% IQE limitation of the conventional fluorescence materials, researchers have incorporated triplet-triplet annihilation molecules into the structures of OLEDs, leveraging the interaction of low triplet energy excitons to generate high-energy singlet excitons [56]. Researchers commonly use anthracene, pyrene, carbazole, benzophenone, and diphenyl sulphone moieties for these purposes, as shown in Figure 5.

24
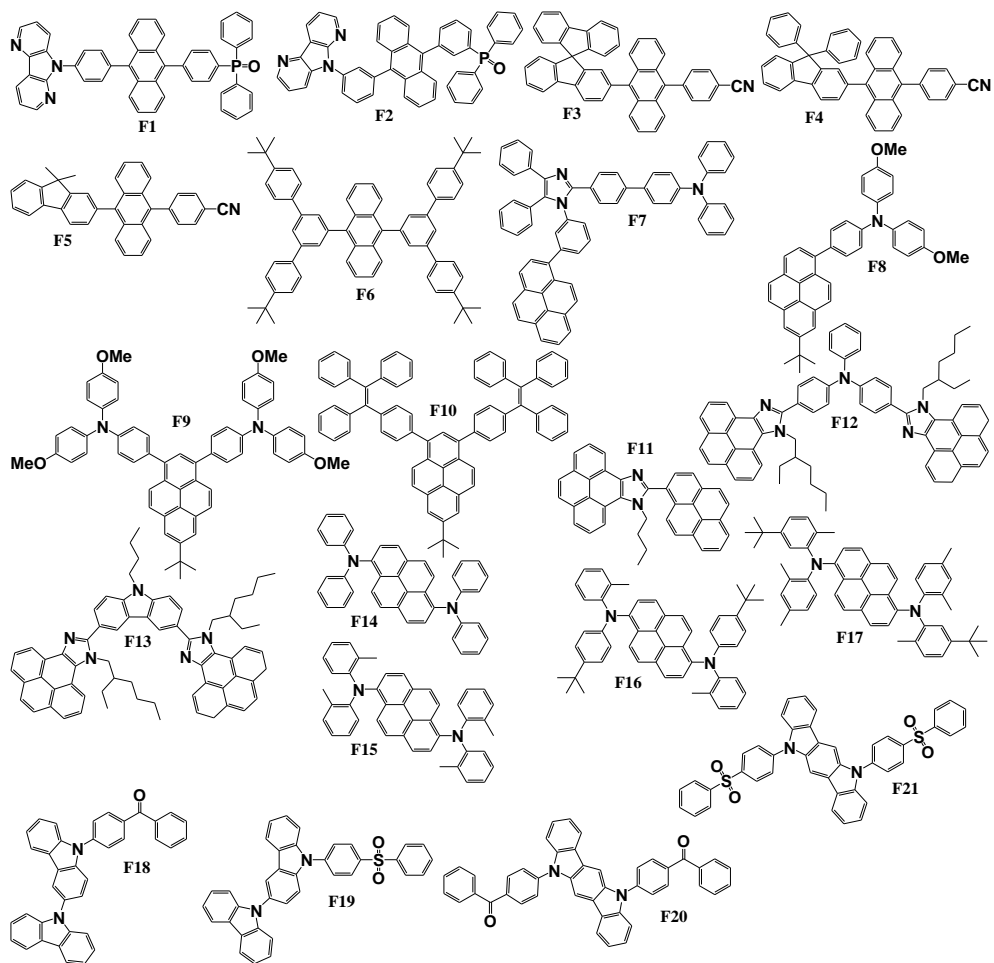
Figure 5. Chemical structures of fluorescent emitters

For instance, S. Ye and his team synthesized and experimented with two asymmetric anthracene materials, namely, **F1** and **F2** [57]. These materials exhibited a maximum EQE of 6.40% and 4.86%, respectively, when utilized in devices, along with deep-blue emissions indicated by the CIE coordinates of (0.151, 0.066) and (0.157, 0.071). L. Xing and his team synthesized and characterized three derivatives featuring the anthracene core and fluorene fragments, namely, **F3**, **F4**, and **F5** [58]. These anthracene derivatives exhibit a highly twisted configuration, resulting in deep-blue light emission, as confirmed by crystallographic analysis. An undoped device constructed with material **F4** as the emitter showcased a maximum EQE of 7.1% with the CIE coordinates of (0.149, 0.104). Notably, even at a high brightness of 1000 cd/m², the EQE was maintained at 6.6%, thus indicating the minimal efficiency roll-off. The excellent electroluminescence (EL) performance is attributed to triplet-triplet annihilation. In contrast, the anthracene-based derivative **F6**, synthesized and studied by Z. Q. Wang and colleagues back in 2011 [59], showed no triplet-triplet annihilation effect, and achieved a lower EQE of 2.2% in a non-doped device configuration.

Despite this, it emitted an even deeper blue light, with CIE coordinates of (0.15, 0.05), which could potentially expand the colour range for the display purposes. Khurram Usman and his team adopted an alternative approach, combining imidazole, triphenylamine, and pyrene units into a single fluorescent donor-acceptor type molecule **F7**, which was tested as an emitter [60]. In a solution-processed non-doped OLED, it exhibited a low V_{ON} of 2.8 V, an EQE of 2.97%, and consistent emission in the deep-blue region with the CIE coordinates of (0.15, 0.13).

Pyrene fragments were also effectively employed by researchers under the leadership of J. Zeng. They combined pyrene with triphenylamine or tetraphenylethylene electron donors, yielding materials **F8**, **F9**, and **F10** [61]. The compounds **F8** and **F10** displayed characteristics of aggregation-induced emission, while **F9** did not exhibit such a behaviour. In OLED applications, the emitter **F8** performed best in a non-doped device configuration, by achieving an EQE of 6.53% and emitting light in the greenish-blue region with the CIE coordinates of (0.18, 0.39). On the other hand, the emitter **F10** demonstrated superior performance when doped into a host material, resulting in a device with an EQE of 7.27% and the emission with the CIE coordinates of (0.18, 0.27), indicative of the blue emission. Jwo-Huei Jou's research team synthesized and characterized pyrene-imidazole hybrids, specifically, **F11**, **F12**, and **F13** [62], which showed a potential as fluorescent emitters. Devices employing the derivatives **F12** and **F13** as the emitters achieved EQE levels of 1.87% and 1.94%, respectively, with the CIE coordinates of (0.157, 0.054) and (0.163, 0.045), signifying a particularly deep blue emission. H. Jung and his team developed and tested pyrene derivatives featuring two diphenylamine moieties **F14**, **F15**, **F16** and **F17**, distinguished by alkyl substitutions [63]. When evaluated as emitters, these derivatives displayed encouraging outcomes with their EQE levels surpassing 7.5%. However, the best performance was exhibited by the device employing the derivative **F17** as a dopant, achieving an EQE of 9.25% with the CIE coordinates of (0.133, 0.145), indicating a blue emission. In pursuit of deep-blue fluorescence, J. Wang and co-workers merged bulky rigid planes of bicarbazole and indolocarbazole as the donors with highly twisted benzophenone and diphenyl sulphone as the acceptors, resulting in the creation of derivatives **F18**, **F19**, **F20** and **F21** [64]. In this application, the indolocarbazole-diphenyl sulphone derivative demonstrated the highest effectiveness. The device utilizing the emitter **F21** achieved an EQE of 4.61% with the CIE coordinates of (0.154, 0.059), thus confirming the deep-blue emission.

Despite the continuous efforts of researchers, these derivatives, particularly anthracene, typically demonstrate low singlet exciton yields, possibly due to robust hole-electron pairing. Consequently, they often encounter the aggregation-caused quenching effect [65]. This phenomenon reduces the device efficiency and compromises the colour purity [65–67]. The development of new fluorescent emitters is crucial for advancing the OLED technology and overcoming the current constraints. In essence, the creation of novel fluorescent emitters fosters innovation in the OLED technology, resulting in the evolution of the display and lighting solutions that are not only more efficient and versatile, but also more cost-effective and sustainable.

2.3. Phosphorescent OLEDs

Over the past few decades, there has been a gradual shift from fluorescence-based to phosphorescence-based devices in the quest for greater efficiencies [33,68–71]. OLEDs incorporating the traditional fluorescent dopants usually achieve a maximum IQE of 25% [4]. However, by utilizing triplet excitons through intersystem singlet-to-triplet crossing in phosphorescent emitters, the IQE value can be increased from 25% to 100% [24,25], as shown in Figure 6.
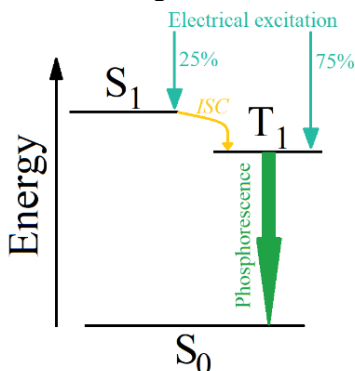
Figure 6. Basic working principle of phosphorescent OLEDs

Through the efficient utilization of triplet excitons, phosphorescent emitters notably amplify the efficiency and luminosity of OLED displays, rendering them well-suited for diverse applications spanning from smartphones to large-scale television screens. Their exceptional performance and energy efficiency have firmly established phosphorescent emitters as fundamental components within the modern OLED technology. Typically, phosphorescent emitters in the form of heavy-metal complexes have been engineered and utilized for second-generation OLEDs [72]. In the development of PhOLEDs, commonly employed commercial emitters include bis(1-phenylisoquinoline)(acetylacetonate)iridium(III) (Ir(piq)$_2$acac), bis(2-phenylbenzothiazolato)(acetylacetonate)iridium(III) (Ir(bt)$_2$(acac)), and tris(1-phenylisoquinoline)iridium(III) (Ir(piq)$_3$) for red devices; bis(2-methyldibenzo[f,h]quinoxaline)(acetylacetonate)iridium(III) (Ir(MDQ)$_2$acac) and tris(2-phenylquinoline)iridium(III) (Ir(2-phq)$_3$) for orange-red devices; bis(4-phenylthieno[3,2-c]pyridinato-N,C2')(acetylacetonate) iridium(III) (PO-01) for yellow devices; tris[2-phenylpyridine]iridium(III) (Ir(ppy)$_3$), bis[2-(2-pyridinyl-N)phenyl-C](acetylacetonato)iridium(III) (Ir(ppy)$_2$acac), and [2-(4- methyl-5-phenyl-2-pyridinyl-κN)phenyl-κC]bis[2-(2-pyridinyl-κN)phenyl-κC] iridium (Ir(ppy)$_2$(bpmp)) for green devices; and bis[2-(4,6-difluorophenyl)pyridinato-C2,N](picolinato)iridium (FIrpic) and bis(2,4-difluorophenylpyridinato)-tetrakis(1-pyrazolyl)borate iridium(III) (FIr6) for blue devices. The structures of these emitters are illustrated in Figure 7.
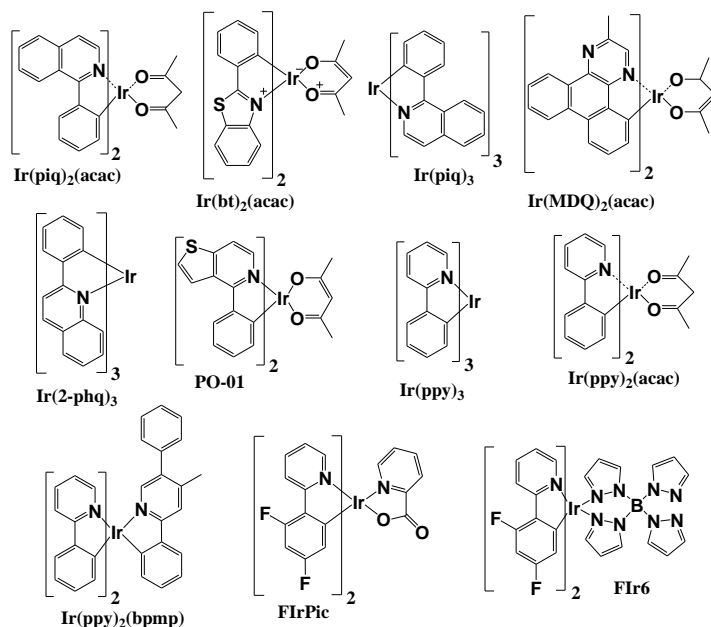
Figure 7. Structures of commercial phosphorescent emitters

Phosphorescent emitters offer an appealing array of the emission colours spanning from red to blue. By integrating yellow and red emitters within a single device, PhOLEDs have been utilized in candlelight-style lighting applications. This approach holds the promise of reducing the potential risks associated with blue emissions to human health, ecosystems, and nocturnal environments, as it effectively eliminates blue light hazards altogether [73]. On the other hand, yellow emitters, when combined with blue emitters, can play a significant role in enhancing the efficiency of white OLEDs [74].

The high internal quantum efficiency and the operational stability observed in emissive complexes of noble metals, particularly iridium [75–78], do not shield PhOLEDs from encountering the typical above mentioned efficiency reduction problems caused by issues such as aggregation-induced quenching, triplet-triplet, and triplet-polaron annihilation, especially as the luminance levels increase [15–18]. To address these challenges, host materials are typically introduced to the emissive layer in order to ensure the even spread of phosphorescent emitters throughout the layer's volume. High-performance PhOLEDs necessitate host materials which would comply with the fundamental requirements, such as an excellent thermal stability and film formation qualities, including a high glass transition temperature [79–84]. The film-forming property ensures the uniform dispersion of guest molecules within the host material, reducing the likelihood of concentration quenching. Additionally, it is crucial for the host material to possess a higher triplet energy value than the emitter in order to ensure the optimal energy transfer from the host to the emitter [85–87]. Thus far, numerous materials meeting the necessary criteria have been synthesized and utilized as the host materials for PhOLEDs, with their structures depicted in Figure 8. As evident from the Figure, the predominant fragments utilized in PhOLED host

materials include carbazole, phenoxazine, different furans, thiophenes, pyrans, pyridines, pyrimidines, etc. Moreover, it is observable that these materials are bipolar, thereby indicating that molecules incorporate both electron-accepting and electron-donating components.

J. Wang and the research team investigated materials **P1**, **P2**, and **P3**, where indolocarbazole serves as an electron donor, while either pyridine or pyrimidine functions as an electron acceptor [88]. Additionally, they employed dibenzofuran as an additional acceptor, which proved beneficial in enhancing both the thermal and the morphological properties. The novel host materials exhibited remarkably high T_g values exceeding 150 °C, along with elevated E_T values of 2.69 eV for **P1**, 2.86 eV for **P2**, and 2.85 eV for **P3**. Among these materials, the derivative **P3** emerged as the most efficient host for the green dopant Ir(ppy)$_3$, achieving impressive CE, PE, and EQE, which reached, respectively, 168.4 cd/A, 203.4 lm/W, and 41.1%. The derivatives **P4** and **P5**, consisting of electron donating carbazole and electron accepting dioxy[2,3-b]pyrazine units, were synthesized and characterized by Yuhuan Chen and team [89]. With high T_g values ranging from 147 to 155 °C, and the triplet energy levels of 2.55 to 2.57 eV, these materials were well-suited for creating thin amorphous films to serve as hosts for the red phosphorescent dopant Ir(piq)$_2$(acac). Between these two materials, **P5** demonstrated a higher efficiency, and the device utilizing this host achieved CE, PE, and EQE values of 9.69 cd/A, 7.27 lm/W, and 13.82%, respectively. The derivatives **P6**, **P7** and **P8**, utilizing the carbazole electron donor in tandem with pyrimidine and pyridine electron acceptors in D-π-A structures, were introduced by the group of researchers led by Z. Huang [90]. All the three materials exhibited high T_g values exceeding 100°C, coupled with sufficiently high E_T levels ranging from 2.58 to 2.75 eV, thereby making them suitable hosts for both the red Ir(piq)$_2$(acac) and green Ir(ppy)$_3$ phosphorescent dopants. The compound **P8** emerged as the most efficient host for both red and green emitters within this group. The green device achieved the maximum CE, PE, and EQE values of 88.15 cd/A, 78.57 lm/W, and 21.79%, respectively. Meanwhile, the red device demonstrated a CE of 21.07 cd/A, a PE of 23.64 lm/W, and an EQE of 25.03%. Qin Zhang with team worked on the novel host materials **P9** and **P10**, based on the carbazole electron donor with pyridine and benzonitrile electron acceptors [91]. Both materials displayed exceptional thermal and morphological characteristics, boasting T_g values exceeding 120°C, thereby enabling their utilization in the formation of stable amorphous layers. Additionally, the derivatives **P9** and **P10** exhibited E_T levels of 2.75 eV and 2.84 eV, respectively. After testing both compounds as hosts for red Ir(piq)$_2$(acac) and green Ir(ppy)$_3$ phosphorescent emitters, the derivative **P10** emerged as the more suitable host for this application. The green device achieved CE, PE, and EQE of 88.32 cd/A, 98.19 lm/W, and 24.3%, while the red device attained values of 22.19 cd/A, 24.38 lm/W, and 25.3%, respectively.
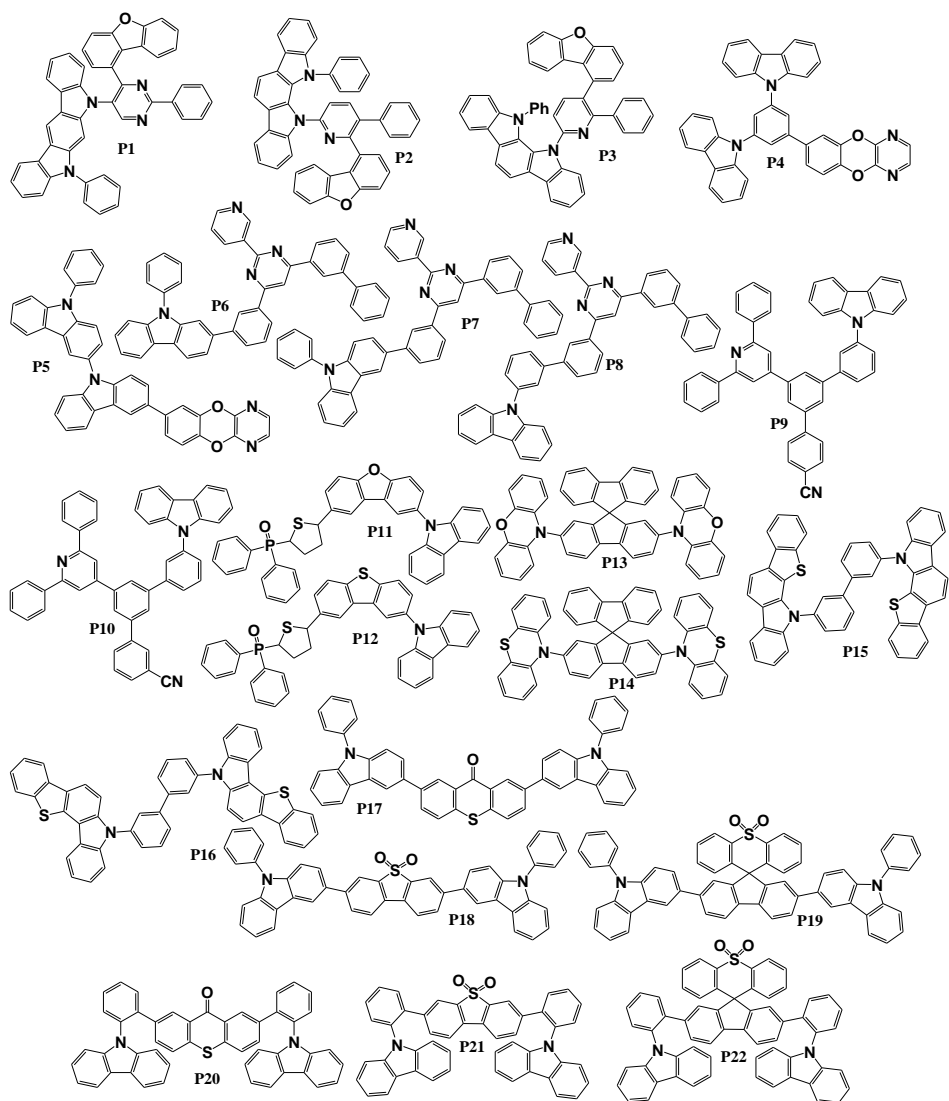
Figure 8. Host materials for phosphorescent OLEDs

An alternative molecular design approach was employed by S. Ryu and colleagues, by combining carbazole, thiophene, and diphenylphosphine oxide fragments with central dibenzofuran or dibenzothiophene moieties in the molecules **P11** and **P12** [92]. DSC analysis of these materials unveiled high glass T_g values of 119 °C for the derivative **P11** and 127 °C for the compound **P12**. Moreover, the materials exhibited E_T levels within the range of 2.52–2.56 eV, thus rendering them well-suited as the potential host materials for the yellow phosphorescent dopant PO-01. Following device testing, OLEDs employing the host **P12** demonstrated superior performance, by achieving PE and EQE values of 65.7 lm/W and 25.4%, respectively. Researchers led by J. Jesuraj obtained the D-A-D-type molecules **P13** and **P14**, employing a central spirobifluorene electron acceptor core paired with phenoxazine

or phenothiazine electron donors [93]. Both compounds **P13** and **P14** exhibited a good thermal stability, with T_d of 415°C and 428°C, respectively, and morphological stability, while boasting T_g values of 198°C and 196°C, respectively. When these materials were employed as hosts for the green triplet emitter Ir(ppy)$_3$, the OLED-utilizing host **P13** demonstrated the CE and EQE values of 28 cd/A and 7.5%, respectively, while the device utilizing the host **P14** showed an efficiency of 37 cd/A and 11%. The derivatives **P15** and **P16**, both utilizing benzothienocarbazole as a main building block, were synthesized and investigated by A. Arai with the team [94]. These derivatives exhibited high T_g values of 166–167 °C, along with elevated E_T levels of 2.7 and 2.8 eV for the materials **P15** and **P16**, respectively, making them suitable candidates for testing as the hosts for the green phosphorescent dopant Ir(ppy)$_3$. After device experiments, the compound **P15** proved to be more effective, by achieving maximum CE, PE, and EQE values of 81.7 cd/A, 87.7 lm/W, and 22.5%, respectively, when utilized in PhOLEDs. P. Gnanasekaran and co-workers designed and synthesized the objective materials **P17** – **P22**. Their approach involved combining thioxanthone, diphenyl sulfone, and spiro[fluorene9,9'-thioxanthene]10',10'-dioxide as the central electron-accepting fragments with phenyl carbazole as the electron donor [95]. The E_T levels for the derivatives **P17**, **P18**, **P19**, **P20**, **P21**, and **P22** were 2.39 eV, 2.13 eV, 2.31 eV, 2.65 eV, 2.45 eV, and 2.47 eV, respectively, thus making them suitable candidates for the application as host materials for the red phosphorescent dopant Ir(piq)$_2$(acac). While the efficiencies of the devices utilizing these six host materials were comparably similar, the highest efficiencies were achieved by the PhOLED utilizing host **P18**, with its maximum CE, PE, and EQE values reaching 11.8 cd/A, 16.2 lm/W, and 21.1%, respectively.

In general, the continuous development of novel host materials is crucial for the progression of the phosphorescent OLED technology. It fosters enhancements in efficiency, stability, reliability, and cost-effectiveness, while also facilitating innovation and customization in the OLED device design.

2.4. Thermally Activated Delayed Fluorescence Based OLEDs

Despite the collaborative efforts of researchers, the persistent challenges of poor stability along with the limited lifespan in blue phosphorescent OLEDs remain significant limitations [96]. Furthermore, as previously noted, the presence of noble metals in phosphorescent materials raises strong environmental concerns and the potential future cost growth for the devices concerned [13,14]. In recent years, there has been a notable shift in focus towards TADF materials. This interest stems from their capacity to convert triplet excitons into emissive singlet excitons through *reverse intersystem crossing* (RISC) without the requirement of noble metal atoms, all the while achieving high EQE levels [97,98]. Figure 9 depicts the basic working principle of TADF OLEDs.
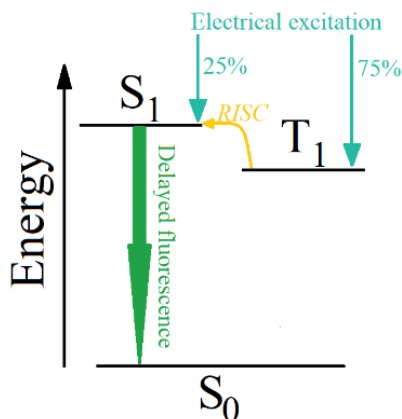
Figure 9. Basic working principle of TADF-based OLEDs

Usually, TADF emitters employ a combination of the electron donor and acceptor in one molecule in such a way that the objective molecule would conform to the basic requirements for TADF emitters, such as: minimally overlapping or not spatially overlapping HOMO and LUMO orbitals, which, in turn, would grant a low difference between the singlet and triplet excited state energy levels (ΔE_{ST}). By achieving the fulfilment of this requirement, an efficient RISC process could be obtained. To achieve this, researchers often utilize a twisted connection between the donor and the acceptor [99–102]. Figure 10 depicts commonly utilized commercial TADF emitters.

Commercially available TADF emitters include red: 2,3,5,6-tetrakis(3,6-dimethylcarbazol-9-yl)-1,4-dicyanobenzene (4CzTPN-Me), 3,7,11-tris(diphenylamino)quinolino[3,2,1-de]acridine-5,9-dione (3DPA-DiKTa), 2-(9-phenyl-9*H*-carbazol-3-yl)-10,10-dioxide-9*H*-thioxanthen-9-one (TXO-PhCz) and 2,6-bis(4-(diphenylamino)phenyl)anthracene-9,10-dione (DPA-Ph-AQ), green: bis(4-(9,9-dimethylacridin-10(9*H*)-yl)phenyl)methanone (DMAC-BP), 10,10'-(4,4'-sulfonylbis(4,1-phenylene))bis(10*H*-phenoxazine) (PXZ-DPS), 3,4,5,6-tetra(9*H*-carbazol-9-yl)phthalonitrile (4CzPN) and 9-(4-(4,6-diphenyl-1,3,5-triazin-2-yl)phenyl)-N3,N3,N6,N6-tetraphenyl-9*H*-carbazole-3,6-diamine (DACT-II) and blue: 9'-(2,12-di-tert-butyl-5,9-dioxa-13b-boranaphtho- [3,2,1-de]anthracen-7-yl)-9,9"-diphenyl-9*H*,9'*H*,9"*H*-3,3':6',3"-tercarbazole (TB-P3Cz), 9-(4-(4,6-diphenyl-1,3,5-triazin-2-yl)phenyl)-3,6-diphenyl-9*H*-carbazole (PCzTrz), 3,3',6,6'-tetrakis(9-phenyl-9*H*-carbazol-3-yl)-spiro-diphenylsulfone (SDPS-4PhCz) and 2-(4-(9,9-dimethylacridin-10(9*H*)-yl)phenyl)thianthrene 5,5,10,10-tetraoxide (ACRDSO2) emitters.
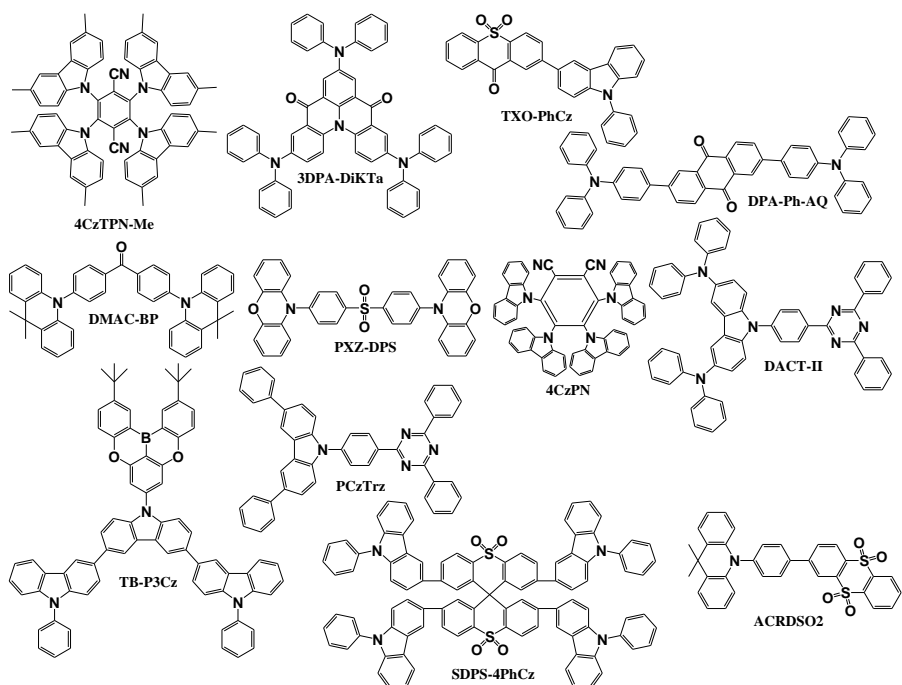
Figure 10. Structures of commercially available TADF emitters

Despite the wide selection of the commercial TADF emitters, obstacles such as the ineffective utilization of triplet excitons and the challenges associated with achieving high PLQY values are those factors which contribute to the reduced overall efficiency seen in TADF-based OLEDs in comparison to the conventional phosphorescent OLEDs. One of the strategies entails the creation of novel TADF molecules, particularly for non-doped OLEDs utilizing materials demonstrating aggregation-induced emission characteristics [103–109]. Some of the newly synthesized TADF emitters are shown in Figure 11.

Z. Hao led a team which designed and synthesized the chiral sulfoximine-based green TADF emitter **TE1**. This emitter exhibited a low ΔE_{ST} of 0.075 eV and an exceptionally high PLQY of 99% [110]. A device incorporating the **TE1** emitter displayed outstanding maximum values of CE, PE, and EQE of 85.6 cd/A, 84.0 lm/W, and 28.5%, respectively. The emitters **TE2**, **TE3**, and **TE4**, designed and studied by F. Hu et al., exhibited small ΔE_{ST} levels ranging from 0.02 to 0.08 eV and showcased distinct prompt and delayed fluorescence features in their overall photoluminescence [111]. Across all the devices, green emission was observed, with OLED using **TE2** serving as the emitter demonstrating superior efficiencies, by achieving a CE of 47.7 cd/A, a PE of 42.9 lm/W, and an EQE of 14.6%. Y. Mei and colleagues developed the TADF emitters **TE5**, **TE6**, and **TE7** by employing the electron donor carbazole and the electron acceptor 10-(pyridin-2-yl)acridin-9(10*H*)-one. These novel materials exhibited high PLQYs ranging from 54% to nearly 100%, and ΔE_{ST} values spanning from 0.15 to 0.26 eV [112]. When employed as emitters in OLEDs, these substances displayed deep-blue emission with a CIE$_y$ value of around 0.1. The most outstanding

characteristics were exhibited by the dopant **TE6** in a device achieving the maximum CE, PE, and EQE values of 33.5 cd/A, 35.3 lm/W, and 33.4%, respectively. Researchers under the leadership of G. Kručaitė synthesized and evaluated the emitters **TE8** and **TE9** by employing an asymmetric molecular structure. They combined carbazole and diphenylamine electron donors with diphenyl sulphone or benzophenone electron acceptors [113]. These materials displayed vastly different ΔE_{ST} levels, measuring 0.29 eV for **TE8**, and 0.04 eV for **TE9**. This difference became evident when the derivatives were utilized as emitters in OLEDs, with **TE9** exhibiting notably better characteristics. The yellow TADF OLED utilizing emitter **TE9** achieved CE, PE, and EQE values of 35.4 cd/A, 46.3 lm/W, and 12.1%, respectively. Z. Xie and colleagues synthesized the emitters **TE10** and **TE11** by merging the acridine and carbazole electron donors with a pyridine-carbonitrile electron acceptor within a single molecule. These innovative derivatives exhibited remarkably high PLQYs ranging from 89% to 95%, coupled with low ΔE_{ST} levels spanning from 0.09 to 0.17 eV [114]. The emitter **TE11**, utilized in an OLED prototype, showcased a green emission and offered superior characteristics, by achieving a CE of 84.1 cd/A, a PE of 64.4 lm/W, and an EQE of 25.3% in a non-doped device configuration.
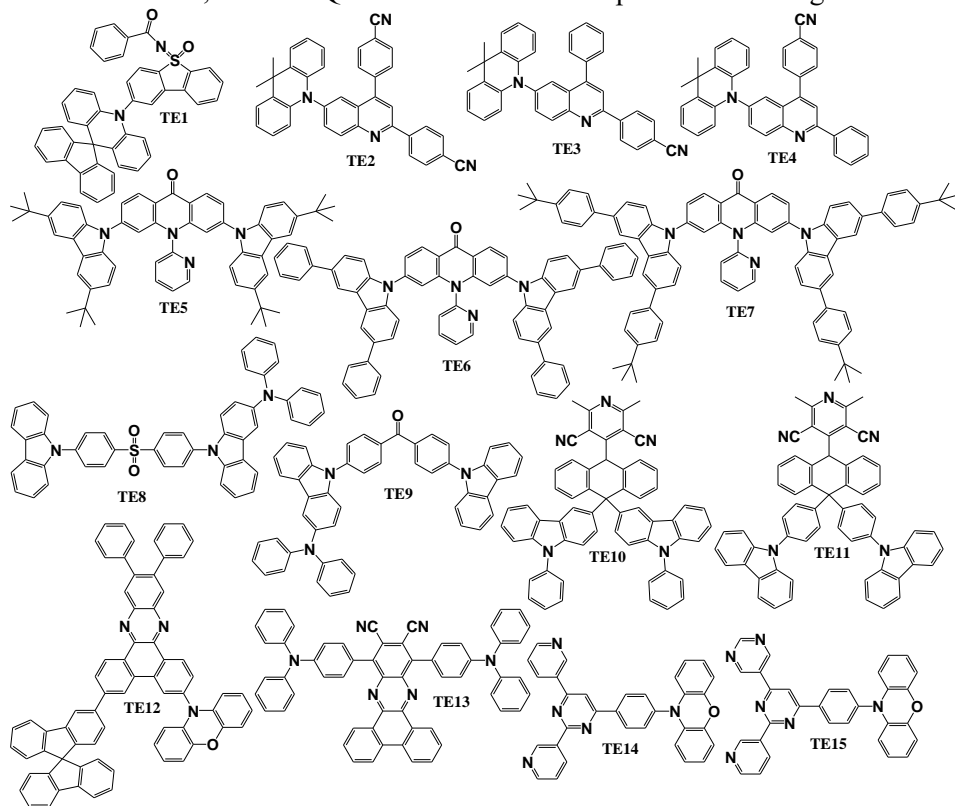
Figure 11. Structures of newly synthesized TADF emitters

J.-X. Chen and colleagues introduced the emitter **TE12** incorporating a rigid D-A backbone and a spirobifluorene moiety [115]. The material exhibited an

34

exceptionally high PLQY of 96% and a low ΔE_{ST} of 0.05 eV, emitting the orange light. In device applications, the emitter **TE12** achieved high CE, PE, and EQE values of 55.7 cd/A, 53.8 lm/W, and 33.4%, respectively. Under the leadership of H. Wang, a scientific team developed a red TADF emitter, **TE13**, featuring two electron-donating triphenylamine segments installed at the para- positions of a fused phenyl ring within the acceptor core, situated between the phenazine and carbonitrile groups [116]. This derivative exhibited a sufficiently low ΔE_{ST} of 0.12 eV and a high PLQY of 94%. In the most efficient OLED configuration, **TE13** demonstrated efficient deep-red electroluminescence, by achieving a maximum EQE of 27.6%, a CE of 13.4 cd/A, and a PE of 12.0 lm/W. Under the leadership of Y.-Z. Shi, the materials **TE14** and **TE15** were synthesized by combining the electron donor phenoxazine, the phenyl separator, and the electron acceptors pyridine and pyrimidine [117]. These novel derivatives exhibited low ΔE_{ST} levels of 0.04–0.05 eV. A device employing the **TE14** emitter attained superior characteristics. In a non-doped configuration, the OLED achieved a CE of 50.5 cd/A, a PE of 53.5 lm/W, and an EQE of 18.8%. Developing novel TADF emitters is essential for the ongoing enhancement of technology, thereby ensuring an improved colour purity, stability, cost-effectiveness, and longevity of the forthcoming devices.

Despite the potential of TADF materials, many TADF OLEDs experience a significant decline in their EQE levels at higher luminance, which is a phenomenon commonly known as the efficiency roll-off [15]. This decline is attributed to various issues such as concentration quenching, singlet-singlet annihilation, triplet-triplet annihilation, and singlet-triplet annihilation, with these effects becoming more pronounced as the exciton lifetime increases [118]. To mitigate the concentration quenching issue, the majority of highly efficient TADF OLEDs integrate TADF molecules into the appropriate host materials. However, due to the limited availability of the host materials tailored for TADF OLEDs [119–121], researchers often resort to using conventional host materials typical in phosphorescent OLEDs [122]. Hence, one of the strategies for addressing efficiency challenges involves developing new host materials specifically designed for TADF OLEDs.

Nevertheless, in contrast to organic emitters, there is a scarcity of reports on suitable host materials, primarily due to challenges in designing hosts with the needed properties, such as high triplet and singlet energies to confine excitons, a sufficient overlap between the PL spectra of the host material and the absorption spectra of the emitter, bipolar characteristics with the appropriate HOMO and LUMO levels relative to the neighbouring layers, inhibited molecular interaction to mitigate concentration quenching, and, preferably, solution-process-ability [123,124]. Figure 12 depicts the chemical structures of the recently developed host materials.

W. Jiang and co-workers developed the host materials **TH1**, **TH2**, and **TH3** by combining a benzonitrile electron acceptor with carbazole-based electron donors [125]. All the newly synthesized materials exhibited high triplet energies exceeding 2.8 eV and demonstrated a good thermal and electrochemical stability. When tested as host materials for the blue dopant 2,3,5,6-tetrakis(3,6-di-tert-butyl-9*H*-carbazol-9-yl)benzonitrile (4TCzBN), the host **TH2** showcased the best characteristics in the

device, by achieving the maximum CE and EQE values of 41.88 cd/A and 22.04%, respectively, along with a low turn-on voltage of 3.5 V.
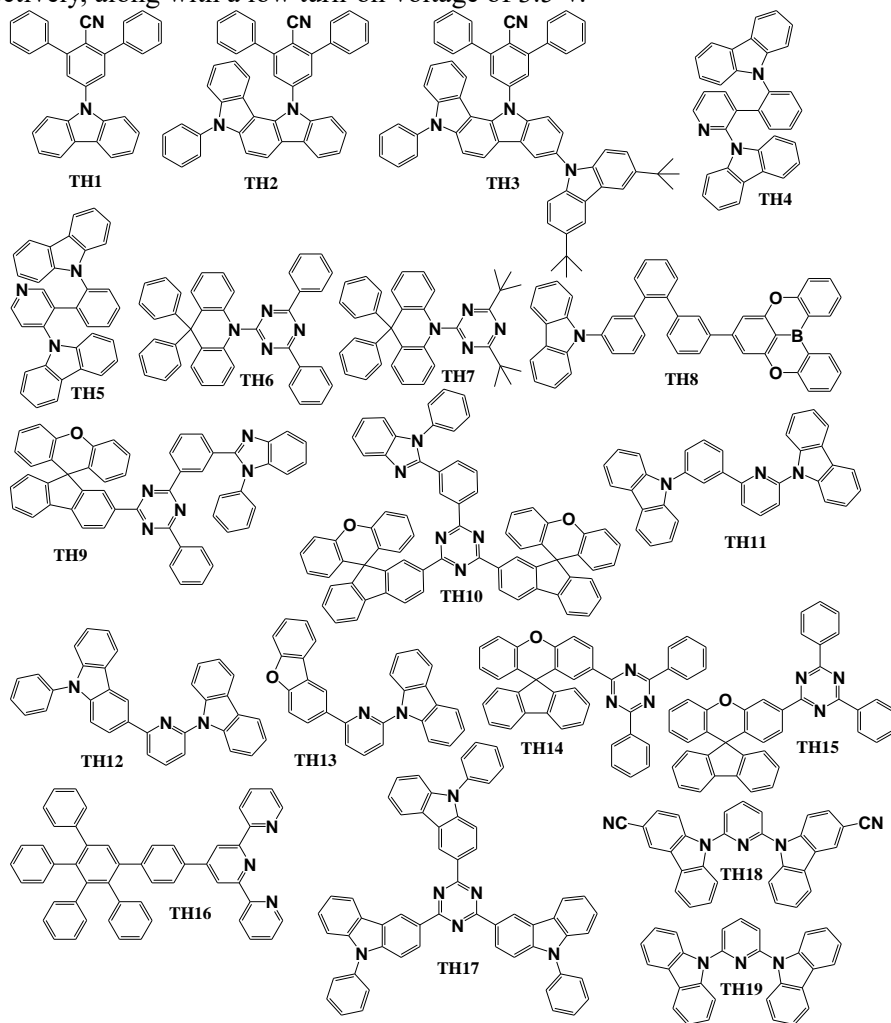
Figure 12. Structures of newly synthesized host materials for TADF OLEDs

A team led by T. H. Ha developed two novel host materials, **TH4** and **TH5**, by utilizing a pyridine electron acceptor core combined with carbazole electron donors linked at different locations [126]. Both host materials underwent testing in OLED devices using a blue 2,4,6-tris(2-(9H-carbazol-9-yl)phenyl)-1,3,5-triazine (TCz-Trz) dopant, with the reference device employing 2,2′-di(9H-carbazol-9-yl)-1,1′-biphenyl (oCBP) as the host material. The device utilizing the host material **TH5** exhibited the best characteristics, by achieving a maximum EQE of 16.2%, while the operational lifetime improved by 88% compared to the reference device. G. Kreiza and his team developed two new host materials, **TH6** and **TH7**, employing a D-A molecular structure with a triazine electron acceptor and an acridine electron donor [127]. Both materials exhibited prominently high E_T values, measuring 3.07 eV for the derivative

TH6 and 3.27 eV for the compound **TH7**. During the characterization of blue OLED devices with a dopant of 10-(4-[1,4]benzoxaborino[2,3,4-kl]phenoxaborin-6-ylphenyl)-10*H*-phenoxazine (OBA-O), a reference device with the host material 3,3′-di(9*H*-carbazol-9-yl)-1,1′-biphenyl (mCBP) was utilized. The device employing the host **TH6** demonstrated the best characteristics, by achieving the maximum CE, PE, and EQE values of 22.5 cd/A, 23.5 lm/W, and 10.2%, respectively. Additionally, this device exhibited a 140% longer lifetime compared to the reference device. The above-mentioned research team led by T. H. Ha employed a different approach, by combining a carbazole electron donor with a 5,9-dioxa-13b-boranaphtho[3,2,1-de]anthracene electron acceptor separated by a terphenyl spacer in the molecule **TH8** [128]. The material exhibited an amorphous structure with a high T_g of 128 °C and demonstrated a high E_T of 3.07 eV and an E_S of 3.18 eV. When incorporated into the device structure as a host material for the green TADF emitter 1,2,3,5-tetrakis(carbazol-9-yl)-4,6-dicyanobenzene (4CzIPN), the OLED achieved the maximum CE and PE values of 70.4 cd/A and 71.3 lm/W, respectively. The maximum EQE achieved was 22.8%, and, at a luminance of 1000 cd/m², a very low roll-off of 5.26% was observed. The materials **TH9** and **TH10**, developed by X. Lu and colleagues, employed a benzimidazole-triazine electron acceptor as the core of the molecule in combination with one or two electron-rich spiro[fluorene-9,9′-xanthene] moieties [129]. Both materials exhibited E_T levels around 2.6 eV and high E_S levels exceeding 3.40 eV. The derivative **TH9** demonstrated a high Tg of 168°C, while no glass transition was observed for the material **TH10**. Both compounds were tested in devices as the host materials for the green TADF emitter BN-TP [130]. The optimal performance was achieved by employing both materials **TH9** and **TH10** in devices at the same time, which resulted in low turn-on voltages of 2.6 V and a maximum EQE of 35.7%. Impressively, EQE could be maintained above 30% even at luminance of 1000 cd/m². Y. Yu and colleagues designed, synthesized, and characterized novel compounds, namely, **TH11**, **TH12**, and **TH13**, based on a central pyridine electron acceptor, and a carbazole or dibenzofuran electron donor [131]. All the materials exhibited amorphous properties, with T_g values of 97°C, 102°C, and 69°C for the derivatives **TH11**, **TH12**, and **TH13**, respectively. Additionally, the compounds demonstrated high E_T values of 2.93 eV, 2.87 eV, and 2.96 eV, in the same order. Upon evaluating these new materials as hosts for the green TADF emitter 4CzIPN, the device with the host material **TH13** exhibited the best overall characteristics. It achieved the maximum CE, PE, and EQE values of 67.8 cd/A, 57.2 lm/W, and 20.3%, respectively, along with a 2.5-times increase in the device lifetime compared to the OLED utilizing the commercial host material CBP. The derivatives **TH14** and **TH15**, incorporating a diphenyltriazine electron acceptor and a spiro[fluorene-9,9'-xanthene] electron donor were synthesized by the research group lead by Q. Liu [132]. Although no T_g values were detected, the high melting point temperatures (T_m) exceeding 295°C suggest a good morphological stability. The compounds **TH14** and **TH15** also exhibited high E_T levels of 2.82 eV and 2.89 eV, respectively. Both derivatives were evaluated as host materials for the green TADF emitter 4CzIPN, with the device utilizing the host material **TH15** demonstrating better characteristics. It achieved the maximum values CE, PE, and EQE of 75.5 cd/A, 55.0 lm/W, and 23.0%, respectively.

P. Palanisamy and colleagues synthesized the material **TH16** incorporating terpyridine and terphenyl fragments, which exhibited high T_g and E_T levels of 176°C and 2.98 eV, respectively [133]. This derivative was employed as a host material for the blue TADF emitter 10-(4-(4,6-diphenyl-1,3,5-triazin-2-yl)phenyl)-9,9-dimethyl-9,10-dihydroacridine (DMAC-TRZ), yielding a solution-processed device with the maximum values CE, PE, and EQE of 45.15 cd/A, 32.95 lm/W, and 22.35%, respectively. X.-H. Zhao and colleagues developed the novel host material **TH17** by employing a central triazine core and three phenylcarbazole fragments. This derivative exhibited a high E_T of 2.88 eV, significant thermal stability with a T_D of 284°C, and maintained stable morphology [134]. The compound **TH17** was assessed in the emissive layer of OLED as a host for the green TADF emitter 9,10-bis(4-(3,6-ditertbutyl-9*H*-carbazol-9-yl)-2,6-dimethyl-phenyl)-9,10-diboraanthracene (tBuCzDBA). The resulting device achieved the maximum CE, PE, and EQE values of 39.8 cd/A, 21.2 lm/W, and 14.0%, respectively. C. Tang and the research team developed and synthesized the derivatives **TH18** and **TH19**, based on pyridine, incorporating carbazole or carbazole-3-carbonitrile fragments. Both materials possessed an amorphous structure, with **TH18** exhibiting a T_g of 75°C, and **TH19** featuring a T_g of 125°C [135]. Additionally, the compounds displayed high E_T levels, measured at 3.00 eV for the derivative **TH18** and 3.02 eV for the material **TH19**. Upon evaluating these materials as hosts for the green TADF emitter 4CzIPN, the device utilizing the host **TH18** showed a slightly better performance, by achieving a CE of 10.6 cd/A and an EQE of 3.0%.

To sum up, each of the OLEDs of the three generations is denoted by not only advantages, but also drawbacks. It is crucial to persist in synthesizing and refining all the three generations of this technology so that to attain the optimal outcomes and facilitate their commercial applications in fluorescent, phosphorescent, and TADF based OLEDs. Through collaborative efforts among researchers, the development of new emissive and host materials holds the promise of unlocking the potential for efficient, dependable, and cost-effective lighting solutions across a broad spectrum of applications.

3. REVIEW OF PUBLISHED ARTICLES

3.1. Pyridinyl-Carbazole Fragments Containing Host Materials for Efficient Green and Blue Phosphorescent OLEDs (Scientific Publication No. 1, Q2, 3 citations)

This chapter is based on the paper published in *Molecules*, **2021**, 26, 15 by *D. Blazevicius, D. Tavgeniene, S. Sutkuviene, E. Zaleckas, M.-R. Jiang, S. S. Swayamprabha, R. A. K. Yadav, J.-H. Jou*, and *S. Grigalevicius* [136].

Throughout this study, the target materials **4** (**H1)** and **5** (**H2)** were synthesized during three sequential synthesis steps, as illustrated in Scheme 1. Initially, 3-iodo-9*H*-carbazole **2** was produced through the iodination method of Tucker [137] by using 9*H*-carbazole **1** as an initial reagent. Subsequently, the key material, 3,3-bis(3-iodo-9-carbazolylmethyl)oxetane **3**, was synthesized by reacting 3,3-bis(chloromethyl)oxetane with an excess of the iodinated derivative **2** in basic conditions and in a presence of phase a transfer catalyst, as described earlier [138]. The desired compounds 3,3-bis[3-(2-methoxy-3-pyridinyl)carbazol-9-ylmethyl]oxetane **4** (**H1)** and 3,3-bis[3-(4-methoxy-3-pyridinyl)carbazol-9-ylmethyl]oxetane **5** (**H2**) were obtained through a Suzuki reaction [139] while applying similar synthetic procedures. Diiodo-compound **3** (1 mol. eq.) was stirred with an excess of the corresponding methoxypyridinylboronic acid (2.5 mol. eq.), potassium hydroxide (5 mol. eq.), and the catalyst bis(triphenylphosphine)palladium (II) chloride (PdCl$_2$(PPh$_3$)$_2$) (0.04 mol. eq.) in a mixture of THF (12 ml) and degassed water (1.5ml) at reflux for 1h. The reactions were executed in nitrogen atmosphere. After the reactions, the mixtures were cooled and filtered. The solvent was evaporated, and the objective products were purified with silica gel column chromatography by using a mixture of ethyl acetate and hexane (vol. ratio 1:7) as an eluent. All the structures of the synthesized derivatives were confirmed through mass spectrometry (MS), as well as by ^{1}H and ^{13}C nuclear magnetic resonance (NMR) spectroscopy. The experimental data aligned well with the theoretically proposed structures.
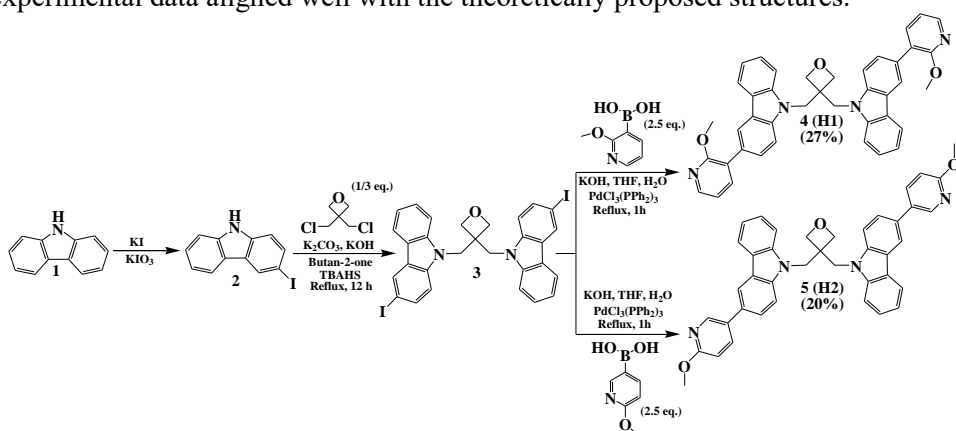
Scheme 1. Synthetic pathway of materials **4** (**H1)** and **5** (**H2)**

The synthesized target derivatives exhibit an excellent solubility in common organic solvents. While electroactive thin layers can be prepared on substrates by using a thermal evaporation technique, the good solubility enables the preparation through the cost-effective spin coating method from a solution. The thermal behaviour of the synthesized host derivatives, **4** (**H1**) and **5** (**H2**), was investigated by using DSC and TGA, with the latter one revealing its remarkable thermal stability. The temperatures of 5% weight loss for **4** (**H1**) and **5** (**H2**) were determined to be 386°C and 361°C, respectively. DSC measurements showed that **4** (**H1**), obtained as a crystalline material after synthesis and purification by silica gel chromatography, exhibited an endothermic melting peak at 257 °C during the first heating. Upon cooling, it transformed into an amorphous material with a high T_g value of 127°C. the subsequent heating cycles detected only the glass transition, with no signals of melting or crystallization. In contrast, **5 (H2)** was obtained as a fully amorphous material, as confirmed by DSC. The thermograms of **5** (**H2**), depicted in Figure 13, revealed only a high T_g of 139°C during both the first and second heating scans. No signals related to crystallization or melting were observed in the temperature range from 0°C to 350°C during the heating and cooling cycles.
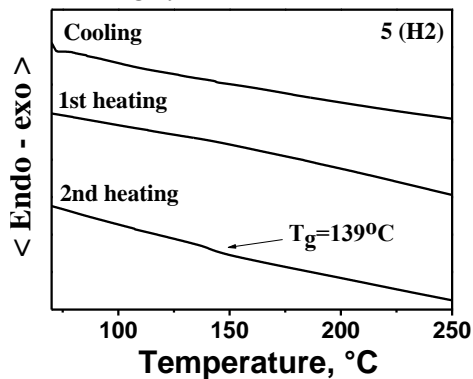
Figure 13. DSC curves of derivative **5** (**H2**)

The low-temperature (77K) photoluminescence (LTPL) spectra were recorded with the aim of determining the triplet state energy values of the pyridinyl-carbazole based derivatives **4 (H1)** and **5 (H2)**. The calculations revealed that the triplet energy values for the compounds **4 (H1)** and **5 (H2)** were 2.82 eV and 2.81 eV, respectively. Notably, these triplet energies surpass those reported for the blue phosphorescent emitter FIrpic (E_T = 2.65 eV) [140] and the green phosphorescent dopant Ir(ppy)$_3$ (E_T = 2.59 eV) [141]. This experimental outcome affirms the suitability of **4 (H1)** and **5 (H2)** as the host materials, thereby establishing their potential in applications for both green and blue phosphorescent organic light-emitting diodes (OLEDs). Table 1 summarises measured the thermal and photophysical properties of the newly synthesized materials.

Table 1. Thermal and photophysical properties of host materials **4 (H1)** and **5 (H2)**

Material	T_d (°C)	T_m (°C)	T_g (°C)	E_T (eV)
4 (H1)	386	257	127	2.82
5 (H2)	361	-	139	2.81

To evaluate the suitability of the prepared derivatives **4 (H1)** and **5 (H2)** as the host materials, green and blue PhOLEDs were fabricated by using blue FIrpic and green Ir(ppy)$_3$ phosphorescent emitters. In Figure 14, the electroluminescent (EL) spectra of devices employing the host material **4 (H1)** are depicted. The spectra of both OLEDs confirm the pure emissions of FIrpic or Ir(ppy)$_3$ dopants, thus indicating the effective energy transfer between the host **4 (H1)** and the respective guest [142]. Notably, no additional emission zones were observed, which signifies that carrier recombination occurs solely within the emitting layer. This observation suggests that exciton diffusion to the hole or electron transporting layers is avoided in the OLED structures [143].
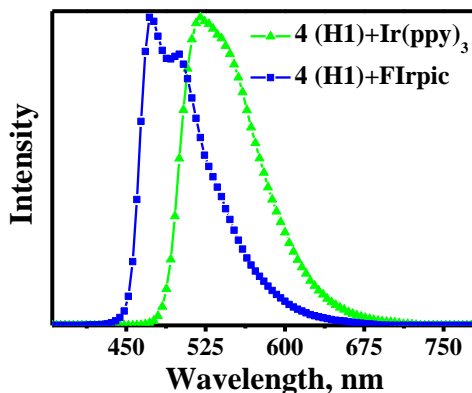
Figure 14. EL spectra of the OLEDs having host material **4 (H1)** doped with blue FIrpic or green Ir(ppy)$_3$ emitter

The host material **5 (H2)** was also utilized in blue and green OLEDs, while incorporating blue FIrpic and green Ir(ppy)$_3$ dopants as the emitters, and the resulting devices demonstrated higher efficiencies than the devices based on the host **4 (H1)**. To optimize the structure of the emissive layer, concentration-dependent experiments involving the FIrpic amount from 15 to 22.5 wt% and the Ir(ppy)$_3$ dopant amount from 7.5 to 15 wt% were employed. Table 2 provides a summary of the OLED characteristics for the investigated **5 (H2)**-based PhOLEDs.

Table 2. Characteristics of devices featuring host **5 (H2)** with FIrpic and Ir(ppy)$_3$ dopants

Host	Dopant	wt%	*PE*, lm/W	*CE*, cd/A	*EQE*, %	L_{MAX}, cd/m^2
			@100 / @1000 cd/m^2			
		15.0	**24.9 / 15.8**	**23.9 / 18.4**	**10.3 / 8.0**	**9173**
	FIrpic	17.5	11.5 / 6.60	12.1 / 9.80	5.1 / 4.1	3317
		20.0	8.50 / 5.70	8.60 / 8.00	3.6 / 3.4	4377
5 (H2)		22.5	5.90 / 11.5	5.70 / 13.1	2.4 / 5.5	10350
		7.50	0.80 / 19.4	0.90 / 24.5	0.3 / 6.8	32390
	Ir(ppy)$_3$	10.0	10.0 / 34.1	10.3 / 33.9	3.3 / 9.4	38980
		12.5	**18.9 / 26.2**	**20.6 / 34.0**	**5.7 / 9.5**	**14170**
		15.0	10.9 / 34.1	10.3 / 33.9	2.3 / 7.4	18980

The OLED with a 15 wt% FIrpic doping ratio exhibited the best characteristics among the blue devices, boasting a current efficiency of 23.9 cd/A, a power efficiency of 24.9 lm/W, and an external quantum efficiency of 10.3% at a brightness of 100 cd/m^2. At a higher brightness level of 1000 cd/m^2, which is crucial for illumination technologies, this device also maintained the highest efficiency of 8.0% (18.4 cd/A, 15.8 lm/W), as compared to all other blue devices, and a maximum luminance exceeding 9170 cd/m^2. In the realm of green devices, it could be noted that PhOLEDs based on the material **5 (H2)** outperformed those utilizing the host derivative **4 (H1)**. Notably, the OLED containing 10 wt% of Ir(ppy)$_3$ doped in the host material **5 (H2)** exhibited superior characteristics, with a current efficiency of 33.9 cd/A, a power efficiency of 34.1 lm/W, and a high external quantum efficiency of 9.4% at a brightness of 1000 cd/m^2, which is essential for lighting applications. The green PhOLED also reached an impressive maximum brightness of almost 39000 cd/m^2.

3.2. Easily Synthesized and Cheap Carbazole- or Phenoxazine-Based Hosts for Efficient Yellow Phosphorescent OLEDs (Scientific Publication No. 2, Q2, 4 citations)

This chapter is based on the paper published in *Optical Materials*, **2021**, 118, 111251 by *D. Blazevicius, G. Krucaite, S. Shahnawaz, S. S. Swayamprabha, E. Zaleckas, J.-H. Jou*, and *S. Grigalevicius* [144].

This study involved the simplification of structures described in the previous chapter and detailed synthesis, characterization, and application of low molecular weight derivatives featuring the carbazole (**7 (H3)**) or phenoxazine (**8 (H4)**) moieties as the host materials for PhOLEDs. The oxetane-based host compounds were prepared through a cost-effective and straightforward one-step synthetic procedure, as illustrated in Scheme 2. The synthesis of 3,3-bis(9-carbazolylmethyl)oxetane **7** (**H3**) involved stirring 9H-carbazole (3.0 g, 0.018 mol), 3,3-bis(chloromethyl)oxetane **6** (0.93 g, 0.006 mol) potassium hydroxide (3.0 g, 0.0537 mol), potassium carbonate (2.475 g, 0.018 mol), and the phase-transfer catalyst tetrabutylammonium hydrogensulfate (TBAHS) in butan-2-one at reflux for 12h. The target material was purified by using silica gel chromatography while using a mixture of ethylacetate and hexane (vol. ratio 1:7) as an eluent. The yield was determined as 0.85 g (29%). This procedure closely resembled the one previously described in [145,146]. 3,3-Bis(10-phenoxazinylmethyl)oxetane **8** (**H4**) was synthesized through a *N*-alkylation reaction of 10H-phenoxazine. 10H-Phenoxazine (0.6 g, 0.00327 mol), potassium tert-butoxide (0.0408 g, 0.00423 mol), and 3,3-bis(chloromethyl)oxetane **6** (0.132 ml, 0.17 g, 0.0011 mol) were refluxed in 5 ml of degassed THF under nitrogen for 12 hours. After monitoring the reaction progress by thin-layer chromatography, the mixture was cooled off and quenched with addition of ice water. The product was extracted with chloroform, and the organic extract was dried over anhydrous Na$_2$SO$_4$. The desired product was then isolated by column chromatography while using silica gel and a 1:7 volume ratio mixture of toluene and hexane as the eluent. The yield was 0.24g (42%) of a pale-yellow material. The structures of the synthesized compounds were confirmed through NMR and MS, and the obtained data aligned well with the theoretically proposed structures.
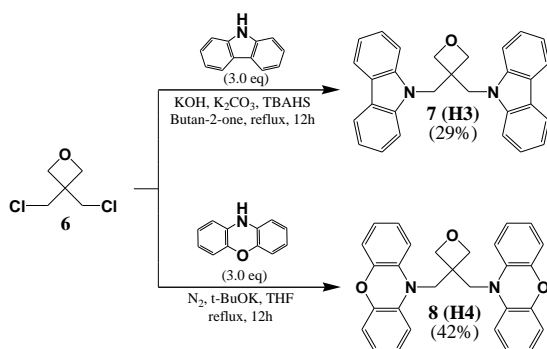
Scheme 2. Synthesis of new host materials **7 (H3)** and **8 (H4)**

The synthesized compounds were soluble in commonly used organic solvents, thus enabling cost-effective layer formation through a spin-coating process from a solution. DSC and TGA were employed to examine the behaviour under heating of the target host derivatives, **7 (H3)** and **8 (H4)**. The results confirmed that these materials exhibit a high thermal stability with a T_d value of 324 °C for the material **7 (H3)** and 314 °C for the derivative **8 (H4)**, as verified by TGA. During DSC measurements, it was discovered that both derivatives **7 (H3)** and **8 (H4)** were obtained as crystalline materials after synthesis and purification. However, they could be transformed into an amorphous state by cooling their melted samples.

Figure 15 displays the DSC thermograms of the derivatives **7 (H3)** (left) and **8 (H4)** (right). For the material **7 (H3)**, an endothermic melting peak was observed at 199 °C during the first heating of the crystalline sample. Subsequently, upon cooling and reheating, the glass-transition was identified at 75 °C. Upon further heating, crystallization of the liquid material was registered at 123 °C, which resulted in the formation of the same crystals obtained through synthesis.
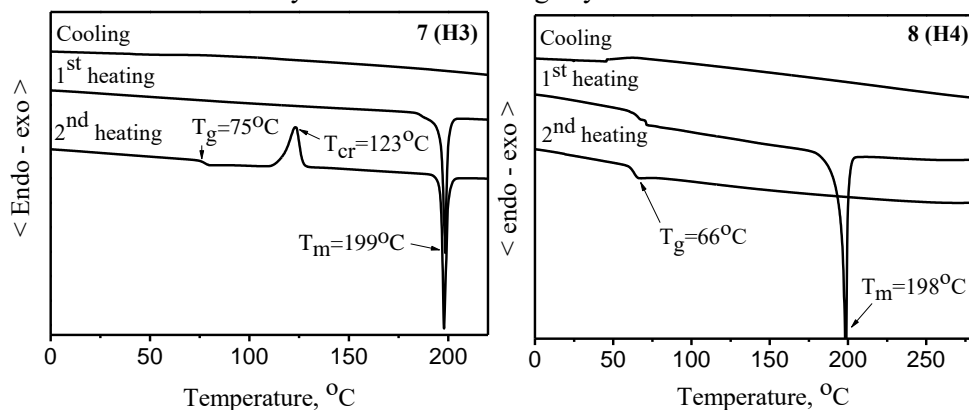
Figure 15. DSC curves of derivatives **7 (H3)** (left) and **8 (H4)** (right)

The DSC measurements for the derivative **8 (H4)** revealed an endothermic melting peak at 198 °C during the first heating of the sample. The melted material was then cooled, thus forming an amorphous state with a T_g of 66 °C, and no subsequent peaks indicating crystallization or melting were detected. These DSC measurements affirm that both materials have the capability to form thin amorphous layers suitable

43

for OLEDs. However, films of the compound **8** (**H4**) are anticipated to demonstrate better stability in the amorphous state based on the absence of crystallization at high temperatures.

The LTPL spectra of the materials were measured at 77K to determine the E_T values of the host derivatives **7 (H3)** and **8** (**H4**). It was determined that the values are 2.95 eV for the compound **7 (H3)**, and 2.73 eV for the derivative **8** (**H4**). Notably, the triplet energy levels for the hosts surpass E_T of 2.21 eV for the well-known yellow phosphorescent dopant PO-01 [147], thus affirming the suitability of these host compounds for the formation of emissive layers in yellow PhOLEDs. All the presently mentioned properties of new derivatives are summarised in Table 3.

Table 3. Thermal and photophysical properties of host materials

Material	T_D (°C)	T_m (°C)	T_{cr} (°C)	T_g (°C)	E_T (eV)
7 (H3)	324	199	123	75	2.95
8 (H4)	314	198	-	66	2.73

To assess the suitability of the hosts for the emitting layers, yellow phosphorescent devices were constructed byt using the above-mentioned PO-01 yellow triplet emitter as a dopant. The multilayer OLED structures were as follows: ITO/PEDOT:PSS/(**7 (H3)** or **8 (H4)**):X wt% PO-01/TPBi/LiF/Al, where X is the dopant concentration. The electroluminescent spectra, shown in Figure 16, demonstrate a singular emission peak for various doping concentrations in devices based on the **7 (H3)** host. In all PhOLEDs, light emission occurs at 570 nm, attributed to the emissions of PO-01. Notably, there is no colour shift observed with the changes in the dopant concentration of the yellow emitter in the host materials **7 (H3)** and **8 (H4)**. The created devices emit the yellow light with the CIE coordinates of (0.49, 0.50) at a luminance of 1000 cd/m^2.
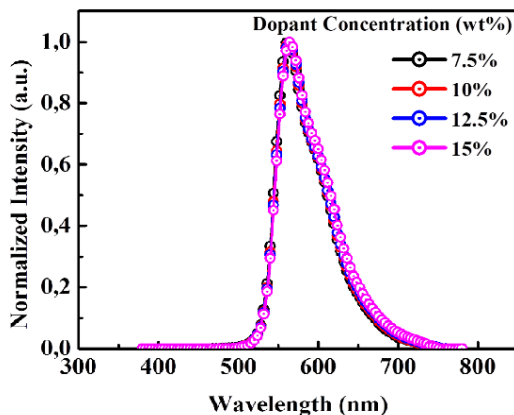
Figure 16. EL spectra of OLEDs having host material **7 (H3)** with yellow PO-01 dopant in emitting layers

The EL properties of the devices were demonstrated in concentration-dependent experiments by using dopant concentrations of 7.5, 10, 12.5, and 15 wt%. The characteristics of resulting devices are presented in Table 4. PhOLEDs based on the derivative **7 (H3)** with various dopant concentrations exhibited similar characteristics.

However, the device having 15 wt% of the dopant in its emissive layer showcased the highest EQE and PE values, measuring 10.6% and 19.2 lm/W, respectively, while simultaneously achieving the highest maximum luminance (L_{max}) of 12250 cd/m². The device with a 7.5% dopant concentration attained the best CE value of 32.0 cd/A. It is notably of importance for the lighting luminance of 1000 cd/m² that the device with 10% dopant concentration in its emissive layer demonstrated superior overall efficiencies, with a PE of 17.3 lm/W, a CE of 30.7 cd/A, and an EQE of 10.3%.

It is evident that devices based on the host **8 (H4)** showed significantly better characteristics compared to those based on the **7 (H3)** host, especially at high brightness levels. The **8 (H4)**-based devices displayed relatively low turn-on voltages ranging from 3.5 to 3.6 V, power efficiencies between 23.1 and 32.2 lm/W, current efficiencies from 26.0 to 35.8 cd/A, and EQE values of 8.1 to 10.9% at a luminance of 100 cd/m². Among them, the device containing 10 wt% of PO-01 demonstrated the best overall characteristics, featuring a current efficiency of 33.1 cd/A, a power efficiency of 22.8 lm/W, and an external quantum efficiency of 10.1% at a luminance of 1000 cd/m², making it well-suited for technological applications for lighting. The OLED achieved a maximum brightness exceeding 23100 cd/m².

Table 4. Characteristics of devices featuring host H3 or H4 with PO-01 dopant

Host	Dopant	wt%	V_{ON}, V	PE, lm/W	CE, cd/A	EQE, %	L_{MAX}, cd/m²
			@100 / @1000 cd/m²				cd/m²
7 (H3)	PO-01	7.50	6.3 / 8.2	16 / 9.9	32 / 25.6	10.5 / 7.9	10760
		10.0	5.6 / 7.4	17.3 / 11.4	30.7 / 26.8	10.3 / 8.5	10600
		12.5	5.1 / 6.7	18.4 / 10.9	30.1 / 23.2	10.5 / 7.5	10700
		15.0	4.8 / 6.3	19.2 / 11.3	29.4 / 22.7	10.6 / 7.5	12250
8 (H4)		7.50	3.5 / 4.9	31.6 / 21.2	34.9 / 32.9	10.6 / 9.9	20520
		10.0	3.5 / 4.6	32.2 / 22.8	35.8 / 33.1	10.9 / 10.1	23190
		12.5	3.6 / 5.1	28.6 / 15.5	32.8 / 25.4	10.1 / 7.9	19470
		15.0	3.5 / 4.7	23.1 / 16.5	26.0 / 24.5	8.1 / 7.7	22360

Based on the obtained experimental results, it is evident that the host material **8 (H4)** exhibits superior film-forming properties and possesses a triplet energy level that aligns more effectively with the PO-01 yellow triplet emitter as a dopant. This compatibility appears to be a contributing factor to the enhanced characteristics observed in OLEDs utilizing the host **8 (H4)**. The data conclusively affirms that this host material, prepared through a straightforward one-step procedure, holds significant potential in the realm of phosphorescent, second-generation device fabrication.

3.3. Highly Efficient Candlelight Organic Light-Emitting Diode with a very Low Color Temperature (Scientific Publication No. 3, Q2, 6 citations)

This chapter is based on the paper published in *Molecules*, **2021**, 26, 24 by *S. Shahnawaz, I. Siddiqui, M. R. Nagar, A. Choudhury, J.-T. Lin, D. Blazevicius, G. Krucaite, S. Grigalevicius*, and *J.-H. Jou* [148].

In this study, the phenoxazine-based derivative **8** (**H4)** was employed as a host for the production of omni-friendly low-colour-temperature candlelight OLEDs. The

derivative was synthesized by using a simple one-step procedure outlined in the previous chapter, as depicted in Scheme 3. Specifically, 3,3-bis(10-phenoxazinylmethyl)oxetane **8 (H4)** was synthesized by N-alkylating 10H-phenoxazine. The reaction involved refluxing 10H-phenoxazine (0.6 g, 0.00327 mol), potassium tert-butoxide (0.0408 g, 0.00423 mol), and 3,3-bis(chloromethyl)oxetane **6** (0.132 ml, 0.17 g, 0.0011 mol) in degassed THF under nitrogen atmosphere for 12 hours. After confirming the completion of the reaction, the mixture was cooled and quenched by adding ice water. The product was extracted with chloroform, and the organic layer was dried over anhydrous Na_2SO_4. The desired compound was then purified by column chromatography while using silica gel as the stationary phase and a 1:7 toluene-to-hexane mixture as the mobile phase. This procedure yielded 0.24 g (42%) of a pale-yellow product.
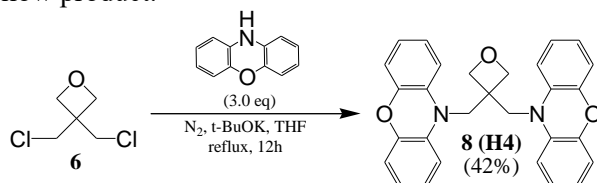
Scheme 3. Synthesis of phenoxazine-based material **8 (H4)**

In the previous chapter, the thermal properties of the material **8 (H4)** were explained. TGA measurements revealed a high thermal stability with a T_d of 314 °C. Although the derivative was initially obtained as a crystalline material with a T_m of 198 °C, the cooling of the melted sample resulted in an amorphous state with a T_g of 66 °C, as verified by DSC.

Figure 17 illustrates photophysical characteristics of commercial host material CBP and **8 (H4)**, utilizing UV-vis absorbance, photoluminescence (PL), and LTPL characterizations. Absorbance, PL, and LTPL (at 77 K) peaks were observed at 320, 395, and 495 nm, respectively, for the derivative **8 (H4)**, whereas the E_g value, derived from the absorbance spectrum, was estimated at 3.85 eV.
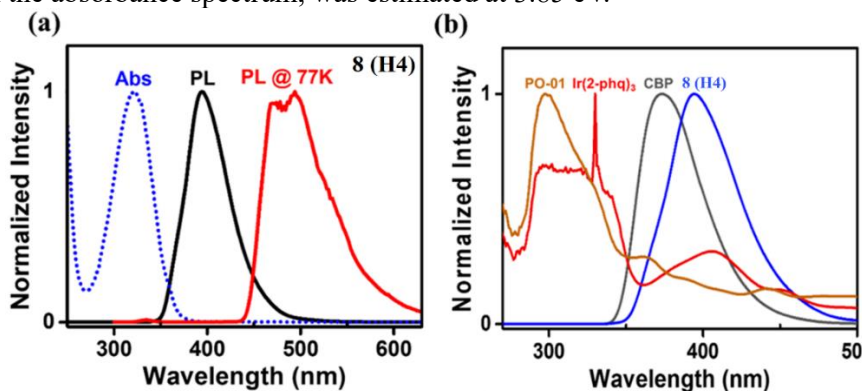
Figure 17. Photophysical characteristics showing (a) Abs, PL and LTPL spectra of **H4**, and (b) the overlapping area between the PL of hosts **8 (H4)** and CBP and the Abs of yellow PO-01 and orange-red Ir(2-phq)₃ dyes

In Figure 17(a), the E_S (3.44 eV) and E_T (2.87 eV) values of the host **8 (H4)** were calculated by using the intercepting wavelength of Abs:PL (360 nm) and Abs:LTPL (436 nm). The formulas for calculating the singlet and triplet energy were as follows:

$$E_S = 1240/\text{intercepting wavelength of UV-vis and PL} \qquad (1)$$

$$E_T = 1240/\text{intercepting wavelength of UV-vis and LTPL} \qquad (2)$$

In Figure 17(b), the plot illustrates the intersection between the normalized PL of the hosts **8 (H4)** and CBP, and the normalized absorbance of the yellow dye PO-01 and the orange-red dye Ir(2-phq)$_3$ incorporated in candlelight organic LEDs. Notably, **8 (H4)** exhibits a larger overlapping area with the absorbance of the yellow dye PO-01 and the orange-red dye Ir(2-phq)$_3$, measuring 20.37 and 31.52 square units, respectively, as opposed to the host CBP with the values of 19.36 and 22.6 square units, respectively.

Cyclic voltammetry (CV) experiments were conducted on **8 (H4)** in dichloromethane during the oxidation scan. The HOMO and LUMO energy levels were determined as -5.39 eV and -1.54 eV, respectively, derived from the CV curve and utilizing the previously calculated E_g of 3.85 eV. Table 5 outlines the photophysical and electrochemical characteristics of the host **8 (H4)**, alongside those of the commercial host derivative CBP [18,71,149].

Table 5. Thermal, electrochemical and photophysical properties of host materials

Material	T_d (ºC)	T_m (ºC)	T_g (ºC)	HOMO (eV)	LUMO (eV)	E_T (eV)	E_S (eV)	E_g (eV)	References
8 (H4)	340	199	66	-5.39	-1.54	2.95	3.44	3.85	[144]
CBP	320	-	62	-6.00	-2.90	2.73	3.49	3.10	[18,71,149]

To assess the performance of the new material **8 (H4)** as a host material, solution-processed candlelight organic LEDs were fabricated. For comparison, an analogical device with the commercial host compound CBP was also assembled, utilizing the emitters PO-01 (yellow) and Ir(2-phq)$_3$ (orange-red) for both **8 (H4)**- and CBP-based candlelight OLEDs. The device structure was configured as ITO/PEDOT:PSS/**8 (H4)** or CBP : PO-01 (10 wt%): Ir(2-phq)$_3$ (x wt%) (x= 7.5, 10.0, 12.5, 15.0)/TPBi/LiF/Al. Figure 18(a) depicts the CIE chromaticity coordinates of the resulting devices.
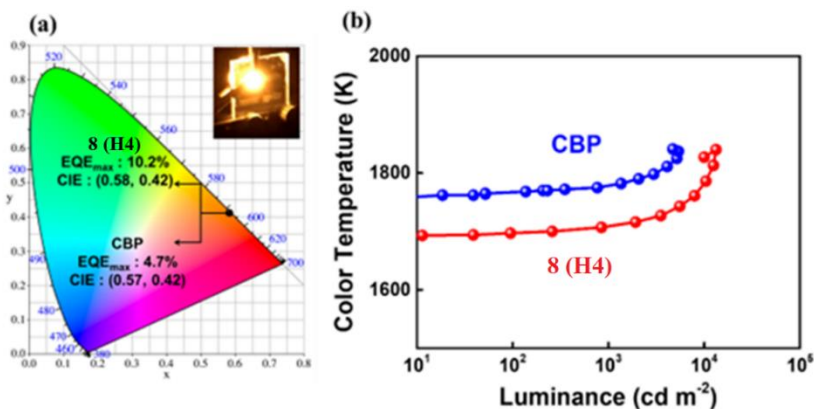
Figure 18. Characteristics of **8** (**H4**)- and CBP-based OLEDs: (a) CIE chromaticity with EQE$_{max}$ and pixel image (inset), and (b) colour temperature dependence on luminance

For the **8** (**H4**)-based device these coordinates were (0.58, 0.42), whereas, for the CBP-based device, they were (0.57, 0.42). The corresponding achieved EQE$_{max}$ values were 10.2% and 4.7%, respectively. The device pixel image (Figure 18(a), inset) depicts the candle-like emission.

The electroluminescent characteristics of candlelight organic LED devices based on **8** (**H4**) and CBP were investigated. A yellow emitter (PO-01) at 10 wt% and an orange-red emitter (Ir(2-phq)$_3$), doped at varying concentrations, were employed.

An increase in the concentration of the orange-red emitter from 7.5 to 15 wt% in **8** (**H4**)-based devices resulted in changes in the maximum PE value from 22.1 to 19.9 lm/W, CE from 20.3 to 18.2 cd/A, EQE from 9.2 to 8.5%, and the colour temperature (CT) from 1,730 to 1,705 K. Conversely, CBP-based devices exhibited changes in PE$_{max}$ from 9.3 to 7.6 lm/W, CE$_{max}$ from 11.8 to 9.3 cd/A, EQE$_{max}$ from 5.0 to 4.0%, and CT from 1,790 to 1,723 K. Notably, the efficiencies and CT were found to be concentration-dependent. Thus, the optimized concentration was determined to be 10 wt% for the orange-red emitter. Moreover, the incorporation of a higher concentration of the highly efficient orange-red emitter and ensuring balanced charge recombination in the emission zone facilitates a reduction in the emission colour temperature [150–152].

Table 6 illustrates the efficiencies of the investigated candlelight organic LED devices based on **8** (**H4**) and CBP, when utilizing 10 wt% of either the yellow emitter PO-01, or the orange-red emitter Ir(2-phq)$_3$.

The **8** (**H4**)-based device exhibited a high luminance of 14,950 cd/m² with a PE$_{max}$ of 24 lm/W, a CE$_{max}$ of 22.4 cd/A, and an EQE$_{max}$ of 10.2% with an impressively low turn-on voltage of 2.8 V. At 100 cd/m², a PE of 22.0 lm/W, CE of 22.4 cd/A, EQE of 10.2%, and a CT of 1,690 K was achieved. Even at a higher luminance level, such as 1,000 cd/m², the efficiencies remained high, thus indicating a low roll-off at a very low CT. These results can be attributed to the balanced charge transport, aligned HOMO, LUMO, and triplet energies, a low hole-injection barrier between the hole

injection layer and the emissive layer, and a large hole-injection barrier between the emissive layer and the electron transport layer.

For comparison, the CBP-based device displayed a L_{max} of 8,393 cd/m², with a PE_{max} of 9.6 lm/W, a CE_{max} of 11.7 cd/A, an EQE_{max} of 6.8%, and a CT as low as 1,768 K with a turn-on voltage of 3.2 V. These values were considerably lower than those of the **8 (H4)**-based counterpart in all aspects, thereby indicating that **8 (H4)**-based devices outperform CBP-based devices by 150%, 91%, and 50% in terms of the PE, CE, and EQE values, respectively, as shown in Figure 19.

Table 6. Characteristics of candlelight OLEDs having 10wt% of PO-01 and 10wt% of Ir(2-phq)$_3$ doped in **8 (H4)** or CBP hosts

Host	V_{ON}, V	PE, lm/W	CE, cd/A	EQE, %	CT, K	L_{MAX}, cd/m^2
		@100 / @1000 cd/m^2 / MAX			@100/@1000cd/m^2	
8 (H4)	2.8	22.0/16.9/23.7	22.4/21.6/22.4	10.2/9.6/10.2	1690 / 1707	14950
CBP	3.2	7.4 /3.9/9.6	10.3/7.4/11.7	4.7/3.2/6.8	1768 / 1782	8393
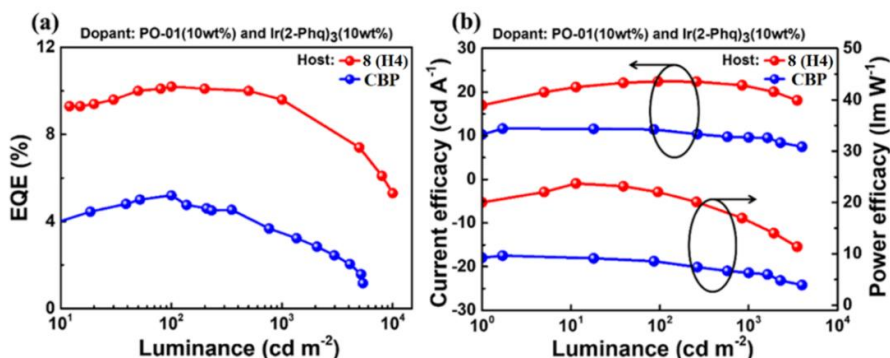
Figure 19. Study of **8 (H4)**- and CBP-based candlelight OLEDs showing (a) EQE dependence on luminance, and (b) power efficacy-luminance-current efficacy curves

In assessing the influence of a lighting source on human health, this study incorporates the maximum permissible exposure limit (MPE) and melatonin suppression sensitivity (MSS). The MPE, as defined by the *International Commission on Non-Ionizing Radiation Protection* (ICNIRP) [153], serves to quantify the hazards associated with blue light, and it can be calculated as follows:

$$MPE = \frac{100}{E_B} \qquad (3)$$

where: E_B – the photo-retinitis or blue light hazard weighted radiation (W/m^2) [154–156]

The melatonin suppression sensitivity after 1.5 hours of exposure (MSS) was introduced by Prof. Jou [157], and it can be calculated with the following equation:

$$MSS = \frac{S_{LC}(\lambda)}{S_{LC}(480)} \times 100 \qquad (4)$$
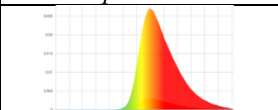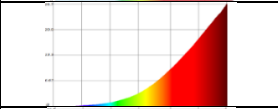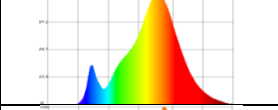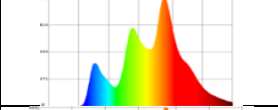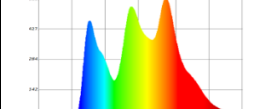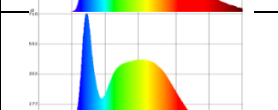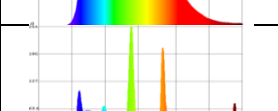
where: $S_{LC}(\lambda)$ – the melatonin suppression spectrum per lux for a given polychromatic light;

   $S_{LC}(480)$ – the melatonin suppression spectrum per lux for a reference blue light of 480 nm.

Table 7 presents the emission spectra, CT, MSS (1.5 hours exposure), and the MPE characteristics of the investigated low colour temperature candlelight OLED in comparison with various commercial lighting sources. These include incandescent bulbs, warm white LEDs and OLEDs, cold white LEDs and OLEDs, as well as CFLs.

It could be observed that the **8 (H4)**-based blue emission-free candlelight OLED boasts a colour temperature of 1,690 K, making it 180 times more friendly in terms of MPE compared to the cold-white CFL with a CT of 5,843 K. Correspondingly, at 100 lx, the MPE was 57,696 s (16 hours) for the studied device, whereas it was only 320 s for the cold-white CFL. Furthermore, the melatonin secretion sensitivity of the studied device at 100 lx (1.33%) is 22.4 times lower than its counterpart cold-white CFL (29.9%) after a 1.5-hour exposure at night.

Table 7. Comparison between the spectrum, CT, MSS (1.5 hours exposure) and MPE of the studied candlelight OLED and the commercial light sources

Light source	Spectrum	CT (K)	MSS (%)	MPE (s) @100 lx
This work		1,690	1.33	57,696
Candle Light		1,884	4.0	2,750
Incandescent Bulb		2,444	11.5	1,100
Warm-white LED		2,704	8.0	1,000
Warm-white OLED		3,080	6.9	1,050
Cold-white OLED		4,034	12.8	590
Cold-white LED		5,549	19.8	380
Cold-white CFL		5,843	29.9	320

In contrast to cold-white LEDs, the studied device demonstrates the MPE and MSS values which are 152 and 15 times better, respectively. Compared to cold-white OLEDs, the candlelight OLED is 98 times more human eye-friendly and 9.6 times more friendly in terms of the inhibition of melatonin secretion. Moreover, the studied device outperforms warm-white LED (CT of 2,704 K) and warm-white organic LED (CT of 3,080 K) by 57.6 / 54.9 and 6 / 5.2 times in terms of the MPE / MSS values, respectively. Additionally, when compared to an incandescent bulb (CT of 2,444 K) and candlelight (CT of 1,884 K), the fabricated candlelight organic LED proves to be 52.4 times more friendly to the human eye and inhibits melatonin secretion 8.6 times less than the incandescent bulb. Furthermore, it is 21 times more human eye-friendly, and it inhibits melatonin secretion by 200% less than the natural candlelight due to the total absence of blue emission.

Therefore, the present study-based candlelight OLED stands out for being free from flickering, scorching, glare, and, importantly, it is potentially more energy-efficient than any commercial lighting sources. The key factors contributing to the enhanced device efficiencies include the outstanding electron-blocking capabilities, the appropriate levels of HOMO, LUMO, and triplet energies, the reduced hole-injection barriers between the host and HIL, and significantly confined light-emitting excitation to the designated recombination zone. This study paves the way for development of highly efficient candlelight OLED lighting devices using cost-effective solution processes.

3.4. A Review of Benzophenone-Based Derivatives for Organic Light-Emitting Diodes (Scientific Publication No. 4, Q1, 3 citations)

This chapter is based on the paper published in *Nanomaterials*, 2024, 14, 4 by *D. Blazevicius*, and *S. Grigalevicius* [158]

In this study, in order to explore more possibilities in improving the efficiency of OLEDs, the synthetic routes, thermal properties, electrochemical behaviour, photoelectrical and photophysical characteristics of benzophenone-based derivatives were examined. Also, we overviewed their application in OLED devices, both as the hosts and the emitters. This chapter provides a systematic review of various device configurations and their corresponding performances. The review is organized into several sections based on the application and structure of benzophenone derivatives, encompassing host materials for phosphorescent emitters, host materials for TADF emitters, D–A type emitters, D–A–D type symmetric structure emitters, D–A–D type asymmetric structure emitters, and emitters featuring dendritic structures.

3.4.1. Benzophenone-based host materials used for phosphorescent emitters

Figure 20 depicts the structures of benzophenone-based derivatives utilized as host materials in PhOLEDs.
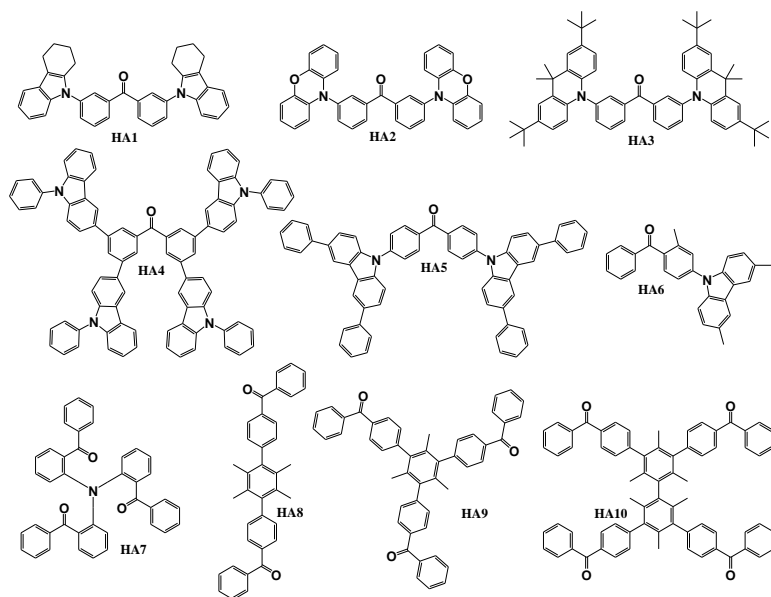
Figure 20. Structures of benzophenone-based materials used as hosts in PhOLEDs [159, 161-164, 166]

The target compounds, **HA1**, **HA2**, and **HA3** [159], were synthesized via the Buchwald–Hartwig [160] amination reaction between 3,3′-dibromobenzophenone and 1,2,3,4-tetrahydrocarbazole for **HA1**, phenoxazine for **HA2**, and 9,9-dimethyl-9,10-dihydroacridine for **HA3**. Additionally, the host material **HA4** [161] was synthesized during the Suzuki coupling reaction [139] between 3,3′,6,6′-tetrabromobenzophenone and 9-phenylcarbazol-3-ylboronic acid. **HA5** [162] was obtained through a Buchwald–Hartwig amination reaction between 4,4'-dibromobenzophenone and 3,6-diphenyl-9*H*-carbazole. Similarly, **HA6** [163] was synthesized by utilizing analogous reaction conditions with 4-bromo-3-methylbenzophenone and 3,6-dimethyl-9*H*-carbazole. **HA7** [164] was obtained via a single-step synthetic procedure involving the Ullmann reaction [165] of iodophenylketone and aminodiphenylketone. The synthesis of the remaining PhOLED host materials, **HA8**, **HA9**, and **HA10** [166], was achieved through a straightforward Friedel−Craft benzoylation reaction [167] conducted in carbon disulfide. Benzoyl chloride, in the presence of AlCl$_3$, reacted with 1,4-diphenyldurene, 1,3,5-triphenylmesitylene, and 3,3′,5,5′-tetraphenylbimesitylene to yield **HA8**, **HA9**, and **HA10**, respectively.

Out of this group of materials, the most notable efficiencies were achieved by utilizing the derivatives **HA5**, **HA6** and **HA8** as hosts for various phosphorescent dopants. Both materials **HA5** and **HA8** showed a high thermal stability with the T_d values of 480 ºC and 337 ºC, respectively. The derivative **HA6**, on the other hand, showed a high T_g value of 131ºC, thereby confirming its tendency to form stable amorphous layers. All the three materials showed high E_T values of 2.69 eV for derivative **HA5**, 3.00 eV for **HA6**, and 2.97 eV for **HA8**. Furthermore, the presently discussed compounds had a large bandgap from 3.10 eV to 3.91 eV. All these

properties were suitable to test the earlier-mentioned materials as hosts for red, orange, yellow, green, and blue phosphorescent emitters. The architectures of devices utilizing the host materials **HA5**, **HA6** and **HA8** are shown in Table 8.

Table 8. Architectures of devices utilizing host materials **HA5**, **HA6** and **HA8**

Device	Device architecture	Reference
D1HA5	ITO/NPB (35nm)/mCP (5nm)/**HA5**:3wt% Ir(ppy)$_2$acac (30 nm)/B3PYMPM (30nm)/LiF (0.5nm)/Al (150nm)	[162]
D2HA5	ITO/NPB (35nm)/mCP (5nm)/**HA5**:3wt% Ir(bzq)2(dipba) (30 nm)/B3PYMPM (30nm)/LiF (0.5nm)/Al (150nm)	[162]
D3HA5	ITO/NPB (35nm)/mCP (5nm)/**HA5**:3wt% Ir(bt)2(dipba) (30 nm)/B3PYMPM (30nm)/LiF (0.5nm)/Al (150nm)	[162]
D1HA6	ITO/TAPC (30nm)/TCTA (10nm)/**HA6**:FIrpic (20nm)/CzPhPy (10nm)/TmPyPB (45nm)/LiF/Al	[163]
D2HA6	ITO/TAPC (30nm)/TCTA (10nm)/**HA6**:Ir(ppy)$_2$(acac) (20nm)/CzPhPy (10nm)/TmPyPB (45nm)/LiF/Al	[163]
D3HA6	ITO/TAPC (30nm)/TCTA (10nm)/**HA6**:Ir(mphmq)$_2$(tmd) (20nm)/HA8 (10nm)/CzPhPy (10nm)/TmPyPB (45nm)/LiF/Al	[163]
D1HA8	ITO/NPB (40nm)/mCP (10nm)/**HA8**:9-10wt%Ir(ppy)$_3$ (30nm)/TmPyPB (45nm)/LiF (2nm)/Al (150nm)	[166]
D4HA8	ITO/NPB (40nm)/mCP (10nm)/**HA8**:9-10wt% PO-01 (30nm)/TmPyPB (45nm)/LiF (2nm)/Al (150nm)	[166]

Table 9 displays the characteristics of phosphorescent OLEDs employing host materials **HA5**, **HA6**, and **HA8**. The utilization of these benzophenone-based hosts yielded efficient PhOLED devices, with their external quantum efficiency surpassing 16%. These host materials were employed across red, orange, yellow, green, and blue devices.

Table 9. Characteristics of PhOLEDs using host materials **HA5**, **HA6**, and **HA8**

Device	Host	Colour	V_{ON}, V	L_{MAX}, cd/m^2	CE, cd/A	PE, lm/W	EQE, %	CIE (x, y)	Reference
D1HA5	**HA5**	Green	2.5	93330	-	99.1	25.1	(0.29, 0.64)	[162]
D2HA5	**HA5**	Orange	2.6	31200	-	61.6	23.1	(0.51, 0.47)	[162]
D3HA5	**HA5**	Red	2.9	10240	-	27.1	22.1	(0.61, 0.36)	[162]
D1HA6	**HA6**	Blue	3.0	-	-	38.2	19.4	(0.16, 0.33)	[163]
D2HA6	**HA6**	Green	2.9	-	-	75.7	21.0	(0.29, 0.64)	[163]
D3HA6	**HA6**	Red	3.1	-	-	30.8	16.5	(0.62, 0.38)	[163]
D1HA8	**HA8**	Green	4.5	3080	46.8	29.1	17.0	(0.30, 0.60)	[166]
D4HA8	**HA8**	Yellow	5.5	3490	50.6	28.9	19.2	(0.47, 0.51)	[166]

Among the red devices, the prototype D3HA5 emerged as the most efficient option, boasting a low V_{ON} of 2.9 V, a high PE of 27.1 lm/W, an EQE of 22.1%, and an L_{MAX} of 10,240 cd/m². The orange device D2HA5 proved most effective, by showcasing the V_{ON}, L_{MAX}, PE, and EQE values of 2.6 V, 31,200 cd/m², 61.6 lm/W, and 23.1%, respectively. Among yellow devices, the prototype D4HA8 stands out with a CE of 50.6 cd/A, a PE of 28.9 lm/W, and an EQE of 19.2%. When comparing green PhOLEDs, the host material **HA5**, which is compatible with the green phosphorus E_T value of 2.69 eV, exhibited a superior efficiency, with PhOLED

D1HA5 achieving a remarkable PE of 99.1 lm/W and an EQE of 25.1%, along with an L_{MAX} exceeding 93,300 cd/m². For blue PhOLEDs, devices utilizing the host material **HA6**, characterized by a high E_T of 3.00 eV as well as exceptional thermal and film-forming properties, demonstrated the best performance. Specifically, the device D1HA6 showcased high PE and EQE values of 38.2 lm/W and 19.4%, respectively.

3.4.2. Benzophenone-based bipolar host materials used for TADF emitters

Figure 21 depicts the structures of benzophenone-based derivatives utilized as the host materials in TADF-based OLED devices. The target compounds **HB1** and **HB2** [168] were synthesized through a straightforward one-step Friedel–Crafts reaction by employing the readily available and cost-effective triphenylamine along with isophthaloyl- or terephthaloyl-dichloride as the starting materials. The remaining host materials **HB3**, **HB4** [169], **HB5** [170], **HB6**, **HB7** [171], and **HB8** [172] were obtained via simple nucleophilic substitution reactions between fluorinated benzophenone and the corresponding amines. For their application as TADF host materials, benzophenone was paired with either electron-rich carbazole, or with phenyl-/naphthyl-amino fragments. The compounds **HB3**, **HB4**, **HB5**, **HB6**, and **HB7** were derived from the reactions of 4,4'-difluorobenzophenone with *N*-phenyl-1-naphthylamine, *N*-phenyl-2-naphthylamine, 3-naphthyl-9*H*-carbazole, 3-phenyl-9*H*-carbazole, and 3-(4-(9*H*-carbazol-9-yl)phenyl)-9*H*-carbazole, respectively. The material **HB8** was synthesized during the reaction between 2,3,4,5,6-pentafluorobenzophenone and 9*H*-carbazole.
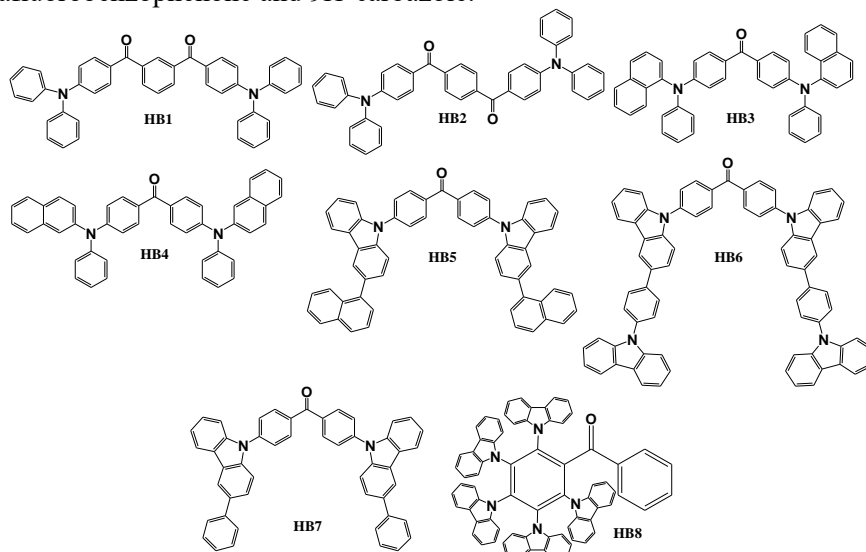
Figure 21. Structures of benzophenone-based materials used as hosts in TADF OLEDs [168–172]

Experiments conducted by various researchers showed that the most efficient host materials in this chapter were **HB3**, **HB6**, and **HB7**. After the investigation of the thermal properties, it was observed that benzophenone-based compounds exhibited a

high heat resistance, with T_d surpassing 277°C for all derivatives, as confirmed by TGA. Additionally, all the three materials demonstrated the capability to form stable amorphous films, whereas the glass transition temperatures, measured by DSC, for the derivatives **HB3**, **HB6**, and **HB7** reached 101°C, 92°C, and 187°C, respectively. Moreover, the presently discussed HB series benzophenone derivatives exhibited E_g values ranging from 2.89 to 4.10 eV, while their triplet state energies ranged from 2.55 eV to 2.64 eV. These properties indicate their potential for application as host materials in green and white TADF OLEDs. The device architectures utilizing the host materials **HB3**, **HB6**, and **HB7** are illustrated in Table 10.

Table 10. Architectures of devices utilizing host materials **HB3**, **HB6**, and **HB7**

Device	Device architecture	Reference
DHB3	ITO/MoO$_3$ (8nm)/NPB (60nm)/TAPC (5nm)/**HB3**:5wt%4CzTPN (5nm)/**HB3** (15nm)/PFBP-2b(20 wt%):TPBi (40nm)/LiF (1nm)/Al	[169]
D1HB6	ITO (125 nm)/PEDOT:PSS (35 nm)/**HB6**:4CzIPN (20 nm)/PO-T2T (10 nm)/TPBi (30 nm)/LiF (1nm)/Al (200 nm)	[171]
D2HB6	ITO (125 nm)/PEDOT:PSS (35 nm)/VPEC (10nm)/**HB6**:4CzIPN(20 nm)/PO-T2T (10 nm)/TPBi (30 nm)/LiF (1nm)/Al (200 nm)	[171]
DHB7	ITO (125 nm)/PEDOT:PSS (35 nm)/**HB7**:4CzIPN (20 nm)/PO-T2T (10nm)/TPBi (30 nm)/LiF (1nm)/Al (200 nm)	[171]

Table 11 displays the measured characteristics of TADF OLED devices utilizing the host materials **HB3**, **HB6**, and **HB7**. The material **HB3** was examined by M. Mahmoudi et al., who determined that the synthesized material could best serve as an exciton modulator between two TADF emitters. By combining orange and blue TADF materials with a new benzophenone-based host, efficient white TADF OLEDs were introduced, with the device DHB3 achieving an EQE of 9.5% along with a high-quality white electroluminescence characterized by the CIE coordinates of (0.32, 0.31), a colour temperature of 4490 K, and a colour rendering index of 80. A team of researchers led by S. Swyamprabha synthesized and characterized new materials with variously substituted carbazoles **HB6** and **HB7**. A green solution-processable OLED, D2HB6, which was fabricated by using the host **HB6** and a cross-linkable hole transport material VPEC, achieved a PE of 63.6 lm/W and an EQE of 25.3%. The derivative **HB7** demonstrated superior effectiveness as a host for a green TADF emitter compared to the lower E_T having material **HB6**.

Table 11. Characteristics of TADF OLED devices using host materials **HB3**, **HB6**, and **HB7**

Device	Host	Colour	V_{ON}, V	L_{MAX}, cd/m^2	CE, cd/A	PE, lm/W	EQE, %	CIE (x, y)	Reference
DHB3	**HB3**	White	3.9	29922	18.6	-	9.5	(0.36, 0.31)	[169]
D1HB6	**HB6**	Green	3.0	16500	70.7	55.6	23.2	(0.28, 0.57)	[171]
D2HB6	**HB6**	Green	2.9	18900	72.3	63.6	25.3	(0.29, 0.58)	[171]
DHB7	**HB7**	Green	2.7	10540	49.2	46.2	15.3	(0.28, 0.57)	[171]

3.4.3. Benzophenone-based emitters employing donor-acceptor molecular structure

Figure 22 depicts the structures of donor-acceptor type molecules explored for their potential as emitters in OLED devices.
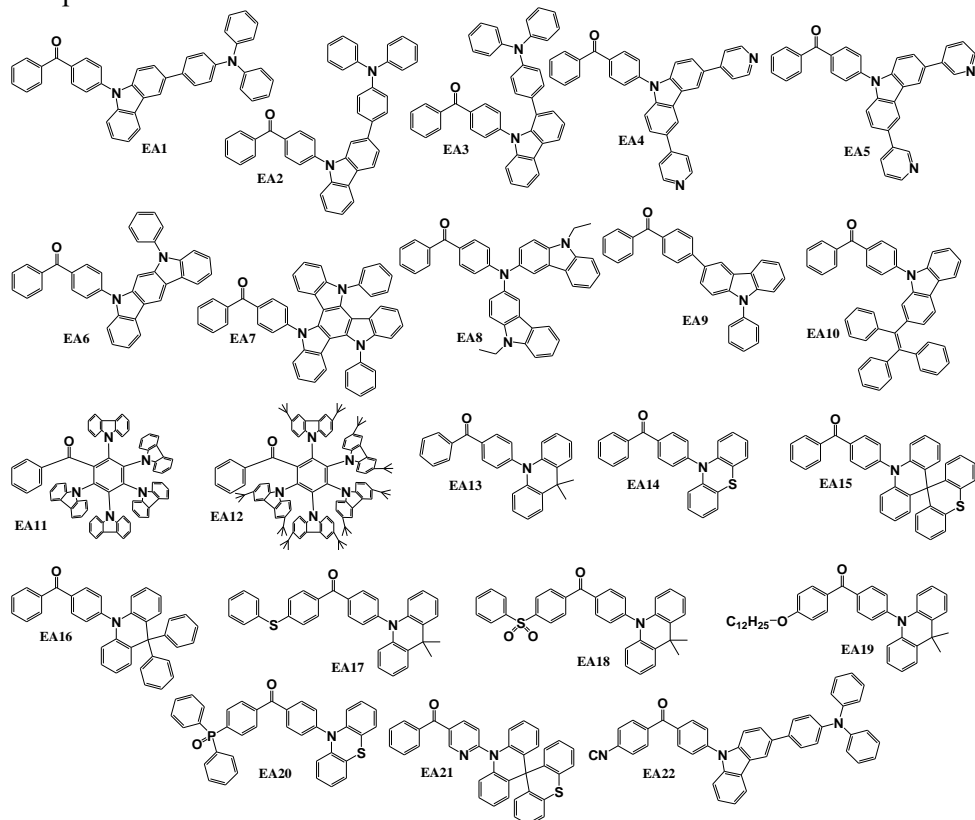
Figure 22. Structures of benzophenone-based D–A materials used as emitters in OLEDs [172–188]

The compounds **EA1**, **EA2**, **EA3** [173], **EA6** [174], **EA7** [175], **EA8** [176], **EA13** [177], **EA14** [178], **EA16** [179], **EA17**, and **EA18** [180] were synthesized by using the Buchwald–Hartwig coupling reaction methodology. The materials **EA4** and **EA5** [181], incorporating 3,6-pyridinyl-9*H*-carbazole substitutions, were synthesized via Suzuki reactions. This process entailed coupling 4-(3,6-dibromocarbazol-yl)benzophenone with 4-pyridinylboronic acid to produce the compound **EA4** and with 3-pyridinylboronic acid to synthesize the derivative **EA5**. The Suzuki coupling method was also utilized for the synthesis of the target materials **EA9** [182] and **EA22** [183]. Benzophenone-based derivatives **EA10** [184], **EA11** [172], **EA12** [185], and **EA19** [186] were synthesized through relatively straightforward catalyst-free nucleophilic substitution reactions. An alternative synthesis approach was employed for the creation of the compounds **EA15** and **EA21** [187], wherein 10*H*-spiro(acridine-9,9'-thioxanthene) was employed in Ullmann reactions with 4-

bromobenzophenone and (6-bromopyridin-3-yl)(phenyl)methanone, respectively. The phosphorus-containing emitter **EA20** [188] was synthesized through a palladium-catalyzed reaction between the intermediate compound 4-iodo-4'-phenothiazin-10yl-benzophenone and diphenylphosphine oxide in the presence of triethylamine.

From this selection of materials, the best efficiencies were achieved by employing the derivatives **EA6**, **EA19**, **EA20**, and **EA21** as TADF emitters in yellow (**EA20**), green (**EA21**), or blue (**EA6**, **EA19**) OLEDs. High thermal stability was confirmed for all the tested materials through TGA measurements. The T_d values ranged from 278°C to 428°C. DSC experiments indicated the formation of stable amorphous layers, with T_g values recorded at 177°C for the derivative **EA6**, 91°C for the material **EA20**, and 102°C for the compound **EA21**. Most of the EA benzophenone derivatives exhibited an E_g of 3.2 eV or lower, suggesting potentially a more efficient TADF process compared to emitters with wider bandgaps. A crucial factor for achieving the TADF effect is the small ΔE_{ST} value facilitating effective reverse intersystem crossing [20]. This metric was evaluated for all benzophenone-based D-A emitters, with the best performers showing ΔE_{ST} levels of 0.09 eV, 0.01 eV, 0.02 eV, and 0.08 eV for the derivatives **EA6**, **EA19**, **EA20**, and **EA21**, respectively. A small ΔE_{ST} is linked to a higher PLQY, thus enabling efficient radiative decay. For the materials **EA6** and **EA21**, the PLQY values were determined to be 62.0% and 98.9%, respectively. Additionally, both prompt and delayed emission components were observed, with the delayed component (R_D) comprising 37.9% and 60.1% of the overall emission for the derivatives **EA6** and **EA21**, respectively. All four top-performing emitters in this study demonstrated TADF properties. The device architectures utilizing emitters **EA6**, **EA19**, **EA20**, and **EA21** are outlined in Table 12.

Table 12. Architectures of devices utilizing emitters **EA6**, **EA19**, **EA20** and **EA21**

Device	Device architecture	Reference
DEA6	ITO/HAT-CN (10nm)/TAPC (30nm)/TCTA(10nm)/DPEPO: 10wt.%**EA6** (40nm)/TmPyB (40nm)/LiF (1nm)/Al (100nm)	[174]
DEA19	ITO/PEDOT:PSS (30nm)/mCP:CzAcSF:**EA19**(40:30:30) (40nm) /DPEPO (10 nm)/TmPyB (50nm)/Liq (1nm)/Al (100nm)	[186]
D1EA20	ITO/PEDOT:PSS (40 nm)/CBP (20nm)/CBP:10wt%**EA20** (15nm)/TPBI (40nm)/Mg:Ag	[189]
D2EA20	ITO/PEDOT:PSS (40nm)/CBP (20nm)/**EA20** (4nm)/2CzTPEPCz (15nm)/TPBI (40nm)/Mg:Ag	[190]
D1EA21	ITO/TAPC (30nm)/mCP (10nm)/**EA21** (20nm)/DPEPO (10nm)/TmPyB (40nm)/LiF/Al	[187]
D2EA21	ITO/TAPC (30nm)/mCP (10nm)/DPEPO:30wt%**EA21** (20nm)/DPEPO (10nm)/TmPyB (40nm)/LiF/Al	[187]

Table 13 displays various characteristics for EA derivatives-based OLEDs. X. Chen et al. developed the most effective yellow OLED device D1EA20, attaining the maximum CE, PE, and EQE values of 73.1 cd/A, 38.2 lm/W, and 26.7%, respectively [189]. J. Zhao et al. utilized the same emitter **EA20** in a white TADF-based prototype D2EA20, thus achieving a high CE of 45.9 cd/A, a PE of 18.0 lm/W, and an EQE of 20.8% [190]. J. Wang and colleagues synthesized the TADF emitter **EA21**,

demonstrating superior efficiency in green light emitting devices. The doped device D2E21 surpassed a luminance of 11000 cd/m^2 with an EQE of 25.6%. Additionally, CE and PE reached 69.8 cd/A and 58.9 lm/W, respectively. The same green TADF emitter also showed exceptional performance in non-doped EMLs, whereas the device D1EA21 achieved the maximum PE, CE, and EQE values of 56.4 cd/A, 43.5 lm/W, and 18.7%, respectively.

Table 13. Characteristics of TADF OLED devices using emitters **EA6**, **EA19**, **EA20**, and **EA21**

Device	Host	Colour	V_{ON}, V	L_{MAX}, cd/m^2	CE, cd/A	PE, lm/W	EQE, %	CIE (x, y)	Reference
DEA6	EA6	Blue	3.2	14724	44.8	45.6	17.7	(0.17, 0.28)	[174]
DEA19	EA19	Blue	4.0	4235	47.7	29.9	20.6	-	[186]
D1EA20	EA20	Yellow	4.4	32590	73.1	38.2	26.7	-	[188]
D2EA20	EA20: 2CzTPEPCz	White	6.1	12310	45.9	18.0	20.8	(0.45, 0.44)	[188]
D1EA21	EA21	Green	3.2	26836	56.4	43.5	18.7	(0.28, 0.53)	[187]
D2EA21	EA21	Green	3.2	11392	69.8	58.9	25.6	(0.24, 0.49)	[187]

In the realm of blue TADF emitters, J. Wang's group successfully combined a benzophenone electron acceptor with an 11-phenyldihydroindolo[2,3-a]carbazole electron donor, thereby yielding the material **EA6**. When applied as a dopant in blue OLED DEA6, it achieved a maximum EQE of 17.7%, as well as luminance exceeding 14000 cd/m^2, with the CE and PE values of 44.8 cd/A and 45.6 lm/W. The most efficient benzophenone derivative used as a blue TADF emitter was **EA19**, synthesized and characterized by J. Zhang and his team. The relatively simple structure of the benzophenone-acridine derivative in blue DEA19 reached the CE, PE, and EQE values of 47.7 cd/A, 29.9 lm/W, and 20.6%, respectively.

3.4.4. Benzophenone-based emitters employing symmetric donor-acceptor-donor structure

Figure 23 illustrates the chemical structures of symmetrical benzophenone-based emitters employing the D–A–D configuration. The material **EB1** [191] was synthesized via the Ullmann reaction between 4,4'-dibromobenzophenone and 3,6-bis(tert-butyl)-9*H*-carbazole. Notably, a significant number of materials were synthesized through the Buchwald–Hartwig amination of 3,3'-dibromobenzophenone or 4,4-dibromobenzophenone, employing diverse electron-donating groups. Tetrahydrocarbazole, phenoxazine, 2,7-ditert-butyl-9,9-dimethylacridine, and 3,6-diphenyl-9*H*-carbazole served as second reactants for the compounds **EB2**, **EB9**, **EB13** [159], and **EB4** [162], respectively. The reaction with carbazole resulted in the material **EB3**, while the reaction with bicarbazole yielded **EB5** [192], whereas 9,9,9'9'-tetramethyl-9,9'10,10'-tetrahydro-2,10'-biacridine led to **EB11** [193].
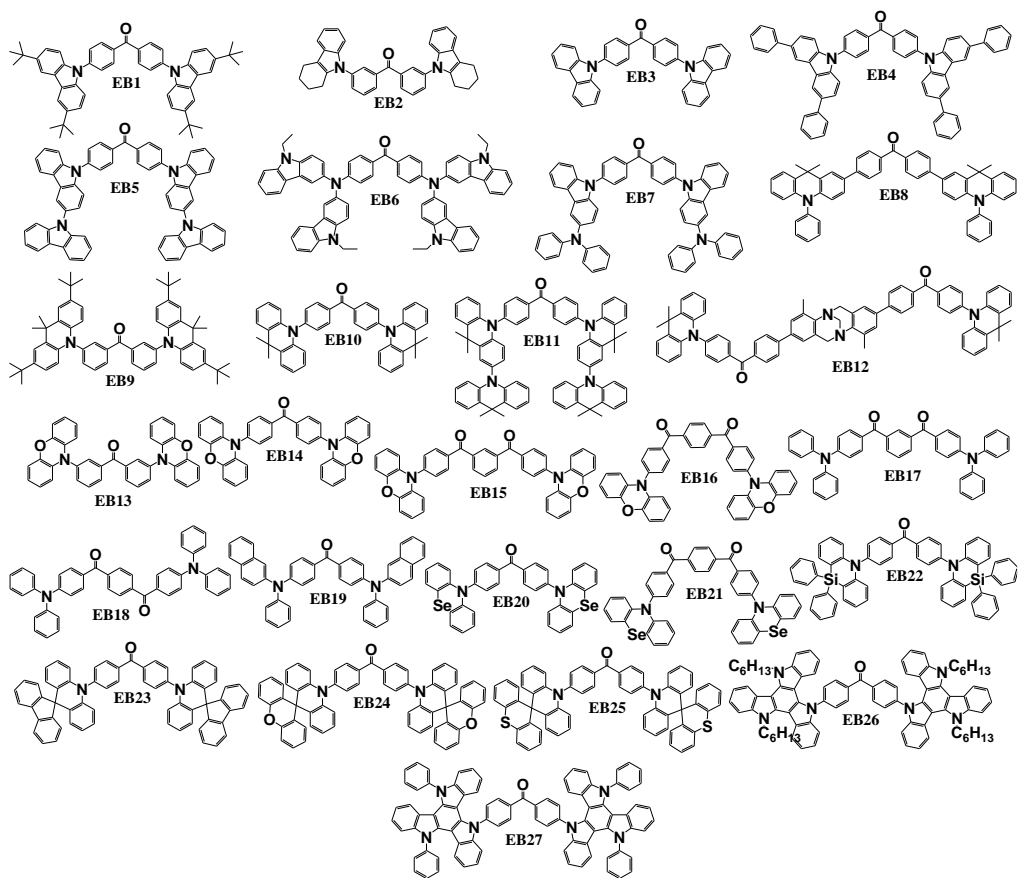
Figure 23. Structures of benzophenone-based D–A–D symmetrical materials used as emitters in OLEDs [159, 162, 168, 176, 191–202]

N-(2-naphthyl)aniline played a crucial role in obtaining **EB19** [194]. Phenoselanazine, azasiline, 10*H*-spiro[acridine-9,9′-fluorene], 10*H*-spiro[acridine-9,9′-xanthene], and 10*H*-spiro[acridine-9,9′-thioxanthene] were utilized for **EB20**, **EB21** [195], **EB22** [196], **EB23**, **EB24**, and **EB25** [197], respectively. The synthesis of the compounds **EB26** and **EB27** [198] involved the use of 5,10-dihexyl-10,15-dihydro-5H-diindolo[3,2-a:3',2'-c]carbazole and 5,10-diphenyl-10,15-dihydro-5H-diindolo[3,2-a:3',2'-c]carbazole as the reactants. The synthesis of the benzophenone derivatives **EB14**, **EB15** and **EB16** [192], which was described in the same publication with the above-mentioned **EB3** and **EB5**, was achieved by using aminations of bis(4-bromobenzoyl)benzenes with two equivalents of phenoxazine. The same reaction methodology was used to obtain the emitter **EB6** [176]. In this case, the amination of 3-iodo-9-ethylcarbazole with 4,4′-diaminobenzophenone took place. ((4,10-Dimethyl-6H,12H-5,11-methanodibenzo[b,f][1,5]diazocine-2,8-diyl)bis(4,1-phenylene))bis((4-bromophenyl)methanone) reacted with 9,9-dimethyl-9,10-dihydroacridine in similar conditions to make up the emitter **EB12** [199]. The material **EB7** [200] was synthesized through a simple nucleophilic substitution of

4,4'-difluorobenzophenone with 3-(*N*,*N*-diphenylamino)carbazole. The Suzuki reaction was chosen as the optimal procedure for obtaining the compound **EB8** [201], by using 4,4'-dibromobenzophenone and 9,9-dimethyl-10-phenyl-2-(4,4,5,5-tetramethyl-1,3,2-dioxaborolan-2-yl)-9,10-dihydroacridine as the initial reactants. **EB10** [202] was synthesized during a *N*,*N*-(2,6-di(3-pentyl)phenyl) imidazolium-catalyzed reaction of 4,4'-dibromobenzophenone and 9,9-dimethyl-9,10-dihydroacridine. Both compounds **EB17** and **EB18** [168] were prepared through a simple one-step Friedel–Crafts reaction, while using commercially available inexpensive starting materials triphenylamine and isophthaloyl dichloride for the compound **EB17** or terephthaloyl dichloride for the emitter **EB18**.

Among this category of materials, the highest efficiencies in devices were demonstrated by **EB5**, **EB20**, **EB23**, **EB24**, and **EB25**. T_d values were reported for the derivatives **EB23**, **EB24** and **EB25**, with all of these exceeding 430°C, which proves the excellent thermal stability. The above-mentioned five symmetrical D–A–D benzophenone derivatives exhibited relatively narrow bandgaps ranging from 3.02 to 3.37 eV. Additionally, the derivatives **EB5**, **EB20**, **EB23**, **EB24**, and **EB25** achieved low ΔE_{ST} levels of 0.14 eV, 0.15 eV, 0.01 eV, 0.01 eV, and 0.01 eV, respectively, which is crucial for enhancing the efficiency of the TADF process. This enhancement is evident as the materials **EB5**, **EB23**, **EB24**, and **EB25** exhibited the PLQY values of 73.0%, 91.0%, 94.0%, and 85.0%, respectively. The involvement of the triplet state in the emission process is apparent for some compounds, observed in **EB23**, **EB24**, and **EB25**, where substantial R_D levels of 55.6%, 54.5%, and 42.8% were identified. All five best-performing emitters in this chapter exhibited TADF properties. The device architectures utilizing the emitters **EB5**, **EB20**, **EB23**, **EB24**, and **EB25** are outlined in Table 14.

Table 14. Architectures of devices utilizing emitters **EB5**, **EB20**, **EB23**, and **EB24**

Device	Device architecture	Reference
DEB5	ITO/α-NPD (35nm)/mCP (5nm)/DPEPO:6 wt%**EB5** (20nm)/DPEPO (10nm)/TPBi (30nm)/LiF (0.8nm)/Al (80 nm)	[192]
DEB20	ITO/α-NPD (40nm)/mCBP:10wt%**EB20** (20nm)/TPBi (40nm)/LiF (0.6nm)/Al (100 nm)	[195]
D1EB23	ITO/HAT-CN (5nm)/NPB (30nm)/mCP (5nm)/**EB23** (20 nm)/PPF (5nm)/TPBi (50nm)/LiF (1nm)/Al (120nm)	[197]
D2EB23	ITO/HAT-CN (5nm)/NPB (30nm)/mCP (5nm)/PPF:30wt%**EB23** (20nm)/ PPF (5nm)/TPBi (50nm)/LiF (1nm)/Al (120nm)	[197]
D1EB24	ITO/HAT-CN (5nm)/NPB (30nm)/mCP (5nm)/**EB24** (20 nm)/PPF (5nm)/TPBi (50nm)/LiF (1nm)/Al (120nm)	[197]
D2EB24	ITO/HAT-CN (5nm)/NPB (30nm)/mCP (5nm)/PPF:30wt%**EB24** (20nm)/PPF (5nm)/TPBi (50nm)/LiF (1nm)/Al (120nm)	[197]
D1EB25	ITO/HAT-CN (5nm)/NPB (30nm)/mCP (5nm)/**EB25** (20nm)/PPF (5nm)/TPBi (50nm)/LiF (1nm)/Al (120nm)	[197]
D2EB25	ITO/HAT-CN (5nm)/NPB (30nm)/mCP (5nm)/PPF:30wt%**EB25** (20nm)/PPF (5nm)/TPBi (50nm)/LiF (1nm)/Al (120nm)	[197]

Table 15 displays the characteristics of the most efficient devices utilizing EB derivatives as emitters. S.J. Lee et al. synthesized and characterized the most efficient

blue TADF emitter described in this chapter, **EB5**, achieving an EQE value of 14.3% and a CE of 25.5 cd/A, when applied in a device. Researchers developed the green TADF emitters **EB20**, **EB23**, **EB24**, and **EB25** with a symmetrical D–A–D structure incorporating a central benzophenone fragment, with all of them achieving over 17% external quantum efficiency. P. Sharif and colleagues synthesized and characterized the derivative **EB20**, which proved highly efficient in green TADF OLED devices. By combining a phenoselenazine electron donor with benzophenone, they synthesized **EB20** and fabricated the DEB20 device, exhibiting an exceptionally high EQE of 30.8% and a CE of 64.0 cd/A.

Table 15. Characteristics of TADF OLED devices using emitters **EB5**, **EB20**, **EB23**, **EB24**, and **EB25**

Device	Emitter	Colour	V_{ON}, V	L_{MAX}, cd/m^2	CE, cd/A	PE, lm/W	EQE, %	CIE (x, y)	Reference
DEB5	**EB5**	Blue	4.4	3900	25.5	-	14.3	(0.17, 0.27)	[192]
DEB20	**EB20**	Green	4.3	17007	64.0	-	30.8	(0.31, 0.53)	[195]
D1EB23	**EB23**	Green	3.2	31713	53.9	48.9	18.6	(0.24, 0.53)	[197]
D2EB23	**EB23**	Green	3.0	48712	90.9	91.2	30.3	(0.25, 0.54)	[197]
D1EB24	**EB24**	Green	3.6	30283	46.8	37.5	17.1	(0.22, 0.46)	[197]
D2EB24	**EB24**	Green	3.2	48515	87.5	85.9	32.2	(0.22, 0.49)	[197]
D1EB25	**EB25**	Green	3.8	25616	49.1	35.7	18.1	(0.22, 0.50)	[197]
D2EB25	**EB25**	Green	3.2	48153	79.8	75.9	28.4	(0.23, 0.50)	[197]

The highest overall efficiencies of green TADF OLEDs using symmetrical D-A-D benzophenone-based emitters were achieved by R. Huang et al., who synthesized and characterized the derivatives **EB23**, **EB24**, and **EB25**. These materials underwent testing in both non-doped and doped emissive layers. The most efficient non-doped device, D1EB23, demonstrated an exceptional performance with the maximum CE, PE, and EQE values reaching 53.9 cd/A, 48.9 lm/W, and 18.6%, respectively. In the doped configuration of the device D2EB23, efficiencies were further elevated, ultimately achieving an impressive CE of 90.9 cd/A, a PE of 91.2 lm/W, and an EQE of 30.3%. While the device D2EB23 attained the highest CE and PE among green devices in this study, the OLED prototype D2EB24, featuring the emitter **EB24** doped in a host material, remained unparalleled with an extraordinary EQE level of 32.2%.

3.4.5. Benzophenone-based emitters employing asymmetric donor-acceptor-donor structure

Figure 24 illustrates the structures of benzophenone-based TADF emitters utilizing an asymmetric D–A–D molecular configuration. Except for one material, all of them incorporated carbazole as one of the electron-donating fragments, alongside other donating moieties, such as 3-substituted carbazole, 9,10-dihydro-9,9-dimethylacridine, spiro[acridine-9,9'-fluorene], and phenoxazine. Notably, the derivative **EC11** stood out by not incorporating carbazole as one of the electron donors; instead, it employed 9,10-dihydro-9,9-dimethylacridine and thianthrene fragments.
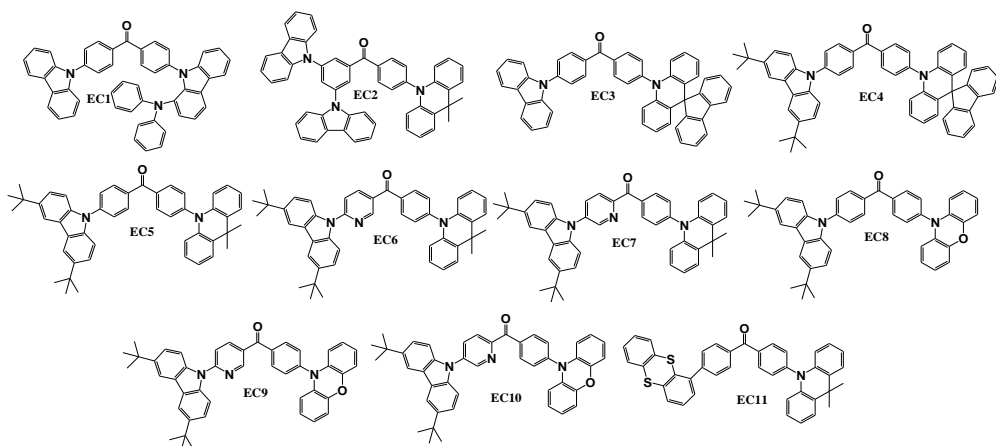
Figure 24. Structures of benzophenone-based D–A–D asymmetrical materials used as emitters in OLEDs [104, 173, 203–205]

The synthesis of the derivatives required at least two synthetic steps. For instance, the derivative **EC1** [173] was synthesized through a two-step Buchwald–Hartwig amination procedure, involving the replacement of one bromine atom in 4,4'-dibromobenzophenone with carbazole, followed by the reaction with 4-(9*H*-carbazol-1-yl)-N,N'-diphenylaniline. The material **EC2** [104] was obtained by reacting (3,5-bis-carbazol-9-yl-phenyl)-(4-bromophenyl)-methanone with 9,10-dihydro-9,9-dimethylacridine under Buchwald–Hartwig reaction conditions. Similarly, the derivatives **EC3** and **EC4** [203] were synthesized through a two-step process involving a nucleophilic substitution reaction followed by a Buchwald–Hartwig reaction. The materials **EC5**–**EC10** were also synthesized by using very similar procedures [204], where the Buchwald–Hartwig reactions of 3,6-di-tert-butyl-9*H*-carbazole with various aromatic ketones were followed by nucleophilic substitution reactions with 9,10-dihydro-9,9-dimethylacridine or phenoxazine. The synthesis of the compound **EC11** involved a two-step process [205] starting with a Suzuki reaction to replace one bromine atom of 4,4'-dibromobenzophenone with a thianthrene moiety, followed by a Buchwald–Hartwig coupling reaction to substitute the second bromine atom with 9,10-dihydro-9,9-dimethylacridine.

Among all these materials, the best efficiencies were achieved by the derivatives **EC2**, **EC3**, **EC4**, and **EC11**. Researchers presented the thermal, electrochemical, photoelectrical, and photophysical properties of these materials. The presently mentioned benzophenone derivatives with an asymmetric D–A–D structure exhibited an exceptional thermal stability, with the T_d values ranging from 309 to 451°C. During DSC experiments, T_g values were recorded at 72°C and 104°C for the materials **EC2** and **EC11**, respectively. The HOMO levels of the materials **EC2**, **EC3**, **EC4**, and their **EC11** values ranged from -5.92 to -5.35, while the LUMO levels varied between -3.04 and -2.61, resulting in the bandgap energies of 2.88 eV or lower, thus facilitating the minimal energy difference between the lowest singlet and triplet states, thus enabling efficient reverse intersystem crossing. Experimental results supported this data, with ΔE_{ST} being 0.10 eV or lower, and resulting in high PLQY for the derivatives

EC3, **EC4**, and **EC11** reaching 90%, 86%, and 76%, respectively. Additionally, these derivatives exhibited aggregation-induced emission properties, with significantly lower PLQY values detected in solutions compared to the film states. The PLQY values for the materials **EC3** and **EC4** detected in solutions were 28% and 25%, respectively, while the material **EC11** exhibited a PLQY value of 17%. Furthermore, the materials **EC3** and **EC4** demonstrated involvement of triplet states in photon generation, as evidenced by R_D levels of 53.3% and 33.0%, respectively, with one of the potential light-generating mechanisms being TADF. The architectures of the devices based on the emitters **EC2**, **EC3**, **EC4**, and **EC11** are presented in Table 16.

Table 16. Architectures of devices utilizing emitters **EC2**, **EC3**, **EC4**, and **EC11**

Device	Device architecture	Reference
DEC2	ITO/HAT-CN (20nm)/TAPC (30nm)/CBP:20wt%**EC2** (25nm)/TmPyPb (40nm)/LiF (1nm)/Al (150nm)	[104]
D1EC3	ITO/HAT-CN (5nm)/NPB (30nm)/mCP (5nm)/**EC3** (20nm)/PPF (5nm)/TPBi (50nm)/LiF (1nm)/Al (120nm)	[203]
D2EC3	ITO/HAT-CN (5nm)/NPB (30nm)/mCP (5nm)/PPF:20wt% **EC3** (20nm)/PPF (5nm)/TPBi (50nm)/LiF (1nm)/Al (120nm)	[203]
D1EC4	ITO/HAT-CN (5nm)/NPB (30nm)/mCP (5nm)/**EC4** (20nm)/PPF (5nm)/TPBi (50nm)/LiF (1nm)/Al (120nm)	[203]
D2EC4	ITO/HAT-CN (5nm)/NPB (30nm)/mCP (5nm)/PPF:20wt% **EC4** (20nm)/PPF (5nm)/TPBi (50nm)/LiF (1nm)/Al (120nm)	[203]
DEC11	ITO/MoO$_3$ (1.2nm)/NPB (44nm)/TCTA (4nm)/mCP (4nm)/mCP:7%wt **EC11** (24 nm)/ TSPO1 (4nm)/TPBi (40nm)/LiF (1.2nm)/Al (400nm)	[205]

Table 17 illustrates the characteristics of the most efficient devices utilizing EC materials as the emitters. The derivative **EC2**, synthesized and characterized by Y. Zhao et al., demonstrated an impressive performance with the CE, PE, and EQE values of 61.8 cd/A, 40.4 lm/W, and 19.7%, respectively, along with an impressive L_{MAX} of 116,000 cd/m^2. R. Huang and colleagues developed the derivatives **EC3** and **EC4**, among which, the TADF emitter **EC3**-based devices exhibited the highest efficiencies in this study, achieving CE, PE, and EQE of 76.9 cd/A, 71.0 lm/W, and 29.0% in the non-doped device D1EC3. Introduction of the host material PPF in the emissive layer (D2EC3) further elevated the efficiencies to 82.9 cd/A CE, 70.1 lm/W PE, and a peak EQE of 33.3%. Although **EC4**-based OLEDs were slightly less efficient, D1EC4 exhibited a remarkably low voltage turn-on (V_{ON}) of 3.0 V and an EQE of 21.6%. D2EC4 demonstrated an impressive EQE of 32.9%, with the CE and PE values of 77.2 cd/A and 65.0 lm/W. Lastly, the TADF emitter **EC11**, designed and synthesized by A. Tomkevičienė and colleagues, featured two electron-donating fragments of thianthrene and 9,10-dihydro-9,9-dimethylacridine. When incorporated into the emissive layer of the device DEC11, it achieved the CE, PE, and EQE values of 57.8 cd/A, 38.8 lm/W, and 22.2%, with L_{MAX} exceeding 15,000 cd/m^2.

Table 17. Characteristics of TADF OLED devices using emitters **EC2**, **EC3**, **EC4**, and **EC11**

Device	Emitter	Colour	V_{ON}, V	L_{MAX}, cd/m^2	CE, cd/A	PE, lm/W	EQE, %	CIE (x, y)	Reference
DEC2	**EC2**	Green	3.6	116000	61.8	40.4	19.7	(0.26, 0.56)	[104]
D1EC3	**EC3**	Green	3.2	78540	76.9	71.0	29.0	(0.21, 0.47)	[203]
D2EC3	**EC3**	Green	3.2	71150	82.9	70.1	33.3	(0.20, 0.42)	[203]
D1EC4	**EC4**	Green	3.0	54450	53.2	51.5	21.6	(0.20, 0.42)	[203]
D2EC4	**EC4**	Green	3.2	42550	77.2	65.0	32.9	(0.19, 0.38)	[203]
DEC11	**EC11**	Green	4.2	15600	57.8	38.8	22.2	(0.18, 0.41)	[205]

In summary, this research indicates that benzophenones with different electron donors demonstrate significant potential as hosts for both PhOLEDs and TADF OLEDs, and hold promise as effective emissive materials for diverse OLED device configurations. Continuous synthesis and investigation of novel benzophenone-based electroactive materials would further enhance the quality and efficiency of future OLED devices.

3.5. Bifunctional Bicarbazole-Benzophenone-Based Twisted Donor–Acceptor–Donor Derivatives for Deep-Blue and Green OLEDs (Scientific Publication No. 5, Q1, 6 citations)

This chapter is based on the paper published in *Nanomaterials*, **2023**, 13, 8 by *P. Gautam, S. Shahnawaz, I. Siddiqui, D. Blazevicius, G. Krucaite, D. Tavgeniene, J.-H. Jou*, and *S. Grigalevicius* [206].

In this study, a carbazole fragment was utilized differently than in the first two chapters of the review of published articles. This time, carbazole in a form of bicarbazole was used as an electron donor in combination with a diphenyl sulfone electron acceptor to produce new bifunctional compounds. The synthesis of bicarbazole-based host materials was conducted during a three-step procedure depicted in Scheme 4. Initially, 3,3'-bicarbazole (**9**) was obtained through the oxidation of carbazole (**1**) with iron (III) chloride. The reaction was carried out for 20 minutes at room temperature. The product was precipitated by using methanol, then filtered and washed again with methanol. The subsequent step involved *N*-alkylation reactions between bicarbazole (**9**) and various alkyl or benzyl bromides, resulting in diverse 9-alkyl-9'*H*-3,3'-bicarbazoles (**10–12**) and 9-benzyl-9'*H*-3,3'-bicarbazole (**13**). These reactions were carried out by adding 1-bromoalkane or benzyl bromide (1 mol. eq.) to a stirred solution of 3,3'-bicarbazole (**9**) (1 mol. eq.) in tetrahydrofuran. The mixture was heated to reflux, and then potassium carbonate (2 mol. eq.) and powdered potassium hydroxide (6 mol. eq.) was added stepwise to deprotonate bicarbazole, this way enhancing its nucleophilic properties. The resulting mixture was left to react for 4 h. After thin-layer chromatography control, the inorganic salts were filtered off. Due to the lack of selectivity in the reactions, both amino groups of bicarbazole simultaneously attacked the electron-deficient carbon of alkyl bromide (or benzyl bromide). As a result, the mixture contained mono-substituted, di-substituted, and unsubstituted bicarbazole. To extract the desired 9-alkyl(or benzyl)-9'*H*-3,3'-bicarbazole compounds, extensive purification by silica gel column chromatography

while using a mixture of THF and hexane as an eluent was needed. The yields of these reactions ranged from 27% to 48%.
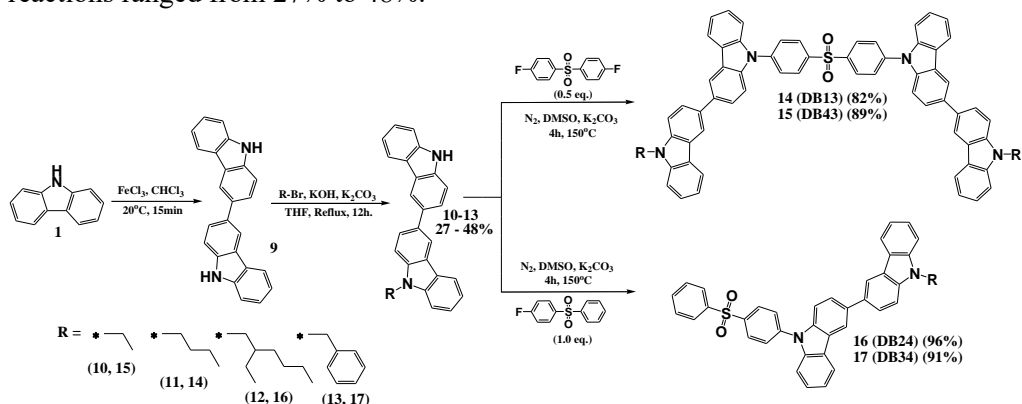
Scheme 4. Synthetic pathway of new diphenyl sulfone-based materials

The final step was comprised of a nucleophilic aromatic substitution of partially substituted bicarbazole with diphenyl sulfone containing one or two fluorine atoms. Bis(4-(9-alkyl(or benzyl)-3,3'-bicarbazol-9'-yl)phenyl)sulfones were synthesized during the following procedure. 9-Alkyl(or benzyl)-9'H-3,3'-bicarbazoles (**10–13**) (1 mol. eq.) and bis(4-fluorophenyl) sulfone (0.5 mol. eq.) or 4-fluorophenyl phenyl sulfone (1 mol. eq.) were stirred in 10 mL of dimethyl sulfoxide (DMSO) at 150 °C under nitrogen atmosphere for 4 h. Potassium carbonate (10 mol. eq.) was also added in this reaction to deprotonate the bicarbazole-based reactant, thereby enhancing its nucleophilic properties and accelerating the reaction. After thin-layer chromatography control, the resulting mixture was cooled down and quenched by the addition of ice water. The organic phase was separated by extracting with chloroform, and the combined organic extract was dried over anhydrous Na_2SO_4. The crude product was purified by silica gel column chromatography while using a mixture of THF and hexane as an eluent. These reactions successfully produced the target materials **14 (DB13)**, **15 (DB43)**, **16 (DB24)**, and **17 (DB34)** with yields ranging from 82% to 96%. MS and NMR spectroscopy were employed to identify the newly synthesized derivatives, with the obtained data aligning well with the proposed structures. Each new derivative **14 (DB13)**, **15 (DB43)**, and **16 (DB24)** possesses an alkyl chain(s) of various lengths with the exception of the compound **17 (DB34)**, which had a benzyl fragment incorporated in its structure. Notably, both **15 (DB43)** and **14 (DB13)** consist of two 3,3'-bicarbazole units, with **14 (DB13)** featuring a longer alkyl chain compared to **15 (DB43)**. In a study by S. Inoue et al., the impact of the alkyl chain length on the solubility of organic compounds was explored [207]. The general trend observed suggests that the longer alkyl chain improves the solubility of the molecule in a compatible solvent.

The electron density contours of the frontier molecular orbitals for the materials **DB13**, **DB24**, **DB34**, and **DB43** are shown in Figure 25. As seen in the figure, all derivatives exhibit twisted spatial structures, resulting in a minimal HOMO-LUMO overlap. This characteristic could facilitate a small gap between the singlet and triplet energy levels, leading to the more efficient utilization of triplet excitons.
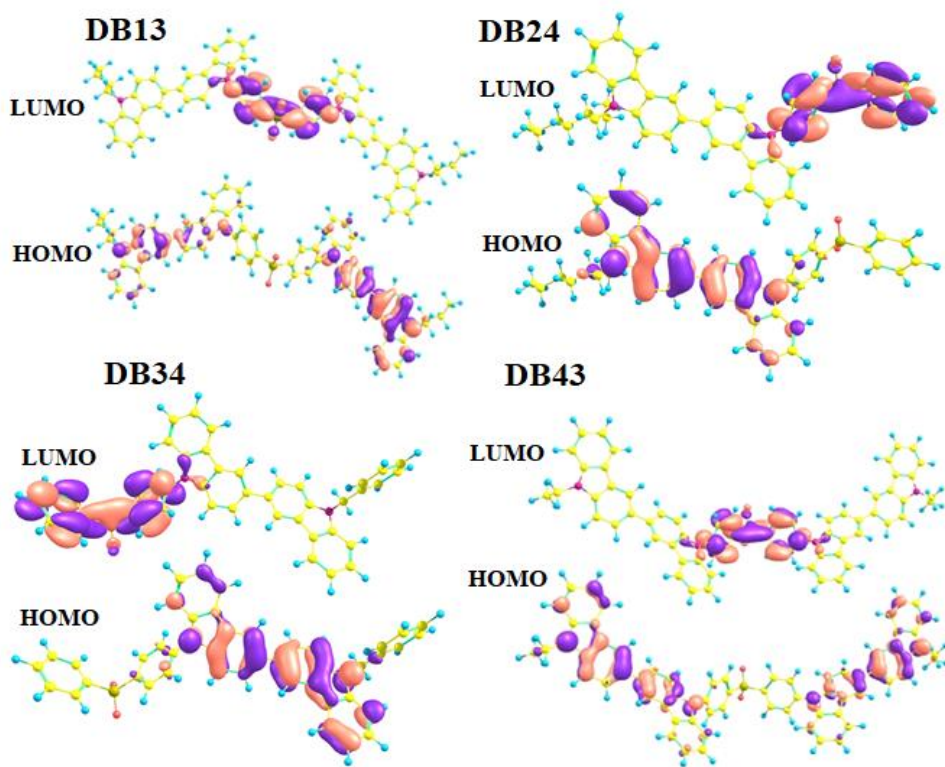
Figure 25. Electron density contours of frontier molecular orbitals and HOMO, LUMO distribution for compounds **14 (DB13)**, **16 (DB24)**, **17 (DB34)**, and **15 (DB43)**.

The behaviour of the synthesized materials **14 (DB13)**, **16 (DB24)**, **17 (DB34)**, and **15** (**DB43)** under heating was examined through DSC and TGA analysis conducted in nitrogen atmosphere. The findings revealed that these compounds possess high thermal stability. In particular, the T_d values for the derivatives **14 (DB13)**, **16 (DB24)**, **17 (DB34)**, and **15** (**DB43)** were determined as 365 °C, 430 °C, 391 °C, and 383 °C, respectively. Notably, the materials **16 (DB24)** and **17 (DB34)** displayed a marginally higher thermal stability, potentially attributed to the presence of one alkyl chain in their structures, opposed to two in the structures of the derivatives **14 (DB13)** and **15** (**DB43)**.

The DSC curves illustrating the second heating scans of the **14 (DB13)**, **15** (**DB43)**, **16 (DB24)**, and **17 (DB34)** samples are depicted in Figure 26. Analysis of the curves reveals distinct T_g levels for these derivatives, with **14 (DB13)** and **17 (DB34)** both exhibiting a high T_g of 154 °C, while **15 (DB43)** has a T_g of 125 °C. In contrast, **16 (DB24)** displays a lower T_g value of 82 °C, attributed to the presence of a branched 2-ethylhexyl group in its structure. The TGA and DSC results collectively support the suitability of these materials for use in the amorphous electroactive layers of OLEDs. The thermal characteristics of the new materials are also presented in Table 18.
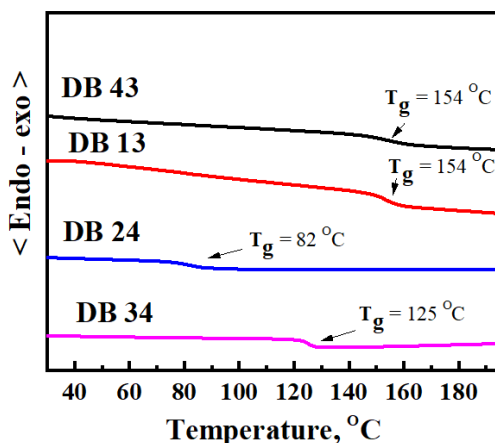
Figure 26. DSC curves of second heating and T_g values of compounds **14 (DB13)**, **15 (DB43)**, **16 (DB24)**, and **17 (DB34)**

The compounds **14 (DB13)**, **15 (DB43)**, **16 (DB24)**, and **17 (DB34)** exhibit high PLQY values of 50.5%, 61.8%, 68.5%, and 66.5%, respectively. These PLQY values are also detailed in Table 8. The UV-absorption spectra of the materials were generated in THF solvent under ambient conditions. The spectra of the prepared solutions were recorded by using a quartz cuvette, revealing absorption peaks around 375 nm for all the compounds. This consistency is expected due to the identical chromophores present in their structures. A Tauc plot for material **14 (DB13)**, shown in Figure 27, was generated based on the absorption wavelength and intensity by using the following equations to determine the E_g values:

$$x = \sqrt{(\alpha \times h\nu)} \tag{5}$$
$$y = h\nu \tag{6}$$

where: α – absorption coefficient;
$h\nu$ – energy.

Identical absorption experiments were conducted, and Tauc plots were constructed for all the materials discussed in this chapter. The determined E_g values for each material are compiled and presented in Table 18.
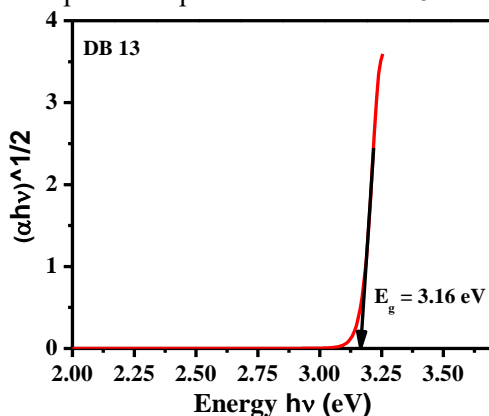
Figure 27. Tauc plot representing the bandgap of compound **14 (DB13)**

In Figure 28 (left), the PL spectrum of **14 (DB13)** is depicted. The PL spectra were generated for all the materials under discussion, revealing the maximum emission wavelengths falling within the 450–470 nm range. The E_S values for the derivatives were calculated by identifying the point of intersection between the PL and absorbance wavelengths. Additionally, the LTPL spectrum, as depicted in Figure 28 (right), was measured to ascertain the E_T value. The same experiments were repeated for all the target materials. The compounds **14 (DB13)**, **15** (**DB43**), **16 (DB24)**, and **17 (DB34)** exhibit elevated triplet energy levels of 2.78, 2.77, 2.80, and 2.77 eV, respectively. These materials could be explored as promising host candidates for both green phosphorescent emitters and green TADF emitters. The singlet and triplet energy values are also provided in Table 18.
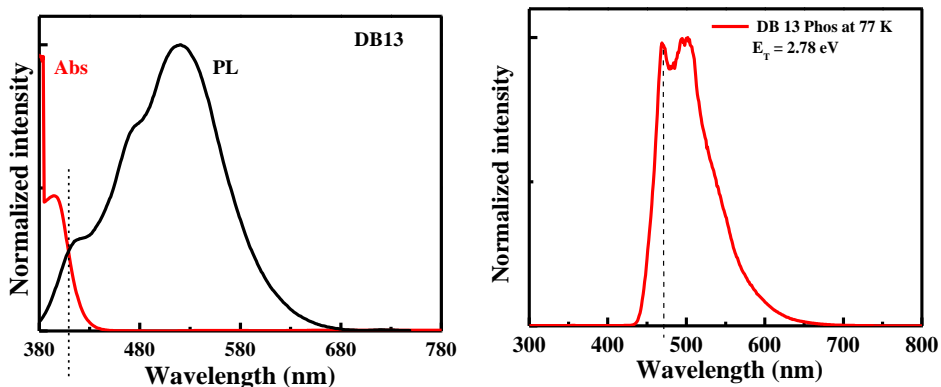
Figure 28. PL (left) and LTPL (right) spectra for compound **14 (DB13)**

Figure 29 displays the results of time-resolved photoluminescence (TRPL) analysis, portraying the photoluminescence decay kinetics. Specifically, the photoluminescence decay time values for **14 (DB13)**, **15** (**DB43**), **16 (DB24)**, and **17 (DB34)** were determined to be in a 2.7–3.3 ns range. Notably, all the compounds exhibit radiative emission with a short decay time, and the corresponding decay values are also outlined in Table 18. The instrument response function (IRF), serving as a control parameter, was measured both before and after each measurement.
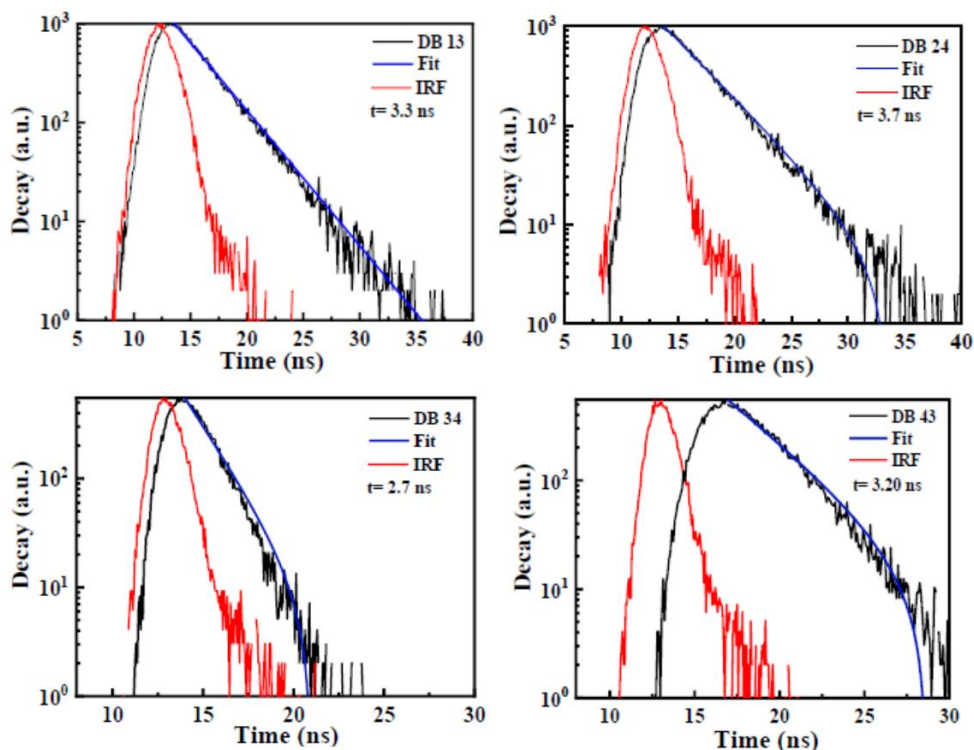
Figure 29. Time-resolved photoluminescence (TRPL) spectra for the PL decay kinetics analysis of the compounds **14 (DB13)**, **15** (**DB43**), **16** (**DB24**), and **17** (**DB34**)

The electrochemical characteristics of the compounds **14 (DB13)**, **15** (**DB43**), **16 (DB24)**, and **17 (DB34)** were assessed through cyclic voltammetry (CV) measurements. The HOMO and LUMO levels were calculated by using the following equations:

$$E_{HOMO} = -[4.4 + E_{onset}^{ox}] \qquad (7)$$
$$E_{LUMO} = E_{HOMO} + E_g \qquad (8)$$

where: E_{onset}^{ox} – onset oxidation potential;

E_g – optical bandgap, derived from Tauc plot.

The calculated HOMO energy levels were -5.73, -5.71, -5.77, and -5.69 eV, while the LUMO levels were -2.57, -2.43, -2.41, and -2.49 eV for **14 (DB13)**, **15** (**DB43**), **16 (DB24)**, and **17 (DB34)**, respectively. The E_g values obtained from the Tauc plot, formed by using Equation (5) for the x value and Equation (6) for the y value, were 3.16, 3.26, 3.30, and 3.28 eV for the compounds **14 (DB13)**, **15** (**DB43**), **16 (DB24)**, and **17 (DB34)**, respectively (refer to Table 18). The HOMO and LUMO levels of the derivatives were found to be suitable for application as both blue emitters and host materials.

Table 18 provides an overview of the photophysical, electrochemical, and thermal properties of **14 (DB13)**, **15** (**DB43**), **16 (DB24)**, and **17 (DB34)**. The table

underscores the high photoluminescence yields of the compounds, as well as the elevated decomposition temperatures, and high glass transition temperatures for the derivatives **14 (DB13)**, **17 (DB34)**, and **15** (**DB43**). Additionally, the compounds exhibit large bandgaps, which makes them well-suited for use in OLEDs, serving both as emitters and hosts.

Table 18. Thermal, photophysical and electrochemical properties of compounds **14 (DB13)**, **15** (**DB43**), **16 (DB24)**, and **17 (DB34)**

Material	T_D (ºC)	T_g (ºC)	E_g, eV	PLQY, %	Decay, ns	HOMO, eV	LUMO, eV	E_S, eV	E_T, eV	ΔE_{ST}, eV
14 (DB13)	430	154	3.16	50.5	3.30	5.73	2.57	3.10	2.78	0.32
15 (**DB43**)	365	154	3.26	66.5	3.30	5.69	2.43	3.23	2.77	0.46
16 (DB24)	391	82	3.30	61.8	3.70	5.71	2.41	3.12	2.77	0.35
17 (DB34)	383	125	3.28	68.5	2.70	5.77	2.49	3.14	2.80	0.34

Blue OLED devices were manufactured to evaluate the new materials **14 (DB13)**, **15** (**DB43**), **16 (DB24)**, and **17 (DB34)** as emitters in combination with the CBP host matrix. After the EL experiments, the derivative **14 (DB13)** proved to be most effective as an emitter within this group of materials. The EL characteristics of OLEDs utilizing the emitter **14 (DB13)**, along with the device characteristics, are depicted in Figure 30 and summarised in Table 19.
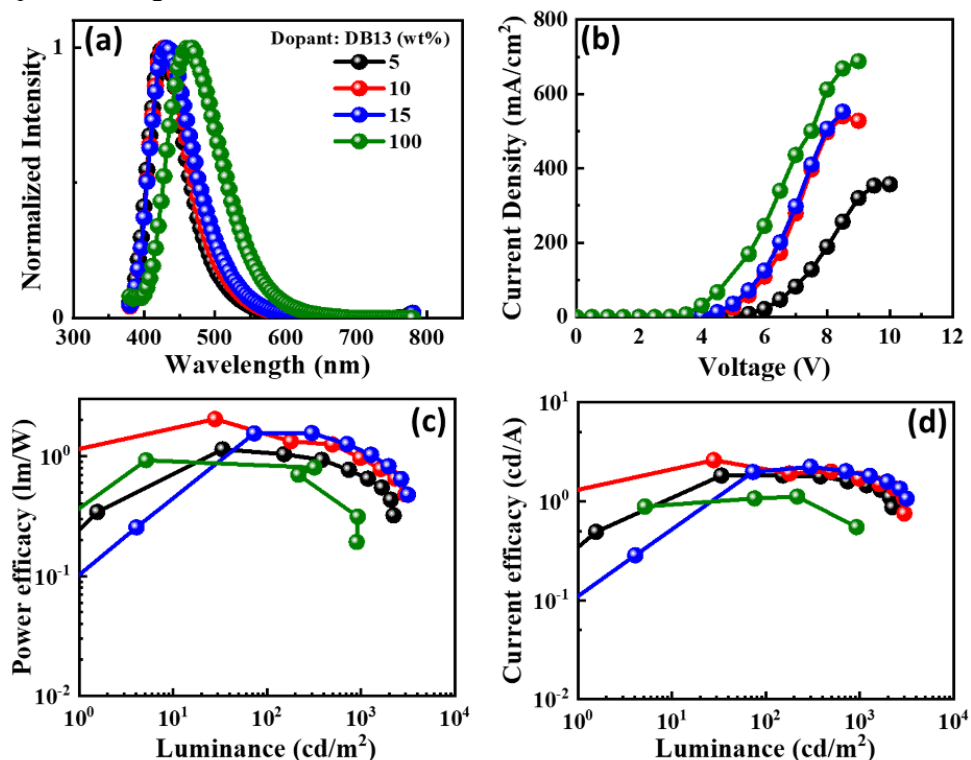
Figure 30. EL properties of **14 (DB13)**-based devices showing (a) EL spectra, (b) current density-voltage, (c) power efficacy-luminance, and (d) current efficacy-luminance characteristics

Table 19. Characteristics of devices utilizing blue fluorescent emitter

Emitter	wt%	V_{ON}, V	PE_{max}, lm/W	CE_{max}, cd/A	EQE_{max}, %	CIE (x, y) @100/1000 cd/m²	L_{MAX}, cd/m²
14 (DB13)	5	4.6	1.1	1.8	3.4	(0.16, 0.08) / (0.16, 0.08)	2230
	10	3.7	2.0	2.5	4.0	(0.16, 0.09) / (0.16, 0.09)	2987
	15	3.5	1.6	2.2	2.9	(0.16, 0.10) / (0.16, 0.10)	3167
	100	3.0	1.0	1.1	0.6	(0.16, 0.20) / -	928

The fabricated OLEDs were configured as either doped or non-doped devices with the following structure: ITO (125 nm)/PEDOT:PSS (35 nm)/host: (x wt%) emitter (x = 5.0, 10, 15, and 100%) (20 nm)/TPBi (40 nm)/LiF (1 nm)/Al (200 nm).

The role of the host material was crucial, and a device based on a 10 wt% **14 (DB13)** emitter in its emissive layer outperformed others, by achieving a PE_{max} of 2.0 lm/W, a CE_{max} of 2.5 cd/A, and a low turn-on voltage of 3.7 eV. Furthermore, the above-mentioned **14 (DB13)**-based device attained the highest EQE_{max} of 4.0%, thus approaching the theoretical limit for fluorescent emitters in deep-blue emission with a CIEy of 0.09. This device exhibited a higher EQE compared to many other fluorescent emitters found in scientific literature [208]. The **14 (DB13)**-based fluorescent OLED not only displayed a deeper blue emission, but also outperformed a recently reported device based on a hybridized local and charge-transfer mechanism [209]. This proves the advantage of twisted D–A–D derivatives as candidates for fluorescent emission

Additionally, all the newly synthesized derivatives were tested as hosts in green phosphorescent and TADF OLEDs, as shown in the energy-level diagrams depicted in Figure 31.
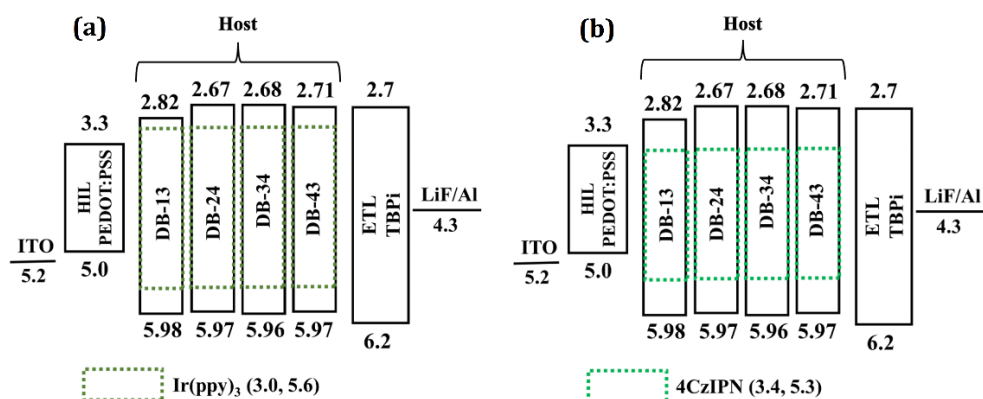
Figure 31. Energy-level diagram (in eV) of green OLEDs containing hosts **14 (DB13)**, **15** (**DB43**), **16 (DB24)**, and **17 (DB34)** doped with commercial phosphorescent emitter Ir(ppy)₃ (a) or commercial TADF emitter 4CzIPN (b)

The compounds **14 (DB13)**, **15** (**DB43**), **16 (DB24)**, and **17 (DB34)** were chosen as the host materials for green OLEDs due to their wide bandgap and high triplet energies. In the context of green OLED applications, second- and third-generation

green emitters, namely, the phosphorescent emitter Ir(ppy)$_3$ and the TADF emitter 4CzIPN, were employed. The structure of these solution-processed green OLEDs was ITO (125 nm)/PEDOT:PSS (35 nm)/host: (x wt%) emitter (host = **14 (DB13)**, **15 (DB43)**, **16 (DB24)**, and **17 (DB34)**) (emitter = Ir(ppy)$_3$ or 4CzIPN) (x = 5, 10, and 12.5 for Ir(ppy)$_3$), (x = 1, 3, and 5% for 4CzIPN) (20 nm)/TPBi (40 nm)/LiF (1 nm)/Al (200 nm).

The electroluminescent spectra of the devices employing the hosts **14 (DB13)**, **16 (DB24)**, and **17 (DB34)**, doped with the green phosphorescent emitter Ir(ppy)$_3$, exhibit peaks around ~540 nm, corresponding to green emission, as shown in Figure 32. The peak observed in the electroluminescence (EL) spectra aligns with the photoluminescence (PL) peak of Ir(ppy)$_3$, suggesting a common emission source [210].
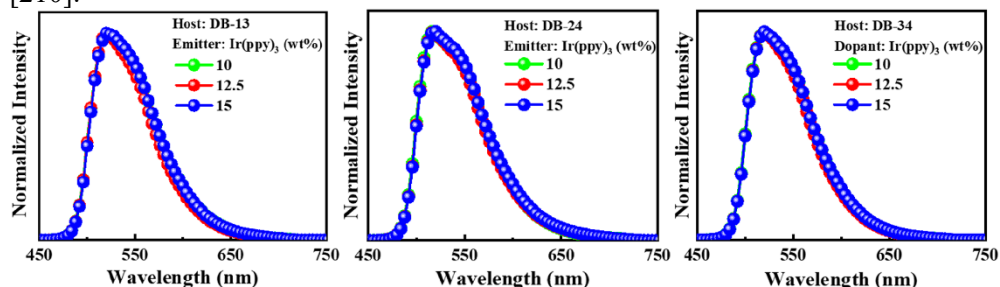
Figure 32. EL spectra of Ir(ppy)$_3$-based OLEDs utilizing hosts **14 (DB13)**, **16 (DB24)** and **17 (DB34)**

The singular EL peak indicates an efficient host-to-guest energy transfer, with the best-performing device being the one having 12.5 wt% Ir(ppy)$_3$ doped in the **14 (DB13)** host. This device achieves a PE$_{max}$ of 45 lm/W, a CE$_{max}$ of 43 cd/A, an EQE$_{max}$ of 10.6%, and an L$_{max}$ value of 37680 cd/m^2, exhibiting a low efficiency roll-off at higher luminance. Table 20 provides a breakdown of the characteristics for green devices, by focusing on the most efficient host material in this group: **14 (DB13)** doped with the commercial phosphorescent green emitter Ir(ppy)$_3$.

Table 20. Characteristics of devices utilizing Ir(ppy)$_3$ emitter doped in **14 (DB13)** host material

Host	Ir(ppy)$_3$ wt%	V$_{ON}$, V	PE, lm/W	CE, cd/A	EQE, %	L$_{MAX}$, cd/m^2
			Max / @1000 cd/m^2			
14 (DB13)	10	2.6	40.0 / 32.1	41.1 / 40.9	11.1 / 11.1	33870
	12.5	3.1	45.4 / 33.4	43.4 / 42.5	10.6 / 10.5	37680
	15	2.5	34.6 / 28.7	35.3 / 33.5	9.5 / 9.4	32300

The superior performance of the **14 (DB13)**-based device may be attributed to its favourable chemical structure, longer aliphatic chains, a high decomposition temperature, a small singlet-triplet energy gap (ΔE_{ST}) promoting the effective triplet exciton utilization, and suitable HOMO-LUMO levels matching those of Ir(ppy)$_3$, thereby facilitating an efficient host-to-guest energy transfer within the emitting layer.

The novel materials **14 (DB13)**, **16 (DB24)**, and **17 (DB34)** were also tested as hosts for the TADF emitter 4CzIPN. Figure 33 depicts the EL spectra of the devices

with a peak around ~530 nm, indicating green emission. The observed peak in the EL spectra closely aligns with the PL peak of 4CzIPN, and any bathochromic shift is only evident with an increase in the doping concentration, thus providing proof of the emission source [211]. Moreover, the singular EL peak mirrors the complete host-to-guest energy transfer.
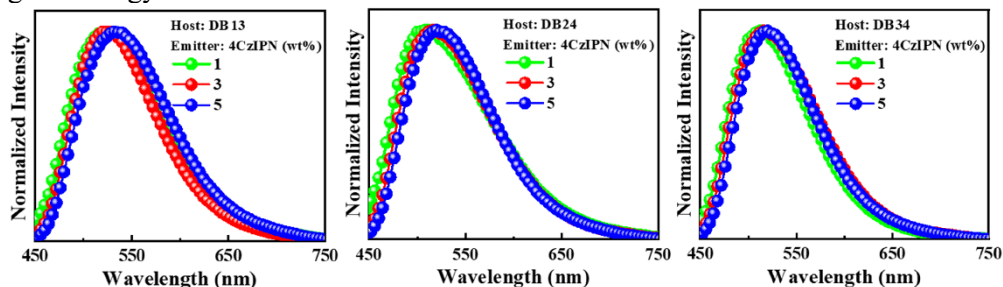
Figure 33. EL spectra of 4CzIPN-based OLEDs utilizing hosts **14 (DB13)**, **16 (DB24)**, and **17 (DB34)**

Among these OLEDs, the device based on the **17 (DB34)** host, doped with 3 wt% of 4CzIPN, outperformed others, by achieving a peak EQE of 10.8%. The detailed OLED characteristics of the devices employing the **17 (DB34)** host are presented in Table 21.

Table 21. Characteristics of devices utilizing 4CzIPN emitter doped in **DB34** host material

Host	4CzIPN wt%	V_{ON}, V	*PE*, lm/W	*CE*, cd/A	*EQE*, %	L_{MAX}, cd/m^2
			Max / @1000 cd/m^2			
17 (DB34)	1	2.7	30.4 / 10.2	27.1 / 14.7	8.9 / 5.0	3782
	3	2.6	37.5 / 15.8	33.5 / 22.6	10.8 / 7.4	9484
	5	2.6	34.7 / 18.9	33.2 / 24.0	10.5 / 7.6	12480

Our TADF-based OLED device utilizing the host material **17 (DB34)** surpassed numerous efficient phosphorescent green devices in terms of EQE [212]. However, its PE and L_{max} were slightly lagging behind the aforementioned devices. This discrepancy may be attributed to triplet-triplet annihilation. Adjustment of the synthesized compounds to further reduce the ΔE_{ST} value could enhance the effective utilization of triplet excitons, potentially leading to improved performance in green OLEDs based on TADF emitters.

3.6. Bicarbazole-Benzophenone-Based Twisted Donor-Acceptor-Donor Derivatives as Blue Emitters for Highly Efficient Fluorescent Organic Light-Emitting Diodes (Scientific Publication No. 6, Q1, 1 citation)

This chapter is based on the paper published in *Nanomaterials*, **2024**, 14, 2 by *D. Blazevicius, I. Siddiqui, P. Gautam, G. Krucaite, D. Tavgeniene, M. R. Nagar, K. Kumar, S. Banik, J.-H. Jou*, and *S. Grigalevicius* [213].

This work also included utilization of bicarbazole, as in the previous chapter, but, this time, instead of diphenyl sulfone, a benzophenone electron acceptor was used in a new series of twisted D–A–D type compounds. These derivatives were synthesised by involving a three-step procedure, similar to the one detailed in the preceding chapter. The synthetic pathway to produce novel materials is illustrated in Scheme 5.
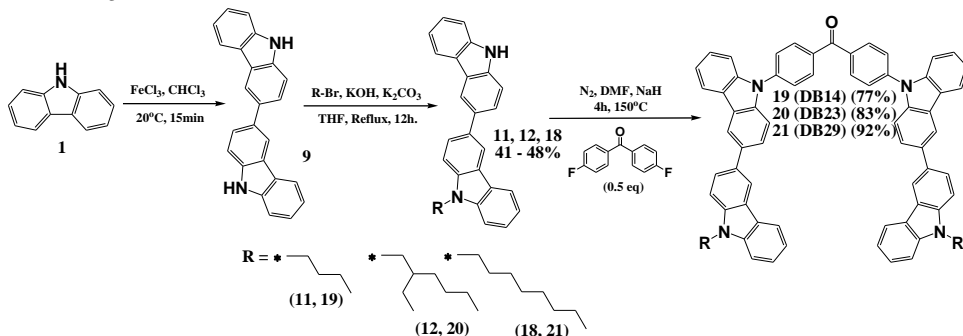
Scheme 5. Synthesis of new benzophenone-based materials

The two initial synthetic steps, involving the production of 3,3′-bicarbazole (**9**) by oxidizing 9*H*-carbazole (**1**) and the reaction of the produced 3,3'-bicarbazole with alkyl bromides, are described in the previous chapter. Finally, the partially alkylated bicarbazoles underwent similar nucleophilic aromatic substitution reactions. In this synthetic step, 9-alkyl-9'*H*-3,3′-bicarbazole (**11, 12, 18**) (1. mol. eq.) and NaH (4 mol. eq.) were stirred in dimethylformamide at room temperature under nitrogen atmosphere for 20 minutes to effectively deprotonate the amino group of bicarbazole, thus boosting its nucleophilic capabilities. Then, 4,4'-difluorobenzophenone (0.5 mol. eq.) was added to the reaction, and the resulting mixture was stirred at 150 °C under nitrogen atmosphere for 4 h. After thin-layer chromatography control, the reaction mixture was cooled and quenched by the addition of ice water. The organic portion of the mixture was isolated via chloroform extraction, and the combined extract was subsequently dried with anhydrous Na_2SO_4. The crude product underwent purification through silica gel column chromatography, while utilizing a mixture of THF and hexane as the eluent. This method reliably produced the intended bicarbazole-based compounds **19** (**DB14**), **20** (**DB23**), and **21 (DB29)**, ranging from 77% to 92% in yield, with their structures validated by MS and NMR spectroscopy.

Figure 34 shows the electron density contours of the frontier molecular orbitals for the compounds **19 (DB14)**, **20 (DB23)**, and **21 (DB29)**. As it can be seen from the illustration, all the materials exhibit a twisted structure, with the spatial separation of HOMO and LUMO indicating donor-acceptor characteristics. In these molecules, the carbazole units function as the donor units, while benzophenone acts as the acceptor.
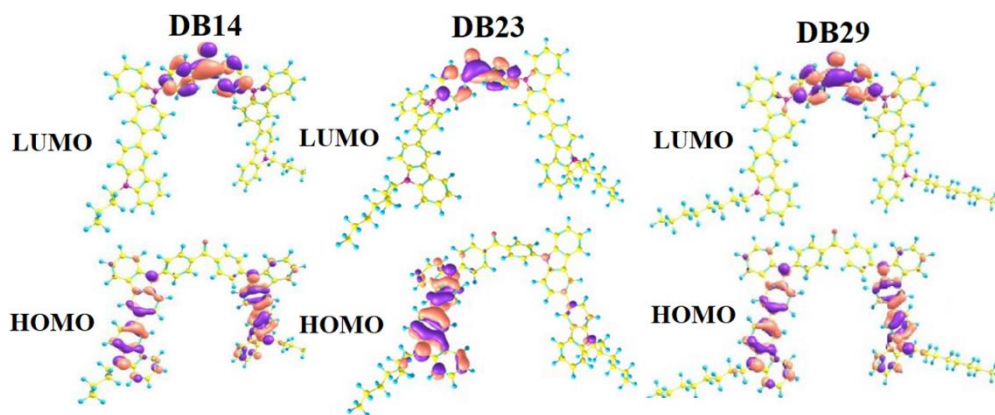
Figure 34. Electron density contours of frontier molecular orbitals of compounds **19** (**DB14**), **20** (**DB23**), and **21** (**DB29**).

The thermal stability characteristics of the materials **19** (**DB14**), **20** (**DB23**), and **21 (DB29)** were investigated under nitrogen atmosphere. The TGA curve for the derivative **19** (**DB14**) is depicted in Figure 35 (left). For **19** (**DB14**), characterized by the shortest alkyl chains, the T_d value at which 5% weight loss occurred was determined to be 462 °C. In contrast, the materials **20** (**DB23**), and **21 (DB29)**, featuring longer aliphatic substitutions, exhibited slightly lower T_d values of 383 °C and 384 °C, respectively. The DSC thermograms of the second heating scans for the compounds **19** (**DB14**), **20** (**DB23**), and **21** (**DB29**) are presented in Figure 35 (right).
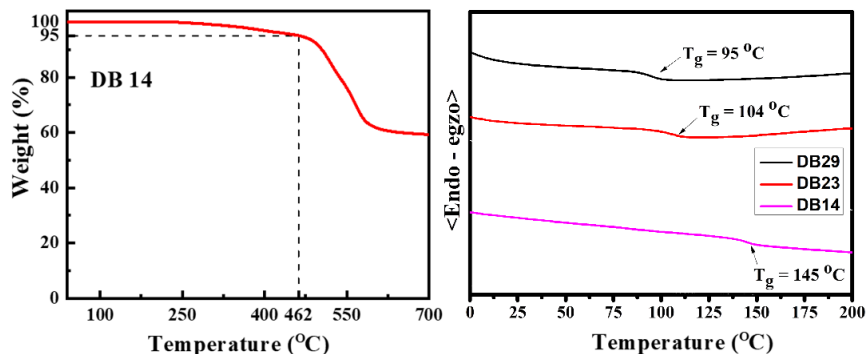
Figure 35. TGA curve of material **19** (**DB14**) (left). Curves of second DSC scans of materials **19** (**DB14**), **20** (**DB23**), and **21** (**DB29**) (right). Heating rate: 10 °C/min

By analysing the DSC curves, it becomes apparent that the novel derivatives exhibit T_g values which directly correspond to the length of their aliphatic substituents. For instance, the material **19** (**DB14**) with the shortest butyl substitution has the highest T_g of 145 °C. This trend persists for compounds featuring longer alkyl groups: the derivatives **20** (**DB23**), and **21** (**DB29**) with 2-ethylhexyl and octyl substitutions, respectively, display T_g values of 104 °C and 95 °C. Hence, these results indicate that the developed compounds demonstrate excellent thermal and morphological stability and are well-suited for use in optoelectronic devices. The values of T_d and T_g are compiled in Table 22.

The derivatives **19** (**DB14**), **20** (**DB23**), and **21 (DB29)** show high PLQY values of 55.6%, 52.0%, and 55.5%, respectively, as summarized in Table 22. The UV-absorption investigations were conducted in the THF solvent under standard conditions. Notably, all the compounds consistently exhibited primary and secondary absorption peaks at around 375 nm and 400 nm. The UV absorption wavelength and intensity were employed to construct Tauc plots for the materials, as shown in Figure 36, by using the values calculated with the above-described Equation (5) for the x-axis, and Equation (6) for the y-axis. The Tauc plots revealed the bandgaps of the investigated compounds, which are 3.05 eV for **19** (**DB14**), 3.08 eV for **20** (**DB23)**, and 3.02 eV for **21 (DB29)** (Table 12).
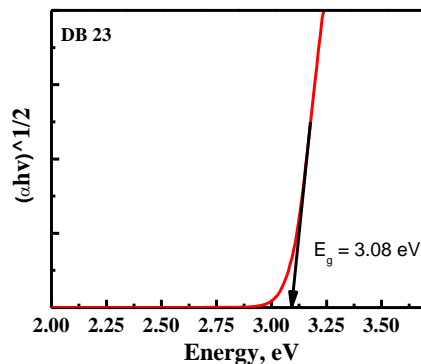
Figure 36. UV-vis absorbance spectra and Tauc plot (inset) represent the absorption wavelength and bandgap of compound **20** (**DB23)**

To determine the triplet energies of the potential emitters, their LTPL spectra were recorded. It is noteworthy that the compounds **19** (**DB14**), **20** (**DB23**), and **21 (DB29)** demonstrated heightened E_T levels of 2.83, 2.84, and 2.73 eV, respectively, as visually depicted in Figure 37. These specific characteristics are also detailed in Table 22. Additionally, in order to determine the singlet state energy values for the newly developed materials, their PL spectra were recorded at room temperature. The E_S values were calculated by determining the intercept of PL and absorbance wavelengths, thus yielding values of 3.32 eV for **19** (**DB14)**, 3.19 eV for **20** (**DB23)**, and 3.22 eV for **21 (DB29)** (refer to Table 22).
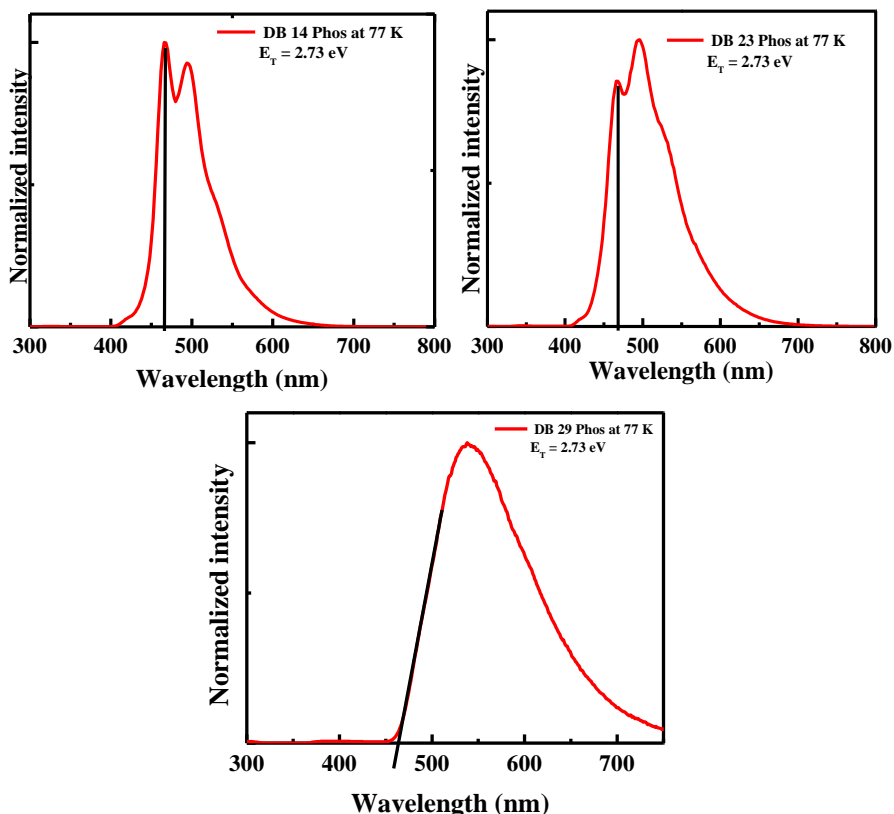
Figure 37. LTPL spectra of derivatives **19** (**DB14**), **20** (**DB23**), and **21 (DB29)** at 77 K

Figure 38 presents the results of TRPL analysis, indicating the PL decay times for the compounds **19** (**DB14**), **20** (**DB23**), and **21 (DB29)** at 3.40, 2.67, and 3.57 ns, respectively. IRF is the instrument response function, which is measured as a control parameter before and after each measurement. It is noteworthy that all the lifetime curves of the materials exhibit a nanosecond-scale component. Typically, the decay lifetime of fluorescent emitters falls within the picosecond range. However, our materials display decay at the nanoscale, thus suggesting a potential utilization of the triplet energy levels.
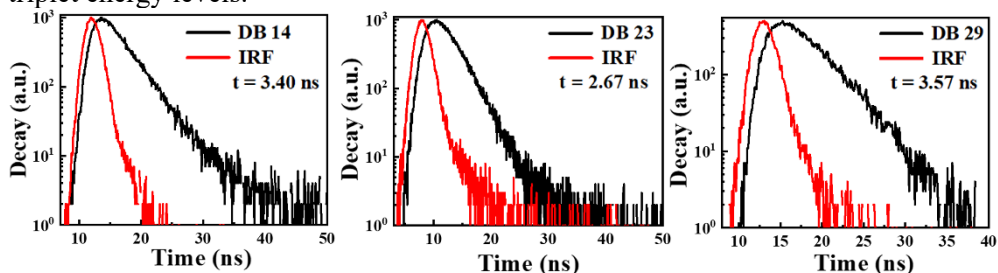
Figure 38. TRPL spectra for the transient decay of materials **19** (**DB14**), **20** (**DB23**), and **21 (DB29)**

The electrochemical characteristics of the compounds **19** (**DB14**), **20** (**DB23**), and **21 (DB29)** were evaluated through CV measurements, as illustrated in Figure 39. By utilizing the obtained oxidation onset values, the HOMO levels were calculated while using Equation (7), and the LUMO levels were determined using equation (8). The calculated HOMO levels were −5.70, −5.63, and −5.66 eV, whereas the corresponding LUMO levels were −2.65, −2.55, and −2.64 eV for the compounds **19** (**DB14**), **20** (**DB23**), and **21** (**DB29**), respectively. These values, along with the previously determined bandgap measurements, are presented in Table 22. It can be asserted that the HOMO and LUMO levels of the compounds are deemed suitable for blue-emitting layers when employing the previously mentioned CBP host material.
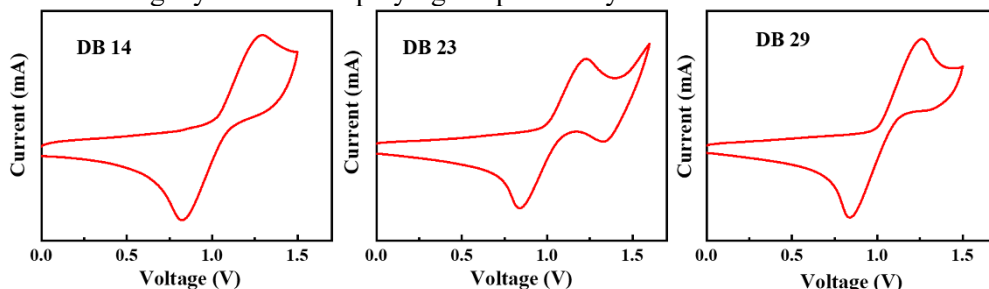
Figure 39. Curves of CV scans of molecules **19** (**DB14**), **20** (**DB23**), and **21 (DB29)**

Table 22. Optoelectronic and thermal characteristics of compounds **19** (**DB14**), **20** (**DB23**), and **21 (DB29)**

Material	T_d (°C)	T_g (°C)	E_g, eV	PLQY, %	Decay, ns	HOMO, eV	LUMO, eV	S_1, eV	T_1, eV	ΔE_{ST}, eV
19 (DB14)	462	145	3.05	55.6	3.40	-5.70	-2.65	3.32	2.83	0.49
20 (DB23)	383	104	3.08	52.0	2.67	-5.63	-2.55	3.19	2.84	0.35
21 (DB29)	384	95	3.08	55.5	3.57	-5.66	-2.64	3.22	2.73	0.49

To assess the performance of the new benzophenone-based derivatives as emitters, OLEDs were fabricated, and the schematic energy level diagram, as presented in Figure 40, outlines the configuration of the devices prepared in this study.
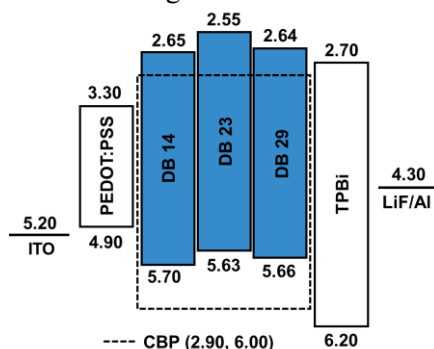
Figure 40. Energy-level diagram of OLEDs using emitters **19** (**DB14**), **20** (**DB23**), and **21 (DB29)** doped in CBP host

These devices incorporated the emitters **19** (**DB14**), **20** (**DB23)** or **21** (**DB29)** doped within a CBP host matrix. The device structure was ITO/PEDOT:PSS/host CBP : emitter **19** (**DB14**), **20** (**DB23)** or **21** (**DB29)** (5, 10, or 15 wt.%)/TPBi/LiF/Al. The EL properties of the devices utilizing the new emitting material **20** (**DB23)** dispersed within the CBP host are depicted in Figure 41.
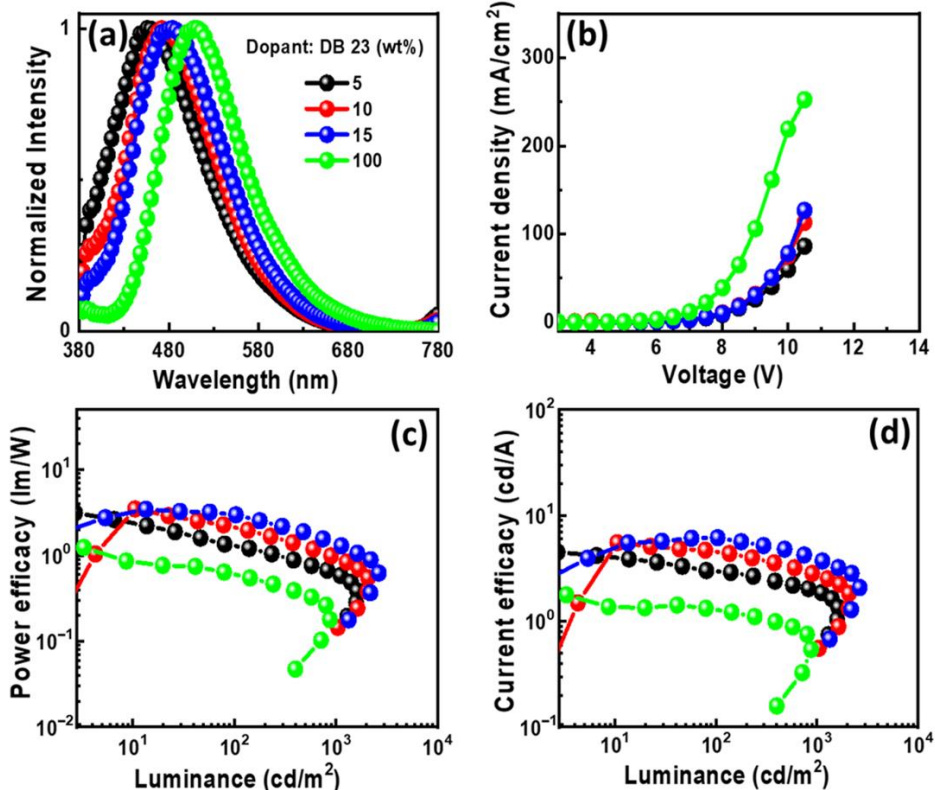
Figure 41. EL characteristics of OLEDs employing emitter **20** (**DB23)** doped in CBP host: (a) EL spectra, (b) current density–voltage, (c) power efficacy–luminance, and (d) current efficacy–luminance characteristics

The corresponding characteristics for each emitter are also presented in Table 23. Within Figure 41, various aspects are illustrated, including the (a) EL spectra, (b) current density–voltage characteristics, (c) power efficacy–luminance characteristics, and (d) current efficacy–luminance characteristics. In Figure 41 (a), the EL spectra of the devices featuring the emitter **20** (**DB23)** display single peaks at around 470 nm, indicating blue emission. The presence of these single peaks suggests the successful completion of the host-to-guest energy transfer. Notably, both doped and non-doped devices exhibit similar EL emission peaks.

Figures 41 (b–d) illustrate the current density–voltage, power efficacy–luminance, and current efficacy-luminance characteristics. Comparatively, the non-doped device shows a significantly lower efficacy than the doped devices, thus emphasizing the crucial role of the host material. The device utilizing a 15 wt% doping concentration of the emitter **20** (**DB23)** achieves a maximum PE of 3.2 lm/W, a

maximum CE of 5.3 cd/A, and an L_{max} of 2076 cd/m^2. Additionally, the device with a 10 wt% doping concentration reveals a remarkable EQE_{max} of 5.3%, surpassing even the theoretical limit for fluorescent emitters [54]. As shown in Table 23, the device based on **20 (DB23)** exhibits the highest EQE among all the devices, surpassing both the prior research and the expected outcomes of this study. This improved performance is likely due to the presence of branched alkyl side chains in the molecule, enhancing the solubility for wet-processed OLEDs and the film-forming properties of the material.

Table 23. Characteristics of devices utilizing blue, fluorescent emitters **19 (DB14)**, **20 (DB23)**, and **21 (DB29)**

Emitter	*wt*, %	V_{ON}, V	PE_{max}, lm/W	CE_{max}, cd/A	EQE_{max}, %	*CIE* (x, y) @100 cd/m^2	L_{MAX}, cd/m^2
19 (DB14)	5	5.0	3.9	6.5	2.7	(0.22, 0.36)	2951
	10	5.1	4.4	7.6	3.3	(0.21, 0.33)	3175
	15	5.9	2.4	4.9	2.4	(0.20, 0.28)	1884
	100	6.1	0.4	0.8	0.4	(0.26, 0.40)	515
20 (DB23)	5	5.7	2.1	3.8	2.3	(0.17, 0.07)	883
	10	5.2	1.7	2.6	5.3	(0.19, 0.22)	1620
	15	5.2	3.2	5.3	2.7	(0.20, 0.27)	2076
	100	5.1	1.0	1.8	0.7	(0.26, 0.44)	875
21 (DB29)	5	5.4	2.1	3.9	2.3	(0.19, 0.22)	1578
	10	5.7	4.4	6.5	3.1	(0.20, 0.27)	2251
	15	4.7	7.9	9.1	4.0	(0.21, 0.31)	2631
	100	4.8	1.4	1.8	0.7	(0.26, 0.44)	884

However, the **21 (DB29)**-based device outperformed others in terms of PE and CE with the values of 7.9 lm/W and 9.1 cd/A, respectively. This superiority can be attributed to its optimal HOMO and LUMO levels, facilitating the efficient host-to-guest energy transfer. Furthermore, the incorporation of two bicarbazole donor moieties led to a balanced charge transfer, thereby further boosting its performance.

3.7. Bicarbazole-Benzophenone Based Twisted Donor-Acceptor Derivatives as Potential Blue TADF Emitters for OLEDs (Scientific Publication No. 7, Q2, 0 citations)

This chapter is based on the paper published in *Molecules*, 2024, 29, 7 by *I. Siddiqui, P. Gautam, D. Blazevicius, J. Jayakumar, S. Lenka, D. Tavgeniene, E. Zaleckas, S.Grigalevicius*, and *J.-H. Jou* [214].

In this study, new electroactive derivatives based on an benzophenone electron acceptor and a bicarbazole electron donor were designed by simplifying the compounds discussed in the previous chapter from the D–A–D type to the D–A type twisted structures. New materials were synthesized by using a three-step process similar to that described in the previous chapters and shown in Scheme 6. Initially, 9*H*-carbazole **1** was oxidised to produce 9*H*,9′*H*-3,3′-bicarbazole (**9**). Then, we used various alkyl bromides and bases to mono-alkylate 9*H*,9′*H*-3,3′-bicarbazole (**9**) in the

THF solution, resulting in the formation of 9-alkyl-9‘*H*-3,3′-bicarbazoles (**10–12, 18, 22, 23**), as described in the previous chapters.
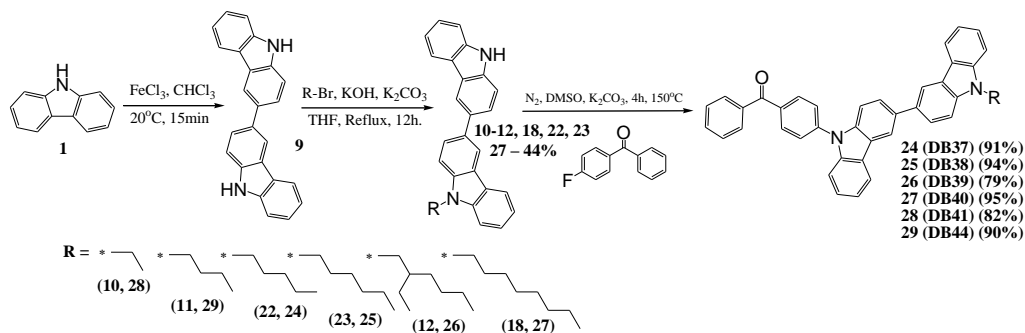
Scheme 6. Synthetic pathway of new benzophenone-bicarbazole-based materials

Finally, the target 4-(9′-alkyl-[3,3′]-bicarbazol-9-yl)benzophenones were synthesized by applying similar synthetic procedures, involving stirring 9-alkyl-9'*H*-3,3′-bicarbazole (**10–12, 18, 22, 23**) (1 mol. eq.) with 4-fluorobenzophenone (1 mol. eq.) in 10 ml of DMSO at 150 °C under inert nitrogen atmosphere with potassium carbonate (1.92 g, 13.90 mmol) present to effectively deprotonate the unsubstituted amino group of bicarbazole derivative and enhance its nucleophilic properties. After 4 h, thin-layer chromatography was used to confirm the completion of the reaction, following which, the reaction mixture was slowly quenched into ice water. The organic phase was extracted through the use of chloroform, and any remaining traces of water in the organic part were removed by drying over anhydrous Na_2SO_4, which was later removed by filtration. The desired product was purified via column silica gel chromatography by using various mixtures of THF and hexane as the mobile phase. These procedures resulted in the yellow target derivatives **24 (DB37)**, **25 (DB38)**, **26 (DB39)**, **27 (DB40)**, **28 (DB41)**, and **29 (DB44)** with yields ranging from 79% to 95%. The mass spectrometry and NMR spectroscopy confirmed the theoretically proposed chemical structures of these new electroactive compounds. The aliphatic chains which are present in the synthesized compounds increased the solubility in common organic solvents, thus offering a cost-effective method for forming thin films through spin-coating from their solutions.

The behaviour under heating of the synthesized materials **24 (DB37)**, **25 (DB38)**, **26 (DB39)**, **27 (DB40)**, **28 (DB41)**, and **29 (DB44)** was investigated by using the DSC and TGA methods, with the samples heated under inert nitrogen atmosphere at a rate of 10 °C/min. It was observed that the target compounds displayed remarkable resistance to heating with all the investigated materials demonstrating T_d values of over 370 °C. The thermograms from the DSC experiments for all the compounds **24 (DB37)**, **25 (DB38)**, **26 (DB39)**, **27 (DB40)**, **28 (DB41)**, and **29 (DB44)** are shown in Figure 42. The results clearly indicate that the T_g values are directly correlated with the length of the alkyl sidechains in the structures. For example, the material **28 (DB41)**, which contains an ethyl group, demonstrated the highest T_g of 102 °C. In contrast, the compounds **29 (DB44)** and **24 (DB37)**, substituted with butyl and pentyl groups, respectively, exhibited slightly lower T_g values of 80 °C and 77 °C. This trend

persists for materials with even longer alkyl groups: the derivatives **25 (DB38)**, **26 (DB39)**, and **27 (DB40)**, which are substituted with hexyl, 2-ethylhexyl, and octyl groups, respectively, displayed the T_g values of 68 °C, 64 °C, and 57 °C. This phenomenon could be attributed to the reduced intermolecular hydrogen bonding as the length of the alkyl chain increases [207]. Results from both TGA and DSC experiments are compiled in Table 24.
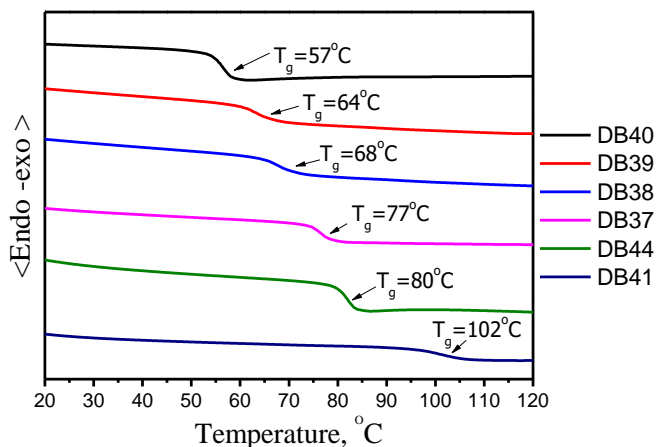
Figure 42. Curves of second DSC scans of materials **24 (DB37)**, **25** (**DB38**), **26** (**DB39**), **27 (DB40)**, **28 (DB41)**, and **29 (DB44)**. Heating rate: 10 ºC/min

The new compounds exhibit heightened PLQY levels ranging from 45.3% to 75.5%, with the values for all the materials summarized in Table 24. As an example, Figure 43 (left) displays the UV-absorption band of the compound **24 (DB37)**. All the derivatives were analysed in the THF solvent under standard conditions while using a quartz cuvette. Notably, each derivative consistently showed two absorption peaks at around 380 and 410 nm, which can be attributed to the presence of identical chromophores within their structures. The Tauc plot for the material **DB37** is shown in Figure 43 (right).
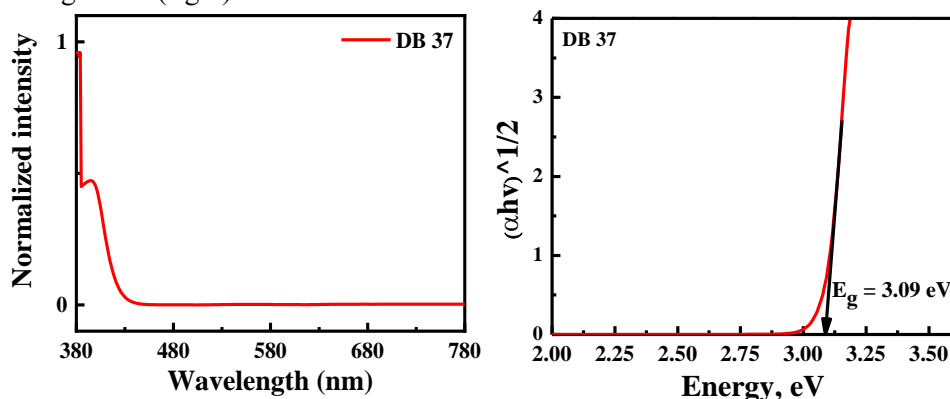
Figure 43. UV-Vis absorbance (left) spectrum and Tauc plot (right) of compound **24 (DB37)**

The Tauc plots were generated for the target compounds by using the UV absorption wavelength and intensity, with the values calculated by using Equations (5) and (6) described above for the x-axis and the y-axis, respectively. The Tauc plots revealed bandgaps for the studied derivatives ranging from 3.07 eV to 3.10 eV. Similar bandgap values were expected since all the derivatives utilize the same chromophores. The electrochemical characteristics of the new derivatives **24 (DB37)**, **25 (DB38)**, **26 (DB39)**, **27 (DB40)**, **28 (DB41)**, and **29 (DB44)** were assessed via CV measurements. The obtained oxidation onset values were utilized to calculate the HOMO levels by using Equation (7), while the determination of the LUMO levels was carried out by using Equation (8). The determined HOMO levels ranged from -5.73 to -5.67, while the LUMO levels ranged from -2.64 to -2.58. These values, along with the E_g levels, are detailed in Table 24. The HOMO and LUMO levels of the compounds were suitable for forming blue-emitting layers in conjunction with the commercial host material CBP.

In Figure 44 (left), the PL spectrum of the derivative **24 (DB37)** is depicted, showing a peak emission wavelength at approximately 510 nm, which is indicative of cyan-blue emission. The E_S values of the potential emitters were calculated by determining the crossing points of the PL and absorbance curves, resulting in the values ranging from 3.04 eV to 3.22 eV. Additionally, the LTPL spectra were recorded to determine the E_T levels with an example of such a spectrum for the material **24 (DB37)**, illustrated in Figure 44 (right). The compounds also exhibited E_T values exceeding 2.75 eV. These values of the singlet ant triplet energy levels suggest their potential suitability as blue emitters. The values of E_S and E_T for the derivatives **24 (DB37)**, **25 (DB38)**, **26 (DB39)**, **27 (DB40)**, **28 (DB41)**, and **29 (DB44)** are listed in Table 24.
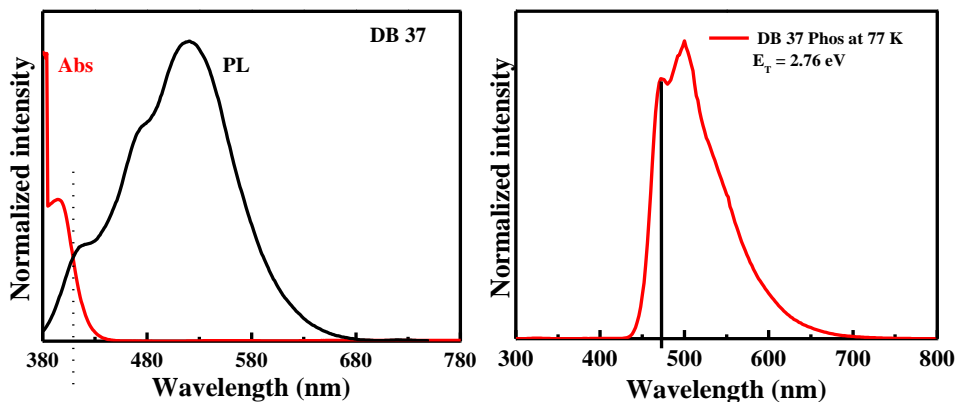
Figure 44. Photoluminescence (left) and low-temperature photoluminescence (right) spectra of material **24 (DB37)**

Figure 45 presents the outcomes of the TRPL experiments, showcasing the photoluminescence decay times for the newly developed emitters. The determined decay times for **24 (DB37)**, **25 (DB38)**, **26 (DB39)**, **27 (DB40)**, **28 (DB41)**, and **29 (DB44)** were 5.53, 1.88, 4.27, 2.41, 2.24, and 6.28 ns, respectively. Typically, the decay lifetime of pure fluorescent emitters falls within the picosecond range; however,

the materials depicted here exhibit significantly longer photoluminescence decay times, thus indicating their potential utilization of triplet excited states as emitters based on the TADF effect [215,216]. The photoluminescence decay times are outlined in Table 24. In the graphs, IRF represents the instrument response function, which was assessed both before and after each measurement as a control parameter.
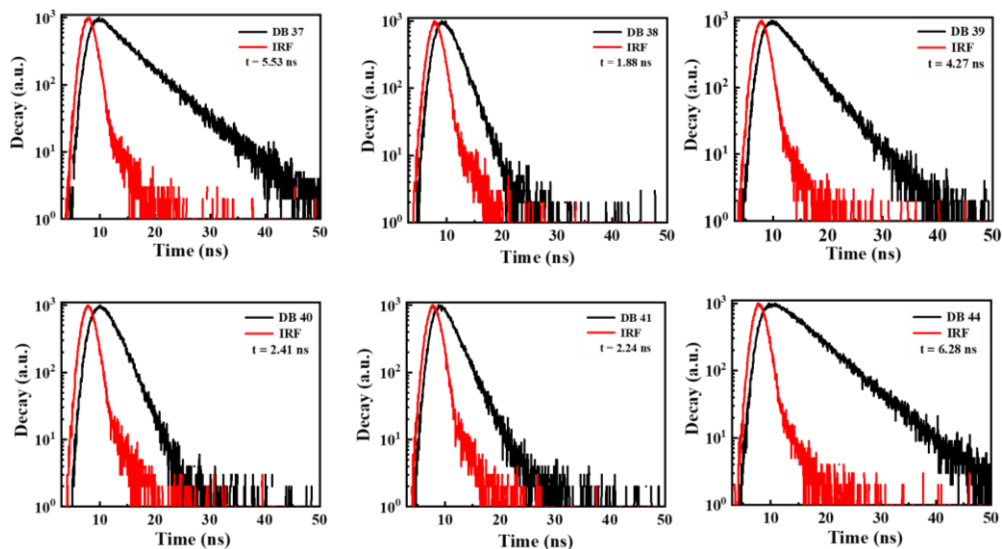
Figure 45. TRPL spectra of compounds **24 (DB37)**, **25** (**DB38**), **26** (**DB39**), **27** (**DB40**), **28** (**DB41**), and **29** (**DB44**)

Table 24. Optoelectronic and thermal characteristics of compounds **24 (DB37)**, **25** (**DB38**), **26** (**DB39**), **27** (**DB40**), **28** (**DB41**), and **29** (**DB44**)

Emitter	T_d (ºC)	T_g (ºC)	E_g, eV	Φ, %	Decay, ns	HOMO, eV	LUMO, eV	E_S, eV	E_T, eV	ΔE_{ST}, eV
24 (DB37)	406	77	3.09	65.5	5.53	-5.67	-2.58	3.04	2.76	0.28
25 (DB38)	398	68	3.09	45.3	1.88	-5.70	-2.61	2.94	2.89	0.05
26 (DB39)	383	64	3.08	75.5	4.27	-5.68	-2.60	3.10	2.81	0.29
27 (DB40)	397	57	3.10	52.5	2.41	-5.69	-2.59	3.06	2.80	0.26
28 (DB41)	374	102	3.09	62.5	2.24	-5.73	-2.64	3.22	2.80	0.42
29 (DB44)	389	80	3.07	68.5	6.28	-5.69	-2.62	3.18	2.82	0.15

Considering the properties of the new benzophenone-based derivatives, it was decided to assess their performance as emitters in solution-processed OLEDs with a simple device structure, as depicted in the energy level diagram shown in Figure 46. These OLED devices incorporate the emitters **24 (DB37)**, **25** (**DB38**), **26** (**DB39**), **27** (**DB40**), **28** (**DB41**), and **29 (DB44)** doped into a CBP host material. The basic device

structures comprise a 125 nm ITO anode layer, followed by a 35 nm PEDOT:PSS hole injection layer, and then a 30 nm emissive layer consisting of a CBP host with dopants (at concentrations of 5%, 10%, 15%, and 100% by weight). For the electron transporting layer, TPBi (32 nm) was used, while lithium fluoride (0.8 nm) served as the electron injecting layer, and aluminium (150 nm) was employed as the cathode.
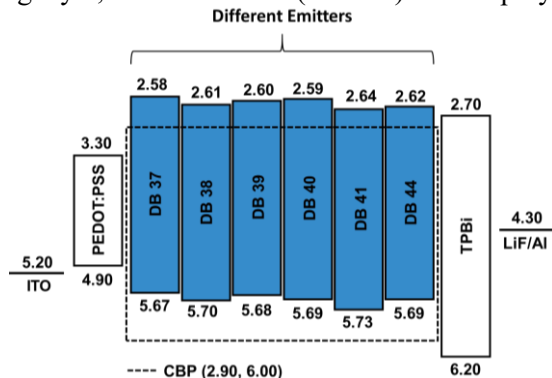
Figure 46. Energy-level diagram illustrating OLEDs incorporating emitters **24 (DB37)**, **25** (**DB38)**, **26** (**DB39)**, **27** (**DB40)**, **28** (**DB41)**, and **29** (**DB44)** doped within the CBP host

Figure 47 visually depicts the EL characteristics of the devices utilizing the most efficient emitter in this study, specifically, **26** (**DB39)**.
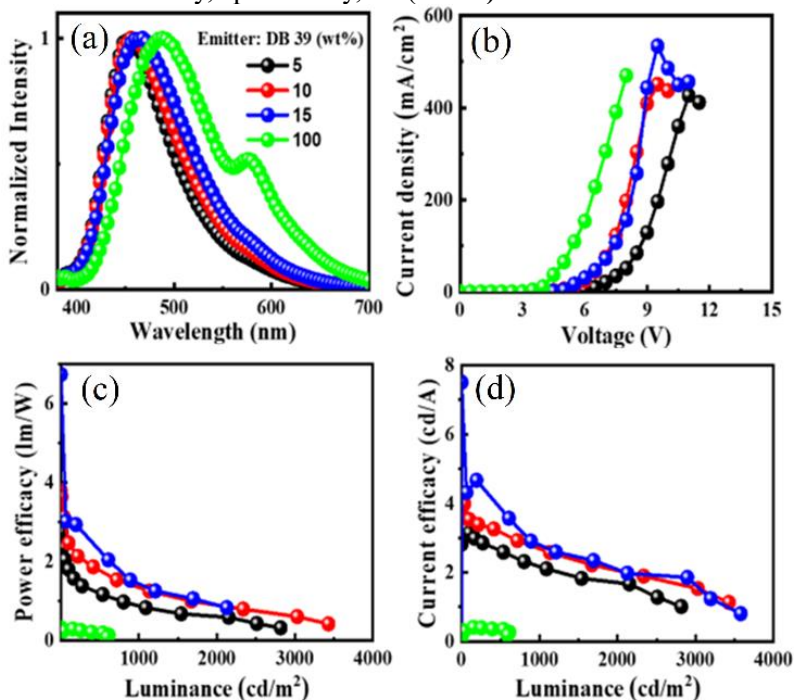
Figure 47. EL properties of the device utilizing emitter **26** (**DB39)**: EL spectra (a), current density-voltage (b), power efficiency-luminance (c), and current efficiency-luminance (d) characteristics

Due to their solubility, all the newly synthesized compounds were suitable for layer preparation via spin-coating. Concentration-dependent experiments were conducted for all the new emissive materials, with proportions ranging from 5 to 100 wt% of each guest in the emissive layer. Figure 47 illustrates the EL spectra of the devices, as well as the current density-voltage and power efficacy-luminance-current efficacy characteristics. The EL properties, including PE, CE, EQE, L_{MAX}, and the CIE colour space coordinates of the devices utilizing the most efficient emitter in this group of materials, specifically, **26 (DB39)**, distributed within the CBP host, are summarized in Table 25.

Table 25. Characteristics of devices utilizing blue emitter **26 (DB39)**

Emitter	wt, %	V_{ON}, V	PE_{max}, lm/W	CE_{max}, cd/A	EQE_{max}, %	CIE (x, y) @100 cd/m^2	L_{MAX}, cd/m^2
26 (DB39)	5	4.0	3.3	3.7	2.1	(0.18, 0.20)	2818
	10	3.5	4.4	4.9	2.2	(0.18, 0.23)	3430
	15	3.9	4.1	5.7	2.7	(0.19, 0.27)	3581
	100	3.4	0.3	0.4	0.4	(0.24, 0.39)	615

In Figure 47(a), the EL spectra of the devices utilizing the **26 (DB39)** dopant reveal peaks within the 460–490 nm range, which is indicative of blue emission. The absence of additional peaks suggests an effective energy transfer from the host to the guest. Figure 47(b)–(d) illustrates the characteristics of the current density as well as the PE and CE dependence on luminance. The undoped device demonstrates a higher current density than the doped devices and a lower efficiency than the doped devices, thereby underscoring the significant influence of the host material. OLEDs based on the emitter **26 (DB39)** exhibit the best efficiencies among all these devices. This enhanced performance can be attributed to the inclusion of the elongated and branched 2-ethylhexyl sidechain in the molecule, potentially improving the solubility to produce wet-processed OLEDs and also contributing to the favourable film-forming characteristics of the derivative [217]. Moreover, the appropriate HOMO and LUMO levels facilitate the effective energy transfer from the host to the dopant, while the combination of the electron-accepting benzophenone fragment with the bicarbazole donor moiety promotes a balanced charge transfer and the efficient utilization of the excitons [218,219]. Specifically, the device containing 10 wt% of the emitter **26 (DB39)** demonstrates the highest PE of 4.4 lm/W, with L_{MAX} reaching 3430 cd/m^2. However, the overall best efficiency is achieved by the device incorporating 15 wt% of the emitter **26 (DB39)** in its emissive layer, and attaining the PE and CE values of 4.1 lm/W and 5.7 cd/A, respectively, while its EQE reached 2.7% with an L_{MAX} of 3581 cd/m^2. The findings of this study indicate the potential of benzophenone and bicarbazole fragments in the synthesis of organic semiconductors and demonstrate how thermal and film-forming properties could be controlled by introducing and modifying alkyl chains within the molecular structure of new compounds.

4. CONCLUSIONS

In summary, the research outcomes presented in this study reveal potential pathways for advancing the OLED technology. Specifically, this work introduces novel material designs applicable to efficient OLEDs, serving as both hosts and emitters, in particular:

1. Oxetane, carbazole and methoxypyridine fragments having materials have been synthesized and characterized. The new materials have been proven to be effective host materials with the top-performing blue device achieving a high external quantum efficiency of 10.3%, and the most efficient green PhOLED showcasing a high external quantum efficiency of 9.4%.

2. Carbazole- or phenoxazine-substituted low molecular weight oxetanes have been synthesized via a simple one-step procedure. The investigation of the materials has revealed that they are suitable to be used as hosts for yellow PhOLEDs, with the most efficient PhOLED exhibiting an external quantum efficiency of 10.9%.

3. A previously synthesized phenoxazine-oxetane derivative was proven to be an effective host material for candlelight OLEDs, with the target device exhibiting an external quantum efficiency of 10.2%, which is much higher than the CBP-based device. The OLED under investigation also exhibited a very low colour temperature of 1690K and a record-breaking maximum permissible exposure limit of 57,696s.

4. By reviewing the recent progress in electroactive benzophenone derivatives, the high potential of the benzophenone fragment in designing efficient host materials and emitters for OLEDs has been proven.

5. Bicarbazole-diphenyl sulfone-based twisted donor-acceptor-donor derivatives have been synthesized and characterized. The high potential of these novel compounds as bi-functional materials was proven by firstly utilizing them as deep-blue emitters, resulting in a device exhibiting an external quantum efficiency of 4.0%. Secondly, the new materials were applied as hosts for green phosphorescent and TADF emitters, resulting in devices demonstrating external quantum efficiencies of 10.6% and 10.8%, respectively.

6. A group of twisted donor-acceptor-donor derivatives, featuring bicarbazole as the electron donor and benzophenone as the electron acceptor, have been synthesized and investigated. It was established that the new materials are highly efficient blue fluorescent emitters, with the most efficient device in this study achieving an external quantum efficiency of 5.3%, and thus challenging the theoretical limit for blue fluorescent devices.

7. A series of electroactive bipolar donor-acceptor type derivatives, utilizing benzophenone and bicarbazole as the main fragments, have been designed, synthesized, and characterized. It has been determined that the new derivatives possess suitable properties to be used as blue fluorescent emitters in OLEDs, with the most efficient device achieving an external quantum efficiency of 2.7%.

Overall, these results have proven the significant potential of phenoxazine- and carbazole-based materials in the manufacturing of OLEDs. This study included promising host materials for PhOLEDs, some of which were synthesized via a cost-effective one-step procedure, thus paving the way for scalable production of the host

materials for yellow and candlelight OLEDs. Additionally, bicarbazole derivatives showed great promise as both blue fluorescent emitters and host materials for green OLEDs. The research also highlighted the crucial role of aliphatic side chains in optimizing the film-forming properties and solubility. However, the efficiency of OLEDs could be further improved by optimizing the device structure and the thicknesses of layers, as well as by reducing ΔE_{ST} for bicarbazole-based compounds through structural modifications to utilize triplet excitons more efficiently.

5. SANTRAUKA

5.1. Įvadas

Nuo pat 1880 m., kai T. Edisonas patentavo kaitinamąją lemputę, siekis sukurti efektyvesnius, įvairioms sritims pritaikomus ir vizualiai patrauklius apšvietimo sprendimus tapo viena svarbiausių nuolatinių inovacijų varomųjų jėgų. Tokie veiksniai, kaip gyventojų skaičiaus augimas, urbanizacija, industrializacija ir platus elektros prietaisų ir technologijų paplitimas lėmė žymų globalaus elektros energijos suvartojimo padidėjimą. Tarptautinės energetikos agentūros duomenimis, pasaulinis elektros energijos vartojimo mastas nuolat didėja, vidutiniškai išaugdamas apie 2 % kasmet per pastarąjį dešimtmetį, dabar siekiantis apie 25 000 teravatvalandžių per metus [1], iš kurių apie 19 % skiriama dirbtiniam apšvietimui [2]. Susirūpinimas dėl ribotų energijos išteklių, poveikio aplinkai ir besitęsiančio energijos suvartojimo bei jos kainų didėjimo [3] pabrėžė būtinumą kurti energiškai efektyvius apšvietimo sprendimus įvairioms pritaikymo sritims, pavyzdžiui, ekranams ir kasdieniniams apšvietimo prietaisams. Organiniai šviestukai (OLED) iškilo kaip potenciali alternatyva po to, kai C. W. Tangas su kolega publikavo savo novatorišką darbą apie organinius šviestukus 1986 m. [4]. OLED technologijos sužavėjo tyrėjus, inžinierius ir vartotojus savo įspūdingu potencialu. Toks didelis susidomėjimas leido šią sritį transformuoti iš paprasto laboratorinio smalsumo į milijardus dolerių siekiančią verslo rinką [5]. OLED prietaisai, kurie naudoja organinius junginius, skleidžiančius šviesą esant elektros srovei, siūlo daug pranašumų, lyginant su tradiciniais šviesos šaltiniais, tokiais kaip kaitinamosios ar fluorescencinės lempos, įskaitant didesnį ryškumą, platesnį žiūrėjimo kampą, energijos efektyvumą, kontrastą, prietaisų plonumą ir lankstumą. Be to, OLED prietaisus galima formuoti naudojant ekonomiškus liejimo ar spausdinimo iš tirpalų procesus, kurie galėtų prisidėti prie šiltnamio efektą sukeliančių išmetamųjų dujų kiekio ir bendro poveikio aplinkai mažinimo.

Per pastarąjį dešimtmetį tiek mokslo bendruomenė, tiek pramonė skyrė daug savo išteklių didelio efektyvumo, ilgaamžių OLED prietaisų plėtrai. Nepaisant neįtikėtinų pasiekimų, kaip daugiau nei 30 % siekiantis išorinis kvantinis efektyvumas (EQE) [6–8] ir 100 lm/W viršijantis energinis efektyvumas (PE) [9–11], vis dar yra iššūkių, kuriuos reikia įveikti, pavyzdžiui, kuriant didelio efektyvumo, ilgaamžius giliai mėlyną šviesą skleidžiančius OLED [12]. Taip pat tauriųjų metalų naudojimas fosforescuojančiose medžiagose kelia susirūpinimą dėl ateities prietaisų kainų bei jų gamybos ir utilizavimo poveikio aplinkai [13,14]. Viena didesnių egzistuojančių problemų – smarkus prietaisų efektyvumo mažėjimas, didėjant skaičiui dėl tripletinių būsenų anihiliacijos, sukelto dėl per didelės spinduolio koncentracijos ar sužadintųjų būvių tarpusavio sąveikos. Šie emisijos gesinimo procesai ypač suaktyvėja ilgėjant eksitonų gyvavimo trukmei fosforescuojančiuose (PhOLED) [15–18] ir termiškai aktyvuotosios uždelstosios fluorescencijos efektu (TADF) pasižyminčiuose OLED prietaisuose [19–21]. Norint įveikti kai kurias minėtų problemų, spinduoliai dažnai disperguojami matricose. Naujų OLED medžiagų, skirtų matricoms ir spinduoliams, kūrimas ir sintezė išlieka ypač svarbūs tolesnio šios technologijos vystymosi uždaviniai.

Darbo tikslas – susintetinti naujus karbazolo ar fenoksazino junginius, ištirti jų savybes ir pritaikyti organinių šviestukų emisinių sluoksnių matricoms ar spinduoliams.

Darbo tikslui pasiekti išsikelti šie uždaviniai:

1. Susintetinti ir ištirti mažamolekulių piridinil-karbazolilo bei oksetano fragmentus turinčius junginius, pritaikyti juos fosforescuojančių organinių šviestukų matricoms.

2. Susintetinti ir ištirti mažamolekulius karbazolo arba fenoksazino junginius, turinčius centrinį oksetano fragmentą. Gautas medžiagas pritaikyti fosforescuojančių organinių šviestukų matricoms.

3. Sukurti žmogui ir aplinkai draugišką žemos skleidžiamos šviesos spalvinės temperatūros, žvakės šviesą skleidžiantį organinį šviestuką, pasitelkiant naujai susintetintą fosforescuojančių spinduolių matricą su fenoksazino fragmentais.

4. Išsamiai apžvelgti benzfenono junginių sintezę, termines, elektrochemines ir fotofizikines savybes. Išnagrinėti ir apibendrinti apžvelgtų junginių potencialą, pritaikant juos kaip organinių šviestukų matricas ar spinduolius.

5. Susintetinti naujus bifunkcius susuktos struktūros bikarbazolildifenilsulfono junginius, ištirti jų savybes ir pritaikyti gilią mėlyną šviesą skleidžiantiems spinduoliams bei žalią šviesą skleidžiančių organinių šviestukų matricoms.

6. Susintetinti ir charakterizuoti susuktos donoro–akceptoriaus–donoro struktūros tipo junginių seriją, turinčių bikarbazolilo elektronų donorą bei benzfenono elektronų akceptorių ir juos išbandyti mėlyną šviesą skleidžiančiais spinduoliais organiniuose šviestukuose.

7. Susintetinti ir ištirti naujus donoro–akceptoriaus tipo junginius, turinčius bikarbazolilo ir benzfenono fragmentus, ir pritaikyti mėlyną šviesą skleidžiančių organinių šviestukų spinduoliams.

Darbo mokslinis naujumas ir ryšys tarp publikacijų

OLED technologijos įprastai skirstomos į tris kartas: 1-osios kartos prietaisai naudoja fluorescuojančius spinduolius, 2-oji karta pasitelkia fosforescuojančius spinduolius, o 3-ioji karta – TADF efektu pasižyminčius spinduolius. Pirmosios kartos fluorescenciniai OLED, esant elektriniam sužadinimui, pasiekia 25 % vidinį kvantinį efektyvumą (IQE), naudodami tik singuletinius emisinius eksitonus [22, 23]. Fosforescuojantys ir TADF spinduoliai turi galimybę pasiekti iki 100 % IQE sėkmingai išnaudodami tripletinius eksitonus emisijos procesui. Fosforescuojantys spinduoliai tai pasiekia naudodami interkombinacinę konversiją iš singuletinės būsenos į tripletinę [24, 25], o TADF spinduoliai, atgalinės interkombinacinės konversijos metu tripletinius eksitonus, naudodami aplinkos šilumą, verčia šiek tiek aukštesnės energijos, fotonus generuojančiais singuletiniais eksitonais [26–32]. Nepaisant to, emisijos pikams slenkant link giliai mėlynos šviesos spalvos srities, nespindulinė fosforescuojančių spinduolių d orbitalių rekombinacija yra linkusi didėti [23, 33–35], o sprendžiant šią problemą, mažamolekulės fluorescuojančios medžiagos plėtojamos dėl jų aukšto skleidžiamos šviesos spalvos grynumo ir žemos kainos [36]. Fosforescuojantys ir TADF emiteriai, siekiant išvengti koncentracinio emisijos

gesinimo, tripletų–tripletų ir singuletų–tripletų anihiliacijos, dažnai disperguojami tinkamose matricose. Šiame darbe medžiagos, paskelbtos disertacijos straipsniuose, tiesiogiai prisideda prie pirmiau išvardytų problemų sprendimo ir padidina visų trijų OLED kartų vertę – dariniai naudojami kaip gilią mėlyną ir mėlyną šviesą skleidžiantys fluorescuojantys spinduoliai arba medžiagos matricos, pritaikytos fosforescuojantiems arba TADF spinduoliams.

Pirmoje publikacijoje aprašoma naujų piridinilkarbazolilo fragmentus turinčių junginių sintezė, savybių tyrimas ir pritaikymas mėlyną ar žalią šviesą skleidžiančiuose PhOLED prietaisuose. Efektyviausias mėlyną šviesą skleidžiantis prietaisas demonstravo aukštą EQE, siekiantį 10,3 %. Efektyviausias žalią šviesą skleidžiantis prototipas pasiekė 9,4 % EQE, esant aukštam 1000 cd/m^2 skaičiui.

Antrojoje publikacijoje buvo pristatyti supaprastintos struktūros, lyginant su pirmąja publikacija, junginių sintezė ir charakterizavimas. Nauji karbazolo ir fenoksazino dariniai išbandyti kaip matricos geltoną šviesą skleidžiančiuose fosforescuojančiuose šviestukuose. Paprastesnė matricos cheminė struktūra nesumažino efektyvumo, o geriausias savybes turėjusio prietaiso EQE buvo 10,9 %.

Trečiajame moksliniame straipsnyje tyrinėtas antrojoje publikacijoje aprašyto fenoksazino junginio pritaikymas žemos skleidžiamos šviesos spalvinės temperatūros organiniuose šviesos dioduose. Gautasis žvakės šviesą skleidžiantis organinis šviesos diodas pasižymėjo rekordine didžiausiąja leidžiamąja poveikio riba naktį, siekiančia 57 700 s. Be to, prietaisas parodė 1690 K siekiančią skleidžiamos šviesos spalvinę temperatūrą, kuri buvo kur kas žemesnė už komercinių apšvietimo prietaisų skleidžiamos šviesos spalvinę temperatūrą. Naujasis OLED pademonstravo EQE, siekiantį 10,2 %, o ši vertė gerokai viršijo prietaiso, naudojančio komercinę matricą 4,4′-di(N-karbazolil)-1,1′-bifenilą (CBP), efektyvumą.

Ketvirtojoje publikacijoje apžvelgtas benzfenono junginių pritaikymas organiniams šviesos diodams, o šis literatūros tyrimas padėjo sukurti molekules, aprašytas vėlesniuose straipsniuose.

Penktajame straipsnyje karbazolo fragmentai naudojami kiek kitaip nei pirmuose dviejuose straipsniuose. Čia karbazolas buvo panaudotas bikarbazolilo fragmento forma, jį derinant su difenilsulfono elektronų akceptoriumi, siekiant išgauti naujas daugiafunkces medžiagas. Maksimalus prietaisų EQE buvo 4,0 %, kai nauji dariniai buvo naudojami giliai mėlynos šviesos spinduoliais, o tai yra labai arti teorinio fluorescuojančių šviesos diodų efektyvumo limito. Panaudojus naujas medžiagas kaip matricas žaliai fosforescuojančiam iridžio spinduoliui, buvo pasiektas maksimalus 45 lm/W PE. Be to, naujos medžiagos buvo naudojamos kaip žalios spalvos šviesą skleidžiančio TADF spinduolio matricos, o suformuoti prietaisai parodė EQE, siekiantį 11%.

Šeštojoje publikacijoje taip pat buvo aprašyti bikarbazolilo dariniai, bet difenilsulfono fragmentas pakeistas benzfenonu, taip sukurta nauja serija susuktos struktūros D-A-D tipo darinių. Efektyviausias OLED šiame tyrime parodė 5,3 % EQE, glaudžiai atitinkantį teorinį efektyvumo limitą, galimą pirmosios kartos prietaisuose.

Septintajame moksliniame straipsnyje analizuojamas šeštosios publikacijos darinių supaprastinimas į susuktos struktūros D-A tipo junginius, pasitelkiant

bikarbazolilą ir benzfenoną kaip pagrindinius molekulių komponentus. Visi junginiai buvo įvertinti kaip potencialūs mėlyną šviesą skleidžiantys spinduoliai iš tirpalų formuojamiems prietaisams. Perspektyviausias OLED, aprašytas šioje publikacijoje, pasiekė maksimalų 2,7 % EQE.

5.2. Paskelbtų mokslinių straipsnių apžvalga

5.2.1. Piridinil-karbazolilo fragmentus turinčios medžiagos efektyvių žalią ir mėlyną šviesą skleidžiančių fosforescuojančių OLED matricoms

Šis skyrius parengtas pagal straipsnį, paskelbtą žurnale *Molecules*, **2021**, 26, 15, *D. Blazevicius, D. Tavgeniene, S. Sutkuviene, E. Zaleckas, M.-R. Jiang, S. S. Swayamprabha, R. A. K. Yadav, J.-H. Jou* and *S. Grigalevicius* [136].

Šios studijos metu tikslinės medžiagos **4 (H1)** ir **5 (H2)** buvo susintetintos trijų stadijų procedūros metu, kaip pavaizduota 7 schemoje. Iš pradžių, 3-jod-9*H*-karbazolas (**2**) buvo pagamintas Tucker jodinimo procedūros [137] metu, naudojant 9*H*-karbazolą (**1**) kaip pradinį reagentą. Kita tarpinė medžiaga – 3,3-di(3-jod-9-karbazolilmetil)oksetanas (**3**) – buvo susintetinta reaguojant 3,3-di(chlormetil)ok-setanui su jodo atomus turinčio darinio 2 pertekliumi, kaip aprašyta anksčiau [138]. Galutinis darinys **4 (H1)** buvo gautas Suzuki reakcijos metu [139], kurioje dalyvavo dijodjunginys 3 ir 2-metoksi-3-piridinilborono rūgšties perteklius. Tikslinis junginys **5 (H2)** taip pat buvo susintetintas Suzuki reakcijos metu reaguojant medžiagai 3 su 6-metoksi-3-piridinilborono rūgšties pertekliumi. Visos susintetintų darinių struktūros buvo patvirtintos naudojant masių spektrometriją (MS), taip pat ^{1}H ir ^{13}C branduolinio magnetinio rezonanso (BMR) spektroskopiją, o gautieji eksperimentiniai duomenys gerai sutapo su sudarytomis tikslinių darinių struktūromis.
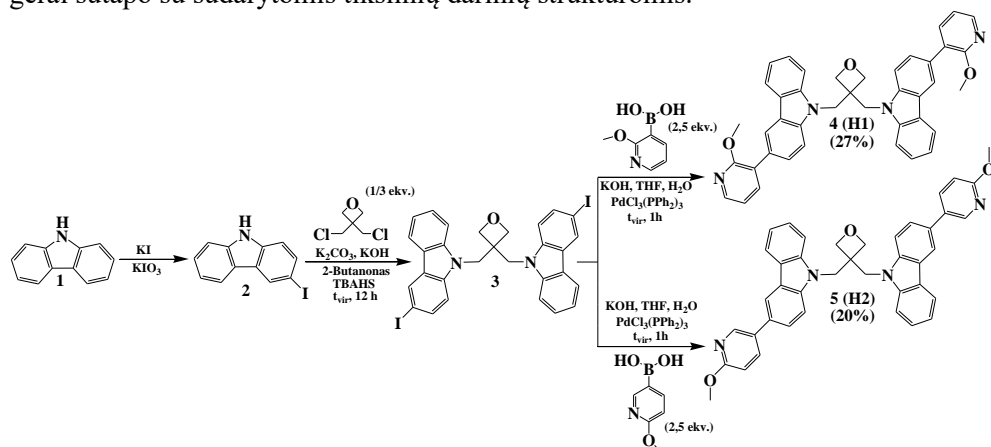
7 schema. Naujų piridinil-karbazolilo darinių **4 (H1)** ir **5 (H2)** sintezė

Naujai susintetintos medžiagos pasižymėjo ypač geru tirpumu įprastuose organiniuose tirpikliuose. Nors šių junginių plonus elektroaktyvius sluoksnius galima formuoti vakuuminio išgarinimo būdu, geras darinių tirpumas leidžia tokius sluoksnius pagaminti ekonomiškesniu liejimo iš tirpalų būdu. Terminės medžiagų **4 (H1)** ir **5 (H2)** charakteristikos buvo tyrinėtos diferencinės skenuojamosios

kalorimetrijos (DSK) ir termogravimetrinės analizės (TGA) metodais, kaitinant bandinius 10 ºC/min greičiu azoto aplinkoje. Temperatūra, kurioje patiriami medžiagų **4 (H1)** ir **5 (H2)** 5 % masės nuostoliai (destrukcijos temperatūra T_d), siekė atitinkamai 386 °C ir 361 °C, kaip parodė TGA eksperimentai. DSK matavimai parodė, kad nors medžiaga **4 (H1)** po sintezės buvo gauta kaip kristalinis darinys su 257 °C siekiančia lydymosi temperatūra (T_m), bet išlydytą bandinį atšaldžius gaunama amorfinio būvio medžiaga su aukšta stiklėjimo temperatūra T_g, siekiančia 127 °C. Kita vertus, junginys **5 (H2)** jau po sintezės buvo gautas kaip amorfinė medžiaga, kurios bandinį kaitinant DSK eksperimentų metu buvo fiksuojamas tik medžiagos stiklėjimas maždaug 139 °C temperatūroje, kaip pavaizduota 48 pav. Terminės abiejų medžiagų charakteristikos apibendrintos 26 lentelėje.
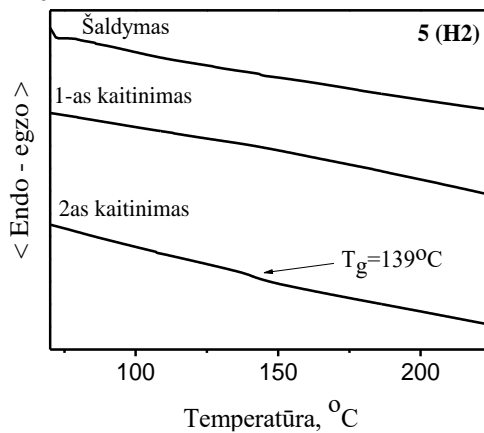
48 pav. Junginio **5** (**H2)** DSK kreivės

Žemos temperatūros fotoliuminescencijos (LTPL) spektrai, užrašyti 77 K temperatūroje, buvo skirti junginių **4 (H1)** ir **5 (H2)** tripletinės būsenos energijai nustatyti, kuri siekė atitinkamai 2,82 eV ir 2,81 eV. Šios vertės buvo didesnės nei mėlyną šviesą skleidžiančio spinduolio FIrpic (E_T = 2,65 eV) [140] ir žalią šviesą skleidžiančio spinduolio Ir(ppy)$_3$ (E_T = 2,59 eV) tripletinės būsenos energijos vertės [141]. Savybių tyrimų rezultatai patvirtino medžiagų **H1** ir **H2** tinkamumą naudoti kaip matricas tiek žaliai, tiek mėlynai fosforescuojantiems OLED prietaisams. Išmatuotos naujai susintetintų medžiagų savybės apibendrintos 26 lentelėje.

26 lentelė. Terminės ir fotofizikinės naujų medžiagų savybės

Medžiaga	T_d (ºC)	T_m (ºC)	T_g (ºC)	E_T (eV)
4 (H1)	386	257	127	2,82
5 (H2)	361	–	139	2,81

Norint įvertinti darinių **4 (H1)** ir **5 (H2)** tinkamumą naudoti kaip matricas, naudojant mėlyną šviesą skleidžiantį FIrpic ir žalią šviesą skleidžiantį Ir(ppy)$_3$ fosforescuojančius spinduolius, buvo pagaminti PhOLED prototipai. Prietaisų, naudojančių **4 (H1)** matricą elektroliuminescencijos (EL) spektrai, užfiksuoti esant 1000 cd/m^2 skaičiui, pavaizduoti 49 pav. Kaip parodyta, abiejų OLED EL spektrai demonstruoja gryną FIrpic arba Ir(ppy)$_3$ spinduolių emisiją, o tai rodo efektyvų energijos perdavimą tarp matricos **4 (H1)** ir atitinkamų spinduolių [142]. Pažymėtina,

kad nebuvo pastebėta jokių papildomų emisijos zonų, o tai reiškia, kad krūvininkų rekombinacija vyksta tik emisiniame sluoksnyje. Tai rodo, kad OLED struktūrose išvengiama eksitonų difuzijos į skyles arba elektronus pernešančius sluoksnius [143].
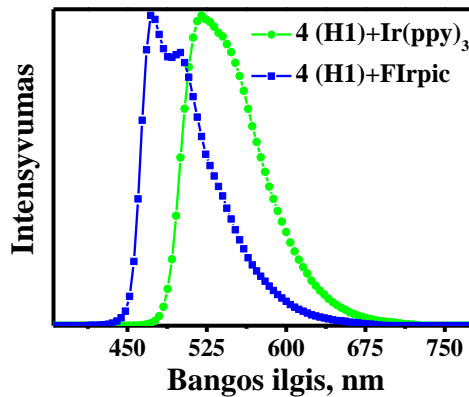
49 pav. OLED prietaisų, naudojančių matricą **4 (H1)** su mėlynos šviesos FIrpic ar žalios šviesos Ir(ppy)$_3$ spinduoliais, EL spektrai

Medžiaga **5** (**H2)** taip pat buvo naudojama mėlyną ir žalią šviesą skleidžiančiuose OLED kaip matrica, kuriuose buvo naudojami jau minėti spinduoliai, o gautų prietaisų efektyvumas buvo didesnis nei prietaisų, kurių matrica buvo medžiaga **4 (H1)**. Siekiant optimizuoti emisinio sluoksnio struktūrą, buvo naudojami spinduolių koncentracijos emisiniame sluoksnyje eksperimentai, kurių metu FIrpic koncentracija buvo keičiama nuo 15 iki 22,5 masės % (m%), o Ir(ppy)$_3$ spinduolio koncentracija svyravo nuo 7,5 iki 15 m%. 27 lentelėje pateikiamos suformuotų PhOLED su matrica **5** (**H2)** charakteristikos.

17 lentelė. PhOLED prototipų, turinčių medžiagos **5** (**H2)** matricą bei FIrpic ar Ir(ppy)$_3$ spinduolius, charakteristikos

Matrica	Spinduolis	m%	*PE*, lm/W	*CE*, cd/A	*EQE*, %	L_{maks}, cd/m^2
			Esant 100 / 1000 cd/m^2			
5 (**H2)**	FIrpic	**15,0**	**24,9 / 15,8**	**23,9 / 18,4**	**10,3 / 8,0**	**9173**
		17,5	11,5 / 6,60	12,1 / 9,80	5,1 / 4,1	3317
		20,0	8,50 / 5,70	8,60 / 8,00	3,6 / 3,4	4377
		22,5	5,90 / 11,5	5,70 / 13,1	2,4 / 5,5	10350
	Ir(ppy)$_3$	7,50	0,80 / 19,4	0,90 / 24,5	0,3 / 6,8	32390
		10,0	10,0 / 34,1	10,3 / 33,9	3,3 / 9,4	38980
		12,5	**18,9 / 26,2**	**20,6 / 34,0**	**5,7 / 9,5**	**14170**
		15,0	10,9 / 34,1	10,3 / 33,9	2,3 / 7,4	18980

OLED su 15 m% spinduolio FIrpic emisiniame sluoksnyje pasižymėjo geriausiomis charakteristikomis tarp mėlyną šviesą skleidžiančių prietaisų. Jo srovės efektyvumas (CE) buvo 23,9 cd/A, PE siekė 24,9 lm/W, o EQE buvo 10,3 %, esant 100 cd/m^2 skaičiui. Esant didesniam, 1000 cd/m^2 skaičiui, itin svarbiam apšvietimo technologijoms, šis prietaisas išlaikė aukščiausią 8,0 % EQE (18,4 cd/A CE, 15,8 lm/W PE), palyginti su visais kitais mėlyną šviesą skleidžiančiais prietaisais, o

maksimalus skaistis ($L_{maks.}$) viršijo 9170 cd/m². Iš žalią šviesą skleidžiančių prietaisų pažymėtina, kad PhOLED prototipai, kurių matricą sudarė medžiaga **5 (H2)**, pranoko tuos, kurie OLED matricoms naudojo darinį **4 (H1)**. PhOLED, kurio emisiniame sluoksnyje buvo 10 m% spinduolio Ir(ppy)₃, disperguoto matricoje **5 (H2)**, pasižymėjo puikiomis charakteristikomis: CE buvo 33,9 cd/A, PE siekė 34,1 lm/W, o EQE pasiekė 9,4 %, esant aukštam 1000 cd/m² skaisčiui, kuris yra reikalingas apšvietimo reikmėms. Žalią šviesą skleidžiantis PhOLED taip pat pasiekė įspūdingą maksimalų skaistį – beveik 39 000 cd/m².

5.2.2. Lengvai susintetinami ir pigūs karbazolo arba fenoksazino dariniai geltoną šviesą skleidžiančių fosforescuojančių OLED matricoms

Šis skyrius parengtas pagal straipsnį, paskelbtą žurnale *Optical Materials*, **2021**, 118, 111251, *D. Blazevicius, G. Krucaite, S. Shahnawaz, S. S. Swayamprabha, E. Zaleckas, J.-H. Jou* ir *S. Grigalevicius* [144].

Šis tyrimas apėmė mažos molekulinės masės oksetano darinių, turinčių karbazolo (**7 (H3)**) arba fenoksazino (**8 (H4)**) fragmentus, sintezę, charakterizavimą ir taikymą PhOLED prietaisų matricoms. Tiksliniai junginiai buvo susintetinti naudojant ekonomišką ir nesudėtingą vienos pakopos sintezę, kaip parodyta 8 schemoje. 3,3-Bis(9-karbazolilmetil)oksetano **7 (H3)** sintezė apėmė 9*H*-karbazolo *N*-alkilinimą, naudojant kalio hidroksidą, kalio karbonatą ir trapfazinį katalizatorių tetrabutilamonio hidrosulfatą (TBAHS) 2-butanone. Ši procedūra labai panaši į anksčiau aprašytą [145, 146]. 3,3-Bis(10-fenoksazinilmetil)oksetanas **8 (H4)** buvo susintetintas naudojantis 10*H*-fenoksazino *N*-alkilinimo reakcija tetrahidrofurane naudojant kalio tretbutoksidą.
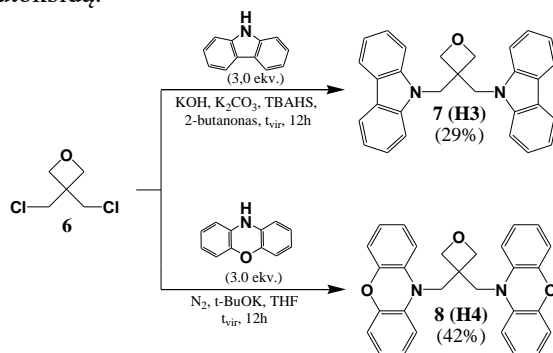
8 schema. Naujų medžiagų matricoms **7 (H3)** ir **8 (H4)** sintezė

Naujai susintetintos medžiagos buvo tirpios įprastuose organiniuose tirpikliuose, o tai leidžia prietaisus formuoti ekonomiškiau – liejant iš tirpalų. Junginių terminės ir morfologinės savybės buvo tyrinėtos TGA ir DSK metodais. TGA tyrimai parodė, kad medžiagų terminis stabilumas ypač aukštas, o jų T_d vertės viršijo 310 °C. DSK matavimų metu paaiškėjo, kad medžiagos **7 (H3)** ir **8 (H4)** po sintezės buvo gautos kaip kristaliniai junginiai, tačiau, išlydžius ir atšaldžius tyrinėjamų medžiagų bandinius, dariniai gali pereiti į amorfinę būseną. Medžiagai **7 (H3)** pirmojo DSK kaitinimo metu buvo užfiksuotas endoterminis lydymosi signalas 199 °C temperatūroje, o išlydytą bandinį atšaldžius, susidarė amorfinė medžiaga su 75 °C

siekiančia T_g. Toliau kaitinant bandinį buvo užfiksuotas kristalizavimasis 123 °C temperatūroje. Darinys **8 (H4)** po reakcijos taip pat buvo gautas kaip kristalinė medžiaga, kurios T_m siekė 198 °C, kaip pavaizduota 50 pav. Išlydytą bandinį atšaldžius, taip pat susidarė amorfinio būvio darinys su 66 °C siekiančia T_g, o toliau kaitinant medžiagą jokie papildomi morfologiniai virsmai nebuvo fiksuojami. Šie DSK matavimų rezultatai patvirtina abiejų medžiagų tinkamumą formuoti plonas amorfines plėveles, bet tikimasi, kad junginys **8 (H4)** suformuos stabilesnius sluoksnius dėl mažesnio polinkio kristalizuotis.
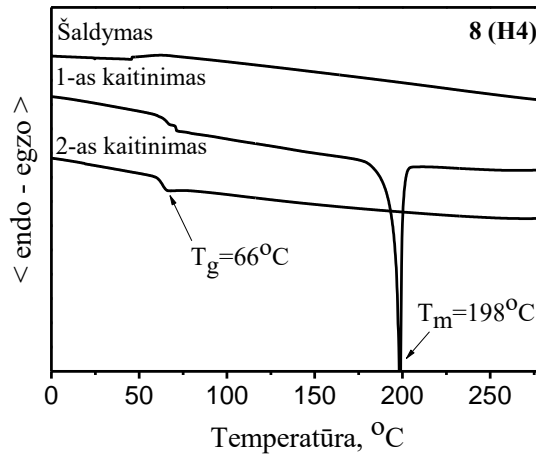
50 pav. Junginio **8 (H4)** DSK kreivės

Siekiant nustatyti junginių **7 (H3)** ir **8 (H4)** E_T vertes, buvo užrašyti LTPL spektrai 77 K temperatūroje. Nustatyta, kad šios vertės siekė 2,95 eV dariniui **7 (H3)** ir 2,73 eV medžiagai **H4**. Abiejų junginių E_T vertės viršija gerai žinomo geltonai fosforescuojančio spinduolio PO-01 E_T, kuri yra 2,21 eV [147], o tai patvirtina medžiagų tinkamumą pritaikyti geltoną šviesą skleidžiančių PhOLED matricoms. Visos išmatuotos junginių savybės pateikiamos 28 lentelėje.

28 lentelė. Terminės ir fotofizikinės medžiagų **H3** ir **H4** savybės

Medžiaga	T_d (°C)	T_m (°C)	T_{cr} (°C)	T_g (°C)	E_T (eV)
7 (H3)	324	199	123	75	2,95
8 (H4)	314	198	–	66	2,73

Norint įvertinti potencialių matricų efektyvumą emisiniuose sluoksniuose, buvo suformuoti geltonai fosforescuojantys prietaisai, naudojant minėtą PO-01 spinduolį. OLED struktūra buvo tokia: ITO/PEDOT:PSS/(**7 (H3)** ir **8 (H4)**):X m% PO-01/TPBi/LiF/Al, čia X – spinduolio koncentracija. Visuose PhOLED buvo skleidžiama 570 nm bangos ilgio emisija, priskiriama geltonai PO-01 skleidžiamai šviesai. Keičiant spinduolio koncentraciją matricose **7 (H3)** ir **8 (H4)**, skleidžiamos šviesos spalvos pokytis nepastebėtas. Sukurti prietaisai skleidžia geltoną šviesą, kurios CIE koordinatės yra (0,49; 0,50), esant 1000 cd/m^2 skaičiui. EL charakteristikos matuotos prietaisams su įvairia spinduolio koncentracija emisiniame sluoksnyje, kurios pateiktos 29 lentelėje. Prietaisai, naudoję junginio **8 (H4)** matricą, pademonstravo geresnes charakteristikas nei matricą **7 (H3)** naudoję OLED. Galima

išskirti 10 m% spinduolio savo emisiniame sluoksnyje turėjusį OLED, kuris pademonstravo CE, PE ir EQE, siekiančius atitinkamai, 33,1 cd/A, 22,8 lm/W ir 10,1 %, esant 1000 cd/m² skaičiui, kuris reikalingas praktiniam taikymui.

29 lentelė. OLED, naudojančių matricas **7 (H3)** arba **8 (H4)** su spinduoliu PO-01, charakteristikos

Matrica	Spinduolis	m%	V_{ON}, V	PE, lm/W	CE, cd/A	EQE, %	L_{maks}, cd/m²
			Esant 100 / 1000 cd/m²				
7 (H3)	PO-01	7,50	6,3 / 8,2	16,0 / 9,9	32,0 / 25,6	10,5 / 7,9	10760
		10,0	5,6 / 7,4	17,3 / 11,4	30,7 / 26,8	10,3 / 8,5	10600
		12,5	5,1 / 6,7	18,4 / 10,9	30,1 / 23,2	10,5 / 7,5	10700
		15,0	4,8 / 6,3	19,2 / 11,3	29,4 / 22,7	10,6 / 7,5	12250
8 (H4)		7,50	3,5 / 4,9	31,6 / 21,2	34,9 / 32,9	10,6 / 9,9	20520
		10,0	**3,5 / 4,6**	**32,2 / 22,8**	**35,8 / 33,1**	**10,9 / 10,1**	**23190**
		12,5	3,6 / 5,1	28,6 / 15,5	32,8 / 25,4	10,1 / 7,9	19470
		15,0	3,5 / 4,7	23,1 / 16,5	26,0 / 24,5	8,1 / 7,7	22360

Remiantis gautais eksperimentiniais rezultatais, akivaizdu, kad medžiaga OLED matricoms **8 (H4)** pasižymi geresnėmis sluoksnių formavimo savybėmis ir turi geriau suderinamą E_T vertę su geltoną šviesą skleidžiančiu spinduoliu PO-01. Šis suderinamumas prisideda prie gerų OLED prietaisų, naudojančių matricą **8 (H4)** charakteristikų. Pažymėtina, kad ši medžiaga gauta naudojant paprastą vienos stadijos sintezę ir turi didelį potencialą fosforescuojančių organinių šviestukų gamybos srityje.

5.2.3. Didelio efektyvumo žvakės šviesą skleidžiantys OLED, pasižymintys ypač žema skleidžiamos šviesos spalvine temperatūra

 Šis skyrius parengtas pagal straipsnį, paskelbtą žurnale *Molecules*, **2021**, 26, 24, *S. Shahnawaz, I. Siddiqui, M. R. Nagar, A. Choudhury, J.-T. Lin, D. Blazevicius, G. Krucaite, S. Grigalevicius and J.-H. Jou* [148].

Šio darbo metu junginys 3,3-bis(10-fenoksazinilmetil)oksetanas **8** (**H4**), kurio sintezė pavaizduota 9 schemoje, buvo panaudotas žmogui ir aplinkai draugiškiems žvakių šviesą skleidžiančiuose OLED. Darinys buvo susintetintas procedūros, aprašytos ankstesniame skyriuje, metu, naudojant paprastą vienos pakopos sintezės būdą. Konkrečiau, 3,3-bis(10-fenoksazinilmetil)oksetanas **8** (**H4**) buvo gautas 10H-fenoksazino N-alkilinimo reakcijos tetrahidrofurane metu, naudojant kalio tretbutoksido bazę.
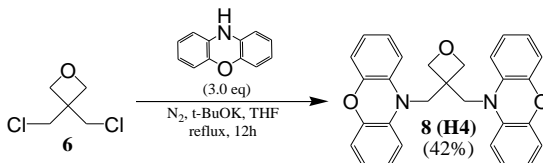
9 schema. Junginio **8** (**H4**) sintezė

Ankstesniame skyrelyje buvo aprašytos **8** (**H4**) terminės savybės, fotofizikinės medžiagos **8** (**H4**) charakteristikos šiame tyrime buvo nagrinėjamos pasitelkiant ultravioletinių spindulių – regimosios šviesos (UV-RŠ) absorbcijos, PL ir LTPL tyrimus. Absorbcijos, PL ir LTPL (esant 77 K) smailių pikai buvo stebimi atitinkamai

esant 320, 395 ir 495 nm, o E_g vertė, gauta iš absorbcijos spektro, siekė 3,85 eV. Junginio **8** (**H4**) E_S (3,44 eV) ir E_T (2,87 eV) vertės buvo apskaičiuotos naudojant atitinkamai absorbcijos PL (360 nm) ir absorbcijos LTPL (436 nm) kreivių susikirtimo taškus. HOMO ir LUMO energijos lygiai siekė atitinkamai –5,39 eV ir –1,54 eV, apskaičiuojant pagal ciklinės voltamperometrijos (CV) kreivę ir anksčiau apskaičiuotą E_g. 30 lentelėje pateikiamas fotofizikinių, elektrocheminių ir terminių **8** (**H4**) savybių palyginimas su komercinės matricos CBP charakteristikomis [18,71,149].

30 lentelė. Medžiagų matricoms terminės, elektrocheminės ir fotofizikinės savybės

Medžiaga	T_d (ºC)	T_m (ºC)	T_g (ºC)	HOMO (eV)	LUMO (eV)	E_T (eV)	E_S (eV)	E_g (eV)	Šaltinis
8 (**H4**)	340	199	66	–5,39	–1,54	2,95	3,44	3,85	[144]
CBP	320	–	62	–6,00	–2,90	2,73	3,49	3,10	[18, 71, 149]

Norint įvertinti matricos **8** (**H4**) efektyvumą, buvo pagaminti iš tirpalų formuojami organiniai žvakės šviesą skleidžiantys šviestukai. Palyginimui taip pat buvo suformuotas analogiškas prietaisas su komercine matrica CBP, naudojant geltoną šviesą skleidžiančio PO-01 ir raudonai oranžinę šviesą skleidžiančio Ir(2-phq)$_3$ spinduolių mišinį. Naudotų prietaisų struktūra buvo ITO/PEDOT:PSS/**8** (**H4**) arba CBP : PO-01 (10 m%):Ir(2-phq)$_3$(x m%) (x = 7,5, 10,0, 12,5, 15,0)/TPBi /LiF/Al. Keičiant Ir(2-phq)$_3$ koncentraciją emisiniame sluoksnyje nuo 7,5 % iki 15,0 %, buvo nustatyta, kad optimizuota šio spinduolio koncentracija, kurioje pasiekiamas aukščiausias OLED efektyvumas, yra 10 %. Gautų prietaisų skleidžiamos šviesos CIE koordinatės ir skleidžiamos šviesos spalvinės temperatūros priklausomybė nuo skaisčio pavaizduotos 51 pav.
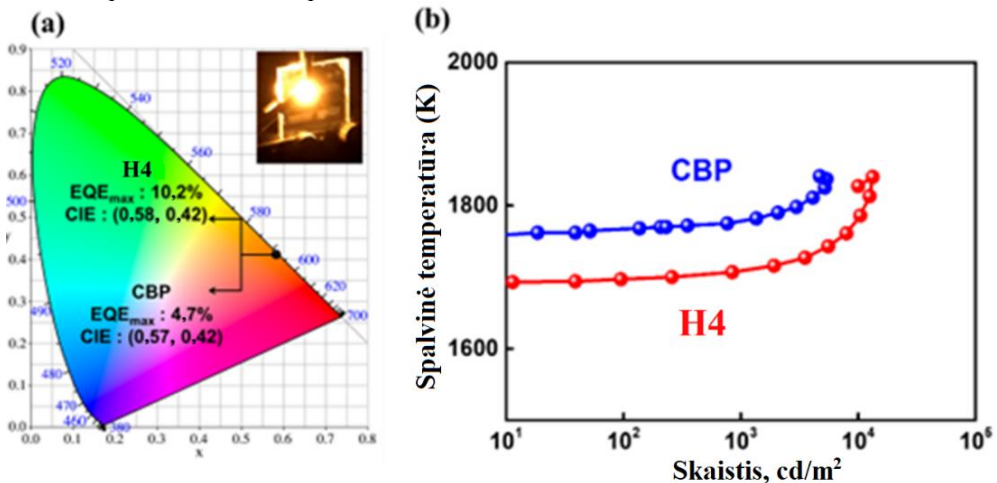
51 pav. 8 (**H4**) arba CBP matricas naudojusių OLED (a) CIE spalvinės koordinatės ir EQE$_{maks.}$ vertės su pikselio nuotrauka (viduje) ir (b) skleidžiamos šviesos spalvinės temperatūros priklausomybė nuo skaisčio

8 (**H4**) junginį kaip matricą naudojančio OLED CIE koordinatės buvo (0,58; 0,42), o CBP matricą naudojančio prietaiso – (0,57, 0,42). Pasiektos EQE$_{maks.}$ vertės buvo ta pačia tvarka 10,2 % ir 4,7 %.

Tirtų žvakės šviesą skleidžiančių organinių šviestukų, kurių matricoms panaudoti **8** (**H4**) ir CBP junginiai, PE, CE, EQE ir skleidžiamos šviesos spalvinės temperatūros (CT) charakteristikos apibendrintos 31 lentelėje. OLED emisiniai sluoksniai suformuoti iš tirpalų, juose naudojant po 10 m% geltonos šviesą skleidžiančio spinduolio PO-01 ir raudonai oranžinę šviesą skleidžiančio spinduolio Ir(2-phq)$_3$.
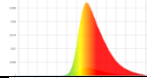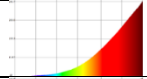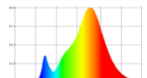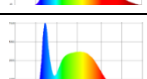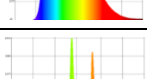
31 lentelė. Žvakės šviesą skleidžiančių po 10 m% PO-01 ir Ir(2-phq)3 spindulių turinčių OLED charakteristikos, matricomis panaudojus **8** (**H4**) arba CBP junginius

Matrica	V_{ON}, V	PE, lm/W	CE, cd/A	EQE, %	CT, K	L_{maks}, cd/m^2
		Esant 100 / 1000 cd/m^2 / MAKS.			Esant 100/1000cd/m^2	
8 (H4)	2,8	22,0/16,9/23,7	22,4/21,6/22,4	10,2/9,6/10,2	1690 / 1707	14950
CBP	3,2	7,4 /3,9/9,6	10,3/7,4/11,7	4,7/3,2/6,8	1768 / 1782	8393

8 (**H4**) matricą naudojęs prietaisas pasižymėjo maksimaliomis PE, CE ir EQE vertėmis, siekiančiomis atitinkamai 23,7 lm/W, 22,4 cd/A ir 10,2 % kartu su 2,8 V įsijungimo įtampa (V_{ON}) ir labai žema CT, kuri buvo vos 1690 K. Net esant didesniam skaičiui, pvz., 1000 cd/m², efektyvumas išliko aukštas, o tai rodo mažą efektyvumo kritimą didėjant skaičiui, kartu išlaikant žemą CT. Palyginimui – CBP matricą naudojęs OLED pateikė daug mažesnes PE, CE ir EQE vertes, tuo pat metu esant didesnei CT.

Vertinant apšvietimo šaltinio įtaką žmonių sveikatai, šis tyrimas įvertina didžiausią leidžiamąją poveikio ribą (MPE) ir melatonino slopinimo jautrumą (MSS). MPE, kaip apibrėžta Tarptautinės apsaugos nuo nejonizuojančiosios spinduliuotės komisijos (ICNIRP) [153], skirta kiekybiškai įvertinti su mėlyna šviesa susijusius pavojus ir parodo didžiausią tam tikros spinduliuotės didžiausiąjį veikimo laiką, kuriuo žmogus gali būti veikiamas be pavojingų padarinių ar akių ir odos pakitimų. Melatonino slopinimo jautrumas po 1,5 h veikimo (MSS) įvertina, kiek tam tikro bangos ilgio spinduliuotė slopina melatonino išsiskyrimą organizme, lyginant su mėlynos šviesos (480 nm) etalonu. Įvairių apšvietimo šaltinių emisijos spektrų, CT, MSS ir MPE palyginimas pateiktas 32 lentelėje. **8** (**H4**) matricą naudojęs mėlynos spinduliuotės neskleidžiančio žvakės šviesos OLED CT yra 1690 K, todėl MPE atžvilgiu jis yra 180 kartų mažiau kenksmingas, palyginti su šaltai baltos šviesos spalvos CFL, kurio CT yra 5 843 K. Be to, esant 100 lx apšvietai, tirto prietaiso MPE buvo 57 696 s (daugiai nei 16 valandų), o šaltai baltos šviesos spalvos CFL – tik 320 s. Tirto prietaiso MSS, esant 100 lx apšvietai, (1,33 %) yra 22,4 karto mažesnis nei šaltai baltą šviesą skleidžiančio CFL (29,9 %) po 1,5 valandos veikimo naktį. Žvakės šviesą skleidžiantis OLED minėtomis charakteristikomis taip pat pranoksta šiltai baltą šviesą skleidžiantį LED, šaltai baltą šviesą skleidžiantį LED, kaitinamąją lemputę ir net natūralią žvakių šviesą.

32 lentelė. Įvairių šviesos šaltinių spektrų, CT, MSS (po 1,5 h) ir MPE charakteristikų palyginimas

Šviesos šaltinis	Spektras	CT (K)	MSS (%)	MPE (s), esant 100 lx
Šis darbas		1690	1,33	57 696
Žvakės šviesa		1884	4,0	2750
Kaitinamoji lemputė		2444	11,5	1100
Šiltai baltos šviesos spalvos LED		2704	8,0	1000
Šaltai baltos šviesos spalvos LED		5549	19,8	380
Šaltai baltos šviesos spalvos CFL		5843	29,9	320

Šiame darbe sukurtas OLED su **8 (H4)** matrica nemirga, nedegina rainelės, neakina ir yra potencialiai energiškai efektyvesnis nei bet kurie komerciniai apšvietimo šaltiniai. Šis tyrimas atveria kelią kurti efektyvius žvakės šviesą skleidžiančius OLED apšvietimo prietaisus, naudojant ekonomiškus prietaisų formavimo iš tirpalų metodus.

5.2.4. Benzfenono darinių, naudojamų organiniams šviestukams apžvalga

Šis skyrius parengtas pagal straipsnį, paskelbtą žurnale *Nanomaterials*, 2024, 14, 4 by *D. Blazevicius and S. Grigalevicius* [158].

Šiame tyrime buvo nagrinėjama benzfenono darinių sintezė, terminės, elektrocheminės, fotoelektrinės ir fotofizikinės savybės. Be to, apžvelgtas jų pritaikymas OLED prietaisuose tiek matricoms, tiek spinduoliams. Šiame skyriuje pateikiama sisteminė įvairių OLED struktūrų ir jų atitinkamų efektyvumų apžvalga. Apžvalga suskirstyta į keletą skyrelių, suskirstytų pagal benzfenono darinių taikymą ir struktūrą, kaip, pavyzdžiui, matricos fosforescuojantiems spinduoliams, matricos TADF spinduoliams, D–A tipo spinduoliai, D–A–D tipo simetrinės struktūros spinduoliai ir D–A–D tipo asimetrinės struktūros spinduoliai.

5.2.4.1. Benzfenono dariniai, skirti fosforescuojančių organinių šviestukų matricoms

Medžiagų su benzfenono fragmentu, pademonstravusių aukščiausią efektyvumą jas pritaikius kaip fosforescuojančių organinių šviestukų matricas, struktūros pavaizduotos 52 pav.
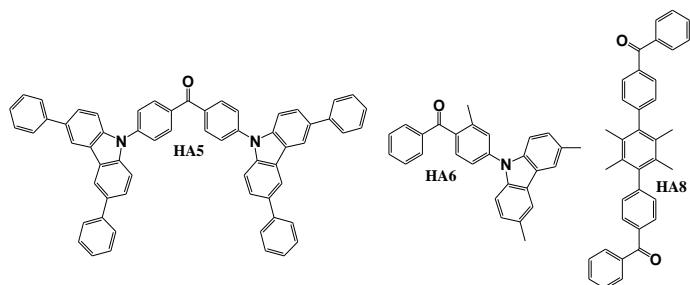
12 pav. Benzfenono dariniai, naudojami PhOLED matricoms [162, 163, 166]

PhOLED, naudojančių matricas **HA5** [162], **HA6** [163] ir **HA8** [166], charakteristikos pateiktos 33 lentelėje. Naudojant šiuos junginius buvo suformuoti veiksmingi PhOLED prietaisai, kurių EQE viršijo 16 %. Šios matricos buvo naudojamos raudoną, oranžinę, geltoną, žalią ir mėlyną šviesą skleidžiančiuose prietaisuose.

33 lentelė. PhOLED prietaisų, naudojančių matricas **HA5**, **HA6** ir **HA8**, charakteristikos

Prietaisas	Matrica	Skleidžiama šviesa	V_{ON}, V	$L_{maks.}$, cd/m²	CE, cd/A	PE, lm/W	EQE, %	CIE (x; y)	Šaltinis
D1HA5	**HA5**	Žalia	2,5	93330	–	99,1	25,1	(0,29; 0,64)	[162]
D2HA5	**HA5**	Oranžinė	2,6	31200	–	61,6	23,1	(0,51; 0,47)	[162]
D3HA5	**HA5**	Raudona	2,9	10240	–	27,1	22,1	(0,61; 0,36)	[162]
D1HA6	**HA6**	Mėlyna	3,0	–	–	38,2	19,4	(0,16; 0,33)	[163]
D2HA6	**HA6**	Žalia	2,9	–	–	75,7	21,0	(0,29; 0,64)	[163]
D3HA6	**HA6**	Raudona	3,1	–	–	30,8	16,5	(0,62; 0,38)	[163]
D1HA8	**HA8**	Žalia	4,5	3080	46,8	29,1	17,0	(0,30; 0,60)	[166]
D4HA8	**HA8**	Geltona	5,5	3490	50,6	28,9	19,2	(0,47; 0,51)	[166]

Tarp raudoną šviesą skleidžiančių prietaisų prototipas D3HA5 demonstravo geriausias charakteristikas, tarp kurių 27,1 lm/W siekiantis PE ir 22,1 % siekiantis EQE. Oranžinę šviesą skleidžiantis prietaisas D2HA5 pasirodė esąs efektyviausias, jo PE ir EQE atitinkamai siekė 61,6 lm/W ir 23,1 %. Tarp geltoną šviesą skleidžiančių prietaisų prototipas D4HA8 išsiskyrė 50,6 cd/A siekiančiu CE, 28,9 lm/W siekiančiu PE ir 19,2 % EQE. Lyginant žalią šviesą skleidžiančių PhOLED matricas, medžiaga HA5 pasižymėjo puikiu efektyvumu, o prietaisas D1HA5 pasiekė puikų 99,1 lm/W PE ir 25,1 % EQE. Tarp mėlyną šviesą skleidžiančių PhOLED prietaisas D1HA6 parodė geriausią efektyvumą su aukštais PE ir EQE – atitinkamai 38,2 lm/W ir 19,4 %.

5.2.4.2. Benzfenono dariniai, skirti TADF organinių šviestukų matricoms

Benzfenono darinių, parodžiusių geriausias charakteristikas, jas pritaikius kaip TADF efektu pasižyminčių spinduolių matricas, struktūros pavaizduotos 53 pav., o TADF OLED prietaisų, naudojančių matricas **HB3** [169], **HB6** ir **HB7** [171], charakteristikos pateiktos 34 lentelėje.
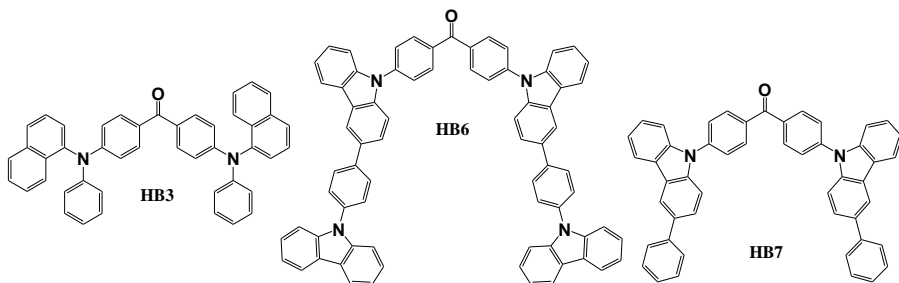
53 pav. Benzfenono dariniai TADF OLED matricoms [169, 171]

34 lentelė. Geriausių TADF OLED, naudojančių benzfenono darinių matricas, charakteristikos

Prietaisas	Matrica	Skleidžiama šviesa	V_{ON}, V	$L_{maks.}$, cd/m²	CE, cd/A	PE, lm/W	EQE, %	CIE (x; y)	Šaltinis
DHB3	**HB3**	Balta	3,9	29922	18,6	–	9,5	(0,36; 0,31)	[169]
D1HB6	**HB6**	Žalia	3,0	16500	70,7	55,6	23,2	(0,28; 0,57)	[171]
D2HB6	**HB6**	Žalia	2,9	18900	72,3	63,6	25,3	(0,29; 0,58)	[171]
DHB7	**HB7**	Žalia	2,7	10540	49,2	46,2	15,3	(0,28; 0,57)	[171]

Medžiaga **HB3** geriausiai pasitarnavo kaip papildomas sluoksnis tarp dviejų skirtingų TADF emisinių sluoksnių. Emisiniuose sluoksniuose panaudojus oranžinę ir mėlyną šviesą skleidžiančius TADF spinduolius, buvo suformuoti efektyvūs baltą šviesą skleidžiantys TADF OLED, o prietaisas DHB3 pasiekė 9,5 % EQE. Medžiagos **HB6** ir **HB7**, savo struktūroje turėjusios įvairiais fragmentais pakeistus karbazolo žiedus, parodė geriausias charakteristikas, kai buvo pritaikytos kaip matricos žalią šviesą skleidžiančiuose, iš tirpalų formuojamuose TADF OLED prietaisuose, iš kurių aukštesniu efektyvumu pasižymėjo šviestukas D2HB6. Šis OLED, turėjęs papildomą skyles pernešantį sluoksnį, paygint su prietaisu D1HB6, pademonstravo 63,6 lm/W siekiantį PE, o EQE buvo 25,3 %.

5.2.4.3. Donoro-akceptoriaus tipo benzfenono dariniai spinduoliams

D-A tipo benzfenono spinduolių, parodžiusių aukščiausią efektyvumą organiniuose šviestukuose, struktūros pavaizduotos 54 paveiksle.
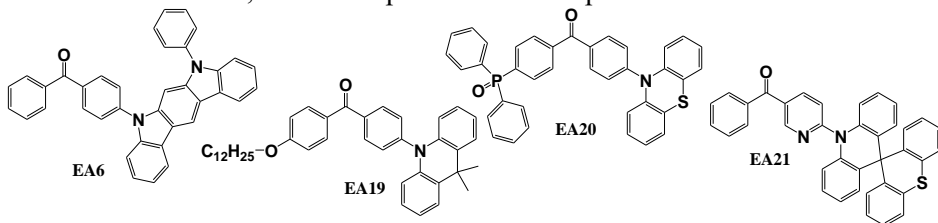
54 pav. D-A tipo benzfenono dariniai OLED spinduoliams [174, 187, 189]

Efektyviausių organinių šviestukų, naudojusių D-A tipo benzfenono spinduolių, charakteristikos pateiktos 35 lentelėje. Efektyviausias geltoną šviesą skleidžiantis prietaisas naudojo darinio **EA20** spinduolį, o prietaiso D1EA20 CE, PE ir EQE siekė atitinkamai 73,1 cd/A, 38,2 lm/W ir 26,7 % [189]. Spinduolis **EA20**, derinamas su

kitu mėlyną šviesą skleidžiančiu TADF spinduoliu baltą šviesą skleidžiančiame šviestuke D2E20, pademonstravo aukštą 45,9 cd/A siekiantį CE, 18,0 lm/W siekiantį PE ir 20,8 % EQE [190]. TADF spinduolis **EA21** [187] parodė geriausias charakteristikas žalią šviesą skleidžiančiuose prietaisuose, o OLED D2E21 pasiekė 25,6 % EQE. Tas pats spinduolis parodė ypač gerą efektyvumą matricos nenaudojančiame prietaise D1EA21, o PE, CE ir EQE siekė atitinkamai 56,4 cd/A, 43,5 lm/W ir 18,7 %. Medžiaga **EA6** [174], sukurta derinant benzfenono elektronų akceptorių ir 11-fenildihidroindolo[2,3-a]karbazolo elektronų donorą, buvo panaudota kaip mėlyną šviesą skleidžiantis spinduolis **EA6** prietaise DEA6, kurio didžiausiasis EQE buvo 17,7 %, o CE ir PE vertės buvo 44,8 cd/A ir 45,6 lm/W. Efektyviausias mėlyną šviesą skleidžiantis D-A tipo TADF benzfenono spinduolis buvo **EA19** [186], o šį spinduolį naudojantis prietaisas DEA19 pasiekė aukštas CE, PE ir EQE reikšmes – atitinkamai 47,7 cd/A, 29,9 lm/W ir 20,6 %.

35 lentelė. TADF OLED, naudojančių spinduolius EA6, EA19, EA20 ir EA21, charakteristikos

Prietaisas	Spinduolis	Skleidžiama šviesa	V_{ON}, V	$L_{maks.}$, cd/m^2	CE, cd/A	PE, lm/W	EQE, %	CIE (x; y)	Šaltinis
DEA6	**EA6**	Mėlyna	3,2	14724	44,8	45,6	17,7	(0,17; 0,28)	[174]
DEA19	**EA19**	Mėlyna	4,0	4235	47,7	29,9	20,6	–	[186]
D1EA20	**EA20**	Geltona	4,4	32590	73,1	38,2	26,7	–	[189]
D2EA20	**EA20**: 2CzTPEPCz	Balta	6,1	12310	45,9	18,0	20,8	(0,45; 0,44)	[190]
D1EA21	**EA21**	Žalia	3,2	26836	56,4	43,5	18,7	(0,28; 0,53)	[187]
D2EA21	**EA21**	Žalia	3,2	11392	69,8	58,9	25,6	(0,24; 0,49)	[187]

5.2.4.4. Donoro-akceptoriaus-donoro tipo simetrinės struktūros benzfenono spinduoliai

D-A-D tipo simetrinės struktūros benzfenono spinduolių, pademonstravusių aukščiausias charakteristikas juos pritaikius organiniuose šviestukuose, struktūros pavaizduotos 55 pav.
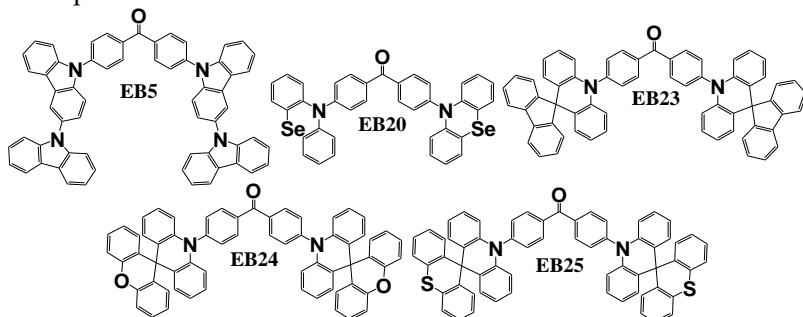
55 pav. D-A-D tipo simetrinės struktūros benzfenono dariniai OLED spinduoliams [192, 195, 197]

Efektyviausių prietaisų, naudojančių D-A-D tipo, simetrinės struktūros benzfenono darinius kaip spinduolius, charakteristikos apibendrintos 36 lentelėje. Darinys **EB5** [192] parodė aukščiausią efektyvumą tarp mėlyną šviesą skleidžiančių

TADF spinduolių, apibendrintų šiame skyriuje. Organinis šviestukas DEB5 pasiekė 14,3 % EQE vertę ir 25,5 cd/A CE. Tyrėjai sukūrė žalią šviesą skleidžiančius, centrinį benzfenono fragmentą turinčius TADF spinduolius **EB20** [195], **EB23**, **EB24** ir **EB25** [197], kurie, pritaikyti prietaisuose, viršijo 17 % EQE net nelegiruotuose prietaisų konfigūracijose. Darinys **EB20**, susintetintas sujungus fenoselenazino elektronų donorą su benzfenono elektronų akceptoriumi, prietaise DEB20 demonstravo išskirtinai aukštą 30,8 % EQE ir CE, siekiantį 64,0 cd/A. Didžiausią bendrą žalią šviesą skleidžiančių TADF OLED efektyvumą, naudojant simetriškus D-A-D tipo benzfenono spinduolius, pasiekė prietaisai, spinduoliais naudoję darinius **EB23**, **EB24** ir **EB25**. Šios medžiagos buvo išbandytos tiek nelegiruotuose (D1EB23, D1EB24, D1EB24), tiek legiruotuose (D2EB23, D2EB24, D2EB24) emisiniuose sluoksniuose.

36 lentelė. TADF OLED, naudojančių spinduolius EB5, EB20, EB23, EB24 ir EB25, charakteristikos

Prietaisas	Spinduolis	Skleidžiama šviesa	V_{ON}, V	$L_{maks.}$, cd/m^2	CE, cd/A	PE, lm/W	EQE, %	CIE (x; y)	Šaltinis
DEB5	**EB5**	Mėlyna	4,4	3900	25,5	–	14,3	(0,17; 0,27)	[192]
DEB20	**EB20**	Žalia	4,3	17007	64,0	–	30,8	(0,31; 0,53)	[195]
D1EB23	**EB23**	Žalia	3,2	31713	53,9	48,9	18,6	(0,24; 0,53)	[197]
D2EB23	**EB23**	Žalia	3,0	48712	90,9	91,2	30,3	(0,25; 0,54)	[197]
D1EB24	**EB24**	Žalia	3,6	30283	46,8	37,5	17,1	(0,22; 0,46)	[197]
D2EB24	**EB24**	Žalia	3,2	48515	87,5	85,9	32,2	(0,22; 0,49)	[197]
D1EB25	**EB25**	Žalia	3,8	25616	49,1	35,7	18,1	(0,22; 0,50)	[197]
D2EB25	**EB25**	Žalia	3,2	48153	79,8	75,9	28,4	(0,23; 0,50)	[197]

Efektyviausias nelegiruotas prietaisas D1EB23 demonstravo išskirtinį našumą – maksimalus CE, PE ir EQE siekė atitinkamai,53,9 cd/A, 48,9 lm/W ir 18,6 %. Prietaiso D2EB23 legiruotoje konfigūracijoje efektyvumas buvo dar didesnis ir pasiektas įspūdingas 90,9 cd/A siekiantis CE, PE buvo 91,2 lm/W, o EQE siekė 30,3 %. Prietaisas D2EB23 pasiekė aukščiausią CE ir PE tarp šiame skyrelyje analizuojamų prietaisų, o OLED prototipas D2EB24, naudojęs legiruotą spinduolį **EB24**, pasiekė aukščiausią 32,2 % EQE.

5.2.4.5. Donoro-akceptoriaus-donoro tipo asimetrinės struktūros benzfenono spinduoliai

D-A-D tipo asimetrinės struktūros benzfenono spinduolių, pademonstravusių geriausią efektyvumą juos pritaikius OLED emisiniuose sluoksniuose, struktūros pavaizduotos 56 pav.
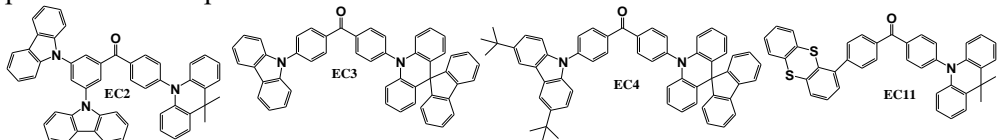
56 pav. D-A-D tipo, asimetrinės struktūros benzfenono dariniai organinių šviestukų spinduoliams [104, 203, 205]

Efektyviausių prietaisų, naudojančių EC medžiagų spinduolius, charakteristikos pateiktos 37 lentelėje. Visi spinduoliai šiame skyrelyje skleidė žalią šviesą. Spinduolis **EC2** [104], panaudotas organiniame šviestuke DEC2, pasiekė aukštas CE, PE ir EQE vertes – atitinkamai 61,8 cd/A, 40,4 lm/W ir 19,7 %. Dariniai **EC3** ir **EC4** [203] taip pat demonstravo aukštą efektyvumą, o iš jų šiek tiek geresnes charakteristikas parodė spinduolis **EC3**. Neleigiruotą emisinį sluoksnį turintis prietaisas D1EC3 demonstravo įspūdingas charakteristikas – CE, PE ir EQE atitinkamai siekė 76,9 cd/A, 71,0 lm/W ir 29,0 %. Spinduolio dispergavimas matricoje šviestuke D2EC3 dar padidino efektyvumą iki 82,9 cd/A CE, 70,1 lm/W PE ir 33,3 % siekiančio EQE. Galiausiai TADF spinduolis EC11 [205], savo struktūroje turintis elektronų donorų tiantreno ir 9,10-dihidro-9,9-dimetilakridino fragmentus, panaudotas prietaiso DEC11 emisiniame sluoksnyje, pasiekė 57,8 cd/A CE, 38,8 lm/W PE ir 22,2 % EQE vertes.

37 lentelė. TADF OLED, naudojančių spinduolius **EC2**, **EC3**, **EC4** ir **EC11**, charakteristikos

Prietaisas	Spinduolis	Skleidžiama šviesa	V_{ON}, V	$L_{maks.}$, cd/m^2	CE, cd/A	PE, lm/W	EQE, %	CIE (x; y)	Šaltinis
DEC2	**EC2**	Žalia	3,6	116000	61,8	40,4	19,7	(0,26; 0,56)	[104]
D1EC3	**EC3**	Žalia	3,2	78540	76,9	71,0	29,0	(0,21; 0,47)	[203]
D2EC3	**EC3**	Žalia	3,2	71150	82,9	70,1	33,3	(0,20; 0,42)	[203]
D1EC4	**EC4**	Žalia	3,0	54450	53,2	51,5	21,6	(0,20; 0,42)	[203]
D2EC4	**EC4**	Žalia	3,2	42550	77,2	65,0	32,9	(0,19; 0,38)	[203]
DEC11	**EC11**	Žalia	4,2	15600	57,8	38,8	22,2	(0,18; 0,41)	[205]

Apibendrinant ši apžvalga parodo, kad benzfenonų dariniai su skirtingais elektronų donorais turi didelį potencialą juos pritaikant PhOLED ir TADF OLED matricoms ar įvairių OLED konstrukcijų spinduoliams. Nuolatinė naujų elektroaktyvių benzfenono darinių sintezė ir tyrimai gali prisidėti prie būsimų OLED prietaisų kokybės ir efektyvumo.

5.2.5. Susuktos struktūros daugiafunkciai bikarbazolilo-difenilsulfono dariniai, giliai mėlyną ir žalią šviesą skleidžiantiems OLED

Šis skyrius parengtas pagal straipsnį, paskelbtą žurnale *Nanomaterials*, **2023**, 13, 8, *P. Gautam, S. Shahnawaz, I. Siddiqui, D. Blazevicius, G. Krucaite, D. Tavgeniene, J.-H. Jou and S. Grigalevicius* [206].

Šio darbo metu buvo susintetinti nauji bikarbazolilo dariniai, turintys centrinį difenilsulfono fragmentą. Sintezei buvo pasitelkta trijų stadijų procedūra, kaip pavaizduota 10 schemoje.

Iš pradžių 3,3'-bikarbazolas (**1**) buvo gautas oksiduojant karbazolą geležies (III) chloridu. Paskui buvo vykdoma *N*-alkilinimo reakcija tetrahidrofurane tarp bikarbazolo (**1**) ir įvairių alkil- arba benzilbromidų, reakcijoje dalyvaujant kalio hidroksidui ir kalio karbonatui. Susidarę įvairūs 9-alkil-9'*H*-3,3'-bikarbazolai (**2-4**) ir 9-benzil-9'*H*-3,3'-bikarbazolas (**5**) dalyvavo paskutinėje sintezės stadijoje, kuri buvo nukleofilinio pakeitimo reakcija su vieną arba du fluoro atomus turinčiu difenilsulfonu. Šių reakcijų, atliktų dimetilsulfokside (DMSO) su kalio karbonatu kaip baze, metu buvo gautos tikslinės medžiagos **14** (**DB13**), **15** (**DB43**), **16** (**DB24**) ir

17 (**DB34**). Naujai susintetintų darinių struktūros buvo identifikuotos naudojant MS spektrometriją ir BMR spektroskopiją, o gauti duomenys sutapo su teoriškai pasiūlytomis struktūromis. Junginiai 14 (**DB13**), 15 (**DB43**) ir 16 (**DB24**) turėjo įvairaus ilgio alifatinę grandinėlę (-es), išskyrus junginį 17 (**DB34**), į kurio struktūrą buvo įtrauktas benzilfragmentas. Inoue ir kt. atliktame tyrime buvo tiriama alkilo grandinėlės ilgio įtaka organinių junginių tirpumui [207]. Pastebėta bendra tendencija rodo, kad ilgesnė alifatinė grandinėlė pagerina molekulės tirpumą suderinamame tirpiklyje.
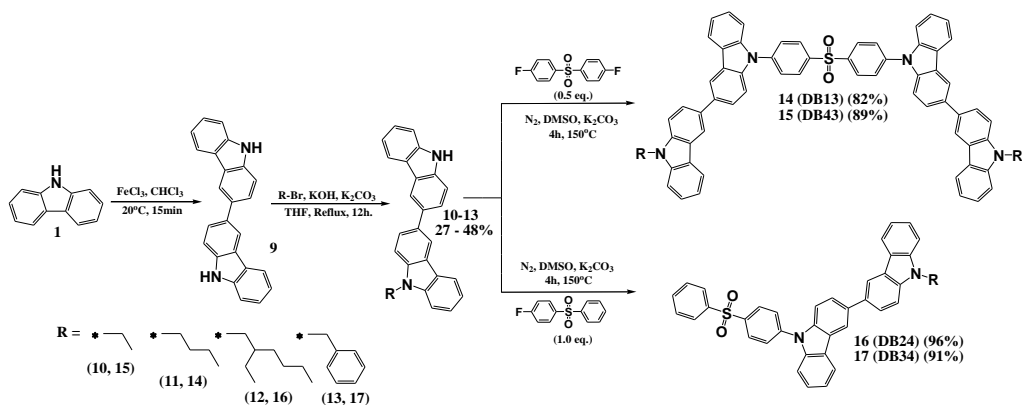
10 schema. Bikarbazolildifenilsulfono darinių sintezė

Naujieji dariniai pasižymėjo aukštomis, 50 % viršijančiomis PLQY vertėmis. Buvo registruojami kiekvienos medžiagos UV-RŠ absorbcijos, PL ir LTPL spektrai, o gauti duomenys panaudoti E_g, E_S ir E_T apskaičiuoti. TRPL matavimai atlikti siekiant nustatyti fotoemisijos gesimo trukmę, o CV matavimai padėjo nustatyti HOMO ir LUMO vertes. Termines savybes ištyrus TGA ir DSK metodais paaiškėjo, kad medžiagos pasižymi aukštu atsparumu kaitinimui ir yra amorfinės, jų T_g vertės yra aukštos. Visos matuotos terminės, fotofizikinės ir elektrocheminės medžiagų savybės apibendrintos 38 lentelėje.

38 lentelė. Terminės, fotofizikinės ir elektrocheminės darinių 14 (**DB13**), 15 (**DB43**), 16 (**DB24**) ir 17 (**DB34**) savybės

Medžiaga	T_D, °C	T_g, °C	E_g, eV	PLQY, %	PL gesimas, ns	HOMO, eV	LUMO, eV	E_S, eV	E_T, eV	ΔE_{ST}, eV
14 (DB13)	430	154	3,16	50,5	3,30	5,73	2,57	3,10	2,78	0,32
15 (DB43)	365	154	3,26	66,5	3,30	5,69	2,43	3,23	2,77	0,46
16 (DB24)	391	82	3,30	61,8	3,70	5,71	2,41	3,12	2,77	0,35
17 (DB34)	383	125	3,28	68,5	2,70	5,77	2,49	3,14	2,80	0,34

Naujų junginių savybės leidžia juos pritaikyti organiniuose šviestukuose tiek spinduoliams, tiek matricoms. Mėlyną šviesą skleidžiantys OLED buvo sukonstruoti pasitelkiant naująsias medžiagas kaip spinduolius, suformuojant legiruotus ir nelegiruotus emisinius sluoksnius turinčius šviestukus, kurių struktūra buvo tokia: ITO (125 nm)/PEDOT:PSS (35 nm)/CBP: x m% spinduolio (x = 5,0, 10, 15, and 100 %) (20 nm)/TPBi (40 nm)/LiF (1 nm)/Al (200 nm). Po EL eksperimentų

efektyviausias darinys šioje taikymo srityje buvo **14** (**DB13**). EL charakteristikos su prietaisų efektyvumo rodikliais pavaizduoti 57 pav. ir 39 lentelėje.
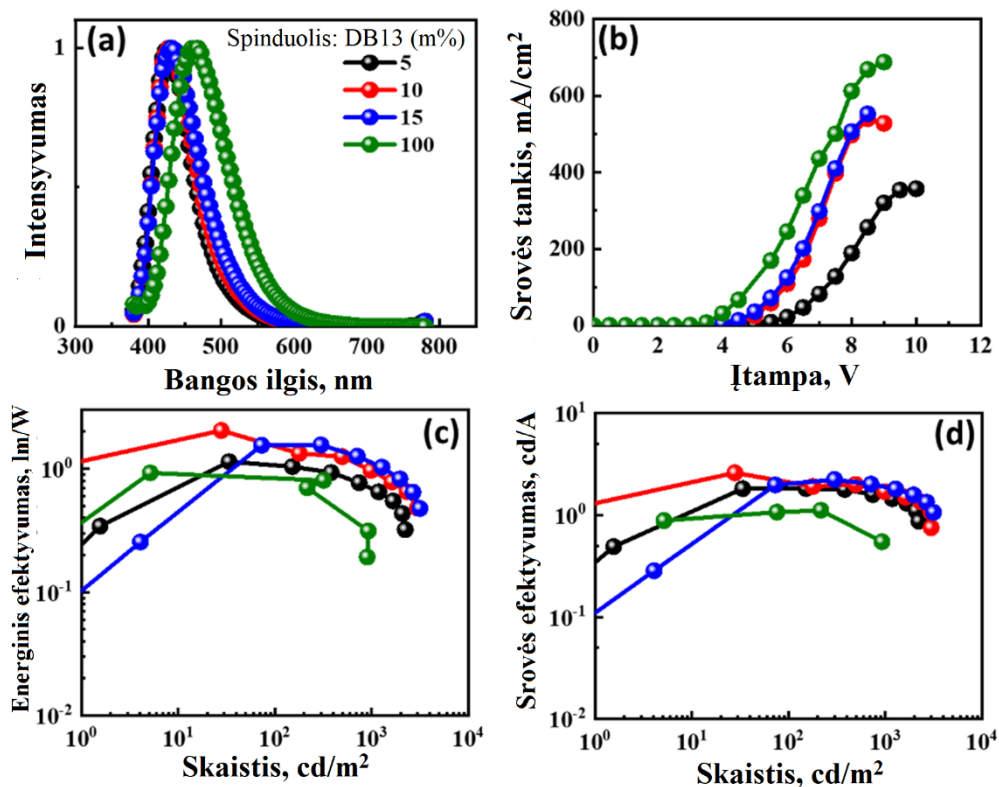
57 pav. Prietaisų, turinčių **14** (**DB13**) spinduolį: (a) EL spektras bei (b) srovės tankio ir įtampos, (c) energinio efektyvumo ir skaičio, (d) srovės efektyvumo ir skaisčio grafikai

39 lentelė. Prietaisų, naudojančių fluorescuojantį **DB13** spinduolį, charakteristikos

Spinduolis	m%	V_{ON}, V	PE_{maks}, lm/W	$CE_{maks.}$, cd/A	EQE_{maks}, %	CIE (x; y), esant 100/1000 cd/m²	L_{maks}, cd/m²
14 (**DB13**)	5	4,6	1,1	1,8	3,4	(0,16; 0,08) / (0,16; 0,08)	2230
	10	3,7	2,0	2,5	4,0	(0,16; 0,09) / (0,16; 0,09)	2987
	15	3,5	1,6	2,2	2,9	(0,16; 0,10) / (0,16; 0,10)	3167
	100	3,0	1,0	1,1	0,6	(0,16; 0,20) / -	928

Nors nelegiruotas prietaisas demonstravo aukštesnį srovės tankį nei legiruoti, bet jo bendras efektyvumas buvo mažesnis. Geriausias charakteristikas pademonstravo prietaisas, savo emisiniame sluoksnyje turintis 10 m% **14** (**DB13**) spinduolio. Maksimalus PE ir CE siekė atitinkamai 2,0 lm/W ir 2,5 cd/A esant žemai 3,7 eV įsijungimo įtampai V_{ON}. Be to, šis prietaisas pasiekė 4,0 % EQE, kuris artėja prie teorinės efektyvumo ribos fluorescuojantiems spinduoliams ir pasižymi giliai mėlyna šviesos emisija.

Be to, junginiai **14** (**DB13**), **15** (**DB43**), **16** (**DB24**) ir **17** (**DB34**) buvo pasirinkti kaip OLED matricos dėl jų plačios draustinės juostos ir aukštos E_T. Žalią šviesą skleidžiančiuose OLED prietaisuose buvo panaudotas tiek fosforescuojantis spinduolis Ir(ppy)₃, tiek TADF spinduolis 4CzIPN. Formuotų prietaisų energinių lygių diagramos pavaizduotos 58 pav., o prietaisų struktūra buvo tokia: ITO (125 nm) / PEDOT: PSS (35 nm) / matrica: x m% spinduolio (matrica = **14** (**DB13**), **15** (**DB43**), **16** (**DB24**) ir **17** (**DB34**)) (spinduolis = Ir(ppy)₃ arba 4CzIPN) (x = 5, 10 ir 12,5 (Ir(ppy)₃)), (x = 1, 3 ir 5 % (4CzIPN)) (20 nm)/TPBi (40 nm)/LiF (1 nm)/Al (200) nm).
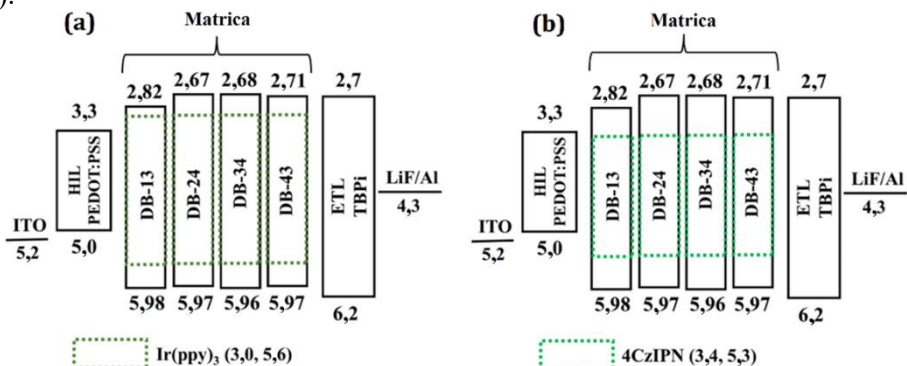
58 pav. Žalią šviesą skleidžiančių, **14** (**DB13**), **15** (**DB43**), **16** (**DB24**) ir **17** (**DB34**) matricas naudojančių OLED energetinių lygių diagramos (eV), naudojant spinduolį (a) Ir(ppy)₃ arba (b) 4CzIPN.

Išbandžius visus naujus junginius žaliai fosforescuojančių šviestukų matricoms, geriausios charakteristikos buvo pasiektos su dariniu **14** (**DB13**). Jį savo struktūroje naudojusių šviestukų efektyvumo rodikliai pateikti 40 lentelėje, iš kurios matyti, kad didžiausias efektyvumas pasiektas prietaiso, savo emisiniame sluoksnyje turėjusio 12,5 m% spinduolio Ir(ppy)₃. Šio prietaiso maksimalus PE buvo 45 lm/W, didžiausias CE – 43 cd/A, o EQE pasiekė 10,6 %. Prietaiso efektyvumas taip pat mažai krito didinant skaistį.

40 lentelė. Prietaisų, naudojančių matricą **14** (**DB13**), legiruotą spinduoliu Ir(ppy)3, charakteristikos

Matrica	Ir(ppy)₃ m%	V_{ON}, V	PE, lm/W	CE, cd/A	EQE, %	$L_{maks.}$, cd/m²
			Maks. / Esant 1000 cd/m²			
14 (**DB13**)	10	2,6	40,0 / 32,1	41,1 / 40,9	11,1 / 11,1	33870
	12,5	3,1	45,4 / 33,4	43,4 / 42,5	10,6 / 10,5	37680
	15	2,5	34,6 / 28,7	35,3 / 33,5	9,5 / 9,4	32300

Naujieji dariniai **14** (**DB13**), **16** (**DB24**) ir **17** (**DB34**) taip pat buvo išbandyti kaip matricos TADF spinduoliui 4CzIPN. Tarp suformuotų prietaisų geriausias charakteristikas demonstravo OLED, turintis 3 m% 4CzIPN spinduolio disperguoto **17** (**DB34**) matricoje. Šio prietaiso PE, CE ir EQE siekė atitinkamai 37,5 lm/W, 33,5 cd/A ir 10,8 %. Detalizuotos prietaisų, naudojančių **17** (**DB34**) matricą, charakteristikos pateiktos 41 lentelėje.

41 lentelė. OLED prietaisų, naudojančių matricą **17** (**DB34**), charakteristikos

Matrica	*4CzIPN* *m*%	V_{ON}, V	*PE*, lm/W	*CE*, cd/A	*EQE*, %	$L_{maks.}$, cd/m²
			Maks. / Esant 1000 cd/m²			
17 (**DB34**)	1	2,7	30,4 / 10,2	27,1 / 14,7	8,9 / 5,0	3782
	3	2,6	37,5 / 15,8	33,5 / 22,6	10,8 / 7,4	9484
	5	2,6	34,7 / 18,9	33,2 / 24,0	10,5 / 7,6	12480

Pagaminto TADF OLED su **17** (**DB34**) matrica EQE viršijo daugelio publikuotų fosforescuojančių OLED prietaisų EQE [212], tačiau PE ir $L_{maks.}$ charakteristikos šiek tiek atsilieka. Tai galima sieti su tripletinių būsenų naikinimo reiškiniu. Susintetintų junginių struktūrų koregavimas, siekiant dar labiau sumažinti ΔE_{ST}, galėtų padėti efektyviau išnaudoti tripletinius eksitonus, o tai gali pagerinti žalią šviesą skleidžiančių TADF OLED veikimą.

5.2.6. Donoro-akceptoriaus-donoro tipo bikarbazolilo-benzfenono medžiagos kaip efektyvūs mėlynai fluorescuojantys organinių šviestukų spinduoliai

Šis skyrius parengtas pagal straipsnį, paskelbtą žurnale *Nanomaterials*, **2024**, 14, 2, *D. Blazevicius, I. Siddiqui, P. Gautam, G. Krucaite, D. Tavgeniene, M. R. Nagar, K. Kumar, S. Banik, J.-H. Jou and S. Grigalevicius* [213].

Šiame darbe buvo susintetinta serija susuktos erdvinės struktūros bikarbazolilbenzfenono medžiagų. Tiksliniai dariniai buvo gauti naudojant trijų pakopų sintezės procedūrą, kaip ir ankstesniame skyriuje, pavaizduotą 11 schemoje.
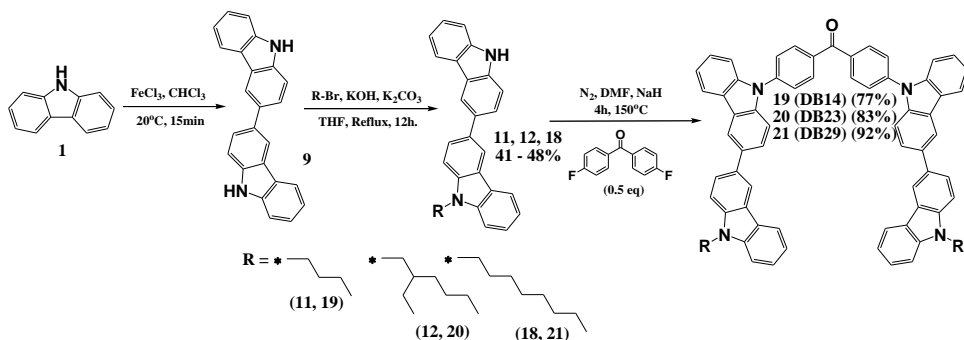
11 schema. Bikarbazolilbenzfenono darinių sintezė

Pirmosios dvi sintezės stadijos, apimančios 3,3'-bikarbazolo (**2**) gavimą oksiduojant 9H-karbazolą (**1**) ir pagaminto 3,3'-bikarbazolo reakciją su alkilbromidais, aprašytos ankstesniame skyriuje. Paskutinėje stadijoje monoalkilpakeistas bikarbazolas reagavo su 4,4′-difluorbenzfenonu DMF tirpale, naudojant natrio hidridą kaip bazę. Gautųjų tikslinių medžiagų teoriškai pateiktos struktūros buvo patvirtintos naudojant MS ir BMR spektroskopiją.

Dariniai **19** (**DB14**), **20** (**DB23**) ir **21** (**DB29**) pasižymėjo aukštomis, 52 % viršijančiomis PLQY vertėmis, o UV-RŠ absorbcijos spektras buvo panaudotas E_g nustatyti, kuris buvo nuo 3,02 eV iki 3,08 eV, o tikslios PLQY ir E_g vertės pateiktos 42 lentelėje. E_S ir E_T vertės buvo nustatytos iš PL ir LTPL spektrų, o fotoliuminescencijos gesimo kinetika tyrinėta TRPL metodu. E_S ir E_T vertės kartu su

fotoliuminescencijos gesimo laiku pateiktos 42 lentelėje. CV matavimai padėjo apskaičiuoti HOMO ir LUMO energines vertes, o terminės naujų medžiagų savybės buvo tyrinėtos TGA ir DSK metodais. TGA tyrimai atskleidė, kad medžiagos pasižymi aukštu terminiu stabilumu, o T_d vertės visoms medžiagoms viršijo 380 ºC. DSK matavimai atskleidė, kad visos tirtos medžiagos yra amorfinės ir pasižymi aukštomis T_g vertėmis. HOMO, LUMO vertės ir terminės medžiagų savybės taip pat apibendrintos 42 lentelėje.

42 lentelė. Optoelektrinės ir terminės medžiagų **19** (**DB14**), **20** (**DB23**) ir **21** (**DB29**) savybės

Medžiaga	T_d (ºC)	T_g (ºC)	E_g, eV	$PLQY$, %	PL gesimas, ns	HOMO, eV	LUMO, eV	E_S, eV	E_T, eV	ΔE_{ST}, eV
19 (**DB14**)	462	145	3,05	55,6	3,40	−5,70	−2,65	3,32	2,83	0,49
20 (**DB23**)	383	104	3,08	52,0	2,67	−5,63	−2,55	3,19	2,84	0,35
21 (**DB29**)	384	95	3,08	55,5	3,57	−5,66	−2,64	3,22	2,73	0,49

Norint įvertinti naujų darinių tinkamumą naudoti spinduoliams, buvo pagaminti OLED prototipai, o jų energinių lygių schema pavaizduota 59 pav.
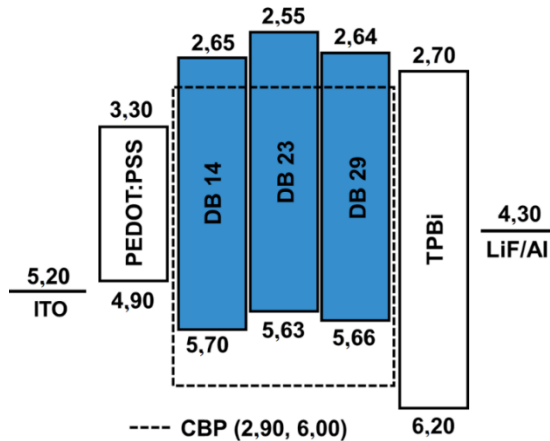
59 pav. Mėlyną šviesą skleidžiančių, **19** (**DB14**), **20** (**DB23**) ir **21** (**DB29**) spinduolius naudojančių OLED energinių lygių diagrama (eV)

Šie prietaisai savo emisiniuose sluoksniuose naudojo spinduolius **19** (**DB14**), **20** (**DB23**) ir **21** (**DB29**), disperguotus CBP matricoje. OLED struktūra buvo ITO/PEDOT:PSS/CBP: spinduolis **19** (**DB14**), **20** (**DB23**) ir **21** (**DB29**) (5, 10, 15 arba 100 m%)/TPBi/LiF/Al. Visų prietaisų skleidžiama emisija buvo apie 470 nm bangos ilgio, kas indikuoja mėlynos spalvos šviesą, o visų šiame tyrime suformuotų OLED prietaisų charakteristikos pateiktos 43 lentelėje.

43 lentelė. OLED prietaisų, naudojančių mėlyną šviesą skleidžiančius fluorescuojančius spinduolius **19** (**DB14**), **20** (**DB23**) ir **21** (**DB29**), charakteristikos

Spinduolis	m%	V_{ON}, V	$PE_{maks.}$, lm/W	$CE_{maks.}$, cd/A	$EQE_{maks.}$, %	CIE (x; y), esant 100 cd/m²	$L_{maks.}$, cd/m²
19 (DB14)	5	5,0	3,9	6,5	2,7	(0,22; 0,36)	2951
	10	5,1	4,4	7,6	3,3	(0,21; 0,33)	3175
	15	5,9	2,4	4,9	2,4	(0,20; 0,28)	1884
	100	6,1	0,4	0,8	0,4	(0,26; 0,40)	515
20 (DB23)	5	5,7	2,1	3,8	2,3	(0,17; 0,07)	883
	10	5,2	1,7	2,6	5,3	(0,19; 0,22)	1620
	15	5,2	3,2	5,3	2,7	(0,20; 0,27)	2076
	100	5,1	1,0	1,8	0,7	(0,26; 0,44)	875
21 (DB29)	5	5,4	2,1	3,9	2,3	(0,19; 0,22)	1578
	10	5,7	4,4	6,5	3,1	(0,20; 0,27)	2251
	15	4,7	7,9	9,1	4,0	(0,21; 0,31)	2631
	100	4,8	1,4	1,8	0,7	(0,26; 0,44)	884

OLED prietaisas, savo emisiniame sluoksnyje naudojęs 10 m% spinduolio **20** (**DB23**) pasiekė aukščiausią EQE šiame tyrime, kuris siekė 5,3 %, o tai net šiek tiek viršija teorinį fluorescuojančių spinduolių efektyvumo limitą [54].

Šis aukštesnis efektyvumas greičiausiai atsiranda dėl ilgų, šakotų alkilo šoninių grandinėlių molekulėje, padidinančių medžiagos tirpumą ir pagerinančių sluoksnių formavimo savybes. Nors **20** (**DB23**) prietaisas pademonstravo didžiausią EQE, OLED, naudojęs **21** (**DB29**) spinduolį, pranoko kitus pagal PE ir CE – atitinkamai 7,9 lm/W ir 9,1 cd/A. Šis pranašumas gali būti siejamas su optimaliais HOMO ir LUMO lygiais, palengvinančiais efektyvų energijos perdavimą iš matricos spinduoliui. Be to, įtraukus du bikarbazolilo elektronų donoro fragmentus, buvo subalansuota krūvio pernaša, dar labiau pagerinant gautų prietaisų efektyvumą.

5.2.7. Donoro-akceptoriaus tipo bikarbazolilo-benzfenono junginiai kaip potencialūs mėlyną šviesą skleidžiantys TADF spinduoliai

Šis skyrius parengtas pagal straipsnį, paskelbtą žurnale *Molecules*, 2024, 29, 7, *I. Siddiqui, P. Gautam, D. Blazevicius, J. Jayakumar, S. Lenka, D. Tavgeniene, E. Zaleckas, S.Grigalevicius and J.-H. Jou* [214].

Šioje tyrimų stadijoje buvo susintetinti nauji elektroaktyvūs junginiai, turintys benzfenono elektronų akceptorių, prijungtą prie bikarbazolilo elektronų donorinio fragmento. Naujieji dariniai buvo susintetinti trijų pakopų sintezės, pavaizduotos 12 schemoje, metu. Iš pradžių 9*H*,9′*H*-3,3′-bikarbazolas (**2**) gautas 9*H*-karbazolą oksidavus geležies (III) chloridu. Toliau gautasis bikarbazolas reagavo su įvairiais alkilbromidais THF tirpale, siekiant išgauti tarpines monopakeistas medžiagas (9-alkil-9'*H*-3,3′-bikarbazolus) **3**-**8**. Paskutinė reakcijos stadija buvo junginių **3**-**8** nukleofilinio pakeitimo reakcija su 4-fluorbenzfenonu DMSO tirpale, naudojant kalio karbonatą kaip bazę, taip gaunant tikslinius darinius **24** (**DB37**), **25** (**DB38**), **26 DB39**), **27** (**DB40**), **28** (**DB41**) ir **29** (**DB44**). MS ir BMR tyrimai patvirtino visų medžiagų struktūras. Susintetintuose junginiuose esančios įvairaus ilgio alifatinės

grandinėlės padidino tirpumą įprastuose organiniuose tirpikliuose ir atvėrė kelią ekonomiškam OLED formavimui iš tirpalų.
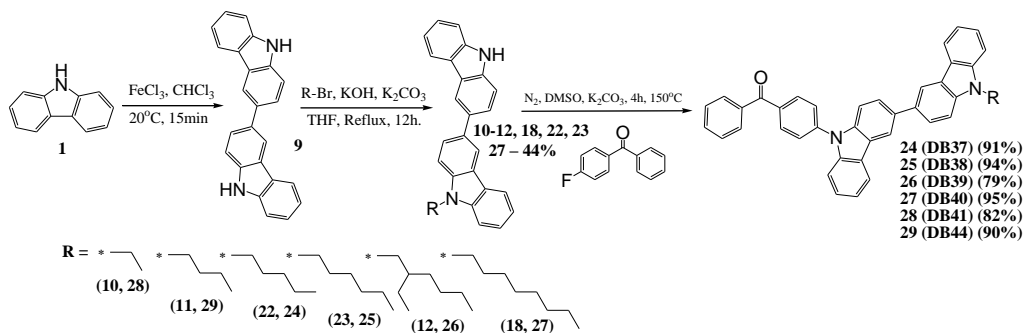
12 schema. D-A struktūros bikarbazolilo junginių sintezė

Terminės ir morfologinės medžiagų **24** (**DB37**), **25** (**DB38**), **26** (**DB39**), **27** (**DB40**), **28** (**DB41**) ir **29** (**DB44**) savybės buvo tiriamos DSK ir TGA metodais, bandinius kaitinant 10 °C/min greičiu azoto aplinkoje. Buvo pastebėta, kad visi tiksliniai junginiai pasižymi aukštomis destrukcijos temperatūromis, viršijančiomis 370 °C. DSK tyrimų antrojo kaitinimo darinių **24** (**DB37**), **25** (**DB38**), **26** (**DB39**), **27** (**DB40**), **28** (**DB41**) ir **29** (**DB44**) termogramos pavaizduotos 60 pav.
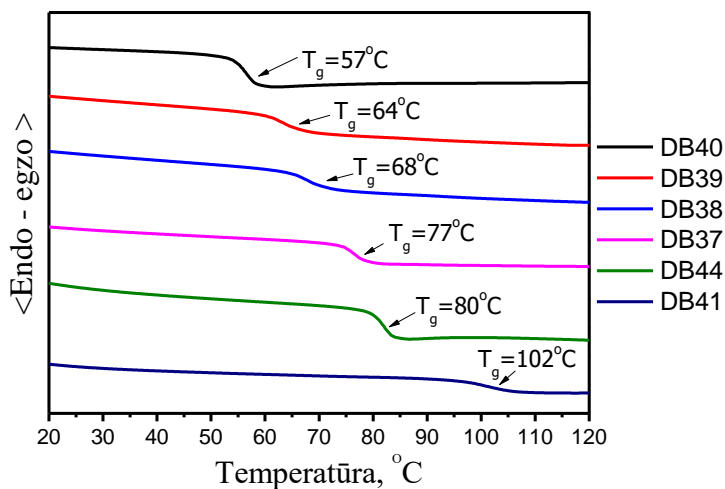
60 pav. Darinių **24** (**DB37**), **25** (**DB38**), **26** (**DB39**), **27** (**DB40**), **28** (**DB41**) ir **29** (**DB44**) antrojo DSK kaitinimo kreivės

Rezultatai rodo, kad medžiagų stiklėjimo temperatūra tiesiogiai priklauso nuo alifatinės grandinėlės ilgio. Pavyzdžiui, trumpiausią etilgrandinėlę turėjęs darinys **28** (**DB41**) pasižymėjo aukščiausia 102 °C siekiančia T_g, kuri mažėjo ilgėjant alifatinei grandinėlei, o ilgiausią oktilgrandinėlę turėjęs darinys pasižymėjo žemiausia T_g, siekiančia 57 °C. Terminės medžiagų savybės pateiktos 44 lentelėje.

Naujos medžiagos PLQY vertės buvo gana nemažos – siekė nuo 45,3 % iki 75,5 %. Visos PLQY vertės pateiktos 44 lentelėje. Tyrinėjant medžiagų UV-RŠ

112

absorbciją, buvo pastebėta, kad visi junginiai demonstruoja du absorbcijos pikus esant 380 nm ir 410 nm. Šio tyrimo duomenys buvo panaudoti nustatant junginių E_g vertes, kurios svyravo nuo 3,07 eV iki 3,10 eV. CV matavimai buvo atlikti siekiant nustatyti HOMO ir LUMO energinius lygmenis, kurie kartu su E_g vertėmis pateikti 44 lentelėje. HOMO ir LUMO vertės buvo tinkamos siekiant junginius pritaikyti kaip spinduolius mėlyną šviesą skleidžiančiuose OLED, emisiniame sluoksnyje kartu naudojant matricą CBP. Darinių PL spektrai buvo užrašyti siekiant nustatyti E_S vertes, naudojant absorbcijos ir PL linijų susikirtimo tašką. E_T vertės dariniams buvo nustatomos naudojant LTPL spektrą ir pirmojo piko liestinės ir x ašies sankirtos tašką. Medžiagų **24** (**DB37**), **2** (**DB38**), **26** (**DB39**), **27** (**DB40**), **28** (**DB41**) ir **29** (**DB44**) E_S ir E_T vertės pateiktos 44 lentelėje. Su visais junginiais taip pat buvo atlikti ir TRPL eksperimentai, siekiant nustatyti fotoliuminescencijos gesimo trukmes, kurios siekė nuo 1,88 ns iki 6,28 ns, o tikslios vertės nurodytos 44 lentelėje.

44 lentelė. Optoelektroninės ir terminės medžiagų **24** (**DB37**), **25** (**DB38**), **26** (**DB39**), **27** (**DB40**), **28** (**DB41**) ir **29** (**DB44**) savybės

Spinduolis	T_d, ℃	T_g, ℃	E_g, eV	$PLQY$, %	PL gesimas, ns	HOMO, eV	LUMO, eV	E_S, eV	E_T, eV	ΔE_{ST}, eV
24 (**DB37**)	406	77	3,09	65,5	5,53	−5,67	−2,58	3,04	2,76	0,28
25 (**DB38**)	398	68	3,09	45,3	1,88	−5,70	−2,61	2,94	2,89	0,05
26 (**DB39**)	383	64	3,08	75,5	4,27	−5,68	−2,60	3,10	2,81	0,29
27 (**DB40**)	397	57	3,10	52,5	2,41	−5,69	−2,59	3,06	2,80	0,26
28 (**DB41**)	374	102	3,09	62,5	2,24	−5,73	−2,64	3,22	2,80	0,42
29 (**DB44**)	389	80	3,07	68,5	6,28	−5,69	−2,62	3,18	2,82	0,15

Atsižvelgiant į naujų benzfenono darinių savybes, buvo nuspręsta įvertinti jų kaip spinduolių veikimą paprastos struktūros, iš tirpalų suformuotose OLED, kurių emisiniai sluoksniai suformuoti iš spinduolių **24** (**DB37**), **25** (**DB38**), **26** (**DB39**), **27** (**DB40**), **28** (**DB41**) ar **29** (**DB44**), disperguotų CBP matricoje. Prietaisų energinių lygių diagrama pavaizduota 61 pav., o prietaisų, naudojančių efektyviausią spinduolį šiame darbe **26** (**DB39**), charakteristikos pateiktos 45 lentelėje.
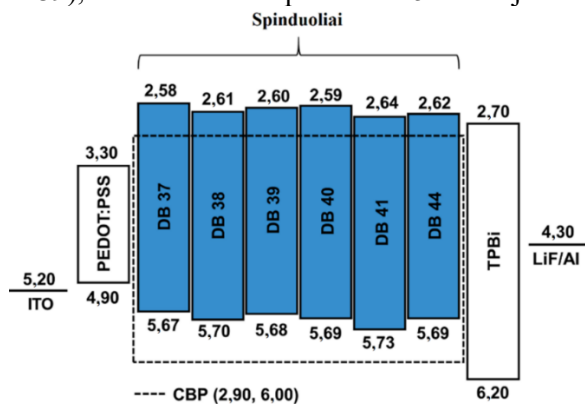
61 pav. Mėlyną šviesą skleidžiančių, **24** (**DB37**), **25** (**DB38**), **26** (**DB39**), **27** (**DB40**), **28** (**DB41**) ar **29** (**DB44**) spinduolius naudojančių OLED sluoksnių energinių lygių diagrama (eV)

Prietaisų struktūras sudaro 125 nm ITO anodo sluoksnis, 35 nm PEDOT: PSS skylių injekcijos sluoksnis, 30 nm emisinis sluoksnis, susidedantis iš CBP matricoje disperguotų spinduolių (5 m%, 10 m%, 15 m% ir 100 m%). Elektronų pernašos sluoksniui buvo naudojamas TPBi (32 nm), ličio fluoridas (0,8 nm) buvo naudojamas kaip elektronų injekcijos sluoksnis, o aliuminis (150 nm) – kaip katodas.

45 lentelė. Prietaisų, savo emisiniame sluoksnyje naudojančių spinduolį **26** (**DB39**), charakteristikos

Spinduo lis	wt, %	V_{ON}, V	$PE_{maks.}$, lm/W	$CE_{maks.}$, cd/A	$EQE_{maks.}$, %	CIE (x, y), esant 100 cd/m^2	$L_{maks.}$, cd/m^2
26 (**DB39**)	5	4,0	3,3	3,7	2,1	(0,18, 0,20)	2818
	10	3,5	4,4	4,9	2,2	(0,18, 0,23)	3430
	15	3,9	4,1	5,7	2,7	(0,19, 0,27)	3581
	100	3,4	0,3	0,4	0,4	(0,24, 0,39)	615

OLED, suformuoti su spinduoliu **26** (**DB39**), parodė geriausias savybes tarp šioje stadijoje pagamintų prietaisų. Šios geresnės charakteristikos gali būti siejamos su ilgos ir šakotos 2-etilheksil alifatinės grandinėlės buvimu medžiagos struktūroje, potencialiai pagerinant junginio tirpumą ir sluoksnių formavimo savybes iš tirpalų liejamiems OLED [217]. Be to, tinkami HOMO ir LUMO lygiai palengvina efektyvų energijos perdavimą iš matricos spinduoliui, o elektronų akceptoriaus benzfenono fragmento ir bikarbazolilo elektronų donoro fragmento derinys subalansuoja krūvio pernašą ir efektyvų eksitonų naudojimą [218,219]. Prietaisas, kurio emisiniame sluoksnyje buvo 10 m% spinduolio **26** (**DB39**), demonstravo didžiausią PE – 4,4 lm/W, bet geriausias bendras efektyvumas buvo pasiektas, kai prietaiso emisiniame sluoksnyje buvo 15 m% spinduolio **26** (**DB39**). Šio prietaiso PE, CE ir EQE pasiekė atitinkamai 4,1 lm/W, 5,7 cd/A ir 2,7 %. Šis tyrimas parodė benzfenono ir bikarbazolilo fragmentų potencialą organinių puslaidininkių sintezėje ir atskleidė, kaip galima kontroliuoti termines bei sluoksnių formavimo savybes naudojant ir modifikuojant alifatines grandinėles naujų junginių struktūroje.

5.3. Išvados

Šioje disertacijoje pateikti rezultatai parodo kelis galimus OLED technologijos tobulinimo būdus. Darbe pristatomos naujos struktūros medžiagos, taikomos efektyvių OLED matricoms ir spinduoliams, pavyzdžiui:

1. Susintetintos ir charakterizuotos naujos medžiagos, turinčios oksetano, karbazolo ir metoksipiridino fragmentus. Įrodyta, kad naujieji dariniai gali būti pritaikomi kaip efektyvios PhOLED matricos. Geriausias mėlyną šviesą skleidžiantis prietaisas demonstravo 10,3 % išorinį kvantinį efektyvumą, o našiausias žalią šviesą skleidžiantis prietaisas parodė 9,4 % išorinį kvantinį efektyvumą.

2. Karbazolu ar fenoksazinu pakeisti mažamolekuliai oksetano dariniai buvo susintetinti paprastos, vienos stadijos sintezės metu. Naujų medžiagų savybių tyrimai parodė, kad jos yra tinkamos geltoną šviesą skleidžiančių PhOLED matricoms, o efektyviausias prietaisas pasiekė 10,9 % išorinį kvantinį efektyvumą.

3. Anksčiau susintetinta fenoksazino ir oksetano fragmentus turinti medžiaga buvo išbandyta kuriant žvakės šviesos OLED. Įrodytas aukštas medžiagos

efektyvumas ją pritaikius kaip matricą – tikslinis prietaisas pasiekė 10,2 % išorinį kvantinį efektyvumą, 1690 K spalvinę temperatūrą ir rekordinę didžiausią leidžiamąją poveikio ribą, siekiančią 57 696 s, šiomis charakteristikomis lenkiant komercinę matricą CBP naudojusį prietaisą.

4. Apžvelgus naujausią elektroaktyvių benzfenono darinių pažangą įrodyta, kad benzfenono fragmentas turi didelį potencialą kuriant efektyvias matricas ir spinduolius OLED technologijai.

5. Susintetinti ir charakterizuoti bikarbazolilo-difenilsulfono dariniai, pasižymintys susukta donoro-akceptoriaus-donoro struktūra. Šių medžiagų daugiafunkciškumas buvo įrodytas juos iš pradžių pritaikant giliai mėlyną šviesą skleidžiantiems spinduoliams, suformuojant 4,0 % išorinį kvantinį efektyvumą pasiekusį prietaisą. Šios medžiagos taip pat parodė gerus rezultatus jas išbandžius žalią šviesą skleidžiančių fosforescuojančių ir TADF OLED matricoms, o efektyviausi prietaisai pasiekė atitinkamai 10,6 % ir 10,8 % siekiantį išorinį kvantinį efektyvumą.

6. Susintetinta ir charakterizuota grupė susuktos donoro-akceptoriaus-donoro struktūros junginių, naudojant bikarbazolą kaip elektronų donorą ir benzfenoną kaip elektronų akceptorių. Nustatyta, kad šios medžiagos yra ypač efektyvūs mėlyną šviesą skleidžiantys fluorescuojantys spinduoliai. Našiausias OLED pasiekė 5,3 % išorinį kvantinį efektyvumą, o tokia vertė yra apylygė teoriniam fluorescuojančių OLED efektyvumo limitui.

7. Susintetinta ir charakterizuota serija elektroaktyvių bipolinių donoro-akceptoriaus struktūros darinių, pasitelkiant benzfenoną ir bikarbazolą kaip pagrindinius fragmentus. Tyrimai parodė, kad naujieji dariniai yra tinkami juos pritaikyti kaip mėlyną šviesą skleidžiančius fluorescuojančius spinduolius, o efektyviausias OLED šiame tyrime rodė 2,7 % išorinį kvantinį efektyvumą.

Pasiekti rezultatai įrodo didelį fenoksazino ir karbazolo medžiagų potencialą didinant OLED prietaisų efektyvumą. Tyrimai apėmė daug žadančias medžiagas, skirtas PhOLED matricoms, kai kurios iš jų susintetintos taikant paprastą vienos stadijos sintezę, potencialiai atveriant kelią didesnės apimties geltoną ar žvakės šviesą skleidžiančių OLED matricų sintezei. Be to, bikarbazolo dariniai parodė aukštą efektyvumą tiek kaip mėlynai fluorescuojantys spinduoliai, tiek kaip žalią šviesą skleidžiančių OLED matricos. Tyrimai taip pat pabrėžė alifatinių grandinėlių vaidmenį optimizuojant sluoksnių formavimo savybes ir darinių tirpumą. Nepaisant pasiektų rezultatų, OLED efektyvumą būtų galima dar labiau pagerinti optimizuojant prietaisų struktūras ir sluoksnių storius, taip pat mažinant bikarbazolo darinių ΔE_{ST} struktūrinių pakeitimų metu, siekiant efektyviau panaudoti tripletinius eksitonus.

REFERENCES

1.   International Energy Agency *Electricity Information: Overview*; Paris, 2021;
2.   SADEGHIAN, O. et al. Unveiling the Potential of Renewable Energy and Battery Utilization in Real-World Public Lighting Systems: A Review. *Renewable and Sustainable Energy Reviews* [interactive]. 2024, *192*, 114241. Access via: doi:10.1016/j.rser.2023.114241.
3.   SADEGHIAN, O. et al. A Comprehensive Review on Energy Saving Options and Saving Potential in Low Voltage Electricity Distribution Networks: Building and Public Lighting. *Sustain Cities Soc* [interactive]. 2021, *72*, 103064. Access via: doi:10.1016/j.scs.2021.103064.
4.   TANG, C.W. and VANSLYKE, S.A. Organic Electroluminescent Diodes. *Appl Phys Lett* [interactive]. 1987, *51*, 913–915. Access via: doi:10.1063/1.98799.
5.   YANG, X. and DING, L. Organic Semiconductors: Commercialization and Market. *Journal of Semiconductors* [interactive]. 2021, *42*, 090201. Access via: doi:10.1088/1674-4926/42/9/090201.
6.   SU, N. et al. High Efficiency Electroluminescence of Orange-Red Iridium(III) Complexes for OLEDs with an EQE over 30%. *Dyes and Pigments* [interactive]. 2021, *195*, 109733. Access via doi:10.1016/j.dyepig.2021.109733.
7.   SHARMA, A. et al. Highly Efficient OLED Device Based on the Double Emissive Layer with an EQE about 39%. *Optik (Stuttg)* [interactive]. 2020, *221*, 165350. Access via: doi:10.1016/j.ijleo.2020.165350.
8.   KISHORE KESEVAN, K. et al. Achieving a 32% EQE Solution-Processed Simple Structure OLED via Exciplex System. *Chemical Engineering Journal* [interactive]. 2022, *435*, 134879. Access via: doi:10.1016/j.cej.2022.134879.
9.   CHEN, C.-H. et al. New Bipolar Host Materials for High Power Efficiency Green Thermally Activated Delayed Fluorescence OLEDs. *Chemical Engineering Journal* [interactive]. 2022, *442*, 136292. Access via: doi:10.1016/j.cej.2022.136292.
10. KUMAR, A. et al. Triarylboron-Based TADF Emitters with Perfluoro Substituents: High-Efficiency OLEDs with a Power Efficiency over 100 Lm W^{-1}. *J Mater Chem C Mater* [interactive]. 2020, *8*, 4253–4263. Access via: doi:10.1039/C9TC06204A.
11. HUANG, C. et al. Hybrid Tandem White OLED with Long Lifetime and 150 Lm W^{-1} in Luminous Efficacy Based on TADF Blue Emitter Stabilized with Phosphorescent Red Emitter. *Adv Opt Mater* [interactive]. 2020, *8*. Access via: doi:10.1002/adom.202000727.
12. SIDDIQUI, I. et al. Status and Challenges of Blue OLEDs: A Review. *Nanomaterials* [interactive]. 2023, *13*, 2521. Access via: doi:10.3390/nano13182521.
13. YANG, X. et al. Strategically Formulating Aggregation-Induced Emission-Active Phosphorescent Emitters by Restricting the Coordination Skeletal Deformation of Pt(II) Complexes Containing Two Independent Monodentate

Ligands. *Adv Opt Mater* [interactive]. 2020, *8*. Access via: doi:10.1002/adom.202000079.

14. RAJAMALLI, P. et al. New Molecular Design Concurrently Providing Superior Pure Blue, Thermally Activated Delayed Fluorescence and Optical Out-Coupling Efficiencies. *J Am Chem Soc* [interactive]. 2017, *139*, 10948–10951. Access via: doi:10.1021/jacs.7b03848.

15. MURAWSKI, C. et al. Efficiency Roll-Off in Organic Light-Emitting Diodes. *Advanced Materials* [interactive]. 2013, *25*, 6801–6827. Access via: doi:10.1002/adma.201301603.

16. REINEKE, S. et al. Triplet-Exciton Quenching in Organic Phosphorescent Light-Emitting Diodes with Ir-Based Emitters. *Phys Rev B* [interactive]. 2007, *75*, 125328. Access via: doi:10.1103/PhysRevB.75.125328.

17. LIGTHART, A. et al. Effect of Triplet Confinement on Triplet–Triplet Annihilation in Organic Phosphorescent Host–Guest Systems. *Adv Funct Mater* [interactive]. 2018, *28*. Access via: doi:10.1002/adfm.201804618.

18. BALDO, M.A. et al. Transient Analysis of Organic Electrophosphorescence. II. Transient Analysis of Triplet-Triplet Annihilation. *Phys Rev B* [interactive]. 2000, *62*, 10967–10977. Access via: doi:10.1103/PhysRevB.62.10967.

19. WANG, Z. et al. Structure–Performance Investigation of Thioxanthone Derivatives for Developing Color Tunable Highly Efficient Thermally Activated Delayed Fluorescence Emitters. *ACS Appl Mater Interfaces* [interactive]. 2016, *8*, 8627–8636. Access via: doi:10.1021/acsami.5b12559.

20. IM, Y. et al. Molecular Design Strategy of Organic Thermally Activated Delayed Fluorescence Emitters. *Chemistry of Materials* [interactive]. 2017, *29*, 1946–1963. Access via: doi:10.1021/acs.chemmater.6b05324.

21. CAI, X. et al. "Rate-Limited Effect" of Reverse Intersystem Crossing Process: The Key for Tuning Thermally Activated Delayed Fluorescence Lifetime and Efficiency Roll-off of Organic Light Emitting Diodes. *Chem Sci* [interactive]. 2016, *7*, 4264–4275. Access via: doi:10.1039/C6SC00542J.

22. SALEHI, A. et al. Recent Advances in OLED Optical Design. *Adv Funct Mater* [interactive]. 2019, *29*. Access via: doi:10.1002/adfm.201808803.

23. LI, L. et al. Blue Organic Light Emitting Diode Materials Based on Different Light-Emitting Groups. *Curr Org Chem* [interactive]. 2023, *27*, 352–362. Access via: doi:10.2174/1385272827666230413083558.

24. WU, H. et al. Progress and Perspective of Polymer White Light-Emitting Devices and Materials. *Chem Soc Rev* [interactive]. 2009, *38*, 3391. Access via: doi:10.1039/b816352a.

25. YERSIN, H. *Highly Efficient OLEDs with Phosphorescent Materials*; John Wiley & Sons, 2008;

26. CHEN, J. et al. Red/Near-Infrared Thermally Activated Delayed Fluorescence OLEDs with Near 100 % Internal Quantum Efficiency. *Angewandte Chemie International Edition* [interactive]. 2019, *58*, 14660–14665. Access via: doi:10.1002/anie.201906575.

27. ALBRECHT, K. et al. Carbazole Dendrimers as Solution-Processable Thermally Activated Delayed-Fluorescence Materials. *Angewandte Chemie International Edition* [interactive]. 2015, *54*, 5677–5682. Access via: doi:10.1002/anie.201500203.

28. ZHANG, Q. et al. Design of Efficient Thermally Activated Delayed Fluorescence Materials for Pure Blue Organic Light Emitting Diodes. *J Am Chem Soc* [interactive]. 2012, *134*, 14706–14709. Access via: doi:10.1021/ja306538w.

29. WU, K. et al. De Novo Design of Excited-State Intramolecular Proton Transfer Emitters via a Thermally Activated Delayed Fluorescence Channel. *J Am Chem Soc* [interactive]. 2018, *140*, 8877–8886. Access via: doi:10.1021/jacs.8b04795.

30. GOUSHI, K. et al. Organic Light-Emitting Diodes Employing Efficient Reverse Intersystem Crossing for Triplet-to-Singlet State Conversion. *Nat Photonics* [interactive]. 2012, *6*, 253–258. Access via: doi:10.1038/nphoton.2012.31.

31. AHN, D.H. et al. Highly Efficient Blue Thermally Activated Delayed Fluorescence Emitters Based on Symmetrical and Rigid Oxygen-Bridged Boron Acceptors. *Nat Photonics* [interactive]. 2019, *13*, 540–546. Access via: doi:10.1038/s41566-019-0415-5.

32. UOYAMA, H. et al. Highly Efficient Organic Light-Emitting Diodes from Delayed Fluorescence. *Nature* [interactive]. 2012, *492*, 234–238. Access via: doi:10.1038/nature11687.

33. XU, H. et al. Recent Progress in Metal–Organic Complexes for Optoelectronic Applications. *Chem. Soc. Rev.* [interactive]. 2014, *43*, 3259–3302. Access via: doi:10.1039/C3CS60449G.

34. DU, C. et al. Rational Molecular Design of Phenanthroimidazole-Based Fluorescent Materials towards High-Efficiency Non-Doped Deep Blue OLEDs. *J. Mater. Chem. C.* [interactive]. 2022, *10*, 14186–14193. Access via: doi:10.1039/D2TC02329F.

35. WANG, Z. et al. Anthracene and Carbazole Based Asymmetric Fluorescent Materials for High-Efficiency Deep-Blue Non-Doped Organic Light Emitting Devices with CIEy=0.06. *Dyes and Pigments* [interactive]. 2022, *199*, 110047. Access via: doi:10.1016/j.dyepig.2021.110047.

36. XING, L. et al. Anthracene-Based Fluorescent Emitters toward Superior-Efficiency Nondoped TTA-OLEDs with Deep Blue Emission and Low Efficiency Roll-Off. *Chemical Engineering Journal* [interactive]. 2021, *421*, 127748. Access via: doi:10.1016/j.cej.2020.127748.

37. HELFRICH, W. et al. Recombination Radiation in Anthracene Crystals. *Phys Rev Lett* [interactive]. 1965, *14*, 229–231. Access via: doi:10.1103/PhysRevLett.14.229.

38. HAYASHI, S. et al. Electroluminescence of Perylene Films with a Conducting Polymer as an Anode. *Jpn J Appl Phys* [interactive]. 1986, *25*, L773. Access via: doi:10.1143/JJAP.25.L773.

39. ADACHI, C. et al. Electroluminescence in Organic Films with Three-Layer Structure. *Jpn J Appl Phys* [interactive]. 1988, *27*, L269. Access via: doi:10.1143/JJAP.27.L269.

40. JI, Y. et al. Improved Performance and Low Cost OLED Microdisplay with Titanium Nitride Anode. *Org Electron* [interactive]. 2014, *15*, 3137–3143. Access via: doi:10.1016/j.orgel.2014.09.001.

41. KIM, S.K. et al. Patternization of Cathode Metal Using Low Surface Energy Organic Molecules in OLED Thermal Evaporation Process. *Journal of Industrial and Engineering Chemistry* [interactive]. 2022, *114*, 213–220. Access via: doi:10.1016/j.jiec.2022.07.011.

42. SONG, M.-G. et al. Highly Reliable and Transparent Al Doped Ag Cathode Fabricated Using Thermal Evaporation for Transparent OLED Applications. *Org Electron* 2020, *76*, 105418. Access via: doi:10.1016/j.orgel.2019.105418.

43. WONG, W.-Y. et al. Functional Metallophosphors for Effective Charge Carrier Injection/Transport: New Robust OLED Materials with Emerging Applications. *J Mater Chem* [interactive]. 2009, *19*, 4457. Access via: doi:10.1039/b819943d.

44. TSAI, M.-J. et al. Solution-Processed High Efficiency OLED Harnessing a Thermally Cross-Linked Hole-Transporting Layer and Exciplex-Forming Emission Layer. *J Mater Chem C Mater* [interactive]. 2023, *11*, 1056–1066. Access via: doi:10.1039/D2TC04638E.

45. KUMAR, K. et al. Decorated Pyridine as Hole Transporting Material (HTM) for Solution-Processed OLEDs. *J Photochem Photobiol A Chem* [interactive]. 2023, *437*, 114380. Access via: doi:10.1016/j.jphotochem.2022.114380.

46. SHAHNAWAZ, S. et al. Hole-Transporting Materials for Organic Light-Emitting Diodes: An Overview. *J Mater Chem C Mater* [interactive]. 2019, *7*, 7144–7158. Access via: doi:10.1039/C9TC01712G.

47. GUO, X. at al. A High Thermal Stability Terpyridine Derivative as the Electron Transporter for Long-Lived Green Phosphorescent OLED. *Org Electron* [interactive]. 2021, *89*, 106048. Access via: doi:10.1016/j.orgel.2020.106048.

48. JAYAKUMAR, J. et al. Highly Thermal Stable Electron-Transporting Materials Using Triptycene Derivatives for OLEDs. *Org Electron* [interactive]. 2021, *88*, 106013. Access via: doi:10.1016/j.orgel.2020.106013.

49. ZHANG, Z. et al. Intermolecular Hydrogen Bond and π-π Stacking Improve Electron Mobility of Phenanthroline-Based Electron-Transporting Materials. *Comput Theor Chem* [interactive]. 2022, *1217*, 113865. Access via: doi:10.1016/j.comptc.2022.113865.

50. PARK, S. et al. New Electron-Transporting Materials Based on Pyrimidine and Thiazolopyridine Moieties for High-Efficiency Organic Light-Emitting Diodes. *physica status solidi (a)* [interactive]. 2024. Access via: doi:10.1002/pssa.202300889.

51. CHEN, L.-L. et al. Molecular Engineering of an Electron-Transport Triarylphosphine Oxide-Triazine Conjugate toward High-Performance Phosphorescent Organic Light-Emitting Diodes with Remarkable Stability. *Sci*

China Chem [interactive]. 2020, *63*, 904–910. Access via: doi:10.1007/s11426-020-9714-0.

52. KUMAR, P. et al. Highly-Efficient OLED with Cesium Fluoride Electron Injection Layer. *Solid State Electron* [interactive]. 2021, *183*, 108031. Access via: doi:10.1016/j.sse.2021.108031.

53. HONG, G. et al. Brief History of OLEDs—Emitter Development and Industry Milestones. *Advanced Materials* [interactive]. 2021, *33*. Access via: doi:10.1002/adma.202005630.

54. LEE, J.-H. et al. Blue Organic Light-Emitting Diodes: Current Status, Challenges, and Future Outlook. *J Mater Chem C Mater* [interactive]. 2019, *7*, 5874–5888. Access via: doi:10.1039/C9TC00204A.

55. ZHU, M. et al. Blue Fluorescent Emitters: Design Tactics and Applications in Organic Light-Emitting Diodes. *Chem Soc Rev* [interactive]. 2013, *42*, 4963. Access via: doi:10.1039/c3cs35440g.

56. KONDAKOV, D.Y. et al. Triplet Annihilation Exceeding Spin Statistical Limit in Highly Efficient Fluorescent Organic Light-Emitting Diodes. *J Appl Phys* [interactive]. 2009, *106*. Access via: doi:10.1063/1.3273407.

57. YE, S. et al. Asymmetric Anthracene Derivatives as Multifunctional Electronic Materials for Constructing Simplified and Efficient Non-Doped Homogeneous Deep Blue Fluorescent OLEDs. *Chemical Engineering Journal* [interactive]. 2020, *393*, 124694. Access via: doi:10.1016/j.cej.2020.124694.

58. XING, L. et al. Anthracene-Based Fluorescent Emitters toward Superior-Efficiency Nondoped TTA-OLEDs with Deep Blue Emission and Low Efficiency Roll-Off. *Chemical Engineering Journal* [interactive]. 2021, *421*, 127748. Access via: doi:10.1016/j.cej.2020.127748.

59. WANG, Z. et al. Efficient and Stable Non-Doped Deep-Blue Organic Light Emitting Diode Based on an Anthracene Derivative. *Sci China Chem* [intertactive]. 2011, *54*, 666–670. Access via: doi:10.1007/s11426-011-4243-9.

60. USMAN, K. et al. Fluorescent Pyrene-Imidazole Material for Deep-Blue Organic Light-Emitting Devices. *Opt Mater (Amst)* [interactive]. 2021, *121*, 111582. Access via: doi:10.1016/j.optmat.2021.111582.

61. ZENG, J. et al. Y-Shaped Pyrene-Based Aggregation-Induced Emission Blue Emitters for High-Performance OLED Devices. *Adv Opt Mater* [interactive]. 2022, *10*. Access via: doi:10.1002/adom.202200917.

62. KUMAR, D. et al. Pyrenoimidazole-Based Deep-Blue-Emitting Materials: Optical, Electrochemical, and Electroluminescent Characteristics. *Chem Asian J* [interactive]. 2013, *8*, 2111–2124. Access via: doi:10.1002/asia.201300271.

63. JUNG, H. et al. High Efficiency and Long Lifetime of a Fluorescent Blue-Light Emitter Made of a Pyrene Core and Optimized Side Groups. *ACS Appl Mater Interfaces* [interactive]. 2018, *10*, 30022–30028. Access via: doi:10.1021/acsami.8b09013.

64. WANG, J. et al. Simple A–D–A Pure Blue Fluorescent Emitters Based on Hybridized Local and Charge-Transfer Excited State for Non-Doped OLEDs with Narrow Full Width at Half-Maximum of 0.20 EV and CIEy<0.06. *Dyes*

and Pigments [interactive]. 2023, *219*, 111586. Access via: doi:10.1016/j.dyepig.2023.111586.

65. LIU, B. et al. Productive Harvesting of Triplet Excitons in Anthracene-Based Emitters toward High-Performance Deep-Blue Nondoped Organic Light-Emitting Diodes. *Mater Today Chem* [interactive]. 2022, *23*, 100630. Access via: doi:10.1016/j.mtchem.2021.100630.

66. LEE, J. et al. *Nat Commun* [interactive]. 2017, *8*, 15566. Access via: doi:10.1038/ncomms15566.

67. CHEN, W.-C. et al. Achieving Efficient Violet-Blue Electroluminescence with CIE_y>0.06 and EQE>6% from Naphthyl-Linked Phenanthroimidazole–Carbazole Hybrid Fluorophores. *Chem Sci* [interactive]. 2017, *8*, 3599–3608. Access via: doi:10.1039/C6SC05619A.

68. BALDO, M.A. et al. Highly Efficient Phosphorescent Emission from Organic Electroluminescent Devices. *Nature* [interactive]. 1998, *395*, 151–154. Access via: doi:10.1038/25954.

69. BALDO, M.A. et al. Very High-Efficiency Green Organic Light-Emitting Devices Based on Electrophosphorescence. *Appl Phys Lett* [interactive]. 1999, *75*, 4–6. Access via: doi:10.1063/1.124258.

70. SUN, Y. et al. Management of Singlet and Triplet Excitons for Efficient White Organic Light-Emitting Devices. *Nature* [interactive]. 2006, *440*, 908–912. Access via: doi:10.1038/nature04645.

71. TAO, Y. et al. Organic Host Materials for Phosphorescent Organic Light-Emitting Diodes. *Chem Soc Rev* [interactive]. 2011, *40*, 2943. Access via: doi:10.1039/c0cs00160k.

72. KAPPAUN, S. et al. Phosphorescent Organic Light-Emitting Devices: Working Principle and Iridium Based Emitter Materials. *Int J Mol Sci* [interactive]. 2008, *9*, 1527–1547. Access via: doi:10.3390/ijms9081527.

73. CHEN, T.-H. et al. Flexible Candlelight Organic LED on Mica. *ACS Appl Electron Mater* [interactive]. 2022, *4*, 2298–2305. Access via: doi:10.1021/acsaelm.2c00123.

74. KONG, F. et al. Pure Hydrocarbon Materials as Highly Efficient Host for White Phosphorescent Organic Light-Emitting Diodes: A New Molecular Design Approach. *Angewandte Chemie International Edition* [interactive]. 2022, *61*. Access via: doi:10.1002/anie.202207204.

75. CAO, L. et al. Efficient and Stable Organic Light-Emitting Devices Employing Phosphorescent Molecular Aggregates. *Nat Photonics* [interactive]. 2021, *15*, 230–237. Access via: doi:10.1038/s41566-020-00734-2.

76. FUSELLA, M.A. et al. Plasmonic Enhancement of Stability and Brightness in Organic Light-Emitting Devices. *Nature* [interactive]. 2020, *585*, 379–382. Access via: doi:10.1038/s41586-020-2684-z.

77. KIM, K.-H. et al. Phosphorescent Dye-Based Supramolecules for High-Efficiency Organic Light-Emitting Diodes. *Nat Commun* [interactive]. 2014, *5*, 4769. Access via: doi:10.1038/ncomms5769.

78. BALDO, M.A. et al. High-Efficiency Fluorescent Organic Light-Emitting Devices Using a Phosphorescent Sensitizer. *Nature* [interactive]. 2000, *403*, 750–753. Access via: doi:10.1038/35001541.

79. JIN, J. et al. Construction of High T_g Bipolar Host Materials with Balanced Electron–Hole Mobility Based on 1,2,4-Thiadiazole for Phosphorescent Organic Light-Emitting Diodes. *Chemistry of Materials* [interactive]. 2014, *26*, 2388–2395. Access via: doi:10.1021/cm403388s.

80. HUANG, X.-L. et al. A High T_g Small-Molecule Arylamine Derivative as a Doped Hole-Injection/Transport Material for Stable Organic Light-Emitting Diodes. *Org Electron* [interactive]. 2018, *58*, 139–144. Access via: doi:10.1016/j.orgel.2018.04.012.

81. L, S. et al. Pronounced Luminescence Efficiency and Thermal Stability of Small Imidazole Architect 2-(1, 4, 5-Triphenyl-1H-Imidazol-2-yl)Phenol for Efficient Non-Doped Blue OLEDs. *J Photochem Photobiol A Chem* [interactive]. 2018, *365*, 232–237. Access via: doi:10.1016/j.jphotochem.2018.08.009.

82. CHIEN, C. et al. Multifunctional Deep-Blue Emitter Comprising an Anthracene Core and Terminal Triphenylphosphine Oxide Groups. *Adv Funct Mater* [interactive]. 2009, *19*, 560–566. Access via: doi:10.1002/adfm.200801240.

83. CHI, Y.J. et al. Increased Electromer Formation and Charge Trapping in Solution-Processed versus Vacuum-Deposited Small Molecule Host Materials of Organic Light-Emitting Devices. *ACS Appl Mater Interfaces* [interactive]. 2017, *9*, 40564–40572. Access via: doi:10.1021/acsami.7b15190.

84. SHIBATA, M. et al. Advantages and Disadvantages of Vacuum-Deposited and Spin-Coated Amorphous Organic Semiconductor Films for Organic Light-Emitting Diodes. *J Mater Chem C Mater* [interactive]. 2015, *3*, 11178–11191. Access via: doi:10.1039/C5TC01911G.

85. WANG, Y. et al. High Triplet Energy Hosts for Blue Organic Light-Emitting Diodes. *Adv Funct Mater* [interactive]. 2021, *31*. Access via: doi:10.1002/adfm.202008332.

86. IDRIS, M. et al. Phenanthro[9,10-*d*]Triazole and Imidazole Derivatives: High Triplet Energy Host Materials for Blue Phosphorescent Organic Light Emitting Devices. *Mater Horiz* [interactive]. 2019, *6*, 1179–1186. Access via: doi:10.1039/C9MH00195F.

87. MAHESHWARAN, A. et al. High Efficiency Deep-Blue Phosphorescent Organic Light-Emitting Diodes with CIE x, y ($\leq$ 0.15) and Low Efficiency Roll-Off by Employing a High Triplet Energy Bipolar Host Material. *Adv Funct Mater* [interactive]. 2018, *28*. Access via: doi:10.1002/adfm.201802945.

88. WANG, J. et al. Novel Bipolar Hosts for Highly Efficient Green Phosphorescent Organic Light-Emitting Diodes with Slow Efficiency Roll-Off. *Dyes and Pigments* [interactive]. 2024, *223*, 111920. Access via: doi:10.1016/j.dyepig.2023.111920.

89. CHEN, Y. et al. Novel Bipolar Host Materials Including Carbazole and Dioxy[2,3-b] Pyrazine Units for Red Phosphorescent Organic Light-Emitting Diodes. *Dyes and Pigments* [interactive]. 2023, *220*, 111684. Access via: doi:10.1016/j.dyepig.2023.111684.

90. HUANG, Z. et al. Highly Efficient Phosphorescent Organic Light-Emitting Diodes with Low Turn-on Voltages Using N-Phenylcarbazole/Pyrimidine-Based Bipolar Host Materials. *Dyes and Pigments* [interactive]. 2024, *222*, 111828. Access via: doi:10.1016/j.dyepig.2023.111828.

91. Zhang, Q. et al. Highly Efficient Red and Green Phosphorescent OLEDs Based on Benzonitrile and Carbazole as Bipolar Host Materials. *Dyes and Pigments* [interactive]. 2024, *222*, 111874. Access via: doi:10.1016/j.dyepig.2023.111874.

92. RYU, S. et al. Synthesis of Dibenzofuran and Dibenzothiophene Derivatives as Yellow Host Materials for Phosphorescent Organic Light-Emitting Diodes. *Synth Met* [interactive]. 2024, *301*, 117538. Access via: doi:10.1016/j.synthmet.2023.117538.

93. JESURAJ, P.J. et al. Intramolecular Charge Transfer-Based Spirobifluorene-Coupled Heteroaromatic Moieties as Efficient Hole Transport Layer and Host in Phosphorescent Organic Light-Emitting Diodes. *Org Electron* [interactive]. 2020, *85*, 105825. Access via: doi:10.1016/j.orgel.2020.105825.

94. ARAI, A. et al. Π-Extended Carbazole Derivatives as Host Materials for Highly Efficient and Long-Life Green Phosphorescent Organic Light-Emitting Diodes. *Chemistry – A European Journal* [interactive]. 2021, *27*, 4971–4976. Access via: doi:10.1002/chem.202005144.

95. GNANASEKARAN, P. et al. Perceiving the Influence of Phenyl-Carbazole Isomers on Sulfone/Thioxanthone-Based D–A–D Hosts: Realizing Efficient Red-Phosphorescent OLEDs. *J Mater Chem C Mater* [interactive]. 2024, *12*, 2203–2215. Access via: doi:10.1039/D3TC04075E.

96. SCHOLZ, S. et al. Degradation Mechanisms and Reactions in Organic Light-Emitting Devices. *Chem Rev* [interactive]. 2015, *115*, 8449–8503. Access via: doi:10.1021/cr400704v.

97. ZHANG, Q. et al. Anthraquinone-Based Intramolecular Charge-Transfer Compounds: Computational Molecular Design, Thermally Activated Delayed Fluorescence, and Highly Efficient Red Electroluminescence. *J Am Chem Soc* [interactive]. 2014, *136*, 18070–18081. Access via: doi:10.1021/ja510144h.

98. SHI, K. et al. High-Efficiency Asymmetric TADF Dendrimers via Promoting Mixing of Multiple Excited States toward Solution-Processed OLEDs with Low Efficiency Rolloff. *ACS Mater Lett* [interactive]. 2024, 1491–1503. Access via: doi:10.1021/acsmaterialslett.4c00273.

99. CHAN, C.-Y. et al. Efficient and Stable Sky-Blue Delayed Fluorescence Organic Light-Emitting Diodes with CIEy below 0.4. *Nat Commun* [interactive]. 2018, *9*, 5036. Access via: doi:10.1038/s41467-018-07482-6.

100. HU, Y.X. et al. Efficient Selenium-Integrated TADF OLEDs with Reduced Roll-Off. *Nat Photonics* [interactive]. 2022, *16*, 803–810. Access via: doi:10.1038/s41566-022-01083-y.

101. SAMANTA, P.K. et al. Up-Conversion Intersystem Crossing Rates in Organic Emitters for Thermally Activated Delayed Fluorescence: Impact of the Nature of Singlet vs Triplet Excited States. *J Am Chem Soc* [interactive]. 2017, *139*, 4042–4051. Access via: doi:10.1021/jacs.6b12124.

102. CHEN, X. et al. Hybridized Local and Charge-Transfer Excited-State Fluorophores through the Regulation of the Donor–Acceptor Torsional Angle for Highly Efficient Organic Light-Emitting Diodes. *CCS Chemistry* [interactive]. 2022, *4*, 1284–1294. Access via: doi:10.31635/ccschem.021.202100900.

103. ZHOU, S.-Y. et al. AIEgens-Lightened Functional Polymers: Synthesis, Properties and Applications. *Chinese Journal of Polymer Science* [interactive]. 2019, *37*, 302–326. Access via: doi:10.1007/s10118-019-2217-0.

104. ZHAO, Y. et al. Thermally Activated Delayed Fluorescence Material with Aggregation-Induced Emission Properties for Highly Efficient Organic Light-Emitting Diodes. *J Mater Chem C Mater* [interactive]. 2018, *6*, 2873–2881. Access via: doi:10.1039/C7TC04934J.

105. WU, J.-L. et al. Thermoresponsive Fluorescent Semicrystalline Polymers Decorated with Aggregation Induced Emission Luminogens. *Chinese Journal of Polymer Science* [interactive]. 2019, *37*, 394–400. Access via: doi:10.1007/s10118-019-2201-8.

106. HUANG, J. et al. Robust Luminescent Small Molecules with Aggregation-Induced Delayed Fluorescence for Efficient Solution-Processed OLEDs. *J Mater Chem C Mater* [interactive] 2019, *7*, 330–339. Access via: doi:10.1039/C8TC04842H.

107. HUANG, J. et al. Highly Efficient Nondoped OLEDs with Negligible Efficiency Roll-Off Fabricated from Aggregation-Induced Delayed Fluorescence Luminogens. *Angewandte Chemie International Edition* [interactive]. 2017, *56*, 12971–12976. Access via: doi:10.1002/anie.201706752.

108. HU, Y.B. et al. Recent Progress in AIE-Active Polymers. *Chinese Journal of Polymer Science* [interactive]. 2019, *37*, 289–301. Access via: doi:10.1007/s10118-019-2221-4.

109. GU, J. et al. Polymers with Aggregation-Induced Emission Characteristics. In *Principles and Applications of Aggregation-Induced Emission*; Springer International Publishing: Cham, 2019; pp. 77–108.

110. HAO, Z. et al. Chiral Sulfoximine-Based TADF Emitter for Circularly Polarized Luminescence and Highly Efficient OLEDs. *Chemical Engineering Journal* [interactive]. 2023, *454*, 140070. Access via: doi:10.1016/j.cej.2022.140070.

111. HU, F. et al. Multifunctional Emitters with TADF, AIE, Polymorphism and High-Contrast Multicolor Mechanochromism: Efficient Organic Light-Emitting Diodes. *Chemical Engineering Journal* [interactive]. 2023, *464*, 142678. Access via: doi:10.1016/j.cej.2023.142678.

112. MEI, Y. et al. Hydrogen Bond Boosts EQEs to 30+% for Acridone-Carbazole Based Deep-Blue TADF Emitters in Simple-Structure OLEDs. *Chemical*

Engineering Journal [interactive]. 2024, *480*, 148351. Access via: doi:10.1016/j.cej.2023.148351.

113. KRUCAITE, G. et al. New Bipolar Derivatives with Diphenylsulfone or Dibenzophenone as TADF Based Emitters for OLEDs. *Org Electron* [interactive]. 2024, *125*, 106981. Access via: doi:10.1016/j.orgel.2023.106981.

114. XIE, Z. et al. Molecular Engineering Enables TADF Emitters Well Suitable for Non-Doped OLEDs with External Quantum Efficiency of Nearly 30%. *Adv Funct Mater* [interactive]. 2022, *32*. Access via: doi:10.1002/adfm.202112881.

115. CHEN, J. et al. Optimizing Intermolecular Interactions and Energy Level Alignments of Red TADF Emitters for High-Performance Organic Light-Emitting Diodes. *Small* [interactive]. 2022, *18*. Access via: doi:10.1002/smll.202201548.

116. WANG, H. et al. A TADF Emitter with Dual Para-Positioned Donors Enables OLEDs with Improved Efficiency and CIE Coordinates Close to the Rec. 2020 Red Standard. *ACS Appl Mater Interfaces* [interactive]. 2023, *15*, 1685–1692. Access via: doi:10.1021/acsami.2c18219.

117. SHI, Y.-Z. et al. Applying Intermolecular Hydrogen Bonding to Exploit TADF Emitters for High-Performance Orange-Red Non-Doped OLEDs. *J Mater Chem C Mater* [interactive]. 2022, *10*, 4717–4722. Access via: doi:10.1039/D1TC03803F.

118. HASAN, M. et al. Exciton–Exciton Annihilation in Thermally Activated Delayed Fluorescence Emitter. *Adv Funct Mater* [interactive]. 2020, *30*. Access via: doi:10.1002/adfm.202000580.

119. WANG, Y. et al. Through Space Charge Transfer for Efficient Sky-Blue Thermally Activated Delayed Fluorescence (TADF) Emitter with Unconjugated Connection. *Adv Opt Mater* [interactive]. 2020, *8*. Access via: doi:10.1002/adom.201901150.

120. CAI, M. et al. Enhancing Spin-Orbital Coupling in Deep-Blue/Blue TADF Emitters by Minimizing the Distance from the Heteroatoms in Donors to Acceptors. *Chemical Engineering Journal* [interactive]. 2021, *420*, 127591. Access via: doi:10.1016/j.cej.2020.127591.

121. CUI, L. et al. Controlling Singlet–Triplet Energy Splitting for Deep-Blue Thermally Activated Delayed Fluorescence Emitters. *Angewandte Chemie International Edition* [interactive]. 2017, *56*, 1571–1575. Access via: doi:10.1002/anie.201609459.

122. CHATTERJEE, T. et al. Perspective on Host Materials for Thermally Activated Delayed Fluorescence Organic Light Emitting Diodes. *Adv Opt Mater* [interactive]. 2019, *7*. Access via: doi:10.1002/adom.201800565.

123. ZHANG, J. et al. Multiplying Phosphine-Oxide Orientation to Enable Ultralow-Voltage-Driving Simple White Thermally Activated Delayed Fluorescence Diodes with Power Efficiency over 100 Lm W $^{-1}$. *Adv Funct Mater* [interactive]. 2022, *32*. Access via: doi:10.1002/adfm.202209163.

124. WALLWORK, N.R. et al. High-Performance Solution-Processed Red Hyperfluorescent OLEDs Based on Cibalackrot. *J Mater Chem C Mater* [interactive]. 2022, *10*, 4767–4774. Access via: doi:10.1039/D1TC04937B.

125. JIANG, W. et al. Novel Benzonitrile-Based AIE Host with High Triplet Energy for Highly Efficient Solution-Processed Blue TADF OLEDs. *Dyes and Pigments* [interactive]. 2023, *210*, 111037. Access via: doi:10.1016/j.dyepig.2022.111037.

126. HA, T.H. et al. Phenylpyridine and Carbazole Based Host Materials for Highly Efficient Blue TADF OLEDs. *Org Electron* [interactive]. 2022, *102*, 106450. Access via: doi:10.1016/j.orgel.2022.106450.

127. KREIZA, G. Ambipolar Hosts for Blue TADF OLEDs: Assessment of the Device Performance and Lifetime. *Org Electron* [interactive]. 2023, *120*, 106849. Access via: doi:10.1016/j.orgel.2023.106849.

128. HA, T.H. et al. Highly Reduced Efficiency Roll-off with 5,9-Dioxa-13b-Boranaphtho[3,2,1-de]Anthracen-Containing Unit on Bipolar Host for Improved OLEDs Device Lifespan. *Org Electron* [interactive]. 2024, *124*, 106960. Access via: doi:10.1016/j.orgel.2023.106960.

129. LU, X. et al. Exciplex Hosts for Constructing Green Multiple Resonance Delayed Fluorescence OLEDs with High Color Purity And Low Efficiency Roll-Offs. *Adv Funct Mater* [interactive]. 2024, 2313897. Access via: doi:10.1002/adfm.202313897.

130. XU, Y. et al. Constructing Organic Electroluminescent Material with Very High Color Purity and Efficiency Based on Polycyclization of the Multiple Resonance Parent Core. *Angewandte Chemie International Edition* [interactive]. 2022, *61*. Access via: doi:10.1002/anie.202204652.

131. HU, Y. et al. Judicious Design of Pyridine-Based Hosts for Stable, Efficient, and Low-Driving Thermally Activated Delayed Fluorescence Organic Light-Emitting Diodes. *Adv Opt Mater* [interactive]. 2024, 2302971. Access via: doi:10.1002/adom.202302971.

132. LIU, Q. et al. Unraveling the Position Effect of Spiroxanthene-Based n-Type Hosts for High-Performance TADF–OLEDs. *Nanomaterials* [interactive]. 2023, *13*, 2517. Access via: doi:10.3390/nano13182517.

133. PALANISAMY, P. et al. Solution-Processed OLEDs Based on a Bipolar AIE Terpyridine Derivative as a Host. *ACS Applied Optical Materials* [interactive]. 2024, *2*, 76–87. Access via: doi:10.1021/acsaom.3c00346.

134. ZHAO, X.-H. et al. A Low-Cost Facile Synthesis of Solution-Processable N-Phenylcarbazole/Triazine Hybrid Host for Orange Thermally-Activated Delayed Fluorescent Organic Light-Emitting Diodes. *physica status solidi (a)* [interactive]. 2024, *221*. Access via: doi:10.1002/pssa.202300687.

135. TANG, C. et al. Carbazole or Carbazole-3-Carbonitrile /Pyridine Host Materials for Efficient Solution-Processable Blue Phosphorescent and Green TADF OLEDs. *Opt Mater (Amst)* [interactive]. 2022, *132*, 112573. Access via: doi:10.1016/j.optmat.2022.112573.

136. BLAZEVICIUS, D. et al. Pyridinyl-Carbazole Fragments Containing Host Materials for Efficient Green and Blue Phosphorescent OLEDs. *Molecules* [interactive]. 2021, *26*, 4615. Access via: doi:10.3390/molecules26154615.

137. TUCKER, S.H. LXXIV.—Iodination in the Carbazole Series. *J. Chem. Soc.* [interactive]. 1926, *129*, 546–553. Access via: doi:10.1039/JR9262900546.

138. GRIGALEVICIUS, S. et al. New Carbazole-Based Copolymers as Amorphous Hole-Transporting Materials for Multilayer Light-Emitting Diodes. *Macromol Chem Phys* [interactive]. 2007, *208*, 349–355. Access via: doi:10.1002/macp.200600498.

139. SUZUKI, A. Organoborane Coupling Reactions (Suzuki Coupling). *Proceedings of the Japan Academy, Series B* [interactive]. 2004, *80*, 359–371. Access via: doi:10.2183/pjab.80.359.

140. LEE, S.J. et al. A Study on the Phosphorescent Blue Organic Light-Emitting Diodes Using Various Host Materials. *Molecular Crystals and Liquid Crystals* [interactive]. 2009, *507*, 345–352. Access via: doi:10.1080/15421400903054287.

141. HAY, P.J. Theoretical Studies of the Ground and Excited Electronic States in Cyclometalated Phenylpyridine Ir(III) Complexes Using Density Functional Theory. *J Phys Chem A* [interactive]. 2002, *106*, 1634–1641. Access via: doi:10.1021/jp013949w.

142. CHANG, C.-H. et al. A New Class of Sky-Blue-Emitting Ir(III) Phosphors Assembled Using Fluorine-Free Pyridyl Pyrimidine Cyclometalates: Application toward High-Performance Sky-Blue- and White-Emitting OLEDs. *ACS Appl Mater Interfaces* [interactive]. 2013, *5*, 7341–7351. Access via: doi:10.1021/am401694s.

143. CHANG, C.-H. et al. Efficient Phosphorescent White Organic Light-Emitting Devices Incorporating Blue Iridium Complex and Multifunctional Orange–Red Osmium Complex. *Org Electron* [interactive]. 2009, *10*, 1235–1240. Access via: doi:10.1016/j.orgel.2009.06.016.

144. BLAZEVICIUS, D. et al. Easily Synthesized and Cheap Carbazole- or Phenoxazine-Based Hosts for Efficient Yellow Phosphorescent OLEDs. *Opt Mater (Amst)* [interactive]. 2021, *118*, 111251. Access via: doi:10.1016/j.optmat.2021.111251.

145. ZOSTAUTIENE, R. et al. Electro-active Oligomers Containing Pendent Carbazolyl or Indolyl Groups as Host Materials for OLEDs. *J Appl Polym Sci* [interactive]. 2011, *122*, 908–913. Access via: doi:10.1002/app.34206.

146. ZOSTAUTIENE, R. et al. Diphenylsilanes Containing Electronically Isolated Carbazolyl Fragments as Host Materials for Light Emitting Diodes. *Synth Met* [interactive]. 2011, *161*, 92–95. Access via: doi:10.1016/j.synthmet.2010.11.003.

147. LI, X.-L. et al. Highly Efficient Single- and Multi-Emission-Layer Fluorescent/Phosphorescent Hybrid White Organic Light-Emitting Diodes with ~20% External Quantum Efficiency. *J Mater Chem C Mater* [interactive]. 2015, *3*, 9233–9239. Access via: doi:10.1039/C5TC02050F.

148. SHAHNAWAZ, S. et al. Highly Efficient Candlelight Organic Light-Emitting Diode with a Very Low Color Temperature. *Molecules* [interactive]. 2021, *26*, 7558. Access via: doi:10.3390/molecules26247558.

149. TSAI, M. -H. et al. 3-(9-Carbazolyl)Carbazoles and 3,6-Di(9-carbazolyl)Carbazoles as Effective Host Materials for Efficient Blue Organic Electrophosphorescence. *Advanced Materials* [interactive]. 2007, *19*, 862–866. Access via: doi:10.1002/adma.200600822.

150. JOU, J. et al. High-Efficiency Wet- and Dry-Processed Green Organic Light Emitting Diodes with a Novel Iridium Complex-Based Emitter. *Adv Opt Mater* [interactive]. 2013, *1*, 657–667. Access via: doi:10.1002/adom.201300172.

151. TAO, P. et al. Facile Synthesis of Highly Efficient Lepidine-Based Phosphorescent Iridium(III) Complexes for Yellow and White Organic Light-Emitting Diodes. *Adv Funct Mater* [interactive]. 2016, *26*, 881–894. Access via: doi:10.1002/adfm.201503826.

152. SHARMA, A. et al. Tuning Photophysical and Electroluminescent Properties of Phenanthroimidazole Decorated Carbazoles with Donor and Acceptor Units: Beneficial Role of Cyano Substitution. *Dyes and Pigments* [interactive]. 2021, *184*, 108830. Access via: doi:10.1016/j.dyepig.2020.108830.

153. International Commission on Non-Ionizing Radiation Protection (ICNIRP) Guidelines on Limits of Exposure to Broad-Band Incoherent Optical Radiation (0.38 to 3 MicroM). International Commission on Non-Ionizing Radiation Protection. *Health Phys.* 1997, *73*, 539–554.

154. O'HAGAN, J.B. et al. Low-Energy Light Bulbs, Computers, Tablets and the Blue Light Hazard. *Eye* [interactive]. 2016, *30*, 230–233. Access via: doi:10.1038/eye.2015.261.

155. BULLOUGH, J.D. The Blue-Light Hazard: A Review. *Journal of the Illuminating Engineering Society* [interactive]. 2000, *29*, 6–14. Access via: doi:10.1080/00994480.2000.10748312.

156. JOU, J.-H. et al. Blue-Hazard-Free Candlelight OLED. *Journal of Visualized Experiments* [interactive]. 2017, 121, e54644. Access via: doi:10.3791/54644.

157. JOU, J.-H. et al. Approach for Fabricating Healthy OLED Light Sources with Visual Quality and Energy-Saving Character. *Org Electron* [interactive]. 2016, *38*, 396–400. Access via: doi:10.1016/j.orgel.2016.09.005.

158. BLAZEVICIUS, D. et al. A Review of Benzophenone-Based Derivatives for Organic Light-Emitting Diodes. *Nanomaterials* [interactive]. 2024, *14*, 356. Access via: doi:10.3390/nano14040356.

159. KERUCKIENE, R. et al. Meta-Substituted Benzophenones as Multifunctional Electroactive Materials for OLEDs. *Dyes and Pigments* [interactive]. 2020, *174*, 108058. Access via: doi:10.1016/j.dyepig.2019.108058.

160. HERAVI, M.M. et al. Buchwald-Hartwig Reaction: An Overview. *J Organomet Chem* [interactive]. 2018, *861*, 17–104. Access via: doi:10.1016/j.jorganchem.2018.02.023.

161. CHIBA, T. et al. A Solution-Processable Small-Molecule Host for Phosphorescent Organic Light-Emitting Devices. *Journal of Photopolymer*

Science and Technology [interactive]. 2016, *29*, 317–321. Access via: doi:10.2494/photopolymer.29.317.

162. LIANG, J. et al. Novel Blue Bipolar Thermally Activated Delayed Fluorescence Material as Host Emitter for High-Efficiency Hybrid Warm-White OLEDs with Stable High Color-Rendering Index. *Adv Funct Mater* [interactive]. 2018, *28*. Access via: doi:10.1002/adfm.201707002.

163. MA, W. et al. Structurally Nontraditional Bipolar Hosts for RGB Phosphorescent OLEDs: Boosted by a "Butterfly-Shaped" Medium-Ring Acceptor. *Angewandte Chemie International Edition* [interactive]. 2022, *61*. Access via: doi:10.1002/anie.202116681.

164. KUMAR, S. et al. One-Shot Triphenylamine/Phenylketone Hybrid as a Bipolar Host Material for Efficient Red Phosphorescent Organic Light-Emitting Diodes. *Synth Met* [interactive]. 2019, *254*, 42–48. Access via: doi:10.1016/j.synthmet.2019.05.015.

165. LIN, H. et al. Recent Synthetic Developments and Applications of the Ullmann Reaction. A Review. *Org Prep Proced Int* [interactive]. 2013, *45*, 341–394. Access via: doi:10.1080/00304948.2013.816208.

166. JHULKI, S. et al. Benzophenones as Generic Host Materials for Phosphorescent Organic Light-Emitting Diodes. *ACS Appl Mater Interfaces* [interactive]. 2016, *8*, 1527–1535. Access via: doi:10.1021/acsami.5b11232.

167. RUEPING, M. et al. A Review of New Developments in the Friedel–Crafts Alkylation – From Green Chemistry to Asymmetric Catalysis. *Beilstein Journal of Organic Chemistry* [interactive]. 2010, *6,* 6. Access via: doi:10.3762/bjoc.6.6.

168. HU, J. et al. Linkage Modes on Phthaloyl/Triphenylamine Hybrid Compounds: Multi-Functional AIE Luminogens, Non-Doped Emitters and Organic Hosts for Highly Efficient Solution-Processed Delayed Fluorescence OLEDs. *Dyes and Pigments* [interactive]. 2017, *137*, 480–489. Access via: doi:10.1016/j.dyepig.2016.10.029.

169. MAHMOUDI, M. et al. Bis(N-Naphthyl-N-Phenylamino)Benzophenones as Exciton-Modulating Materials for White TADF OLEDs with Separated Charge and Exciton Recombination Zones. *Dyes and Pigments* [interactive]. 2022, *197*, 109868. Access via: doi:10.1016/j.dyepig.2021.109868.

170. SUDHEENDRAN SWYAMPRABHA, S. et al. Novel Carbazole Host Materials for Solution Processed TADF Organic Light Emitting Diodes. *Dyes and Pigments* [interactive]. 2023, *208*, 110821. Access via: doi:10.1016/j.dyepig.2022.110821.

171. NAGAR, M.R. et al. Solution Processable Carbazole-Benzophenone Derivatives as Bipolar Hosts Enabling High-Efficiency Stable Green TADF Organic LEDs. *J Mater Chem C Mater* [interactive]. 2023, *11*, 1579–1592. Access via: doi:10.1039/D2TC04820E.

172. WANG, F. et al. Twisted Penta-Carbazole/Benzophenone Hybrid Compound as Multifunctional Organic Host, Dopant or Non-doped Emitter for Highly Efficient Solution-Processed Delayed Fluorescence OLEDs. *Chin J Chem* [interactive]. 2018, *36*, 241–246. Access via: doi:10.1002/cjoc.201700703.

173.	MA, F. et al. Adjusting the Photophysical Properties of AIE-Active TADF Emitters from through-Bond to through-Space Charge Transfer for High-Performance Solution-Processed OLEDs. *Dyes and Pigments* [interactive]. 2021, *188*, 109208. Access via: doi:10.1016/j.dyepig.2021.109208.

174.	WANG, J. et al. Effective Design Strategy for Aggregation-Induced Emission and Thermally Activated Delayed Fluorescence Emitters Achieving 18% External Quantum Efficiency Pure-Blue OLEDs with Extremely Low Roll-Off. *ACS Appl Mater Interfaces* [interactive]. 2021, *13*, 57713–57724. Access via: doi:10.1021/acsami.1c17449.

175.	LIU, Y. et al. Triazatruxene-Based Thermally Activated Delayed Fluorescence Small Molecules with Aggregation-Induced Emission Properties for Solution-Processable Nondoped OLEDs with Low Efficiency Roll-Off. *J Mater Chem C Mater* [interactive]. 2019, *7*, 9719–9725. Access via: doi:10.1039/C9TC02927C.

176.	TANI, K. et al. Carbazole and Benzophenone Based Twisted Donor–Acceptor Systems as Solution Processable Green Thermally Activated Delayed Fluorescence Organic Light Emitters. *Chem Lett* [interactive]. 2018, *47*, 1236–1239. Access via: doi:10.1246/cl.180438.

177.	JING, Y.-Y. et al. Triptycene-Imbedded Thermally Activated Delayed Fluorescence Emitters with Excellent Film Morphologies for Applications in Efficient Nondoped and Doped Organic Light-Emitting Devices. *Chemical Engineering Journal* [interactive]. 2021, *413*, 127418. Access via: doi:10.1016/j.cej.2020.127418.

178.	AIZAWA, N. et al. Aggregation-Induced Delayed Fluorescence from Phenothiazine-Containing Donor–Acceptor Molecules for High-Efficiency Non-Doped Organic Light-Emitting Diodes. *Polym J* [interactive]. 2017, *49*, 197–202. Access via: doi:10.1038/pj.2016.82.

179.	WU, L. et al. Using Fluorene to Lock Electronically Active Moieties in Thermally Activated Delayed Fluorescence Emitters for High-Performance Non-Doped Organic Light-Emitting Diodes with Suppressed Roll-Off. *Chem Sci* [interactive]. 2021, *12*, 1495–1502. Access via: doi:10.1039/D0SC05631F.

180.	MA, M. Low Efficiency Roll-off Thermally Activated Delayed Fluorescence Emitters for Non-Doped OLEDs: Substitution Effect of Thioether and Sulfone Groups. *Dyes and Pigments* [interactive] 2021, *194*, 109649. Access via: doi:10.1016/j.dyepig.2021.109649.

181.	RAJAMALLI, P. et al. Pyridine-Functionalized Carbazole Donor and Benzophenone Acceptor Design for Thermally Activated Delayed Fluorescence Emitters in Blue Organic Light-Emitting Diodes. *J Photonics Energy* [interactive]. 2018, *8*, 1. Access via: doi:10.1117/1.JPE.8.032106.

182.	WANG, J. et al. Ultrapure Deep-Blue Aggregation-Induced Emission and Thermally Activated Delayed Fluorescence Emitters for Efficient OLEDs with CIE_y<0.1 and Low Efficiency Roll-Offs. *J Mater Chem C Mater* [interactive]. 2022, *10*, 3163–3171. Access via: doi:10.1039/D1TC05497J.

183.	NIE, X. et al. Modulation of OLED Efficiency *via* a Combination of Aromatic Electrophilic Directing and Intramolecular Charge Transfer. *J Mater Chem C*

Mater [interactive]. 2021, *9*, 15698–15706. Access via: doi:10.1039/D1TC04156H.

184. Ho, C.-Y. et al. Triphenylethene-Carbazole-Based Molecules for the Realization of Blue and White Aggregation-Induced Emission OLEDs with High Luminance. *Org Electron* [interactive]. 2022, *108*, 106571. Access via: doi:10.1016/j.orgel.2022.106571.

185. KREIZA, G. et al. Suppression of Benzophenone-Induced Triplet Quenching for Enhanced TADF Performance. *J Mater Chem C Mater* [interactive]. 2019, *7*, 11522–11531. Access via: doi:10.1039/C9TC02408E.

186. ZHANG, J. et al. Simple-Structured Blue Thermally Activated Delayed Fluorescence Emitter for Solution-Processed Organic Light-Emitting Diodes with External Quantum Efficiency of over 20%. *ACS Appl Mater Interfaces* [interactive]. 2021, *13*, 12305–12312. Access via: doi:10.1021/acsami.1c00412.

187. WANG, L. et al. Achieving Enhanced Thermally Activated Delayed Fluorescence Rates and Shortened Exciton Lifetimes by Constructing Intramolecular Hydrogen Bonding Channels. *ACS Appl Mater Interfaces* [interactive]. 2019, *11*, 45999–46007. Access via: doi:10.1021/acsami.9b16073.

188. XIE, Z. et al. Hydrogen-Bonding-Assisted Intermolecular Charge Transfer: A New Strategy to Design Single-Component White-Light-Emitting Materials. *Adv Funct Mater* [interactive]. 2017, *27,* 1703918. Access via: doi:10.1002/adfm.201703918.

189. CHEN, X. et al. An Efficient Yellow Thermally Activated Delayed Fluorescence Emitter with Universal Applications in Both Doped and Non-Doped Organic Light-Emitting Diodes. *Mater Chem Front* [interactive]. 2018, *2*, 1017–1023. Access via: doi:10.1039/C8QM00064F.

190. ZHAO, J. et al. Efficient Triplet Harvesting in Fluorescence–TADF Hybrid Warm-White Organic Light-Emitting Diodes with a Fully Non-Doped Device Configuration. *J Mater Chem C Mater* [interactive]. 2018, *6*, 4257–4264. Access via: doi:10.1039/C8TC01210E.

191. HUANG, B. et al. Thermally Activated Delayed Fluorescence Materials Based on Benzophenone Derivative as Emitter for Efficient Solution-Processed Non-Doped Green OLED. *Dyes and Pigments* [interactive]. 2016, *133*, 380–386. Access via: doi:10.1016/j.dyepig.2016.06.025.

192. LEE, S.Y. et al. Luminous Butterflies: Efficient Exciton Harvesting by Benzophenone Derivatives for Full-Color Delayed Fluorescence OLEDs. *Angewandte Chemie International Edition* [interactive]. 2014, *53*, 6402–6406. Access via: doi:10.1002/anie.201402992.

193. LIU, Y. et al. A Novel Donor Moiety 9,9,9′9′-Tetramethyl-9,9′10,10′-Tetrahydro-2,10′-Biacridine *via* One-Pot C–H Arylation for TADF Emitters and Their Application in Highly Efficient Solution-Processable OLEDs. *J Mater Chem C Mater* [interactive]. 2020, *8*, 8971–8979. Access via: doi:10.1039/D0TC01612H.

194.   SUN, J. et al. A Purely Organic D-π-A-π-D Emitter with Thermally Activated Delayed Fluorescence and Room Temperature Phosphorescence for near-White OLED. *Chinese Chemical Letters* [interactive]. 2021, *32*, 1367–1371. Access via: doi:10.1016/j.cclet.2020.09.060.

195.   SHARIF, P. et al. Rational Molecular Design Enables Efficient Blue TADF−OLEDs with Flexible Graphene Substrate. *Adv Funct Mater* [interactive]. 2022, *32*, 2207324. Access via: doi:10.1002/adfm.202207324.

196.   SUN, J.W. et al. Azasiline-Based Thermally Activated Delayed Fluorescence Emitters for Blue Organic Light Emitting Diodes. *J Mater Chem C Mater* [interactive]. 2017, *5*, 1027–1032. Access via: doi:10.1039/C6TC04653C.

197.   HUANG, R. et al. Creating Efficient Delayed Fluorescence Luminogens with Acridine-Based Spiro Donors to Improve Horizontal Dipole Orientation for High-Performance OLEDs. *Chemical Engineering Journal* [interactive]. 2022, *435*, 134934. Access via: doi:10.1016/j.cej.2022.134934.

198.   CHEN, Y. et al. Triazatruxene-Based Small Molecules with Thermally Activated Delayed Fluorescence, Aggregation-Induced Emission and Mechanochromic Luminescence Properties for Solution-Processable Nondoped OLEDs. *J Mater Chem C Mater* [interactive]. 2018, *6*, 12503–12508. Access via: doi:10.1039/C8TC04721A.

199.   WU, Z.-L. et al. Tröger's Base-Derived Thermally Activated Delayed Fluorescence Dopant for Efficient Deep-Blue Organic Light-Emitting Diodes. *Molecules* [interactive]. 2023, *28*, 4832. Access via: doi:10.3390/molecules28124832.

200.   TAVGENIENE, D. et al. 3-(N,N-Diphenylamino)Carbazole Donor Containing Bipolar Derivatives with Very High Glass Transition Temperatures as Potential TADF Emitters for OLEDs. *Coatings* [interactive]. 2022, *12*, 932. Access via: doi:10.3390/coatings12070932.

201.   CAI, X. et al. Singlet–Triplet Splitting Energy Management via Acceptor Substitution: Complanation Molecular Design for Deep-Blue Thermally Activated Delayed Fluorescence Emitters and Organic Light-Emitting Diodes Application. *Adv Funct Mater* [interactive] 2016, *26*, 8042–8052. Access via: doi:10.1002/adfm.201603520.

202.   ZHANG, Q. et al. Nearly 100% Internal Quantum Efficiency in Undoped Electroluminescent Devices Employing Pure Organic Emitters. *Advanced Materials* [interactive]. 2015, *27*, 2096–2100. Access via: doi:10.1002/adma.201405474.

203.   HUANG, R. et al. Sky-Blue Aggregation-Induced Delayed Fluorescence Luminogens with High Horizontal Dipole Orientation for Efficient Organic Light-Emitting Diodes. *Chin J Chem* [interactive]. 2023, *41*, 527–534. Access via: doi:10.1002/cjoc.202200543.

204.   MA, F. et al. Molecular Engineering of Thermally Activated Delayed Fluorescence Emitters with Aggregation-Induced Emission via Introducing Intramolecular Hydrogen-Bonding Interactions for Efficient Solution-Processed Nondoped OLEDs. *ACS Appl Mater Interfaces* [interactive]. 2020, *12*, 1179–1189. Access via: doi:10.1021/acsami.9b17545.

205. TOMKEVICIENE, A. et al. Thianthrene and Acridan-Substituted Benzophenone or Diphenylsulfone: Effect of Triplet Harvesting via TADF and Phosphorescence on Efficiency of All-Organic OLEDS. *Org Electron* [interactive]. 2019, *70*, 227–239. Access via: doi:10.1016/j.orgel.2019.04.025.

206. GAUTAM, P. et al. Bifunctional Bicarbazole-Benzophenone-Based Twisted Donor–Acceptor–Donor Derivatives for Deep-Blue and Green OLEDs. *Nanomaterials* [interactive]. 2023, *13*, 1408. Access via: doi:10.3390/nano13081408.

207. INOUE, S. et al. Effects of Substituted Alkyl Chain Length on Solution-Processable Layered Organic Semiconductor Crystals. *Chemistry of Materials* [interactive]. 2015, *27*, 3809–3812. Access via: doi:10.1021/acs.chemmater.5b00810.

208. YANG, X. et al. Recent Advances of the Emitters for High Performance Deep-Blue Organic Light-Emitting Diodes. *J Mater Chem C Mater* [interactive]. 2015, *3*, 913–944. Access via: doi:10.1039/C4TC02474E.

209. TIAN, X. et al. Novel Deep Blue LE-Dominated HLCT Excited State Design Strategy and Material for OLED. *Molecules* [interactive]. 2021, *26*, 4560. Access via: doi:10.3390/molecules26154560.

210. HEDLEY, G.J. et al. Ultrafast Luminescence in Ir(ppy)3. *Chem Phys Lett* [interactive]. 2008, *450*, 292–296. Access via: doi:10.1016/j.cplett.2007.11.028.

211. WANG, P. et al. The Electroluminescence Mechanism of Solution-Processed TADF Emitter 4CzIPN Doped OLEDs Investigated by Transient Measurements. *Molecules* [interactive]. 2016, *21*, 1365. Access via: doi:10.3390/molecules21101365.

212. YOOK, K.S. et al. Small Molecule Host Materials for Solution Processed Phosphorescent Organic Light-Emitting Diodes. *Advanced Materials* [interactive]. 2014, *26*, 4218–4233. Access via: doi:10.1002/adma.201306266.

213. BLAZEVICIUS, D. et al. Bicarbazole-Benzophenone-Based Twisted Donor-Acceptor-Donor Derivatives as Blue Emitters for Highly Efficient Fluorescent Organic Light-Emitting Diodes. *Nanomaterials* [interactive]. 2024, *14*, 146. Access via: doi:10.3390/nano14020146.

214. SIDDIQUI, I. et al. Bicarbazole-Benzophenone Based Twisted Donor-Acceptor Derivatives as Potential Blue TADF Emitters for OLEDs. *Molecules* [interactive]. 2024, *29*, 1672. Access via: doi:10.3390/molecules29071672.

215. LI, F. et al. Singlet and Triplet to Doublet Energy Transfer: Improving Organic Light-Emitting Diodes with Radicals. *Nat Commun* [interactive]. 2022, *13*, 2744. Access via: doi:10.1038/s41467-022-29759-7.

216. CHEN, C. et al. Intramolecular Charge Transfer Controls Switching Between Room Temperature Phosphorescence and Thermally Activated Delayed Fluorescence. *Angewandte Chemie International Edition* [interactive]. 2018, *57*, 16407–16411. Access via: doi:10.1002/anie.201809945.

217. LIU, X. et al. Improving Film Uniformity and Interface Solvent Resistance to Realize Multilayer Printing of OLED Devices. *J Mater Chem C Mater* [interactive]. 2024, *12*, 4070–4084. Access via: doi:10.1039/D3TC04465C.

218. WANG, G. et al. *Colloquium*: Excitons in Atomically Thin Transition Metal Dichalcogenides. *Rev Mod Phys* [interactive]. 2018, *90*, 021001. Access via: doi:10.1103/RevModPhys.90.021001.

219. TROVATELLO, C. et al. The Ultrafast Onset of Exciton Formation in 2D Semiconductors. *Nat Commun* [interactive]. 2020, *11*, 5277. Access via: doi:10.1038/s41467-020-18835-5.

Pyridinyl-Carbazole Fragments Containing Host Materials for Efficient Green and Blue Phosphorescent OLEDs

Dovydas Blazevicius [1], Daiva Tavgeniene [1], Simona Sutkuviene [2], Ernestas Zaleckas [3], Ming-Ruei Jiang [4], Sujith Sudheendran Swayamprabha [4], Rohit Ashok Kumar Yadav [4], Jwo-Huei Jou [4,*] and Saulius Grigalevicius [1,*]

[1] Department of Polymer Chemistry and Technology, Kaunas University of Technology, Radvilenu Plentas 19, LT50254 Kaunas, Lithuania; dovydas.blazevicius@ktu.lt (D.B.); daiva.tavgeniene@ktu.lt (D.T.)
[2] Department of Biochemistry, Faculty of Natural Sciences, Vytautas Magnus University, Vileikos Str. 8, LT44404 Kaunas, Lithuania; Simona.Sutkuviene@vdu.lt
[3] Institute of Agricultural Engineering and Safety, Agriculture Academy, Vytautas Magnus University, Studentu Str. 15A-212, Akademija, LT53362 Kauno Distr., Lithuania; zerniukas@yahoo.co.uk
[4] Department of Materials Science and Engineering, National Tsing-Hua University, No. 101, Kaungfu Rd. Hsin-Chu 30013, Taiwan; g8ai5up@gmail.com (M.-R.J.); sujithsudheendran.s@gmail.com (S.S.S.); rohitakyadav@gmail.com (R.A.K.Y.)
* Correspondence: jjou@mx.nthu.edu.tw (J.-H.J.); saulius.grigalevicius@ktu.lt (S.G.)

Abstract: Pyridinyl-carbazole fragments containing low molar mass compounds as host derivatives **H1** and **H2** were synthesized, investigated, and used for the preparation of electro-phosphorescent organic light-emitting devices (PhOLEDs). The materials demonstrated high stability against thermal decomposition with the decomposition temperatures of 361–386 °C and were suitable for the preparation of thin amorphous and homogeneous layers with very high values of glass transition temperatures of 127–139 °C. It was determined that triplet energy values of the derivatives are, correspondingly, 2.82 eV for the derivative **H1** and 2.81 eV for the host **H2**. The new derivatives were tested as hosts of emitting layers in blue, as well as in green phosphorescent OLEDs. The blue device with 15 wt.% of the iridium(III)[bis(4,6-difluorophenyl)-pyridinato-$N,C2'$]picolinate (FIrpic) emitter doping ratio in host material **H2** exhibited the best overall characteristics with a power efficiency of 24.9 lm/W, a current efficiency of 23.9 cd/A, and high value of 10.3% of external quantum efficiency at 100 cd/m^2. The most efficient green PhOLED with 10 wt% of Ir(ppy)$_3$ {tris(2-phenylpyridine)iridium(III)} in the **H2** host showed a power efficiency of 34.1 lm/W, current efficiency of 33.9 cd/A, and a high value of 9.4% for external quantum efficiency at a high brightness of 1000 cd/m^2, which is required for lighting applications. These characteristics were obtained in non-optimized PhOLEDs under an ordinary laboratory atmosphere and could be improved in the optimization process. The results demonstrate that some of the new host materials are very promising components for the development of efficient phosphorescent devices.

Keywords: carbazole; triplet energy; amorphous film; current efficiency; host material; emitter

1. Introduction

OLEDs (organic light-emitting devices) receive a lot of attention due to their growing applications in solid-state lighting devices, as well as in flat-panel display technologies [1]. The OLED-based displays are already demonstrated in the market starting from the last several years, and lighting technologies were also presented rapidly [2,3]. In the emerging technologies of organic electronics, phosphorescent organic light-emitting diodes (PhOLEDs) are among the most mature devices. In such a type of device, discovered in 1998, the emitting layer is constituted of a heavy-metal complex emitter dispersed within a host material in order to harvest both singlet and triplet excitons. This technique allows the PhOLED to reach an internal quantum efficiency (IQE) of 100%, whereas the IQE of

a fluorescent OLED is only 25%. At this time, the phosphorescent derivatives are ideal for the production of the devices with high efficiency due to the exploitation of singlet and triplet excitons of the emitters simultaneously through intersystem crossing [4–7]. In the phosphorescent OLEDs (PhOLEDs), the mentioned triplet emitters in layers are dispersed as emitting guests in host materials to decrease quenching due to relatively long excited-state lifetimes of the triplet emitting materials and to reduce triplet-triplet annihilation. For these reasons, the required host derivatives are widely synthesized and investigated for the production of the PhOLEDs [8–10].

It is important for the efficient electro-phosphorescence that the triplet level energy of a used host derivative would be higher than that of the used triplet dopant to prevent reverse energy transmittance from the emitter back to the host and to confine as many as possible triplet excitons on guest structures [11–13]. Another requirement for the effective operation of the PhOLEDs is the ability of the host to create amorphous and stable layers with high values of the glass transition temperature. The film-forming property ensures that the guest molecules stay uniformly dispersed in the host material to decrease the possibility of concentration quenching.

It was described earlier that various compounds containing electronically isolated indolyl and/or carbazolyl substituents have rather large values of the triplet energy and are useful amorphous hosts for the PhOLEDs [14–18]. Here, we describe new well soluble pyridinyl-carbazole-based host materials for solution-processed emitting layers of the electro-phosphorescent technologies. The bipolar nature of the aromatic chromophore of the derivatives is responsible for bipolar charge transfer in the emitting layer. On the other hand, the oxetane unit in the structure affects the high glass transition temperature of the materials, as well as improved film-forming properties.

2. Experimental

2.1. Preparation of the Objective Materials

9H-carbazole (**1**), 3,3-bis(chlormethyl)oxetane, boronic acid of 2-methoxy-3-pyridine, 6-boronic acid of 6-methoxy-3-pyridine, KOH, K_2CO_3, butan-2-one, tetrahydrofuran (THF), and catalyst $PdCl_2(PPh_3)_2$ were received from Aldrich and used without purification.

The 3-Iodo-9H-carbazole (**2**) was synthesized by using Tucker's method [19].

The 3,3-Di(3-iodo-9-carbazolylmethyl)oxetane (**3**) was prepared by reaction of the 3,3-di(chloromethyl)oxetane and 3-iodo-9H-carbazole (**2**) by using the procedure we described earlier [20].

The 3,3-Bis [3-(2-methoxy-3-pyridinyl)carbazol-9-ylmethyl]oxetane (**H1**): 3,3-Bis(3-iodocarbazol-9-ylmethyl)oxetane **3** (0.8 g, 0.0012 mol), 2-methoxy-3-pyridinylboronic acid (0.46 g, 0.03 mol), potassium hydroxide (0.34 g, 0.006 mol), and catalyst $PdCl_2(PPh_3)_2$ (0.034 g, 0.000048 mol) were stirred in mixture of THF (12 mL) and degassed water (1.5 mL) at reflux for 1 h. After the TLC test, the reaction mixture was cooled and filtered. Solvents were removed by evaporation. The objective product was separated by silica gel chromatography. A mixture of ethyl acetate and hexane (vol. ratio 1:7) was used as eluent. Yield: 0.32 g (27%) of yellow material. M.p.: 257 °C (DSC). ^{1}H NMR (400 MHz, CDCl$_3$, δ, ppm): 8.23 (s, 2H, Ar), 8.17 (t, 4H, Ar, J = 7.2 Hz), 7.71 (dd, 2H, Ar, J$_1$ = 1.6 Hz, J$_2$ = 7.2 Hz), 7.65 (dd, 2H, Ar, J$_1$ = 1.4 Hz, J$_2$ = 8.6 Hz), 7.46 (t, 2H, Ar, J = 7.6 Hz), 7.37–7.25 (m, 6H, Ar), 7.01 (m, 2H, Ar), 4.73 (s, 4H, -N-CH$_2$-), 4.70 (s, 4H, -CH$_2$-O-), 4.00 (s, 6H, CH$_3$-O-). ^{13}C NMR (400 MHz, CDCl$_3$) δ 161.05, 145.25, 141.80, 140.88, 138.80, 130.96, 128.49, 127.54, 126.31, 125.18, 123.45, 121.35, 120.75, 119.96, 117.21, 108.84, 108.44, 75.93, 53.61, 50.74, 47.53. MS (APCI$^+$, 20 V): 653.19 ([M + Na]$^+$, 100%).

The 3,3-Bis [3-(4-methoxy-3-pyridinyl)carbazol-9-ylmethyl]oxetane (**H2**): 3,3-Bis(3-iodocarbazol-9-ylmethyl)oxetane **3** (0.8 g, 0.0012 mol), 6-methoxy-3-pyridinylboronic acid (0.46 g, 0.03 mol), potassium hydroxide (0.34 g, 0.006 mol) and catalyst $PdCl_2(PPh_3)_2$ (0.034 g, 0.000048 mol) were stirred into a mixture of THF (12 mL) and degassed water (1.5 mL) at reflux for 1 h. After the TLC test, the reaction mixture was cooled and filtered. The solvent was evaporated and the objective product was separated by silica gel column

chromatography using the mixture of ethyl acetate and hexane (vol. ratio 1:7) as an eluent. Yield: 0.23 g (20%) of yellow amorphous material. T_g = 139 °C (DSC). ^{1}H NMR (400 MHz, CDCl$_3$, δ, ppm): 8.47 (d, 2H, Ar, J = 2.4 Hz), 8.25 (d, 2H, Ar, J = 1.2 Hz), 8.17 (d, 2H, Ar, J = 7.6 Hz), 7.89 (dd, 2H, Ar, J$_1$ = 2.4 Hz, J$_2$ = 8.4 Hz), 7.59 (dd, 2H, Ar, J$_1$ = 2 Hz, J$_2$ = 8.4 Hz), 7.46 (t, 2H, Ar, J = 7.4 Hz), 7.37–7.28 (m, 6H, Ar), 6.85 (d, 2H, Ar, J = 8.8 Hz), 4.73 (s, 4H, -CH$_2$-N-), 4.68 (s, 4H, -CH$_2$-O-), 4.00 (s, 6H, CH$_3$-O-). ^{13}C NMR (400 MHz, CDCl$_3$) δ 163.27, 144.97, 141.83, 140.82, 137.73, 130.71, 129.97, 126.52, 125.17, 124.00, 123.28, 120.77, 120.04, 118.74, 110.81, 109.18, 108.88, 75.94, 53.58, 50.76, 47.47. MS (APCI$^+$, 20 V): 653.23 ([M + Na]$^+$, 100%).

2.2. Instrumentation and Structures of the PhOLEDs

The Bruker Avance III (400 MHz) apparatus was used for recording ^{1}H and ^{13}C nuclear magnetic resonance (NMR) spectra. The data are provided as chemical shifts (δ) in ppm against trimethylsilane. The Waters ZQ 2000 mass spectrometer was utilized for recording mass spectra.

The TGAQ50 apparatus was used for TGA (thermo-gravimetric analyses). The Bruker Reflex II DSC apparatus was utilized for differential scanning calorimetry (DSC) measurements. The TGA and DSC measurements were performed at a heating rate of 10 °C/min in a nitrogen atmosphere.

The PhOLED devices were fabricated on cleaned indium tin oxide (ITO) sputtered glass substrates. The soap solution, deionized water, acetone, and alcohol were used for cleaning the substrates, followed by ultraviolet ozone treatment. The energy levels and structure of blue and green devices using host **H1** are shown in Figure 1 as an example.
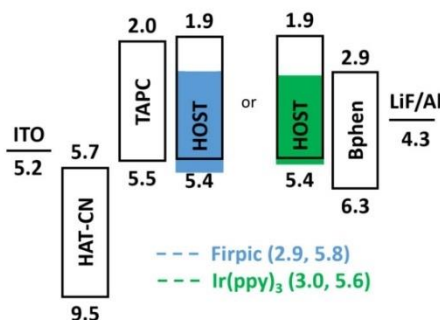
Figure 1. Structure and energy levels of blue and green PhOLEDs with host **H1**.

All the described OLEDs were formed from ITO (125 nm) as an anode, a layer of 1,4,5,8,9,11-hexaazatriphenylenehexacarbonitrile (HAT-CN, 30 nm) for hole injection, and a hole transporting layer of 1,1-bis[(di-4-tolylamino)phenyl]cyclohexane (TPC, 20 nm). The layers of HAT-CN and TPC were prepared by the thermal evaporation technique. A single emissive layer was used in all the OLEDs with different doping concentrations of phosphorescent blue FIrpic emitter or green Ir(ppy)$_3$ emitter dispersed in the host materials **H1** or **H2**. The emitting layers of 50 nm were prepared by spin-coating from chloroform solutions (formed at 2000–2500 rpm for 20 s). The 4,7-Diphenyl-1,10-phenanthroline (Bphen, 20 nm) was thermally evaporated for the electron transporting layer. LiF (1 nm) was formed by evaporation as an electron injecting layer (EIL), and Al (100 nm) was evaporated as a cathode in structures of all the OLEDs, as demonstrated in Figure 1.

Characteristics of the prepared devices were registered at room temperature. The current–voltage (I–V) measurements were performed with the Keithley 2400 electrometer

137

Minolta CS-100. A Photo Research PR-655 spectro-radiometer was utilized for measurements of luminance, chromaticity coordinates (CIE), and spectra of the electroluminescence.

As it could be seen from the energy levels presented in Figure 1, the HOMO and LUMO energy values of the new host materials **H1** and **H2** were 5.4 and 1.9 eV, respectively, and were very similar due to similar chemical structures of the synthesized materials. The energy levels are not exactly the same as that of the used dopants but are still suitable for the preparation of the host–quest systems in the emitting layers by using the blue FIrpic or green Ir(ppy)$_3$ emitters.

3. Results and Discussions

The objective host materials **H1** and **H2** were synthesized during the three synthesis steps, as shown in Scheme 1. The 3-Iodo-9H-carbazole (**2**) was firstly obtained by using the 9H-carbazole (**1**) iodination method of Tucker [19]. The 3,3-Di(3-iodo-9-carbazolylmethyl)oxetane (**3**), as a key material, was then made by the reaction of 3,3-di(chloromethyl)oxetane with an excess of the iodo-derivative **2** under basic conditions in the presence of the phase transfer catalyst—tetrabutylammonium hydrogensulfate. The objective compound **H1** was received by Suzuki reaction of the diiodo-compound **3** with an excess of 2-methoxy-3-pyridinylboronic acid. Derivative **H2** was also prepared by Suzuki reaction of the bi(3-iodocarbazole) derivative **3**. In this reaction, an excess of 6-methoxy-3-pyridinylboronic acid was used. All the prepared derivatives were confirmed by MS spectrometry, ^{1}H, and ^{13}C NMR spectroscopy. All these practically obtained data are in good agreement with theoretically developed structures.
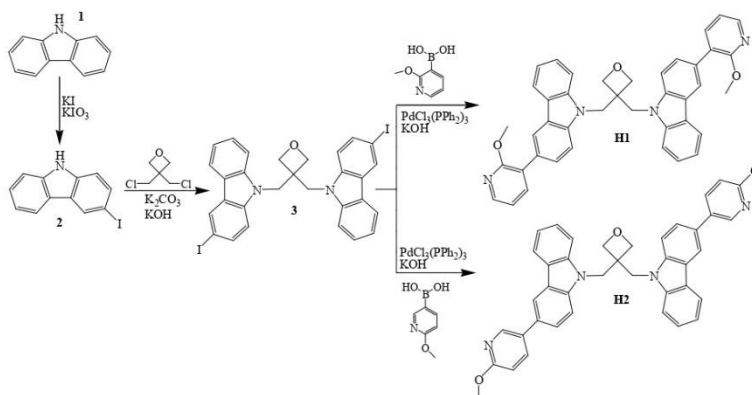
Scheme 1. Synthetic pathway of materials **H1** and **H2**.

The synthesized objective derivatives are well soluble in conventional organic solvents. The thermal evaporation technique could be used for the preparation of electroactive thin layers on substrates from these derivatives. The thin films could also be prepared by cheap spin coating from the solution method.

The behavior under thermal treatment of the synthesized objective host derivatives **H1** and **H2** was established by DSC and TGA. It was demonstrated that the derivatives obviously have high thermal stability. The temperature of 5% weight loss for the compounds **H1** and **H2** was 386 °C and 361 °C, respectively, as confirmed by TGA with a heating rate of 10 °C/min. It could be mentioned that the material with 2-methoxy-3-pyridinylcarbazole fragments has higher thermal stability than that of an analogous material with 4-methoxy-

3-pyridinyl substituents. The TGA curves are presented as Supplementary Materials for the publication.

The derivative **H1** was obtained as crystalline material after its synthesis and purification by silica gel chromatography, as confirmed by DSC. During the first heating, the endothermic melting peak of the crystals was observed at 257 °C, as shown in Figure 2. When the melted sample was cooled down, it formed an amorphous material with a high glass transition temperature (T_g) of 127 °C. Only the glass transition was also registered at the second heating of the material. No other signals due to melting or crystallization were observed by further heating of the used sample.
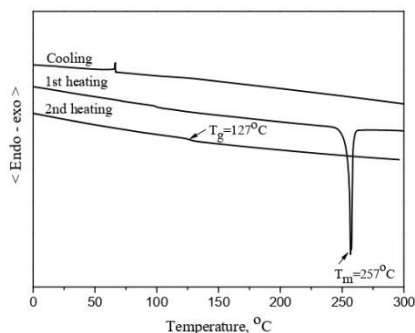
Figure 2. DSC curves of the material **H1**.

On the other hand, the compound **H2** was obtained as fully amorphous material after its synthesis, as confirmed by the DSC. The thermo-grams of the compound **H2** are shown in Figure 3. During the first and second heating scans, only the high glass transition temperature (T_g) of 139 °C was detected for the compound. Crystallization or melting signals were not registered during these heating/cooling scans in the area from 0 °C to 350 °C.
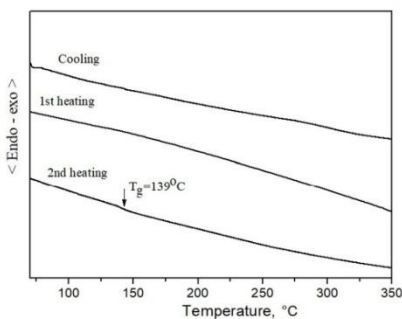
Figure 3. DSC curves of the derivative **H2**.

Phosphorescent spectra, which were registered at 77 K, aimed to establish triplet energies of the host derivatives **H1** and **H2**. The spectra are presented as Supplementary Materials for the publication. It was calculated that values of the triplet energy are 2.82 eV

for derivative **H1** and 2.81 eV for compound **H2**. The triplet energies of the hosts are higher than those declared for blue or green phosphorescent dopants, thus confirming their suitability as emitting hosts in green as well as in blue phosphorescent OLEDs applications.

To demonstrate the performance of the prepared derivatives **H1** and **H2** as emitting hosts, green and blue PhOLEDs were formed by using blue FIrpic and also green Ir(ppy)$_3$ phosphorescent emitters. Figure 4 demonstrates the electroluminescent (EL) spectra of the devices using the host material **H1**, which were registered at a brightness of 1000 cd/m^2. As it could be seen from the Figure, the EL spectra of both the OLEDs confirmed pure emissions of, correspondingly, FIrpic or Ir(ppy)$_3$ dopants, confirming the presence of suitable energy transfer between the host **H1** and the guests [21]. No additional emission zones were registered, demonstrating that the carrier recombination is located within the emitting layer and that the exciton diffusion to the hole or electron transporting layers is avoided in the OLEDs structures [22].
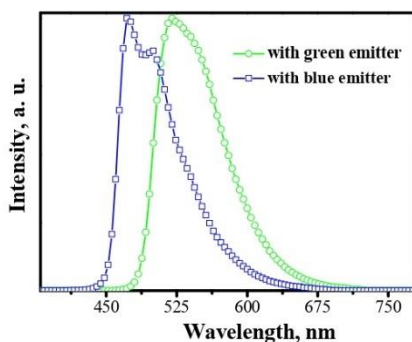
Figure 4. EL spectra of the OLEDs with host material **H1** with blue FIrpic or green Ir(ppy)$_3$ dopants in emitting layers.

The low molar mass host material **H1** was firstly tested in a concentration-dependent OLED formation with phosphorescent green Ir(ppy)$_3$ dopant. The electro-phosphorescence of the devices was seen to originate only from the quest at different voltages in all the concentration-dependent OLEDs. No host and transporting layer compound molecular emission was observed from the devices, confirming the suitable energy transfer and/or charge transfer from the host material to the dopant and also the efficient transfer of holes as well as electrons into the emission layer. It was established that 12.5 wt.% of Ir(ppy)$_3$ with green OLED demonstrated the best characteristics. Figure 5 presents the performance of the device. The green device showed a low turn-on voltage of 3 V, 49.8 cd/A of maximum current efficiency, maximum power efficiency of 33.2 lm/W, and 28,390 cd/m^2 exceeding maximal brightness. At a higher brightness of 1000 cd/m^2, which is required for illumination technologies, this device also demonstrated the highest efficiency of 34.6 cd/A (24.5 lm/W) between all the green OLEDs using host material **H1**.

140
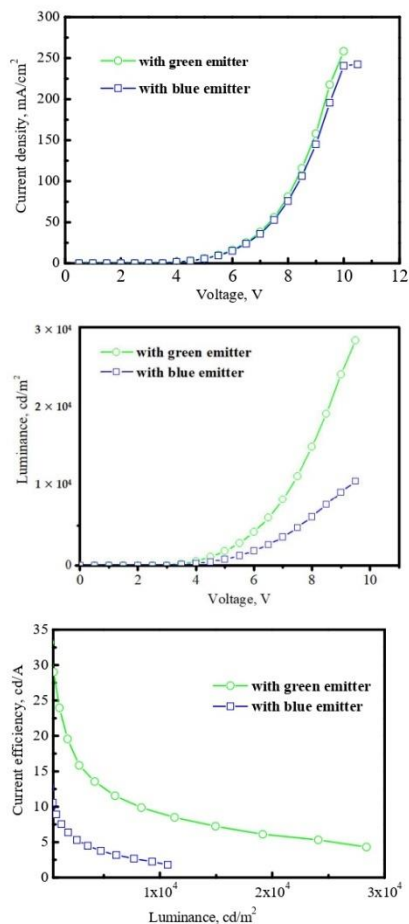
Figure 5. Characteristics of OLEDs with host **H1** with Ir(ppy)$_3$ or FIrpic dopants in emitting layers.

To demonstrate the characteristics of the compound **H1** as a host of blue OLEDs, phosphorescent devices were formed by taking blue FIrpic dopant as the guest. The structure of the produced OLED is also described in the Experimental part. The material **H1** was also tested in concentration-dependent emitting layers. As it could be seen from Figure 5, the blue OLED with 20 wt.% of FIrpic as the dopant demonstrated the best overall characteristics with a low turn-on voltage of ca. 3 V, 18.3 cd/A of maximum current efficiency, maximum power efficiency of 12.7 cd/A, and 10,700 cd/m^2 exceeding maximum brightness. The efficiency roll-off at a high current, which is typical for phosphorescent

devices, was also seen here; however, at 1000 cd/m^2, brightness, a rather high efficiency of about 13.7 cd/A (8.3 lm/W) was still registered in the blue device.

The other host material, **H2**, was also applied in blue devices by using blue FIrpic dopant as the emitter. In order to optimize the concentration of the dopant in the emitting layer, **H2** was applied as the host in concentration-dependent experiments with the FIrpic amount ranging from 15 to 22.5 wt.%. Table 1 summarizes the OLED characteristics and efficiencies of the investigated PhOLEDs. It was observed that the OLED with 15 wt.% of the FIrpic doping ratio demonstrated the best characteristics with 23.9 cd/A of current efficiency, 24.9 lm/W of power efficiency, and high external quantum efficiency of 10.3% at a brightness of 100 cd/m^2. At a higher brightness of 1000 cd/m^2, which is desired for illumination technologies, this device also had the highest efficiency of 8.0% (18.4 cd/A, 15.8 lm/W) among all the blue devices using host **H2**. The maximum luminance of the OLED exceeded 9170 cd/m^2.

Table 1. Characteristics of devices with host **H2** with Ir(ppy)$_3$ and FIrpic dopants.

Device	Dopant	Dopant, wt.%	OV, V	PE, lm/W	CE, cd/A	EQE, %	CIE$_{xy}$ Coordinates	Max Luminance, cd/m^2
			@100/1000/10,000 cd/m^2					
I-1	Firpic	15	3.0/3.7/-	24.9/15.8/-	23.9/18./-	10.3/8.0/-	(0.18, 0.39)/(0.18, 0.39)/-	9173
I-2	Firpic	17.5	3.3/4.7/-	11.5/6.6/-	12.1/9.8/-	5.1/4.1/-	(0.18, 0.4)/(0.18, 0.4)/-	3317
I-3	Firpic	20	3.2/4.4/-	8.5/5.7/-	8.6/8.0/-	3.6/3.4/-	(0.18, 0.38)/(0.18, 0.38)/-	4377
I-4	Firpic	22.5	2.8/3.6/6.8	5.9/11.5/2.6	5.7/13.1/5.7	2.4/5.5/-	(0.18, 0.4)/(0.18, 0.4)/-	10,350
II-1	Ir(ppy)$_3$	7.5	3.2/3.8/5.3	0.8/19.4/19.6	0.9/24.5/32.7	0.3/6.8/9.1	(0.32, 0.62)/(0.33, 0.62)/(0.33, 0.61)	32,390
II-2	Ir(ppy)$_3$	10	2.6/3.1/4.3	10/34.1/23.9	10.3/33.9/32.2	3.3/9.4/8.9	(0.34, 0.6)/(0.34, 0.61)/(0.34, 0.61)	38,980
II-3	Ir(ppy)$_3$	12.5	3.3/4.1/6.7	18.9/26.2/8.8	20.6/34/18.5	5.7/9.5/7.8	(0.33, 0.61)/(0.33, 0.61)/-	14,170
II-4	Ir(ppy)$_3$	15	2.6/3.1/4.3	10.9/34.1/23.9	10.3/33.9/32.2	2.3/7.4/6.9	(0.34, 0.6)/(0.34, 0.61)/(0.34, 0.61)	18,980

The host material **H2** was also applied as a component of green PhOLEDs in concentration-dependent tests with the Ir(ppy)$_3$ dopant amount in the range from 7.5 to 15 wt%. Table 1 summarizes the properties of the PhOLEDs. It can be mentioned that material **H2**-based green PhOLEDs had reasonable better performance than that of derivative **H1** using OLEDs. The devices with host **H2,** using dopant concentration ranging from 10 to 15 wt%., demonstrated rather low turn-on voltages of 2.6–3.3 V, power efficiencies of 26.2–34.1 lm/W, current efficiencies of 10.3–20.6 cd/A, and high external quantum efficiencies of 3.3–5.7% at a brightness of 100 cd/m^2. As it could be observed, the 10 wt.% of Ir(ppy)$_3$ containing OLED had the best characteristics with a current efficiency of 33.9 cd/A, power efficiency of 34.1 lm/W, and high external quantum efficiency of 9.4% at 1000 cd/m^2 brightness, which is applied for illumination applications. The maximal brightness of the OLED reached almost 39,000 cd/m^2.

It should be mentioned that these properties were demonstrated in non-optimized test PhOLEDs under an ordinary laboratory atmosphere. The PhOLEDs characteristics could be further modified by an optimization of the film thicknesses as well as layers formation conditions. It could be seen that the efficiency of all the presented devices decreases rapidly with the increase in luminance or current density. The phenomenon of organic light-emitting diodes is termed the efficiency roll-off. In particular, phosphorescent organic light-emitting diodes are known to have higher efficiency but tend to exhibit higher efficiency roll-off compared with fluorescent organic light-emitting diodes. The efficiency drops at higher luminance occur due to lack of exciton confinement in the emitting layer and exciton quenching induced by high exciton density [3,4].

4. Conclusions

Novel host derivatives were prepared during the three-step process procedure by using carbazole and methoxypyridine as building fragments. Values of triplet energy of the derivatives were 2.82 eV for **H1** and 2.81 eV for **H2**. The host materials demonstrate high thermal stability and form amorphous and homogeneous layers with very high glass transition temperatures of 127 °C for **H1** and 139 °C for **H2**. The derivatives were applied as host materials for blue or green PhOLEDs by using blue triplet dopant of

142

iridium(III)[bis(4,6-difluorophenyl)-pyridinato-*N,C2'*]picolinate or green dopant of tris(2-phenylpyridine)iridium(III) (Ir(ppy)$_3$) as phosphorescent guests. The blue device with 15 wt.% of the FIrpic emitter in host material **H2** exhibited the best overall characteristics, with a current efficiency of 23.9 cd/A, power efficiency of 24.9 lm/W, and high external quantum efficiency of 10.3% at a brightness of 100 cd/m^2. The most efficient green PhOLED device with 10 wt.% of Ir(ppy)$_3$ in host **H2** demonstrated a current efficiency of 33.9 cd/A, power efficiency of 34.1 lm/W, and high external quantum efficiency of 9.4% at high 1000 cd/m^2 brightness used in technologies of illumination. These properties were demonstrated in non-optimized PhOLEDs, under an ordinary laboratory atmosphere and could be improved in the optimization process. The obtained results confirmed that some of the new host materials are promising components for the development of highly efficient phosphorescent devices.

References

1. So, F.; Kido, J.; Burrows, P. Organic light-emitting devices for solid-state lighting. *MRS Bull.* **2008**, *33*, 663–669. [CrossRef]
2. Lee, G.-H.; Moon, H.; Kim, H.; Lee, G.H.; Kwon, W.; Yoo, S.; Myung, D.; Yun, S.H.; Bao, Z.; Hahn, S.K. Multifunctional materials for implantable and wearable photonic healthcare devices. *Nat. Rev. Mater.* **2020**, *5*, 149–165. [CrossRef]
3. Reineke, S.; Thomschke, M.; Lussem, B.; Leo, K. White organic light-emitting diodes: Status and perspective. *Rev. Mod. Phys.* **2013**, *85*, 1245. [CrossRef]
4. Chen, Y.; Wei, X.; Li, Z.; Liu, Y.; Liu, J.; Wang, R.; Wang, P.; Yamada-Takamura, Y.; Wang, Y. n-Doping-induced efficient electron-injection for high efficiency inverted organic light-emitting diodes based on thermally activated delayed fluorescence emitter. *J. Mat. Chem. C* **2017**, *5*, 8400–8407. [CrossRef]
5. Lee, J.-H.; Chen, C.-H.; Lee, P.-H.; Lin, H.-Y.; Leung, M.-K.; Chiu, T.-L.; Lin, C.-F. Blue organic light-emitting diodes: Current status, challenges, and future outlook. *J. Mater. Chem. C* **2019**, *7*, 5874–5888. [CrossRef]
6. Peng, C.C.; Yang, S.Y.; Li, H.C.; Xie, G.H.; Cui, L.S.; Zou, S.N.; Poriel, C.; Jiang, Z.Q.; Liao, L.S. Highly Efficient Thermally Activated Delayed Fluorescence via an Unconjugated Donor–Acceptor System Realizing EQE of Over 30%. *Adv. Mater.* **2020**, *32*, 2003885. [CrossRef]
7. Zhang, Q.; Zhou, Q.; Cheng, Y.; Wang, L.; Ma, D.; Jing, X. Highly Efficient Green Phosphorescent Organic Light-Emitting Diodes Based on CuI Complexes. *Adv. Mater.* **2004**, *16*, 432–436. [CrossRef]
8. Sicard, L.J.; Li, H.-C.; Wang, Q.; Liu, X.-Y.; Jeannin, O.; Rault-Berthelot, J.; Liao, L.-S.; Jiang, Z.-Q.; Poriel, C. C1-Linked Spirobifluorene Dimers: Pure Hydrocarbon Hosts for High-Performance Blue Phosphorescent OLEDs. *Angew. Chem. Int. Ed.* **2019**, *58*, 3848–3853. [CrossRef] [PubMed]
9. Tao, Y.; Wang, Q.; Yang, C.; Wang, Q.; Zhang, Z.; Zou, T.; Qin, J.; Ma, D. A simple carbazole/oxadiazole hybrid molecule: An excellent bipolar host for green and red phosphorescent OLEDs. *Angew. Chem. Int. Ed.* **2008**, *47*, 8104–8107. [CrossRef] [PubMed]
10. Holder, E.; Langeveld, B.M.W.; Schubert, U.S. New trends in the use of transition metal–ligand complexes for applications in electroluminescent devices. *Adv. Mater.* **2005**, *17*, 1109–1121. [CrossRef]

11. Kula, S.; Szlapa-Kula, A.; Kotowicz, S.; Filapek, M.; Bujak, K.; Siwy, M.; Janeczek, H.; Mackowski, S.; Schab-Balcerzak, E. Phenanthro[9,10-*d*]imidazole with thiophene rings toward OLEDs application. *Dye. Pigment.* **2018**, *159*, 646–654. [CrossRef]

12. Avilov, I.; Marsal, P.; Bredas, J.-L.; Beljonne, D. Quantum-Chemical Design of Host Materials for Full-Color Triplet Emission. *Adv. Mater.* **2004**, *16*, 1624–1629. [CrossRef]

13. Ulbricht, C.; Beyer, B.; Friebe, C.; Winter, A.; Schubert, U.S. Recent developments in the application of phosphorescent iridium (III) complex systems. *Adv. Mater.* **2009**, *21*, 4418–4441. [CrossRef]

14. Jou, J.H.; Wang, W.B.; Shen, S.M.; Kumar, S.; Lai, I.M.; Shyue, J.J.; Lengvinaite, S.; Zostautiene, R.; Grazulevicius, J.V.; Grigalevicius, S.; et al. Highly efficient blue organic light-emitting diode with an oligomeric host having high triplet-energy and high electron mobility. *J. Mat. Chem.* **2011**, *21*, 9546–9552. [CrossRef]

15. Chang, C.-H.; Griniene, R.; Su, Y.-D.; Yeh, C.-C.; Kao, H.-C.; Grazulevicius, J.V.; Volyniuk, D.; Grigalevicius, S. Efficient red phosphorescent OLEDs employing carbazole-based materials as the emitting host. *Dye. Pigment.* **2015**, *122*, 257–263. [CrossRef]

16. Tavgeniene, D.; Krucaite, G.; Baranauskyte, U.; Wu, J.-Z.; Su, H.-Y.; Huang, C.-W.; Chang, C.-H.; Grigalevicius, S. Phenanthro [9,10-d] imidazole based new host materials for efficient red phosphorescent OLEDs. *Dye. Pigment.* **2017**, *137*, 615–621. [CrossRef]

17. Lengvinaite, S.; Grazulevicius, J.V.; Grigalevicius, S.; Lai, Y.M.; Wang, W.B.; Jou, J.H. Polyethers containing 2-phenylindol-1-yl moieties as host materials for light emitting diodes. *Synth. Met.* **2010**, *160*, 1793–1796. [CrossRef]

18. Chou, H.H.; Cheng, C.H. A highly efficient universal bipolar host for blue, green, and red phosphorescent OLEDs. *Adv. Mater.* **2010**, *22*, 2468–2471. [CrossRef] [PubMed]

19. Tucker, S.H. LXXIV.—Iodination in the carbazole series. *J. Chem. Soc.* **1926**, *129*, 546–553. [CrossRef]

20. Grigalevicius, S.; Ma, L.; Qian, G.; Xie, Z.; Forster, M.; Scherf, U. New Carbazole-Based Copolymers as Amorphous Hole-Transporting Materials for Multilayer Light-Emitting Diodes. *Macromol. Chem. Phys.* **2007**, *208*, 349–355. [CrossRef]

21. Chang, C.-H.; Wu, Z.-J.; Chiu, C.-H.; Liang, Y.-H.; Tsai, Y.-S.; Liao, J.-L.; Chi, Y.; Hsieh, H.-Y.; Kuo, T.-Y.; Lee, G.-H.; et al. A new class of sky-blue-emitting Ir (III) phosphors assembled using fluorine-free pyridyl pyrimidine cyclometalates: Application toward high-performance sky-blue-and white-emitting OLEDs. *ACS Appl. Mater. Interfaces* **2013**, *5*, 7341–7351. [CrossRef] [PubMed]

22. Chang, C.-H.; Lin, Y.-H.; Chen, C.-C.; Chang, C.-K.; Wu, C.-C.; Chen, L.-S.; Wu, W.-W.; Chi, Y. Efficient phosphorescent white organic light-emitting devices incorporating blue iridium complex and multifunctional orange–red osmium complex. *Org. Electron.* **2009**, *10*, 1235–1240. [CrossRef]

144

ELSEVIER

Research Article

Easily synthesized and cheap carbazole- or phenoxazine-based hosts for efficient yellow phosphorescent OLEDs

Dovydas Blazevicius[a], Gintare Krucaite[a], Shahnawaz Shahnawaz[b], Sujith Sudheendran Swayamprabha[b], Ernestas Zaleckas[c], Jwo-Huei Jou[b,*], Saulius Grigalevicius[a,**]

[a] Department of Polymer Chemistry and Technology, Kaunas University of Technology, Radvilenu Plentas 19, LT50254, Kaunas, Lithuania
[b] Department of Materials Science and Engineering, National Tsing-Hua University, No.101, Kaungfu Rd, Hsin-Chu, 30013, Taiwan
[c] Vytautas Magnus University, Agriculture Academy, Institute of Agricultural Engineering and Safety, Studentu 15A-204, LT-53362, Akademija, Kauno r., Lithuania

ARTICLE INFO

ABSTRACT

Carbazole (H1) or phenoxazine (H2) based low molecular weight derivatives as host materials were synthesized, characterized and applied in formation of phosphorescent organic light emitting diodes (PhOLEDs). The compounds demonstrate high thermal stability and are suitable for formation of thin homogeneous amorphous layers. It was established that values of triplet energies were, correspondingly, 2.95 eV for the host H1 and 2.73 eV for the host material H2. The compounds were used as hosts for yellow PhOLEDs with iridium (III) bis (4-phenylthieno[3,2-c]pyridinato-N,C2′)acetyl-acetonate (PO-01) as the guests. The most efficient H1 host material based yellow PhOLED demonstrated EQE of 10.6%, power efficiency of 19.2 lm·W^{-1} and current efficiency of 29.4 cd A^{-1} at 100 cd m^{-2}, with a maximum luminance of 12250 cd m^{-2}. The analogous host H2 based devices exhibited noticeably better characteristics than those of host H1 containing PhOLEDs. The most efficient device with host H2 demonstrated very low turn-on voltage of 3.5 V, power efficiency of 32.2 lm/W, current efficiency of 35.8 cd/A and external quantum efficiency of 10.9% at brightness of 100 cd/m^2.

1. Introduction

Organic light-emitting devices (OLEDs) have been widely investigated due to their potential using in energy-saving lighting technologies as well as in new-generation flat-panel displays [1–6]. Some OLED based devices, for example smart phones, have been already commercialized. Phosphorescent OLEDs are attracting more and more attention because IQE (internal quantum efficiency) of the devices can achieve 100% by harvesting of both triplet and singlet excitons through the intersystem crossing and reverse intersystem crossing mechanisms [7–11]. Yellow phosphorescent emitters based PhOLED devices take an important role in the high-efficiency WOLEDs (white organic light emitting diodes) as well as in full color display applications [12–16].

The PhOLEDs are usually fabricated by using host-dopant structure to avoid triplet-triplet annihilation in the emitting layer. The hosts are as important as the phosphorescent emitters (dopants) and have significant effects on the electroluminescence characteristics of the devices [17–19]. The suitable hosts must demonstrate the following requirements: (1) high value of triplet energy to assure energy transfer from the host material to a phosphorescent dopant; (2) appropriate levels of HOMO/LUMO energies for effective injection of charge; (3) high values of glass transition as well as thermal decomposition temperatures to maintain OLED stability; (4) balanced electron and hole transport capability for broad exciton recombination zone in emitter layer [20–22].

It was earlier described in scientific literature that various materials having phenothiazinyl, indolyl or carbazolyl chromophorests demonstrate rather large values of triplet energies and are suitable hosts and/or hole transporting compounds for the second generation OLED devices [23–27]. Here, we present easily prepared and cheap carbazole- or phenoxazine -based host derivatives, which are synthesized by simple one step reaction procedure, for the solution processed yellow second generation devices.

PO-01

PEDOT:PSS

TPBi
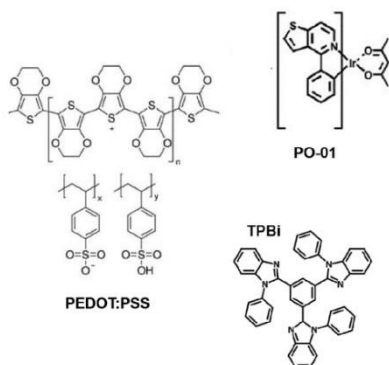
Scheme 1. Chemical structures of the materials used for preparation of PhOLEDs.
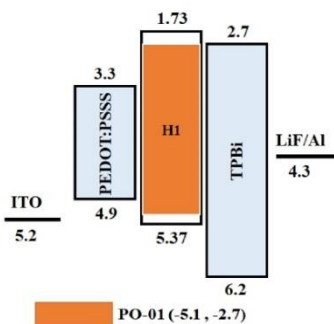
Scheme 2. Structure and energy-level diagram of host **H1**-based yellow PhOLED.

2. Experimental

2.1. Synthesis of the host derivatives

10H-Phenoxazine, 9H-carbazole, 3,3-bis(chloromethyl)oxetane, KOH, K_2CO_3, butan-2-one, tetrahydofuran (THF), tetra-*n*-butylammonium hydrogen sulfate (TBAHS) and potassium *tert*-butoxide have been purchased from Aldrich and used without an additional purification.

3,3-Bis(9-carbazolylmethyl)oxetane (**H1**) was synthesized by using similar procedures as we described earlier [28, 29]. M.p.: 199 °C (DSC). MS (APCI$^+$, 20 V): 455.01 ([M+K]$^+$, 100%). ^{1}H NMR (400 MHz, CDCl$_3$-d_6, δ, p.m.): 8.16 (d, 4H, Ar, $J = 6.4$ Hz), 7.45 (t, 4H, Ar, $J = 6.0$ Hz), 7.32–7.27 (m, 8H, Ar), 4.69 (s, 4H, -N-CH$_2$-), 4.67 (s, 4H, -CH$_2$-O-). ^{13}C NMR (400 MHz, CDCl$_3$-d_6, δ, p.m.): 141.44, 126.15, 123.36, 120.66, 119.78, 108.73, 75.99, 50.76, 47.37.

3,3-Bis(phenoxazin-10-ylmethyl)oxetane (**H2**). 10H-phenoxazine

(0.6g, 0.00327mol), potassium *tert*-butoxide (0.0408g, 0.00423mol) and 3,3-bis(chloromethyl)oxetane (0.132 ml, 0,17g, 0,0011mol) were refluxed in 5 ml of degassed THF under nitrogen for 12h. After control of the reaction by TLC, the mixture has been cooled and quenched by using ice water. The product was extracted by chloroform. The organic fraction was dried with anhydrous Na$_2$SO$_4$. The objective product was separated by column silica gel chromatography using the toluene and hexane (vol. ratio 1:7) mixture of as an eluent. Yield: 0.24g (42%) of yellowish crystals. M.p.: 198 °C (DSC). MS (APCI$^+$, 20 V): 448.63 ([M$^+$], 100%). ^{1}H NMR (400 MHz, DMSO-d_6, δ, p.m.): 6.94 (d, 4H, Ar, $J = 8.0$ Hz), 6.87–6.83 (m, 4H, Ar), 6.75–6.71 (m, 8H, Ar), 4.35 (s, 4H, -N-CH$_2$-), 4.03 (s, 4H, -CH$_2$-O-). ^{13}C NMR (400 MHz, CDCl$_3$-d_6, δ, p.m.): 144.85, 135.01, 124.37, 122.07, 116.11, 113.19, 75.35, 48.85, 44.80.

2.2. Preparation of the PhOLED devices

The chemical structures of the materials employed in this work for preparation of OLED devices are shown in Scheme 1.

The ITO sputtered glass substrates with high transmission have been obtained from Shine Materials Technology. Hole injection material PEDOT: PSS {poly(3,4-ethylene-dioxythiophene)-*co*-(styrene-sulfonate)} was obtained from Sigma Aldrich (USA). The iridium based yellow emitter **PO-01** (iridium (III) bis (4-phenylthieno[3,2-*c*]pyridinato-N,C2′)acetyl-acetonate), 2,2′,2″-(1,3,5-benzinetriyl)-tris(1-phenyl-1-H-benzimidazole) (TPBi) and LiF were purchased from Shine Materials Technology (Taiwan). The highly pure (>99.99%) aluminium ingots were purchased from Showa Chemicals. The host materials 3,3-bis(9-carbazolylmethyl)oxetane (**H1**) and 3,3-bis(phenoxazin-10-ylmethyl) oxetane (**H2**) were prepared and characterized as it is described below.

The PhOLED devices were fabricated on cleaned substrate. The cleaning was done with soap solution, deionized water, acetone, alcohol and ultraviolet ozone treatment. Structure and energy-level diagram of host **H1**-based device is shown in Scheme 2 as an example. The studied devices composed of indium tin oxide (ITO, 125 nm) as an anode layer, hole injection layer (HIL) of PEDOT:PSS (formed at 4000 rpm for 20s), single emissive layer (EML) with different doping concentration of yellow emitter **PO-01** in host **H1** or **H2**, electron transporting layer (ETL) of thermally evaporated 1,3,5-tris(N-phenylbenzimidazol-2-yl)benzene (TPBi), lithium fluoride (LiF, 1 nm) as an electron injecting layer (EIL) and aluminium (Al, 100 nm) as a cathode. The emitting layers were prepared by spin-coating from chloroform solutions (formed at 2500 rpm for 20 s).

The characteristics of all the described OLEDs were measured at room temperature. A Keithley 2400 computer mounted electrometer Minolta CS-100 was used to determine the characteristics of current-voltage (I–V). The luminance, chromaticity coordinates (CIE) and spectra of the electroluminescence of the formed devices have been obtained by exploitation of Photo Research PR-655 spectro-radiometer.

3. Results and discussion

Preparation of the oxetane-based host compounds was organized by the cheap and simple one step synthetic procedure, which is demonstrated in Scheme 3. 3,3-Bis(9-carbazolylmethyl)oxetane (**H1**) has been obtained by N-alkylation reaction of 9H-carbazole using potassium hydroxide, potassium carbonate and phase-transfer catalyst TBAHS in butan-2-one. The used procedure was similar to that which we described earlier [28,29]. The oxetane was used earlier for preparation of electroactive oligomers. 3,3-Bis(10-phenoxazinylmethyl)oxetane (**H2**) was prepared by N-alkylation reaction of 10H-phenoxazine in THF using potassium *tert*-butoxide. Structures of the objective compounds have been confirmed by using NMR spectroscopy as well as mass spectrometry. The practically obtained data were in good agreement with the theoretically proposed structures.

The synthesized compounds have been soluble in widely used organic solvents. Electroactive thin layers on substrates from these

2

146
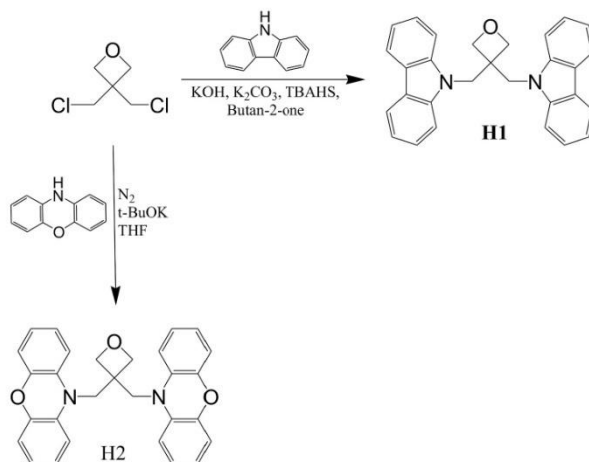
Scheme 3. Synthetic scheme of the host compounds **H1** and **H2**.

(a)

(b)
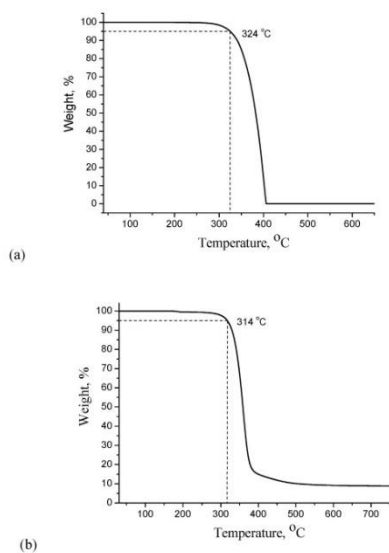
Fig. 1. TGA curves of the objective derivatives **H1** (a) and **H2** (b).
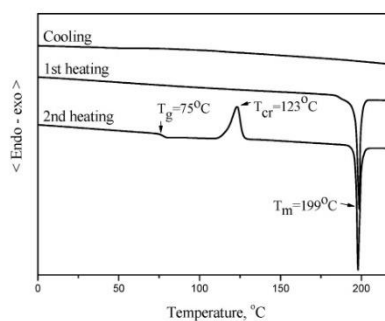
Fig. 2. DSC curves of the material **H1**.

compounds could be formed by thermal evaporation as well as by cheap spin coating from solution method.

DSC and TGA were used in order to investigate behaviour under heating of the objective host derivatives **H1** and **H2**. It was confirmed that the materials have characteristic of high thermal stability. As it is obvious from Fig. 1, temperatures of weight loss of 5% for derivatives **H1** and **H2** were 324 °C and 314 °C, respectively, as confirmed by the TGA method. It should be stated that the compound having carbazol-9-yl chromophores shows a little higher thermal stability than that of the similar compound with 10-phenoxazinyl fragments.

Both the derivatives **H1** and **H2** were obtained as crystalline materials from eluent solutions after column chromatography; however, they could be transferred to glassy state from their melted samples by cooling in air or in atmosphere of liquid nitrogen.

3
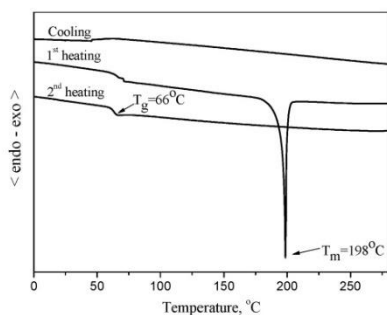
Fig. 3. DSC curves of the material **H2**.

Table 1
EL characteristics of devices using host **H1**.

Doping conc. (wt%)	@100/1000 cd/m²				Maxi. Lumi.(cd m⁻²)
	OV [V]	PE[lm W⁻¹]	CE[cd A⁻¹]	EQE [%]	
7.5	6.3/ 8.2	16/9.9	32/25.6	10.5/ 7.9	10760
10	5.6/ 7.4	17.3/ 11.4	30.7/ 26.8	10.3/ 8.5	10600
12.5	5.1/ 6.7	18.4/ 10.9	30.1/ 23.2	10.5/ 7.5	10700
15	4.8/ 6.3	19.2/ 11.3	29.4/ 22.7	10.6/ 7.5	12250

The DSC thermos-grams of derivative **H1** are shown in Fig. 2. An endothermic melting peak has been recorded at 199 °C, when the semicrystalline sample was heated during 1st heating. The melted sample was then cooled down and heated again, and the glass-transition phenomenon was recorded at 75 °C. However, on further heating crystallization of the liquid material was registered at 123 °C with formation of the same crystals, which were obtained after synthesis of the compound by using crystallization from eluent solution ($T_m = 199$ °C).

The results of DSC measurements of derivative **H2** are shown in Fig. 3. In the case, endothermic peak of the melting was registered at 198 °C, when crystals of **H2** sample were heated. The melted material was cooled down and formed an amorphous state. During the second heating of the sample only the glass-transition was determined at 66 °C and no peaks of crystallization and melting appeared on further heating. The DSC measurements confirm that both the objective materials could form thin amorphous layers for application in OLEDs formation, however the films of compound **H2** should demonstrate higher stability in the amorphous state according to the measurements due to absence of crystallization at high temperature.

Phosphorescent spectra of the materials were measured at 77K in order to establish values of triplet energies of the host derivatives **H1** and **H2**. It has been found that these values are 2.95 eV for compound **H1** and 2.73 eV for derivative **H2**. As it could be stated the triplet energy

gaps for the hosts are higher than those of yellow phosphorescent dopants, thus confirming application of these host compounds for emitting layers of yellow PhOLEDs.

To evaluate suitability of the hosts for emitting layers, yellow phosphorescent devices have been formed by using well known **PO-01** yellow triplet emitter as a dopant. Structures of the multilayer OLEDs were as follows: ITO/PEDOT:PSS/(**H1** or **H2**):X wt% of **PO-01**/TPBi/LiF/Al, where X denotes dopant concentration into host. Details of preparation of the OLEDs are presented in Experimental part. The electroluminescent (EL) properties of the devices for 7.5, 10, 12.5, and 15 wt% dopant concentration were demonstrated. A reference device without host materials **H1** and **H2** was also prepared, but its efficiency was very weak perhaps due to triplet-triplet annihilation in the emitting layer.

The EL characteristics of devices using host **H1** and their corresponding values have been shown in Table 1 and Fig. 4.

The EL spectra (Fig. 4) show primary emission peaks for different doping concentrations in **H1** host based devices. All the PhOLEDs emit light at 570 nm, which is due to the emissions of PO-01. They do not show any colours shift while changing the dopant concentration of the yellow emitter. The fabricated devices emitted yellow light having CIE coordinates of (0.49, 0.50) with broad spectra from 400 to 750 nm at 1000 cd m⁻² luminance.

The 15 wt% dopant concentration device exhibited excellent performance with EQE value of 10.6%, power efficiency (PE) of 19.2 lm·W⁻¹, and CE of 29.4 cd A⁻¹ at 100 cd m⁻², with a maximal brightness of 12250 cd m⁻². It could be also mentioned that this device exhibits PE of 11.3 lm·W⁻¹, CE of 22.7 cd A⁻¹ at a luminance of 1000 cd m⁻². For the 12.5 wt% dopant concentration the device shows PE, CE, and EQE of 18.4 lm·W⁻¹, 30.1 cd A⁻¹ and 10.5% at 100 cd m⁻² with a maximum luminance of 10700 cdm⁻², respectively. The 10 wt% dopant concentration-based device reveals PE of 17.3 lm·W⁻¹, CE of 30.7 cd A⁻¹, and EQE of 10.3%. It also depicts PE, CE, and EQE of 11.4 lm·W⁻¹, 26.8 cd A⁻¹ and 8.5% at 100 cd m⁻², respectively. The device based on 7.5% dopant has a maximal brightness of 10760 cdm⁻² and PhOLED with 15% of the dopant exhibited a maximal brightness of 12250 cdm⁻².

The host material **H2** was also characterized as host compound of yellow PhOLED devices in concentration-dependent investigations with the **PO-01** triplet emitter by using the amount in the range from 7.5 to 15 wt%. Details of preparation of the OLEDs were the same as mentioned in Experimental part. Table 2 and Fig. 5 show characteristics of the devices. All the devices also emit light with maxima at 570 nm, which is due to the emissions from the quest **PO-01**. They do not demonstrate any colours shift while changing the dopant concentration of the phosphorescent emitter.

It could be observed that host **H2**-based devices demonstrated noticeably better characteristics than those of **H1** host component based PhOLEDs, especially at high brightness. The devices with host **H2** had rather low values of turn-on voltages of 3.5–3.6 V, power efficiencies of 23.1–32.2 lm/W, current efficiencies of 26.0–35.8 cd/A and EQE of 8.1–10.9% at luminance of 100 cd/m². As it demonstrated by the data shown in Table 2, the 10 wt% of **PO-01** containing device exhibited the best overall characteristics with value of current efficiency of 33.1 cd/A, power efficiency of 22.8 lm/W and external quantum efficiency of 10.1% at luminance of 1000 cd/m², which is useful for illumination technological applications. The maximal brightness of the OLED exceeded 23100 cd/m². According to the obtained result the host material **H2** demonstrate better film forming properties and has triplet energy level, which is suited better for the **PO-01** yellow triplet emitter

148
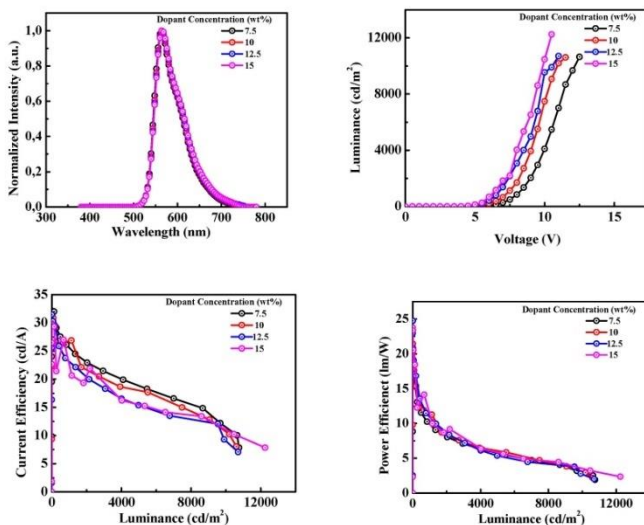
Fig. 4. PhOLED characteristics of host **H1**-based yellow devices with **PO-01** guest.

Table 2
EL characteristics of devices using host **H2**.

Doping concentration. (wt%)	@100/1000 cd/m²					Maximum. Luminance.(cd m⁻²)
	OV[V]	PE[lm W⁻¹]	CE[cd A⁻¹]	EQE[%]	CIExy coordinates	
7.5	3.5/4.9	31.6/21.2	34.9/32.9	10.6/9.9	(0.49,0.51)/(0.49,0.51)	20520
10	3.5/4.6	32.2/22.8	35.8/33.1	10.9/10.1	(0.49,0.5)/(0.49,0.5)	23190
12.5	3.6/5.1	28.6/15.5	32.8/32.8	10.1/7.9	(0.5,0.5)/(0.49,0.5)	19470
15	3.5/4.7	23.1/16.5	26.0/24.5	8.1/7.7	(0.5,0.5)/(0.5,0.5)	22360

as a dopant. It seems that due to the reasons the OLEDs using host **H2** demonstrate better characteristics. The data confirm that the host material, which is prepare by simple one step procedure, has big potential in the field of preparation of phosphorescent, second generation devices.

In conclusion, the host materials were synthesized during cheap, one step procedure by using carbazole (**H1**) or phenoxazine (**H2**) as building blocks. Triplet energy values of the compounds were 2.95 eV for **H1** and 2.73 eV for **H2**. The derivatives formed homogeneous amorphous films having values of glass transition temperatures of 75 °C for **H1** and 66 °C for **H2**. The compounds were investigated as host components for yellow phosphorescent OLEDs by using yellow triplet dopant of iridium (III) bis (4-phenylthieno[3,2-c]pyridinato-N,C2')acetyl-acetonate (**PO-01**) as the phosphorescent guest. The devices with the host of 3,3-bis(phenoxazin-10-ylmethyl)oxetane (**H2**) exhibited the best overall characteristics. The most efficient yellow PhOLED using the host had low turn-on voltage of 3.5 V, power efficiency of 32.2 lm/W, current efficiency of 35.8 cd/A and EQE of 10.9% at luminance of 100 cd/m². The maximum

brightness of the device exceeded 23100 cd/m².

CRediT authorship contribution statement

Dovydas Blazevicius: Investigation. **Gintare Krucaite:** Investigation. **Shahnawaz Shahnawaz:** Investigation. **Sujith Sudheendran Swayamprabha:** Writing – original draft. **Ernestas Zaleckas:** Formal analysis, Investigation. **Jwo-Huei Jou:** Writing – review & editing. **Saulius Grigalevicius:** Writing – review & editing.

Declaration of competing interest

The authors declare that they have no known competing financial interests or personal relationships that could have appeared to influence the work reported in this paper.

149
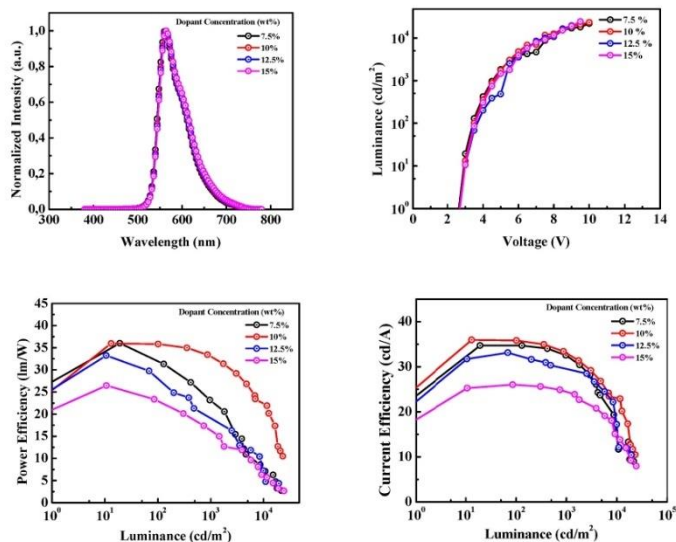
Fig. 5. PhOLED characteristics of host **H2**-based yellow devices with **PO-01** guest.

References

[1] A. Pazini, L. Maqueira, H.C. Avila, et al., Tetrahedron Lett. 59 (2018) 2994.
[2] D.M. Sun, Z.J. Ren, S.K. Yan, J. Mater. Chem. C 6 (2018) 4800.
[3] T.T. Yang, H.X. Xu, K.X. Wang, et al., Dyes Pigments 153 (2018) 67.
[4] M.A. Baldo, D.F. O'Brien, Y. You, et al., Nature 395 (1998) 151.
[5] Y.W. Liu, X.F. Wei, Z.Y. Li, et al., Adv. Opt. Mater. 6 (2018), 1800978.
[6] S. Ohisa, T. Takahashi, M. Igarashi, et al., Adv. Funct. Mater. 29 (2019), 1808022.
[7] S. Wang, Y. Zhang, W. Chen, et al., Chem. Commun. 51 (2015), 11972.
[8] G.H. Kim, R. Lampande, M.J. Park, et al., J. Phys. Chem. C 118 (2014), 28757.
[9] Y. Tao, C. Yang, J. Qin, Chem. Soc. Rev. 40 (2011) 2943.
[10] H. Nakanotani, K. Masui, J. Nishide, et al., Sci. Rep. 3 (2013) 2127.
[11] S.E. Jang, C.W. Joo, K.S. Yook, et al., Synth. Met. 160 (2010) 1184.
[12] B.-Y. Ren, R.-D. Guo, D.-K. Zhong, et al., Inorg. Chem. 56 (2017) 8397.
[13] S. Reineke, F. Lindner, G. Schwartz, et al., Nature 459 (2009) 234.
[14] S. Gong, Y. Chen, C. Yang, et al., Adv. Mater. 22 (2010) 5370.
[15] B.H. Zhang, et al., Adv. Mater. 24 (2012) 1873.
[16] S. Wang, et al., iScience 6 (2018) 128.
[17] C. Adachi, M.A. Baldo, M.E. Thompson, et al., J. Appl. Phys. 90 (2001) 5048.
[18] Y. Tao, Q. Wang, C. Yang, et al., Angew. Chem. Int. Ed. 47 (2008) 8104.
[19] E. Holder, B.M.W. Langeveld, U.S. Schubert, Adv. Mater. 17 (2005) 1109.
[20] C. Adachi, R.C. Kwong, P. Djurovich, et al., Appl. Phys. Lett. 79 (2001) 2082.
[21] I. Avilov, P. Marsal, J.-L. Bredas, D. Beljonne, Adv. Mater. 16 (2004) 1624.
[22] C. Ulbricht, B. Beyer, C. Friebe, et al., Adv. Mater. 21 (2009) 4418.
[23] J.H. Jou, W.B. Wang, S.M. Shen, et al., J. Mater. Chem. 21 (2011) 9546.
[24] J.-H. Jou, T.-H. Li, C.-C. An, et al., Organic Electronics 24 (2015) 254.
[25] G. Blazys, S. Grigalevicius, J.V. Grazulevicius, et al., Journal of Photochemistry and Photobiology A-Chemistry 174 (2005) 1.
[26] S. Kumar, C.-C. An, S. Sahoo, et al., J. Mater. Chem. C 5 (2017) 9854.
[27] C.-H. Chang, R. Griniene, Y.-D. Su, Dyes Pigments 122 (2015) 257.
[28] R. Zostautiene, J.V. Grazulevicius, Y.M. Lai, et al., Synth. Met. 161 (2011) 92.
[29] R. Zostautiene, D. Mazetyte, J.V. Grazulevicius, et al., J. Appl. Polym. Sci. 122 (2011) 908.

6

150

Article

Highly Efficient Candlelight Organic Light-Emitting Diode with a Very Low Color Temperature

Shahnawaz [1], Iram Siddiqui [1], Mangey Ram Nagar [1], Abhijeet Choudhury [1], Jin-Tin Lin [1], Dovydas Blazevicius [2], Gintare Krucaite [2], Saulius Grigalevicius [2,*] and Jwo-Huei Jou [1,*]

1   Department of Materials Science and Engineering, National Tsing Hua University, Hsinchu 30044, Taiwan; shaan88usmani@gapp.nthu.edu.tw (S.); iramsidd29@gmail.com (I.S.); mangeyrnagar@gmail.com (M.R.N.); abhijeetchoudhury101@gmail.com (A.C.); s10030267@gmail.com (J.-T.L.)
2   Department of Polymer Chemistry and Technology, Kaunas University of Technology, Radvilenu Plentas 19, LT50254 Kaunas, Lithuania; dovydas.blazevicius@ktu.lt (D.B.); gintare.krucaite@ktu.lt (G.K.)
*   Correspondence: saulius.grigalevicius@ktu.lt (S.G.); jjou@mx.nthu.edu.tw (J.-H.J.)

Abstract: Low color temperature candlelight organic light-emitting diodes (LEDs) are human and environmentally friendly because of the absence of blue emission that might suppress at night the secretion of melatonin and damage retina upon long exposure. Herein, we demonstrated a lighting device incorporating a phenoxazine-based host material, 3,3-bis(phenoxazin-10-ylmethyl)oxetane (BPMO), with the use of orange-red and yellow phosphorescent dyes to mimic candlelight. The resultant BPMO-based simple structured candlelight organic LED device permitted a maximum exposure limit of 57,700 s, much longer than did a candle (2750 s) or an incandescent bulb (1100 s) at 100 lx. The resulting device showed a color temperature of 1690 K, which is significantly much lower than that of oil lamps (1800 K), candles (1900 K), or incandescent bulbs (2500 K). The device showed a melatonin suppression sensitivity of 1.33%, upon exposure for 1.5 h at night, which is 66% and 88% less than the candle and incandescent bulb, respectively. Its maximum power efficacy is 23.1 lm/W, current efficacy 22.4 cd/A, and external quantum efficiency 10.2%, all much higher than the CBP-based devices. These results encourage a scalable synthesis of novel host materials to design and manufacture high-efficiency candlelight organic LEDs.

Keywords: phenoxazine; amorphous layer; efficiency; host derivative; light emitting diode

1. Introduction

The white lighting sources with high color temperature consist of blue light enriched emission, responsible for blue hazards especially at dawn-, dusk-, and night-time, that may lead to serious human health disorders such as retinal cell damage and melatonin suppression, increasing insomnia, obesity, or even cancer risk [1–10]. Moreover, blue-emission can cause ecological disruptions as well as discoloring well-known paintings [11,12]. The same views about the dangers posed by the blue hazard have also been echoed by various governmental and scientific organizations [13–16].

The scientific community has been demanding more research in development of blue-emission less low color temperature lighting. Interestingly, the emission spectra of the candles and old incandescent light lamps have generally emitted moderately lower blue-emission. However, the flickering nature of the candles, along with the energy-inefficient nature of both light sources, resists the devices to be reintroduced in the commercial market [4,11,12,17]. To eradicate such issues, candlelight-style lighting sources were introduced.

The next-generation organic LED lighting systems can generate the blue-free emission candlelight-style lighting that provides a pleasant sensation for the users due to its glare-free Lambertian quality [1]. Candlelight-style organic LEDs are human and environmentally

friendly due to the absence of blue emission that might suppress the secretion of melatonin and damage retina upon long exposure at night.

Jou and co-workers were one of the first to report a psychologically friendly organic LED lighting device with a power efficacy (PE) of 11.9 lm/W at 100 cd/m^2 and external quantum efficiency (EQE) of 6.4% [18]. In 2017, they reported a low-cost solution-processable organic LED with a power efficacy of 7.2 lm/W at a low-color temperature of 1807 K [2]. There have been extensive research efforts to develop next generation-al human-friendly low color temperature devices.

To achieve highly efficient and cost-effective organic LEDs, different research groups have reported numerous effective host-guest device structures to overcome exciton quenching in the emissive region, enabling high-performance electroluminescent (EL) devices [19–25]. The host materials play an essential role in the overall EL characteristic of organic LEDs [26–29]. Developing a suitable host material is highly essential to pose following properties as (1) appropriate frontier energy-levels HOMO/LUMO for aligning host-guest molecules, helping in the formation and harvesting the radiative excitons in the emissive region, (2) efficient triplet energy-level corresponding to the guest molecules, assuring complete energy transfer from host to guest materials, (3) efficient charge transfer capabilities, improving the charge transfer and charge recombination in the host-guest system, and (4) high glass-transition temperature and thermal-decomposition temperatures to attain good thin-films morphology to realize highly stable organic LEDs. The carbazolyl, indolyl, and phenothiazinyl chromophores display enormous triplet energies and appropriate host materials for the dry-processed organic LED devices [20,30–33]. However, they encounter problems in solution-processed organic LEDs, inspiring us to search for novel solution-processable host materials with desired characteristics.

Herein, we report easily synthesized and cheap phenoxazine-based host material synthesized by modest one-step reaction technique and utilized in the fabrication of solution-processed organic LED devices [34–37]. We fabricated solution-processable candlelight organic LED devices using host materials 3,3-bis(phenoxazin-10-ylmethyl)oxetane (BPMO) and 4,4′-Bis(N-carbazolyl)-1,1′-biphenyl (CBP) along with an orange-red tris(2-phenylquinoline)iridium(III) (Ir(2-phq)$_3$) and a yellow emitter iridium(III) bis(4-phenylthieno [3,2–c]pyridinato-N,C2′)acetylacetonate (PO-01) resulting in a simpler device architecture. The BPMO-based device showed a maximum luminance (L$_{max}$) of 14,950 cd/m^2 (equivalent to 16,500 candles in an area of 1 m^2) PE$_{max}$ of 24 lm/W, current efficacy (CE$_{max}$) of 22.4 cd/A and EQE$_{max}$ of 10.2% with a low CT of 1690 K at a voltage (2.9 V). While CBP-based device displayed L$_{max}$ 8393 cd/m^2 with PE$_{max}$ of 9.6 lm/W, CE$_{max}$ 11.7 cd/A, EQE$_{max}$ 6.8%, and CT as low as 1768 K at 3.5 V that is much lower than its counterpart.

Furthermore, the resulting solution-processed organic LED device is the first reported low CT with a record-break maximum permissible exposure limit (MPE) at 100 lx, 57,696 s comparative to a candle (2750 s) and an incandescent bulb (1100 s). Moreover, it exhibits 1.33% melatonin suppression sensitivity (MSS) upon exposure for 1.5 h at night at 100 lx, 66%, and 88% less than a candle and incandescent bulb, respectively.

2. Result and Discussion

2.1. Synthesis

The phenoxazine-based host material was prepared using an approach similar to our previously reported work [37] which was carried out by the simple one-step synthetic route as shown in Scheme 1. 3,3-Bis(phenoxazin-10-ylmethyl)oxetane (BPMO) host was obtained by N-alkylation reaction of phenoxazine (1) with 3,3-bis(chloromethyl)oxetane using potassium tert-butoxide in tetrahydrofuran (THF). Mass and NMR spectroscopy had recognized the presence of the newly synthesized derivative. The data were found to be well in line with the proposed structure (See details Section 3.1).
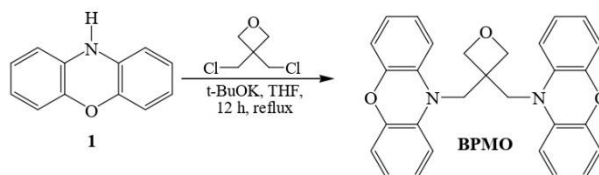
Scheme 1. Synthesis route of phenoxazine-based compound BPMO.

2.2. Theoretical Analysis

In order to better understand the link between photophysical and electronic characteristics of the synthesized host material BPMO, the theoretical calculation was carried out based on Gaussian software, density functional theory (DFT). Figure 1 shows the electron density distributions of the frontier molecular orbitals. The molecular structure is distributed by the highest occupied molecular orbitals (HOMO) and the lowest unoccupied molecular orbitals (LUMO). For BPMO, the HOMO/LUMO values estimated are −5.1/−0.7 eV, while the singlet and triplet energy are 3.7 and 3.0 eV, respectively (Table 1). Therefore, the BPMO host has 0.68 eV singlet-triplet splitting energy.
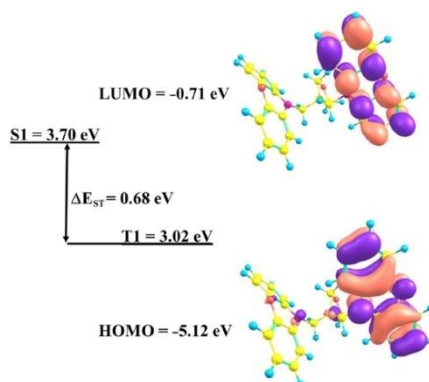
Figure 1. The HOMO (−5.1 eV), LUMO (−0.7 eV), and triplet energy (3.0 eV) of BPMO host theoretically calculated using DFT.

Table 1. A comprehensive list of photophysical and electrochemical properties of hosts BPMO and CBP for emission wavelength, melting temperature, glass-transition temperature, decomposition temperature, HOMO, LUMO, singlet/triplet energies, and bandgap.

Material	λ_{em} [a] (nm)	Tm [b] (°C)	T_g [c] (°C)	T_d [d] (°C)	HOMO [e] (eV)	LUMO [e] (eV)	HOMO [f] (eV)	LUMO [f] (eV)	E_t [g] (eV)	E_s [g] (eV)	E_t [h] (eV)	E_s [h] (eV)	Band Gap [i] (eV)	Refs.
BPMO	393	199	63	340	5.12	0.71	5.39	1.54	3.02	3.70	2.87	3.44	3.85	[37]
CBP	369	-	62	320	-	-	6.0	2.9	2.56	3.49	2.6	-	3.1	[38–40]

[a] Photoluminescence peak; [b] melting temperature; [c] glass transition temperature; [d] decomposition temperature; [e] HOMO and LUMO were calculated by DFT. [f] the redox potential obtained using a cyclic voltammetry (CV) technique gives HOMO and LUMO. [g] Calculated triplet (E_t) and singlet (E_s) energy by DFT. [h] Calculated triplet (E_t) and singlet (E_s) energy by UV-vis and low-temperature PL.. [i] Optical energy band gap.

153

2.3. Thermal Characteristics

The as-reported material BPMO possesses a very high thermal stability and crystallinity. Its melting point as 198 °C and the glass transition temperature (T_g) as 66 °C was recorded using (TGA). While (DSC) characterization confirmed the high crystallinity of the host materials [37] (See details Section 3.2).

2.4. Photophysical and Electrochemical Characteristics

Figure 2 shows the photophysical and electroluminescent (EL) characteristics of the host CBP and BPMO using UV-vis absorbance (Abs), photoluminescence (PL), and low-temperature phosphorescence (LTPL) characterizations. Abs, PL, and LTPL (at 77 K) spectra were observed at 320, 395, and 495 nm, respectively. The optical energy bandgap (E_g) of 3.85 eV for BPMO was estimated by absorbance peak. Figure 2a shows the singlet (3.44 eV), and triplet energy (2.87 eV) (see Table 1) of the host BPMO calculated using the intercepting wavelength of Abs: PL (360 nm) and Abs: LTPL (436 nm). The formula for calculating singlet and triplet energy is

Singlet: 1240/intercepting wavelength of UV-vis: PL
Triplet: 1240/intercepting wavelength of UV-vis: LTPL
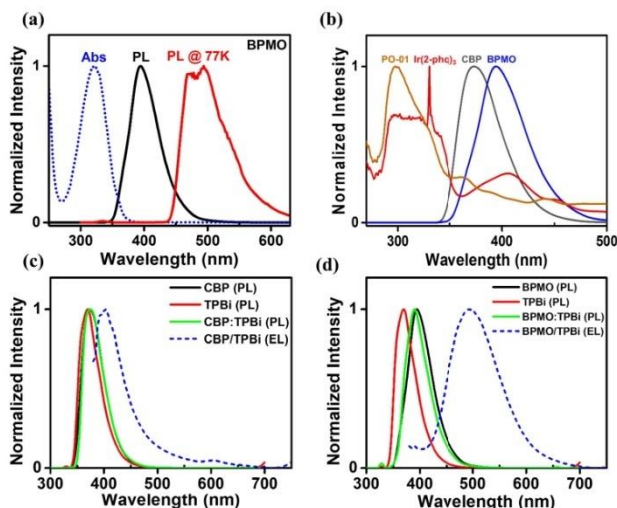
Figure 2. The photophysical and electroluminescent (EL) characteristics showing (**a**) singlet (3.44 eV) and triplet energy (2.87 eV) of the host BPMO measured using Abs/PL and PL/PL (at 77 K) spectrum, respectively. (**b**) The overlapping area between PL of hosts BPMO and CBP and Abs of yellow (PO-01) and orange-red (Ir(2-phq)₃) dye. BPMO shows the larger overlapping area, (**c**) and (**d**) show a larger redshift between the PL and EL spectra for host BPMO than CBP. The shifting is observed between the individual and mixture of host BPMO/CBP and electron-transporting layer (ETL) TPBi, respectively.

Figure 2b shows the overlapping area between normalized PL of hosts BPMO and CBP and normalized Abs of yellow (PO-01) and orange-red (Ir(2-phq)₃) dye incorporated in the candlelight organic LED devices. BPMO shows the larger overlapping area with the absorbance of yellow dye (PO-01) and orange-red dye (Ir(2-phq)₃) as 20.37 and 31.52 square units, respectively, in lieu of host CBP (19.36 and 22.6 square units).

154

Furthermore, Figure 2c,d shows a more significant redshift between the PL and EL spectra for host BPMO than CBP. The shifting is observed between the individual (BPMO/CBP and TPBi) and mixture (BPMO/CBP:TPBi) of the host and electron-transporting layer (ETL). A comparative redshift suggests the possibility of exciplex formation between the host BPMO and ETL TPBi (See details Section 3.2)

Figure S1 shows the cyclic voltammetry (CV) curve of BPMO in dichloromethane (DCM) for the oxidation scan. The HOMO and LUMO were calculated as −5.39 eV and −1.54 eV, respectively, from the CV curve, using the optical energy bandgap (E_g) 3.85 eV.

Table 1 represents the photophysical and electrochemical characteristics of the host BPMO and commercial host CBP [38–40] (See details Section 3.2).

2.5. Charge Transporting Properties (HOD/EOD)

The charge transport characteristics of the host and guest materials play a vital role in deciding effective organic LEDs performance. The hole-only and electron-only devices were fabricated based on CBP and BPMO hosts to determine their carrier mobilities.

Figure 3a shows the schematic energy level diagrams of hole-only and electron-only devices. The devices were configured as

Hole-only device: ITO (125 nm)/PEDOT:PSS (35 nm)/TAPC (20 nm)/CBP or BPMO (20 nm)/TAPC (20 nm)/Al (200 nm)

Electron-only device: ITO (125 nm)/TPBi (35 nm)/CBP or BPMO (20 nm)/TPBi (40 nm)/LiF (1 nm)/Al (200 nm).
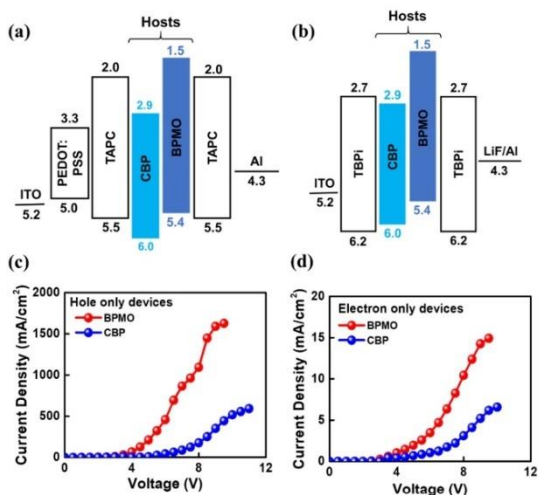
Figure 3. Schematic energy level diagrams of (**a**) hole-only, (**b**) electron-only devices, current-density-voltage curves of BPMO- and CBP-based (**c**) hole-only devices, and (**d**) electron-only devices. The cures reveal that BPMO host composing device has better charge-carrier mobility than CBP.

Figure 3c,d shows the current-density-voltage curves of BPMO- and CBP-based hole-only devices and BPMO- and CBP-based electron-only devices, respectively. The current density-voltage results from the hole-only device suggest that BPMO displays much better (almost 3 times) hole-transporting characteristics than CBP. Moreover, from an electron-

only device, BPMO displays better electron-transporting properties as compared with the CBP.

Moreover, BPMO shows bipolar nature, i.e., the hole and electron current densities are comparably equivalent, indicating balanced charge transport in organic LEDs.

2.6. Electroluminescent Properties

Solution-processed candlelight organic LED devices using host materials BPMO and CBP had been fabricated. Figure 4a shows the schematic energy level diagram using emitters PO-01 (yellow) and Ir(2-phq)$_3$ (orange-red) for BPMO- and CBP-based candlelight organic LED. The device structure is configured as ITO/PEDOT:PSS/BPMO or CBP: PO-01 (10 wt%): Ir(2-phq)$_3$ (x wt%) (x = 7.5, 10.0, 12.5, 15.0)/TPBi/LiF/Al. The materials utilized and the device fabrication are discussed in Schemes S3 and S4, respectively.
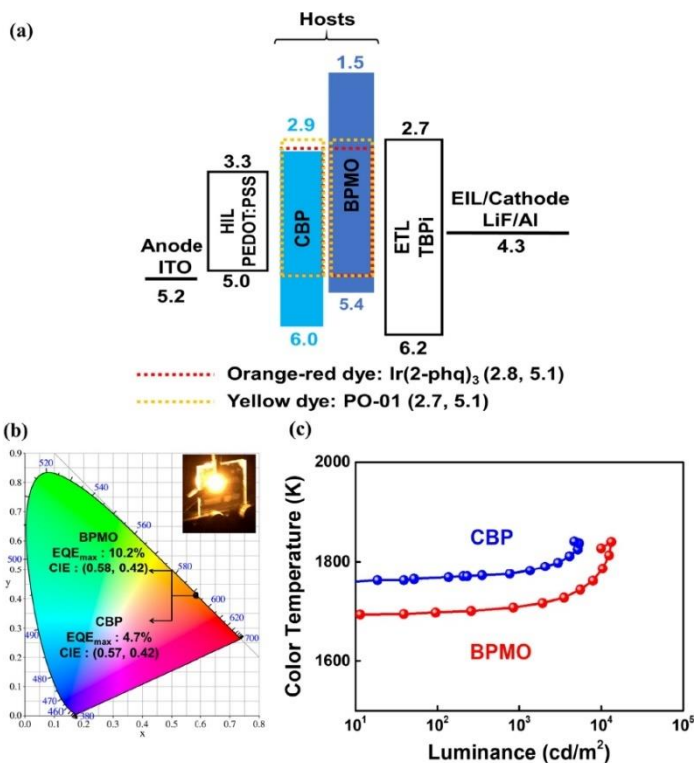
Figure 4. BPMO- and CBP-based candlelight organic LED showing (**a**) schematic energy level diagram using emitters PO-01 (yellow) and Ir(2-phq)$_3$ (orange-red), (**b**) CIE chromaticity with achieved maximum EQE and device pixel image (inset figure), and (**c**) color-temperature variation with luminance.

Figure 4b shows the CIE chromaticity coordinates for BPMO-based device as (0.58, 0.42) and CBP-based device as (0.57, 0.42). The corresponding maximum EQE (EQE_{max}) achieved were 10.2% and 4.7%, respectively. The device pixel image (inset figure) shows the candlelight emission.

Figure 4c shows the color-temperature (CT) variation with luminance for BPMO- and CBP-based devices. It can be seen that for the same luminance, CBP-based shows higher CT than BPMO-based device. The color temperature varies from 1690 to 1827 K for BPMO-based, while from 1751 to 1841 K for CBP-based candlelight organic LED, indicating the usefulness of BPMO as a host for candlelight organic LED.

The electroluminescent properties were studied for BPMO- (Figure S3a) and CBP-based (Figure S4a) candlelight organic LED devices. The yellow emitter (PO-01) at 10 wt% and orange-red emitter (Ir(2-phq)$_3$) were utilized and doped with different concentrations, as shown in Table S1.

It is observed that the EL spectra showed a bathochromic shift on increasing the concentration of orange-red emitter from 7.5 to 15 wt% (Figures S3b and S4b). For BPMO-based devices, the maximum power efficacy (PE_{max}) changes from 22.1 to 19.9 lm/W, current efficacy (CE_{max}) from 20.3 to 18.2 cd/A, external quantum efficiencies (EQE_{max}) from 9.2 to 8.5%, and CT from 1730 to 1705 K. While CBP-based devices exhibit changes in PE_{max} from 9.3 to 7.6 lm/W, CE_{max} from 11.8 to 9.3 cd/A, EQE_{max} from 5.0 to 4.0%, and CT from 1790 to 1723 K (Figures S3c–d and S4c–d). It is observed that the efficiencies and CT are concentration dependent. Therefore, the optimized concentration is 10 wt% for the orange-red emitter. Furthermore, we can reduce the candlelight color temperature by incorporating a higher concentration of orange-red emitter, utilizing highly efficient orange-red emitter, and balanced charge recombination in the emission zone [41–43].

Table 2 shows the power efficacy (PE), current efficacy (CE), EQE, color-temperature (CT) of studied BPMO- and CBP-based candlelight organic LED using (at 10 wt%) yellow (PO-01) and orange-red (Ir(2-phq)$_3$) emitters at 100, 1000 cd/m^2, and the peak efficiency luminance (at max). The BPMO-based device shows a high luminance of 14,950 cd/m^2 with PE_{max} of 24 lm/W, CE_{max} of 22.4 cd/A, and EQE_{max} of 10.2% at a very low voltage (2.9 V). At 100 cd/m^2, a 22.0 lm/W PE, 22.4 cd/A CE, 10.2 % EQE, 1690 K CT is obtained at 3.2 V. Even at higher luminance, i.e., at 1000 and 10,000 cd/m^2, the efficiencies are pronounced indicative of low roll-off at a very low CT. The results may be attributed to the balanced-charge transport, aligned HOMO, LUMO, and triplet energies, a low hole-injection barrier between HIL and emissive layer (EML), and a large hole-injection barrier between EML and ETL.

Table 2. Power efficacy (PE), current efficacy (CE), EQE, color-temperature (CT) of studied BPMO- and CBP-based candlelight organic LED using (at 10 wt%) yellow (PO-01) and orange-red (Ir(2-phq)$_3$) emitters.

Hosts.	Emitter (wt%)		DV (V)	OV (V)	PE (lm/W)	CE (cd/A)	EQE (%)	CT (K)	CIE	L_{max} (cd/m^2)
	PO-01	Ir(2-phq)$_3$		@100/1000/10,000/max. (cd/m^2)						
BPMO	10	10	2.8	3.2/4.1/6.4/2.9	22.0/16.9/5.6/23.7	22.4/21.6/11.6/22.4	10.2/9.6/5.3/10.2	1690/1707/1786	(0.58, 0.42)/(0.58, 0.42)/(0.57, 0.43)	14,950
CBP	10	10	3.2	4.1/5.7/-/3.5	7.4/3.9/-/9.6	10.3/7.4/-/11.7	4.7/3.2/-/6.8	1768/1782/-	(0.57, 0.42)/(0.57, 0.42)/-	8393

While CBP-based device displayed luminance as high as 8393 cd/m^2 with PE_{max} of 9.6 lm/W, CE_{max} 11.7 cd/A, EQE_{max} 6.8%, and CT as low as 1768 K at 3.5 V that is much lower than its counterpart in all respect suggesting BPMO-based devices are 150, 91, and 50% better in terms of PE, CE, and EQE, respectively (Figure 5b,d).
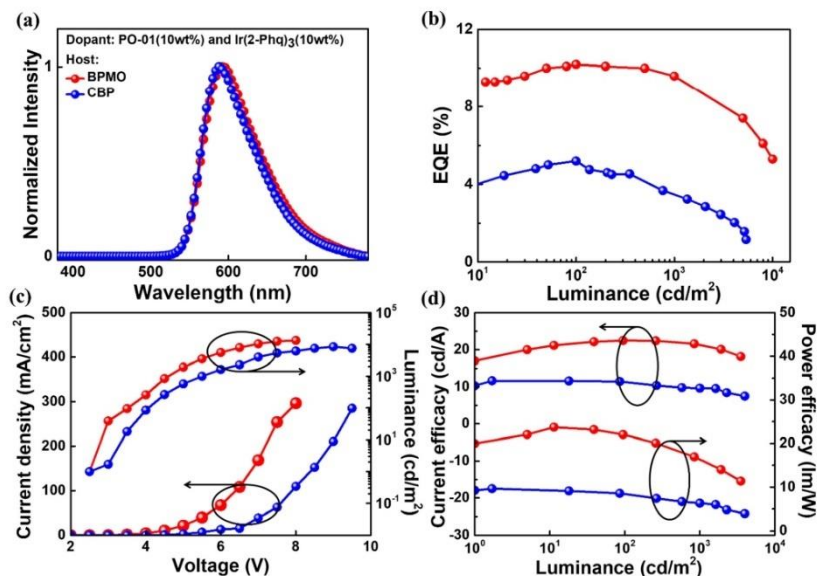
Figure 5. The studied BPMO- and CBP-based candlelight organic LEDs with (at 10 wt%) yellow and (at 10 wt%) orange-red emitter showing (**a**) the electroluminescent spectra, (**b**) variation of EQE with respect to luminance, (**c**) luminance-voltage-current density (L–V–J), (**d**) power efficacy-luminance-current-efficacy curve. The BPMO-based organic LED device shows better performance compared to the CBP-based device.

Figure 5c shows the current-density curves concerning voltages. The BPMO-based device possesses higher current density and luminance than the CBP-based device, indicative of the high carrier mobility of BPMO. Such devices may show a better injection of positive charge carriers and efficient exciton generation in the emissive zone [44,45]. However, increasing the voltage increases the current density and luminance decreases due to charge imbalance and the influence of exciton quenching [46].

Figure 5b displays the external quantum efficiencies curves concerning luminance for the candlelight organic LED devices having different hosts, i.e., BPMO and CBP. Candlelight organic LED devices fabricated with BPMO possesses higher EQE as compared with control device fabricated using CBP. Moreover, it can be observed that the EQE increases as the luminance increases up to a certain level, and afterward, EQE starts decreasing because of charge imbalance and exciton quenching [47–49]. Figure 5a exhibits electroluminescence spectra of candlelight organic LED fabricated with different host BPMO and CBP. It is observed that the EL spectra of BPMO-based candlelight organic LED are slightly red-shifted as compared with CBP-based devices, which is attributed to high hole mobility of BPMO and formation of excitons at ETL/EML interface [50–52].

For achieving higher efficiency, the device is optimized by varying the thickness of the electron-transport layer (ETL). The EL properties of studied organic LED devices are shown in Figure 6, and the values are summarized in Table 3. Figure 6 shows the studied BPMO- and CBP-based candlelight organic LEDs with (at 10 wt%) yellow and (at 10 wt%) orange-red emitter by varying electron transporting layer (ETL) thickness. Negligible change is

158

observed in EL spectra on varying thickness from 45–55 nm (Figure 6a). Figure 6b displays that EQE increases on increasing the thickness, which may be attributed to microcavity changes in the fabricated organic LED device.
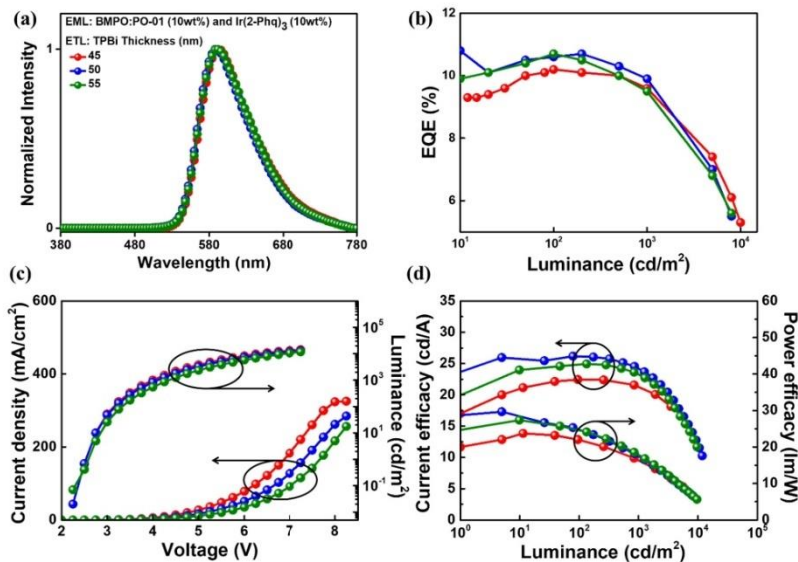
Figure 6. The studied BPMO- and CBP-based candlelight organic LEDs with (at 10 wt%) yellow and (at 10 wt%) orange-red emitter by varying electron transporting layer (ETL) thickness showing (**a**) the electroluminescent spectra, (**b**) variation of EQE with respect to luminance, (**c**) luminance-voltage-current density (L–V–J), (**d**) power efficacy-luminance-current-efficacy curve. The device with 55 nm thickness shows better performance among all.

Table 3. Effects of ETL (TPBi) thickness on power efficacy (PE), current efficacy (CE), EQE, color-temperature (CT) of studied BPMO- and CBP-based candlelight organic LED using (at 10 wt%) yellow (PO-01) and orange-red (Ir(2-phq)$_3$) emitters.

ETL (nm)	DV (V)	OV (V)	PE (lm/W)	CE (cd/A)	EQE (%)	CT (K)	CIE	L_{max} (cd/m^2)
				@100/1000/10,000/max. (cd/m^2)				
45	2.8	3.2/4.1/6.4/2.9	22.0/16.9/5.6/23.1	22.4/21.6/11.6/22.1	10.2/9.6/5.3/9.5	1690/1707/1786/-	(0.58, 0.42)/(0.58, 0.42)/(0.57, 0.43)	14,950
50	2.8	3.2/4.1/6.6	24.7/17.9/5.4/24.8	24.8/23.3/11.3/28.8	10.6/9.9/-/10.6	1785/1795/1898/-	(0.57, 0.43)/(0.57, 0.43)/-	13,520
55	2.9	3.3/4.6/7.1	22.9/10.4/4.9/23.7	24.2/15.3/11/24.2	10.7/6.7/-/10.7	1732/1744/1837/-	(0.57, 0.43)/(0.57, 0.43)/-	13,250

Figure 6c shows that the thicker the device is, the lower is the current density and luminance attributed to the imbalanced charge carriers that may cause a bulk majority carrier leading to non-radiation recombination [53–55].

Figure 6d demonstrates that the PE and CE meaningfully changed depending on the thickness of electron transport layers [56–58], i.e., increases with increasing the thickness of ETL. The PE$_{max}$ varies from 23.1 to 24.8 lm/W and CE$_{max}$ from 22.1 to 28.8 cd/A as the thickness of the ETL increases from 40 to 50 nm, which may be due to balanced charge-

carriers in the emissive region. However, further increasing the thickness to 55 nm, a drop in PE and CE may be attributed to variations in trap densities in the ETL that may limit the charge transport and cause the charge imbalance in the emissive region [59–61].
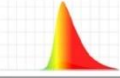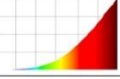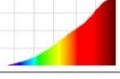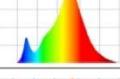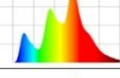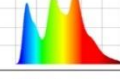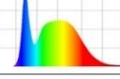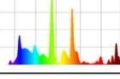
Moreover, the color temperature of candlelight organic LED increases from 1690 to 1785 K as the thickness increases from 45 to 50 nm, which may be attributed to the changes in the recombination zone position in the emissive layer [62,63].

2.7. Comparison between the Studied Very Low Color-Temperature Candlelight Organic LED and Commercial Luminaires

Table 4 shows the comparison between the spectrum, color temperature (CT), melatonin suppression sensitivity (MSS) (1.5 h exposure), and maximum permissible exposure limit (MPE) of the studied very low color temperature candlelight organic LED and the commercial luminaires, including, incandescent bulbs, warm white LEDs, and organic LEDs, cold white LEDs, and organic LEDs, and CFLs.

Table 4. Comparison between the spectrum (350–780 nm), color temperature (CT), melatonin suppression sensitivity (MSS) (1.5 h exposure), and maximum permissible exposure limit (MPE) of the studied very low color temperature candlelight organic LED and the commercial luminaires.

Light Source	Spectrum	CT (K)	MSS (%)	MPE (s) @100 lx
This work		1690	1.33	57,696
Candle Light		1884	4.0	2750
Incandescent Bulb		2444	11.5	1100
Warm-white LED		2704	8.0	1000
Warm-white organic LED		3080	6.9	1050
Cold-white organic LED		4034	12.8	590
Cold-white LED		5549	19.8	380
Cold-white CFL		5843	29.9	320

The blue-emission-free BPMO-based candlelight organic LED possesses a color temperature of 1690 K, 180 times friendlier to the cold-white CFL (CT of 5843 K) (See Section 3.5 for theoretical calculations). Correspondingly, at 100 lx, the MPE is 57,696 s (16 h) and 320 s, respectively. The melatonin secretion sensitivity (1.33%) at 100 lx of the studied device is 22.4 times friendlier than its counterpart cold-white CFL (29.9%) upon exposure for 1.5 h at night.

In contrast to cold-white LEDs, the studied device exhibits 152 times retina pleasant and 15 times amicable to MSS. While, for cold white organic LEDs, the candlelight organic LED is 98 times human eye-friendly and 9.6 times friendlier to melatonin secretion.

Moreover, the studied device is 57.6/54.9, and 6/5.2 times enhanced than warm-white LED (CT of 2704 K) and warm-white organic LED (CT of 3080 K) in terms of MPE/MSS, respectively.

Furthermore, the fabricated candlelight organic LED is far better than incandescent bulb (CT of 2444 K) and candle light (CT of 1884 K) in prospects of both the retina damage and melatonin suppression, i.e., 52.4 times human eye-friendly and 8.6 times melatonin generation-friendly than the incandescent bulb, while 21 times human eye-friendly and 200% more melatonin generation-friendly than candle-light due to the absence of blue-emission.

Therefore, the studied candlelight organic LED is free from flickering, scorching, glare, and, most importantly, PM 2.5, perhaps, significantly energy-efficient than any commercial luminaires.

Figure 7 shows the reported color temperature (at 100 cd/m^2) for a solution and dry-processed candlelight organic LED devices: the CT vs. CE plot displaying the lowest color temperature achieved with high CE compared to most other reports and the CT vs. PE plot displaying a high PE of 22.0 lm/W at 1690 K CT. Most devices are reported using tandem or complex device structures with more than two dopant and/or extra transporting layers. A few published papers showed candlelight organic LED fabricated via a dry process. Furthermore, a comparatively studied and reported candlelight organic LEDs showing their fabrication method, color temperature, power efficacy, current efficacy, and the respective references are revealed in Table S2.
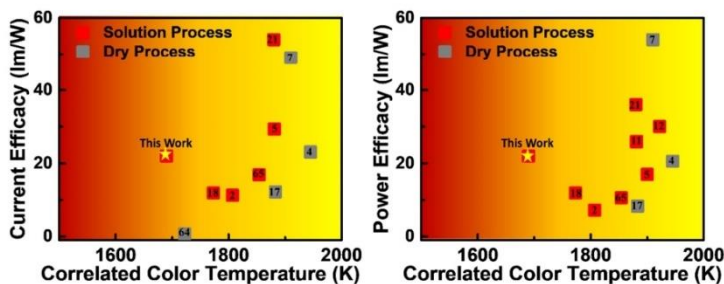
Figure 7. The reported color temperature (at 100 cd/m^2) for the solution and dry-processed candlelight organic LED devices against current efficacy and power efficacy [2,4,5,7,11,12,17,18,21,64,65].

Therefore, this work may direct the field specialists to synthesize novel potential host materials to fabricate low-cost and energy-efficient blue-emission-free organic LED devices for solid-state lighting applications.

161

3. Materials and Methods

3.1. Synthesis

The as-synthesized material 3,3-bis(phenoxazin-10-ylmethyl)oxetane (BPMO) was used as the host material. The material was synthesized using silica gel column chromatography and the yield is found to be 0.24 g (42%) of yellowish crystals. The melting point is found to be at 199 °C through DSC calculation. The complete synthesis of material is described in our previously reported journal [37].

3.2. Characterization and Measurements

Thermogravimetric analysis (TGA) was conducted on TGAQ50 equipment (Verder Scientific, Haan, Germany). The TGA and DSC curves were recorded at a 10 °C/min heating rate in a nitrogen environment. A Bruker Reflex II thermos-system was used to perform differential scanning calorimetry (DSC) measurements [37]. Phosphorescence characteristic of BPMO was recorded in THF solution on a Hitachi F-7000 fluorescence spectrophotometer (Edinburgh Intruments Ltd, Livingston, United Kingdom) with a delay time of 6.25 ms at low-temperature 77 K to determine the triplet energy (E_t). The photophysical measurement (UV-vis and photoluminescence (PL)) of the host materials BPMO and CBP was performed on Metertech SP-8001 (SHISHIN TECHNOLOGY CO., LTD., Taipei, Taiwan) and JASCO FP-6500 (JASCO FP-6500, Tokyo, Japan) . The tetrahydrofuran (THF) was used as a solvent to analyze the photophysical behavior at room temperature in quartz cuvettes. The solvent was purchased from commercial resources. The host materials BPMO and CBP solutions with solvent THF were prepared 1 mg/mL to measure UV-vis and PL. The instrument's excitation wavelength and scan speeds were 350 nm and 10 nm/min, respectively. The electrochemical measurements (cyclic voltammetry, CV) were executed on CH instruments CH1604A electrochemical workstation (Artisan technology group, Champaign County, Illinois, United States) using three-electrode assembly, including a glassy carbon working electrode, an auxiliary platinum electrode, and a non-aqueous Ag/AgCl reference electrode. The measurement was performed at an ambient temperature under a nitrogen atmosphere in dichloromethane (DCM) using 0.1 M tetrabutylammonium perchlorate (Bu_4NClO_4) as the corresponding electrolyte CH-instruments CH1604A potentiostat.

3.3. Materials

In this research, the sputtered indium tin oxide (ITO) of glass substrates with a sheet resistance of 25 sq^{-1} was purchased from Shine Materials Technology Co. Ltd., Taiwan. The hole-transport/-injection (HTL/HIL) material, i.e., poly(3,4-ethylene-dioxythiophene)-poly-(styrenesulfonate) (PEDOT:PSS), was acquired from UniRegion Bio-tech (UR-AI 4083, Hsinchu, Taiwan). The host material 3,3-bis(phenoxazin-10-ylmethyl)oxetane (BPMO) is synthesized in our laboratory. Phenoxazine (1), 3,3-bis(chloromethyl)oxetane, THF, and potassium tert-butoxide were purchased from Aldrich and used as received. Other organic small molecules used for this work such as the one we used as a host (control part) material 4,4′-Bis(N-carbazolyl)-1,1′-biphenyl (CBP), guest materials iridium(III)bis(4-phenylthieno[3,2-c]pyridinato-N,C2′)acetylacetonate (PO-01), Tris(2-phenylquinoline) iridium(III) (Ir(2-phq)$_3$, electron-transport material (ETM) 1,3,5-tris(N-phenylbenzimidazol-2-yl)benzene (TPBi), and an electron injection material lithium fluoride (LiF) were purchased from Shine Materials Technology Co. Ltd, Taiwan. Furthermore, aluminum ingots (Al) used as cathode were acquired from Showa Chemicals, Japan.

3.4. Device Fabrication and Characterization

The displayed highly efficient candlelight organic LEDs with very low-color temperature were fabricated in the following conventional structure: ITO (125 nm)/PEDOT:PSS (35 nm)/CBP or BPMO: 10 wt% PO-01 and x wt% Ir(2-phq)$_3$ (20 nm)/TPBi (40 nm)/LiF (1 nm)/Al (200 nm). Indium tin oxide (ITO) of work function 5.2 eV sputtered on the glass substrate is used as an anode for the device. A hole-injection/-transporting material PEDOT:PSS with HOMO, LUMO 5.0, 3.3 eV, respectively, is spin-coated at 4000 rpm for the

162

20 s and heated for 10 min at 120 °C. Meanwhile, an emissive layer solution is prepared by dissolving the organic materials CBP, BPMO, PO-01, Ir(2-phq)$_3$ in tetrahydrofuran (THF) and sonicated for 30 min at 60 °C. Once the solutions are completely dissolved and cooled, they are filtered separately. Two distinct EML solutions are prepared, one with CBP as a host and the other as BPMO. 10 wt% PO-01 and different concentrations of Ir(2-phq)$_3$ such as 7.5, 10, 12.5, and 15 wt% were mixed in two host solutions and named as EML1 (with CBP) and EML2 (BPMO), keeping CBP as a control part for the experiment. The as-prepared EMLs are spin-coated at 2500 rpm at ambient temperature for 20 s on the pre-deposited PEDOT:PSS, and the devices are kept in sample boxes for further processes. The entire spin-coating process is performed in an inert environment of the glove box. Subsequently, the devices are transferred to a pre-loaded thermal evaporation chamber. Once the vacuum is reached below 10^{-6} torr, TPBi, LiF, and Al deposition is performed for the defined layer thicknesses. Further, the fabricated devices are kept in a mini-chamber of the glove box and taken for testing one at a time. The current-voltage-luminance (J-V-L) measurement is done by a Keithley source measurement unit (Keithley 2400). The CIE chromatic coordinates, electroluminescence spectra, and luminance are determined using a Photo Research PR-655 spectrum scan and CS100A luminance meter. The device emission area is defined as the overlapping area of the visible cathode, and the anode is used as 9 mm^2. All the measured luminance is taken in forward directions. The entire testing process is performed in a closed dark room in an ambient environment.

3.5. Theoretical Calculation of MSS and MPE

3.5.1. Maximum Permissible Exposure-Limit (MPE)

The maximum permissible exposure-limit (MPE) presented by the international Commission on Non-radiation Protection Council (ICNIRP) [66] is used to quantify the blue light hazards, which can be calculated as following:

$$MPE = \frac{100}{E_B} \tag{1}$$

where E_B is the photo-retinitis or blue light hazard weighted radiation (W/m^2) [12,67,68].

3.5.2. Melatonin Suppression Sensitivity

The melatonin suppression sensitivity (MSS) was presented by Prof. Jou [69,70], which can be calculated by the following formula:

$$MSS = \frac{S_{LC}(\lambda)}{S_{LC}(480)} \times 100\% \tag{2}$$

where S_{LC} is the melatonin suppression spectrum per lux for a given polychromatic light, relative to that for a reference blue light of 480 nm.

4. Conclusions

We reported a solution-processable candlelight organic LED with a very low color-temperature via a simpler device architecture. The device consists of a phenoxazine-based host BPMO along with an orange-red and a yellow dye, Ir(2-phq)$_3$ and PO-01, respectively. The study shows a color temperature of 1690 K, which is significantly lower than the oil lamps (1800 K), candles (1900 K), and incandescent bulbs (2444 K). Furthermore, at 100 lx, a record-breaking maximum permissible exposure limit of 57,696 s is obtained along with 1.33% melatonin suppression sensitivity upon exposure for 1.5 h at night. Moreover, BPMO-based candlelight organic LED device enhanced a 200, 120, and 120% in PE, CE, and EQE at 100 cd/m^2, respectively, concerning CBP. The fundamental elements underlying better device efficiencies have excellent electron-blocking abilities, suitable HOMO, LUMO, and triple energy levels, decreased hole-injection barrier between host and HIL, and substantially confined light-emitting excitation to the required recombination

163

zone; moreover, the BPMO-based candlelight organic LED. This work will enable the fabrication of highly efficient candlelight organic LED lighting devices with the feasibility of solution processes.

Supplementary Materials: The following are available online, Figure S1: cyclic voltammetry (CV) curve showing one-step oxidation of the host BPMO, Figure S2: the chemical structure of HIL (PEDOT:PSS), host (BPMO and CBP), yellow emitter (PO-01), orange-red emitter (Ir(2-phq)$_3$), and ETL (TPBi) materials incorporated in this research, Figure S3: the studied BPMO-based candlelight organic LEDs with (at 10 wt%) yellow and (at 7.5, 10 and 12.5 wt%) orange-red emitter, Figure S4: the studied CBP-based candlelight organic LEDs with (at 10 wt%) yellow and (at 7.5, 10 and 12.5 wt%) orange-red emitter, Table S1: power efficacy (PE), current efficacy (CE), EQE, color-temperature (CT) of studied BPMO- and CBP-based candlelight organic LED, Table S2: a comparative study of the studied and reported candlelight organic LEDs showing the fabrication method, color temperature, power efficacy, current efficacy.

Author Contributions: Investigation, S., I.S., M.R.N., A.C., J.-T.L., D.B., and G.K.; writing—original draft preparation, S., S.G. and I.S.; writing—review and editing, J.-H.J. and S.G. All authors have read and agreed to the published version of the manuscript.

Conflicts of Interest: The authors declare no conflict of interest.

Sample Availability: Samples of the compounds BPMO are available from the authors.

References

1. Jou, J.H.; Yu, H.H.; Tung, F.C.; Chiang, C.H.; He, Z.K.; Wei, M.K. A replacement for incandescent bulbs: High-efficiency blue-hazard free organic light-emitting diodes. *J. Mater. Chem. C* **2017**, *5*, 176–182. [CrossRef]
2. Jou, J.H.; Singh, M.; Song, W.C.; Liu, S.H. Printable candlelight-style organic light-emitting diode. In *IOP Conference Series: Materials Science and Engineering, Proceedings of the 5th International Conference on Manufacturing, Optimization, Industrial and Material Engineering, Bali, Indonesia, 1–2 April 2016*; Volume 215, p. 012022. Available online: https://iopscience.iop.org/article/10.1088/1757-899X/215/1/012022/meta (accessed on 2 December 2021).
3. Jou, J.H.; Chen, P.W.; Chen, Y.L.; Jou, Y.C.; Tseng, J.R.; Wu, R.Z.; Hsieh, C.Y.; Hsieh, Y.C.; Joers, P.; Chen, S.H.; et al. OLEDs with chromaticity tunable between dusk-hue and candle-light. *Org. Electron.* **2013**, *14*, 47–54. [CrossRef]
4. Sun, Q.; Hu, Y.; Dai, Y.; Ma, D. Low color-temperature, high color rendering index hybrid white organic light-emitting diodes by the effective control of exciton recombination zone. *J. Mater. Chem. C* **2017**, *5*, 8022–8026. [CrossRef]
5. Jou, J.H.; Su, Y.T.; Liu, S.H.; He, Z.K.; Sahoo, S.; Yu, H.H.; Chen, S.Z.; Wang, C.W.; Lee, J.R. Wet-process feasible candlelight OLED. *J. Mater. Chem. C* **2016**, *4*, 6070–6077. [CrossRef]
6. van Bommel, W.J.M. Non-visual biological effect of lighting and the practical meaning for lighting for work. *Appl. Ergon.* **2006**, *37*, 461–466. [CrossRef]
7. Hu, Y.; Zhang, T.; Chen, J.; Ma, D.; Cheng, C.H. Hybrid organic light-emitting diodes with low color-temperature and high efficiency for physiologically-friendly night illumination. *Isr. J. Chem.* **2014**, *54*, 979–985. [CrossRef]
8. Pauley, S.M. Lighting for the human circadian clock: Recent research indicates that lighting has become a public health issue. *Med. Hypotheses* **2004**, *63*, 588–596. [CrossRef] [PubMed]
9. Lockley, S.W.; Brainard, G.C.; Czeisler, C.A. High sensitivity of the human circadian melatonin rhythm to resetting by short wavelength light. *J. Clin. Endocrinol. Metab.* **2003**, *88*, 4502–4505. [CrossRef]
10. Light Emitting Diodes (LEDs) and the Blue Light Risk. Points de Vue, International Review of Ophthalmic Optics. Available online: https://www.pointsdevue.com/article/light-emitting-diodes-leds-and-blue-light-risk (accessed on 24 June 2021).
11. Jou, J.H.; Hsieh, C.Y.; Tseng, J.R.; Peng, S.H.; Jou, Y.C.; Hong, J.H.; Shen, S.M.; Tang, M.C.; Chen, P.C.; Lin, C.H. Candle light-style organic light-emitting diodes. *Adv. Funct. Mater.* **2013**, *23*, 2750–2757. [CrossRef]
12. Jou, J.H.; Singh, M.; Su, Y.T.; Liu, S.H.; He, Z.K. Blue-hazard-free candlelight OLED. *J. Vis. Exp.* **2017**, *121*, e54644. [CrossRef]
13. Blue Light Has a Dark Side—Harvard Health. Available online: https://www.health.harvard.edu/staying-healthy/blue-light-has-a-dark-side (accessed on 26 June 2021).
14. AMA Adopts Guidance to Reduce Harm from High Intensity Street Lights. American Medical Association. Available online: https://www.ama-assn.org/press-center/press-releases/ama-adopts-guidance-reduce-harm-high-intensity-street-lights (accessed on 26 June 2021).

15. 64% of People Unaware of Blue Light Impact on Skin. News, Unilever Global Company Website. Available online: https://www.unilever.com/news/press-releases/2020/sixty-four-percent-of-people-unaware-of-blue-light-impact-on-skin.html (accessed on 26 June 2021).

16. Health Effects of Lighting Systems Using Light-Emitting Diodes (LEDs). LEDs & Blue Light. Available online: https://www.anses.fr/en/content/leds-blue-light (accessed on 26 June 2021).

17. Gong, Y.; Liu, J.; Zhang, Y.; He, G.; Lu, Y.; Fan, W.B.; Yuan, W.Z.; Sun, J.Z.; Zhang, Y. AIE-active, highly thermally and morphologically stable, mechanochromic and efficient solid emitters for low color temperature OLEDs. *J. Mater. Chem. C* **2014**, *2*, 7552–7560. [CrossRef]

18. Jou, J.H.; Tang, M.C.; Chen, P.C.; Wang, Y.S.; Shen, S.M.; Chen, B.R.; Lin, C.H.; Wang, W.B.; Chen, S.H.; Chen, C.T.; et al. Organic light-emitting diode-based plausibly physiologically-friendly low color-temperature night light. *Org. Electron.* **2012**, *13*, 1349–1355. [CrossRef]

19. Swayamprabha, S.S.; Dubey, D.K.; Shahnawaz; Yadav, R.A.K.; Nagar, M.R.; Sharma, A.; Tung, F.C.; Jou, J.H. Approaches for Long Lifetime Organic Light Emitting Diodes. *Adv. Sci.* **2021**, *8*, 2002254. [CrossRef]

20. Jou, J.H.; Li, T.H.; Kumar, S.; An, C.C.; Agrawal, A.; Chen, S.Z.; Fang, P.H.; Krucaite, G.; Grigalevicius, S.; Grazulevicius, J.; et al. Enabling high-efficiency organic light-emitting diodes with a cross-linkable electron confining hole transporting material. *Org. Electron.* **2015**, *24*, 254–262. [CrossRef]

21. Jou, J.H.; Chen, S.H.; Shen, S.M.; Jou, Y.C.; Lin, C.H.; Peng, S.H.; Hsia, S.P.; Wang, C.W.; Chen, C.C.; Wang, C.C. High efficiency low color-temperature organic light-emitting diodes with a blend interlayer. *J. Mater. Chem.* **2011**, *21*, 17850–17854. [CrossRef]

22. Zhao, F.; Ma, D. Approaches to high performance white organic light-emitting diodes for general lighting. *Mater. Chem. Front.* **2017**, *1*, 1933–1950. [CrossRef]

23. Jou, J.H.; Kumar, S.; Agrawal, A.; Li, T.H.; Sahoo, S. Approaches for fabricating high efficiency organic light emitting diodes. *J. Mater. Chem. C* **2015**, *3*, 2974–3002. [CrossRef]

24. Shahnawaz; Swayamprabha, S.S.; Nagar, M.R.; Yadav, R.A.K.; Gull, S.; Dubey, D.K.; Jou, J.H. Hole-transporting materials for organic light-emitting diodes: An overview. *J. Mater. Chem. C* **2019**, *7*, 7144–7158. [CrossRef]

25. Hwang, J.; Lee, C.; Jeong, J.E.; Kim, C.Y.; Woo, H.Y.; Park, S.; Cho, M.J.; Choi, D.H. Rational Design of Carbazole- And Carboline-Based Polymeric Host Materials for Realizing High-Efficiency Solution-Processed Thermally Activated Delayed Fluorescence Organic Light-Emitting Diode. *ACS Appl. Mater. Interfaces* **2020**, *12*, 8485–8494. [CrossRef] [PubMed]

26. Tao, Y.; Wang, Q.; Yang, C.; Wang, Q.; Zhang, Z.; Zou, T.; Qin, J.; Ma, D. A simple carbazole/oxadiazole hybrid molecule: An excellent bipolar host for green and red phosphorescent OLEDs. *Angew. Chemie. Int. Ed.* **2008**, *47*, 8104–8107. [CrossRef]

27. Holder, E.; Langeveld, B.M.W.; Schubert, U.S. New trends in the use of transition metal-ligand complexes for applications in electroluminescent devices. *Adv. Mater.* **2005**, *17*, 1109–1121. [CrossRef]

28. Adachi, C.; Baldo, M.A.; Thompson, M.E.; Forrest, S.R. Nearly 100% internal phosphorescence efficiency in an organic light emitting device. *J. Appl. Phys.* **2001**, *90*, 5048–5051. [CrossRef]

29. Wang, J.; Li, Y.; Chen, L.; Deng, Y.; Peng, Y.; Lu, F.; Zhu, W. High-performance hybrid white organic light-emitting diodes with bipolar host material and thermally activated delayed fluorescent emitter. *Opt. Mater.* **2020**, *100*, 109673. [CrossRef]

30. Jou, J.H.; Wang, W.B.; Shen, S.M.; Kumar, S.; Lai, I.M.; Shyue, J.J.; Lengvinaite, S.; Zostautiene, R.; Grazulevicius, J.V.; Grigalevicius, S.; et al. Highly efficient blue organic light-emitting diode with an oligomeric host having high triplet-energy and high electron mobility. *J. Mater. Chem.* **2011**, *21*, 9546–9552. [CrossRef]

31. Kumar, S.; An, C.C.; Sahoo, S.; Griniene, R.; Volyniuk, D.; Grazulevicius, J.V.; Grigalevicius, S.; Jou, J.H. Solution-processable naphthalene and phenyl substituted carbazole core based hole transporting materials for efficient organic light-emitting diodes. *J. Mater. Chem. C* **2017**, *5*, 9854–9864. [CrossRef]

32. Chang, C.H.; Griniene, R.; Su, Y.D.; Yeh, C.C.; Kao, H.C.; Grazulevicius, J.V.; Volyniuk, D.; Grigalevicius, S. Efficient red phosphorescent OLEDs employing carbazole-based materials as the emitting host. *Dye Pigment.* **2015**, *122*, 257–263. [CrossRef]

33. Blazys, G.; Grigalevicius, S.; Grazulevicius, J.V.; Gaidelis, V.; Jankauskas, V.; Kampars, V. Phenothiazinyl-containing aromatic amines as novel amorphous molecular materials for optoelectronics. *J. Photochem. Photobiol. A Chem.* **2005**, *174*, 1–6. [CrossRef]

34. Ulbricht, C.; Beyer, B.; Friebe, C.; Winter, A.; Schubert, U.S. Recent developments in the application of phosphorescent iridium(III) complex systems. *Adv. Mater.* **2009**, *21*, 4418–4441. [CrossRef]

35. Avilov, I.; Marsal, P.; Brédas, J.L.; Beljonne, D. Quantum-chemical design of host materials for full-color triplet emission. *Adv. Mater.* **2004**, *16*, 1624–1629. [CrossRef]

36. Adachi, C.; Kwong, R.C.; Djurovich, P.; Adamovich, V.; Baldo, M.A.; Thompson, M.E.; Forrest, S.R. Endothermic energy transfer: A mechanism for generating very efficient high-energy phosphorescent emission in organic materials. *Appl. Phys. Lett.* **2001**, *79*, 2082–2084. [CrossRef]

37. Blazevicius, D.; Krucaite, G.; Shahnawaz, S.; Swayamprabha, S.S.; Zaleckas, E.; Jou, J.-H.; Grigalevicius, S. Easily synthesized and cheap carbazole- or phenoxazine-based hosts for efficient yellow phosphorescent OLEDs. *Opt. Mater.* **2021**, *118*, 111251. [CrossRef]

38. Baldo, M.A.; Forrest, S.R. Transient analysis of organic electrophosphorescence: I. Transient analysis of triplet energy transfer. *Phys. Rev. B* **2000**, *62*, 10958. [CrossRef]

165

39. Tsai, M.H.; Hong, Y.H.; Chang, C.H.; Su, H.C.; Wu, C.C.; Matoliukstyte, A.; Simokaitiene, J.; Grigalevicius, S.; Grazulevicius, J.V.; Hsu, C.P. 3-(9-carbazolyl)carbazoles and 3,6-Di(9-carbazolyl)carbazoles as effective host materials for efficient blue organic electrophosphorescence. *Adv. Mater.* **2007**, *19*, 862–866. [CrossRef]

40. Tao, Y.; Yang, C.; Qin, J. Organic host materials for phosphorescent organic light-emitting diodes. *Chem. Soc. Rev.* **2011**, *40*, 2943–2970. [CrossRef]

41. Sharma, A.; Balasaravanan, R.; Thomas, K.R.J.; Ram, M.; Kumar Dubey, D.; Ashok, R.; Yadav, K.; Jou, J.-H. Tuning photophysical and electroluminescent properties of phenanthroimidazole decorated carbazoles with donor and acceptor units: Beneficial role of cyano substitution. *Dye Pigment.* **2021**, *184*, 108830. [CrossRef]

42. Tao, P.; Li, W.-L.; Zhang, J.; Guo, S.; Zhao, Q.; Wang, H.; Wei, B.; Liu, S.-J.; Zhou, X.-H.; Yu, Q.; et al. Facile Synthesis of Highly Efficient Lepidine-Based Phosphorescent Iridium(III) Complexes for Yellow and White Organic Light-Emitting Diodes. *Adv. Funct. Mater.* **2016**, *26*, 881–894. [CrossRef]

43. Jou, J.-H.; Yang, Y.-M.; Chen, S.-Z.; Tseng, J.-R.; Peng, S.-H.; Hsieh, C.-Y.; Lin, Y.-X.; Chin, C.-L.; Shyue, J.-J.; Sun, S.-S.; et al. High-Efficiency Wet- and Dry-Processed Green Organic Light Emitting Diodes with a Novel Iridium Complex-Based Emitter. *Adv. Opt. Mater.* **2013**, *1*, 657–667. [CrossRef]

44. Na, J.; Bi, S.; Jiang, C.; Song, J. Achieving the hypsochromic electroluminescence of ultraviolet OLED by tuning excitons relaxation. *Org. Electron.* **2020**, *82*, 105718. [CrossRef]

45. Wang, Z.B.; Helander, M.G.; Liu, Z.W.; Greiner, M.T.; Qiu, J.; Lu, Z.H. Controlling carrier accumulation and exciton formation in organic light emitting diodes. *Appl. Phys. Lett.* **2010**, *96*, 043303. [CrossRef]

46. Takahashi, J.-I. Theory of carrier accumulation in organic heterojunctions. *Org. Electron.* **2019**, *65*, 26–30. [CrossRef]

47. Poriel, C.; Rault-Berthelot, J. Designing Host Materials for the Emissive Layer of Single-Layer Phosphorescent Organic Light-Emitting Diodes: Toward Simplified Organic Devices. *Adv. Funct. Mater.* **2021**, *31*, 2010547. [CrossRef]

48. Wang, Y.; Yun, J.H.; Wang, L.; Lee, J.Y. High Triplet Energy Hosts for Blue Organic Light-Emitting Diodes. *Adv. Funct. Mater.* **2021**, *31*, 2008332. [CrossRef]

49. Yun, J.H.; Lim, J.; Chung, W.J.; Lee, J.Y. Exciton stabilizing high triplet energy n-type hosts for blue phosphorescent organic light-emitting diodes. *Dye Pigment.* **2021**, *190*, 109297. [CrossRef]

50. Liu, B.; Wang, L.; Gao, D.; Xu, M.; Zhu, X.; Zou, J.; Lan, L.; Ning, H.; Peng, J.; Cao, Y. Harnessing charge and exciton distribution towards extremely high performance: The critical role of guests in single-emitting-layer white OLEDs. *Mater. Horizons* **2015**, *2*, 536–544. [CrossRef]

51. Liu, J.; Zhang, H.; Dong, H.; Meng, L.; Jiang, L.; Jiang, L.; Wang, Y.; Yu, J.; Sun, Y.; Hu, W.; et al. High mobility emissive organic semiconductor. *Nat. Commun.* **2015**, *6*, 10032. [CrossRef]

52. Movla, H. Influence of the charge carrier mobility on the dynamic behavior and performance of the single-layer OLED. *Optik* **2015**, *126*, 5237–5240. [CrossRef]

53. Schols, S.; Verlaak, S.; Rolin, C.; Cheyns, D.; Genoe, J.; Heremans, P. An Organic Light-Emitting Diode with Field-Effect Electron Transport. *Adv. Funct. Mater.* **2008**, *18*, 136–144. [CrossRef]

54. Soman, A.; Unni, K.N.N. Enhancement in electron transport and exciton confinement in OLEDs: Role of n-type doping and electron blocking layers. *Eur. Phys. J. Appl. Phys.* **2019**, *86*, 10201. [CrossRef]

55. Wei, C.; Zhuang, J.; Zhang, D.; Guo, W.; Yang, D.; Xie, Z.; Tang, J.; Su, W.; Zeng, H.; Cui, Z. Pyridine-Based Electron-Transport Materials with High Solubility, Excellent Film-Forming Ability, and Wettability for Inkjet-Printed OLEDs. *ACS Appl. Mater. Interfaces* **2017**, *9*, 38716–38727. [CrossRef]

56. Kim, J.-H.; Park, J.-W. Designing an electron-transport layer for highly efficient, reliable, and solution-processed organic light-emitting diodes. *J. Mater. Chem. C* **2017**, *5*, 3097–3106. [CrossRef]

57. Earmme, T.; Jenekhe, S.A. High-performance multilayered phosphorescent OLEDs by solution-processed commercial electron-transport materials. *J. Mater. Chem.* **2012**, *22*, 4660–4668. [CrossRef]

58. Oh, J.-H.; Park, J.-W. Designing a solution-processable electron transport layer for transparent organic light-emitting diode. *Org. Electron.* **2021**, *96*, 106252. [CrossRef]

59. Ding, R.; Dong, F.-X.; An, M.-H.; Wang, X.-P.; Wang, M.-R.; Li, X.-B.; Feng, J.; Sun, H.-B. High-Color-Rendering and High-Efficiency White Organic Light-Emitting Devices Based on Double-Doped Organic Single Crystals. *Adv. Funct. Mater.* **2019**, *29*, 1807606. [CrossRef]

60. Wang, Y.; Dai, Y.; Ma, D. Electron Transport Characteristics in Bepp2:Liq Thin Film and Its Influence on Electroluminescent Device Performance. *J. Phys. Chem. C* **2020**, *124*, 7661–7667. [CrossRef]

61. Ding, R.; Feng, J.; Dong, F.-X.; Zhou, W.; Liu, Y.; Zhang, X.-L.; Wang, X.-P.; Fang, H.-H.; Xu, B.; Li, X.-B.; et al. Highly Efficient Three Primary Color Organic Single-Crystal Light-Emitting Devices with Balanced Carrier Injection and Transport. *Adv. Funct. Mater.* **2017**, *27*, 1604659. [CrossRef]

62. Shelhammer, D.; Cao, X.A.; Liu, N.; Wang, H.J.; Zhou, Y.M. Doping effects and stability of calcium in organic electron-transport materials. *Org. Electron.* **2020**, *84*, 105799. [CrossRef]

63. Angel, F.A.; Wallace, J.U.; Tang, C.W. Effect of lithium and silver diffusion in single-stack and tandem OLED devices. *Org. Electron.* **2017**, *42*, 102–106. [CrossRef]

166

64. Korshunov, V.M.; Chmovzh, T.N.; Knyazeva, E.A.; Taydakov, I.V.; Mikhalchenko, L.V.; Varaksina, E.A.; Saifutyarov, R.S.; Avetissov, I.C.; Rakitin, O.A. A novel candle light-style OLED with a record low colour temperature. *Chem. Commun.* **2019**, *55*, 13354–13357. [CrossRef]

65. Singh, M.; Jou, J.H.; Sahoo, S.; Sujith, S.; He, Z.K.; Krucaite, G.; Grigalevicius, S.; Wang, C.W. High light-quality OLEDs with a wet-processed single emissive layer. *Sci. Rep.* **2018**, *8*, 7133. [CrossRef]

66. Guidelines on Limits of Exposure for Broad-Band Incoherent Optical Radiation (0.38 to 3 µm). *Health Phys.* **1997**, *73*, 539–554. Available online: https://www.icnirp.org/cms/upload/publications/ICNIRPbroadband.pdf (accessed on 28 July 2021).

67. Bullough, J.D. The Blue-Light Hazard: A Review. *J. Illum. Eng. Soc.* **2013**, *29*, 6–14. [CrossRef]

68. O'Hagan, J.B.; Khazova, M.; Price, L.L. Low-energy light bulbs, computers, tablets and the blue light hazard. *Eye* **2016**, *30*, 230–233. [CrossRef] [PubMed]

69. US20120303282A1—Melatonin Suppression Extent Measuring Device—Google Patents. Available online: https://patents.google.com/patent/US20120303282 (accessed on 28 July 2021).

70. Jou, J.H.; He, Z.K.; Su, Y.T.; Tsai, Y.F.; Wu, C.H. Approach for fabricating healthy OLED light sources with visual quality and energy-saving character. *Org. Electron.* **2016**, *38*, 396–400. [CrossRef]

167

Review

A Review of Benzophenone-Based Derivatives for Organic Light-Emitting Diodes

Dovydas Blazevicius * and Saulius Grigalevicius *

Department of Polymer Chemistry and Technology, Kaunas University of Technology,
Radvilenu Plentas 19, LT50254 Kaunas, Lithuania
* Correspondence: dovydas.blazevicius@ktu.lt (D.B.); saulius.grigalevicius@ktu.lt (S.G.)

Abstract: Organic light-emitting diodes (OLEDs) have garnered considerable attention in academic and industrial circles due to their potential applications in flat-panel displays and solid-state lighting technologies, leveraging the advantages offered by organic electroactive derivatives over their inorganic counterparts. The thin and flexible design of OLEDs enables the development of innovative lighting solutions, facilitating the creation of customizable and contoured lighting panels. Among the diverse electroactive components employed in the molecular design of OLED materials, the benzophenone core has attracted much attention as a fragment for the synthesis of organic semiconductors. On the other hand, benzophenone also functions as a classical phosphor with high intersystem crossing efficiency. This characteristic makes it a compelling candidate for effective reverse intersystem crossing, with potential in leading to the development of thermally activated delayed fluorescent (TADF) emitters. These emitting materials witnessed a pronounced interest in recent years due to their incorporation in metal-free electroactive frameworks and the capability to convert triplet excitons into emissive singlet excitons through reverse intersystem crossing (RISC), consequently achieving exceptionally high external quantum efficiencies (EQEs). This review article comprehensively overviews the synthetic pathways, thermal characteristics, electrochemical behaviour, and photophysical properties of derivatives based on benzophenone. Furthermore, we explore their applications in OLED devices, both as host materials and emitters, shedding light on the promising opportunities that benzophenone-based compounds present in advancing OLED technology.

Keywords: donor–acceptor–donor (D–A–D) derivatives; organic light-emitting diode (OLED); high efficiency; emission; thermal analysis; synthesis

1. Introduction

Since C. W. Tang's groundbreaking research in 1986 [1], there has been significant interest in organic light-emitting diodes (OLEDs) for several decades. Their potential applications span a wide range including full-colour flat-panel displays, smart watches, smartphones, large-screen televisions, and solid-state lighting, attracting attention in both scientific and industrial domains [2–8]. Today, OLEDs have evolved into a crucial commercial venture, driven by their notable advantages in terms of brightness, wide-angle viewability, power efficiency, contrast ratio, and other factors [9–20]. Flexibility stands out as an additional attribute in their technological arsenal, unmatched by any of the other existing technologies [21,22]. Predictably, the relentless pursuit of superior OLED materials continues, driven by the quest for enhanced efficiency when incorporated into devices.

Originally, OLEDs were simple devices with a single emissive layer placed between a cathode and an anode, deposited on a transparent substrate-like glass. As interest in the technology grew, and the pursuit of higher efficiency intensified, additional layers were introduced to optimize the flow of electrons and holes to the emissive layer. This is where excitons form, leading to photon generation during the recombination process. In Figure 1, we illustrate a modern multi-layer OLED structure. Beginning with a transparent substrate,

an anode is deposited, typically made of the low-resistance transparent material indium tin oxide (ITO). Subsequently, hole injection (HIL) and hole transporting (HTL) layers are added. For these layers, materials with high hole mobility and robust electron-donating properties are chosen. Following that, the emissive layer (EML) is introduced, composed either of the emitting material alone or doped within a host matrix. Materials in this layer commonly feature both electron-donating and electron-accepting groups, essential for an efficient recombination process. The primary purpose of the host material is to effectively transfer charge to the emitter while avoiding various emission-quenching mechanisms. OLED emitters are categorized into three generations: 1st-generation fluorescent, 2nd-generation phosphorescent, and 3rd-generation thermally activated delayed fluorescence (TADF) phenomena featuring emitters. Moving forward, electron transporting (ETL) and electron injection (EIL) layers are applied, performing the opposite functions to HTL and HIL. These layers utilize materials with high electron mobility and robust electron-accepting properties. Finally, a cathode, often made of aluminium, is deposited. Presently, there is a diverse range of OLED structures, some incorporating even more layers (electron/hole blocking, multiple charge-transporting layers, etc.) than the example provided. This complexity aims to achieve well-aligned energy levels for each layer with its adjacent layers, thereby minimizing energy barriers for charge carrier transport and achieving more efficient OLED devices.
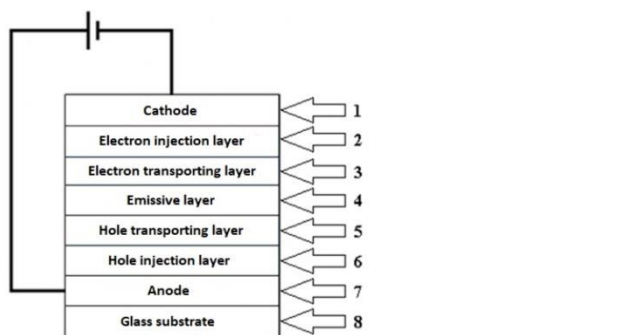
Figure 1. Structure of organic light-emitting diode.

In past decades, there has been a progressive transition from fluorescence- to phospho-rescence-based devices in the pursuit of higher efficiencies [23–27]. OLEDs utilizing conventional fluorescent emitters typically exhibit a maximum internal quantum efficiency (IQE) of 25% [1]. IQE can be elevated from 25% to 100% by harnessing triplet excitons through the use of intersystem singlet-to-triplet crossing in phosphorescent emitters [28,29]. Despite the high internal quantum efficiency and operational stability of emissive iridium or platinum complexes [30–33], phosphorescent OLEDs (PhOLEDs) encounter significant efficiency roll-off due to issues like aggregation-caused quenching and triplet–triplet and triplet–polaron annihilation [34–37]. As a result, host–guest systems are commonly employed to disperse phosphorescent emitters into host matrices. To achieve high-performance PhOLEDs, host materials must be ingeniously designed to adhere to fundamental principles such as good thermal stability and film formation quality [38–43] and a sufficiently high triplet energy to prevent reverse energy transfer from emitter to host [44–46]. Nevertheless, the persistent issue of poor stability of blue phosphorescent OLEDs remains a significant constraint [47,48]. The presence of noble metals in phosphorescent materials raises an undeniable challenge to the future costs of devices and environmental considerations [49,50]. In recent years, there has been a notable focus on TADF emitters. This interest arises from their utilization in

metal-free electroactive frameworks and their ability to upconvert full triplet excitons into emissive singlet excitons through reverse intersystem crossing (RISC), thereby achieving ultrahigh external quantum efficiencies (EQEs) [51–57]. Despite the promise of TADF materials, many TADF OLEDs encounter same quenching and triplet–triplet (or singlet–triplet) annihilation problems as PhOLEDs, due to a long exciton lifetime [58–60]. Consequently, to address the concentration quenching problem, many TADF molecules also need to be incorporated into suitable host matrices. However, because of a limited selection of TADF-specific host materials [61–63], researchers often utilize conventional host materials common to phosphorescent OLEDs [64]. Therefore, one approach to overcoming efficiency challenges is the design of new host materials specifically tailored for TADF OLEDs. Another approach involves the development of new TADF molecules, especially for non-doped OLEDs based on materials exhibiting aggregation-induced emission (AIE) characteristics [65–71].

Units derived from benzophenone, shown in Figure 2, are renowned for their efficient intersystem crossing (ISC) capability, attributed to robust spin–orbit coupling [72]. This characteristic renders them highly appealing as acceptor blocks for the fabrication of TADF emitters. Notably, benzophenone is recognized for its stability as an acceptor [73]. Furthermore, benzophenone functions as a classical phosphor with a high intersystem crossing efficiency, potentially leading to effective reverse intersystem crossing with a small ΔE_{ST} [74]. The benzophenone framework not only serves as an electron-deficient core by integrating various donor units to create molecules with small ΔE_{ST} and intramolecular charge transfer (CT) states [75], but it also features a highly twisted geometry, reducing intermolecular interactions and the self-quenching effect [76,77]. Owing to the properties of benzophenone, most of its derivatives have found applications in emissive layers of OLEDs both as a host or as an emitter.
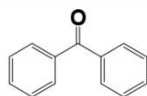
Figure 2. Chemical structure of benzophenone.

In this review article, we examine the synthetic pathways, thermal characteristics, electrochemical behaviour, photoelectrical, and photophysical properties of derivatives based on benzophenone. Additionally, we explore their applications in OLED devices, both as host materials as well as emitters. This article will systematically review various device structures and their corresponding performances. This review is structured into several sections based on the application and structure of benzophenone derivatives, including the following: host materials for phosphorescent emitters, host materials for TADF emitters, donor–acceptor (D–A)-type emitters, donor–acceptor–donor (D–A–D)-type symmetric structure emitters, D–A–D-type asymmetric structure emitters, as well as emitters having dendritic structures.

2. Benzophenone-Based Host Materials Used for Phosphorescent Emitters

Scheme 1 illustrates the configurations of benzophenone-based derivatives, employed as host materials in PhOLED devices. The objective compounds HA1, HA2, and HA3 [78] were obtained using Buchwald–Hartwig [79] amination reaction between 3,3′-dibromobenzophenone and 1,2,3,4-tetrahydrocarbazole for HA1, phenoxazine for HA2, and 9,9-dimethyl-9,10-dihydroacridine for HA3. The host material HA4 [80] was synthesized by utilizing Suzuki coupling reaction [81] between 3,3′,6,6′-tetrabromobenzophenone and 9-phenyl-9H-carbazol-3-ylboronic acid. To obtain the target compound HA5 [82], Buchwald–Hartwig amination reaction of 4,4′-dibromobenzophenone with a 3,6-diphenyl-9H-carbazole donor unit was used. Material HA6 [83] was synthesized utilizing similar reaction conditions between 4-bromo-3-methylbenzophenone and 3,6-dimethyl-9H-carbazole. The host material HA7 [84] was acquired through a single-step synthetic procedure employing Ullmann

reaction [85] between iodophenylketone and aminodiphenylketone. The synthesis of the remaining PhOLED host materials HA8, HA9, and HA10 [86] was easily achieved through a simple Friedel–Crafts benzoylation reaction [87] carried out in carbon disulfide. Benzoyl chloride, in the presence of AlCl₃, reacted with 1,4-diphenyldurene, 1,3,5-triphenylmesitylene, and 3,3′,5,5′-tetraphenylbimesitylene to yield HA8, HA9, and HA10, respectively.
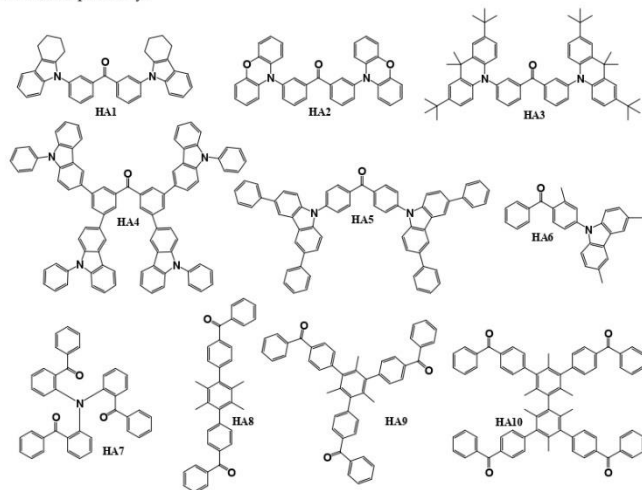
Scheme 1. Structures of benzophenone-based materials used as hosts in PhOLEDs.

Thermal, electrochemical, photoelectrical, and photophysical properties of the materials HA1–HA10 are displayed in Table 1. The thermal properties were investigated for all the objective materials. All the derivatives showed good thermal stability with high thermal decomposition temperatures (T_D) of 218–553 °C, as confirmed by thermogravimetric analysis (TGA). Differential scanning calorimetry (DSC) measurements showed that the derivatives HA1, HA4, HA6, HA7, and HA10 were fully amorphous materials with glass transition temperatures (T_G) of 55–188 °C. Only melting temperatures (T_M) of 118–370 °C were detected for other presented materials. During cooling, crystallization temperatures (T_{Cr}) of 62 °C and 269 °C were detected for compounds HA2 and HA3, respectively. For this group of materials, HOMO levels were measured to be from −5.80 eV to −4.74 eV and LUMO levels were in a region of −2.80 eV to −1.83 eV, attributed to bandgap energies (E_g) of 2.72–3.93 eV. Benzophenone-based PhOLED host materials showed high triplet state energy (E_T) levels, which were in a range of 2.53 eV–3.02 eV. Regarding photoluminescence quantum yield, materials with this metric measured demonstrated 15–24.4% quantum yield from film (Φ_{PL} film) and 3–15.3% quantum yield from solution (Φ_{PL} sol). In terms of photoluminescence quantum yield, materials with this metric measured showed a range of 15% to 24.4% in film (Φ_{PL} film) and 3% to 15.3% in solution (Φ_{PL} sol). All these properties were suitable to test the materials as hosts for various phosphorescent emitters.

171

Table 1. Thermal, electrochemical, photoelectrical, and photophysical properties of materials HA1–HA10.

	T_M, °C	T_G, °C	T_{Cr}, °C	T_D, °C	E_g, eV	E_s, eV	E_T, eV	ΔE_{ST}, eV	HOMO, eV	LUMO, eV	Φ_{PL} Film, %	Φ_{PL} Sol., %
HA1	–	91	–	312	3.21	–	3.02	–	−5.17	−2.03	20	3
HA2	118	–	62	218	3.05	–	2.65	–	−4.74	−2.19	15	12
HA3	342	–	269	389	3.66	2.70	2.66	0.04	−4.78	−2.02	16	6
HA4	–	188	–	553	3.00	–	2.61	–	−5.80	−2.80	–	–
HA5	370	–	–	480	3.52	2.83	2.69	0.14	−5.77	−2.25	24.4	15.3
HA6	–	131	–	–	3.10	3.70	3.00	0.70	−5.60	−2.50	–	–
HA7	–	55	–	339	2.72	2.77	2.53	0.24	−5.51	−2.79	–	–
HA8	272	–	–	337	3.91	–	2.97	–	−5.80	−1.89	–	–
HA9	291	–	–	445	3.93	–	2.97	–	−5.76	−1.83	–	–
HA10	–	122	–	466	3.91	–	2.95	–	−5.78	−1.87	–	–

Architectures of devices utilizing host materials HA1–HA10 are shown in Table 2. While all the devices used indium tin oxide (ITO) as the anode, hole-transporting layers (HTLs) had more variability. All the reviewed devices used two HTLs of different derivatives stacked on top of each other. Various materials were used in forming HTLs, such as 1,1-bis[[di-4-tolylamino)phenyl]cyclohexane (TAPC), 1,3-bis(N-carbazolyl)benzene (mCP), poly(3,4-ethylenedioxythiophene):polystyrene sulfonate (PEDOT:PSS), N,N′-di(1-naphthyl)-N,N′-diphenyl-(1,1′-biphenyl)-4,4′-diamine (NPB), tris(4-carbazoyl-9-ylphenyl)- amine (TCTA), and 1,4,5,8,9,11-hexaazatriphenylenehexacarbonitrile (HAT-CN). In emissive layers, iridium-based phosphorescent emitters were doped in host materials HA1–HA10, using various doping concentrations. Bis(1-phenylisoquinoline)(acetylacetonate) iridium(III) (Ir(piq)2acac), bis[2-(3,5-dimethylphenyl)-4-methyl-quinoline](acetylacetonate) iridium(III) (Ir(mphmq)2(tmd)), bis(2-methyldibenzo[f,h]quinoxaline)(acetylacetonate)iridium(III) (Ir(MDQ)2acac), bis(2-benzo[b]thiophen-2-yl-pyridine)(acetylacetonate)iridium(III) (Ir(btp)2acac), and bis(2-benzothiozolato-phenyl)(pylbenzamidinate)iridium(III) (Ir(bt) (dipba)) were used for red, bis(7,8-benzoquinolinato)(N,N′-diisopropylbenzamidine) iridium (III) (Ir(bzq)2(dipba)) for orange, bis(4-phenylthieno[3,2-c]pyridinato-N,C2′) (acetylacetonate) iridium(III) (PO-01) for yellow, bis[2-(2-pyridinyl-N)phenyl-C](acetylacetonato) iridium(III) (Ir(ppy)2acac) and tris(2-phenylpyridine)iridium(III) (Ir(ppy)3) for green, and bis[2-(4,6-difluorophenyl)pyridinato-C2,N](picolinato)iridium (FIrpic) for blue devices. For electron-transporting layers (ETLs), 4,6-bis(3,5-di(pyridin-3-yl)phenyl)-2-methylpyrimidine (B3PYMPM), 4,6-bis(3-(9H-carbazol-9-yl)phenyl)pyrimidine (CzPhPy), and 1,3,5-tris(3-pyridyl-3-phenyl)benzene (TmPyPB) were used. Additionally, 4,7-diphenyl-1,10-phenan- throline (Bphen), lithium fluoride (LiF), lithium-8-hydroxyquinolinolate (Liq), or caesium carbonate (Cs_2CO_3) were deposited as electron-injecting layers (EILs). Lastly, all of the devices mentioned in this section used aluminium (Al) as a cathode.

Table 2. Architectures of devices utilizing host materials HA1–HA10.

Device with HA Host	Device Architecture
DHA3	ITO/TAPC (50 nm)/mCP (10 nm)/**HA3**:7 wt% Ir(piq)2acac (30 nm)/Bphen (50 nm)/LiF (1 nm)/Al (100 nm)
DHA4	ITO (130 nm)/PEDOT:PSS (30 nm)/TFB (20 nm)/**HA4**:8 wt% Ir(ppy)3/Cs_2CO_3:Al (100 nm)
D1HA5	ITO/NPB (35 nm)/mCP (5 nm)/**HA5**:3 wt% Ir(ppy)2acac (30 nm)/B3PYMPM (30 nm)/LiF (0.5 nm)/Al (150 nm)
D2HA5	ITO/NPB (35 nm)/mCP (5 nm)/**HA5**:3 wt% Ir(bzq)2(dipba) (30 nm)/B3PYMPM (30 nm)/LiF (0.5 nm)/Al (150 nm)
D3HA5	ITO/NPB (35 nm)/mCP (5 nm)/**HA5**:3 wt% Ir(bt)2(dipba) (30 nm)/B3PYMPM (30 nm)/LiF (0.5 nm)/Al (150 nm)

Table 2. *Cont.*

Device with HA Host	Device Architecture
D1HA6	ITO/TAPC (30 nm)/TCTA (10 nm)/**HA6**:FIrpic (20 nm)/CzPhPy (10 nm)/TmPyPB (45 nm)/LiF/Al
D2HA6	ITO/TAPC (30 nm)/TCTA (10 nm)/**HA6**:Ir(ppy)$_2$(acac) (20 nm)/CzPhPy (10 nm)/TmPyPB (45 nm)/LiF/Al
D3HA6	ITO/TAPC (30 nm)/TCTA (10 nm)/**HA6**: Ir(mphmq)$_2$(tmd) (20 nm)/HA8 (10 nm)/CzPhPy (10 nm)/TmPyPB (45 nm)/LiF/Al
DHA7	ITO/HAT-CN (10 nm)/TAPC (65 nm)/TCTA (10 nm)/**HA7**:10 wt% Ir(MDQ)2acac (30 nm)/TmPyPb (55 nm)/Liq (1 nm)/Al (110 nm)
D1HA8	ITO/NPB (40 nm)/mCP (10 nm)/**HA8**:9–10 wt% Ir(ppy)$_3$ (30 nm)/TmPyPB (45 nm)/LiF (2 nm)/Al (150 nm)
D2HA8	ITO/NPB (40 nm)/mCP (10 nm)/**HA8**:9–10 wt% Ir(btp)$_2$acac (30 nm)/TmPyPB (45 nm)/LiF (2 nm)/Al (150 nm)
D3HA8	ITO/NPB (40 nm)/mCP (10 nm)/**HA8**:9–10 wt% FIrpic (30 nm)/TmPyPB (45 nm)/LiF (2 nm)/Al (150 nm)
D4HA8	ITO/NPB (40 nm)/mCP (10 nm)/**HA8**:9–10 wt% PO-01 (30 nm)/TmPyPB (45 nm)/LiF (2 nm)/Al (150 nm)
D1HA9	ITO/NPB (40 nm)/mCP (10 nm)/**HA9**:9–10 wt% Ir(ppy)$_3$ (30 nm)/TmPyPB (45 nm)/LiF (2 nm)/Al (150 nm)
D2HA9	ITO/NPB (40 nm)/mCP (10 nm)/**HA9**:9–10 wt% Ir(btp)$_2$acac (30 nm)/TmPyPB (45 nm)/LiF (2 nm)/Al (150 nm)
D3HA9	ITO/NPB (40 nm)/mCP (10 nm)/**HA9**:9–10 wt% FIrpic (30 nm)/TmPyPB (45 nm)/LiF (2 nm)/Al (150 nm)
D4HA9	ITO/NPB (40 nm)/mCP (10 nm)/**HA9**:9–10 wt% PO-01 (30 nm)/TmPyPB (45 nm)/LiF (2 nm)/Al (150 nm)
D1HA10	ITO/NPB (40 nm)/mCP (10 nm)/**HA10**:9–10 wt% Ir(ppy)$_3$ (30 nm)/TmPyPB (45 nm)/LiF (2 nm)/Al (150 nm)
D2HA10	ITO/NPB (40 nm)/mCP (10 nm)/**HA10**:9–10 wt% Ir(btp)$_2$acac (30 nm)/TmPyPB (45 nm)/LiF (2 nm)/Al (150 nm)
D3HA10	ITO/NPB (40 nm)/mCP (10 nm)/**HA10**:9–10 wt% FIrpic (30 nm)/TmPyPB (45 nm)/LiF (2 nm)/Al (150 nm)
D4HA10	ITO/NPB (40 nm)/mCP (10 nm)/**HA10**:9–10 wt% PO-01 (30 nm)/TmPyPB (45 nm)/LiF (2 nm)/Al (150 nm)

Characteristics of phosphorescent OLED devices using host materials HA1–HA10 are shown in Table 3. Overall, the utilization of benzophenone-based host materials resulted in efficient PhOLED devices with the external quantum efficiency of most devices exceeding 10%. Host materials HA1–HA10 were used for red, orange, yellow, green, and blue devices. Comparison of the red devices with each other showed that the most efficient prototype was D3HA5, which has a demonstrated low turn-on voltage (V_{ON}) of 2.9 V, high power efficiency (PE) of 27.1 lm/W, and external quantum efficiency (EQE) of 22.1%, as well as a maximum brightness (L_{MAX}) of 10,240 cd/m^2. For the orange emitter, only 3,6-diphenylcarbazol-9-yl-substituted host HA5 was used. The device D2HA5 demonstrated a V_{ON}, L_{MAX}, PE, and EQE of 2.6 V, 31,200 cd/m^2, 61.6 lm/W, and 23.1%, respectively, with CIExy coordinates of (0.51, 0.47). Between yellow devices, prototype D4HA8 stood out the most and outperformed devices D4HA9 and D4HA10. That could be attributed to the structure of host material HA8 which utilizes two benzophenone fragments compared to the three of HA9 and four of HA10. Diode D4HA8 demonstrated a current efficiency (CE) of 50.6 cd/A, PE of 28.9 lm/W, and EQE of 19.2%. Comparing green PhOLEDs, two carbazole fragments having the host material HA5 outperformed other host materials that had one or four carbazole fragments (HA4, HA6) or without carbazole fragments (HA8, HA9, HA10). Furthermore, the suitability of derivative HA5 (E_T = 2.69 eV) for green phosphors could be ascribed to the highest efficiency observed in the devices. PhOLEDs with a D1HA5 host demonstrated a very high PE of 99.1 lm/W and excellent EQE of 25.1% with their L_{MAX} exceeding 93,300 cd/m^2. When comparing blue PhOLEDs, devices using host material HA6 with a high E_T of 3.00 eV and excellent thermal and film forming properties exhibited the best characteristics. Device D1HA6 displayed a high PE and EQE of 38.2 lm/W and 19.4%, respectively.

173

Table 3. Characteristics of phosphorescent OLED devices using host materials HA1–HA10.

Device	Host	Colour	V_{ON}, V	L_{MAX}, cd/m^2	CE, cd/A	PE, lm/W	EQE, %	CIE (x, y)
DHA3	HA3	Red	–	1094	5.6	5.30	8.60	(0.68, 0.32)
DHA4	HA4	Green	–	–	–	22.0	14.6	–
D1HA5	HA5	Green	2.5	93,330	–	99.1	25.1	(0.29, 0.64)
D2HA5	HA5	Orange	2.6	31,200	–	61.6	23.1	(0.51, 0.47)
D3HA5	HA5	Red	2.9	10,240	–	27.1	22.1	(0.61, 0.36)
D1HA6	HA6	Blue	3.0	–	–	38.2	19.4	(0.16, 0.33)
D2HA6	HA6	Green	2.9	–	–	75.7	21.0	(0.29, 0.64)
D3HA6	HA6	Red	3.1	–	–	30.8	16.5	(0.62, 0.38)
DHA7	HA7	Red	4.0	3876	20.6	12.6	16.1	–
D1HA8	HA8	Green	4.5	3080	46.8	29.1	17.0	(0.30, 0.60)
D2HA8	HA8	Red	5.0	905	5.5	2.2	5.9	(0.65, 0.32)
D3HA8	HA8	Blue	5.5	708	10.9	4.6	5.3	(0.17, 0.32)
D4HA8	HA8	Yellow	5.5	3490	50.6	28.9	19.2	(0.47, 0.51)
D1HA9	HA9	Green	4.5	4940	45.6	31.9	15.6	(0.31, 0.60)
D2HA9	HA9	Red	4.5	1840	13.2	9.2	10.8	(0.67, 0.33)
D3HA9	HA9	Blue	4.5	1010	9.3	3.7	4.5	(0.17, 0.32)
D4HA9	HA9	Yellow	4.5	6480	50.8	31.9	18.5	(0.48, 0.51)
D1HA10	HA10	Green	4.5	5020	37.5	26.2	12.1	(0.31, 0.60)
D2HA10	HA10	Red	4.0	1820	19.9	15.6	13.7	(0.67, 0.33)
D3HA10	HA10	Blue	5.5	473	8.5	4.9	4.0	(0.19, 0.32)
D4HA10	HA10	Yellow	4.5	10,700	30.5	21.3	10.7	(0.48, 0.52)

3. Benzophenone-Based Bipolar Host Materials Used for TADF Emitters

Scheme 2 illustrates the configurations of benzophenone-based derivatives, employed as host materials in TADF OLED devices. Objective compounds HB1 and HB2 [88] were synthesized via a straightforward one-step Friedel–Crafts reaction utilizing readily available, cost-effective triphenylamine and isophthaloyl or terephthaloyl dichloride as initial reagents. All the remaining host materials HB3, HB4 [89], HB5 [90], HB6, HB7 [91], and HB8 [92] were obtained by simple nucleophilic substitution reactions between fluorinated benzophenone and corresponding amines. For application as TADF host materials, benzophenone was combined either with carbazole or phenyl-/naphtyl- amino fragments as electron donors. 4,4′-Difluorobenzophenone reactions with N-phenyl-1-naphtylamine, N-phenyl-2-naphtylamine, 3-naphtyl-9H-carbazole, 3-phenyl-9H-carbazole, and 3-(4-(9H-carbazol-9-yl)phenyl)-9H-carbazole yielded compounds HB3, HB4, HB5, HB6, and HB7, respectively. Material HB8 was obtained during reaction between 2,3,4,5,6-pentafluorobenzophenone and 9H-carbazole.

174
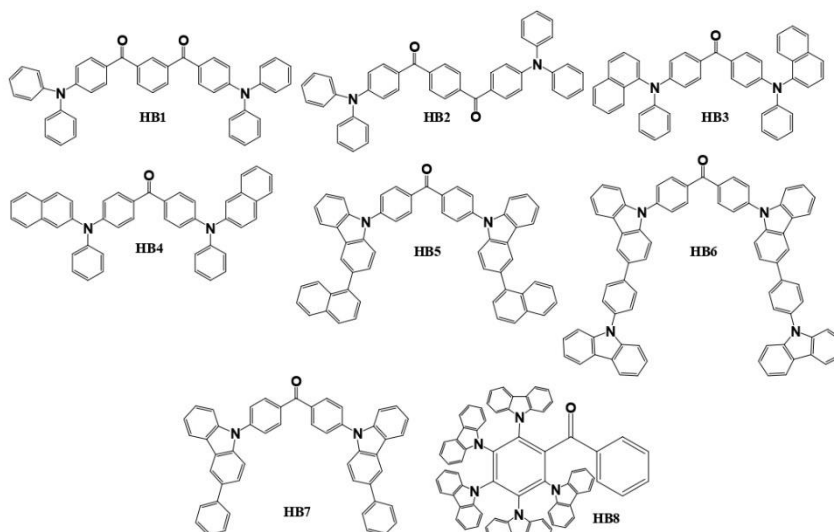
Scheme 2. Structures of benzophenone-based materials used as hosts in TADF OLEDs.

Table 4 presents the thermal, electrochemical, photoelectrical, and photophysical properties of materials HB1 to HB8. During the investigation of thermal properties, it was noticed that most of the benzophenone-based compounds were resistant to heat with thermal decomposition temperatures ranging from 277 °C to as high as 497 °C. Most of the same materials also possessed the ability to form stable amorphous films with glass transition temperatures ranging from 90 °C to 187 °C. At the same time, HB series benzophenone derivatives had optical bandgap energies of 2.70–4.10 eV, singlet state energy (E_S) levels of 2.37–3.07 eV, and triplet state energies ranging from 2.32 eV to 2.64 eV. Notably, carbazole-substituted derivatives HB5-HB8 demonstrated higher E_T levels.

Table 4. Thermal, electrochemical, photoelectrical, and photophysical properties of materials HB1–HB8.

	T_M, °C	T_G, °C	T_{Cr}, °C	T_D, °C	E_g, eV	E_S, eV	E_T, eV	ΔE_{ST}, eV	HOMO, eV	LUMO, eV	Φ_{PL} Film, %	Φ_{PL} Sol., %	
												N_2	O_2
HB1	–	90	–	436	2.84	2.59	2.38	0.21	−5.31	−2.47	75	46	–
HB2	–	92	–	416	2.70	2.37	2.32	0.05	−5.32	−2.62	2	2	–
HB3	218	101	203	411	2.89	3.07	2.55	0.52	−5.13	−1.47	9	9	–
HB4	241	107	–	428	2.78	3.00	2.53	0.47	−5.08	−1.53	13	13	–
HB5	–	156	–	–	3.33	2.91	2.61	0.30	−5.38	−2.05	–	–	–
HB6	123	92	–	277	4.10	2.97	2.64	0.33	−6.15	−2.63	–	–	–
HB7	366	187	–	371	4.00	2.95	2.60	0.35	−6.05	−2.45	–	–	–
HB8	–	–	–	497	2.80	2.61	2.60	0.01	−5.35	−2.55	–	8	6

The configurations of devices employing host materials HB1 to HB8 are illustrated in Table 5. All the manufactured devices used an ITO anode. To lower the hole injection barrier, molybdenum (VI) oxide (MoO$_3$) was used as a hole injection layer (HIL) for devices DHB3 and DHB4. The most popular material of choice for the formation of hole-transporting layers was PEDOT:PSS. NPB, TAPC, or a cross-linkable molecule 3,6-bis(4-vinylphenyl)-9-ethylcarbazole (VPEC), were also employed for HTLs in some cases. Each device utilized one or two hole-transporting layers (HTLs). The chosen TADF emitters included orange 1,2,3,5-tetrakis(carbazol-9-yl)-4,6-dicyanobenzene (4CzTPN), green 2,3,5,6-tetracarbazole-4-cyano-pyridine (4CzCNPy), and blue 10,10′-(perfluoro-[1,10-biphenyl]-4,4′-diyl)bis(2,7-ditert-butyl-9,9-dimethyl-9,10-dihydro-acridine) (PFBP-2b). The electron-transporting layers utilized compounds such as TmPyPB, TPBi, and 2,4,6-tris[3-(diphenylphosphinyl)phenyl]-1,3,5-triazine (PO-T2T). Finally, for all devices under investigation, a combination of LiF as the electron-injecting layer and an Al cathode was employed.

Table 5. Architectures of devices utilizing host materials HB1–HB8.

Device	Device Architecture
DHB1	ITO/PEDOT:PSS (40 nm)/**HB1**:10 wt% 4CzCNPy (35–40 nm)/TmPyPB (60 nm)/LiF (0.8 nm)/Al (120 nm)
DHB2	ITO/PEDOT:PSS (40 nm)/**HB2**:10 wt% 4CzCNPy (35–40 nm)/TmPyPB (60 nm)/LiF (0.8 nm)/Al (120 nm)
DHB3	ITO/MoO$_3$ (8 nm)/NPB (60 nm)/TAPC (5 nm)/**HB3**:5 wt% 4CzTPN (5 nm)/**HB3** (15 nm)/ PFBP-2b(20 wt%):TPBi (40 nm)/LiF (1 nm)/Al
DHB4	ITO/MoO$_3$ (8 nm)/NPB (60 nm)/TAPC (5 nm)/**HB4**:5 wt% 4CzTPN (5 nm)/**HB4**(15 nm)/ PFBP-2b(20 wt%):TPBi (40 nm)/LiF (1 nm)/Al
DHB5	ITO (125 nm)/PEDOT:PSS (30 nm)/**HB5**:15 wt% 4CzIPN (20 nm)/TPBi (30 nm)/LiF (1.0 nm)/Al (150 nm)
D1HB6	ITO (125 nm)/PEDOT:PSS (35 nm)/**HB6**:4CzIPN (20 nm)/PO-T2T (10 nm)/TPBi (30 nm)/LiF (1 nm)/Al (200 nm)
D2HB6	ITO (125 nm)/PEDOT:PSS (35 nm)/VPEC (10 nm)/**HB6**:4CzIPN (20 nm) /PO-T2T (10 nm)/TPBi (30 nm)/LiF (1 nm)/Al (200 nm)
DHB7	ITO (125 nm)/PEDOT:PSS (35 nm)/**HB7**:4CzIPN (20 nm)/PO-T2T (10 nm)/TPBi (30 nm)/LiF (1 nm)/Al (200 nm)
DHB8	ITO/PEDOT:PSS (40 nm)/**HB8**:10 wt% 4CzCNPy (40 nm)/TmPyPB (60 nm)/LiF (0.8 nm)/Al (100 nm)

Measured characteristics of TADF OLED devices employing host materials HB1–HB8 are shown in Table 6. Most of the HB materials were used to dope green TADF emitters, except benzophenone derivatives HB3 and HB5, which were used in combination with orange and sky blue dopants to achieve white emission. Hu and co-authors investigated electron-donating triphenylamino and electron-accepting phthaloyl moieties having compounds HB1 and HB2. When these materials were used as hosts for the green TADF emitter, compound HB1 prevailed as a more effective choice that could be explained by higher singlet and triplet energy levels which enhance energy transfer efficiency and effectively prevent reverse energy transfer from the green TADF emitter to the TADF host, resulting in a CE, PE, and EQE of 43.5 cd/A, 33.3 lm/W, and 13.0% for device DHB1, respectively. Materials HB3 and HB4 were investigated by Mahmoudi et al. They found that the best use of the synthesized materials would be as exciton modulators between two TADF emitters. By combining orange and blue TADF materials with the new benzophenone-based hosts, efficient white TADF OLEDs were introduced with the EQE for devices DHB3 and DHB4 reaching 9.5% and 7.1%, respectively. Device-utilizing compound HB3 showed higher-quality white electroluminescence, which is defined by CIE coordinates of (0.32, 0.31), a colour temperature of 4490 K, and a colour-rendering index of 80. A team of researchers led by Swyamprabha synthesized and characterized 3-naphtyl-9H-carbazole-substituted derivative HB5. The green TADF OLED device showed a maximum CE, PE, and EQE of 9.5 cd/A, 8.4 lm/W and 2.8%, respectively. The same researchers continued their work and synthesized new materials HB6 and HB7 with different substituents at the carbazole core. At last, green solution-processable OLEDs were also fabricated with a cross-linkable

hole transport material VPEC and realized PE of 63.6 lm/W with an EQE of 25.3% for device D2HB7, which was more effective than an analogical device with a lower E_T having host material HB6. Wang et al. introduced a new penta-carbazole-substituted benzophenone derivative HB8, which has also been tested as a host material for the green TADF emitter. Device DHB8 displayed a yellowish-green emission, possessing CIE coordinates of (0.34, 0.58), aligning with the emission characteristics of 4CzCNPy [93]. The OLED achieved a maximum current and external quantum efficiency, reaching 38.3 cd/A and 12.5%, respectively.

Table 6. Characteristics of TADF OLED devices using host materials HB1–HB8.

Device	Host	Colour	V_{ON}, V	L_{MAX}, cd/m^2	CE, cd/A	PE, lm/W	EQE, %	CIE (x, y)
DHB1	HB1	Green	3.5	20,322	43.5	33.3	13.0	(0.32, 0.60)
DHB2	HB2	Green	3.2	15,510	29.3	25.4	9.0	(0.33, 0.58)
DHB3	**HB3**	**White**	**3.9**	**29,922**	**18.6**	**–**	**9.5**	**(0.36, 0.31)**
DHB4	HB4	White	3.6	15,350	13.8	–	7.1	(0.32, 0.31)
DHB5	HB5	Green	3.4	8601	9.5	8.4	2.8	(0.31, 0.59)
D1HB6	HB6	Green	3.0	16,500	70.7	55.6	23.2	(0.28, 0.57)
D2HB6	**HB6**	**Green**	**2.9**	**18,900**	**72.3**	**63.6**	**25.3**	**(0.29, 0.58)**
DHB7	HB7	Green	2.7	10,540	49.2	46.2	15.3	(0.28, 0.57)
DHB8	HB8	Green	3.7	22,004	38.3	–	12.5	(0.34, 0.58)

Characteristics of best performing white and green devices are highlighted in bold.

4. Benzophenone-Based Emitters Employing a D–A Molecular Structure

Scheme 3 illustrates the structures of donor–acceptor-type molecules reviewed for their application as emitters in OLED devices. These materials typically exhibit a structure where one part of the molecule has a higher electron-donating ability, while another part has a higher electron-accepting ability. The compounds EA1, EA2, EA3 [94], EA6 [95], EA7 [96], EA8 [97], EA13 [98], EA14 [99], EA16 [100], EA17, and EA18 [101] were synthesized using the Buchwald–Hartwig coupling reaction methodology. Specifically, EA1, EA2, and EA3 were obtained in the reaction of 4-bromobenzophenone with 3-(4-(diphenylamino)phenyl)-9H-carbazole, 2-(4-(diphenylamino)phenyl)-9H-carbazole, and 1-(4-(diphenylamino)phenyl)-9H-carbazole, respectively. EA6 and EA7 were derived from the reactions of 4-bromobenzophenone with 11-phenyldihydroindolo[2,3-a]carbazole or N,N′-diphenyltriazatruxene. EA8 resulted from the reaction of 4-aminobenzophenone with 3-iodo-9-ethylcarbazole. Emitters EA13, EA14, and EA16 were synthesized through the reactions of 4-bromobenzophenone with 9,9-dimethyl-9,10-dihydroacridine, 10H-phenothiazine, or 9,9-diphenyl-9,10-dihydroacridine, respectively. Lastly, employing 9,9-dimethyl-9,10-dihydroacridine in reaction with (4-bromophenyl)(4-(phenylthio)phenyl)methanone resulted in EA17 and 9,9-dimethyl-9,10-dihydroacridine reaction with (4-bromophenyl)(4-(phenylsulfonyl)phenyl)methanone, which was used to obtain EA18. Materials EA4 and EA5 [102], featuring 3,6-pyridinyl-9H-carbazole substitutions, were synthesized through Suzuki reactions. This involved the coupling of 4-(3,6-dibromocarbazol-yl)benzophenone with 4-pyridinylboronic acid for the production of compound EA4 or with 3-pyridinylboronic acid for the synthesis of derivative EA5. The Suzuki coupling method was also employed for the synthesis of target materials EA9 [103] and EA22 [104]. For EA9, the reaction involved 4-bromobenzophenone with 9-phenylcarbazole-3-boronic acid pinacol ester. For derivative EA22, the initial reagents selected were 4-(4-(3-bromo-9H-carbazol-9-yl)benzoyl)benzonitrile and (4-(diphenylamino)phenyl)boronic acid. Benzophenone-based derivatives EA10 [105], EA11 [92], EA12 [106], and EA19 [107] were synthesized through relatively straightforward catalyst-free nucleophilic substitution reactions. For EA10, the initial reactants included 4-fluorobenzophenone and triphenyl-2-(9H-carbazol-2-yl)ethylene.

177

The synthesis of material EA11 is detailed in a previous section under the name HB8. The objective compound EA12 was obtained by reacting of 2,3,4,5,6-pentafluorobenzophenone with 3,6-bis(tert-butyl)-9H-carbazole. Emitter EA19 was prepared through the reaction of (4-(dodecyloxy)phenyl)(4′-fluorophenyl)methanone with 9,9-dimethyl-9,10-dihydroacridine. An alternative synthesis approach was employed for the creation of compounds EA15 and EA21 [108]. In this scenario, 10H-spiro(acridine-9,9′-thioxanthene) was employed in Ullmann reactions with 4-bromobenzophenone and (6-bromopyridin-3-yl)(phenyl)methanone, respectively. The phosphorus-containing emitter EA20 [109] was synthesized through a palladium-catalysed reaction between the intermediate compound 4-iodo-4′-phenothiazin-10yl-benzophenone and diphenylphosphine oxide in the presence of triethylamine.
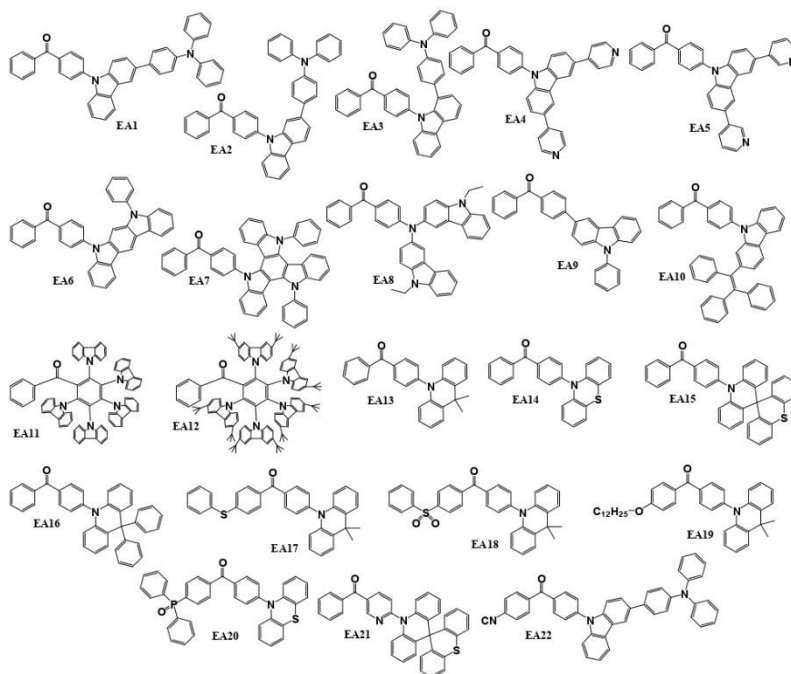
Scheme 3. Structures of benzophenone-based D–A materials used as emitters in OLEDs.

The thermal, electrochemical, photoelectrical, and photophysical properties of materials EA1–EA22 are provided in Table 7. All the tested materials exhibited good thermal stability, as verified by the TGA measurements conducted on the samples. The thermal decomposition temperatures for these materials ranged from 278 °C to 497 °C. DSC experiments showed that most of the tested materials were capable of forming stable amorphous layers with glass transition temperatures of 80–194 °C. By analysing the HOMO–LUMO gap (energy bandgap E_g), it was seen that most of the EA series derivatives demonstrated E_g levels of around 3 eV or slightly lower. Only materials EA4 and EA5 showed significantly higher E_g levels of around 4 eV, which might lead to less efficient TADF processes compared to emitters with smaller bandgaps [59]. A crucial characteristic for achievement

of the TADF effect is a small energy difference between the singlet and triplet states (ΔE_{ST}), which facilitates effective reverse intersystem crossing, allowing the conversion of triplet excitons to singlet excitons, which is essential for delayed fluorescence [59]. This metric was measured for all benzophenone-based D–A emitters. From 22 derivatives described in this section, 17 of them demonstrated ΔE_{ST} levels of 0.10 eV or lower. Higher singlet–triplet energy difference-having derivatives could be suffering from an ineffective TADF process, thus lowering the overall performance of the devices. A small ΔE_{ST} is associated with a higher photoluminescence quantum yield (Φ_{PL}), as it facilitates efficient radiative decay from the triplet state to the ground state. We can compare materials EA1, EA2, and EA3 since experiments with them were executed under the same conditions. The biggest ΔE_{ST} of 0.37 eV having derivative EA2 showed the lowest quantum yield (Φ_{PL}) of 20% in thin film. On the other hand, the narrowest singlet–triplet energy gap of just 0.02 eV was measured for compound EA3, which exhibited the highest Φ_{PL} of 50%. This trend could be observed in other pairings of similarly structured materials that were characterized under the same conditions such as EA4 and EA5 as well as EA15 and EA21. Oxygen molecules can quench the triplet states involved in the TADF process [110]. This quenching effect can lead to a decrease in the efficiency of delayed fluorescence and, consequently, reduced performance of TADF-based devices. Triplet state involvement in overall emission is proven by this way for benzophenone derivatives EA5, EA6, EA8, and EA11. In the cases of materials EA6, EA13, EA15, EA16, and EA21, prompt and delayed components of emissions were detected with the ratio of the delayed component in overall emission (R_D) ranging from 37.9% to 81.3%. All emitters described in this section, except fluorescent EA10, exhibited TADF properties.

Table 7. Thermal, electrochemical, photoelectrical, and photophysical properties of materials EA1–EA22.

	T_M, °C	T_G, °C	T_D, °C	E_g, eV	E_S, eV	E_T, eV	ΔE_{ST}, eV	HOMO, eV	LUMO, eV	Φ_{PL} Film, %		Φ_{PL} Sol., %		R_D, %
										N_2	O_2	N_2	O_2	
EA1	–	90	367	2.39	2.81	2.55	0.26	−5.55	−3.16	42.0	–	12.4	–	–
EA2	–	148	377	2.43	2.81	2.44	0.37	−5.58	−3.15	20.0	–	–	–	–
EA3	–	–	407	2.33	2.78	2.76	0.02	−5.51	−3.18	50.0	–	–	–	–
EA4	–	–	–	3.94	–	–	0.06	−5.83	−1.89	23.4	19.1	56.0	18.0	–
EA5	–	–	–	4.02	–	–	0.07	−5.99	−1.97	21.0	17.3	52.0	10.0	–
EA6	–	177	278	3.00	2.92	2.83	0.09	−5.45	−2.45	62.0	–	–	–	37.9
EA7	–	145	379	2.72	2.68	2.59	0.06	−5.37	−2.65	51.0	–	14.0	–	–
EA8	135	–	–	2.60	–	–	0.24	−5.20	−2.60	76.0	70	–	–	–
EA9	–	155	311	3.09	2.97	2.55	0.42	−5.66	−2.57	50.8	–	–	–	–
EA10	200	107	341	–	3.66	2.57	1.09	–	–	–	–	–	–	–
EA11	–	–	497	2.80	2.61	2.60	0.01	−5.35	−2.55	24.0	–	8.0	6.0	–
EA12	–	194	420	2.80	2.86	2.76	0.10	−5.90	−3.10	28.0	–	8.4	–	–
EA13	–	–	297	2.87	2.90	2.81	0.09	−5.06	−2.19	75.0	–	–	–	81.3
EA14	–	–	–	2.60	–	–	0.07	–	–	31.0	–	–	–	–
EA15	–	165	372	2.91	–	–	0.09	−5.11	−1.98	75.7	–	–	–	66.3
EA16	–	–	–	2.64	2.14	2.13	0.01	−5.70	−3.06	47.0	–	–	–	70.2
EA17	–	–	367	2.31	2.64	2.63	0.008	−5.24	−2.93	90.1	–	–	–	–
EA18	–	80	350	2.01	2.03	2.02	0.005	−5.24	−3.23	39.7	–	–	–	–
EA19	–	–	355	3.20	2.64	2.63	0.01	−4.93	−1.73	–	–	–	–	–
EA20	–	91	428	2.3	2.61	2.59	0.02	−5.50	−3.20	–	–	–	–	–
EA21	–	102	389	2.81	–	–	0.08	−5.12	−2.22	98.9	–	–	–	60.1
EA22	–	–	460	2.07	2.56	2.47	0.09	−5.02	−2.95	63.0	–	41.0	–	–

Architectures of devices utilizing emitters EA1–EA22 are displayed in Table 8. As it was mentioned in earlier sections, all of the devices formed with the D–A-type benzophenone emitters used an ITO anode and Al cathode except for EA20-based devices, which used cathodes made of a blend of magnesium and silver. To lower the hole injection barrier, hole-injecting material MoO_3 was used in some devices. Hole-transporting layers were made utilizing PEDOT:PSS, NPB, TAPC, HAT-CN, TCTA, 9-(4-tert-butylphenyl)-3,6-bis(triphenylsilyl)-9H-carbazole (CzSi), mCP, 3,3′-di(9H-carbazol-9-yl)-1,1′-biphenyl (mCBP), 4,4′-bis(9-carbazolyl)-1,1′-biphenyl (CBP), or N,N′-bis(naphthalen-1-yl)-N,N′-bis(phenyl)-2,2′-dimethylbenzidine (α-NPD). Doped and non-doped emissive layers (EMLs) were used during studies of the devices. In the case of doped devices, host materials bis[2-(diphenylphosphino)phenyl]ether oxide (DPEPO), 3,6-di(9-carbazolyl)-9-(2-ethylhexyl) carbazole (TCzl), mCP, bis-4-(N-carbazolyl)phenyl)phenylphosphine oxide (BCPO), 10-(4-(4-(9H-carbazol-9-yl)phenylsulfonyl)phenyl)-9,9-dimethyl- 9,10-dihydroacridine (CzAcSF), and CBP were used. To achieve desirable emission, an additional emitter, 9,9′-((2-(4′-(9H-carbazol-9-yl)-[1,10-biphenyl]-4-yl)ethene-1,1-diyl)bis(4,1-phenylene))bis(9H-carbazole) (2CzTPEPCz), was used in tandem with emissive material EA20. To balance the flow of electrons, TBPi, TmPyPB, DPEPO, and B3PyPB were applied for electron-transporting layers. In order to make a lower electron injection barrier, LiF, Cs_2CO_3, or Liq were used for EILs in some cases as it can be seen in Table 8.

Table 8. Architectures of devices utilizing the emitters EA1–EA22.

Device	Device Architecture
DEA1	ITO/PEDOT:PSS (40 nm)/**EA1** (40 nm)/TPBi (30 nm)/Cs_2CO_3 (2 nm)/Al (100 nm)
DEA2	ITO/PEDOT:PSS (40 nm)/**EA2** (40 nm)/TPBi (30 nm)/Cs_2CO_3 (2 nm)/Al (100 nm)
DEA3	ITO/PEDOT:PSS (40 nm)/**EA3** (40 nm)/TPBi (30 nm)/Cs_2CO_3 (2 nm)/Al (100 nm)
DEA4	ITO/NPB (30 nm)/TAPC (20 nm)/mCP (10 nm)/DPEPO:7 wt% **EA4** (30 nm)/ TPBi (40 nm)/LiF (0.8 nm)/Al (100 nm)
DEA5	ITO/NPB (30 nm)/TAPC (20 nm)/mCP (10 nm)/DPEPO:7 wt% **EA5** (30 nm)/ TPBi (40 nm)/LiF (0.8 nm)/Al (100 nm)
DEA6	ITO/HAT-CN (10 nm)/TAPC (30 nm)/TCTA (10 nm)/DPEPO:10 wt% **EA6** (40 nm)/TmPyPB (40 nm)/LiF (1 nm)/Al (100 nm)
DEA7	ITO/PEDOT:PSS (25 nm)/**EA7** (25 nm)/TmPyPB (55 nm)/LiF (1 nm)/Al (150 nm)
DEA8	ITO (50 nm)/PEDOT:PSS (30 40 nm)/TCzl:5 wt% **EA8**/TPBi (50 nm)/Liq (1 nm)/Al (80 nm)
DEA9	ITO/TAPC (40 nm)/TCTA (20 nm)/**EA9** (40 nm)/TmPyPB (50 nm)/LiF (1 nm)/Al (100 nm)
DEA10	ITO (120 nm)/TAPC:20 wt%MoO_3 (20 nm)/TAPC (20 nm)/TCTA (10 nm)/**EA10** (20 nm)/ CBP (2 nm)/TmPyPB (50 nm)/LiF (1.2 nm)/Al (120 nm)
DEA11	ITO/PEDOT:PSS (40 nm)/mCP:10 wt% **EA11** (40 nm)/TmPyPB (60 nm)/LiF (0.8 nm)/Al (100 nm)
D1EA12	ITO/NPB (30 nm)/TCTA (20 nm)/CzSi (10 nm)/**EA12** (20 nm)/DPEPO (10 nm)/TPBi (30 nm)/LiF (1 nm)/Al (100 nm)
D2EA12	ITO/NPB (30 nm)/TCTA (20 nm)/CzSi (10 nm)/DPEPO:20 wt% **EA12** (20 nm)/ DPEPO (10 nm)/TPBi (30 nm)/LiF (1 nm)/Al (100 nm)
D1EA13	ITO/MoO_3 (1 nm)/TAPC (50 nm)/mCP (10 nm)/**EA13** (30 nm)/DPEPO (10 nm)/ TmPyPB (30 nm)/LiF (1 nm)/Al (100 nm)
D2EA13	ITO/MoO_3 (1 nm)/TAPC (50 nm)/mCP (10 nm)/BCPO:20 wt% **EA13** (30 nm)/DPEPO (10 nm) /TmPyPB (30 nm)/LiF (1 nm)/Al (100 nm)
DEA14	ITO (100 nm)/α-NPD (40 nm)/mCBP (10 nm)/**EA14** (15 nm)/B3PyPB (55 nm)/Liq (1 nm)/Al (80 nm)
D1EA15	ITO/TAPC (30 nm)/mCP (10 nm)/**EA15** (20 nm)/DPEPO (10 nm)/TmPyPB (40 nm)/LiF/Al
D2EA15	ITO/TAPC (30 nm)/mCP (10 nm)/DPEPO:30 wt% **EA15** (20 nm)/DPEPO (10 nm)/TmPyPB (40 nm)/LiF/Al
DEA16	ITO/TAPC (40 nm)/TCTA (10 nm)/mCP (10 nm)/**EA16**/TmPyPb (40 nm)/LiF (1 nm)/Al (120 nm)

180

Table 8. *Cont.*

Device	Device Architecture
D1EA17	ITO/PEDOT:PSS (40 nm)/TAPC (20 nm)/**EA17** (20 nm)/TmPyPB (40 nm)/LiF (1 nm)/Al (200 nm)
D2EA17	ITO/PEDOT:PSS (40 nm)/TAPC (20 nm)/CBP:5 wt% **EA17** (20 nm)/TmPyPB (40 nm)/LiF (1 nm)/Al (200 nm)
D1EA18	ITO/PEDOT:PSS (40 nm)/TAPC (20 nm)/**EA18** (20 nm)/TmPyPB (40 nm)/LiF (1 nm)/Al (200 nm)
D2EA18	ITO/PEDOT:PSS (40 nm)/TAPC (20 nm)/CBP:5 wt% **EA18** (20 nm)/TmPyPB (40 nm)/LiF (1 nm)/Al (200 nm)
DEA19	ITO/PEDOT:PSS (30 nm)/mCP:CzAcSF:**EA19**(40:30:30) (40 nm) /DPEPO (10 nm)/TmPyPB (50 nm)/Liq (1 nm)/Al (100 nm)
D1EA20	ITO/PEDOT:PSS (40 nm)/CBP (20 nm)/CBP:10 wt% **EA20** (15 nm)/TPBi (40 nm)/Mg:Ag
D2EA20	ITO/PEDOT:PSS (40 nm)/CBP (20 nm)/**EA20** (4 nm)/2CzTPEPCz (15 nm)/TPBi (40 nm)/Mg:Ag
D1EA21	ITO/TAPC (30 nm)/mCP (10 nm)/**EA21** (20 nm)/DPEPO (10 nm)/TmPyPB (40 nm)/LiF/Al
D2EA21	ITO/TAPC (30 nm)/mCP (10 nm)/DPEPO:30 wt% **EA21** (20 nm)/DPEPO (10 nm)/TmPyPB (40 nm)/LiF/Al
DEA22	ITO/TAPC (30 nm)/TCTA (10 nm)/mCP:5 wt% **EA22** (20 nm)/TmPyPb (40 nm)/LiF (1 nm)/Al

Various metrics of the OLEDs using EA derivatives are shown in Table 9. Green light emission of the D–A-type benzophenone derivatives was the most common result for 19 of the 28 single-emitter devices described in this section. There also were reported six blue, three yellow, and one white OLED prototype using materials of this group. The EQE exhibited by the devices ranged widely from 1.8% to 26.7%. The most effective yellow OLED device was achieved by Chen and colleagues and reached a maximum CE, PE, and EQE of 73.1 cd/A, 38.2 lm/W, and 26.7%, respectively [111]. For all the emitters used in yellow OLED devices, the TADF effect was confirmed. Zhao et al. successfully applied the same emitter EA20 in the white TADF OLED prototype D2EA20 and achieved a high CE of 45.9 cd/A, PE of 18.0 lm/W, and EQE of 20.8% [112]. Ho and co-workers synthesized and characterized triphenylethene-carbazole-substituted benzophenone derivative EA10. A big ΔE_{ST} gap of 1.09 eV could not enable the TADF process in this case. The green OLED device with DEA10 achieved an EQE of 1.7% and high luminance of 11,802 cd/m^2. Ma et al. tested three different benzophenone-carbazole materials EA1, EA2, and EA3 with different positions of triphenylamine moiety in the structures. The most efficient TADF emitter was compound EA3, which in a green device DEA3, reached an external quantum efficiency of 7.6%. Kreiza and colleagues also achieved good results utilizing a benzophenone-based D–A TADF emitter EA12. Non-doped green OLED device D1EA12 achieved a CE, PE, and EQE of 19.0 cd/A, 14.9 lm/W, and 10.3%. By doping the mentioned emitter in a DPEPO host, characteristics were enhanced by the authors with 34.9 cd/A, 27.3 lm/W, and 12.5% for device D2EA12. Ma and co-workers presented another very efficient green light-emitting sulfone group-enriched benzophenone TADF emitter EA18. Luminance of the doped device D2EA18 surpassed 30,000 cd/m^2 with an EQE reaching 20.6%. Other characteristics were also impressive with a CE reaching 64.6 cd/A and PE being 75.1 lm/W. Meanwhile, the similarly structured green TADF emitter EA17 obtained by the same researchers was less efficient in doped devices, which could be attributed to the absence of a sulfone group. However, it was impressive when applied in non-doped EMLs: device D1EA17 achieved a maximum PE, CE, and EQE of 53.7 cd/A, 52.7 lm/W, and 17.3%, respectively. In the realm of green light-emitting devices, the TADF emitter EA21, which had one of its benzophenone phenyl rings replaced with pyridine and was characterized by Wang and co-workers, demonstrated superior efficiency. Luminance of the doped device D2E21 surpassed 11,000 cd/m^2, while its EQE was 25.6%. Other characteristics were also impressive with a CE and PE reaching 69.8 cd/A and 58.9 lm/W. The same green TADF emitter was also unrivalled when applied in non-doped EML. Device D1EA21 achieved a maximum PE, CE, and EQE of 56.4 cd/A, 43.5 lm/W, and 18.7%. These characteristics were considerably higher than those of devices D1EA15 and D2EA15, which used pyridine-unmodified green TADF emitter EA15. The benzophenone

fragment was also successfully applied in the synthesis of blue TADF emitters. A group of researchers led by J. Wang successfully combined a benzophenone electron acceptor with the 11-phenyldihydroindolo[2,3-a]carbazole electron donor and obtained material EA6. When applied as a dopant in blue OLED DEA6, a maximum EQE of 17.7% and luminance of over 14,000 cd/m^2 were obtained. Other efficiencies such as the CE and PE were 44.8 cd/A and 45.6 lm/W, respectively. However, the most efficient benzophenone derivative used as a blue TADF emitter was EA19, characterized by J. Zhang and his group of scientists. A relatively simple structure of a benzophenone-acridine derivative was applied for a blue DEA19 device and reached a CE of 47.7 cd/A, PE of 29.9 lm/W, and EQE of 20.6%

Table 9. Characteristics of OLED devices using emitters EA1–EA22.

Device	Emitter	Colour	V_{ON}, V	L_{MAX}, cd/m^2	CE, cd/A	PE, lm/W	EQE, %	CIE (x, y)
DEA1	EA1	Green	3.9	615	8.00	4.20	3.40	(0.27, 0.43)
DEA2	EA2	Blue	4.4	568	3.90	1.70	1.80	(0.21, 0.29)
DEA3	EA3	Green	3.8	1472	17.9	11.2	7.60	(0.26, 0.42)
DEA4	EA4	Blue	5.5	663	7.30	4.20	5.00	(0.18, 0.21)
DEA5	EA5	Blue	6.0	605	3.10	1.60	2.10	(0.19, 0.22)
DEA6	EA6	Blue	3.2	14,724	44.8	45.6	17.7	(0.17, 0.28)
DEA7	EA7	Green	2.5	>10,000	20.9	21.8	6.40	–
DEA8	EA8	Green	–	–	–	–	6.90	–
DEA9	EA9	Blue	4.0	10,754	23.3	19.3	9.50	(0.15, 0.15)
DEA10	EA10	Green	3.1	11,802	4.10	3.60	1.70	(0.23, 0.37)
DEA11	EA11	Green	4.7	17,353	24.8	–	8.90	(0.25, 0.48)
D1EA12	EA12	Green	3.8	2544	19.0	14.9	10.3	(0.26, 0.47)
D2EA12	EA12	Green	4.1	568	34.9	27.3	12.5	(0.23, 0.41)
D1EA13	EA13	Green	3.9	3006	18.2	14.1	6.59	(0.26, 0.47)
D2EA13	EA13	Green	3.2	13,280	44.4	45.0	15.2	(0.27, 0.50)
DEA14	EA14	Yellow	–	–	–	–	7.60	–
D1EA15	EA15	Green	3.2	6823	34.7	30.1	14.2	(0.20, 0.39)
D2EA15	EA15	Green	3.2	15,047	53.4	48.8	21.2	(0.21, 0.42)
DEA16	EA16	Green	3.0	–	32.7	34.3	12.9	(0.21, 0.42)
D1EA17	EA17	Green	2.5	21,243	53.7	52.7	17.3	(0.31, 0.54)
D2EA17	EA17	Green	3.2	11,977	49.6	48.6	17.7	(0.24, 0.49)
D1EA18	EA18	Yellow	2.5	11,949	8.90	7.99	3.35	(0.48, 0.50)
D2EA18	EA18	Green	2.7	31,115	64.6	75.1	20.6	(0.37, 0.55)
DEA19	**EA19**	**Blue**	**4.0**	**4235**	**47.7**	**29.9**	**20.6**	**–**
D1EA20	EA20	Yellow	4.4	32,590	73.1	38.2	26.7	–
D2EA20	EA20:2CzTPEPCz	White	6.1	12,310	45.9	18.0	20.8	(0.45, 0.44)
D1EA21	EA21	Green	3.2	26,836	56.4	43.5	18.7	(0.28, 0.53)
D2EA21	**EA21**	**Green**	**3.2**	**11,392**	**69.8**	**58.9**	**25.6**	**(0.24, 0.49)**
DEA22	EA22	Green	3.3	–	48.4	46.1	15.6	–

Characteristics of best performing blue and green devices are highlighted in bold.

5. Benzophenone-Based Emitters Employing a Symmetric D–A–D Structure

Chemical structures of symmetrical benzophenone-based emitters employing donor–acceptor–donor (D–A–D) structures are shown in Scheme 4. These compounds possess a molecular configuration comprising two separate donor segments enveloping a central acceptor moiety, establishing a conjugated system characterized by alternating donor and acceptor units. The materials described in this section have a mostly central benzophenone fragment with various carbazole substituents as in the case for compounds EB1–EB7. Acridine was also a popular fragment as an electron donor for five of the described materials EB8–EB12. Phenoxazine was a key element in four structures (EB13–EB16), and phenyl- or naphtyl- amines were used in three molecules, namely EB17–EB19. In addition, various other electron donors, such as spiro-, phenoselanazine, tri-azatruxene, and some others have been utilized. Material EB1 [113] was synthesized by utilizing Ullmann reaction between 4,4′-dibromobenzophenone and 3,6-bis(tert-butyl)-9H-carbazole. A significant number of the EB materials was synthesized through the Buchwald–Hartwig amination of 3,3′-dibromobenzophenone or 4,4′-dibromobenzophenone, employing various electron-donating fragments. For example, for the synthesis of compounds EB2, EB9, EB13 [78], and EB4 [81], tetrahydrocarbazole, phenoxazine, 2,7-ditert-butyl-9,9-dimethylacridine, and 3,6-diphenyl-9H-carbazole, respectively, served as the second reactant. The reactions of dibromobenzophenone with carbazole resulted in material EB3, with bicarbazole yielded EB5 [73], and with 9,9,9′9′-tetramethyl-9,9′10,10′-tetrahydro-2,10′-biacridine—EB11 [114]. N-(2-naphthyl)aniline played a crucial role in obtaining EB19 [115]. Phenoselanazine, azasiline, 10H-spiro[acridine-9,9′-fluorene], 10H-spiro[acridine-9,9′-xanthene], and (10H-spiro[acridine-9,9′-thioxanthene]) were utilized for the preparation of EB21 [116], EB22 [117], EB23, EB24, and EB25 [118], respectively. The synthesis of compounds EB26 and EB27 [119] involved the use of 5,10-dihexyl-10,15-dihydro-5H-diindolo[3,2-a:3′,2′-c]carbazole and 5,10-diphenyl-10,15-dihydro-5H-diindolo[3,2-a:3′,2′-c]carbazole as reactants. The synthesis of the benzophenone derivatives EB14, EB15, and EB16 [75], which was described in the same publication as for the earlier mentioned EB3 and EB5, was achieved using aminations of bis(4-bromobenzoyl)benzenes with two equivalents of phenoxazine. The same reaction methodology was used to obtain emitter EB6 [97]. In this case, amination of 3-iodo-9-ethylcarbazole with 4,4′-diaminobenzophenone took place. ((4,10-Dimethyl-6H,12H-5,11-methanodibenzo[b,f][1,5]diazocine-2,8-diyl)bis(4,1-phenylene))bis((4-bromophenyl)methanone) reacted with 9,9-dimethyl-9,10-dihydroacridine under similar conditions to prepare emitter EB12 [120]. Material EB7 [121] was synthesized during a simple nucleophilic substitution of 4,4′-diflourobenzophenone with 3-(N,N-diphenylamino)carbazole. Suzuki reaction was chosen as the best procedure for obtaining compound EB8 [122] from 4,4′-dibromobenzophenone and 9,9-dimethyl-10-phenyl-2-(4,4,5,5-tetramethyl-1,3,2-dioxaborolan-2-yl)-9,10-dihydroacridine as initial reactants. EB10 [123] was synthesized during the N,N-(2,6-di(3-pentyl)phenyl) imidazolium-catalysed reaction of 4,4′-dibromobenzophenone with 9,9-dimethyl-9,10-dihydroacridine. Two compounds EB17 and EB18 [88] were obtained through a simple one-step Friedel–Crafts reaction by using commercially available cheap starting materials triphenylamine (TPA) and, correspondingly, isophthaloyl dichloride for compound EB17 or terephthaloyl dichloride for emitter EB18.
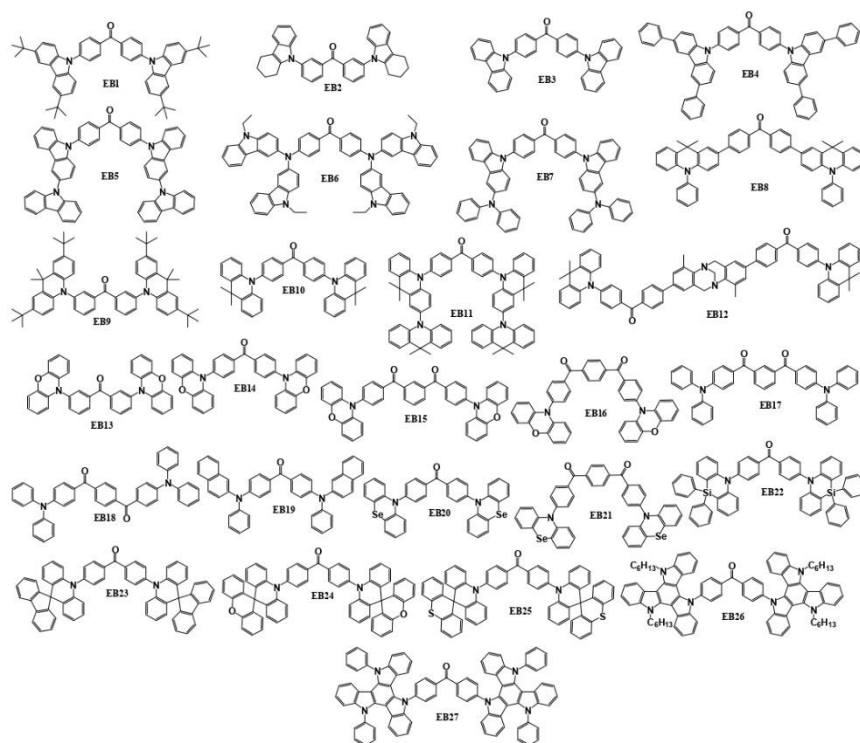
Scheme 4. Structures of benzophenone-based symmetrical D–A–D materials used as emitters in OLEDs.

Table 10 depicts thermal, electrochemical, and photophysical properties of the mentioned light-emitting symmetrical benzophenone materials EB1–EB27. The destruction temperatures were reported for eighteen compounds described in this section. Even though EB13 had a lowest T_D of 218 °C owing to two phenoxazine fragments, it was still high enough to cope with conditions of the device forming and operating, especially bearing in mind a high melting temperature of 118 °C for the compound. All the other presented emitters here were characterized by a T_D of 270 °C or higher. Glass transition temperatures for derivatives EB1, EB2, EB7, EB17, EB18, EB19, EB26, and EB27 were registered at 90 °C or higher, so these emitters could form stable amorphous layers. Crystalline benzophenone-based materials EB4, EB9, and EB22 demonstrated melting temperatures of 300 °C or higher as it was confirmed by DSC. Examining the HOMO–LUMO gap (energy bandgap E_g), it becomes evident that the majority of the symmetrical D–A–D benzophenone derivatives exhibit measured or calculated E_g levels in the region of 2.47–3.37 eV. Only EB9 presented a distinctly elevated E_g level of 3.66 eV. This could be the reason of decreased quantum yield and less effective TADF processes, when compared to emitters possessing smaller bandgaps. Achieving a low ΔE_{ST} is essential in the development of an emitter to enhance

the efficiency of the TADF process, as it is evident from the data of Table 10, where materials EB11, EB14, EB23, EB24, and EB25 with ΔE_{ST} values of 0.03 eV or lower demonstrate a Φ_{PL} exceeding 70% in a nitrogen atmosphere. The participation of the triplet state in the emission process was also demonstrated for some compounds. For example, this was observed in EB6, where the overall Φ_{PL} substantially decreased upon exposure to oxygen. In addition, in derivatives EB1, EB12, EB23, EB24, and EB25, substantial R_D levels were identified. All emitters described in this section, except fluorescent EB2 and EB9, exhibited TADF properties.

Table 10. Thermal, electrochemical, and photophysical properties of materials EB1–EB27.

	T_M, °C	T_G, °C	T_{Cr}, °C	T_D, °C	E_g, eV	E_S, eV	E_T, eV	ΔE_{ST}, eV	HOMO, eV	LUMO, eV	Φ_{PL} Film, %		Φ_{PL} Sol., %	R_D, %
											N_2	O_2		
EB1	–	107	–	384	2.95	2.62	2.47	0.15	−5.16	−2.21	13.1	–	2.20	87.8
EB2	–	91	–	312	3.21	–	3.02	–	−5.17	−2.03	20.0	–	3.00	–
EB3	–	–	–	–	3.10	2.89	3.10	0.21	−5.74	−2.64	55.0	–	21.0	–
EB4	370	–	–	480	3.30	2.83	2.69	0.14	−5.77	−2.25	24.4	–	15.3	–
EB5	–	–	–	–	3.02	3.02	2.88	0.14	−5.65	−2.63	73.0	–	38.0	–
EB6	–	–	–	–	2.60	–	–	0.29	−5.10	−2.50	73.0	37.0	–	–
EB7	–	159	–	398	2.79	–	–	–	−5.58	−2.79	–	–	–	–
EB8	–	–	–	–	–	–	–	0.39	–	–	53.0	–	–	7.5
EB9	342	–	269	389	3.66	2.70	2.66	0.04	−4.78	−219	16.0	–	6.00	–
EB10	–	–	–	410	–	2.76	2.69	0.07	–	–	90.0	–	–	–
EB11	–	–	–	433	2.82	–	–	0.03	−5.16	−2.34	89.1	–	–	–
EB12	–	–	–	270	2.86	2.81	2.68	0.13	−5.26	−2.40	31.5	–	–	32.7
EB13	118	–	62	218	3.05	–	2.65	–	−4.74	−2.19	15.0	–	12.0	–
EB14	–	–	–	–	2.52	2.61	2.58	0.03	−5.44	−2.92	70.0	–	44.0	–
EB15	–	–	–	–	2.61	2.62	2.52	0.10	−5.64	−3.03	71.0	–	36.0	–
EB16	–	–	–	–	2.49	2.59	2.53	0.06	−5.62	−3.13	36.0	–	10.0	–
EB17	–	90	–	436	2.84	2.59	2.38	0.21	−5.31	−2.47	75.0	–	46.0	–
EB18	–	92	–	416	2.70	2.37	2.32	0.05	−5.32	−2.62	39.0	–	2.00	–
EB19	–	99	–	440	2.90	2.66	2.47	0.19	−5.51	−2.60	16.3	–	–	–
EB20	–	–	–	–	–	2.84	2.69	0.15	–	–	7.60	–	–	–
EB21	–	–	–	–	–	2.84	2.69	0.15	–	–	8.50	–	–	–
EB22	300	–	–	495	2.94	2.71	2.64	0.07	−5.49	−2.55	70.0	–	–	–
EB23	–	–	–	445	3.37	2.62	2.61	0.01	−5.42	−2.05	91.0	–	–	55.6
EB24	–	–	–	477	3.32	2.64	2.63	0.01	−5.42	−2.10	94.0	–	–	54.5
EB25	–	–	–	500	3.32	2.64	2.63	0.01	−5.43	−2.11	85.0	–	–	42.8
EB26	–	>95	–	>400	2.47	2.55	2.47	0.13	−5.30	−2.83	22.0	–	0.80	–
EB27	–	>95	–	>400	2.59	2.58	2.48	0.13	−5.33	−2.77	24.2	–	1.90	–

The majority of the D–A–D benzophenone-based derivatives were tested as emitters in OLEDs, whose structures are illustrated in Table 11. The dominant choice for anode in these devices was also ITO. To ease the energy barrier, such hole-injecting materials as Mo_2O_3, rhenium (VI) oxide (ReO$_3$), and MoO_3 were used. NPB, α-NPD, mCP, PEDOT:PSS, TAPC, HAT-CN, or TCTA were chosen for the formation of hole-transporting layers. To further elevate the efficiency of the devices, well-known host materials diphenyl[4-(triphenylsilyl)phenyl]phosphine oxide (TSPO1), DPEPO, TCzl, 9-(3-(9H-carbazol-9-yl)phenyl)-9H-carbazole-3-carbonitrile (mCPCN), 2,8-bis(diphenyl-phosphoryl)-dibenzo[b,d]furan (PPF), mCP, mCBP, CBP, and some others were used in emissive layers. To achieve desired white-light OLEDs, some phosphorescent emitters such as Ir(ppy)$_2$(acac) or Ir(bt)$_2$(dipba) were used in conjunction with benzophenone derivative EB4. Electron transport layers were made from DPEPO, TPBi, B3PYMPM, TmPyPB, BPhen, PPF, or

TSPO1. Also, LiF, Liq, and rubidium carbonate (Rb_2CO_3) were used as electron-injecting materials. For all the devices described in this section, aluminium cathodes were used.

Table 11. Architectures of devices utilizing the D–A–D emitters EB1–EB27.

Device with EB Emitter	Device Architecture
DEB3	ITO/α-NPD (35 nm)/mCP (5 nm)/DPEPO:6 wt% **EB3** (20 nm)/ DPEPO (10 nm)/TPBi (30 nm)/LiF (0.8 nm)/Al (80 nm)
D1EB4	ITO/NPB (35 nm)/mCP (5 nm)/**EB4** (30 nm)/B3PYMPM (30 nm)/LiF (0.5 nm)/Al (150 nm)
D2EB4	ITO/NPB (35 nm)/mCP (5 nm)/**EB4**:0.5%wt Ir(ppy)$_2$(acac)/**EB4**:0.8 wt% Ir(bt)$_2$(dipba) (30 nm)/ B3PYMPM (30 nm)/LiF (0.5 nm)/Al (150 nm)
DEB5	ITO/α-NPD (35 nm)/mCP (5 nm)/DPEPO:6 wt% **EB5** (20 nm)/DPEPO (10 nm)/ TPBi (30 nm)/LiF (0.8 nm)/Al (80 nm)
DEB6	ITO(50 nm)/PEDOT:PSS (30 40 nm)/TCzl:15 wt% **EB6**/TPBi (70 nm)/Liq (1 nm)/Al (80 nm)
DEB8	ITO/TAPC (25 nm)/CBP:3 wt% **EB8** (35 nm)/TmPyPB (55 nm)/LiF (1 nm)/Al
DEB9	ITO/TAPC (50 nm)/mCP (10 nm)/**EB9** (30 nm)/Bphen (50 nm)/LiF (1 nm)/Al (100 nm)
DEB10	ITO/MoO$_3$ (1 nm)/mCP (40 nm)/**EB10** (30 nm)/TBPi (50 nm)/LiF (1 nm)/Al
DEB11	ITO/PEDOT:PSS (40 nm)/mCPCN:25 wt% **EB11** (45 nm)/ DPEPO (10 nm)/TmPyPB (40 nm)/Liq (1.2 nm)/Al (120 nm)
DEB12	ITO/HAT-CN (5 nm)/TAPC (30 nm)/TCTA (5 nm)/mCP (5 nm)/PPF:20% **EB12**(30 nm)/ PPF (10 nm)/Bphen (30 nm)/Liq (1 nm)/Al (100 nm)
DEB14	ITO/α-NPD (40 nm)/mCP:6 wt% **EB14** (20 nm)/TPBi (40 nm)/LiF (0.8 nm)/Al (80 nm)
DEB15	ITO/α-NPD (40 nm)/**EB15** (20 nm)/TPBi (40 nm)/LiF (0.8 nm)/Al (80 nm)
DEB16	ITO/α-NPD (40 nm)/mCBP:6 wt% **EB16** (20 nm)/TPBi (40 nm)/LiF (0.8 nm)/Al (80 nm)
DEB16EB5	ITO/α-NPD (35 nm)/mCBP:18 wt% **EB16** (4 nm)/PPF:6 wt%**EB5** (14 nm)/PPF (40 nm)/LiF (0.8 nm)/Al (80 nm)
DEB17	ITO/PEDOT:PSS (40 nm)/**EB17** (35–40 nm)/TmPyPB (60 nm)/LiF (0.8 nm)/Al (120 nm)
DEB18	ITO/PEDOT:PSS (40 nm)/**EB18** (35–40 nm)/TmPyPB (60 nm)/LiF (0.8 nm)/Al (120 nm)
DEB19	ITO/Mo$_2$O$_3$ (4 nm)/mCP (30 nm)/mCP:15 wt% **EB19** (30 nm)/TmTyPB (60 nm)/LiF (1.5 nm)/Al (100 nm)
DEB20	ITO/α-NPD (40 nm)/mCBP:10 wt% **EB20** (20 nm)/TPBi (40 nm)/LiF (0.6 nm)/Al (100 nm)
DEB21	ITO/α-NPD (40 nm)/mCBP:10 wt% **EB21** (20 nm)/TPBi (40 nm)/LiF (0.6 nm)/Al (100 nm)
DEB22	ITO (70 nm)/4 wt%ReO$_3$:mCP (45 nm)/mCP (15 nm)/mCP:TSPO1:16 wt%**EB22** (15 nm)/ TSPO1 (15 nm)/4 wt%Rb$_2$CO$_3$:TSPO1 (50 nm)/Al (100 nm)
D1EB23	ITO/HAT-CN (5 nm)/NPB (30 nm)/mCP (5 nm)/**EB23** (20 nm)/PPF (5 nm)/TPBi (50 nm)/LiF (1 nm)/Al (120 nm)
D2EB23	ITO/HAT-CN (5 nm)/NPB (30 nm)/mCP (5 nm)/PPF:30 wt% **EB23** (20 nm)/ PPF (5 nm)/TPBi (50 nm)/LiF (1 nm)/Al (120 nm)
D1EB24	ITO/HAT-CN (5 nm)/NPB (30 nm)/mCP (5 nm)/**EB24** (20 nm)/PPF (5 nm)/TPBi (50 nm)/LiF (1 nm)/Al (120 nm)
D2EB24	ITO/HAT-CN (5 nm)/NPB (30 nm)/mCP (5 nm)/PPF:30 wt% **EB24** (20 nm)/PPF (5 nm)/ TPBi (50 nm)/LiF (1 nm)/Al (120 nm)
D1EB25	ITO/HAT-CN (5 nm)/NPB (30 nm)/mCP (5 nm)/**EB25** (20 nm)/PPF (5 nm)/TPBi (50 nm)/LiF (1 nm)/Al (120 nm)
D2EB25	ITO/HAT-CN (5 nm)/NPB (30 nm)/mCP (5 nm)/PPF:30 wt% **EB25** (20 nm)/PPF (5 nm)/ TPBi (50 nm)/LiF (1 nm)/Al (120 nm)
D1EB26	ITO/PEDOT:PSS (25 nm)/**EB26** (25 nm)/TmPyPB (55 nm)/LiF (1 nm)/Al (150 nm)

186

Table 11. *Cont.*

Device with EB Emitter	Device Architecture
D2EB26	ITO/PEDOT:PSS (25 nm)/G3-tCbz:30 wt% **EB26** (25 nm)/TmPyPB (55 nm)/LiF (1 nm)/Al (150 nm)
D1EB27	ITO/PEDOT:PSS (25 nm)/**EB27** (25 nm)/TmPyPB (55 nm)/LiF (1 nm)/Al (150 nm)
D1EB27	ITO/PEDOT:PSS (25 nm)/G3-tCbz:30 wt% **EB27** (25 nm)/TmPyPB (55 nm)/LiF (1 nm)/Al (150 nm)

This section reviews all devices constructed by researchers utilizing benzophenone-based emitters EB1–EB27 with a D–A–D structure, and the characteristics of these devices are detailed in Table 12. The combination of a central benzophenone electron-accepting group with various electron donors yielded red, yellow, green, and blue emitters. Utilization of the described compounds with phosphorescent emitters or other benzophenone-based materials also resulted in white light emission. Lee et al. reported the red-emitting material EB15. Device DEB15, which utilized the mentioned TADF emitter, exhibited a low turn-on voltage of 2.8 V, CE of 11.1 cd/A, and EQE of 4.2%. Additionally, maximum luminance of the device exceeded 50,000 cd/m^2. The same authors introduced blue TADF emitters EB3 and EB5, which in devices achieved EQE values of 8.1% and 14.3%, respectively, with the latter one being the most efficient blue OLED in this D–A–D group. They also presented a green TADF emitter EB14, which attained an EQE of 10.7% in its device, and a yellow TADF emitter EB16, which reached an EQE of 6.9%. Liang and co-workers presented material EB4 which can act as a host and as an emitter at the same time. For example, device D1EB4 with non-doped emitter EB4 demonstrated a PE and EQE of 6.9 lm/W and 4.0%, respectively. By combining phosphorescent emitters Ir(ppy)$_2$(acac) and Ir(bt)$_2$(dipba) with the compound EB4, device D2EB4 achieved white emission and demonstrated an exceptionally high current efficiency of 48.6 cd/A and external quantum efficiency of 25.6%. By utilizing the symmetrical D–A–D structure, researchers developed nine green TADF emitters EB6, EB10, EB11, EB14, EB20, EB21, EB23, EB24, and EB25, which achieved over 10% external quantum efficiency. EB6, designed by Tani and colleagues, was used in an emissive layer of the TADF device DEB6 and achieved an EQE of 10.4%. Zhang and collaborators employed a straightforward structural derivative EB10 as a non-doped TADF emitter. The resultant device exhibited excellent PE and EQE values of 59.0 lm/W and 18.0%, respectively. Liu and colleagues created a structurally similar derivative EB11, where they replaced the acridine electron donor with a biacridine fragment. This modification led to a notable improvement in the EQE, reaching 22.5%, along with an impressive CE of 69.3 cd/A. Derivatives EB20 and EB21, which were characterized by Sharif and co-workers, also were highly efficient when applied in green TADF OLED devices. By combining phenoselenazine electron donors with benzophenone, researchers synthesized EB20 and fabricated the DEB20 device, which exhibited an exceptionally high EQE of 30.8% and a CE of 64.0 cd/A. In comparison, the DEB21 device, which employed derivative EB21 with an additional ketone group as the emitter, achieved a lower EQE of 18.8% but with a higher CE of 73.5 cd/A. The highest overall efficiencies of green TADF OLEDs by utilizing symmetrical D–A–D benzophenone-based emitters were achieved by Huang et al., who synthesized and characterized derivatives EB23, EB24, and EB25. These materials underwent testing in both non-doped and doped emissive layers. The most efficient non-doped device D1EB23 demonstrated exceptional performance with a maximal CE, PE, and EQE reaching 53.9 cd/A, 48.9 lm/W and 18.6%, respectively. In the doped device D2EB23, efficiencies were further elevated, achieving an impressive CE of 90.9 cd/A, PE of 91.2 lm/W, and EQE of 30.3%. If the device D2EB23 attained the highest CE and PE values among the green devices described in this section, the OLED D2EB24 with emitter EB24 doped in a host material remained unparalleled with an extraordinary high EQE level of 32.2%.

187

**Table 12.** Characteristics of OLED devices using emitters EB1–EB27.

Device	Emitter	Colour	V_{ON}, V	L_{MAX}, cd/m^2	CE, cd/A	PE, lm/W	EQE, %	CIE (x, y)
DEB3	EB3	Blue	4.3	510	9.30	–	8.10	(0.16, 0.14)
D1EB4	EB4	Blue	3.2	5516	–	6.90	4.00	(0.15, 0.26)
D2EB4	EB4/Ir(ppy)$_2$(acac)/ Ir(bt)$_2$(dipba)	White	2.7	25,540	48.6	–	25.6	(0.41, 0.46)
DEB5	**EB5**	**Blue**	**4.4**	**3900**	**25.5**	**–**	**14.3**	**(0.17, 0.27)**
DEB6	EB6	Green	–	–	–	–	10.4	
DEB8	EB8	Blue	–	–	–	–	8.90	(0.14, 0.16)
DEB9	EB9	Green	7.5	114	11.8	9.30	1.93	(0.37, 0.57)
DEB10	EB10	Green	2.6	45,300		59.0	18.0	(0.26, 0.55)
DEB11	EB11	Green	4.4	7173	69.3	–	22.5	(0.29, 0.54)
DEB12	EB12	Green	5.3	3524	11.0	6.90	3.90	(0.28, 0.51)
DEB14	EB14	Green	3.2	86,100	35.9	–	10.7	(0.37, 0.58)
DEB15	EB15	Red	2.8	50,820	11.1	–	4.20	(0.58, 0.36)
DEB16	EB16	Yellow	3.6	57,120	20.1	–	6.90	(0.49, 0.51)
DEB16/EB5	EB16/EB5	White	5.0	9800	16.4	–	6.70	(0.32, 0.39)
DEB17	EB17	Blue	3.9	10,005	4.80	2.70	2.40	(0.15, 0.28)
DEB18	EB18	Green	3.8	7354	10.8	4.70	2.70	(0.33, 0.51)
DEB19	EB19	Blue	3.9	1387	2.74	2.20	1.69	(0.16, 0.21)
DEB20	EB20	Green	4.3	17,007	64.0	–	30.8	(0.31, 0.53)
DEB21	EB21	Green	5.4	16,883	73.5	–	18.8	(0.33, 0.48)
DEB22	EB22	Blue	3.6	2021	–	–	11.4	(0.17, 0.31)
D1EB23	EB23	Green	3.2	31,713	53.9	48.9	18.6	(0.24, 0.53)
D2EB23	EB23	Green	3.0	48,712	90.9	91.2	30.3	(0.25, 0.54)
D1EB24	EB24	Green	3.6	30,283	46.8	37.5	17.1	(0.22, 0.46)
D2EB24	**EB24**	**Green**	**3.2**	**48,515**	**87.5**	**85.9**	**32.2**	**(0.22, 0.49)**
D1EB25	EB25	Green	3.8	25,616	49.1	35.7	18.1	(0.22, 0.50)
D2EB25	EB25	Green	3.2	48,153	79.8	75.9	28.4	(0.23, 0.50)
D1EB25	EB25	Yellow	2.6	>10,000	17.8	20.0	5.90	(0.41, 0.54)
D2EB25	EB25	Yellow-green	2.8	>10,000	48.1	47.8	15.9	(0.37, 0.53)
D1EB26	EB26	Yellow-green	2.7	>10,000	18.9	19.2	6.00	(0.38, 0.55)
D2EB26	EB26	Green	2.8	>10,000	46.4	47.2	15.4	(0.34, 0.53)

Characteristics of best performing blue and green devices are highlighted in bold.

Within the realm of blue TADF emitters described in this section, aside from the previously mentioned derivatives EB3 and EB5, notable efficiencies were also observed by using EB8 and EB22 emitters in TADF-based OLEDs. The compound EB8, presented by Cai and colleagues, achieved an EQE of 8.90% in the DEB8 device. Another team led by Sun developed and utilized the TADF emitter EB22 as crucial element in the construction of the DEB22 device, displaying a V_{ON} of 3.6 V, an L_{MAX} of 2021 cd/m^2, and an EQE of 11.4%. The previously mentioned EB5 emitter proved to be the most effective blue TADF emitter in this section. When integrated into a device, it exhibited a CE of 25.5 cd/A, an EQE of 14.3%, and a maximum luminance of 3900 cd/m^2.

188

6. Benzophenone-Based TADF Emitters Employing an Asymmetric D–A–D Structure

Structures of benzophenone-based TADF emitters having asymmetric D–A–D molecular configurations are shown in Scheme 5. Except for one material, all others utilized carbazol-9-yl as one of the electron-donating fragments in conjunction with a benzophenone acceptor, along with other donating moieties like 3-substituted carbazole, 9,10-dihydro-9,9-dimethylacridine, spiro[acridine-9,9′-fluorene], or phenoxazine. Only the derivative EC11 did not incorporate carbazole as one of the electron donors, but employed 9,10-dihydro-9,9-dimethylacridine and thianthrene fragments. To obtain the derivatives presented in this section, at least two synthetic steps were required. Derivative EC1 [94] was synthesized through a two-step Buchwald–Hartwig amination procedure, involving the replacement of one bromine atom in 4,4′-dibromobenzophenone with carbazole by following reaction with 4-(9H-carbazol-1-yl)-N,N′-diphenylaniline. Material EC2 [66] was obtained by reaction between (3,5-bis-carbazol-9-yl-phenyl)-(4-bromophenyl)-methanone and 9,10-dihydro-9,9-dimethylacridine under Buchwald–Hartwig reaction conditions. Derivatives EC3 and EC4 [124] were created through the two-step synthesis process. Initially, the fluorine atom of 4-bromo-4′-fluorobenzophenone was reacted with spiro[acridine-9,9′-fluorene] using a nucleophilic substitution reaction. Subsequently, the bromine atom was replaced with carbazole or 3,6-di-tert-butylcarbazole during Buchwald–Hartwig reaction. Materials EC5–EC10 were synthesized using very similar procedures [125]. In the initial step, 3,6-di-tert-butyl-9H-carbazole underwent Buchwald–Hartwig reaction with (4-bromophenyl)(4-fluorophenyl)methanone, (6-bromopyridin-3-yl)(4-fluorophenyl)methanone, or (5-bromopyridin-2-yl)(4-fluorophenyl)methanone, resulting in intermediate compounds. Subsequently, nucleophilic substitution reactions of 9,10-dihydro-9,9-dimethylacridine were employed with, correspondingly, (4-(3,6-di-tert-butyl-9H-carbazol-9-yl)phenyl)(4-fluorophenyl)methanone, (6-(3,6-di-tert-butyl-9H-carbazol-9-yl)pyridin-3-yl)(4-fluorophenyl)methanone, and (5-(3,6-di-tert-butyl-9H-carbazol-9-yl)pyridin-2-yl)(4-fluorophenyl)methanone, to yield compounds EC5, EC6, and EC7, respectively. Utilizing the same reactions with phenoxazine instead of 9,10-dihydro-9,9-dimethylacridine resulted in compounds EC8, EC9, and EC10, respectively. The synthesis of derivative EC11 also involved a two-step process [126]. Initially, one bromine atom of 4,4′-dibromobenzophenone was replaced with a thianthrene moiety through a Suzuki reaction. Subsequently, the second bromine atom was substituted with 9,10-dihydro-9,9-dimethylacridine in a Buchwald–Hartwig cross-coupling reaction.
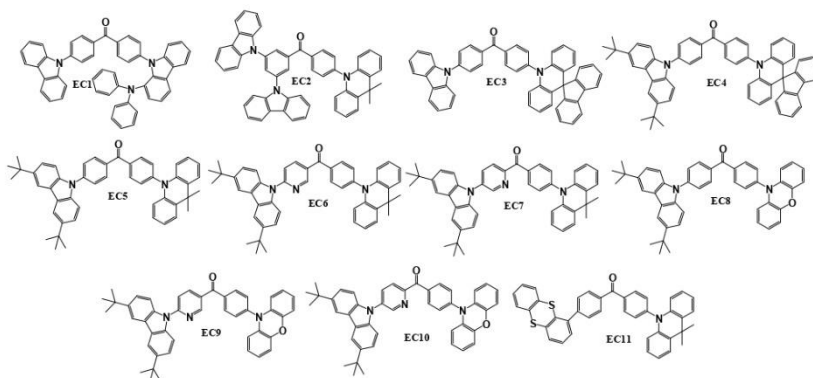
Scheme 5. Structures of benzophenone-based asymmetrical D–A–D materials used as emitters in OLEDs.

189

Table 13 presents the thermal, electrochemical, and photophysical properties of materials EC1–EC11. The asymmetric D–A–D-type benzophenone derivatives exhibited exceptional thermal stability, with a T_D ranging from 309 to 451 °C, as verified through TGA measurements. It is reported that for materials EC2 and EC11, during DSC experiments, T_G values were registered at 72 °C and 104 °C, respectively. The HOMO levels of materials EC1–EC11 ranged from −5.92 to −5.23, while the LUMO levels varied between −3.09 and −2.61. The energy difference between HOMO and LUMO levels for all the materials discussed in this section was 2.88 eV or lower. This small bandgap facilitates a minimal energy difference between the lowest singlet and triplet states, enabling efficient reverse intersystem crossing. Experimental results support this, with the ΔE_{ST} being 0.10 eV or lower, resulting in a high Φ_{PL} ranging from 33.2% to 90.0%. EC3 to EC11 derivatives exhibited aggregation-induced emission properties with lower Φ_{PL} values detected in solutions compared to film states. Additionally, materials EC1 and EC3 to EC10 demonstrated significant involvement of triplet states in photon generation, as evidenced by a R_D ranging from 33.0% to 89.7% with one of the potential light-generating mechanisms being TADF.

Table 13. Thermal, electrochemical, and photophysical properties of materials EC1–EC11.

	T_M, °C	T_G, °C	T_D, °C	E_g, eV	E_S, eV	E_T, eV	ΔE_{ST}, eV	HOMO, eV	LUMO, eV	Φ_{PL} Film, %	Φ_{PL} Sol., %	R_D, %
EC1	–	–	433	2.30	2.75	2.71	0.04	−5.36	−3.06	57	–	78.9
EC2	–	72	309	2.76	2.82	2.72	0.10	−5.37	−2.61	–	–	–
EC3	–	–	417	2.53	2.67	2.66	0.013	−5.35	−2.82	90	28	53.3
EC4	–	–	451	2.58	2.71	2.66	0.05	−5.36	−2.78	86	25	33.0
EC5	–	–	404	2.36	2.81	2.71	0.10	−5.35	−2.99	46.7	1.2	76.4
EC6	–	–	414	2.30	2.69	2.65	0.04	−5.36	−3.06	66.8	3.4	89.7
EC7	–	–	416	2.25	2.59	2.56	0.03	−5.34	−3.09	53.3	0.5	83.3
EC8	–	–	391	2.34	2.58	2.52	0.06	−5.26	−2.92	33.2	0.6	75.3
EC9	–	–	400	2.26	2.57	2.54	0.03	−5.25	−2.99	48.4	0.9	88.2
EC10	–	–	403	2.19	2.41	2.38	0.03	−5.23	−3.04	35.3	0.8	82.7
EC11	190	104	416	2.88	2.85	2.79	0.06	−5.92	−3.04	76	17	–

Every benzophenone derivative presented in this section underwent testing as an emitter in OLED devices, with their structures depicted in Table 14. Consistent with earlier sections, ITO was the only selection for the anode in these devices. To reduce the energy barrier for holes, the device DEC11 utilized MoO_3 as the hole-injecting material. For this device or others, a stack of one to three layers of hole-transporting materials was employed, featuring layers composed of PEDOT:PSS, HAT-CN, TAPC, TCTA, NPB, or mCP. While most devices using EC1-EC11 emitters employed non-doped configurations, some of them also utilized the host–guest approach. Specifically, the host material CBP was applied in device DEC2, and PPF was employed for D2EC3 and D2EC4. TPBi, TmPyPb, and PPF were employed as electron-transporting layers, while Cs_2CO_3 and LiF served as electron-injecting materials. For all the devices discussed in this section, the Al cathode was the only option.

Table 14. Architectures of the devices utilizing emitters EC1–EC11.

Device	Device Architecture
DEC1	ITO/PEDOT:PSS (40 nm)/**EC1** (40 nm)/TPBi (30 nm)/Cs_2CO_3 (2 nm)/Al (100 nm)
DEC2	ITO/HAT-CN (20 nm)/TAPC (30 nm)/CBP:20 wt% **EC2** (25 nm)/TmPyPb (40 nm)/LiF (1 nm)/Al (150 nm)
D1EC3	ITO/HAT-CN (5 nm)/NPB (30 nm)/mCP (5 nm)/**EC3** (20 nm)/PPF (5 nm)/TPBi (50 nm)/LiF (1 nm)/Al (120 nm)

Table 14. *Cont.*

Device	Device Architecture
D2EC3	ITO/HAT-CN (5 nm)/NPB (30 nm)/mCP (5 nm)/PPF:20 wt% **EC3** (20 nm)/ PPF (5 nm)/TPBi (50 nm)/LiF (1 nm)/Al (120 nm)
D1EC4	ITO/HAT-CN (5 nm)/NPB (30 nm)/mCP (5 nm)/**EC4** (20 nm)/PPF (5 nm)/TPBi (50 nm)/LiF (1 nm)/Al (120 nm)
D2EC4	ITO/HAT-CN (5 nm)/NPB (30 nm)/mCP (5 nm)/PPF:20 wt% **EC4** (20 nm)/ PPF (5 nm)/TPBi (50 nm)/LiF (1 nm)/Al (120 nm)
DEC5	ITO/PEDOT:PSS (40 nm)/**EC5** (40 nm)/TPBi (30 nm)/Cs$_2$CO$_3$ (2 nm)/Al (100 nm)
DEC6	ITO/PEDOT:PSS (40 nm)/**EC6** (40 nm)/TPBi (30 nm)/Cs$_2$CO$_3$ (2 nm)/Al (100 nm)
DEC7	ITO/PEDOT:PSS (40 nm)/**EC7** (40 nm)/TPBi (30 nm)/Cs$_2$CO$_3$ (2 nm)/Al (100 nm)
DEC8	ITO/PEDOT:PSS (40 nm)/**EC8** (40 nm)/TPBi (30 nm)/Cs$_2$CO$_3$ (2 nm)/Al (100 nm)
DEC9	ITO/PEDOT:PSS (40 nm)/**EC9** (40 nm)/TPBi (30 nm)/Cs$_2$CO$_3$ (2 nm)/Al (100 nm)
DEC10	ITO/PEDOT:PSS (40 nm)/**EC10** (40 nm)/TPBi (30 nm)/Cs$_2$CO$_3$ (2 nm)/Al (100 nm)
DEC11	ITO/MoO$_3$ (1.2 nm)/NPB (44 nm)/TCTA (4 nm)/mCP (4 nm)/mCP:7%wt **EC11** (24 nm)/ TSPO1 (4 nm)/TPBi (40 nm)/LiF (1.2 nm)/Al (400 nm)

All the recently presented derivatives EC1–EC11 underwent testing as emitters in devices and the characteristics of these OLEDs are detailed in Table 15. Although most of these devices displayed green emission, there were exceptions such as DEC8, which emitted yellow light, and DEC9 as well as DEC10, which emitted orange light. Ma and co-workers successfully synthesized and characterized an EC1 derivative, revealing noteworthy characteristics. The mentioned emitter was integrated into the non-doped emissive layer of device DEC1, which demonstrated a CE of 35.5 cd/A, PE of 22.3 lm/W, and EQE of 13.3%. Another derivative EC2, synthesized and characterized by Zhao et al., showcased impressive performance with CE, PE, and EQE values of 61.8 cd/A, 40.4 lm/W, and 19.7%, respectively, as well as with an impressive L$_{MAX}$ of 116,000 cd/m^2. Huang's team developed derivatives EC3 and EC4. Among them, TADF emitter EC3-based devices exhibited the highest efficiencies between devices described in this section, achieving a CE, PE, and EQE of 76.9 cd/A, 71.0 lm/W and 29.0%, respectively, in the non-doped device D1EC3. Introducing host material PPF in the emissive layer of the D2EC3 further elevated efficiencies to 82.9 cd/A for CE, 70.1 lm/W for PE, and a peak EQE reaching 33.3%. Although EC4 using OLEDs were slightly less efficient, D1EC4 exhibited a remarkably low V$_{ON}$ of 3.0 V and EQE of 21.6%. D2EC4 demonstrated an impressive EQE of 32.9%, with CE and PE values of 77.2 cd/A and 65.0 lm/W, respectively. The emitting materials EC5–EC10 were meticulously designed, synthesized, and tested by Ma and colleagues in non-doped OLED prototypes. These materials combined a 3,6-di-tert-butylcarbazole donor with various other donors such as 9,10-dihydro-9,9-dimethylacridine (EC5, EC6, EC7) or phenoxazine (EC8, EC9, EC10) with acceptors like benzophenone (EC5, EC8), phenyl(3-pyridyl)methanone (EC6, EC9), or phenyl(2-pyridyl)methanone (EC7, EC10). For instance, the incorporation of 9,10-dihydro-9,9-dimethylacridine TADF moiety in benzophenone-based TADF emitter EC5 led to the device DEC5 having a PE, CE, and EQE of 14.3 cd/A, 6.4 lm/W, and 6.70%, respectively. The incorporation of a pyridinyl fragment in TADF emitter EC6 significantly improved efficiencies in its corresponding device DEC6, reaching a CE of 35.4 cd/A, PE of 15.9 lm/W, and EQE of 11.4%. A phenoxazine fragment in benzophenone derivative EC8 resulted in a yellow TADF OLED device that achieved an EQE of 4.8%. An introduction of the pyridinyl fragment in compound EC9 elevated the efficiency of the orange TADF device DEC9, demonstrating a CE, PE, and EQE values of table21.6 cd/A, 6.80 lm/W, and 9.40%, respectively. Finally, the last TADF emitter of the group EC11, designed and synthesized by Tomkeviciene and colleagues, featured two electron-donating fragments of thianthrene and 9,10-dihydro-9,9-dimethylacridine. When incorporated into the emissive

191

layer of device DEC11, CE, PE, and EQE values of 57.8 cd/A, 38.8 lm/W, and 22.2% with an L_{MAX} exceeding 15,000 cd/m^2 were achieved.

Table 15. Characteristics of OLED devices using emitters EC1–EC11.

Device	Emitter	Colour	V_{ON}, V	L_{MAX}, cd/m^2	CE, cd/A	PE, lm/W	EQE, %	CIE (x, y)
DEC1	EC1	Green	3.8	1738	35.5	22.3	13.3	(0.29, 0.48)
DEC2	EC2	Green	3.6	116,000	61.8	40.4	19.7	(0.26, 0.56)
D1EC3	EC3	Green	3.2	78,540	76.9	71.0	29.0	(0.21, 0.47)
D2EC3	EC3	Green	3.2	71,150	82.9	70.1	33.3	(0.20, 0.42)
D1EC4	EC4	Green	3.0	54,450	53.2	51.5	21.6	(0.20, 0.42)
D2EC4	**EC4**	**Green**	**3.2**	**42,550**	**77.2**	**65.0**	**32.9**	**(0.19, 0.38)**
DEC5	EC5	Green	4.5	2599	14.3	6.40	6.70	(0.28, 0.47)
DEC6	EC6	Green	4.2	6726	35.4	15.9	11.4	(0.34, 0.51)
DEC7	EC7	Green	4.3	3832	23.8	10.7	9.10	(0.39, 0.56)
DEC8	EC8	Yellow	4.8	3658	12.4	4.30	4.80	(0.41, 0.55)
DEC9	EC9	Orange	4.6	8085	21.6	6.80	9.40	(0.47, 0.51)
DEC10	EC10	Orange	4.7	6551	14.5	4.20	6.90	(0.53, 0.46)
DEC11	EC11	Green	4.2	15,600	57.8	38.8	22.2	(0.18, 0.41)

Characteristics of best performing device are highlighted in bold.

7. Benzophenone-Based TADF Emitters Employing a Dendritic Structure

The structures of dendritic benzophenone-based TADF emitters are illustrated in Scheme 6. In the case of materials ED9 and ED10, researchers employed a donor–acceptor (D–A) dendritic structure, while all other materials featured donor–acceptor–donor (D–A–D) dendritic structures. The benzophenone as an electron acceptor was paired with either 9,10-dihydro-9,9-dimethylacridine or 9H-carbazole. Additionally, these electron donors were further substituted with diverse alkyl or aryl groups. Material ED1 [113] was synthesized during Ulmann reaction between 3,6-bis(3,6-di-tert-butylcarbazol-9-yl)carbazole and 4,4′-dibromobenzophenone. ED2, ED3, and ED4 [127] derivatives were acquired through N-arylation reactions involving 4,4′-diiodobenzophenone. The reaction with 3,6-bis(3,6-dimethylcarbazol-9-yl)carbazole resulted in ED2, while ED3 was obtained by using 3,6-bis(3,6-dimethoxycarbazol-9-yl)carbazole, and ED4 was derived in the reaction with 3,6-bis(3,6-diphenylcarbazol-9-yl)carbazole. ED5 and ED6 [128] compounds were synthesized using a closely related procedure but with distinct carbazole-based reactants. Specifically, 3,6-bis(carbazol-9-yl)carbazole was employed to produce ED5, while ED6 was derived from 3,6-bis(3,6-di(carbazol-9-yl)carbazol-9-yl)carbazole. For the synthesis of derivatives ED7 and ED8 [129], Ulmann reactions were employed with bis(4-(2,7-diiodo-9,9-dimethylacridin-10(9H)-yl)phenyl)methanone. The reaction with 3,6-di-tert-butylcarbazole resulted in ED7, and the reaction with 3,6-bis(3,6-di-tert-butylcarbazol-9-yl)carbazole produced material ED8. Compounds ED9 and ED10 [108] were also synthesized through the Ullmann reaction procedure, when 3,6-bis(3,6-di-tert-butylcarbazol-9-yl)carbazole reacted with the 4-bromobenzophenone to yield material ED9 and with (6-bromopyridin-3-yl)(phenyl)methanone to yield derivative ED10.

192
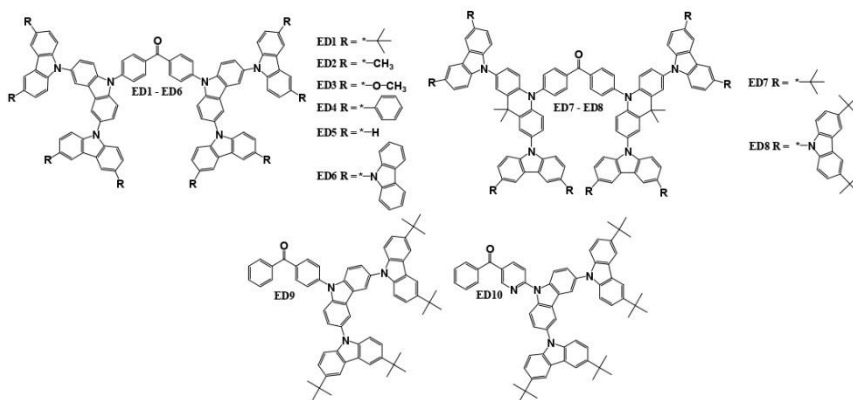
Scheme 6. Structures of benzophenone-based dendritic materials used as emitters in OLEDs.

The thermal, electrochemical, and photophysical characteristics of the emitting materials ED1–ED10 are presented in Table 16. The dendritic benzophenone derivatives displayed remarkable thermal stability with the measured T_D for the tested materials exceeding 470 °C. In the cases of materials ED1, ED7, and ED8, DSC experiments confirmed only a T_G of 218 °C, 283 °C, and 289 °C, respectively. The HOMO levels for materials EC1–EC11 ranged from −5.87 to −5.04, while the LUMO levels varied between −3.09 and −2.03. The energy gap between the HOMO and LUMO levels for all discussed materials in this section was lower than 3.12 eV. This narrow gap facilitates a minimal energy difference between the lowest singlet and triplet states, promoting efficient reverse intersystem crossing. Experimental findings corroborated this, with a ΔE_{ST} of 0.15 eV or lower, and a high Φ_{PL} of up to 77.0% was obtained. Specifically, derivatives ED1, ED4, ED5, and ED6 exhibited aggregation-induced emission properties with lower Φ_{PL} values observed in solutions as compared to film states. Furthermore, materials ED1–ED6, ED9, and ED10 demonstrated the involvement of triplet states in photon generation, as indicated by the R_D ranging from 9.0% to 64.5%. One of the potential light-generating mechanisms could be TADF in the case.

Table 16. Thermal, electrochemical, and photophysical properties of materials ED1–ED10.

	T_M, °C	T_G, °C	T_D, °C	E_g, eV	E_S, eV	E_T, eV	ΔE_{ST}, eV	HOMO, eV	LUMO, eV	Φ_{PL} Film, %	Φ_{PL} Sol., %	R_D, %
ED1	–	218	–	2.73	2.80	2.72	0.08	−5.82	−3.09	74.0	49.0	45.9
ED2	–	–	–	2.74	2.82	2.73	0.09	−5.72	−2.98	34.0	48.0	17.6
ED3	–	–	–	2.67	2.65	2.54	0.11	−5.43	−2.76	17.0	74.0	5.90
ED4	–	–	–	2.92	2.83	2.69	0.14	−5.81	−2.89	41.0	32.0	17.1
ED5	–	–	–	2.96	2.84	2.72	0.12	−5.87	−2.91	33.4	23.6	40.1
ED6	–	–	–	3.06	2.84	2.74	0.10	−5.73	−2.67	21.1	14.7	64.5
ED7	313	283	471	2.58	2.69	2.58	0.11	−5.12	−2.54	77.0	–	–
ED8	367	289	507	2.56	2.84	2.69	0.15	−5.25	−2.69	75.0	–	–
ED9	–	–	493	3.01	–	–	0.13	−5.04	−2.03	21.7	–	18.4
ED10	–	–	522	3.12	–	–	0.11	−5.05	−2.17	36.5	–	9.00

193

All in this section, the described dendritic benzophenone derivatives underwent testing as emitters in OLED devices, and their structures are illustrated in Table 17. As in previous sections, ITO was consistently chosen as the anode material for these devices. The devices utilized one or a stack of two layers of hole-transporting materials, incorporating layers made of PEDOT:PSS, poly(9-vinylcarbazole) (PVK), TAPC, or mCP. While most devices incorporating emitters ED1-ED10 adopted non-doped configurations, devices D2ED9 and D2ED10 employed the host–guest approach with the host material DPEPO. The electron-transporting layers featured TPBi, TmPyPb, 2,7-bis(diphenylphosphoryl)-9,9'-spirobi[fluorene] (SPPO13), and DPEPO, while Cs_2CO_3, calcium (Ca), Liq, or LiF were employed as electron-injecting materials. In all the devices discussed in this section, the exclusive choice for the cathode was Al.

Table 17. Architectures of devices utilizing emitters ED1–ED10.

Device	Device Architecture
D1ED1	ITO/PEDOT:PSS (40 nm)/**ED1** (40 nm)/TPBI (30 nm)/Cs_2CO_3 (2 nm)/Al (120 nm)
D2ED1	ITO/PEDOT:PSS (50 nm)/PVK (20 nm)/**ED1** (25 nm)/SPPO13 (40 nm)/LiF (0.5 nm)/Al (80 nm)
DED2	ITO/PEDOT:PSS (50 nm)/PVK (20 nm)/**ED2** (25 nm)/SPPO13 (40 nm)/LiF (0.5 nm)/Al (80 nm)
DED3	ITO/PEDOT:PSS (50 nm)/PVK (20 nm)/**ED3** (25 nm)/SPPO13 (40 nm)/LiF (0.5 nm)/Al (80 nm)
DED4	ITO/PEDOT:PSS (50 nm)/PVK (20 nm)/**ED4** (25 nm)/SPPO13 (40 nm)/LiF (0.5 nm)/Al (80 nm)
DED5	ITO/PEDOT:PSS (70 nm)/PVK (20 nm)/**ED5** (30 nm)/TPBi (40 nm)/Ca (10 nm)/Al (80 nm)
DED6	ITO/PEDOT:PSS (70 nm)/PVK (20 nm)/**ED6** (30 nm)/TPBi (40 nm)/Ca (10 nm)/Al (80 nm)
DED7	ITO/PEDOT:PSS (30 nm)/**ED7** (70 nm)/TPBi (40 nm)/Liq (2 nm)/Al
DED8	ITO/PEDOT:PSS (30 nm)/**ED8** (70 nm)/TPBi (40 nm)/Liq (2 nm)/Al
D1ED9	ITO/TAPC (30 nm)/mCP (10 nm)/**ED9** (20 nm)/DPEPO (30 nm)/DPEPO (10 nm)/TmPyPB (40 nm)/LiF/Al
D2ED9	ITO/TAPC (30 nm)/mCP (10 nm)/DPEPO:30 wt% **ED9** (20 nm)/DPEPO (30 nm)/DPEPO (10 nm)/TmPyPB (40 nm)/LiF/Al
D1ED10	ITO/TAPC (30 nm)/mCP (10 nm)/**ED10** (20 nm)/DPEPO (30 nm)/DPEPO (10 nm)/TmPyPB (40 nm)/LiF/Al
D2ED10	ITO/TAPC (30 nm)/mCP (10 nm)/DPEPO:30 wt% **ED10** (20 nm)/DPEPO (30 nm)/DPEPO (10 nm)/TmPyPB (40 nm)/LiF/Al

Table 18 presents the characteristics of OLED devices utilizing emitters ED1–ED10. Consistent with preceding sections, most of these devices emitted a green light, except for the yellow-emitting OLED with methoxy-substituted derivative ED3 and the blue-emitting device with derivative ED9 employing a D–A structure. Material ED1 exhibited a CE and EQE of 9.2 cd/A and 4.3%, respectively, in device D1ED1. Matsuoka et al. further explored this TADF derivative, optimizing layer structures in device D2ED1 to achieve the highest CE, PE, and EQE of 46.6 cd/A, 40.7 lm/W, and 17%, respectively, between non-doped devices of this section. The same research team also synthesized and characterized derivatives ED2, ED3, and ED4. Green devices DED2 and DED4 were less efficient than D2ED2 with EQEs of 9.0% and 8.8%, respectively. This difference may be attributed to substituting groups of outermost carbazoles in the structures. The only yellow device, DED3 of this section, demonstrated a CE of 17.7 cd/A, PE of 19.0 lm/W, and EQE of 6.4%. Matsuoka and team investigated dendritic TADF materials ED5 and ED6 [130]. When applied in emissive layers, emitter ED5 proved more effective than the additional carbazole fragments having derivative ED6. Device DED5 reached a maximum CE, PE, and EQE of 14.0 cd/A, 11.5 lm/W, and 5.7%, respectively. Li and co-workers developed and tested new benzophenone-acridine TADF cored dendritic materials ED7 and ED8. The derivative ED7, with fewer carbazole fragments, proved more efficient, reaching a maximum EQE of 12.0% compared to 5.20%, demonstrated by device DED8. Moreover, device DED7 exhibited an

L_{MAX} of over 10,000 cd/m^2. Wang et al. designed and synthesized D–A-type carbazole-dendronized TADF emitting materials ED9 and ED10. Non-doped emitter ED9, utilized in the blue device D1ED9, achieved a CE, PE, and EQE of 9.70 cd/A, 6.10 lm/W, and 4.2%, respectively. Doping ED9 in host material DPEPO significantly increased the efficiency of D2ED9, demonstrating a CE of 28.5 cd/A, PE of 24.9 lm/W, and EQE of 13.4%. Compound ED10, designed by changing the benzophenone electron acceptor with 3-benzoylpyridine, proved more efficient. In a non-doped configuration, device D1ED10 achieved a CE, PE, and EQE of 24.0 cd/A, 15.6 lm/W, and 8.50%, respectively. By introducing host material DPEPO in the emissive layer, the highest efficiency described in this section was achieved in D2ED10, demonstrating CE of 44.4 cd/A, PE of 42.8 lm/W, and EQE of 18.9% for the green-blue device.

Table 18. Characteristics of OLED devices using emitters ED1–ED10.

Device	Emitter	Colour	V_{ON}, V	L_{MAX}, cd/m^2	CE, cd/A	PE, lm/W	EQE, %	CIE (x, y)
D1ED1	ED1	Green	4.5	4200	9.20	–	4.30	(0.26, 0.46)
D2ED1	**ED1**	**Green**	**2.7**	**4639**	**46.6**	**40.7**	**17.0**	**(0.27, 0.52)**
DED2	ED2	Green	2.6	661	23.5	25.0	9.00	(0.28, 0.48)
DED3	ED3	Yellow	2.5	1017	17.7	19.0	6.40	(0.44, 0.51)
DED4	ED4	Green	2.7	965	22.7	20.0	8.80	(0.30, 0.48)
DED5	ED5	Green	3.4	–	14.0	11.5	5.70	(0.26, 0.48)
DED6	ED6	Green	3.7	–	8.70	6.60	3.60	(0.28, 0.43)
DED7	ED7	Green-yellow	4.8	>10,000	–	–	12.0	(0.38, 0.56)
DED8	ED8	Green	7.7	2512	–	–	5.20	(0.32, 0.51)
D1ED9	ED9	Blue	4.4	1290	9.70	6.10	4.20	(0.19, 0.36)
D2ED9	**ED9**	**Blue**	**3.0**	**2189**	**28.5**	**24.9**	**13.4**	**(0.18, 0.33)**
D1ED10	ED10	Green	4.4	5949	24.0	15.6	8.50	(0.26, 0.50)
D2ED10	ED10	Green-blue	3.0	3867	44.4	42.8	18.9	(0.20, 0.38)

Characteristics of best performing green and blue devices are highlighted in bold.

8. Concluding Remarks

This review delves into the recent advancements in electroactive materials derived from benzophenone, providing meticulous attention to their synthesis and physical properties and the performance of organic light-emitting diodes incorporating these derivatives. Benzophenone-based materials exhibit versatile roles, serving as host materials for phosphorescent or TADF emitters, as well as functioning as emitting materials, including those with a TADF effect. A number of derivatives based on benzophenone have proven highly efficient as host materials for phosphorescent emitters, significantly improving the quantum efficiency and reducing the driving voltage of the organic light-emitting devices. Notably, benzophenone materials featuring two 3,6-diphenylcarbazole fragments have demonstrated an exceptional effectiveness for red, orange, and green phosphorescent OLEDs (PhOLEDs), achieving respective EQEs of 22.1%, 23.1%, and 25.1%. For blue phosphorescent emitters, the most suitable host exhibited a donor–acceptor (D–A) structure, incorporating one dimethylcarbazole fragment and achieving a device with an EQE of 19.4%. In the realm of green TADF materials, benzophenone derivatives with two 3-(4-(9H-carbazol-9-yl)phenyl)-9H-carbazole fragments emerged as highly effective hosts, resulting in a device with an EQE of 25.3%. Additionally, the substitution of benzophenone with N-phenyl-1-naphthylamine enabled the creation of a TADF host-emitter, successfully applied to a white OLED device with an EQE of 9.5%. Substituted benzophenones as light-emitting materials span the spectrum of light emission ranging from red to blue, which is achieved through the modification and incorporation of various moieties into the benzophenone

backbone. Among the array of benzophenone-based TADF materials, derivatives employing donor–acceptor (D–A) structures proved highly effective as emitters for green and yellow TADF OLEDs, boasting EQE levels of 25.6% and 26.7%, respectively. This structural type demonstrated optimal suitability for application as blue TADF materials with acridine-substituted benzophenone serving as an emitter for blue TADF OLEDs, achieving an impressive EQE of 20.6%. In the case of symmetrical D–A–D structure benzophenone-based TADF emitters, their EQE reached 14.3% for blue and a remarkable 32.2% for green devices. The efficiency of green devices was further enhanced with asymmetrical D–A–D structured benzophenones by incorporating carbazole and 10H-spiro[acridine-9,9′-fluorene] electron donors. A derivative with this emitter demonstrated a device EQE of 33.3%. Researchers also aimed to achieve stable, long-lasting, non-doped TADF OLED devices by designing carbazole-dendronized benzophenone derivatives. The most efficient green OLED of this type exhibited an EQE of 17.0%. Therefore, benzophenones substituted with various electron donors are promising as emitters and hosts for various configurations of OLED devices, and further research in the field of new benzophenone-based electroactive materials is actively ongoing in order to improve the characteristics of future OLED devices.

References

1. Tang, C.W.; VanSlyke, S.A. Organic electroluminescent diodes. *Appl. Phys. Lett.* **1987**, *51*, 913–915. [CrossRef]
2. Luo, Y.-J.; Lu, Z.-Y.; Huang, Y. Triplet fusion delayed fluorescence materials for OLEDs. *Chin. Chem. Lett.* **2016**, *27*, 1223–1230. [CrossRef]
3. Zeng, H.; Huang, Q.; Liu, J.; Huang, Y.; Zhou, J.; Zhao, S.; Lu, Z. A Red-Emissive Sextuple Hydrogen-Bonding Self-Assembly Molecular Duplex Bearing Perylene Diimide Fluorophores for Warm-White Organic Light-Emitting Diode Application. *Chin. J. Chem.* **2016**, *34*, 387–396. [CrossRef]
4. Zhang, Z.; Li, W.; Ye, K.; Zhang, H. Synthesis, Structure and Properties of a Novel Benzothiazole-based Diboron-Bridged π-Conjugated Ladder. *Acta Chim. Sin.* **2016**, *74*, 179. [CrossRef]
5. Huang, H.; Liu, L.; Wang, J.; Zhou, Y.; Hu, H.; Ye, X.; Ye, X.; Liu, G.; Xu, Z.; Xu, H.; et al. Aggregation caused quenching to aggregation induced emission transformation: A precise tuning based on BN-doped polycyclic aromatic hydrocarbons toward subcellular organelle specific imaging. *Chem. Sci.* **2022**, *13*, 3129–3139. [CrossRef]
6. Zhong, J.; Han, M.; Li, C.; Li, R.; He, H. Facile and scalable fabrication process of electroluminescent filament with high luminescent efficiency. *Mater. Lett.* **2023**, *350*, 134868. [CrossRef]
7. Im, Y.; Byun, S.Y.; Kim, J.H.; Lee, D.R.; Oh, C.S.; Yook, K.S.; Lee, J.Y. Recent Progress in High-Efficiency Blue-Light-Emitting Materials for Organic Light-Emitting Diodes. *Adv. Funct. Mater.* **2017**, *27*, 1603007. [CrossRef]
8. Root, S.E.; Savagatrup, S.; Printz, A.D.; Rodriquez, D.; Lipomi, D.J. Mechanical Properties of Organic Semiconductors for Stretchable, Highly Flexible, and Mechanically Robust Electronics. *Chem. Rev.* **2017**, *117*, 6467–6499. [CrossRef]
9. Kraft, A.; Grimsdale, A.C.; Holmes, A.B. Electroluminescent Conjugated Polymers—Seeing Polymers in a New Light. *Angew. Chem. Int. Ed.* **1998**, *37*, 402–428. [CrossRef]
10. Bernius, M.T.; Inbasekaran, M.; O'Brien, J.; Wu, W. Progress with Light-Emitting Polymers. *Adv. Mater.* **2000**, *12*, 1737–1750. [CrossRef]
11. Mitschke, U.; Bäuerle, P. The electroluminescence of organic materials. *J. Mater. Chem.* **2000**, *10*, 1471–1507. [CrossRef]
12. Shirota, Y. Organic materials for electronic and optoelectronic devices. *J. Mater. Chem.* **2000**, *10*, 1–25. [CrossRef]
13. Hung, L.S.; Chen, C.H. Recent progress of molecular organic electroluminescent materials and devices. *Mater. Sci. Eng. R Rep.* **2002**, *39*, 143–222. [CrossRef]
14. Kulkarni, A.P.; Tonzola, C.J.; Babel, A.; Jenekhe, S.A. Electron Transport Materials for Organic Light-Emitting Diodes. *Chem. Mater.* **2004**, *16*, 4556–4573. [CrossRef]

15. Hughes, G.; Bryce, M.R. Electron-transporting materials for organic electroluminescent and electrophosphorescent devices. *J. Mater. Chem.* **2005**, *15*, 94. [CrossRef]

16. Shirota, Y.; Kageyama, H. Charge Carrier Transporting Molecular Materials and Their Applications in Devices. *Chem. Rev.* **2007**, *107*, 953–1010. [CrossRef] [PubMed]

17. Hwang, S.-H.; Moorefield, C.N.; Newkome, G.R. Dendritic macromolecules for organic light-emitting diodes. *Chem. Soc. Rev.* **2008**, *37*, 2543. [CrossRef] [PubMed]

18. Zhu, M.; Yang, C. Blue fluorescent emitters: Design tactics and applications in organic light-emitting diodes. *Chem. Soc. Rev.* **2013**, *42*, 4963. [CrossRef]

19. Zhou, S.; Liu, X.; Yan, H.; Chen, Z.; Liu, Y.; Liu, S. Highly efficient GaN-based high-power flip-chip light-emitting diodes. *Opt. Express* **2019**, *27*, A669. [CrossRef] [PubMed]

20. Zhou, S.; Liu, X.; Yan, H.; Gao, Y.; Xu, H.; Zhao, J.; Quan, Z.; Gui, C.; Liu, S. The effect of nanometre-scale V-pits on electronic and optical properties and efficiency droop of GaN-based green light-emitting diodes. *Sci. Rep.* **2018**, *8*, 11053. [CrossRef]

21. Wang, Z.B.; Helander, M.G.; Qiu, J.; Puzzo, D.P.; Greiner, M.T.; Hudson, Z.M.; Wang, S.; Liu, Z.W.; Lu, Z.H. Unlocking the full potential of organic light-emitting diodes on flexible plastic. *Nat. Photonics* **2011**, *5*, 753–757. [CrossRef]

22. Kim, J.-J.; Han, M.-K.; Noh, Y.-Y. Flexible OLEDs and organic electronics. *Semicond. Sci. Technol.* **2011**, *26*, 030301. [CrossRef]

23. Baldo, M.A.; O'Brien, D.F.; You, Y.; Shoustikov, A.; Sibley, S.; Thompson, M.E.; Forrest, S.R. Highly efficient phosphorescent emission from organic electroluminescent devices. *Nature* **1998**, *395*, 151–154. [CrossRef]

24. Baldo, M.A.; Lamansky, S.; Burrows, P.E.; Thompson, M.E.; Forrest, S.R. Very high-efficiency green organic light-emitting devices based on electrophosphorescence. *Appl. Phys. Lett.* **1999**, *75*, 4–6. [CrossRef]

25. Sun, Y.; Giebink, N.C.; Kanno, H.; Ma, B.; Thompson, M.E.; Forrest, S.R. Management of singlet and triplet excitons for efficient white organic light-emitting devices. *Nature* **2006**, *440*, 908–912. [CrossRef]

26. Tao, Y.; Yang, C.; Qin, J. Organic host materials for phosphorescent organic light-emitting diodes. *Chem. Soc. Rev.* **2011**, *40*, 2943. [CrossRef] [PubMed]

27. Xu, H.; Chen, R.; Sun, Q.; Lai, W.; Su, Q.; Huang, W.; Liu, X. Recent progress in metal–organic complexes for optoelectronic applications. *Chem. Soc. Rev.* **2014**, *43*, 3259–3302. [CrossRef]

28. Wu, H.; Ying, L.; Yang, W.; Cao, Y. Progress and perspective of polymer white light-emitting devices and materials. *Chem. Soc. Rev.* **2009**, *38*, 3391. [CrossRef]

29. Yersin, H. *Highly Efficient OLEDs with Phosphorescent Materials*; John Wiley & Sons: Hoboken, NJ, USA, 2008.

30. Cao, L.; Klimes, K.; Ji, Y.; Fleetham, T.; Li, J. Efficient and stable organic light-emitting devices employing phosphorescent molecular aggregates. *Nat. Photonics* **2021**, *15*, 230–237. [CrossRef]

31. Fusella, M.A.; Saramak, R.; Bushati, R.; Menon, V.M.; Weaver, M.S.; Thompson, N.J.; Brown, J.J. Plasmonic enhancement of stability and brightness in organic light-emitting devices. *Nature* **2020**, *585*, 379–382. [CrossRef]

32. Kim, K.-H.; Lee, S.; Moon, C.-K.; Kim, S.-Y.; Park, Y.-S.; Lee, J.-H.; Woo Lee, J.; Huh, J.; You, Y.; Kim, J.-J. Phosphorescent dye-based supramolecules for high-efficiency organic light-emitting diodes. *Nat. Commun.* **2014**, *5*, 4769. [CrossRef] [PubMed]

33. Baldo, M.A.; Thompson, M.E.; Forrest, S.R. High-efficiency fluorescent organic light-emitting devices using a phosphorescent sensitizer. *Nature* **2000**, *403*, 750–753. [CrossRef] [PubMed]

34. Murawski, C.; Leo, K.; Gather, M.C. Efficiency Roll-Off in Organic Light-Emitting Diodes. *Adv. Mater.* **2013**, *25*, 6801–6827. [CrossRef] [PubMed]

35. Reineke, S.; Walzer, K.; Leo, K. Triplet-exciton quenching in organic phosphorescent light-emitting diodes with Ir-based emitters. *Phys. Rev. B* **2007**, *75*, 125328. [CrossRef]

36. Ligthart, A.; de Vries, X.; Zhang, L.; Pols, M.C.W.M.; Bobbert, P.A.; van Eersel, H.; Coehoorn, R. Effect of Triplet Confinement on Triplet–Triplet Annihilation in Organic Phosphorescent Host–Guest Systems. *Adv. Funct. Mater.* **2018**, *28*, 1804618. [CrossRef]

37. Zhang, J.; Wang, L.; Zhong, A.; Huang, G.; Wu, F.; Li, D.; Teng, M.; Wang, J.; Han, D. Deep red PhOLED from dimeric salophen Platinum(II) complexes. *Dye. Pigment.* **2019**, *162*, 590–598. [CrossRef]

38. Jin, J.; Zhang, W.; Wang, B.; Mu, G.; Xu, P.; Wang, L.; Huang, H.; Chen, J.; Ma, D. Construction of High Tg Bipolar Host Materials with Balanced Electron–Hole Mobility Based on 1,2,4-Thiadiazole for Phosphorescent Organic Light-Emitting Diodes. *Chem. Mater.* **2014**, *26*, 2388–2395. [CrossRef]

39. Huang, X.-L.; Zou, J.-H.; Liu, J.-Z.; Jin, G.; Li, J.-B.; Yao, S.-L.; Peng, J.-B.; Cao, Y.; Zhu, X.-H. A high Tg small-molecule arylamine derivative as a doped hole-injection/transport material for stable organic light-emitting diodes. *Org. Electron.* **2018**, *58*, 139–144. [CrossRef]

40. Sarala, L.; Babu Yathirajula, R.; Gopikrishna, P.; Elaiyappillai, E.; Bella, A.; Sundar, M.S.; Iyer, P.K.; Johnson, P.M. Pronounced luminescence efficiency and thermal stability of small imidazole architect 2-(1,4,5-triphenyl-1H-imidazol-2-yl)phenol for efficient non-doped blue OLEDs. *J. Photochem. Photobiol. A Chem.* **2018**, *365*, 232–237. [CrossRef]

41. Chien, C.; Chen, C.; Hsu, F.; Shu, C.; Chou, P.; Lai, C. Multifunctional Deep-Blue Emitter Comprising an Anthracene Core and Terminal Triphenylphosphine Oxide Groups. *Adv. Funct. Mater.* **2009**, *19*, 560–566. [CrossRef]

42. Cho, Y.J.; Taylor, S.; Aziz, H. Increased Electromer Formation and Charge Trapping in Solution-Processed versus Vacuum-Deposited Small Molecule Host Materials of Organic Light-Emitting Devices. *ACS Appl. Mater. Interfaces* **2017**, *9*, 40564–40572. [CrossRef]

43. Shibata, M.; Sakai, Y.; Yokoyama, D. Advantages and disadvantages of vacuum-deposited and spin-coated amorphous organic semiconductor films for organic light-emitting diodes. *J. Mater. Chem. C* **2015**, *3*, 11178–11191. [CrossRef]

44. Wang, Y.; Yun, J.H.; Wang, L.; Lee, J.Y. High Triplet Energy Hosts for Blue Organic Light-Emitting Diodes. *Adv. Funct. Mater.* **2021**, *31*, 2008332. [CrossRef]

45. Idris, M.; Coburn, C.; Fleetham, T.; Milam-Guerrero, J.; Djurovich, P.I.; Forrest, S.R.; Thompson, M.E. Phenanthro [9,10-*d*]triazole and imidazole derivatives: High triplet energy host materials for blue phosphorescent organic light emitting devices. *Mater. Horiz.* **2019**, *6*, 1179–1186. [CrossRef]

46. Maheshwaran, A.; Sree, V.G.; Park, H.; Kim, H.; Han, S.H.; Lee, J.Y.; Jin, S. High Efficiency Deep-Blue Phosphorescent Organic Light-Emitting Diodes with CIE *x*, *y* (≤0.15) and Low Efficiency Roll-Off by Employing a High Triplet Energy Bipolar Host Material. *Adv. Funct. Mater.* **2018**, *28*, 1802945. [CrossRef]

47. Lee, J.; Jeong, C.; Batagoda, T.; Coburn, C.; Thompson, M.E.; Forrest, S.R. Hot excited state management for long-lived blue phosphorescent organic light-emitting diodes. *Nat. Commun.* **2017**, *8*, 15566. [CrossRef] [PubMed]

48. Scholz, S.; Kondakov, D.; Lussem, B.; Leo, K. Degradation Mechanisms and Reactions in Organic Light-Emitting Devices. *Chem. Rev.* **2015**, *115*, 8449–8503. [CrossRef] [PubMed]

49. Yang, X.; Yue, L.; Yu, Y.; Liu, B.; Dang, J.; Sun, Y.; Zhou, G.; Wu, Z.; Wong, W. Strategically Formulating Aggregation-Induced Emission-Active Phosphorescent Emitters by Restricting the Coordination Skeletal Deformation of Pt(II) Complexes Containing Two Independent Monodentate Ligands. *Adv. Opt. Mater.* **2020**, *8*, 2000079. [CrossRef]

50. Rajamalli, P.; Senthilkumar, N.; Huang, P.-Y.; Ren-Wu, C.-C.; Lin, H.-W.; Cheng, C.-H. New Molecular Design Concurrently Providing Superior Pure Blue, Thermally Activated Delayed Fluorescence and Optical Out-Coupling Efficiencies. *J. Am. Chem. Soc.* **2017**, *139*, 10948–10951. [CrossRef] [PubMed]

51. Chen, J.; Tao, W.; Chen, W.; Xiao, Y.; Wang, K.; Cao, C.; Yu, J.; Li, S.; Geng, F.; Adachi, C.; et al. Red/Near-Infrared Thermally Activated Delayed Fluorescence OLEDs with Near 100% Internal Quantum Efficiency. *Angew. Chem. Int. Ed.* **2019**, *58*, 14660–14665. [CrossRef]

52. Albrecht, K.; Matsuoka, K.; Fujita, K.; Yamamoto, K. Carbazole Dendrimers as Solution-Processable Thermally Activated Delayed-Fluorescence Materials. *Angew. Chem. Int. Ed.* **2015**, *54*, 5677–5682. [CrossRef]

53. Zhang, Q.; Li, J.; Shizu, K.; Huang, S.; Hirata, S.; Miyazaki, H.; Adachi, C. Design of Efficient Thermally Activated Delayed Fluorescence Materials for Pure Blue Organic Light Emitting Diodes. *J. Am. Chem. Soc.* **2012**, *134*, 14706–14709. [CrossRef]

54. Wu, K.; Zhang, T.; Wang, Z.; Wang, L.; Zhan, L.; Gong, S.; Zhong, C.; Lu, Z.-H.; Zhang, S.; Yang, C. De Novo Design of Excited-State Intramolecular Proton Transfer Emitters via a Thermally Activated Delayed Fluorescence Channel. *J. Am. Chem. Soc.* **2018**, *140*, 8877–8886. [CrossRef]

55. Goushi, K.; Yoshida, K.; Sato, K.; Adachi, C. Organic light-emitting diodes employing efficient reverse intersystem crossing for triplet-to-singlet state conversion. *Nat. Photonics* **2012**, *6*, 253–258. [CrossRef]

56. Ahn, D.H.; Kim, S.W.; Lee, H.; Ko, I.J.; Karthik, D.; Lee, J.Y.; Kwon, J.H. Highly efficient blue thermally activated delayed fluorescence emitters based on symmetrical and rigid oxygen-bridged boron acceptors. *Nat. Photonics* **2019**, *13*, 540–546. [CrossRef]

57. Uoyama, H.; Goushi, K.; Shizu, K.; Nomura, H.; Adachi, C. Highly efficient organic light-emitting diodes from delayed fluorescence. *Nature* **2012**, *492*, 234–238. [CrossRef] [PubMed]

58. Wang, Z.; Li, Y.; Cai, X.; Chen, D.; Xie, G.; Liu, K.; Wu, Y.-C.; Lo, C.-C.; Lien, A.; Cao, Y.; et al. Structure–Performance Investigation of Thioxanthone Derivatives for Developing Color Tunable Highly Efficient Thermally Activated Delayed Fluorescence Emitters. *ACS Appl. Mater Interfaces* **2016**, *8*, 8627–8636. [CrossRef] [PubMed]

59. Im, Y.; Kim, M.; Cho, Y.J.; Seo, J.-A.; Yook, K.S.; Lee, J.Y. Molecular Design Strategy of Organic Thermally Activated Delayed Fluorescence Emitters. *Chem. Mater.* **2017**, *29*, 1946–1963. [CrossRef]

60. Cai, X.; Li, X.; Xie, G.; He, Z.; Gao, K.; Liu, K.; Chen, D.; Cao, Y.; Su, S.-J. Rate-limited effect' of reverse intersystem crossing process: The key for tuning thermally activated delayed fluorescence lifetime and efficiency roll-off of organic light emitting diodes. *Chem. Sci.* **2016**, *7*, 4264–4275. [CrossRef] [PubMed]

61. Wang, Y.; Huang, C.; Ye, H.; Zhong, C.; Khan, A.; Yang, S.; Fung, M.; Jiang, Z.; Adachi, C.; Liao, L. Through Space Charge Transfer for Efficient Sky-Blue Thermally Activated Delayed Fluorescence (TADF) Emitter with Unconjugated Connection. *Adv. Opt. Mater.* **2020**, *8*, 1901150. [CrossRef]

62. Cai, M.; Auffray, M.; Zhang, D.; Zhang, Y.; Nagata, R.; Lin, Z.; Tang, X.; Chan, C.-Y.; Lee, Y.-T.; Huang, T.; et al. Enhancing spin-orbital coupling in deep-blue/blue TADF emitters by minimizing the distance from the heteroatoms in donors to acceptors. *Chem. Eng. J.* **2021**, *420*, 127591. [CrossRef]

63. Cui, L.; Nomura, H.; Geng, Y.; Kim, J.U.; Nakanotani, H.; Adachi, C. Controlling Singlet–Triplet Energy Splitting for Deep-Blue Thermally Activated Delayed Fluorescence Emitters. *Angew. Chem. Int. Ed.* **2017**, *56*, 1571–1575. [CrossRef]

64. Chatterjee, T.; Wong, K. Perspective on Host Materials for Thermally Activated Delayed Fluorescence Organic Light Emitting Diodes. *Adv. Opt. Mater.* **2019**, *7*, 1800565. [CrossRef]

65. Zhou, S.-Y.; Wan, H.-B.; Zhou, F.; Gu, P.-Y.; Xu, Q.-F.; Lu, J.-M. AIEgens-lightened Functional Polymers: Synthesis, Properties and Applications. *Chin. J. Polym. Sci.* **2019**, *37*, 302–326. [CrossRef]

66. Zhao, Y.; Wang, W.; Gui, C.; Fang, L.; Zhang, X.; Wang, S.; Chen, S.; Shi, H.; Tang, B.Z. Thermally activated delayed fluorescence material with aggregation-induced emission properties for highly efficient organic light-emitting diodes. *J. Mater. Chem. C Mater.* **2018**, *6*, 2873–2881. [CrossRef]

67. Wu, J.-L.; Zhang, C.; Qin, W.; Quan, D.-P.; Ge, M.-L.; Liang, G.-D. Thermoresponsive Fluorescent Semicrystalline Polymers Decorated with Aggregation Induced Emission Luminogens. *Chin. J. Polym. Sci.* **2019**, *37*, 394–400. [CrossRef]

68. Huang, J.; Xu, Z.; Cai, Z.; Guo, J.; Guo, J.; Shen, P.; Wang, Z.; Zhao, Z.; Ma, D.; Tang, B.Z. Robust luminescent small molecules with aggregation-induced delayed fluorescence for efficient solution-processed OLEDs. *J. Mater. Chem. C Mater.* **2019**, *7*, 330–339. [CrossRef]

69. Huang, J.; Nie, H.; Zeng, J.; Zhuang, Z.; Gan, S.; Cai, Y.; Guo, J.; Su, S.; Zhao, Z.; Tang, B.Z. Highly Efficient Nondoped OLEDs with Negligible Efficiency Roll-Off Fabricated from Aggregation-Induced Delayed Fluorescence Luminogens. *Angew. Chem. Int. Ed.* **2017**, *56*, 12971–12976. [CrossRef] [PubMed]

70. Hu, Y.B.; Lam, J.W.Y.; Tang, B.Z. Recent Progress in AIE-active Polymers. *Chin. J. Polym. Sci.* **2019**, *37*, 289–301. [CrossRef]

71. Gu, J.; Qin, A.; Tang, B.Z. Polymers with Aggregation-Induced Emission Characteristics. In *Principles and Applications of Aggregation-Induced Emission*; Springer International Publishing: Cham, Switzerland, 2019; pp. 77–108. [CrossRef]

72. Zhao, W.; He, Z.; Lam, J.W.Y.; Peng, Q.; Ma, H.; Shuai, Z.; Bai, G.; Hao, J.; Tang, B.Z. Rational Molecular Design for Achieving Persistent and Efficient Pure Organic Room-Temperature Phosphorescence. *Chem* **2016**, *1*, 592–602. [CrossRef]

73. Kearns, D.R.; Case, W.A. Investigation of Singlet → Triplet Transitions by the Phosphorescence Excitation Method. III. Aromatic Ketones and Aldehydes. *J. Am. Chem. Soc.* **1966**, *88*, 5087–5097. [CrossRef]

74. Yuan, W.Z.; Shen, X.Y.; Zhao, H.; Lam, J.W.Y.; Tang, L.; Lu, P.; Wang, C.; Liu, Y.; Wang, Z.; Zheng, Q.; et al. Crystallization-Induced Phosphorescence of Pure Organic Luminogens at Room Temperature. *J. Phys. Chem. C* **2010**, *114*, 6090–6099. [CrossRef]

75. Lee, S.Y.; Yasuda, T.; Yang, Y.S.; Zhang, Q.; Adachi, C. Luminous Butterflies: Efficient Exciton Harvesting by Benzophenone Derivatives for Full-Color Delayed Fluorescence OLEDs. *Angew. Chem. Int. Ed.* **2014**, *53*, 6402–6406. [CrossRef] [PubMed]

76. Guo, J.; Li, X.-L.; Nie, H.; Luo, W.; Hu, R.; Qin, A.; Zhao, Z.; Su, S.-J.; Tang, B.Z. Robust Luminescent Materials with Prominent Aggregation-Induced Emission and Thermally Activated Delayed Fluorescence for High-Performance Organic Light-Emitting Diodes. *Chem. Mater.* **2017**, *29*, 3623–3631. [CrossRef]

77. Guo, J.; Li, X.; Nie, H.; Luo, W.; Gan, S.; Hu, S.; Hu, R.; Qin, A.; Zhao, Z.; Su, S.; et al. Achieving High-Performance Nondoped OLEDs with Extremely Small Efficiency Roll-Off by Combining Aggregation-Induced Emission and Thermally Activated Delayed Fluorescence. *Adv. Funct. Mater.* **2017**, *27*, 1606458. [CrossRef]

78. Keruckiene, R.; Keruckas, J.; Cekaviciute, M.; Volyniuk, D.; Lee, P.-H.; Chiu, T.-L.; Lee, J.-H.; Grazulevicius, J.V. Meta-Substituted benzophenones as multifunctional electroactive materials for OLEDs. *Dye. Pigment.* **2020**, *174*, 108058. [CrossRef]

79. Heravi, M.M.; Kheilkordi, Z.; Zadsirjan, V.; Heydari, M.; Malmir, M. Buchwald-Hartwig reaction: An overview. *J. Organomet. Chem.* **2018**, *861*, 17–104. [CrossRef]

80. Chiba, T.; Fukada, A.; Igarashi, M.; Hikichi, T.; Ohisa, S.; Pu, Y.-J.; Kido, J. A Solution-Processable Small-Molecule Host for Phosphorescent Organic Light-Emitting Devices. *J. Photopolym. Sci. Technol.* **2016**, *29*, 317–321. [CrossRef]

81. Suzuki, A. Organoborane coupling reactions (Suzuki coupling). *Proc. Jpn. Acad. Ser. B* **2004**, *80*, 359–371. [CrossRef]

82. Liang, J.; Li, C.; Zhuang, X.; Ye, K.; Liu, Y.; Wang, Y. Novel Blue Bipolar Thermally Activated Delayed Fluorescence Material as Host Emitter for High-Efficiency Hybrid Warm-White OLEDs with Stable High Color-Rendering Index. *Adv. Funct. Mater.* **2018**, *28*, 1707002. [CrossRef]

83. Ma, W.; Bin, Z.; Yang, G.; Liu, J.; You, J. Structurally Nontraditional Bipolar Hosts for RGB Phosphorescent OLEDs: Boosted by a 'Butterfly-Shaped' Medium-Ring Acceptor. *Angew. Chem. Int. Ed.* **2022**, *61*, e202116681. [CrossRef] [PubMed]

84. Kumar, S.; Li, D.; Wang, Y.-K.; Yuan, Y.; Khan, A.; Jiang, Z.-Q.; Liao, L.-S. One-shot triphenylamine/phenylketone hybrid as a bipolar host material for efficient red phosphorescent organic light-emitting diodes. *Synth. Met.* **2019**, *254*, 42–48. [CrossRef]

85. Lin, H.; Sun, D. Recent Synthetic Developments and Applications of the Ullmann Reaction. A Review. *Org. Prep. Proced. Int.* **2013**, *45*, 341–394. [CrossRef] [PubMed]

86. Jhulki, S.; Seth, S.; Ghosh, A.; Chow, T.J.; Moorthy, J.N. Benzophenones as Generic Host Materials for Phosphorescent Organic Light-Emitting Diodes. *ACS Appl. Mater. Interfaces* **2016**, *8*, 1527–1535. [CrossRef] [PubMed]

87. Rueping, M.; Nachtsheim, B.J. A review of new developments in the Friedel–Crafts alkylation—From green chemistry to asymmetric catalysis. *Beilstein J. Org. Chem.* **2010**, *6*, 6. [CrossRef] [PubMed]

88. Hu, J.; Zhang, X.; Zhang, D.; Cao, X.; Jiang, T.; Zhang, X.; Tao, Y. Linkage modes on phthaloyl/triphenylamine hybrid compounds: Multi-functional AIE luminogens, non-doped emitters and organic hosts for highly efficient solution-processed delayed fluorescence OLEDs. *Dye. Pigment.* **2017**, *137*, 480–489. [CrossRef]

199

89. Mahmoudi, M.; Keruckas, J.; Volyniuk, D.; Andrulevičienė, V.; Keruckienė, R.; Narbutaitis, E.; Chao, Y.-C.; Rutkis, M.; Grazulevicius, J.V. Bis(N-naphthyl-N-phenylamino)benzophenones as exciton-modulating materials for white TADF OLEDs with separated charge and exciton recombination zones. *Dye. Pigment.* **2022**, *197*, 109868. [CrossRef]

90. Sudheendran Swyamprabha, S.; Kishore Kesavan, K.; Siddiqui, I.; Blazevicius, D.; Jayachandran, J.; Eidimtas, M.; Nayak, S.R.; Nagar, M.R.; Yadav, R.A.K.; Krucaite, G.; et al. Novel carbazole host materials for solution processed TADF Organic Light Emitting Diodes. *Dye. Pigment.* **2023**, *208*, 110821. [CrossRef]

91. Nagar, M.R.; Kumar, K.; Blazevicius, D.; Beresnevicite, R.; Krucaite, G.; Tavgeniene, D.; Hao, C.T.; Banik, S.; Jou, J.-H.; Grigalevicius, S. Solution processable carbazole-benzophenone derivatives as bipolar hosts enabling high-efficiency stable green TADF organic LEDs. *J. Mater. Chem. C Mater.* **2023**, *11*, 1579–1592. [CrossRef]

92. Wang, F.; Cao, X.; Mei, L.; Zhang, X.; Hu, J.; Tao, Y. Twisted penta-Carbazole/Benzophenone Hybrid Compound as Multifunctional Organic Host, Dopant or Non-doped Emitter for Highly Efficient Solution-Processed Delayed Fluorescence OLEDs. *Chin. J. Chem.* **2018**, *36*, 241–246. [CrossRef]

93. Tang, C.; Yang, T.; Cao, X.; Tao, Y.; Wang, F.; Zhong, C.; Qian, Y.; Zhang, X.; Huang, W. Tuning a Weak Emissive Blue Host to Highly Efficient Green Dopant by a CN in Tetracarbazolepyridines for Solution-Processed Thermally Activated Delayed Fluorescence Devices. *Adv. Opt. Mater.* **2015**, *3*, 786–790. [CrossRef]

94. Ma, F.; Ji, H.; Zhang, D.; Xue, K.; Zhang, P.; Qi, Z.; Zhu, H. Adjusting the photophysical properties of AIE-active TADF emitters from through-bond to through-space charge transfer for high-performance solution-processed OLEDs. *Dye. Pigment.* **2021**, *188*, 109208. [CrossRef]

95. Wang, J.; Zhang, J.; Jiang, C.; Yao, C.; Xi, X. Effective Design Strategy for Aggregation-Induced Emission and Thermally Activated Delayed Fluorescence Emitters Achieving 18% External Quantum Efficiency Pure-Blue OLEDs with Extremely Low Roll-Off. *ACS Appl. Mater. Interfaces* **2021**, *13*, 57713–57724. [CrossRef] [PubMed]

96. Liu, Y.; Wu, X.; Chen, Y.; Chen, L.; Li, H.; Wang, W.; Wang, S.; Tian, H.; Tong, H.; Wang, L. Triazatruxene-based thermally activated delayed fluorescence small molecules with aggregation-induced emission properties for solution-processable nondoped OLEDs with low efficiency roll-off. *J. Mater. Chem. C Mater.* **2019**, *7*, 9719–9725. [CrossRef]

97. Tani, K.; Yashima, T.; Miyanaga, K.; Hori, K.; Goto, K.; Tani, F.; Habuka, Y.; Suzuki, K.; Shizu, K.; Kaji, H. Carbazole and Benzophenone Based Twisted Donor–Acceptor Systems as Solution Processable Green Thermally Activated Delayed Fluorescence Organic Light Emitters. *Chem. Lett.* **2018**, *47*, 1236–1239. [CrossRef]

98. Jing, Y.-Y.; Tao, X.-D.; Yang, M.-X.; Chen, X.-L.; Lu, C.-Z. Triptycene-imbedded thermally activated delayed fluorescence emitters with excellent film morphologies for applications in efficient nondoped and doped organic light-emitting devices. *Chem. Eng. J.* **2021**, *413*, 127418. [CrossRef]

99. Aizawa, N.; Tsou, C.-J.; Park, I.S.; Yasuda, T. Aggregation-induced delayed fluorescence from phenothiazine-containing donor–acceptor molecules for high-efficiency non-doped organic light-emitting diodes. *Polym. J.* **2017**, *49*, 197–202. [CrossRef]

100. Wu, L.; Wang, K.; Wang, C.; Fan, X.-C.; Shi, Y.-Z.; Zhang, X.; Zhang, S.-L.; Ye, J.; Zheng, C.-J.; Li, Y.-Q.; et al. Using fluorene to lock electronically active moieties in thermally activated delayed fluorescence emitters for high-performance non-doped organic light-emitting diodes with suppressed roll-off. *Chem. Sci.* **2021**, *12*, 1495–1502. [CrossRef]

101. Ma, M.; Li, J.; Liu, D.; Li, D.; Dong, R.; Mei, Y. Low efficiency roll-off thermally activated delayed fluorescence emitters for non-doped OLEDs: Substitution effect of thioether and sulfone groups. *Dye. Pigment.* **2021**, *194*, 109649. [CrossRef]

102. Rajamalli, P.; Martir, D.R.; Zysman-Colman, E. Pyridine-functionalized carbazole donor and benzophenone acceptor design for thermally activated delayed fluorescence emitters in blue organic light-emitting diodes. *J. Photonics Energy* **2018**, *8*, 1. [CrossRef]

103. Wang, J.; Yang, Y.; Jiang, C.; He, M.; Yao, C.; Zhang, J. Ultrapure deep-blue aggregation-induced emission and thermally activated delayed fluorescence emitters for efficient OLEDs with CIE$_y$ < 0.1 and low efficiency roll-offs. *J. Mater. Chem. C Mater.* **2022**, *10*, 3163–3171. [CrossRef]

104. Nie, X.; Wang, T.; Huang, W.; Su, H.; Chen, B.; Zhang, X.; Zhang, G. Modulation of OLED efficiency via a combination of aromatic electrophilic directing and intramolecular charge transfer. *J. Mater. Chem. C Mater.* **2021**, *9*, 15698–15706. [CrossRef]

105. Ho, C.-Y.; Krucaite, G.; Beresneviciute, R.; Blazevicius, D.; Lin, W.-H.; Lu, J.-C.; Lin, C.-Y.; Grigalevicius, S.; Chang, C.-H. Triphenylethene-carbazole-based molecules for the realization of blue and white aggregation-induced emission OLEDs with high luminance. *Org. Electron.* **2022**, *108*, 106571. [CrossRef]

106. Kreiza, G.; Banevičius, D.; Jovaišaitė, J.; Maleckaitė, K.; Gudeika, D.; Volyniuk, D.; Gražulevičius, J.V.; Juršėnas, S.; Kazlauskas, K. Suppression of benzophenone-induced triplet quenching for enhanced TADF performance. *J. Mater. Chem. C Mater.* **2019**, *7*, 11522–11531. [CrossRef]

107. Zhang, J.; Wei, Q.; Fei, N.; Zhao, M.; Xie, L.; Cao, L.; Zhang, X.; Xie, G.; Wang, T.; Ge, Z. Simple-Structured Blue Thermally Activated Delayed Fluorescence Emitter for Solution-Processed Organic Light-Emitting Diodes with External Quantum Efficiency of over 20%. *ACS Appl. Mater. Interfaces* **2021**, *13*, 12305–12312. [CrossRef] [PubMed]

108. Wang, L.; Cai, X.; Li, B.; Li, M.; Wang, Z.; Gan, L.; Qiao, Z.; Xie, W.; Liang, Q.; Zheng, N.; et al. Achieving Enhanced Thermally Activated Delayed Fluorescence Rates and Shortened Exciton Lifetimes by Constructing Intramolecular Hydrogen Bonding Channels. *ACS Appl. Mater. Interfaces* **2019**, *11*, 45999–46007. [CrossRef] [PubMed]

109. Xie, Z.; Huang, Q.; Yu, T.; Wang, L.; Mao, Z.; Li, W.; Yang, Z.; Zhang, Y.; Liu, S.; Xu, J.; et al. Hydrogen-Bonding-Assisted Intermolecular Charge Transfer: A New Strategy to Design Single-Component White-Light-Emitting Materials. *Adv. Funct. Mater.* **2017**, *27*, 1703918. [CrossRef]

110. Wilkinson, F.; Abdel-Shafi, A.A. Mechanism of Quenching of Triplet States by Molecular Oxygen: Biphenyl Derivatives in Different Solvents. *J. Phys. Chem. A* **1999**, *103*, 5425–5435. [CrossRef]

111. Chen, X.; Yang, Z.; Xie, Z.; Zhao, J.; Yang, Z.; Zhang, Y.; Aldred, M.P.; Chi, Z. An efficient yellow thermally activated delayed fluorescence emitter with universal applications in both doped and non-doped organic light-emitting diodes. *Mater. Chem. Front.* **2018**, *2*, 1017–1023. [CrossRef]

112. Zhao, J.; Yang, Z.; Chen, X.; Xie, Z.; Liu, T.; Chi, Z.; Yang, Z.; Zhang, Y.; Aldred, M.P.; Chi, Z. Efficient triplet harvesting in fluorescence–TADF hybrid warm-white organic light-emitting diodes with a fully non-doped device configuration. *J. Mater. Chem. C Mater.* **2018**, *6*, 4257–4264. [CrossRef]

113. Huang, B.; Ban, X.; Sun, K.; Ma, Z.; Mei, Y.; Jiang, W.; Lin, B.; Sun, Y. Thermally activated delayed fluorescence materials based on benzophenone derivative as emitter for efficient solution-processed non-doped green OLED. *Dye. Pigment.* **2016**, *133*, 380–386. [CrossRef]

114. Liu, Y.; Yin, Z.; Wang, X.; Baranoff, E.; Zhou, D.; Zhang, K.; Ren, Z.; Wang, S.; Zhu, W.; Wang, Y. A novel donor moiety 9,9,9′9′-tetramethyl-9,9′10,10′-tetrahydro-2,10′-biacridine via one-pot C–H arylation for TADF emitters and their application in highly efficient solution-processable OLEDs. *J. Mater. Chem. C Mater.* **2020**, *8*, 8971–8979. [CrossRef]

115. Sun, J.; Jia, J.; Zhao, B.; Yang, J.; Singh, M.; An, Z.; Wang, H.; Xu, B.; Huang, W. A purely organic D-π-A-π-D emitter with thermally activated delayed fluorescence and room temperature phosphorescence for near-white OLED. *Chin. Chem. Lett.* **2021**, *32*, 1367–1371. [CrossRef]

116. Sharif, P.; Alemdar, E.; Ozturk, S.; Caylan, O.; Haciefendioglu, T.; Buke, G.; Aydemir, M.; Danos, A.; Monkman, A.P.; Yildirim, E.; et al. Rational Molecular Design Enables Efficient Blue TADF−OLEDs with Flexible Graphene Substrate. *Adv. Funct. Mater.* **2022**, *32*, 2207324. [CrossRef]

117. Sun, J.W.; Baek, J.Y.; Kim, K.-H.; Huh, J.-S.; Kwon, S.-K.; Kim, Y.-H.; Kim, J.-J. Azasiline-based thermally activated delayed fluorescence emitters for blue organic light emitting diodes. *J. Mater. Chem. C Mater.* **2017**, *5*, 1027–1032. [CrossRef]

118. Huang, R.; Chen, H.; Liu, H.; Zhuang, Z.; Wang, J.; Yu, M.; Yang, D.; Ma, D.; Zhao, Z.; Tang, B. Creating efficient delayed fluorescence luminogens with acridine-based spiro donors to improve horizontal dipole orientation for high-performance OLEDs. *Chem. Eng. J.* **2022**, *435*, 134934. [CrossRef]

119. Chen, Y.; Wang, S.; Wu, X.; Xu, Y.; Li, H.; Liu, Y.; Tong, H.; Wang, L. Triazatruxene-based small molecules with thermally activated delayed fluorescence, aggregation-induced emission and mechanochromic luminescence properties for solution-processable nondoped OLEDs. *J. Mater. Chem. C Mater.* **2018**, *6*, 12503–12508. [CrossRef]

120. Wu, Z.-L.; Lv, X.; Meng, L.-Y.; Chen, X.-L.; Lu, C.-Z. Tröger's Base-Derived Thermally Activated Delayed Fluorescence Dopant for Efficient Deep-Blue Organic Light-Emitting Diodes. *Molecules* **2023**, *28*, 4832. [CrossRef] [PubMed]

121. Tavgeniene, D.; Beresneviciute, R.; Blazevicius, D.; Krucaite, G.; Jacunskaite, G.; Sudheendran Swayamprabha, S.; Jou, J.-H.; Grigalevicius, S. 3-(N,N-Diphenylamino)carbazole Donor Containing Bipolar Derivatives with Very High Glass Transition Temperatures as Potential TADF Emitters for OLEDs. *Coatings* **2022**, *12*, 932. [CrossRef]

122. Cai, X.; Gao, B.; Li, X.; Cao, Y.; Su, S. Singlet–Triplet Splitting Energy Management via Acceptor Substitution: Complanation Molecular Design for Deep-Blue Thermally Activated Delayed Fluorescence Emitters and Organic Light-Emitting Diodes Application. *Adv. Funct. Mater.* **2016**, *26*, 8042–8052. [CrossRef]

123. Zhang, Q.; Tsang, D.; Kuwabara, H.; Hatae, Y.; Li, B.; Takahashi, T.; Lee, S.Y.; Yasuda, T.; Adachi, C. Nearly 100% Internal Quantum Efficiency in Undoped Electroluminescent Devices Employing Pure Organic Emitters. *Adv. Mater.* **2015**, *27*, 2096–2100. [CrossRef]

124. Huang, R.; Yang, Z.; Chen, H.; Liu, H.; Tang, B.Z.; Zhao, Z. Sky-Blue Aggregation-Induced Delayed Fluorescence Luminogens with High Horizontal Dipole Orientation for Efficient Organic Light-Emitting Diodes. *Chin. J. Chem.* **2023**, *41*, 527–534. [CrossRef]

125. Ma, F.; Zhao, G.; Zheng, Y.; He, F.; Hasrat, K.; Qi, Z. Molecular Engineering of Thermally Activated Delayed Fluorescence Emitters with Aggregation-Induced Emission via Introducing Intramolecular Hydrogen-Bonding Interactions for Efficient Solution-Processed Nondoped OLEDs. *ACS Appl. Mater. Interfaces* **2020**, *12*, 1179–1189. [CrossRef] [PubMed]

126. Tomkeviciene, A.; Matulaitis, T.; Guzauskas, M.; Andruleviciene, V.; Volyniuk, D.; Grazulevicius, J.V. Thianthrene and acridan-substituted benzophenone or diphenylsulfone: Effect of triplet harvesting via TADF and phosphorescence on efficiency of all-organic OLEDS. *Org. Electron.* **2019**, *70*, 227–239. [CrossRef]

127. Matsuoka, K.; Albrecht, K.; Nakayama, A.; Yamamoto, K.; Fujita, K. Highly Efficient Thermally Activated Delayed Fluorescence Organic Light-Emitting Diodes with Fully Solution-Processed Organic Multilayered Architecture: Impact of Terminal Substitution on Carbazole–Benzophenone Dendrimer and Interfacial Engineering. *ACS Appl. Mater. Interfaces* **2018**, *10*, 33343–33352. [CrossRef] [PubMed]

128. Albrecht, K.; Yamamoto, K. Dendritic Structure Having a Potential Gradient: New Synthesis and Properties of Carbazole Dendrimers. *J. Am. Chem. Soc.* **2009**, *131*, 2244–2251. [CrossRef]

201

129. Li, Y.; Xie, G.; Gong, S.; Wu, K.; Yang, C. Dendronized delayed fluorescence emitters for non-doped, solution-processed organic light-emitting diodes with high efficiency and low efficiency roll-off simultaneously: Two parallel emissive channels. *Chem. Sci.* **2016**, *7*, 5441–5447. [CrossRef]
130. Matsuoka, K.; Albrecht, K.; Yamamoto, K.; Fujita, K. Mulifunctional Dendritic Emitter: Aggregation-Induced Emission Enhanced, Thermally Activated Delayed Fluorescent Material for Solution-Processed Multilayered Organic Light-Emitting Diodes. *Sci. Rep.* **2017**, *7*, 41780. [CrossRef]

202

Article

Bifunctional Bicarbazole-Benzophenone-Based Twisted Donor–Acceptor–Donor Derivatives for Deep-Blue and Green OLEDs

Prakalp Gautam [1,†], Shahnawaz [1,†], Iram Siddiqui [1,†], Dovydas Blazevicius [2,†], Gintare Krucaite [2], Daiva Tavgeniene [2], Jwo-Huei Jou [1,*] and Saulius Grigalevicius [2,*]

[1] Department of Materials Science and Engineering, National Tsing Hua University, No. 101, Section 2, Guangfu Rd., East District, Hsinchu 30013, Taiwan
[2] Department of Polymer Chemistry and Technology, Kaunas University of Technology, Radvilenu Plentas 19, LT50254 Kaunas, Lithuania
* Correspondence: jjou@mx.nthu.edu.tw (J.-H.J.); saulius.grigalevicius@ktu.lt (S.G.)
† These authors contributed equally to this work.

Abstract: Organic light-emitting diodes (OLEDs) have played a vital role in showing tremendous technological advancements for a better lifestyle, due to their display and lighting technologies in smartphones, tablets, television, and automotive industries. Undoubtedly, OLED is a mainstream technology and, inspired by its advancements, we have designed and synthesized the bicarbazole-benzophenone-based twisted donor–acceptor–donor (D-A-D) derivatives, namely DB13, DB24, DB34, and DB43, as bi-functional materials. These materials possess high decomposition temperatures (>360 °C) and glass transition temperatures (~125 °C), a high photoluminescence quantum yield (>60%), wide bandgap (>3.2 eV), and short decay time. Owing to their properties, the materials were utilized as blue emitters as well as host materials for deep-blue and green OLEDs, respectively. In terms of the blue OLEDs, the emitter DB13-based device outperformed others by showing a maximum EQE of 4.0%, which is close to the theoretical limit of fluorescent materials for a deep-blue emission ($CIE_y = 0.09$). The same material also displayed a maximum power efficacy of 45 lm/W as a host material doped with a phosphorescent emitter $Ir(ppy)_3$. Furthermore, the materials were also utilized as hosts with a TADF green emitter (4CzIPN) and the device based on DB34 displayed a maximum EQE of 11%, which may be attributed to the high quantum yield (69%) of the host DB34. Therefore, the bi-functional materials that are easily synthesized, economical, and possess excellent characteristics are expected to be useful in various cost-effective and high-performance OLED applications, especially in displays.

Keywords: bi-functional D-A-D derivatives; deep-blue emission; phosphorescent and TADF green OLEDs; high-efficiency

1. Introduction

Organic light-emitting diodes (OLEDs) technology has outperformed other technologies in recent decades [1–10]. OLEDs are the ultimate technology for display and are moving rapidly into lighting. At present, there is an intensive need for high-performance deep-blue emitters for full-color displays and solid-state lightings [11–18]. Deep-blue emissions tend to reduce not only the number of pixels required for blue emission but also the cost of the device. For the same purpose, the realization of high-efficiency and stable deep-blue fluorophores is essential, satisfying the National Television System Committee (NTSC) standard [19–23] of the deep-blue Commission International de l'Eclairage (CIE) coordinates ($CIE_y \leq 0.1$). To realize the same, several phosphorescent-based emitters were developed [24–26]. However, as the emission peaks shift towards the deep-blue region, the nonradiative transition rate of metal d-orbitals tends to increase, making it difficult to

achieve high efficiency [24–27]. In order to solve the problem, small-molecule fluorescent materials are being re-developed due to their high color purity and low cost [28].

To date, several reports have presented deep-blue materials based on anthracenes [29–32], pyrenes [33–37] and fluorenes [38–43]. However, these derivatives, especially anthracene, generally exhibit low singlet-exciton yields, which may be caused by strong electron–hole pairing. As a result, they usually suffer from an aggregation-caused quenching (ACQ) effect [44]. This effect diminishes the device efficiency and causes the color purity to deteriorate [44–46].

Herein, we introduce a series of donor–acceptor–donor (D-A-D) twisted derivatives based on bicarbazole and benzophenone moieties. While the D-A-D architecture approach reduces the radiative lifetime as low as is feasible [47], the twisted D-A-D architecture tends to exhibit good intermolecular charge transfer and a small ΔE_{ST}. In addition, bicarbazole, due to its high energy absorption and emission capability, was paired with a strong electron-acceptor benzophenone moiety for effective charge confinement within the emission layer [47–51]. We demonstrated that twisted D-A-D derivatives could provide good thermal and morphological stability and prevent the ACQ by diminishing the electron–hole pairing in the solid state [52]. Hence, a series of four compounds, namely DB13, DB24, DB34, and DB43, was synthesized and investigated. DB13 displayed a maximum EQE of 4.0% for a deep-blue emission. Some of the derivatives also performed as good host materials to realize high-efficiency green phosphorescent as well as TADF-based OLEDs.

2. Experimental Section

2.1. Instrumentation

Thermogravimetric analysis (TGA) was performed on a TGAQ50 apparatus (Verder Scientific Haan, Haan, Germany). The TGA and DSC curves were recorded in a nitrogen atmosphere at a heating rate of 10 °C/min. Differential scanning calorimetry (DSC) measurements were carried out using a Bruker Reflex II thermos-system (Bruker, Berlin, Germany). UV–visible spectroscopy was performed using an HP-8453 diode array spectrometer (Agilent Technology Inc., Hachioji, Tokyo, Japan) to measure the absorption spectra of the compounds. In addition, the Tauc plot was derived using the absorbance wavelength. Photoluminescence (PL) spectra were recorded using the Aminco-Bowman Series 2 luminescence spectrometer (Agilent Technology Inc., Hachioji, Tokyo, Japan). Low-temperature PL (LTPL) was recorded using a Hitachi F-7000 fluorescence spectrophotometer (Edinburgh Instruments Ltd., Livingston, UK). LTPL was performed at a low temperature of 77K to obtain the singlet energy of the compounds. Cyclic voltammetry (CV) was carried out using the CH instrument CH1604A potentiostat Annatech Co., Ltd., Taipei, Taiwan). The highest occupied molecular orbital (HOMO) levels were calculated using results of the CV measurement. Time-resolved photoluminescent measurements were performed on an Edinburgh instrument spectrometer FLS980 (Edinburgh Instruments Ltd., Livingston, UK) in order to determine the decay time of the compounds.

2.2. Device Fabrication

A pre-patterned ITO glass substrate was utilized for the fabrication of OLED devices. The substrate was cleaned using acetone and isopropyl alcohol (IPA) for 30 min each at 50 and 60 °C, respectively. The substrates were then transferred to the preheated UV chamber for 10 min of UV treatment. The layer deposition took place in a glove box under an inert atmosphere. The hole injection layer (PEDOT:PSS) was spin-coated at 4000 rpm for 20 s and the substrates were heated at 130 °C for 10 min. An emissive layer was then spin-coated on the cooled substrates at 2500 rpm for 20 s. The substrates were then transferred to the thermal evaporation chamber where electron-injection/-transport layer and aluminium cathode were deposited at a vacuum of 10^{-6} torr. The substrates were kept under a vacuum in a mini chamber of the glove box and individually taken for testing. The testing was carried out in a completely dark room under ambient conditions. The current-density–voltage–luminance (J-V-L) characteristics were recorded using a CS-100A luminescence spectrophotometer, while power efficacy–luminance–current characteristics were recorded using a PR-655 spectrophotometer. The Keithley voltmeter was used to measure the current–voltage (I-V) characteristics. The device

area was 0.09 cm^{-2}. External quantum efficiency (EQE) of the devices was calculated using the method described in the literature [53].

3. Result and Discussion

The synthesis of bicarbazole-based host materials was carried out by the three-step synthetic route as shown in Figure 1. The 3,3′-Bicarbazole (**1**) was obtained by oxidizing carbazole with iron (III) chloride. Various 9-alkyl-9′H-3,3′-bicarbazoles (**2–4**) and 9-benzyl-9′H-3,3′-bicarbazole (**5**) were obtained by the N-alkylation reaction between the bicarbazole **1** and corresponding alkyl or benzyl bromide, using potassium hydroxide and potassium carbonate in tetrahydrofuran (THF). The last step was the nucleophilic aromatic substitution of partially alkylated bicarbazole.

This was calculated using the method described in the literature, with one or two fluorine atoms containing diphenyl sulfone. The mentioned reactions were carried out in DMSO using potassium carbonate as a base and resulted in objective materials DB13 (**7**), DB24 (**8**), DB34 (**9**), and DB43 (**6**). The newly synthesized derivatives were identified by mass spectrometry and NMR spectroscopy. The data were found to be in good agreement with the proposed structure.
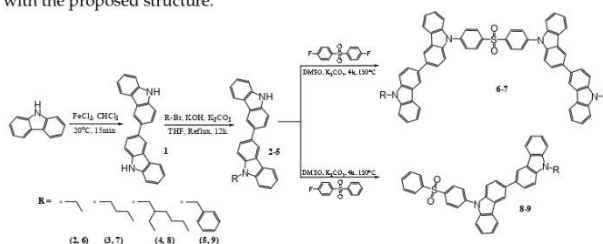
Figure 1. Synthetic pathway of materials DB13 (**7**), DB24 (**8**), DB34 (**9**), and DB43 (**6**).

Figure 2 shows the exact chemical structures of the derivatives in order to demonstrate the different length of alkyl chains in the group DB13 (**7**), DB24 (**8**), and DB43 (**6**). The compound DB34 has in its structure the benzyl fragment. The compounds DB43 and DB13 consist of two 3,3′-bicarbazole units, where DB13 has a longer alkyl chain than that of DB43. Inoue et al. reported the effect of an alkyl chain's length on the solubility of the organic compounds. The longer the alkyl chain, the better the solubility of the molecule in a suitable solvent [54].
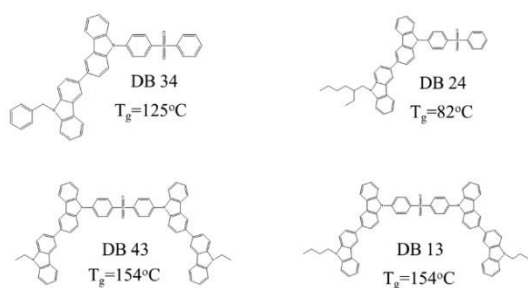
Figure 2. Exact chemical structures of the bicarbazole-benzophenone-based derivatives DB34, DB24, DB43, and DB13.

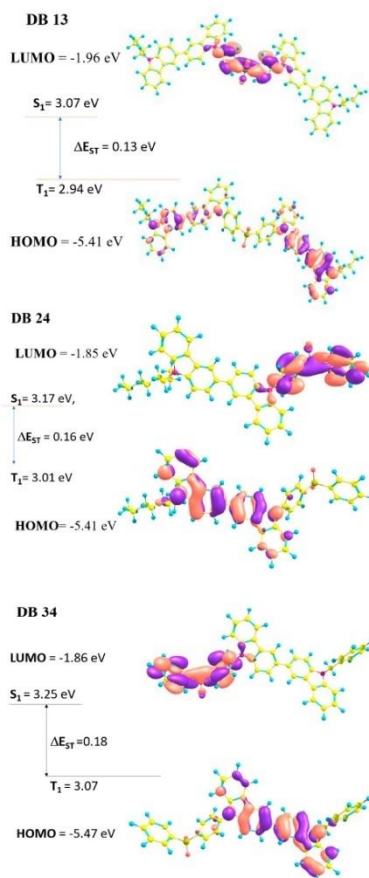### 3.1. Characteristics of the Presented Materials

3.1.1. DFT Calculations

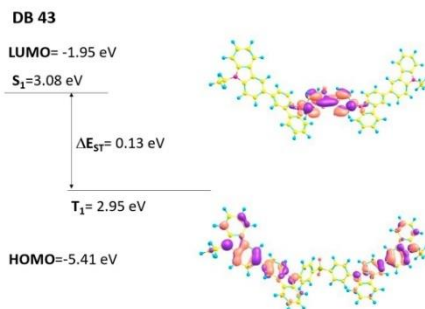The electron density contours of frontier molecular orbitals (FMO) and HOMO, LUMO, singlet, triplet, and singlet–triplet energy gap electron distribution of the compounds DB13, DB24, DB34, and DB43 are shown in Figure 3 and provided in Table 1. The theoretically measured values of the compounds DB13, DB24, DB34, and DB43 show HOMO, LUMO, and the energy gap between singlet and triplet (ΔE_{ST}) and singlet and triplet energies. All the materials show a small ΔE_{ST} (<0.2 eV), referring to the effective utilization of triplet-level excitons. The HOMO and LUMO levels are suitable for developing blue OLEDs and also for use as host materials for OLED devices.

DB 13

LUMO = -1.96 eV

S_1 = 3.07 eV

ΔE_{ST} = 0.13 eV

T_1 = 2.94 eV

HOMO = -5.41 eV

DB 24

LUMO = -1.85 eV

S_1 = 3.17 eV,

ΔE_{ST} = 0.16 eV

T_1 = 3.01 eV

HOMO = -5.41 eV

DB 34

LUMO = -1.86 eV

S_1 = 3.25 eV

ΔE_{ST} = 0.18

T_1 = 3.07

HOMO = -5.47 eV

Figure 3. *Cont.*

206

DB 43

LUMO= -1.95 eV

S_1=3.08 eV

ΔE_{ST}= 0.13 eV

T_1= 2.95 eV

HOMO=-5.41 eV

Figure 3. Electron density contours of frontier molecular orbitals (FMO) and HOMO, LUMO, singlet, triplet, and singlet–triplet energy gap electron distribution of the compounds DB13, DB24, DB34, and DB43.

Table 1. The excitation wavelength (λ_{ex}), emission wavelength (λ_{em}), bandgap (E_g), PLQY (Φ), decay time, theoretical and calculated HOMO-LUMO levels, values of singlet energy (S_1) and triplet energy (T_1), singlet–triplet energy gap (ΔE_{ST}), decomposition temperatures (T_d) and glass-transition temperatures (T_g) of the compounds DB13, DB24, DB34 and DB43.

Emitter	λ_{ex} (nm)	λ_{em} (nm)	E_g (eV)	Φ (%)	Decay (ns)	HOMO (eV)		LUMO (eV)		S_1 (eV)		T_1 (eV)		ΔE_{ST} (eV)		T_d (°C)	T_g (°C)
						Theo.	Cal.	Theo.	Cal.	Theo.	Cal.	Theo.	Cal.	Theo.	Cal.		
DB 13	365.2	465.4	3.16	50.5	3.30	5.41	5.73	1.96	2.57	3.07	3.10	2.94	2.78	0.13	0.32	430	154
DB 24	375.4	462.5	3.30	61.8	3.70	5.41	5.71	1.85	2.41	3.17	3.17	3.01	2.77	0.16	0.35	391	82
DB 34	363.0	462.0	3.28	68.5	2.70	5.47	5.77	1.86	2.49	3.25	3.14	3.07	2.80	0.18	0.34	383	125
DB 43	366.9	463.2	3.26	66.5	3.30	5.41	5.69	1.95	2.43	3.08	3.23	2.95	2.77	0.13	0.46	365	154

3.1.2. Photophysical Properties

The compounds DB13, DB24, DB34, and DB43 possess a high photoluminescence quantum yield (PLQY) of 50.5, 61.8, 68.5 and 66.5%, respectively. The values of PLQYs are also tabulated in Table 1.

The UV abs (Figure 4a–d) of the compounds DB13, DB24, DB34, and DB43 were examined using tetrahydrofuran (THF) solvent under ambient conditions. The spectra of the prepared solutions were recorded using the quartz cuvette. The absorption peaks were observed at around 375 nm for all the compounds. This is understandable, because all the derivatives have the same chromophores in their structures. A Tauc plot (Figure 4e–h) was prepared with the absorption wavelength and intensity, using the following equations:

$$\text{x-axis: } (\alpha \times h\nu)^{1/2} \tag{1}$$

$$\text{y-axis: } h\nu \tag{2}$$

where α is the absorption coefficient and $h\nu$ is the energy ($h\nu = 1240/\text{wavelength}$).

The maximal absorbance wavelength was utilized as the excitation wavelength for measuring photoluminescence. The excitation wavelengths and bandgap are presented in Table 1. The singlet energies calculated are shown in the Supplementary File (Figure S1).
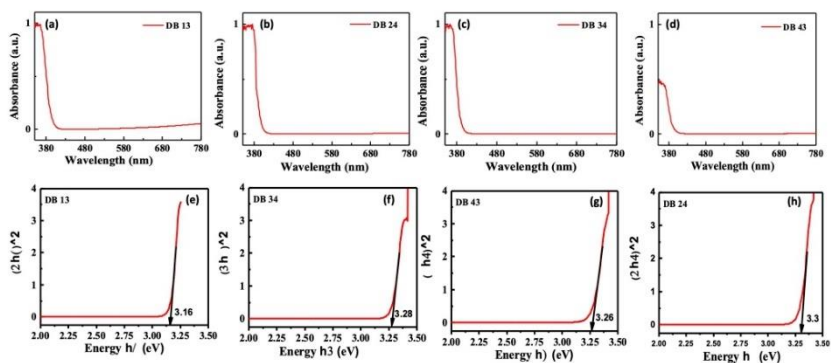
207

Figure 4. (**a–d**) Ultraviolet–visible absorbance (UV abs) spectra and (**e–h**) Tauc plot, represent the absorption wavelength and bandgap, respectively, of the compounds DB13, DB24, DB34 and DB43.

Figure 5 shows the PL spectra of the compounds DB13, DB24, DB34, and DB43, demonstrating the emission wavelength maxima in the region of 450–470 nm. The low-temperature photoluminescence (LTPL) spectra, which are presented in Figure 6, were also measured to determine the triplet energies. The compounds DB13, DB24, DB34, and DB43 possess high triplet energy levels of 2.78, 2.77, 2.80, and 2.77 eV, respectively, and could be tested as suitable host materials for green phosphorescent emitters, as well as for green TADF emitters. The values of triplet energies are also tabulated in Table 1.
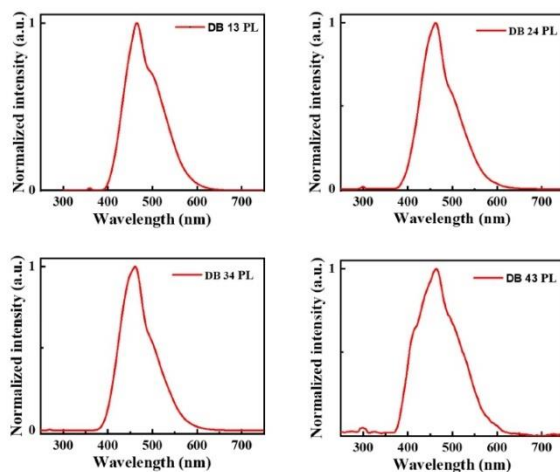
Figure 5. Photoluminescence (PL) spectra of the compounds DB13, DB24, DB34, and DB43.
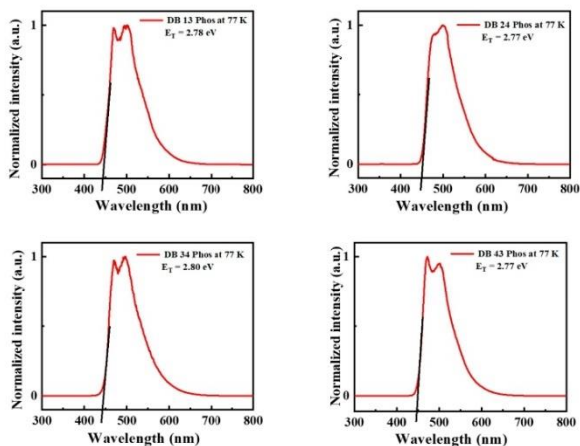
Figure 6. Low–temperature photoluminescence (LTPL) spectra at 77 K of the compounds DB13, DB24, DB34 and DB43.

Figure 7 shows the time-resolved photoluminescence (TRPL) analysis representing the decay time of the compounds. The time values of 3.3, 3.7, 2.7, and 3.2 ns were determined for DB13, DB24, DB34, and DB43, respectively. It could be seen that all the compounds emit radiatively, with a short decay time. The decay values are provided in Table 1. IRF corresponds to the instrument response function that was measured before and after each measurement as a control parameter.

3.1.3. Electrochemical Properties

Electrochemical characteristics of the compounds DB 13, DB 24, DB 34, and DB 43 were estimated using cyclic voltammetry (CV) measurements, which are shown in Figure 8. The HOMO levels were calculated using Equation (3):

$$\mathrm{E}_{\mathrm{HOMO}} = -\left[4.4 + E_{onset}^{ox}\right] \tag{3}$$

The LUMO levels were calculated using the following Equation (4):

$$\mathrm{E}_{\mathrm{LUMO}} = \mathrm{E}_{\mathrm{HOMO}} + E_g \tag{4}$$

where E_g is the bandgap calculated using the Tauc plot. The calculated HOMO energy levels were found to be -5.73, -5.71, -5.77, and -5.69 eV and the LUMO levels were found to be -2.57, -2.41, -2.49, and -2.43 eV for, correspondingly, DB 13, DB 24, DB 34, and DB 43. The bandgap was obtained using the plot of Equations (1) and (2) and was found to be 3.16, 3.30, 3.28, and 3.26 eV for the compounds DB 13, DB 24, DB 34 and DB 43, respectively (Table 1). The HOMO and LUMO levels of the derivatives were found to be very suitable for blue emitters, as well as for host materials.

209
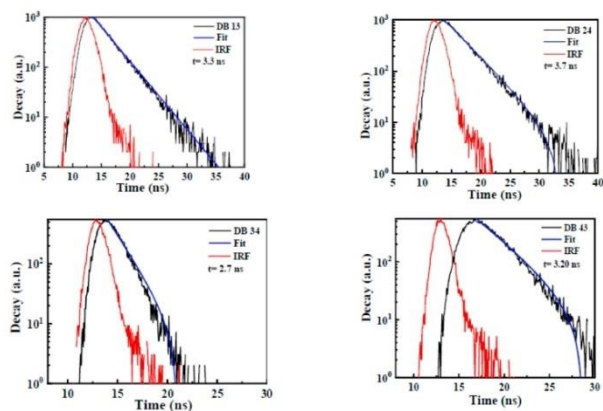
Figure 7. Time-resolved photoluminescence (TRPL) spectra for the PL decay kinetics analysis of the compounds DB 13, DB 24, DB 34, and DB 43.

3.1.4. Thermal Properties

The behavior under heating of the synthesized materials DB13, DB24, DB34, and DB43 was studied using DSC and TGA under a nitrogen atmosphere. It was established that the objective compounds demonstrate very high thermal stability. Data from the TGA analyses are shown in Figure 9. The temperatures of a 5% weight loss (T_d) for derivatives DB13, DB24, DB34, and DB43 were 365 °C, 430 °C, 391 °C and 383 °C, respectively, as confirmed by TGA at a heating rate of 10 °C/min (Figure 9). It could be observed that materials DB13 and DB43 have slightly lower thermal stability, probably due to the presence of two alkyl chains in their structures.
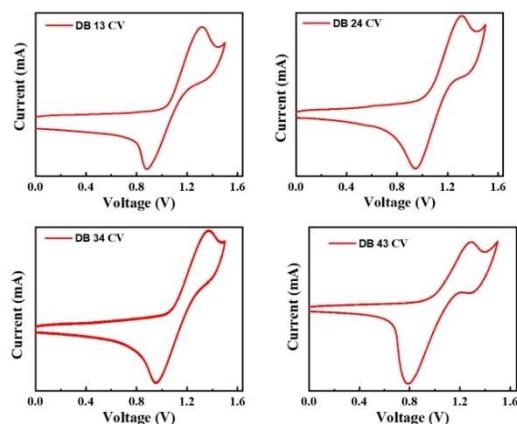
Figure 8. Cyclic voltammetry scans for calculation of HOMO levels of the compounds DB13, DB24, DB34 and DB43.
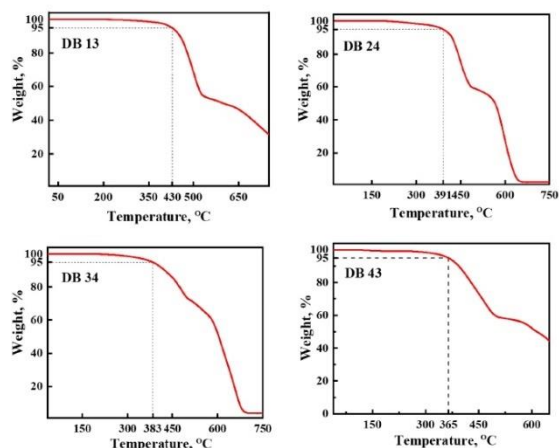
Figure 9. Data of thermogravimetric analysis (TGA) of the compounds DB13, DB24, DB34 and DB43.

The DSC curves of the second heating of compounds DB13, DB24, DB34, and DB43 are presented in Figure 10. It can be clearly seen from the curves that some of the new derivatives have very high glass transition temperatures (T_g), of 154 °C for DB13, and also 154 °C for DB34 and 125 °C for DB43. The material DB24 demonstrated a lower glass transition temperature of 82 °C, due to the branched 2-ethylhexyl group, which is in the structure of the derivative and decreases its morphological stability. Therefore, the TGA and DSC results confirm that many of the materials are well suited for application in the amorphous electroactive layers of OLED devices.
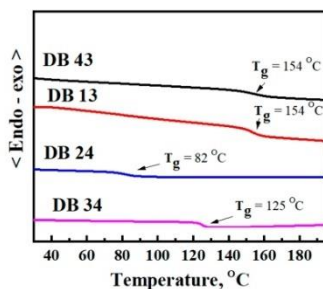
Figure 10. DSC curves of second heating for estimating glass transition temperatures (T_g) of the compounds DB13, DB24, DB34, and DB43.

Table 1 shows the photophysical, electrochemical and thermal properties of the compounds DB13, DB24, DB34, and DB43. The table demonstrates that the compounds possess high photoluminescence yields, high decomposition temperatures and also high glass transition temperatures for derivatives DB13, DB34 and DB43. The compounds also have

large bandgaps, which are suitable for the application of the materials in OLEDs as an emitter as well as a host.

3.2. Structure and Characterization of Electroluminescent OLED Devices

The schematic energy-level diagram in eV of blue OLED devices fabricated in this work by utilizing the emitters DB13, DB24, DB34 and DB43 doped in the commercial 4,4′-Bis(N-carbazolyl)-1,1′-biphenyl (CBP) host matrix is shown in Figure 11. The fabricated devices were composed as doped devices, having the structure: ITO (125 nm)/PEDOT:PSS (35 nm)/host: (x wt%) emitter (x = 5.0, 10, and 15%) (20 nm)/TPBi (40 nm)/LiF (1 nm)/Al (200 nm).

The electroluminescence (EL) spectra of the emitters doped in the CBP host matrix, and the characteristics of the devices are shown in Figures 12–15 and also provided in Table 2. Each figure shows (a) the EL spectra, (b) current-density–voltage, (c) luminance–voltage, (d) power-efficacy–luminance and (e) current-efficacy–luminance characteristics.
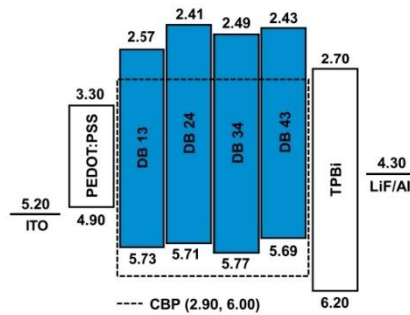
Figure 11. Energy-level diagram in eV of the solution-processed blue OLED devices containing emitters DB 13, DB 24, DB 34, and DB 43 doped in CBP host material.

Table 2. Electroluminescent (EL) characteristics of the devices with emitters DB34, DB24, DB43 and DB13 doped in CBP host matrix at varying concentrations, displaying turn-on voltage at luminance >1 cd m^{-2}, power efficacy, current efficacy, external quantum efficiency, CIE, and maximal luminance.

Emitter	Concentration (wt%)	Turn-on Voltage (V_{on})	Power Efficacy (lm/W)	Current Efficacy (cd/A)	EQE (%)	CIE	Max Luminance (cd/m^2)
			@100/1000 cd/m^2 and Max				
DB34	5.0	4.2	0.7/-/0.8	1.1/-/1.2	2.3/-/2.3	(0.16, 0.07)/-	589
	10	4.0	0.8/-/0.8	1.2/-/1.2	2.0/-/2.0	(0.16, 0.08)/-	631
	15	3.8	0.8/-/1.0	1.3/-/1.4	1.8/-/2.0	(0.16, 0.09)/-	599
	100	3.4	0.2/-/0.3	0.2/-/0.3	0.1/-/0.2	(0.19, 0.24)/-	179
DB 24	5.0	5.1	0.8/-/0.8	1.5/-/1.5	2.5/-/2.5	(0.16, 0.08)/-	724
	10	3.9	0.8/-/0.8	1.2/-/1.2	1.7/-/1.8	(0.16, 0.09)/-	830
	15	3.7	0.9/-/1.0	1.4/-/1.4	1.6/-/1.6	(0.16, 0.11)/-	867
	100	3.1	0.3/-/0.3	0.4/-/0.4	0.2/-/0.2	(0.19, 0.21)/-	238
DB 43	5.0	4.6	0.6/-/0.9	1.1/-/1.4	1.3/-/1.6	(0.17, 0.11)/-	631
	10	4.1	0.9/-/1.2	1.5/-/1.7	1.6/-/1.4	(0.18, 0.14)/-	715
	15	4.0	0.9/-/1.2	1.5/-/1.6	1.2/-/1.2	(0.19, 0.16)/-	892
	100	3.2	0.2/-/0.3	0.2/-/0.3	0.1/-/0.1	(0.25, 0.34)/-	278

Table 2. *Cont.*

Emitter	Concentration (wt%)	Turn-on Voltage (V_{on})	Power Efficacy (lm/W)	Current Efficacy (cd/A)	EQE (%)	CIE	Max Luminance (cd/m^2)
			@100/1000 cd/m^2 and Max				
DB 13	5.0	4.6	1.1/0.7/1.1	1.8/1.5/1.8	3.2/2.5/3.4	(0.16, 0.08)/ (0.16, 0.08)/-	2230
	10	3.7	1.7/ 1.0/ 2.0	2.3/ 1.7/ 2.5	3.4/2.5/4.0	(0.16, 0.09)/ (0.16, 0.09)/-	2987
	15	3.5	1.6/1.1/1.6	2.0/1.9/2.2	2.8/2.5/2.9	(0.16, 0.10)/ (0.16, 0.10)/-	3167
	100	3.0	0.9/-/1.0	1.1/-/1.1	0.6/-/0.6	(0.16, 0.2)/-	928
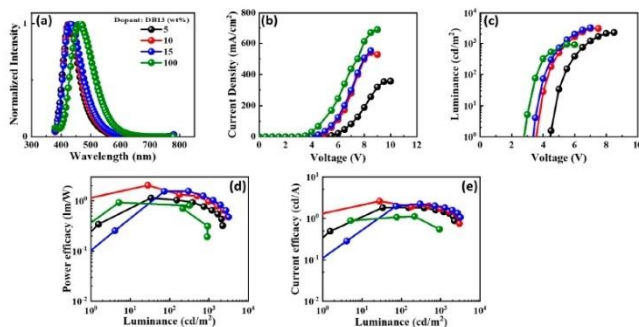
Figure 12. The electroluminescent (EL) properties of the device with emitter DB13 doped in CBP host matrix at varying concentrations showing (**a**) EL spectra, (**b**) current density–voltage, (**c**) luminance–voltage, (**d**) power efficacy–luminance, and (**e**) current efficacy–luminance characteristics.
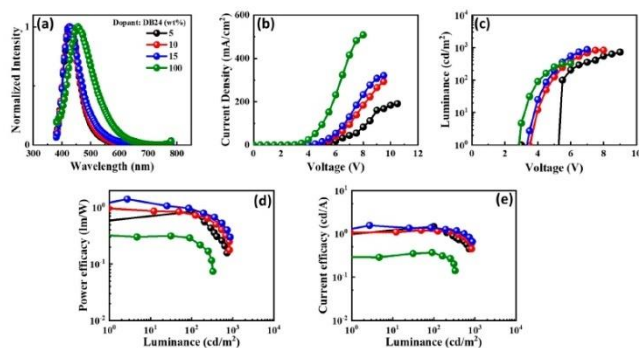
Figure 13. The electroluminescent (EL) properties of the device with emitter DB24 doped in CBP host matrix at varying concentrations showing (**a**) EL spectra, (**b**) current density–voltage, (**c**) luminance–voltage, (**d**) power efficacy–luminance, and (**e**) current efficacy–luminance characteristics.
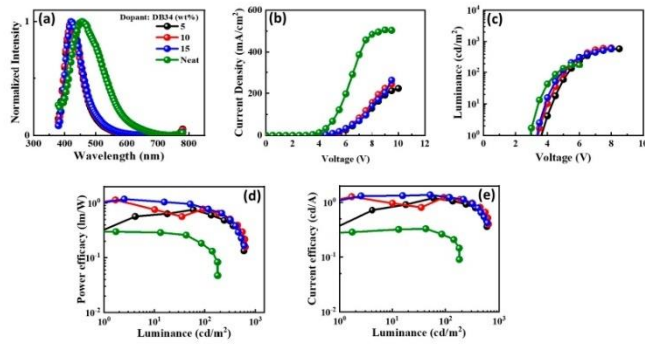
Figure 14. The electroluminescent (EL) properties of the device with emitter DB34 doped in CBP host matrix at varying concentrations showing (**a**) EL spectra, (**b**) current density–voltage, (**c**) luminance–voltage, (**d**) power efficacy–luminance, and (**e**) current efficacy–luminance characteristics.
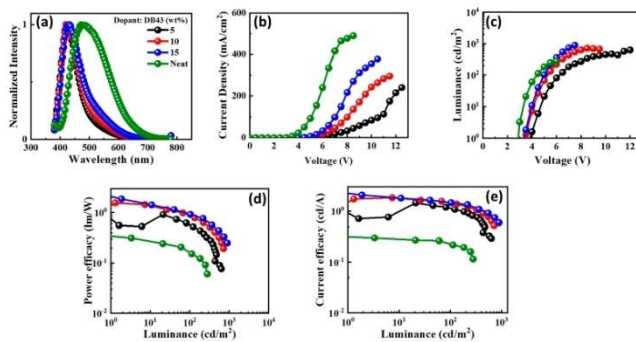
Figure 15. The electroluminescent (EL) properties of the device with emitter DB43 doped in CBP host matrix at varying concentrations showing (**a**) EL spectra, (**b**) current density–voltage, (**c**) luminance–voltage, (**d**) power efficacy–luminance, and (**e**) current efficacy–luminance characteristics.

It can be seen from Figures 12–15 that the EL spectra of emitters DB13, DB24, DB34, and DB43 peak in the region 430–450 nm, with an indication of the blue emission. The presence of a single peak indicates the complete host–guest energy transfer. The EL emission wavelength of the devices was close to the PL spectra of the used emitter, indicating the origin of emission from the material. Both doped and non-doped devices showed a similar EL emission peak. Figures 12–15 also show the characteristics of current-density–luminance-voltage and power-efficacy–luminance–current-efficacy. The non-doped devices showed a current density higher than that of the doped devices and the efficacies were lower than those of the doped devices. Therefore, the role of the host was significant and a 10 wt% DB13 emitter-based device outperformed other devices by displaying a maximum power efficacy (PE_{max}) of 2.0 lm/W, and current efficacy (CE_{max}) of 2.5 cd/A with a turn-on voltage of 3.7 eV. Moreover, the DB13-based device also displayed the highest EQE_{max} of 4.0%, which is close to the theoretical limit of fluorescent emitters for a deep-blue emission,

with a CIE_y of 0.09. This device demonstrated a higher EQE as compared with many other fluorescent emitters which are reviewed in the scientific literature [55]. The DB13-based fluorescent OLED displayed an even deeper blue emission and better performance than the recently reported device, based on the hybridized local and charge-transfer (HLCT) mechanism [56]. As reported, the enhancement was attributed to the LE-dominated HLCT state; however, the power and current efficiencies were significantly lower than in this report. The above statement shows that twisted D-A derivatives prove to be better candidates for fluorescent emission.

As shown in Table 2, the device with the DB13 emitter shows the highest PE, CE and EQE among all the devices. The results may be connected to the presence of two alkyl chains in the molecule, which improves the solubility of the material for the wet-processed device fabrication, a high glass-transition temperature (T_g), high decomposition temperature (T_d), suitable HOMO and LUMO levels, enabling efficient host–guest energy transfer and the presence of two bicarbazole donor moieties for balanced charge transfer. Moreover, the incorporation of the benzophenone moiety into the chemical structure may have resulted in the deep-blue emission from the OLED device.

Furthermore, owing to the wide bandgap and high triplet energies of the compounds DB13, DB24, DB34 and DB43, they were utilized as host materials for the application in green OLEDs. For the same purpose, the green emitters of generation two and three, i.e., the phosphorescent emitter $Ir(ppy)_3$ and TADF emitter 4CzIPN, respectively, were utilized. Figure 16 shows the energy-level diagram in eV of the solution-processed green OLED devices consisting of hosts DB13, DB24, DB34, and DB43, doped with the green commercial phosphorescent emitter $Ir(ppy)_3$ and TADF emitter 4CzIPN. The device structure was therefore composed as ITO (125 nm)/PEDOT:PSS (35 nm)/host: (x wt%) emitter (host = DB13, DB24, DB34, and DB43) (emitter = $Ir(ppy)_3$ or 4CzIPN) (x = 10, 12.5 and 5% for $Ir(ppy)_3$), (x = 1, 3 and 5% for emitter 4CzIPN) (20 nm)/TPBi (40 nm)/LiF (1 nm)/Al (200 nm).
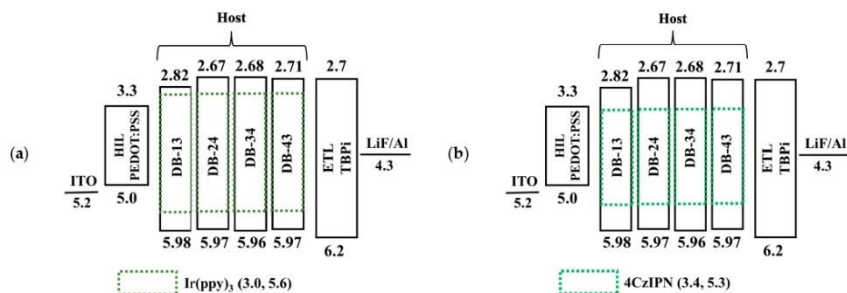

Figure 16. Energy-level diagram in eV of the solution-processed green OLED devices containing hosts DB13, DB24, DB34, and DB43, doped with commercial (**a**) phosphorescent green emitter $Ir(ppy)_3$ and (**b**) commercial TADF green emitter 4CzIPN.

Figures S2–S4 show the electroluminescent characteristics of devices based on the hosts DB13, DB24 and DB34, doped with the green phosphorescent emitter $Ir(ppy)_3$. Figures S2a, S3a and S4a show the EL spectra of the devices peaking at ~540 nm with the green emission. The peak from the EL spectra of the devices is similar to the PL peak of $Ir(ppy)_3$, indicating the origin of the emission [57]. The single EL peak resembles the complete host-to-guest energy transfer. Figures S2b–e, S3b–e, and S4b–e show the luminance–voltage and efficiencies curves. Amongst all of these, a 12.5 wt% $Ir(ppy)_3$ doped in a DB13-based device showed the best performance, with a PE_{max} of 45 lm/W, CE_{max} of 43 cd/A, EQE_{max} of 10.6%, and L_{max} of 37680 cd/m^2, with a low roll-off at higher luminance value.

Table 3 shows the OLED characteristics of green devices based on hosts DB13, DB24, DB34, and DB43. doped with the commercial phosphorescent green emitter Ir(ppy)$_3$. The good performance of the device using DB13 may be due to its suitable chemical structure, longer aliphatic chains, high decomposition temperature, small singlet–triplet energy gap (ΔE_{ST}), i.e., effective triplet exciton utilization, and suitable HOMO-LUMO levels, compared to those of Ir(ppy)$_3$, which enabled an efficient host-to-guest energy transfer in the emitting layer. Devices using other compounds have also shown comparable efficiencies. However, the DB43-based OLED has shown poorer performance, which might be attributed to the large ΔE_{ST}, disabling the use of triplet excitons.

Table 3. Electroluminescent (EL) characteristics of the devices with hosts DB13, DB24, DB34, and DB43, doped with green phosphorescent emitter Ir(ppy)$_3$ at varying concentrations, displaying turn-on voltage, power efficacy, current efficacy, external quantum efficiency, CIE, and luminance.

Host	Ir(ppy)$_3$ Doping con. (wt%)	Turn-on Voltage (V)	PE$_{max}$/CE$_{max}$/ EQE$_{max}$ (lm/W/cd/A/%)	PE$_{100}$/CE$_{100}$/ EQE$_{100}$ (lm/W/cd/A/%)	PE$_{1,000}$/CE$_{1,000}$/ EQE$_{1000}$ (lm/W/cd/A/%)	PE$_{10,000}$/CE$_{10,000}$/ EQE$_{10,000}$ (lm/W/cd/A/%)	CIE$_{xy}$ Coordinates	Maxi. Lum. (cd/m^2)
	10	2.6	40.0/41.1/11.1	39.8/40.6/11.0	32.1/40.9/11.1	17.2/ 32.8/ 8.9	(0.32, 0.62)/(0.32, 0.62)/(0.32, 0.62)	33,870
DB 13	12.5	3.1	45.4/43.4/ 10.6	40.0/43.3/ 10.6	33.4/ 42.5 /10.5	20.8/ 36.4/ 8.7	(0.31, 0.62)/ (0.31, 0.62)/ (0.31, 0.63)	37,680
	15	2.5	34.6/35.3/ 9.5	34.6/33.7/ 9.1	28.7/33.5/ 9.4	17.5/ 29.5/ 7.9	(0.32, 0.62)/ (0.32, 0.62)/ (0.32, 0.62)	32,300
	10	2.8	37.8/32.5/ 9.0	30.9/32.4/ 8.9	24.2/30.9/ 8.5	11.4/ 21.8/ 6.0	(0.32, 0.62)/ (0.31, 0.62)/ (0.31, 0.62)	1410
DB 24	12.5	2.9	30.8/28.3/ 7.8	28.7/28.4/ 7.8	21.2/27.0/ 7.4	9.5 /18.2/ 5.0	(0.32, 0.62)/ (0.31, 0.62)/ (0.31, 0.62)	16,960
	15	2.8	25.7/26.2/ 7.2	23.3/26.0/ 7.2	16.8/24.1/ 6.6	6.4/ 14.3/ 3.9	(0.32, 0.62)/ (0.32, 0.62)/ (0.31, 0.62)	16,200
	10	2.6	37.9/36.2/ 9.8	33/ 34.7/ 9.4	27.1/34.5/ 9.3	12.8/ 24.5/ 6.6	(0.32, 0.62)/ (0.32, 0.62)/ (0.32, 0.62)	22,570
DB 34	12.5	2.8	32.7/32.8/ 8.7	31.6/32.2/ 8.7	24.3/30.9/ 8.3	9.8/ 18.7/ 5.1	(0.31, 0.62)/ (0.31, 0.62)/ (0.31, 0.63)	21,430
	15	2.9	20.2/21.0/ 5.7	18.7/20.8/ 5.6	14.5/20.8/ 5.6	7.3/ 15.1/ 4.1	(0.32, 0.62)/ (0.32, 0.62)/ (0.32, 0.62)	22,100

Figures S5–S7 show the OLED characteristics of devices based on the hosts DB13, DB24 and DB34, doped with the green TADF emitter 4CzIPN. Figures S5a, S6a, and S7a show the EL spectra of the devices peaking at ~530 nm with the green emission. The peak from the EL spectra of the devices is like the PL peak of 4CzIPN, and the bathochromic shift is only observed with increasing doping concentration, indicative of the origin of emission [58]. In addition, the single EL peak resembles the complete host-to-guest energy transfer. Figures S2b–e, S3b–e, and S4b–e show the luminance–voltage and efficiencies curves. Amongst all of these, a device based on a 3wt% 4CzIPN emitter in DB34 host outperformed other devices, with an EQE$_{max}$ of 10.8%, which is higher than that of the many described efficient phosphorescent green devices [59]. However, the PE and luminance are slightly lower than those of the mentioned devices. The possible reason might be attributed to triplet–triplet annihilation (TTA). Further reducing ΔE_{ST} in the synthesized compounds may enable the effective utilization of triplet excitons and may result in better performance of the TADF-based green OLEDs. Table 4 shows the comprehensive list of OLED characteristics of the described devices using hosts DB13, DB24 and DB34.

216

Table 4. Electroluminescent (EL) characteristics of the devices with hosts DB13, DB24 and DB34, doped with green commercial TADF emitter 4CzIPN at varying concentrations, displaying turn-on voltage, power efficacy, current efficacy, external quantum efficiency, CIE, and maximal luminance.

Host	4CzIPN Doping con. (wt%)	Turn-on Voltage (V)	PE_{max}/ CE_{max}/EQE_{max} (lm/W/cd/A/ %)	PE_{100}/CE_{100}/ EQE_{100} (lm/W/cd/A/ %)	$PE_{1,000}$/$CE_{1,000}$/ EQE_{1000} (lm/W/cd/A/ %)	CIE_{xy} Coordinates	Maxi. Lum. (cd/m^2)
DB 13	1	3.2	16.6/15.8/4.8	7.9/11.1/3.6	4.1/8.5/3.1	(0.32, 0.51)/(0.29, 0.46)	3108
	3	3.8	24.9/22.2/6.7	12.1/15.5/4.7	2.3/4.8/1.5	(0.32, 0.55)/(0.29, 0.51)	5869
	5	2.9	16.2/15.7/4.7	14.1/15.7/4.7	6.6/11.7/3.6	(0.35, 0.55)/(0.34, 0.54)	712
DB 24	1	3.1	-/-/-	10.1/12.9/4.6	3.7/7.0/2.7	(0.29, 0.47)/(0.27, 0.42)	2823
	3	2.8	22.9/23.1/7.7	20.7/23.1/7.7	12.1/17.3/5.8	(0.31, 0.52)/(0.30, 0.51)	6231
	5	2.8	18.4/20.5/6.6	18.4/20.5/6.6	10.8/15.5/5.0	(0.31, 0.54)/(0.31, 0.53)	7689
DB 34	1	2.7	30.4/27.1/8.9	21.3/23.1/7.7	10.2/14.7/5.0	(0.27, 0.51)/(0.26, 0.49)	3782
	3	2.6	37.5/33.5/10.8	32.0/32.6/10.6	15.8/22.6/7.4	(0.30, 0.54)/(0.29, 0.53)	9484
	5	2.6	34.7/33.2/10.5	34.7/33.2/10.5	18.9/24.0/7.6	(0.30, 0.55)/(0.29, 0.55)	12480

4. Conclusions

The newly synthesized bicarbazole-benzophenone-based materials possess a large bandgap and high triplet energy, which support their bifunctionality both as an emitter and a host material for OLED applications. Moreover, the materials demonstrate good thermal and morphological stability with very high decomposition temperatures and also high glass-transition temperatures for some compounds as well as short decay time, as confirmed by high PLQY. Two aliphatic chains having the compound DB13 displayed better device performance than their counterparts, probably due to its better solubility and film-forming properties. The bicarbazole-benzophenone-bicarbazole D-A-D-based emitter displayed an EQE_{max} of 4.0% for a deep-blue emission (CIE_y 0.09), which confirms its large potential as a deep-blue emitter. On the other hand the developed emitter has better first-generation OLED characteristics than those of the well-known carbazole-benzophenone-carbazole based device, probably due to its better film-forming properties.

Some of the compounds have also shown promising results as host materials for green phosphorescent as well as TADF-based OLEDs. The host DB13-based device showed a PE_{max} of 45 lm/W and low roll-off for the phosphorescent green OLED, while the host DB34-based TADF device outperformed all the devices, with an EQE_{max} of 10.8%, which is even slightly higher than that of the mentioned phosphorescence-based green devices. These results reveal that some of these cost-effective materials possess excellent photophysical, electrochemical, and thermal properties, and can be applicable to a variety of display and solid-state lighting applications, especially in TVs, laptops, desktops, mobile phones, and interior lightings, etc. Moreover, the efficiency of the devices could be enhanced by further reducing ΔE_{ST} and effectively utilizing triplet-state excitons in order for use in high-power applications such as headlights and street lights, etc. We believe that this research will provide a good pathway for the development of future products for academics as well as for industry.

References

1. Chan, C.-Y.; Cui, L.-S.; Uk Kim, J.; Nakanotani, H.; Adachi, C.; Chan, C.; Cui, L.; Kim, J.U.; Nakanotani, H.; Adachi, C. Rational Molecular Design for Deep-Blue Thermally Activated Delayed Fluorescence Emitters. *Adv. Funct. Mater.* **2018**, *28*, 1706023. [CrossRef]
2. Nayak, S.R.; Siddiqui, I.; Shahnawaz; Jou, J.-H.; Vaidyanathan, S. Diphenylimidazole Based Fluorophores for Explosive Chemosensors and as Efficient Host Materials for Green Phosphorescent Organic Light Emitting Diodes. *ACS Appl. Opt. Mater.* **2022**, *1*, 94–106. [CrossRef]
3. Solanki, J.D.; Siddiqui, I.; Gautam, P.; Gupta, V.K.; Jou, J.H.; Surati, K.R. Blue Fluorescent Zinc(II) Complexes Bearing Schiff Base Ligand for Solution-Processed Organic Light-Emitting Diodes with CIEy ≤ 0.09. *Opt. Mater.* **2022**, *134*, 113222. [CrossRef]
4. Nayak, S.R.; Shahnawaz; Siddiqui, I.; Jou, J.H.; Patel, S.; Vaidyanathan, S. Multifunctional 4,5-Diphenyl-1 H-Imidazole-Based Luminogens as Near UV/Deep Blue Emitters/Hosts for Organic Light-Emitting Diodes and Selective Picric Acid Detection. *J. Phys. Chem. C* **2022**, *127*, 499–515. [CrossRef]
5. Sharma, A.; Thomas, K.R.J.; Kesavan, K.K.; Siddiqui, I.; Nagar, M.R.; Jou, J.H. Effect of Positional Isomerism on the Functional Properties of Carbazole-Phenanthroimidazole-Triphenylamine Triads. *Dye. Pigment.* **2021**, *196*, 109744. [CrossRef]
6. Shahnawaz; Siddiqui, I.; Nagar, M.R.; Choudhury, A.; Lin, J.T.; Blazevicius, D.; Krucaite, G.; Grigalevicius, S.; Jou, J.H. Highly Efficient Candlelight Organic Light-Emitting Diode with a Very Low Color Temperature. *Molecules* **2021**, *26*, 7558. [CrossRef]
7. De, J.; Sarkar, I.; Yadav, R.A.K.; Bala, I.; Gupta, S.P.; Siddiqui, I.; Jou, J.H.; Pal, S.K. Luminescent Columnar Discotics as Highly Efficient Emitters in Pure Deep-Blue OLEDs with an External Quantum Efficiency of 4.7%. *Soft Matter* **2022**, *18*, 4214–4219. [CrossRef]
8. Singh, K.; Siddiqui, I.; Sridharan, V.; Kumar Yadav, R.A.; Jou, J.H.; Adhikari, D. Aggregation-Induced Enhanced Emission-Active Zinc(II) β-Diketiminate Complexes Enabling High-Performance Solution-Processable OLEDs. *Inorg. Chem.* **2021**, *60*, 19128–19135. [CrossRef]
9. Sharma, A.; Thomas, K.R.J.; Kesavan, K.K.; Siddiqui, I.; Ram Nagar, M.; Jou, J.H. Effect of Cyano on the Functional Properties of Phenanthroimidazole-Substituted Carbazole Derivatives. *ACS Appl. Electron. Mater.* **2021**, *3*, 3876–3888. [CrossRef]
10. Girase, J.D.; Tagare, J.; Shahnawaz; Nagar, M.R.; Siddiqui, I.; Jou, J.H.; Patel, S.; Vaidyanathan, S. Deep-Blue Emitters (CIEy ~0.07) Based on Phenanthroimidazole: Remarkable Substitution Effects at the N1 Position of Imidazole on the Excited States and Electroluminescence Properties. *Dye. Pigment.* **2021**, *196*, 109791. [CrossRef]
11. Chaskar, A.; Chen, H.-F.; Wong, K.-T. Bipolar Host Materials: A Chemical Approach for Highly Efficient Electrophosphorescent Devices. *Wiley Online Libr.* **2011**, *23*, 3876–3895. [CrossRef] [PubMed]
12. Han, C.; Zhao, Y.; Xu, H.; Chen, J.; Deng, Z.; Ma, D.; Li, Q.; Yan, P. A Simple Phosphine-Oxide Host with a Multi-Insulating Structure: High Triplet Energy Level for Efficient Blue Electrophosphorescence. *Chem.-A Eur. J.* **2011**, *17*, 5800–5803. [CrossRef] [PubMed]
13. Chien, C.H.; Chen, C.K.; Hsu, F.M.; Shu, C.F.; Chou, P.T.; Lai, C.H. Multifunctional Deep-Blue Emitter Comprising an Anthracene Core and Terminal Triphenylphosphine Oxide Groups. *Adv. Funct. Mater.* **2009**, *19*, 560–566. [CrossRef]
14. Tao, Y.; Wang, Q.; Yang, C.; Zhong, C.; Qin, J.; Ma, D. Multifunctional Triphenylamine/Oxadiazole Hybrid as Host and Exciton-Blocking Material: High Efficiency Green Phosphorescent OLEDs Using Easily Available and Common Materials. *Adv. Funct. Mater.* **2010**, *20*, 2923–2929. [CrossRef]
15. Sudheendran Swayamprabha, S.; Kumar Dubey, D.; Ashok Kumar Yadav, R.; Ram Nagar, M.; Sharma, A.; Tung, F.-C.; Jou, J.-H.; Sudheendran Swayamprabha, S.; Dubey, D.K.; K Yadav, R.A.; et al. Approaches for Long Lifetime Organic Light Emitting Diodes. *Adv. Sci.* **2021**, *8*, 2002254. [CrossRef]
16. Devesing Girase, J.; Rani Nayak, S.; Tagare, J.; Shahnawaz; Ram Nagar, M.; Jou, J.H.; Vaidyanathan, S. Solution-Processed Deep-Blue (Y~0.06) Fluorophores Based on Triphenylamine-Imidazole (Donor-Acceptor) for OLEDs: Computational and Experimental Exploration. *J. Inf. Disp.* **2022**, *23*, 53–67. [CrossRef]
17. Anupriya; Thomas, K.R.J.; Nagar, M.R.; Shahnawaz; Jou, J.H. Phenanthroimidazole Substituted Imidazo[1,2-a]Pyridine Derivatives for Deep-Blue Electroluminescence with CIEy~0.08. *J. Photochem. Photobiol. A Chem.* **2022**, *423*, 113600. [CrossRef]

218

18. Liu, H.; Kang, L.; Li, J.; Liu, F.; He, X.; Ren, S.; Tang, X.; Lv, C.; Lu, P. Highly Efficient Deep-Blue Organic Light-Emitting Diodes Based on Pyreno[4,5-d]Imidazole-Anthracene Structural Isomers. *J. Mater. Chem. C Mater.* **2019**, *7*, 10273–10280. [CrossRef]

19. Kim, S.K.; Yang, B.; Ma, Y.; Lee, J.H.; Park, J.W. Exceedingly Efficient Deep-Blue Electroluminescence from New Anthracenes Obtained Using Rational Molecular Design. *J. Mater. Chem.* **2008**, *18*, 3376–3384. [CrossRef]

20. Liu, X.; Li, J.; Qiu, X.; Ye, X.; Xu, L.; Hu, D. Highly Efficient Non-Doped Deep-Blue OLED with NTSC CIEy and Negligible Efficiency Roll-off Based on Emitter Possessing Hydrogen Bond and Hybridized Excited State. *Dye. Pigment.* **2022**, *200*, 110135. [CrossRef]

21. Kamino, B.A.; Chang, Y.L.; Lu, Z.H.; Bender, T.P. Phthalonitrile Based Fluorophores as Fluorescent Dopant Emitters in Deep-Blue OLEDs: Approaching the NTSC Standard for Blue. *Org. Electron.* **2012**, *13*, 1479–1485. [CrossRef]

22. Tan, Y.; Zhao, Z.; Shang, L.; Liu, Y.; Wei, C.; Li, J.; Wei, H.; Liu, Z.; Bian, Z.; Huang, C. A Novel Bipolar D–π–A Type Phenanthroimidazole/Carbazole Hybrid Material for High Efficiency Nondoped Deep-Blue Organic Light-Emitting Diodes with NTSC CIEy and Low Efficiency Roll-Off. *J. Mater. Chem. C Mater.* **2017**, *5*, 11901–11909. [CrossRef]

23. Lee, J.H.; Chen, C.H.; Lee, P.H.; Lin, H.Y.; Leung, M.K.; Chiu, T.L.; Lin, C.F. Blue Organic Light-Emitting Diodes: Current Status, Challenges, and Future Outlook. *J. Mater. Chem. C Mater.* **2019**, *7*, 5874–5888. [CrossRef]

24. Zhu, M.; Yang, C. Blue Fluorescent Emitters: Design Tactics and Applications in Organic Light-Emitting Diodes. *Chem. Soc. Rev.* **2013**, *42*, 4963–4976. [CrossRef]

25. Xu, H.; Chen, R.; Sun, Q.; Lai, W.; Su, Q.; Huang, W.; Liu, X. Recent Progress in Metal–Organic Complexes for Optoelectronic Applications. *Chem. Soc. Rev.* **2014**, *43*, 3259–3302. [CrossRef]

26. Du, C.; Lu, T.; Cheng, Z.; Chang, Y.; Liu, H.; Wang, J.; Wan, L.; Lv, Y.; Lu, P. Rational Molecular Design of Phenanthroimidazole-Based Fluorescent Materials towards High-Efficiency Non-Doped Deep Blue OLEDs. *J. Mater. Chem. C Mater.* **2022**, *10*, 14186–14193. [CrossRef]

27. Wang, Z.; Yang, T.; Dong, S.; Wen, Z.; Xu, H.; Miao, Y.; Wang, H.; Yu, J. Anthracene and Carbazole Based Asymmetric Fluorescent Materials for High-Efficiency Deep-Blue Non-Doped Organic Light Emitting Devices with CIEy = 0.06. *Dyes Pigment.* **2022**, *199*, 110047. [CrossRef]

28. Xing, L.; Zhu, Z.L.; He, J.; Qiu, Z.; Yang, Z.; Lin, D.; Chen, W.C.; Yang, Q.; Ji, S.; Huo, Y.; et al. Anthracene-Based Fluorescent Emitters toward Superior-Efficiency Nondoped TTA-OLEDs with Deep Blue Emission and Low Efficiency Roll-Off. *Chem. Eng. J.* **2021**, *421*, 127748. [CrossRef]

29. Wang, Z.; Zheng, C.; Liu, H.; Ou, X.; Zhang, X. Efficient and Stable Non-Doped Deep-Blue Organic Light Emitting Diode Based on an Anthracene Derivative. *Sci. China Chem.* **2011**, *54*, 666–670. [CrossRef]

30. Zheng, C.; Zhao, W.; Wang, Z.; Huang, D.; Ye, J.; Ou, X.; Zhang, X.; Lee, C.; Lee, S. Highly Efficient Non-Doped Deep-Blue Organic Light-Emitting Diodes Based on Anthracene Derivatives. *J. Mater. Chem.* **2010**, *20*, 1560–1566. [CrossRef]

31. Chem, J.M.; Kim, S.H.; Cho, I.; Sim, M.K.; Park, S.; Park, S.Y. Highly Efficient Deep-Blue Emitting Organic Light Emitting Diode Based on the Multifunctional Fluorescent Molecule Comprising Covalently Bonded Carbazole and Anthracene Moieties. *J. Mater. Chem.* **2011**, *21*, 9139–9148. [CrossRef]

32. Kotchapradist, P.; Prachumrak, N.; Tarsang, R.; Jungsuttiwong, S.; Keawin, T.; Sudyoadsuk, T.; Promarak, V. Pyrene-Functionalized Carbazole Derivatives as Non-Doped Blue Emitters for Highly Efficient Blue Organic Light-Emitting Diodes. *J. Mater. Chem. C* **2013**, *1*, 4916–4924. [CrossRef]

33. Figueira-Duarte, T.M.; Del Rosso, P.G.; Trattnig, R.; Sax, S.; List, E.J.W.; Mullen, K. Designed Suppression of Aggregation in Polypyrene: Toward High-Performance Blue-Light-Emitting Diodes. *Adv. Mater.* **2010**, *22*, 990–993. [CrossRef] [PubMed]

34. Figueira-Duarte, T.M.; Simon, S.C.; Wagner, M.; Druzhinin, S.I.; Zachariasse, K.A.; Müllen, K. Polypyrene Dendrimers. *Angew. Chem. Int. Ed.* **2008**, *47*, 10175–10178. [CrossRef]

35. Kumar, D.; Thomas, K.R.J.; Lin, C.C.; Jou, J.H. Pyrenoimidazole-Based Deep-Blue-Emitting Materials: Optical, Electrochemical, and Electroluminescent Characteristics. *Chem. Asian J.* **2013**, *8*, 2111–2124. [CrossRef]

36. Jou, J.; Chen, Y.; Tseng, J.; Wu, R.Z.; Shyue, J.J.; Thomas, K.J.; Kapoor, N.; Chen, C.T.; Lin, Y.P.; Wang, P.H.; et al. The Use of a Polarity Matching and High-Energy Exciton Generating Host in Fabricating Efficient Purplish-Blue OLEDs from a Sky-Blue Emitter. *J. Mater. Chem.* **2012**, *22*, 15500–15506. [CrossRef]

37. Hu, L.; Wu, Z.; Wang, X.; Ma, Y.; Guo, T.; Ying, L.; Peng, J.; Cao, Y. Deep-Blue Light-Emitting Polyfluorenes with Asymmetrical Naphthylthio-Fluorene as Chromophores. *J. Polym. Sci. A Polym. Chem.* **2019**, *57*, 171–182. [CrossRef]

38. Lee, J.Y.; Lee, K.H.; Kwon, Y.S.; Lee, J.Y.; Kang, S.; Yook, K.S.; Jeon, S.O.; Yoon, S.S. Highly Efficient Blue Organic Light-Emitting Diodes Based on 2-(Diphenylamino)Fluoren-7-Ylvinylarene Derivatives That Bear a Tert-Butyl Group. *Chem.-A Eur. J.* **2011**, *17*, 12994–13006. [CrossRef]

39. Lai, W.Y.; Zhu, R.; Fan, Q.L.; Hou, L.T.; Cao, Y.; Huang, W. Monodisperse Six-Armed Triazatruxenes: Microwave-Enhanced Synthesis and Highly Efficient Pure-Deep-Blue Electroluminescence. *Macromolecules* **2006**, *39*, 3707–3709. [CrossRef]

40. Lai, W.Y.; He, Q.Y.; Zhu, R.; Chen, Q.Q.; Huang, W. Kinked Star-Shaped Fluorene/ Triazatruxene Co-Oligomer Hybrids with Enhanced Functional Properties for High-Performance, Solution-Processed, Blue Organic Light-Emitting Diodes. *Adv. Funct. Mater.* **2008**, *18*, 265–276. [CrossRef]

41. You, A.; Be, M.A.Y.; In, I. High Efficiency Deep-Blue Organic Light- Emitting Diode with a Blue Dye in Low- Polarity Host. *Appl. Phys. Lett.* **2008**, *92*, 193314. [CrossRef]

42. Wang, L.; Jiang, Y.; Luo, J.; Zhou, Y.; Zhou, J.; Wang, J.; Pei, J.; Cao, Y. Highly Efficient and Color-Stable Deep-Blue Organic Light-Emitting Diodes Based on a Solution-Processible Dendrimer. *Adv. Mater.* **2009**, *21*, 4854–4858. [CrossRef] [PubMed]

43. Liu, B.; Yu, Z.W.; He, D.; Li, M.D.; Xie, W.F.; Tong, Q.X. Productive Harvesting of Triplet Excitons in Anthracene-Based Emitters toward High-Performance Deep-Blue Nondoped Organic Light-Emitting Diodes. *Mater. Today Chem.* **2022**, *23*, 100630. [CrossRef]

44. Chen, W.-C.; Yuan, Y.; Ni, S.-F.; Tong, Q.-X.; Wong, F.-L.; Lee, C.-S. Achieving Efficient Violet-Blue Electroluminescence with CIE y < 0.06 and EQE > 6% from Naphthyl-Linked Phenanthroimidazole-Carbazole Hybrid Fluorophores. *Chem. Sci.* **2017**, *8*, 3599–3608. [CrossRef] [PubMed]

45. Lee, J.; Jeong, C.; Batagoda, T.; Coburn, C.; Thompson, M.E.; Forrest, S.R. ARTICLE Hot Excited State Management for Long-Lived Blue Phosphorescent Organic Light-Emitting Diodes. *Nat. Commun.* **2017**, *8*, 15566. [CrossRef] [PubMed]

46. Yiu, T.C.; Gnanasekaran, P.; Chen, W.-L.; Lin, W.-H.; Lin, M.-J.; Wang, D.-Y.; Lu, C.-W.; Chang, C.-H.; Chang, Y.J. Multifaceted Sulfone–Carbazole-Based D–A–D Materials: A Blue Fluorescent Emitter as a Host for Phosphorescent OLEDs and Triplet–Triplet Annihilation Up-Conversion Electroluminescence. *ACS Appl. Mater. Interfaces* **2022**, *15*, 1748–1761. [CrossRef]

47. Lin, S.L.; Chan, L.H.; Lee, R.H.; Yen, M.Y.; Kuo, W.J.; Chen, C.T.; Jeng, R.J. Highly Efficient Carbazole-π-Dimesitylborane Bipolar Fluorophores for Nondoped Blue Organic Light-Emitting Diodes. *Adv. Mater.* **2008**, *20*, 3947–3952. [CrossRef]

48. Xin, J.; Li, Z.; Liu, Y.; Liu, D.; Zhu, F.; Wang, Y.; Yan, D. High-Efficiency Non-Doped Deep-Blue Fluorescent Organic Light-Emitting Diodes Based on Carbazole/Phenanthroimidazole Derivatives. *J. Mater. Chem. C* **2020**, *8*, 10185–10190. [CrossRef]

49. Yang, H.; Peng, X.; Cao, C.; Wu, L.; Chen, N.; Zhang, X.; Xie, W.; Tong, Q.; Wu, Z. A Deep Blue Fluorescent Emitter Functioning as Host Material in Highly Efficient Phosphorescent and Hybrid White Organic Light-Emitting Devices. *Org. Electron.* **2020**, *85*, 105848. [CrossRef]

50. Xu, J.; Liu, H.; Li, J.; Zhao, Z.; Tang, B.Z. Multifunctional Bipolar Materials Serving as Emitters for Efficient Deep-Blue Fluorescent OLEDs and as Hosts for Phosphorescent and White OLEDs. *Adv. Opt. Mater.* **2021**, *9*, 2001840. [CrossRef]

51. Singh, G.; Bhalla, V.; Kumar, M. Carbazole-Functionalized Polyphenylene-Decorated Solid State Emissive D–A–D Molecules: Reduced Donor–Acceptor Interaction and Enhanced Emission in the Solid State. *Phys. Chem. Chem. Phys.* **2015**, *17*, 22079–22089. [CrossRef] [PubMed]

52. Pereira, D.D.S.; Monkman, A.P. Methods of analysis of organic light emitting diodes. *Disp. Imaging* **2017**, *2*, 323–337.

53. Inoue, S.; Minemawari, H.; Tsutsumi, J.; Chikamatsu, M.; Yamada, T.; Horiuchi, S.; Tanaka, M.; Kumai, R.; Yoneya, M.; Hasegawa, T. Effects of Substituted Alkyl Chain Length on Solution-Processable Layered Organic Semiconductor Crystals. *Chem. Mater.* **2015**, *27*, 3809–3812. [CrossRef]

54. Yang, X.; Xu, X.; Zhou, G. Recent advances of the emitters for high performance deep-blue organic light-emitting diodes. *J. Mater. Chem. C* **2015**, *3*, 913–9440. [CrossRef]

55. Tian, X.; Sheng, J.; Zhang, S.; Xiao, S.; Gao, Y.; Liu, H.; Yang, B. A Novel Deep Blue LE-Dominated HLCT Excited State Design Strategy and Material for OLED. *Molecules* **2021**, *26*, 4560. [CrossRef]

56. Hedley, G.J.; Ruseckas, A.; Samuel, I.D.W. Ultrafast Luminescence in Ir(Ppy)3. *Chem. Phys. Lett.* **2008**, *450*, 292–296. [CrossRef]

57. Wang, P.; Zhao, S.; Xu, Z.; Qiao, B.; Long, Z.; Huang, Q. The Electroluminescence Mechanism of Solution-Processed TADF Emitter 4CzIPN Doped OLEDs Investigated by Transient Measurements. *Molecules* **2016**, *21*, 1365. [CrossRef]

58. Yook, K.P.; Lee, J.Y. Small Molecule Host Materials for Solution Processed Phosphorescent Organic Light-Emitting Diodes. *Adv. Mater.* **2014**, *26*, 4218–4233. [CrossRef]

59. Krucaite, G.; Grigalevicius, S. 2,7(3,6)-Diaryl(arylamino)-substituted Carbazoles as Components of OLEDs: A Review of the Last Decade. *Materials* **2021**, *14*, 6754. [CrossRef]

60. Romero, B.; Schaer, M.; Leclerc, M.; Ades, D.; Siove, A.; Zuppiroli, L. The role of carbazole in organic light-emitting devices. *Synth. Met.* **1996**, *80*, 271–277. [CrossRef]

61. Vaitkeviciene, V.; Grigalevicius, S.; Grazulevicius, J.; Jankauskas, V.; Syromyatnikov, V. Hole-transporting [3,3']bicarbazolyl-based polymers and well-defined model compounds. *Eur. Polymer J.* **2006**, *42*, 2254–2260. [CrossRef]

Article

Bicarbazole-Benzophenone-Based Twisted Donor-Acceptor-Donor Derivatives as Blue Emitters for Highly Efficient Fluorescent Organic Light-Emitting Diodes

Dovydas Blazevicius [1,†], Iram Siddiqui [2,†], Prakalp Gautam [2], Gintare Krucaite [1], Daiva Tavgeniene [1], Mangey Ram Nagar [2], Krishan Kumar [3], Subrata Banik [4], Jwo-Huei Jou [2,*] and Saulius Grigalevicius [1,*]

1 Department of Polymer Chemistry and Technology, Kaunas University of Technology, Radvilenu Plentas 19, LT50254 Kaunas, Lithuania
2 Department of Materials Science and Engineering, National Tsing Hua University, No. 101, Section 2, Guangfu Rd., East District, Hsinchu 30013, Taiwan
3 School of Chemical Sciences, Indian Institute of Technology—Mandi, Kamand 175005, Himachal Pradesh, India
4 Department of Chemistry, School of Chemical and Biotechnology, SASTRA Deemed University, Thanjavur 613401, Tamil Nadu, India
* Correspondence: jjou@mx.nthu.edu.tw (J.-H.J.); saulius.grigalevicius@ktu.lt (S.G.)
† These authors contributed equally to this work.

Abstract: This paper delves into the development of a group of twisted donor-acceptor-donor (D-A-D) derivatives incorporating bicarbazole as electron donor and benzophenone as electron acceptor for potential use as blue emitters in OLEDs. The derivatives were synthesized in a reaction of 4,4'-difluorobenzophenone with various 9-alkyl-9'H-3,3'-bicarbazoles. The materials, namely, **DB14**, **DB23**, and **DB29**, were designed with different alkyl side chains to enhance their solubility and film-forming properties of layers formed using the spin-coating from solution method. The new materials demonstrate high thermal stabilities with decomposition temperatures >383 °C, glass transition temperatures in the range of 95–145 °C, high blue photoluminescence quantum yields (>52%), and short decay times, which range in nanoseconds. Due to their characteristics, the derivatives were used as blue emitters in OLED devices. Some of the OLEDs incorporating the **DB23** emitter demonstrated a high external quantum efficiency (EQE$_{max}$) of 5.3%, which is very similar to the theoretical limit of the first-generation devices.

Keywords: donor-acceptor-donor (D-A-D) derivatives; blue organic light-emitting diode (OLED); high efficiency; blue emission; thermal analysis

1. Introduction

Organic light-emitting diodes (OLEDs) have ushered in a technological revolution with their remarkable impact on diverse sectors of our daily lives. These versatile devices, known for their outstanding display and lighting capabilities, have become indispensable components in different technologies including smartphones, tablets, televisions, and automotive applications [1–6]. OLEDs are steadily advancing in terms of their performance, longevity, and production processes [7–9]. To provide displays and energy-efficient lighting solutions, blue OLEDs are an essential technological component. Despite their significance, the development of blue OLEDs has posed persistent challenges owing to the inherent instability of blue-emitting materials [10–12]. Recent research efforts have resulted in notable progress in the domain of promising host derivatives for the blue devices, offering promising avenues to overcome the efficiency limitations and reaching high internal quantum efficiency [13–16]. Simultaneously, scientists and engineers have made noteworthy strides in the creation of novel organic emitters tailored for blue OLEDs [17–19]. These emitters

were engineered to deliver high efficiency, exceptional color purity, and a narrow emission bandwidth, addressing the demands of modern OLED technology [20–23].

OLED technologies have been generally divided into three generations, depending on the characteristics of the used emitting material, which determines the properties of the diode. First-generation devices use fluorescent emitters [24], second-generation devices use phosphorescent emitters, and third-generation OLEDs are from materials which has a thermally activated delayed fluorescence (TADF) effect. Upon electrical excitation, only 25% of formed excitons in first-generation fluorescent OLEDs are singlet and emissive. The other 75% are of triplet multiplicity and are not involved in light emission [25,26]. Recently, we published carbazole-diphenyl sulfone-carbazole (D-A-D) bipolar blue light emitting materials for first-generation OLEDs. One device outperformed others by showing a peak external quantum efficiency (EQE_{max}) of 4.0% for deep-blue emission ($CIE_y = 0.09$) [27].

In this research article, we present a group of twisted D-A-D compounds incorporating bicarbazole and benzophenone fragments that have also been developed for potential use as blue-emitting layers for the OLEDs. These derivatives include 4,4′-bis(9′-butyl-[3,3′]-bicarbazol-9-yl)benzophenone (**DB14**), 4,4′-bis(9′-{2-ethylhexyl}-[3,3′]- bicarbazol-9-yl)benzophenone (**DB23**), and 4,4′-bis(9′-octyl-[3,3′]-bicarbazol-9-yl)benzophenone (**DB29**). The compounds were designed with different alkyl side chains, which determine the film-forming and solubility properties of the blue emitters. Some of the OLED devices based on the bicarbazole and benzophenone fragments containing D-A-D emitters demonstrated promising performance as compared with the carbazole-diphenyl sulfone-carbazole-based emitters. Specifically, one device, producing a greenish-blue emission with a CIE_y coordinate of (0.22, 0.22), exhibited an EQE_{max} of 5.3%, which is very similar to the theoretical limit of the first-generation devices [10].

2. Experimental Section

2.1. Instruments

Thermogravimetric analysis (TGA) of all compounds was carried out using a TGAQ50 instrument (Verder Scientific Haan, Haan, Germany). Both TGA and differential scanning calorimetry (DSC) profiles were recorded under a nitrogen atmosphere at a controlled heating rate of 10 °C/min. For differential scanning calorimetry (DSC), measurements were carried out on Bruker Reflex II thermos-system (Bruker, Berlin, Germany). UV–visible spectroscopy was carried out using an HP-8453 diode array spectrometer (Agilent Technology Inc., Hachioji, Tokyo, Japan) to capture the absorption spectra of the compounds. Moreover, the Tauc plot was generated using the absorbance wavelength data. Photoluminescence (PL) spectra were captured utilizing the Aminco-Bowman Series 2 luminescence spectrometer (Agilent Technology Inc., Hachioji, Tokyo, Japan). For low-temperature PL (LTPL), a Hitachi F-7000 fluorescence spectrophotometer (Hitachi High-Tech, Tokyo, Japan) was employed. The LTPL measurements were performed at a temperature of 77 K to ascertain the singlet energy of the compounds. Cyclic voltammetry (CV) experiments were conducted using the CH instrument CH1604A potentiostat (Annatech Co., Ltd., Taipei, Taiwan). Time-resolved photoluminescence measurements were executed using an Edinburgh instrument spectrometer FLS980 (Edinburgh Instruments Ltd., Livingston, UK) to accurately determine the decay time of the compounds.

2.2. Synthesis and Structure Characterization of the Materials

Carbazole (**1**), benzylbromide, bromoethane, 1-bromobutane, 1-bromohexane, 2-ethylhexylbromide, 1-bromooctane, ferric chloride ($FeCl_3$), potassium hydroxide (KOH), K_2CO_3, NaH, sodium sulphate (Na_2SO_4), 4,4′-difluorobenzophenone, chloroform, dimethyl formamide (DMF), and tetrahydrofuran (THF) were purchased from Aldrich and used as received.

3,3′-Bicarbazole (**2**) was prepared by oxidation of carbazole using $FeCl_3$ as it was reported in the literature [28].

9-Butyl-9′H-3,3′-bicarbazole (**3**): 1-bromobutane (0.82 g, 6.0 mmol) was added to a stirred solution of 3,3′-bicarbazole (**2**) (2.00 g, 6.0 mmol) in 50 mL of tetrahydrofuran. The reaction mixture was refluxed, and then potassium carbonate (1.66 g, 12.0 mmol) and powdered KOH (2.02 g, 36.1 mmol) were added stepwise. The resulting mixture reacted for 4 h. After TLC test, the inorganic materials were filtered off and the organic derivatives were purified using silica gel column chromatography. A mixture of tetrahydrofuran and hexane (vol. ratio 1:5) was used as an eluent. Yield: 0.96 g (41%) of yellowish material. ^{1}H NMR (400 MHz, CDCl$_3$, δ, m.d.): 8.29 (s, 2H), 8.11–8.06 (m, 2H), 7.73–7.67 (m, 2H), 7.41–7.32 (m, 6H), 7.17 (t, 2H, J = 7.2 Hz), 4.29 (t, 2H, J = 7.2 Hz), 1.79 (quint, 2H, J = 7.2 Hz), 1.38–1.29 (m, 2H), 0.87 (t, 3H, J = 7.2 Hz). ^{13}C NMR (400 MHz, CDCl$_3$, δ, m.d.): 139.64, 138.56, 133.33, 125.94, 125.86, 125.72, 125.57, 124.00, 123.61, 123.43, 123.08, 120.51, 120.46, 119,51, 119.03, 119.00, 118.92, 118.82, 110.83, 110.77, 108.95, 108.86, 42.99, 31.25, 20.65, 13.97. MS (APCI$^+$, 20 V): 339.10 ([M + H], 100%).

9-(2-Ethylhexyl)-9′H-3,3′-bicarbazole (**4**) was prepared by a similar method which was published earlier [27].

9-Octyl-9′H-3,3′-bicarbazole (**5**): 1-Bromooctane (1.16 g, 6.0 mmol) was added to a stirred solution of 3,3′-bicarbazole (**2**) (2.00 g, 6.0 mmol) in 50 mL of tetrahydrofuran. The mixture was heated to reflux, and then potassium carbonate (1.66 g, 12.0 mmol) and powdered KOH (2.02 g, 36.2 mmol) were added stepwise. The resulting mixture reacted for 4 h. After TLC test, the inorganic compounds were filtered off and the organic materials were separated using silica gel column chromatography. A mixture of tetrahydrofuran and hexane (vol. ratio 1:7) was used as an eluent. Yield: 1.15 g (43%) of yellowish material. ^{1}H NMR (400 MHz, CDCl$_3$, δ, m.d.): 8.45 (d, 2H, J = 8.0 Hz), 8.25–8.20 (m, 2H), 8.04 (s, 1H), 7.87 (d, 1H, J = 8.0 Hz), 7.83 (dd, 1H, J_1 = 8.4 Hz, J_2 = 1.6 Hz), 7.56–7.50 (m, 3H), 7.48 (d, 3H, J = 7.2 Hz), 7.31 (t, 2H, J = 8.0 Hz), 4.37 (t, 2H, J = 7.0 Hz), 1.95 (qu, 2H, J = 7.3 Hz), 1.48–1.30 (m, 10H), 0.92 (t, 3H, J = 7.0 Hz). ^{13}C NMR (400 MHz, CDCl$_3$, δ, m.d.): 140.94, 140.02, 139.62, 138.53, 133.30, 125.94, 125.85, 125.70, 125.56, 124.00, 123.61, 123.42, 123.08, 120.49, 120.45, 120.40, 119.51, 119.00, 118.92, 118.79, 110.80, 110.74, 108.92, 108.83, 43.25, 31.85, 29.45, 29.23, 29.08, 27.39, 22.65, 14.12. MS (APCI$^+$, 20 V): 444.67 ([M + H], 100%).

4,4′-Bis(9′-butyl-[3,3′]-bicarbazol-9-yl)benzophenone (**DB14**): 9-Butyl-9′H-3,3′-bicarbazole (**3**) (0.40 g, 1.0 mmol) and NaH (0.10 g, 4.1 mmol) were stirred in 6 mL of DMF at room temperature under nitrogen for 20 min. Then, 4,4′-difluorobenzophenone (0.11 g, 0.5 mmol) was added to the reaction, and the resulting mixture was stirred at 150 °C under nitrogen for 4 h. After TLC control, the reaction mixture was cooled and quenched by the addition of ice water. The product was extracted using chloroform. The combined extract was dried over anhydrous Na$_2$SO$_4$. The crude product was purified using silica gel column chromatography using the mixture of THF and hexane (vol. ratio 1:3) as an eluent. Yield: 0.38 g (77%) of yellow amorphous material. T_g = 145 °C (DSC). ^{1}H NMR (400 MHz, CDCl$_3$, δ, m.d.): 8.51–8.41 (m, 4H), 8.30–8.23 (m, 6H), 7.91–7.83 (m, 8H), 7.71 (d, 2H, J = 8.4 Hz), 7.65 (d, 2H, J = 8.4 Hz), 7.57–7.38 (m, 10H), 7.32–7.29 (m, 4H), 4.42–4.36 (m, 4H), 1.98–1.91 (m, 4H), 1.51–1.45 (m, 4H), 1.01 (t, 6H, J = 7.4 Hz). MS (APCI$^+$, 20 V): 954.8 ([M + H], 100%).

4,4′-Bis(9′-[2-ethylhexyl]-[3,3′]-bicarbazol-9-yl)benzophenone (**DB23**): 9-[2-Ethylhexyl]-9′H-3,3′-bicarbazole (**4**) (0.40 g, 0.9 mmol) and NaH (0.10 g, 4.1 mmol) were stirred in 6 mL of DMF at room temperature under nitrogen for 20 min. Then, 4,4′-difluorobenzophenone (0.10 g, 0.5 mmol) was added to the reaction, and the resulting mixture was stirred at 150 °C under nitrogen for 4 h. After TLC control, the reaction mixture was cooled and quenched by the addition of ice water. The product was extracted using chloroform. The combined extract was dried over anhydrous Na$_2$SO$_4$. The crude product was purified using silica gel column chromatography using the mixture of THF and hexane (vol. ratio 1:5) as an eluent. Yield: 0.40 g (83%) of yellow amorphous material. T_g = 104 °C (DSC). ^{1}H NMR (400 MHz, CDCl$_3$-, δ, m.d.): 8.51–8.45 (m, 4H), 8.31–8.22 (m, 6H), 7.91–7.79 (m, 8H), 7.76–7.70 (m, 4H), 7.66–7.36 (m, 14H), 4.27–4.23 (m, 4H), 1.90–1.87 (m, 2H), 1.47–1.29 (m, 16H), 1.00–0.90 (m, 12H). ^{13}C NMR (400 MHz, CDCl$_3$, δ, m.d.): 195.67, 141.42, 140.70, 140.22, 135.79, 132.79, 131.96, 129.44, 128.17, 127.18, 126.36, 126.13, 125.75, 125.49, 125.45, 124.56, 124.19, 123.42,

223

122.98, 120.77, 120.41, 119.02, 118.92, 118.82, 118.77, 110.08, 109.95, 109.27, 109.13, 47.57, 39.50, 31.06, 28.89, 24.45, 23.10, 14.09, 10.96. MS (APCI$^+$, 20 V): 1066.55 ([M + H], 100%).

4,4′-Bis(9′-octyl-[3,3′]-bicarbazol-9-yl)benzophenone (**DB29**): 9-Octyl-9′H-3,3′-bicarbazole (**5**) (0.40 g, 0.9 mmol) and NaH (0.10 g, 4.1 mmol) were stirred in 6 mL of DMF at room temperature under nitrogen for 20 min. Then, 4,4′-difluorobenzophenone (0.10 g, 0.5 mmol) was added to the reaction and the resulting mixture was stirred at 150 °C under nitrogen for 4 h. After TLC control, the reaction mixture was cooled and quenched by the addition of ice water. The product was extracted using chloroform. The combined extract was dried over anhydrous Na$_2$SO$_4$. The crude product was purified using silica gel column chromatography using the mixture of THF and hexane (vol. ratio 1:5) as an eluent. Yield: 0.44 g (92%) of yellow amorphous material. T$_g$ = 95 °C (DSC). ^{1}H NMR (400 MHz, CDCl$_3$-, δ, m.d.): 8.50 (dd, 4H, J_1 = 15.2 Hz, J_2 = 1.6 Hz), 8.30 (d, 2H, J = 7.6 Hz), 8.27–8.24 (m, 6H), 7.91–7.86 (m, 8H), 7.71 (d, 2H, J = 8.4 Hz), 7.66 (d, 2H, J = 8.0 Hz), 7.56–7.47 (m, 8H), 7.42 (t, 2H, J = 7.2 Hz), 7.33–7.29 (m, 2H), 4.38 (t, 4H, J = 7.2 Hz), 1.99–1.92 (m, 4H), 1.48–1.30 (m, 20H), 0.92 (t, 6H, J = 6.6 Hz). ^{13}C NMR (400 MHz, CDCl$_3$, δ, m.d.): 194.51, 142.04, 140.96, 140.71, 139.74, 139.28, 135.78, 135.41, 132.84, 131.97, 126.38, 126.34, 126.15, 125.79, 125.49, 124.57, 124.20, 123.48, 123.03, 120.78, 120.66, 120.50, 119.02, 118.85, 110.09, 109.97, 109.00, 108.87, 43.26, 31.85, 29.45, 29.23, 29.08, 27.39, 22.65, 14.12. MS (APCI$^+$, 20 V): 1067.78 ([M + H], 100%).

2.3. Device Fabrication

OLED devices were fabricated utilizing a pre-sputtered ITO glass substrate. The substrate underwent a thorough cleaning process, including 30 min treatments with acetone and isopropyl alcohol (IPA) at elevated temperatures of 50 and 60 °C. Subsequently, the substrates were transferred to a UV chamber that was preheated, and exposed to UV light for 10 min. The deposition of layers occurred within a glove box, maintaining an inert atmosphere. The hole injection layer (PEDOT:PSS) was spin-coated onto the substrates for 20 s at 4000 rpm, followed by a 10 min heating step at 130 °C. Subsequently, the cooled substrates were subjected to a 20-s spin-coating process at 2500 rpm for the emissive layer. The subsequent stages encompassed the thermal evaporation of the electron-injecting/transporting layer and aluminum cathode within a vacuum of 1.33×10^{-4} Pa. The substrates remained under vacuum conditions within a mini chamber in the glove box to preserve their quality until individual testing. All testing protocols were executed in a completely dark environment under ambient conditions. The CS-100A luminescence spectrophotometer was employed for recording the current density–voltage–luminance (J-V-L) characteristics, while the PR-655 spectrophotometer was used for power efficacy–luminance–current characteristics. A Keithley voltmeter was utilized to measure the current–voltage (I-V) characteristics. The device area was determined to be 0.09 cm^2. The EQE of the devices was computed following the methodology outlined in the relevant literature, meticulously adhering to this approach during the testing and analysis procedures [20].

3. Results and Discussion

A three-step synthetic pathway was employed to synthesize the bicarbazole-based materials, as is demonstrated in Scheme 1.

3,3′-Bicarbazole (**2**) was synthesized through the oxidation of 9H-carbazole (**1**) using iron (III) chloride, as is described in the ESI file. Various 9-alkyl-9′H-3,3′-bicarbazoles (**3–5**) were prepared via N-alkylation reactions between a bicarbazole and the corresponding alkyl bromides, utilizing potassium hydroxide and potassium carbonate in tetrahydrofuran (THF). The next step involved the nucleophilic aromatic substitution of partially alkylated bicarbazole with 4,4′-difluorobenzophenone. This reaction was conducted in DMF, employing sodium hydride as a base, yielding the desired materials. This multi-step process resulted in the successful synthesis of the targeted bicarbazole-based compounds. The values of glass transition temperatures are influenced by the distinct alkyl chains in the chemical structures of materials **DB14**, **DB23**, and **DB29**. The derivative **DB14**, character-

ized by the shortest butyl alkyl chain, exhibited the highest glass transition temperature at 145 °C. The elongation of the alkyl chain led to decreased but still suitable T_g values for device forming, with **DB23** and **DB29** showing temperatures of 105 °C and 95 °C, respectively, as verified by DSC.
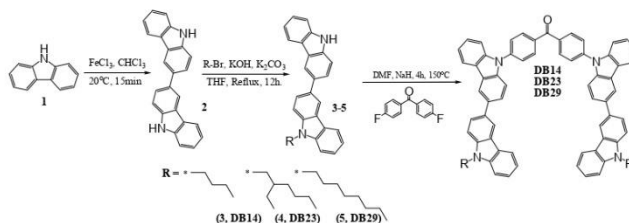
Scheme 1. Synthetic pathway of **DB14**, **DB23**, and **DB29**.

3.1. Material Characteristics

3.1.1. DFT Calculations

Theoretical calculations were carried out to establish a relation between the electrochemical properties and geometries of the synthesized compounds. All calculations were carried out using Gaussian09.0D [29]. The polarizable continuum model, which Gaussian09 uses by default, was employed for the solvent adjustments [30]. In all compounds, HOMO was found to be located over the peripheral carbazole units, while LUMO was found to be spread over the central benzophenone unit. The HOMO/LUMO distributions ensure that the present molecules have donor-acceptor characteristics, in which carbazole units act as donor units and benzophenone acts as an acceptor unit. The values of HOMO/LUMO were theoretically calculated to be −5.39/−2.28, −5.40/−2.28, and −5.40/−2.26 eV for **DB14**, **DB23**, and **DB29**, respectively. Further, the singlet and triplet energies were very crucial for the designed emitters to evaluate their potential for optoelectronic devices; hence, the singlet and triplet energy levels of all synthesized compounds were established through TD-DFT calculations. All compounds showed high triplet energies of about 2.65 eV, which indicated that these molecules have the potential to be used in the emitting layer of OLEDs. The HOMO/LUMO and singlet/triplet energies of **DB23** are shown in Figure 1. Similarly, the theoretical results for **DB13** and **DB29** are presented in Figure S1 of ESI. All theoretical results are also tabulated in Table 1.

3.1.2. Photophysical Properties

The derivatives **DB14**, **DB23**, and **DB29** exhibit substantial photoluminescence quantum yields (PLQY) of 55.6, 52.0, and 55.5%, respectively. The PLQY values are summarized in Table 1. The UV-absorption bands of these compounds are demonstrated in Figure 2. The materials were investigated using tetrahydrofuran (THF) solvent under typical conditions. Notably, all compounds displayed primary and secondary absorption peaks consistently at around 375 and 400 nm. The UV absorption wavelength and intensity were also used to construct the Tauc plots for the materials (Figure 2) using the following values: $(\alpha \times h\nu)^{1/2}$ for the x-axis and $h\nu$ for the y-axis, where α is the intensity and $h\nu$ is the energy ($h\nu = 1240/\text{wavelength}$). The Tauc plots demonstrated the bandgaps of the investigated compounds, which are 3.05 eV for **DB14**, 3.08 eV for **DB23**, and 3.02 eV for **DB29** (Table 1).
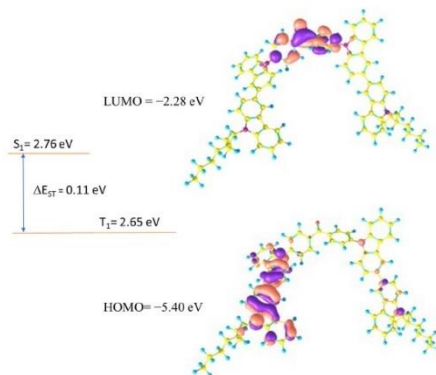
Figure 1. Electron density contours of FMO and theoretically calculated electronic properties of the compound **DB23**.

Table 1. Optoelectronic and thermal characteristics of the derivatives **DB14**, **DB23**, and **DB29**.

Emitter	λ_{ex} (nm)	λ_{em} (nm)	E_g (eV)	Φ (%)	Decay (ns)	Homo (eV)		Lumo (eV)		S_1 (eV)		T_1 (eV)		ΔE_{ST}		T_d (°C)	T_g (°C)
						Th.	Ca.	Th.	Ca.	Th.	Ca.	Th.	Ca.	Th.	Ca.		
DB14	366.7, 383.2	401.7	3.05	55.6	3.40	−5.39	−5.70	−2.28	−2.65	2.76	3.32	2.65	2.83	0.11	0.49	462	145
DB23	380.0, 393.8	412.8	3.08	52.0	2.67	−5.40	−5.63	−2.28	−2.55	2.76	3.19	2.65	2.84	0.11	0.35	383	104
DB29	382.7, 411.7	413.3	3.02	55.5	3.57	−5.40	−5.66	−2.26	−2.64	2.78	3.22	2.66	2.73	0.12	0.49	384	95

λ_{ex}: excitation wavelength; λ_{em}: emission wavelength; E_g: bandgap; Φ: photoluminescence yield; S_1: singlet energy; T_1: triplet energy; ΔE_{ST}: singlet-triplet energy gap; T_d: decomposition temperature; T_g: glass transition temperature; Th.: theoretical value; Ca.: calculated value.
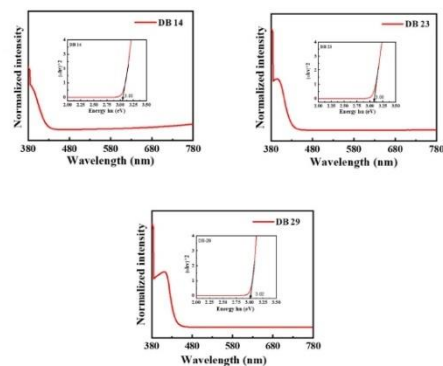
Figure 2. Ultraviolet-visible absorbance spectra and Tauc plots (inset) of the compounds **DB14**, **DB23**, and **DB29**.

For the measurements of photoluminescence, the maxima absorbance wavelengths were employed as the wavelengths for excitation, which are shown in Table 1. In Figure 3, the photoluminescence (PL) spectra of the derivatives **DB14**, **DB23**, and **DB29** are depicted. They show very similar emission bands for all compounds with maxima wavelengths of approximately 400 nm due to the similar electronic structure of the derivatives.
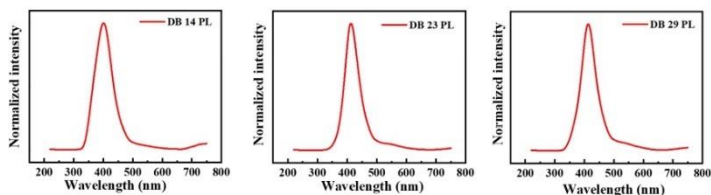

Figure 3. Photoluminescence (PL) spectra of the derivatives **DB14**, **DB23**, and **DB29**.

Moreover, to establish the triplet energies of the potential emitters, photoluminescence (LTPL) spectra at low temperature were also recorded. Notably, the compounds **DB14**, **DB23**, and **DB29** exhibited elevated triplet energies of 2.83, 2.84, and 2.73 eV, respectively, as visually represented in Figure 4. These specific characteristics are also included in Table 1 for reference.
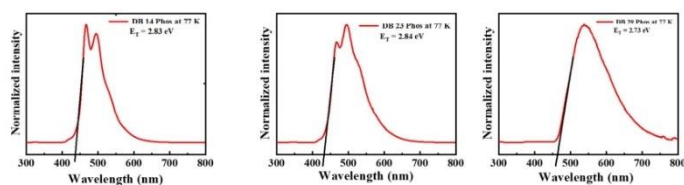
Figure 4. LTPL spectra of the derivatives **DB14**, **DB23**, and **DB29** at 77 K of the compounds.

In Figure 5, the time-resolved photoluminescence (TRPL) analysis illustrates the values of the decay times for the **DB14**, **DB23**, and **DB29** compounds, which were 3.40, 2.67, and 3.57 ns, respectively. It could be stated that all lifetime curves of the materials demonstrate a nanosecond-scale component. Usually, the decay lifetime of fluorescent emitters ranges in picoseconds. However, our materials demonstrate decay in the nanoscale, also indicating a possible use of triplet energy levels.
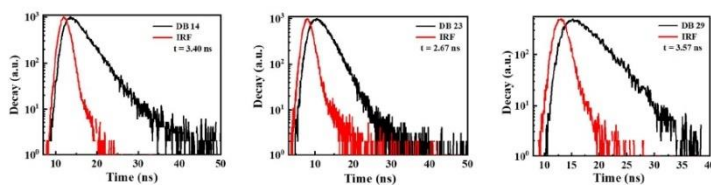

Figure 5. TRPL spectra for the transient decay of the materials **DB14**, **DB23**, and **DB29**. IRF is the instrument response function, which is measured as a control parameter before and after each measurement.

227

3.1.3. Electrochemical Properties

The electrochemical attributes of the **DB14**, **DB23**, and **DB29** compounds were assessed through cyclic voltammetry (CV) measurements, which are depicted in Figure 6. By using the obtained oxidation onset values, the HOMO levels were calculated using Equation (1) and the LUMO levels were calculated using Equation (2), according to the method described in the literature [31,32]:

$$E_{HOMO} = -[4.4 + E^{ox}_{onset}] \tag{1}$$

$$E_{LUMO} = E_{HOMO} + E_g \tag{2}$$
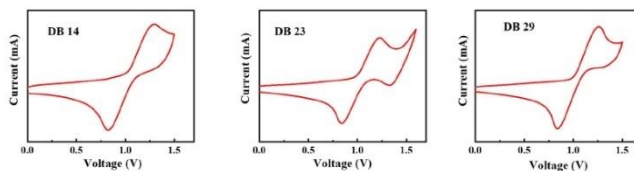
Figure 6. Curves of CV scans of the molecules **DB14**, **DB23**, and **DB29**.

The calculated HOMO levels were -5.70, -5.63, and -5.66 eV, while the corresponding LUMO levels were -2.65, -2.55, and -2.64 eV for the **DB14**, **DB23**, and **DB29** compounds, respectively. These values along with the earlier bandgap measurements are presented in Table 1. It could be stated that the HOMO and LUMO levels of the compounds are found to be suitable for blue-emitting layers using the earlier-mentioned CBP host material.

3.1.4. Thermal Properties

The characteristics of thermal stability of the materials **DB14**, **DB23**, and **DB29** were examined in a nitrogen atmosphere. The curves of the thermogravimetric analysis (TGA) are presented in Figure 7. For **DB14**, having the shortest alkyl chains, the temperature at which 5% weight loss occurred, i.e., the decomposition temperature (T_d), was obtained at 462 °C during heating. The materials **DB23** and **DB29**, featuring lengthier aliphatic substitutions, exhibited a lower thermal stability, with T_d values of 383 °C and 384 °C, respectively. These findings demonstrate that the new materials have very good thermal stability as emitting materials for application in OLED devices.
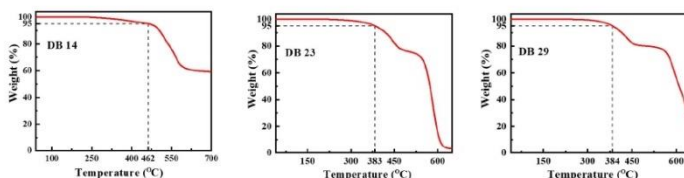

Figure 7. Curves of the TGA measurements of the materials **DB14**, **DB23**, and **DB29**.

The DSC thermograms of second heating for the **DB14**, **DB23**, and **DB29** compounds are displayed in Figure 8. Notably, upon analyzing the second heating curves, it becomes evident that the novel derivatives exhibit glass transition temperatures (T_g) that directly correlate with the length of their alkyl substituents. For instance, the **DB14** material with the shortest butyl substitution has the highest glass transition temperature of 145 °C. This trend persists also for compounds featuring more extended alkyl groups: the **DB23** and **DB29** derivatives with 2-ethylhexyl and octyl substitutions, respectively, display glass transition

228

temperatures of 104 °C and 95 °C. Hence, these results indicated that the developed compounds demonstrate a high thermal stability and are suitable for optoelectronic devices. The comprehensive T_d and glass transition temperature (T_g) values are compiled in Table 1.
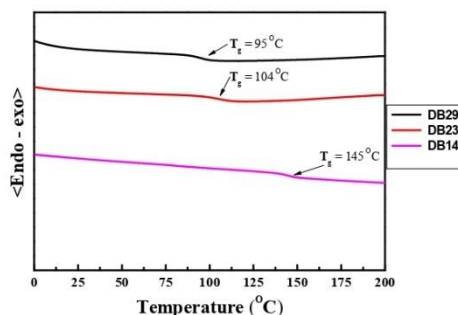

Figure 8. DSC curves of second heating of the materials **DB14**, **DB23**, and **DB29**.

3.1.5. Electroluminescent Properties

The schematic energy level diagram in Figure 9 illustrates the configuration of OLED devices prepared in this study. These devices incorporated the emitters **DB14**, **DB23**, and **DB29** doped within a CBP host matrix. The device structure comprised ITO/PEDOT:PSS/host CBP: emitter **DB14**, **DB23**, or **DB29** (5, 10, or 15wt.%)/TPBi/LiF/Al.
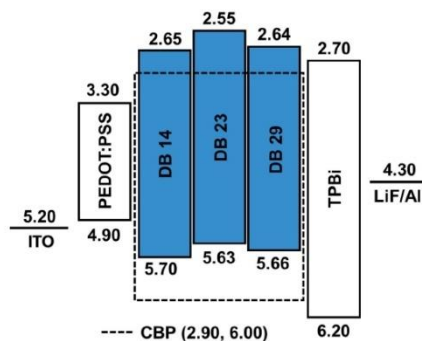
Figure 9. Energy-level diagram of the OLEDs using the emitters **DB14**, **DB23**, and **DB29** doped in CBP host.

The electroluminescence (EL) properties of the devices using the new emitting materials dispersed within the CBP host are shown in Figures 10–12. The corresponding characteristics for each emitter are also detailed in Table 2. Within each figure, various aspects are illustrated: (a) EL spectra, (b) current density–voltage characteristics, (c) luminance–voltage characteristics, (d) power efficacy–luminance characteristics, and € current efficacy–luminance characteristics.
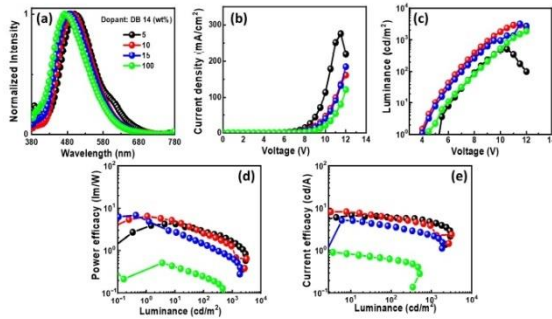
229

Figure 10. EL properties of the devices using the emitter **DB14** doped in CBP host: (**a**) EL spectra, (**b**) current density–voltage, (**c**) luminance–voltage, (**d**) power efficacy–luminance, and (**e**) current efficacy–luminance characteristics.
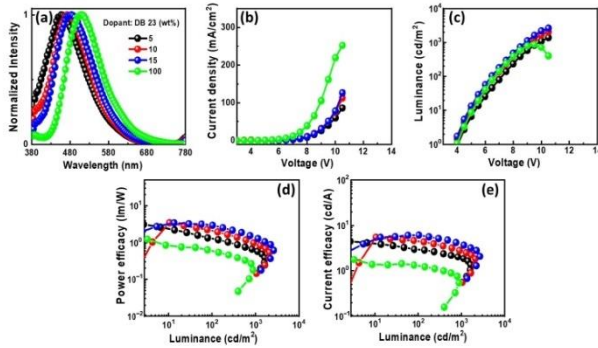

Figure 11. The EL properties of the OLEDs using emitting material **DB23** doped in CBP host: (**a**) EL spectra, (**b**) current density–voltage, (**c**) luminance–voltage, (**d**) power efficacy–luminance, and (**e**) current efficacy–luminance characteristics.

In Figure 10a, the EL spectra of the OLEDs with **DB14** exhibit peaks around 480 nm, indicating blue emission. The presence of sole peaks implies the successful energy transfer between host and guest. The emission wavelength in the EL of the devices undergoes a shift when compared with the PL spectra of the **DB14** emitter, indicating the influence of the CBP host on emission. An evident emission spectrum of the emitter becomes apparent with an increase in the concentration of the **DB14** dopant. Notably, both non-doped and doped devices exhibit very similar EL emission peaks. In Figure 10b–e, the current density–luminance–voltage and power efficacy–luminance–current efficacy characteristics are depicted. The non-doped device exhibits a significantly lower efficacy compared to the doped devices, highlighting the substantial role of the host material. Consequently, a device based on a 10 wt% doping concentration surpasses others in terms of power efficacy, showcasing a PE_{max} of 4.4 lm/W, a CE_{max} of 7.6 cd/A, an EQE_{max} of 3.3%, and an L_{max} of 3175 cd/m^2 at a turn-on voltage of 5.1 V.
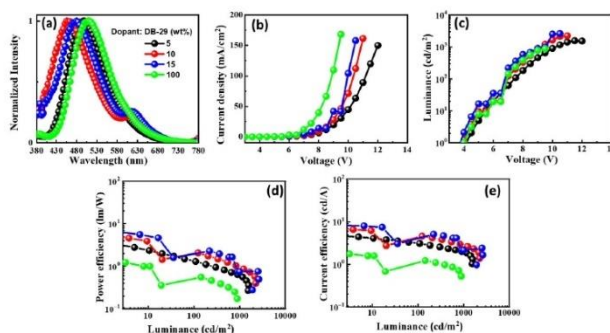
230

Figure 12. The EL characteristics of the OLEDs with emitter **DB29** doped in CBP host material: (**a**) EL spectra, (**b**) current density–voltage, (**c**) luminance–voltage, (**d**) power efficacy–luminance, and (**e**) current efficacy–luminance characteristics.

Table 2. EL properties of the OLEDs with the emitting materials **DB14**, **DB29**, and **DB23** doped in CBP host matrix.

Emitter	Concentration of Emitter in the Host Material (wt%)	Turn-On Voltage (V_{on}) [a]	Power Efficacy (lm/W)	Current Efficacy (cd/A)	EQE (%)	CIE	Max Luminance (cd/m²)
			@100/1000 cd/m² and Max				
DB-14	5.0	5.0	2.9/1.6/3.9	6.1/4.7/6.5	2.6/2.2/2.7	(0.22, 0.36)/(0.21, 0.32)/-	2951
	10	5.1	2.6/1.3/4.4	5.7/3.9/7.6	2.6/2.0/3.3	(0.21, 0.33)/(0.20, 0.29)/-	3175
	15	5.9	1.4/1.3/2.4	3.7/2.3/4.9	1.9/1.4/2.4	(0.20, 0.28)/(0.19, 0.24)/-	1884
	100	6.1	0.2/-/0.4	0.6/-/0.8	0.3/-/0.4	(0.26, 0.40)/-	515
DB-29	5.0	5.4	0.3/0.6/2.1	3.1/2.0/3.9	2.0/1.4/2.3	(0.19, 0.22)/(0.22, 0.22)/-	1578
	10	5.7	1.7/1.0/4.4	3.7/2.8/6.5	2.0/1.7/3.1	(0.20, 0.27)/(0.23, 0.25)/-	2251
	15	4.7	1.0/0.3/7.9	2.3/1.0/9.1	1.1/0.5/4.0	(0.21, 0.31)/(0.22, 0.27)/-	2631
	100	5.8	0.4/-/1.4	0.8/-/1.8	0.3/-/0.7	(0.26, 0.44)/-	884
DB-23	5.0	5.7	1.3/0.6/2.1	3.0/1.9/3.8	1.9/1.4/2.3	(0.17, 0.07)	883
	10	**5.2**	**1.4/0.8/1.7**	**2.4/1.7/2.6**	**5.1/3.5/5.3**	**(0.19, 0.22)/(0.22, 0.22)/-**	**1620**
	15	5.2	2.2/1.0/3.2	4.6/2.8/5.3	2.5/1.7/2.7	(0.20, 0.27)/(0.23, 0.25)/-	2076
	100	5.1	0.6/-/1.0	1.3/-/1.8	0.5/-/0.7	(0.26, 0.44)/-	875

[a] Turn-on voltage at luminance >1 cd m².

In Figure 11a, the EL spectra of the devices with **DB23** exhibit single peaks at around 470 nm, indicating blue emission. The presence of single peaks suggests the successful host–guest energy transfer completion. The emission wavelength in the EL of the devices undergoes a shift when compared with the PL spectra of the **DB23** emitter, indicating the influence of the CBP host on emission. An evident emission spectrum of the emitter becomes apparent with an increase in the concentration of the **DB23** dopant. Notably, both doped and non-doped devices exhibit similar EL emission peaks. Figure 11b–e demonstrate current density–luminance–voltage and power efficacy–luminance–current efficacy characteristics. Comparatively, the non-doped device shows a considerably lower efficacy than the doped devices, demonstrating the crucial role of the host material. The device utilizing a 15 wt% doping concentration of the emitter has a maxima PE_{max} of 3.2 lm/W, a CE_{max} of 5.3 cd/A, and an L_{max} of 2076 cd/m² at a voltage of 5.1 V. Additionally, the device having a 10 wt% doping concentration reveals a remarkable EQE_{max} of 5.3%, even surpassing the theoretical limit for fluorescent emitters. The emitter **DB23**-based device stands out in comparison to the others.

The EL spectra of the **DB29**-based device exhibit a blue shift with increasing doping concentration, in contrast to the non-doped device, as can be seen in Figure 12a. The EL spectra maxima change from approximately 490 nm to 430 nm in the region of blue

231

emission. Single peaks of the emissions signify the achievement of complete energy transfer between host and guest. The emission wavelength in the EL of the devices undergoes a shift when compared with the PL spectra of the **DB29** emitter, indicating the influence of the CBP host on emission. An evident emission spectrum of the emitter becomes apparent with an increase in the concentration of the **DB29** dopant. Figure 12b–e illustrate the current density–luminance–voltage and power efficacy–luminance–current efficacy characteristics. The non-doped device showcases a more favorable current density–voltage characteristic compared to the doped devices, although its efficacy is considerably lower than that of its doped counterparts. Consequently, the role of the host material is pronounced, leading to the prominence of the device with a 15 wt% doping concentration. This device outperforms others in terms of power efficacy, exhibiting a PE_{max} of 7.9 lm/W, a CE_{max} of 9.1 cd/A, an EQE_{max} of 4.0%, and an L_{max} of 2631 cd/m^2 at a voltage of 4.7 V. Impressively, this device showcases the highest PE and CE values among all.

As depicted in Table 2, the **DB23**-based device exhibits the highest EQE among all devices, surpassing both previous research and the outcomes of this study. This enhanced performance could be attributed to the inclusion of the branched alkyl side chains in the molecule, which likely contributed to improved molecule solubility for the fabrication of wet-processed OLED devices and the film-forming properties of the material. Nevertheless, the PE and CE of the **DB29**-based device demonstrated superior performance. This can be attributed to its appropriate HOMO and LUMO levels, which facilitated the efficient host–guest energy transfer. Additionally, the incorporation of two donor moieties of the bicarbazole contributed to a balanced charge transfer, further enhancing its performance.

4. Conclusions

In conclusion, this study presents an exploration of twisted donor-acceptor-donor compounds, specifically bicarbazole-benzophenone-bicarbazole-based compounds, as potential blue emitters for blue OLEDs. The synthesized emitters **DB14**, **DB23**, and **DB29**, were systematically designed with tailored alkyl side chains to enhance their film-forming and solubility properties. The investigation encompassed thorough characterization, including photo-physical analysis to determine photoluminescence quantum yields, UV absorption, and emission characteristics. Electrochemical measurements provided insights into HOMO and LUMO energy levels, while a thermal analysis unveiled the remarkable thermal stability of the compounds. The OLED devices incorporating these emitters demonstrated noteworthy performance, with **DB23** exhibiting the highest EQE among all devices, reaching a peak value of 5.3%. The study also highlighted the significant influence of host–guest energy transfer, optimal doping concentrations, and molecular structures on device efficiency. Notably, the research outcomes underscore the considerable potential of the newly developed D-A-D derivatives in advancing OLED technology. This work contributes to the ongoing progress of OLED materials and their applications, offering insights into the design of efficient blue emitters. This research not only contributes to the understanding of advanced OLED materials but also provides insights into designing efficient blue emitters for future display and lighting applications, thereby advancing the field of organic electronics.

Author Contributions: Investigation, D.B., I.S., P.G., M.R.N., D.T., K.K. and G.K.; writing—original draft preparation, D.B., I.S., P.G. and S.B.; writing—review and editing, J.-H.J. and S.G. All authors have read and agreed to the published version of the manuscript.

Data Availability Statement: The data presented in this study are available on request from the corresponding authors.

Conflicts of Interest: The authors declare no conflicts of interest.

References

1. Sasabe, H.; Kido, J. Development of High Performance OLEDs for General Lighting. *J. Mater. Chem. C* **2013**, *1*, 1699–1707. [CrossRef]
2. Reineke, S.; Lindner, F.; Schwartz, G.; Seidler, N.; Walzer, K.; Lüssem, B.; Leo, K. White Organic Light-Emitting Diodes with Fluorescent Tube Efficiency. *Nature* **2009**, *459*, 234–238. [CrossRef] [PubMed]
3. Park, S.W.; Kim, D.; Rhee, Y.M. Overcoming the Limitation of Spin Statistics in Organic Light Emitting Diodes (OLEDs): Hot Exciton Mechanism and Its Characterization. *Int. J. Mol. Sci.* **2023**, *24*, 12362. [CrossRef]
4. Zhou, Z.; Xie, X.; Sun, Z.; Wang, X.; An, Z.; Huang, W. Recent advances in metal-free phosphorescent materials for organic light-emitting diodes. *J. Mater. Chem. C* **2023**, *11*, 3143–3161. [CrossRef]
5. Chen, Y.-T.; Wen, S.-W.; Liao, P.-H.; Lee, W.-K.; Lee, C.-C.; Huang, C.-W.; Yang, Y.-H.; Lin, K.-C.; Chang, C.-J.; Su, G.-D.; et al. Reflective 3D pixel configuration for enhancing efficiency of OLED displays. *Org. Electron.* **2022**, *103*, 106451. [CrossRef]
6. Huang, Y.; Xu, H.; Ye, Z. Image quality evaluation for OLED-based smart-phone displays at various lighting conditions. *Displays* **2021**, *70*, 102115. [CrossRef]
7. Gupta, N.; Nagar, M.R.; Anamika; Gautam, P.; Maiti, B.; Jou, J.-H.; Kuila, B.K. Triazine and Thiophene-Containing Conjugated Polymer Network Emitter-Based Solution-Processable Stable Blue Organic LEDs. *ACS Appl. Polym. Mater.* **2022**, *5*, 130–140. [CrossRef]
8. Kawamura, Y.; Yanagida, S.; Forrest, S.R. Energy Transfer in Polymer Electrophosphorescent Light Emitting Devices with Single and Multiple Doped Luminescent Layers. *J. Appl. Phys.* **2002**, *92*, 87–93. [CrossRef]
9. Tavgeniene, D.; Krucaite, G.; Baranauskyte, U.; Wu, J.Z.; Su, H.Y.; Huang, C.W.; Chang, C.H.; Grigalevicius, S. Phenanthro[9,10-d]imidazole based new host materials for efficient red phosphorescent OLEDs. *Dye. Pigment.* **2017**, *137*, 615–621. [CrossRef]
10. Lee, J.-H.; Chen, C.-H.; Lee, P.-H.; Lin, H.-Y.; Leung, M.-K.; Chiu, T.-L.; Lin, C.-F. Blue Organic Light-Emitting Diodes: Current Status, Challenges, and Future Outlook. *J. Mater. Chem. C* **2019**, *7*, 5874–5888. [CrossRef]
11. Peng, F.; Zhong, W.; He, J.; Zhong, Z.; Guo, T.; Ying, L. Effect of Alkyl Side Chain Length on the Electroluminescent Performance of Blue Light-Emitting Poly(Fluorene-Co-Dibenzothiophene-S,S-Dioxide). *Dye. Pigment.* **2021**, *187*, 109139. [CrossRef]
12. Jiang, J.; Lee, J.Y. Degradation mechanisms and lifetime extending strategy of phosphorescent and thermally activated delayed-fluorescence organic light-emitting diodes. *Mater. Today* **2023**, *68*, 204–233. [CrossRef]
13. Bommireddy, P.R.B.; Musalikunta, C.S.; Lee, Y.-W.; Suh, Y.; Godumala, M.; Park, S.-H. Recent Endeavors and Perspectives in Developing Solution-Processable Host Materials for Thermally Activated Delayed Fluorescence Organic Light-Emitting Diodes. *J. Mater. Chem. C* **2023**, *11*, 13603–13624. [CrossRef]
14. Chatterjee, T.; Wong, K. Perspective on host materials for thermally activated delayed fluorescence organic light emitting diodes. *Adv. Opt. Mater.* **2019**, *7*, 1800565. [CrossRef]
15. Li, N.; Fang, Y.; Li, L.; Zhao, H.; Quan, Y.; Ye, S.; Fan, Q.; Huang, W. A universal solution-processable bipolar host based on triphenylamine and pyridine for efficient phosphorescent and thermally activated delayed fluorescence OLEDs. *J. Lumin.* **2018**, *199*, 465–474. [CrossRef]
16. Ahn, D.H.; Moon, J.S.; Kim, S.W.; Lee, S.Y.; Karthik, D.; Lee, J.Y.; Kwon, J.H. Effect of various host characteristics on blue thermally activated delayed fluorescent devices. *Org. Electron.* **2018**, *59*, 39–44. [CrossRef]
17. Gu, J.; Shi, W.; Zheng, H.; Chen, G.; Wei, B.; Wong, W.-Y. The Novel Organic Emitters for High-Performance Narrow-Band Deep Blue OLEDs. *Top. Curr. Chem.* **2023**, *381*, 26. [CrossRef]
18. Wu, S.; Aonuma, M.; Zhang, Q.; Huang, S.; Nakagawa, T.; Kuwabara, K.; Adachi, C. High-efficiency deep-blue organic light-emitting diodes based on a thermally activated delayed fluorescence emitter. *J. Mater. Chem. C* **2014**, *2*, 421–424. [CrossRef]
19. Huang, B.; Ban, X.; Sun, K.; Ma, Z.; Mei, Y.; Jiang, W.; Lin, B.; Sun, Y. Thermally activated delayed fluorescence materials based on benzophenone derivative as emitter for efficient solution-processed non-doped green OLED. *Dye. Pigment.* **2016**, *133*, 380–386. [CrossRef]
20. Krucaite, G.; Grigalevicius, S. A review on low-molar-mass carbazole- based derivatives for organic light emitting diodes. *Synth. Met.* **2019**, *247*, 90–108. [CrossRef]
21. Teng, J.-M.; Wang, Y.-F.; Chen, C.-F. Recent progress of narrowband TADF emitters and their applications in OLEDs. *J. Mater. Chem. C* **2020**, *8*, 11340–11353. [CrossRef]
22. Bas, E.E.; Ulukan, P.; Monari, A.; Aviyente, V.; Catak, S. Photophysical Properties of Benzophenone-Based TADF Emitters in Relation to Their Molecular Structure. *J. Phys. Chem. A* **2022**, *126*, 473–484. [CrossRef] [PubMed]
23. Bui, T.-T.; Goubard, F.; Ibrahim-Ouali, M.; Gigmes, D.; Dumur, F. Recent advances on organic blue thermally activated delayed fluorescence (TADF) emitters for organic light-emitting diodes (OLEDs). *Beilstein J. Org. Chem.* **2018**, *14*, 282–308. [CrossRef] [PubMed]
24. Lee, S.Y.; Yasuda, T.; Yang, Y.S.; Zhang, Q.; Adachi, C. Luminous Butterflies: Efficient Exciton Harvesting by Benzophenone Derivatives for Full-Color Delayed Fluorescence OLEDs. *Angew. Chem. Int. Ed.* **2014**, *53*, 6402–6406. [CrossRef] [PubMed]
25. Salehi, A.; Fu, X.; Shin, D.; So, F. Recent Advances in OLED Optical Design. *Adv. Funct. Mater.* **2019**, *29*, 1808803. [CrossRef]
26. Li, L.; Zhu, X.; Sun, S.; Zhang, C.; Yang, B.; Liu, S.; Liu, Z. Blue Organic Light Emitting Diode Materials based on Different Light-emitting Groups. *Curr. Org. Chem.* **2023**, *27*, 352–362. [CrossRef]

27. Gautam, P.; Shahnawaz; Siddiqui, I.; Blazevicius, D.; Krucaite, G.; Tavgeniene, D.; Jou, J.H.; Grigalevicius, S. Bifunctional Bi-carbazole-Benzophenone-Based Twisted Donor–Acceptor–Donor Derivatives for Deep-Blue and Green OLEDs. *Nanomaterials* **2023**, *13*, 1408. [CrossRef]

28. Vaitkeviciene, V.; Grigalevicius, S.; Grazulevicius, J.; Jankauskas, V.; Syromyatnikov, V. Hole-transporting [3,3′]bicarbazolyl-based polymers and well-defined model compounds. *Eur. Polym. J.* **2006**, *42*, 2254–2260. [CrossRef]

29. Frisch, M.J.; Trucks, G.W.; Schlegel, H.B.; Scuseria, G.E.; Robb, M.A.; Cheeseman, J.R.; Scalmani, G.; Barone, V.; Petersson, G.A.; Nakatsuji, H.; et al. *Gaussian 16, Revision B.01*; Gaussian, Inc.: Wallingford, CT, USA, 2016. Available online: https://www.scirp.org/(S(lz5mqp453ed%20snp55rrgjct55))/reference/referencespapers.aspx?referenceid=2418053 (accessed on 24 October 2023).

30. Tomasi, J.; Mennucci, B.; Cammi, R. Quantum Mechanical Continuum Solvation Models. *Chem. Rev.* **2005**, *105*, 2999–3094. [CrossRef]

31. De Leeuw, D.; Simenon, M.; Brown, A.; Einerhand, R. Stability of n-type doped conducting polymers and consequences for polymeric microelectronic devices. *Synth. Met.* **1997**, *87*, 53–59. [CrossRef]

32. Zhao, L.; Liu, Y.; Wang, N.; Fan, S.; Wang; Zhang, X.; Huang, W. Novel Hyperbranched Polymers as Host Materials for Green Thermally Activated Delayed Fluorescence OLEDs. *Chin. J. Polym. Sci.* **2017**, *35*, 490–502. [CrossRef]

Article

Bicarbazole-Benzophenone Based Twisted Donor-Acceptor Derivatives as Potential Blue TADF Emitters for OLEDs

Iram Siddiqui [1,†], Prakalp Gautam [1], Dovydas Blazevicius [2,†], Jayachandran Jayakumar [1], Sushanta Lenka [1], Daiva Tavgeniene [2], Ernestas Zaleckas [3], Saulius Grigalevicius [2,*] and Jwo-Huei Jou [1,*]

[1] Department of Materials Science and Engineering, National Tsing Hua University, Hsinchu 30044, Taiwan; jayakumar@mx.nthu.edu.tw (J.J.); sushantalenka1@gmail.com (S.L.)
[2] Department of Polymer Chemistry and Technology, Kaunas University of Technology, Radvilenu Plentas 19, LT-50254 Kaunas, Lithuania; daiva.tavgeniene@ktu.lt (D.T.)
[3] Department of Agricultural Engineering and Safety, Agriculture Academy, Vytautas Magnus University, Studentu Str. 11, Akademija, LT-53361 Kaunas, Lithuania
* Correspondence: saulius.grigalevicius@ktu.lt (S.G.); jjou@mx.nthu.edu.tw (J.-H.J.)
† These authors contributed equally to this work.

Abstract: Over the past few decades, organic light-emitting diodes (OLEDs) find applications in smartphones, televisions, and the automotive sector. However, this technology is still not perfect, and its application for lighting purposes has been slow. For further development of the OLEDs, we designed twisted donor-acceptor-type electroactive bipolar derivatives using benzophenone and bicarbazole as building blocks. Derivatives were synthesized through the reaction of 4-fluorobenzophenone with various mono-alkylated 3,3′-bicarbazoles. We have provided a comprehensive structural characterization of these compounds. The new materials are amorphous and exhibit suitable glass transition temperatures ranging from 57 to 102 °C. They also demonstrate high thermal stability, with decomposition temperatures reaching 400 °C. The developed compounds exhibit elevated photoluminescence quantum yields (PLQY) of up to 75.5% and favourable HOMO-LUMO levels, along with suitable triplet-singlet state energy values. Due to their good solubility and suitable film-forming properties, all the compounds were evaluated as blue TADF emitters dispersed in commercial 4,4′-bis(N-carbazolyl)-1,10-biphenyl (CBP) host material and used for the formation of emissive layer of organic light-emitting diodes (OLEDs) in concentration-dependent experiments. Out of these experiments, the OLED with 15 wt% of the emitting derivative 4-(9′-[2-ethylhexyl]-[3,3′]-bicarbazol-9-yl)benzophenone exhibited superior performance. It attained a maximum brightness of 3581 cd/m², a current efficacy of 5.7 cd/A, a power efficacy of 4.1 lm/W, and an external quantum efficacy of 2.7%.

Keywords: organic light-emitting diode (OLED); blue TADF emitters; Donor-Acceptor (D-A) materials; benzophenone-based derivatives

1. Introduction

In recent decades, there has been significant and swift advancement in organic light-emitting diode (OLED) technology, transforming it into a multi-billion-dollar market [1]. Its applications have expanded across various domains, encompassing high-contrast flat-panel displays, smartwatches, smartphones, and big-screen television sets. In addition, solid-state lighting is attracting growing interest in both industrial and scientific domains [2–7]. OLED devices offer superior features such as high colour purity, reduced weight, lower power consumption, faster response, and flexibility, surpassing capabilities offered by existing technologies [8–11].

Until now, the prevailing commercial OLED devices were based on phosphorescent materials containing noble metals like platinum and iridium [12]. The incorporation of atoms of noble metals into the structures of phosphorescent materials presents a notable

obstacle not only to the future manufacturing expenses of devices but also prompts environmental concerns [13,14]. Moreover, there is a tendency to increase the nonradiative transition rate of phosphorescent metal complex d-orbitals when the emission peaks are shifting to the blue region of emission, posing challenges in achieving both high efficiency and stability in blue phosphorescent OLEDs [15–20]. To address these challenges, there is a renewed focus on the development of small-molecule fluorescent materials, primarily due to their high colour purity and cost-effectiveness [21]. In recent years, there has also been considerable attention focused on thermally activated delayed fluorescence (TADF) materials. This is due to absence of metal atoms in their structures and their capability to employ reverse intersystem crossing (RISC), resulting in the up-conversion of triplet excitons to emissive singlet excitons, leading to significantly enhanced external quantum efficiencies (EQEs) [22–28]. However, numerous TADF OLEDs face challenges including triplet-triplet and singlet-triplet annihilation, as well as concentration quenching. These issues can be attributed to prolonged exciton lifetimes, leading to a notable decrease in efficiency as luminance increases [29–31].

A crucial requirement for TADF OLED emitters to function efficiently is achieving the smallest possible singlet-triplet energy splitting (ΔE_{ST}). This can be accomplished through molecular design strategies aimed at maximizing the separation between the highest occupied molecular orbital (HOMO) and the lowest unoccupied molecular orbital (LUMO). One effective approach is the incorporation of highly twisted donor and acceptor structure in the derivatives [30,32,33]. Benzophenone and its derivatives having strong electron-withdrawing capabilities, effective intersystem crossing due to robust spin-orbit coupling and twisted configuration offer the potential for developing efficient TADF emitters with shorter exciton lifetimes through smart molecular design [34–42]. Carbazole derivatives, widely recognized for their electron-rich nature, were extensively employed as electron donors in a wide range of optoelectronic devices, serving as both host materials and emitters in various configurations. This is due to the capacity of 9H-carbazole for facile functionalization across multiple sites, tuneable electronic and optical properties, robust electrochemical and thermal stability, and high photoluminescence quantum yield [43–49]. Materials exhibiting both favourable film-forming properties and solubility in common organic solvents are extensively explored in the scientific and technological sectors. This interest stems from the fact that low molar-mass organic derivatives, also called molecular glasses, demonstrate capability to form transparent, stable, and homogenous amorphous layers from their solutions [50,51]. Both benzophenone-based as well as carbazole-based derivatives are valued for their ability to create stable amorphous layers characterized by high glass transition temperatures as reported in the literature [52,53]. Solubility in common organic solvents of new materials enables solution-based manufacturing processes, such as blade or spin coating, and inkjet printing, which are simpler, more cost-effective, and more scalable than the usual vacuum evaporation method [54–57].

In this study, we present the synthesis, investigation, and application of new bipolar electroactive compounds with benzophenone and 3,3′-bicarbazole fragments acting as electron acceptors and electron donors, respectively. The donor-acceptor type twisted molecules demonstrated their efficacy as blue TADF emitters in organic LEDs. The selection of alkyl sidechains, including ethyl, butyl, pentyl, hexyl, 2-ethylhexyl, and octyl was aimed at optimizing their film-forming properties, solubility, and solution processability [58].

2. Results and Discussion

2.1. Synthesis

Novel electroactive bicarbazole-based derivatives were synthesized via a three-step procedure illustrated in Scheme 1. Initially, 9H-carbazole underwent oxidation with iron (III) chloride to yield 9H,9′H-3,3′-bicarbazole (**2**). Subsequently, various alkyl bromides were utilized for mono-alkylation of the 9H,9′H-3,3′-bicarbazole (**2**) in THF solution, resulting in the production of 9-alkyl-9′H-3,3′-bicarbazoles (**3–8**) in the presence of potassium hydroxide and potassium carbonate. Finally, the obtained bicarbazole derivatives (**3–8**)

underwent nucleophilic substitution reactions with 4-fluorobenzophenone in DMSO in the presence of potassium carbonate, leading to the formation of the target derivatives **DB37**, **DB38**, **DB39**, **DB40**, **DB41**, and **DB44**. The chemical structures of these new electroactive compounds were confirmed using mass spectrometry and NMR spectroscopy, demonstrating excellent alignment with the theoretical structures. The aliphatic chains present in the synthesized target compounds contributed to increased solubility in commonly used organic solvents, consistent with the findings of Inoue et al. regarding the relationship between alkyl chain length and the solubility of organic materials [56]. The solubility of the presented materials in appropriate solvents was enhanced by extending the length of the alkyl chain. While the thermal evaporation method could be suitable for the formation of thin layers for devices using these electroactive compounds, the good solubility of the new materials allows a cost-effective alternative method for forming thin films through spin coating from their solutions.
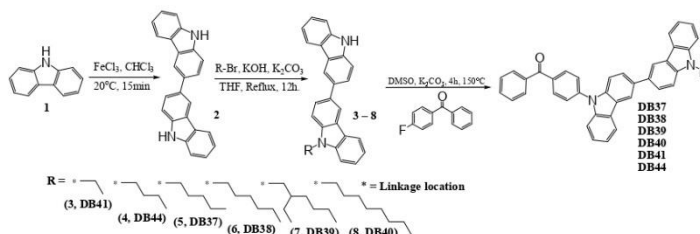
Scheme 1. Synthesis of target compounds **DB37**, **DB38**, **DB39**, **DB40**, **DB41** and **DB44**.

2.2. Thermal and Morphological Properties

The response of the synthesized materials **DB37–DB41** and **DB44** to heating was investigated using DSC and TGA methods, heating the samples under an inert nitrogen atmosphere. Following TGA experiments conducted at a heating rate of 10 °C/min. It was observed that the target compounds exhibit remarkable stability under heating. As depicted in Figure 1, the TGA curve of compound **DB37** illustrates a temperature of 5% weight loss (T_d) at 406 °C. Similarly, derivatives **DB41** and **DB44** demonstrated stability under heating with respective T_d values of 374 °C and 389 °C. Materials **DB38**, **DB39**, and **DB40**, which feature longer aliphatic groups, exhibited comparable thermal stability, reaching T_d values of 398 °C, 383 °C, and 397 °C, respectively. The TGA curves of all the investigated derivatives are provided in Figure S1 of the Supplementary Material for the publication.
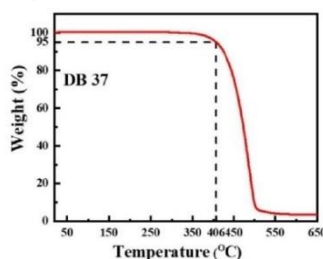

Figure 1. TGA curve (red) of compound **DB37**. Heating rate: 10 °C/min.

Figure 2 displays the thermograms of DSC experiments conducted forn all the compounds **DB37**–**DB41** and **DB44**, with sample sizes varying from 2.6 to 4.8 mg. Upon examining the second heating curve, it becomes evident that the glass transition temperatures (T_g) are influenced by the length of the alkyl sidechains of the compounds. For instance, material **DB41**, containing an ethyl group, exhibited a notably high T_g of 102 °C, determined by a slow endothermic dip in the curve of the second heating. Conversely, compounds **DB44** and **DB37**, which were substituted with butyl and pentyl groups, respectively, displayed slightly lower T_g values of 80 °C and 77 °C. This trend persists for materials featuring even longer alkyl groups: derivatives **DB38**, **DB39**, and **DB40**, substituted with hexyl, 2-ethylhexyl, and octyl groups respectively, exhibited glass transition temperatures of 68 °C, 64 °C, and 57 °C. This phenomenon could be explained by reduced intermolecular hydrogen bonding as length of the alkyl chain increases [59]. In summary, the findings from the TGA and DSC experiments affirm the suitability of these materials for amorphous electroactive layers of OLED devices. All the thermal characteristics are also presented in Table 1.
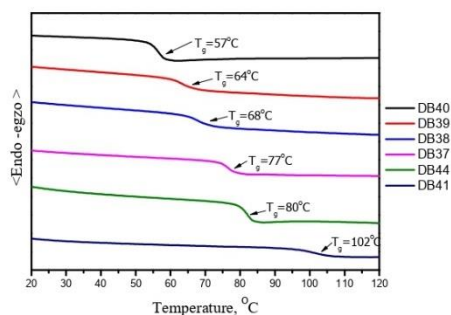

Figure 2. DSC thermograms from the second heating cycle of the target compounds. Heating rate: 10 °C/min.

Table 1. Characteristics of the derivatives **DB37**, **DB38**, **DB39**, **DB40**, **DB41** and **DB44**.

Emitter	λ_{ex} (nm)	λ_{em} (nm)	Φ (%)	Homo (eV)	Lumo (eV)	E_g (eV)	Decay (ns)	S_1 (eV)	T_1 (eV)	ΔE_{ST}	T_d (°C)	T_g (°C)
DB37	384.5, 395.6	509	65.5	−5.67	−2.58	3.09	5.53	3.04	2.76	0.28	406	102
DB38	383.5, 400	510	45.3	−5.70	−2.61	3.09	1.88	2.94	2.89	0.05	398	80
DB39	382.7, 400	528	75.5	−5.68	−2.60	3.08	4.27	3.10	2.81	0.29	383	77
DB40	384.5, 408.2	513	52.5	−5.69	−2.59	3.10	2.41	3.06	2.80	0.26	397	68
DB41	381.0, 399.7	528	62.5	−5.73	−2.64	3.09	2.24	3.22	2.80	0.42	374	64
DB44	383.9, 398.6	529	68.5	−5.69	−2.62	3.07	6.28	3.18	2.82	0.15	389	57

λ_{ex}: Excitation Wavelength; λ_{em}: Emission Wavelength; Φ: Photoluminescence Yield; E_g: Bandgap S_1: Singlet Energy; T_1: Triplet Energy; ΔE_{ST}: Singlet-Triplet Energy Gap; T_d: Destruction temperature; T_g: Glass Transition Temperature.

2.3. Electrochemical and Photo-Physical Properties

The compounds **DB37**, **DB38**, **DB39**, **DB40**, **DB41**, and **DB44** demonstrate elevated photoluminescence quantum yields (PLQY) of 65.5%, 45.3%, 75.5%, 52.5%, 62.5%, and 68.5%, respectively. Summarized values of PLQY can be found in Table 1. Figure 3 illustrates the UV-absorption bands of compound **DB37** as an example. All the UV-absorption bands and Tauc plots for all the compounds are illustrated in Figure S2 of the Supplementary Material of the article. The derivatives were examined in THF solvent under standard conditions using a quartz cuvette.
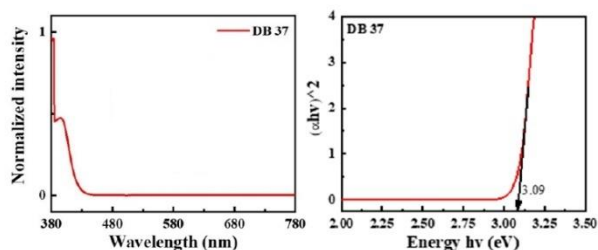
Figure 3. UV-Vis absorbance spectrum (**left**) and tauc plot (**right**) of the compound **DB37**.

Notably, each of the derivatives consistently displayed two absorption peaks around 380 and 410 nm, attributed to the presence of identical chromophores within their structures. Tauc plots for objective compounds were generated by employing the UV absorption wavelength and intensity using equations $(\alpha \times h\nu)^{1/2}$ and $h\nu$ for the x-axis and y-axis, respectively, where α denotes intensity and $h\nu$ stands for energy ($h\nu = 1240/\text{wavelength}$), as it is described in literature [60]. The Tauc plots unveiled bandgaps for the studied derivatives: **DB37**, **DB38**, and **DB41** had a bandgap of 3.09 eV, **DB40** had a bandgap of 3.10 eV, **DB39** had a bandgap of 3.08 eV, and **DB44** had a bandgap of 3.07 eV (see Table 1). The bandgap energy exhibited by the materials was nearly identical, with a maximum difference of 0.03 eV, which aligns closely with the possible measurement discrepancies. Similar bandgap values are acceptable since all the derivatives utilize the same chromophores.

Figure 4 illustrates the evaluation of the electrochemical characteristics of **DB37**, **DB38**, **DB39**, **DB40**, **DB41**, and **DB44** through CV measurements. Obtained oxidation onset values were used for calculations of HOMO levels, employing equation $E_{HOMO} = -[4.4 + E^{ox}_{onset}]$, while the determination of LUMO levels was accomplished using equation $E_{LUMO} = E_{HOMO} + E_g$ following the methodology described in the literature [18,61,62]. The determined HOMO levels for **DB37**, **DB38**, **DB39**, **DB40**, **DB41**, and **DB44** were −5.67, −5.70, −5.68, −5.69, −5.73, and −5.69, respectively. Meanwhile, LUMO levels were, in the same order, −2.58, −2.61, −2.60, −2.59, −2.64, and −2.62. These values, along with E_g levels, are outlined in Table 1. HOMO and LUMO levels of the compounds are appropriate for forming blue-emitting layers in tandem with the commercial host material CBP.

In Figure 5 (left), the PL spectrum of the **DB37** compound is presented, displaying emission wavelength maximum at about 510 nm with cyan blue emission. Singlet state energies of the potential emitters were calculated by utilizing the crossing points of PL and absorbance charts, resulting in values of 3.04 eV for **DB37**, 2.94 eV for **DB38**, 3.10 eV for **DB39**, 3.06 eV for **DB40**, 3.22 eV for **DB41**, and 3.18 eV for **DB44** (see Table 1).

Additionally, low-temperature photoluminescence (LTPL) spectra were registered to ascertain the triplet energy levels. The spectrum for **DB37** is depicted in Figure 5 (right) as an example. The compounds **DB37**, **DB38**, **DB39**, **DB40**, **DB41**, and **DB44** demonstrate elevated levels of triplet energy at 2.76, 2.89, 2.81, 2.80, 2.80, and 2.82 eV, respectively,

239

suggesting their potential suitability as blue emitters. The LTPL spectra of all the objective derivatives are presented in Figure S3 of Supplementary Material, and the triplet state energy values are listed in Table 1.
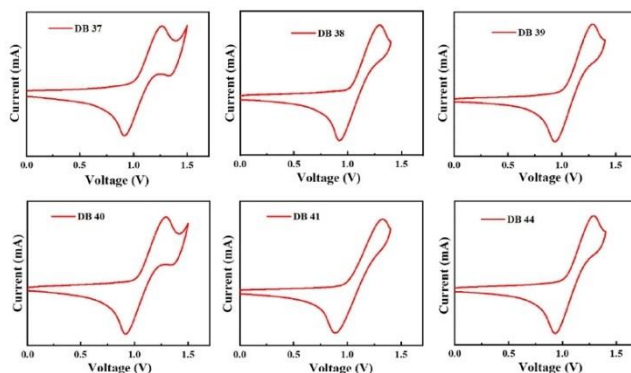

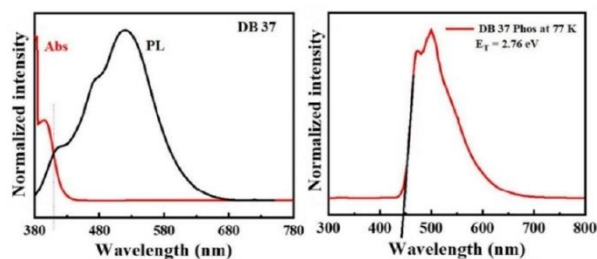**Figure 4.** Curves of CV scans of the materials **DB37**, **DB38**, **DB39**, **DB40**, **DB41**, and **DB44**.

Figure 5. Photoluminescence (**left**) and low-temperature photoluminescence (**right**) spectra of the material **DB37**.

Figure 6 displays the results of the time-resolved photoluminescence (TRPL) experiments illustrating the decay times of photoluminescence for the new emitters. The determined values of the time for **DB37**, **DB38**, **DB39**, **DB40**, **DB41**, and **DB44** were 5.53, 1.88, 4.27, 2.41, 2.24, and 6.28 ns, respectively. Typically, the decay lifetime of fluorescent emitters falls within the picosecond range. However, the presented materials exhibit decay on the nanosecond scale, suggesting the potential utilization of triplet excited states as TADF-based emitters [63,64]. The photoluminescence decay times are detailed in Table 1. In the graphs, IRF denotes the instrument response function, which was measured both prior to and following each measurement as a control parameter.
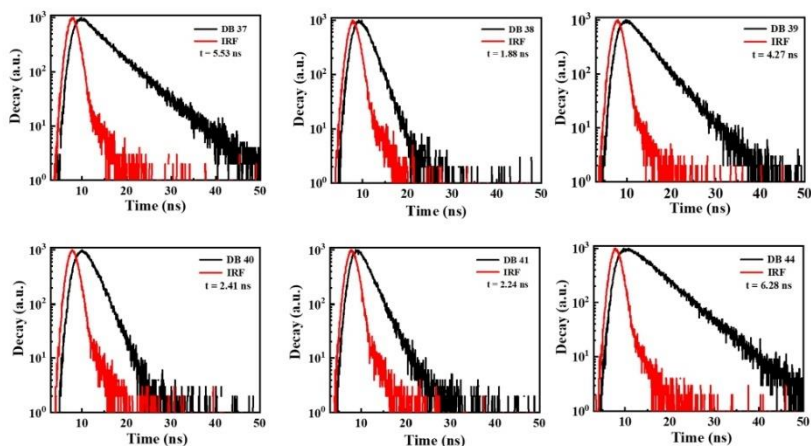
Figure 6. TRPL spectra of the compounds **DB37**, **DB38**, **DB39**, **DB40**, **DB41**, and **DB44**.

2.4. Electroluminescent Properties

The OLED device architecture utilized in this study is represented by the energy level diagram depicted in Figure 7. These devices incorporate emitters **DB37**, **DB38**, **DB39**, **DB40**, **DB41**, and **DB44** doped in a CBP host material. The straightforward device structures consisted of a 125 nm ITO anode layer, followed by a 35 nm PEDOT:PSS hole injection layer (HIL), and subsequently a 30 nm emissive layer (EML) comprising a CBP host with dopants **DB37**, **DB38**, **DB39**, **DB40**, **DB41**, or **DB44** (at concentrations of 5%, 10%, 15%, and 100% by weight). As for the electron transporting layer (ETL), 1,3,5-tris(N-phenyl-benzimidazol-2-yl)benzene (TPBi, 32 nm) was employed, while lithium fluoride (LiF, 0.8 nm) served as the electron injecting layer (EIL), and aluminium (Al, 150 nm) was used as the cathode layer.
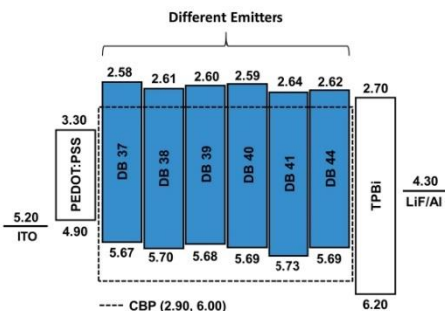

Figure 7. Energy-level diagram of the OLEDs employing the emitters **DB37**, **DB38**, **DB39**, **DB40**, **DB41**, and **DB44** doped in the CBP host.

All the new objective compounds, owing to their solubility, were suitable for layer preparation through spin-coating and were examined as emitters dispersed in a CBP

host for the OLEDs. All new emissive materials underwent concentration-dependent experiments with proportions of 5, 10, 15, or 100 wt% of each guest in the emissive layer. The electroluminescence (EL) properties, like power efficacy (PE), current efficacy (CE), EQE, maximum luminance (L_{MAX}), and the International Commission on Illumination (CIE) colour space coordinates of the devices utilizing the newly introduced emitting materials distributed within the CBP host, along with the respective non-doped devices, are outlined in Table 2. Furthermore, Figure 8 visually represents the EL characteristics of devices employing the most efficient emitter, **DB39**. The Figure illustrates the EL spectra of the devices, current density-voltage-luminance, and power efficacy-luminance-current efficacy characteristics. The same characteristics of OLEDs using other emitters **DB37**, **DB38**, **DB40**, **DB41**, and **DB44** are depicted in Figures S4–S8 in the Supplementary Material of this article.

Table 2. EL characteristics of the OLEDs containing emitting materials **DB37**, **DB38**, **DB39**, **DB40**, **DB41**, and **DB44**.

Emitter	Concentration (wt%)	Turn-On Voltage (Von) [a]	Power Efficacy (lm/W) @100 cd/m²/@1000 cd/m²/max	Current Efficacy (cd/A) @100 cd/m²/@1000 cd/m²/max	EQE (%) @100 cd/m²/@1000 cd/m²/max	CIE_xy @100 cd/m²/@1000 cd/m²	L_Max (cd/m²)
DB37	5.0	4.0	2.1/1.1/3.4	3.4/2.4/3.9	2.1/1.6/2.1	(0.17, 0.22)/(0.17, 0.30)	3449
	10	3.5	2.5/1.3/3.4	3.5/2.5/3.8	1.8/1.5/1.9	(0.18, 0.26)/(0.18, 0.23)	3658
	15	3.4	2.8/1.5/3.6	3.7/2.7/4.0	1.7/1.5/1.8	(0.19, 0.28)/(0.18, 0.25)	3464
	100	3.1	0.3/-/-	0.3/-/-	0.1/-/-	(0.24, 0.40)/-	616
DB38	5.0	3.9	1.9/1.0/3.4	3.1/2.2/3.8	1.9/1.5/1.9	(0.18, 0.22)/(0.17, 0.20)	2801
	10	3.5	2.7/1.4/2.9	3.7/2.7/3.8	2.0/1.6/1.9	(0.18, 0.25)/(0.18, 0.22)	3430
	15	3.4	2.8/1.5/3.5	3.6/2.8/4.2	1.7/1.6/1.8	(0.19, 0.27)/(0.18, 0.24)	3555
	100	3.2	0.2/-/-	0.3/-/-	0.1/-/-	(0.22, 0.38)/-	618
DB39	5.0	4.0	1.8/0.9/3.3	3.1/2.2/3.7	2.0/1.6/2.1	(0.18, 0.20)/(0.17, 0.18)	2818
	10	3.5	2.5/1.3/4.4	3.5/2.7/4.9	2.0/1.8/2.2	(0.18, 0.23)/(0.18, 0.21)	3430
	15	3.9	3.0/1.4/4.1	4.4/2.8/5.7	2.2/1.6/2.7	(0.19, 0.27)/(0.19, 0.24)	3581
	100	3.4	0.3/-/-	0.4/-/-	0.4/-/-	(0.24, 0.39)/-	615
DB40	5.0	4.2	2.0/1.1/2.1	3.4/2.4/3.4	2.2/1.6/2.3	(0.17, 0.22)/(0.17, 0.20)	3166
	10	3.5	2.8/1.5/2.9	3.8/2.8/3.7	2.0/1.7/2.0	(0.18, 0.25)/(0.18, 0.22)	3840
	15	3.3	2.8/1.6/2/8	3.6/2.8/3.6	1.8/1.6/1.8	(0.18, 0.27)/(0.18, 0.24)	3950
	100	3.2	0.2/-/-	0.3/-/-	0.1/-/-	(0.22, 0.38)/-	685
DB41	5.0	4.4	1.6/0.8/1.9	2.9/1.9/3.1	1.9/1.3/2.0	(0.18, 0.21)/(0.18, 0.19)	2687
	10	3.8	2.4/1.1/2.4	3.6/2.5/3.6	2.0/1.5/2.0	(0.19, 0.26)/(0.19, 0.23)	3347
	15	3.5	2.6/1.3/2.7	3.6/2.5/3.6	1.7/1.1/1.8	(0.20, 0.28)/(0.19, 0.24)	3128
	100	3.1	0.2/-/-	0.3/-/-	0.1/-/-	(0.30, 0.45)/-	486
DB44	5.0	4.8	1.6/0.7/1.6	3.3/2.2/3.3	2.3/-/2.3	(0.17, 0.20)/-	1718
	10	4.0	2.1/0.8/2.7	3.9/2.3/4.1	2.1/1.4/2.3	(0.18, 0.24)/(0.18, 0.22)	1283
	15	3.8	2.1/0.5/2.3	3.6/1.5/3.7	1.9/-/2.0	(0.19, 0.26)/-	1275
	100	5.1	-/-/-	-/-/-	-/-/-	-/-	55

[a] Turn-on voltage at luminance > 1 cd/m². Characteristics of best-performing device are highlighted in grey.

In Figure 8a, the EL spectra of devices incorporating the **DB39** dopant demonstrate peaks within the 460–490 nm range, indicating emission in the blue region. The absence of additional peaks implies effective energy transfer from the host to the guest. Evidently, both undoped and doped OLEDs demonstrate comparable EL emission peaks. Figure 8b–e illustrate the characteristics of current density, luminance, voltage and power efficiency-luminance-current efficiency. The undoped device exhibits a higher current density than the doped devices and correspondingly demonstrates lower efficiency than the doped devices, highlighting the significant influence of the host material. As depicted in Table 2, the OLED based on **DB39** displays the best efficiencies out of all these devices. This enhanced performance can be attributed to the inclusion of the elongated and branched 2-ethylhexyl sidechain in the molecule, potentially improving solubility for the production of wet-processed OLEDs and contributing to the favourable film-forming characteristics

of the derivative [65]. Moreover, appropriate HOMO and LUMO levels facilitate effective energy transfer from host to dopant, while the combination of the electron-accepting benzophenone fragment with the bicarbazole donor moiety promotes balanced charge transfer and efficient utilization of excitons [66,67]. Specifically, the device containing 10 wt% of emitter **DB39** demonstrates the highest PE of 4.4 lm/W with a L_{MAX} reaching 3430 cd/m^2. However, the overall best efficiency is achieved by the device incorporating 15wt% of emitter **DB39** in its emissive layer, attaining PE and CE values of 4.1 lm/W and 5.7 cd/A, respectively, while EQE reached 2.7% with L_{MAX} of 3581 cd/m^2. The findings of this study indicate the potential utility of benzophenone and bicarbazole fragments in the synthesis of organic semiconductors and also demonstrates how thermal and film-forming properties could be controlled by introducing and modifying alkyl chains within the molecular structure of the new materials.
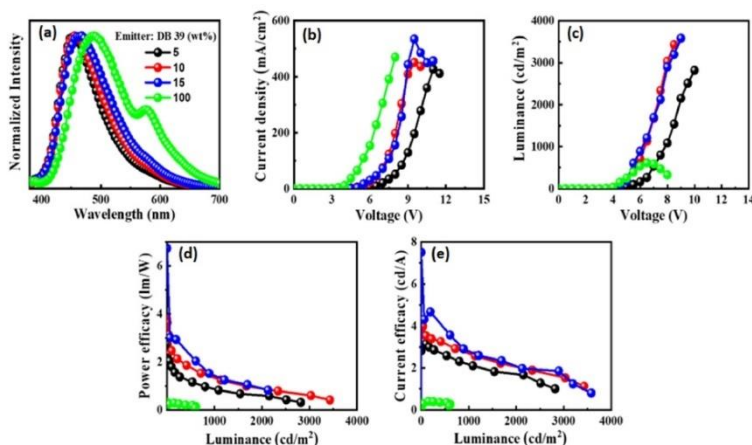
Figure 8. The EL characteristics of the device with pure emitter DB39 or doped within a CBP host material at different concentrations of the DB39: EL spectra (**a**), current density-voltage (**b**), luminance-voltage (**c**), power efficiency-luminance (**d**), and current efficiency-luminance (**e**) characteristics.

3. Materials and Methods

3.1. Instrumentation

The recording of ^{1}H and ^{13}C nuclear magnetic resonance (NMR) spectra was conducted with the Bruker Avance III (400 MHz) instrument (Bruker, Berlin, Germany). Chemical shifts (δ, ppm) are presented relative to the trimethylsilane standard. Mass spectra were acquired using the Waters ZQ 2000 mass spectrometer (Waters, Milford, CT, USA). Thermogravimetric analysis (TGA) was carried out utilizing the TGAQ50 analyser (Verder Scientific Haan, Haan, Germany), while thermograms of differential scanning calorimetry (DSC) were recorded using the Bruker Reflex II DSC apparatus (Bruker, Berlin, Germany). For both types of thermal analysis, a heating rate of 10 °C/min in a nitrogen atmosphere was selected. Ultraviolet-visible (UV–vis) spectroscopy was performed using the HP-8453 diode array spectrometer (Agilent Technology Inc., Hachioji, Tokyo, Japan), and the resultant absorbance wavelengths were used to generate the Tauc plot. An Aminco-Bowman Series 2 spectrofluorometer (Agilent Technology Inc., Hachioji, Tokyo, Japan) were used to record photoluminescence (PL) spectra. Low-temperature PL (LTPL) spectra at 77 K to determine triplet energy was recorded with a Hitachi F-7000 fluorescence spectrophotometer

(Edinburgh Instruments Ltd., Livingston, UK). The CH instrument CH1604A potentiostat (Annatech Co., Ltd., Taipei, Taiwan) was used to perform cyclic voltammetry (CV), and based on these results, HOMO levels were calculated. Time-resolved photoluminescence (TRPL) experiments, aiming to determine compound decay time, were conducted with an Edinburgh instrument FLS980 spectrometer (Edinburgh Instruments Ltd., Livingston, UK).

3.2. Synthesis and Structural Analysis

Carbazole (**1**), 1-bromooctane, 2-ethylhexylbromide, 1-bromohexane, 1-bromopentane, 1-bromobutane, bromoethane, $FeCl_3$, KOH, K_2CO_3, Na_2SO_4, 4-fluorobenzophenone, chloroform, dimethyl sulfoxide (DMSO), and tetrahydrofuran (THF) were bought from Aldrich and used without further purification.

9H,9′H-3,3′-Bicarbazole (**2**), was synthesized using 9H-carbazole as a starting material and $FeCl_3$ as an oxidising agent, as described earlier [68].

9-Ethyl-9′H-3,3′-bicarbazole (**3**) was synthesized by partially alkylating 9H,9′H-3,3′-bicarbazole (**2**), as it was described previously [69].

9-Butyl-9′H-3,3′-bicarbazole (**4**) was also synthesized by partially alkylating 9H,9′H-3,3′-bicarbazole (**2**) as it was described previously [69].

9-Pentyl-9′H-3,3′-bicarbazole (**5**). 9H,9′H-3,3′-bicarbazole (**2**) (2.00 g, 6.02 mmol) was dissolved in 50 mL of tetrahydrofuran, and 1-bromopentane (0.91 g, 6.02 mmol) was subsequently added. Potassium carbonate (1.66 g, 12.04 mmol) and powdered potassium hydroxide (2.02 g, 36.12 mmol) were gradually introduced while the solution was stirred continuously and heated to boiling temperature. After 4 h, TLC analysis was conducted, and the solution was filtered using a paper filter. The pure product was then isolated through column chromatography using tetrahydrofuran/hexane (volume ratio 1:5) as the mobile phase and silica gel as the stationary phase. The yield obtained was 1.06 g (44%) of pale-yellow material. ^{1}H NMR (400 MHz, CDCl$_3$, δ, m.d.): 8.47 (d, 2H, J = 10 Hz), 8.26 (d, 1H, 7.6 Hz), 8.23 (d, 1H, 8.0 Hz), 7.96 (s, 1H), 7.88 (d, 1H, J = 8.4 Hz), 7.84 (dd, 1H, J$_1$ = 8.4 Hz, J$_2$ = 1.6 Hz), 7.58–7.53 (m, 2H), 7.50–7.47 (m, 3H), 7.43 (d, 1H, J = 8 Hz), 7.33 (t, 2H, J = 7.2 Hz), 4.37 (t, 2H, J = 7.0 Hz), 1.96 (qu, 2H, J = 7.2 Hz), 1.49–1.41 (m, 4H), 0.96 (t, 3H, J = 7.2 Hz). ^{13}C NMR (101 MHz, CDCl$_3$, δ, m.d.): 140.98, 140.04, 139.65, 138.56, 133.33, 125.95, 125.87, 125.75, 125.60, 124.00, 123.61, 123.44, 123.10, 120.53, 120.47, 119.52, 119.02, 118.91, 118.83, 110.86, 110.79, 108.97, 108.87, 43.23, 29.50, 28.81, 22.58, 14.05.

9-Hexyl-9′H-3,3′-bicarbazole (**6**). 9H,9′H-3,3′-bicarbazole (**2**) (2.00 g, 6.02 mmol) was dissolved in 50 mL of tetrahydrofuran, and 1-bromohexane (0.99 g, 6.02 mmol) was subsequently added. Potassium carbonate (1.66 g, 12.04 mmol) and powdered potassium hydroxide (2.02 g, 36.12 mmol) were gradually introduced while the solution was stirred continuously and heated to boiling temperature. After 4 h, TLC analysis was conducted, and the solution was filtered using a paper filter. The pure product was then isolated through column chromatography using tetrahydrofuran/hexane (volume ratio 1:7) as the mobile phase and silica gel as the stationary phase. The yield obtained was 1.00 g (40%) of pale-yellow material. ^{1}H NMR (400 MHz, CDCl$_3$, δ, m.d.): 8.46 (d, 2H, J = 9.8 Hz), 8.25 (d, 1H, J = 8.0 Hz), 8.22 (d, 1H, J = 7.6 Hz), 7.99 (s, 1H), 7.88 (dd, 1H, J$_1$ = 8.4 Hz, J$_2$ = 1.6 Hz), 7.83 (dd, 1H, J$_1$ = 8.4 Hz, J$_2$ = 2.0 Hz), 7.57–7.43 (m, 6H), 7.32 (t, 2H, J = 7.4 Hz), 4.37 (t, 2H, J = 7.2 Hz), 1.95 (qu, 2H, J = 7.4 Hz), 1.50–1.33 (m, 6H), 0.94 (t, 3H, J = 7.2 Hz). ^{13}C NMR (101 MHz, CDCl$_3$, δ, m.d.): 140.97, 140.03, 139.64, 138.55, 134.13, 133.32, 125.95, 125.87, 125.73, 125.58, 124.00, 123.61, 123.44, 123.10, 120.51, 120.46, 119.51, 119.01, 118.91, 118.81, 110.83, 110.76, 108.95, 108.85, 43.26, 31.67, 29.05, 27.06, 22.62, 14.10.

9-(2-Ethylhexyl)-9′H-3,3′-bicarbazole (**7**) was synthesized by partially alkylating 9H,9′H-3,3′-bicarbazole (**2**), as it was described previously [67].

9-Octyl-9′H-3,3′-bicarbazole (**8**) was synthesized by partially alkylating 9H,9′H-3,3′-bicarbazole (**2**), as it was described previously [70].

4-(9′-Ethyl-[3,3′]-bicarbazol-9-yl)benzophenone (**DB41**) was synthesized by stirring 9-ethyl-9′H-3,3′-bicarbazole (**3**) (0.50 g, 1.39 mmol) with 4-fluorobenzophenone (0.28 g, 1.39 mmol) in 10 mL of DMSO at 150 °C under an inert nitrogen atmosphere with potas-

sium carbonate (1.92 g, 13.90 mmol) present. After 4 h, TLC was used to confirm the completion of the reaction, following slowly which the reaction mixture was slowly added to ice water. Chloroform was employed to extract the organic phase, and any remaining water traces in the organic phase were removed by adding anhydrous Na_2SO_4, which was filtered off later. The desired product was purified via column chromatography using tetrahydro-furan/hexane (volume ratio 1:3) as the mobile phase and silica gel as the stationary phase, resulting in a yellow amorphous material with a yield of 0.62 g (82%). $T_g = 102\ °C$ (DSC). ^{1}H NMR (400 MHz, $CDCl_3$, δ, m.d.): 8.48 (dd, 2H, $J_1 = 11.2$ Hz, $J_2 = 1.6$ Hz), 8.28 (d, 1H, J = 7.6 Hz), 8.24 (d, 1H, J = 7.6 Hz), 8.14 (d, 2H, J = 8.4 Hz), 7.97–7.95 (m, 1H), 7.89–7.81 (m, 4H), 7.69–7.65 (m, 2H), 7.61 (dd, 2H, $J_1 = 8.0$ Hz, $J_2 = 1.6$ Hz), 7.58–7.45 (m, 6H), 7.40 (t, 1H, J = 7.4 Hz), 7.33–7.30 (m, 1H), 4.46 (q, 2H, J = 7.2 Hz), 1.52 (t, 3H, J = 7.2 Hz). ^{13}C NMR (101 MHz, $CDCl_3$, δ, m.d.): 195.66, 141.81, 140.73, 140.46, 139.31, 139.21, 137.51, 135.97, 135.32, 132.95, 132.65, 131.95, 130.07, 128.49, 126.33, 126.21, 126.11, 125.81, 125.52, 124.51, 124.13, 123.59, 123.15, 120.69, 120.61, 120.56, 119.09, 119.00, 118.89, 110.07, 109.94, 108.73, 108.62, 37.69, 13.89. MS ($APCI^+$, 20 V): 540.26 ([M + H], 100%).

4-(9′-Butyl-[3,3′]-bicarbazol-9-yl)benzophenone (**DB44**) was synthesized by stirring 9-butyl-9′H-3,3′-bicarbazole (**3**) (0.50 g, 1.29 mmol) with 4-fluorobenzophenone (0.26 g, 1.29 mmol) in 10 mL of DMSO at 150 °C under an inert nitrogen atmosphere with potassium carbonate (1.78 g, 12.90 mmol) present. After 4 h, TLC was used to confirm the completion of the reaction, following which the reaction mixture was slowly added to ice water. Chloroform was employed to extract the organic phase, and any remaining water traces in the organic phase were removed by adding anhydrous Na_2SO_4, which was filtered off later. The desired product was purified via column chromatography using tetrahydro-furan/hexane (volume ratio 1:5) as the mobile phase and silica gel as the stationary phase, resulting in a yellow amorphous material with a yield of 0.66 g (90%). $T_g = 82\ °C$ (DSC). ^{1}H NMR (400 MHz, $CDCl_3$, δ, m.d.): 8.49 (dd, 2H, $J_1 = 8.4$ Hz, $J_2 = 1.6$ Hz), 8.29 (d, 1H, J = 7.6 Hz), 8.25 (d, 1H, J = 7.6 Hz), 8.14 (d, 2H, J = 7.2 Hz), 7.97 (d, 2H, J = 7.2 Hz), 7.89–7.84 (m, 2H), 7.82 (d, 2H, 8.4 Hz), 7.69–7.65 (m, 2H), 7.63–7.58 (m, 3H), 7.56–7.47 (m, 4H), 7.40 (t, 1H, J = 7.4 Hz), 7.31 (t, 1H, J = 7.6 Hz), 4.39 (t, 2H, J = 7.2 Hz), 1.95 (qu, 2H, J = 7.4 Hz), 1.48 (sext, 2H, J = 7.4 Hz), 1.02 (t, 3H, J = 7.4 Hz). ^{13}C NMR (101 MHz, $CDCl_3$, δ, m.d.): 196.66, 141.81, 140.98, 140.73, 139.74, 139.31, 137.53, 135.96, 135.33, 132.89, 132.66, 131.96, 130.08, 128.50, 126.34, 126.21, 126.11, 125.78, 125.49, 124.52, 124.15, 123.48, 123.04, 120.71, 120.62, 120.50, 119.01, 118.86, 110.08, 109.96, 108.99, 108.87, 43.00, 31.23, 20.64, 13.96. MS ($APCI^+$, 20 V): 568.39 ([M + H], 100%).

4-(9′-Pentyl-[3,3′]-bicarbazol-9-yl)benzophenone (**DB37**) was synthesized by stirring 9-pentyl-9′H-3,3′-bicarbazole (**3**) (0.50 g, 1.24 mmol) with 4-fluorobenzophenone (0.25 g, 1.24 mmol) in 10 mL of DMSO at 150 °C under an inert nitrogen atmosphere with potassium carbonate (1.72 g, 12.40 mmol) present. After 4 h, TLC was used to confirm the completion of the reaction, following which the reaction mixture was slowly added to ice water. Chloroform was employed to extract the organic phase, and any remaining water traces in the organic phase were removed by adding anhydrous Na_2SO_4, which was filtered off later. The desired product was purified via column chromatography using tetrahydro-furan/hexane (volume ratio 1:5) as the mobile phase and silica gel as the stationary phase, resulting in a yellow amorphous material with a yield of 0.66 g (91%). $T_g = 77\ °C$ (DSC). ^{1}H NMR (400 MHz, $CDCl_3$, δ, ppm): 8.47 (dd, 2H, $J_1 = 13.4$ Hz, $J_2 = 1.4$ Hz), 8.28 (d, 1H, J = 7.6 Hz), 8.23 (d, 1H, J = 7.6 Hz), 8.14 (d, 2H, J = 8.4 Hz), 7.97–7.94 (m, 2H), 7.88–7.81 (m, 4H), 7.69–7.65 (m, 2H), 7.62–7.57 (m, 3H), 7.55–7.46 (m, 4H), 7.39 (t, 1H, J = 7.4 Hz), 7.30 (t, 1H, J = 7.4 Hz), 4.38 (t, 2H, J = 7.2 Hz), 1.96 (qu, 2H, J = 7.2 Hz), 1.47–1.39 (m, 4H), 0.94 (t, 3H, J = 7.0 Hz). ^{13}C NMR (101 MHz, $CDCl_3$, δ, m.d.): 195.65, 141.80, 140.95, 140.71, 139.72, 139.29, 137.51, 135.95, 135.31, 132.86, 132.66, 131.96, 130.07, 128.49, 126.33, 126.20, 126.10, 125.78, 125.48, 124.50, 124.13, 123.46, 123.02, 120.69, 120.61, 120.48, 118.99, 118.84, 110.07, 109.94, 108.97, 108.85, 43.23, 29.49, 28.78, 22.54, 14.01. MS ($APCI^+$, 20 V): 582.34 ([M + H], 100%).

245

4-(9′-Hexyl-[3,3′]-bicarbazol-9-yl)benzophenone (**DB38**) was synthesized by stirring 9-hexyl-9′H-3,3′-bicarbazole (**3**) (0.50 g, 1.20 mmol) with 4-fluorobenzophenone (0.24 g, 1.20 mmol) in 10 mL of DMSO at 150 °C under an inert nitrogen atmosphere with potassium carbonate (1.66 g, 12.00 mmol) present. After 4 h, TLC was used to confirm the completion of the reaction, following which the reaction mixture was slowly added to ice water. Chloroform was employed to extract the organic phase, and any remaining water traces in the organic phase were removed by adding anhydrous Na_2SO_4, which was filtered off later. The desired product was purified via column chromatography using tetrahydrofuran/hexane (volume ratio 1:7) as the mobile phase and silica gel as the stationary phase, resulting in a yellow amorphous material with a yield of 0.67 g (94%). T_g = 68 °C (DSC). ^{1}H NMR (400 MHz, CDCl$_3$, δ, ppm): 8.48 (dd, 2H, J_1 = 12.4 Hz, J_2 = 1.6 Hz), 8.28 (d, 1H, 7.6 Hz), 8.23 (d, 1H, J = 8.0 Hz), 8.14 (d, 2H, J = 8.8 Hz), 7.97–7.95 (m, 2H), 7.88–7.81 (m, 4H), 7.69–7.65 (m, 2H), 7.62–7.58 (m, 3H), 7.56–7.45 (m, 4H), 7.39 (t, 1H, J = 7.2 Hz), 7.30 (t, 1H, J = 7.2 Hz), 4.38 (t, 2H, J = 7.2 Hz), 1.95 (qu, 2H, J = 7.4 Hz), 1.49–1.33 (m, 6H), 0.92 (t, 3H, J = 7.0 Hz). ^{13}C NMR (101 MHz, CDCl$_3$-*d$_6$*, δ, m.d.): 196.04, 141.80, 140.95, 140.70, 140.22, 139.01, 137.50, 135.95, 135.32, 132.86, 132.66, 131.97, 130.07, 128.55, 128.48, 127.24, 126.33, 126.21, 126.10, 125.77, 125.48, 124.49, 123.45, 123.01, 120.69, 120.62, 120.48, 119.00, 118.83, 110.07, 109.94, 108.97, 108.84, 43.26, 31.63, 29.03, 27.02, 22.60, 14.06. MS (APCI$^+$, 20 V): 596.36 ([M + H], 100%).

4-(9′-{2-Ethylhexyl}-[3,3′]-bicarbazol-9-yl)benzophenone (**DB39**) was synthesized by stirring 9-{2-ethylhexyl}-9′H-3,3′-bicarbazole (**3**) (0.50 g, 1.13 mmol) with 4-fluorobenzophenone (0.23 g, 1.13 mmol) in 10 mL of DMSO at 150 °C under an inert nitrogen atmosphere with potassium carbonate (1.56 g, 11.30 mmol) present. After 4 h, TLC was used to confirm the completion of the reaction, following which the reaction mixture was slowly added to ice water. Chloroform was employed to extract the organic phase, and any remaining water traces in the organic phase were removed by adding anhydrous Na_2SO_4, which was filtered off later. The desired product was purified via column chromatography using tetrahydrofuran/hexane (volume ratio 1:7) as the mobile phase and silica gel as the stationary phase, resulting in a pale-yellow amorphous material with a yield of 0.56 g (79%). T_g = 64 °C (DSC). ^{1}H NMR (400 MHz, CDCl$_3$, δ, ppm): 8.48 (dd, 2H, J_1 = 15.2 Hz, J_2 = 1.6 Hz), 8.28 (d, 1H, J = 7.6 Hz), 8.14 (d, 2H, J = 8.8 Hz), 7.97–7.95 (m, 2H), 7.86–7.81 (m, 4H), 7.69–7.65 (m, 2H), 7.62–7.58 (m, 3H), 7.55–7.45 (m, 4H), 7.40 (t, 1H, J = 7.2 Hz), 7.30 (t, 1H, J = 8.0 Hz), 4.26–4.23 (m, 2H), 2.21–2.13 (m, 1H), 1.50–1.31 (m, 8H), 0.98 (t, 3H, J = 7.4 Hz), 0.93 (t, 3H, J = 7.2 Hz). ^{13}C NMR (101 MHz, CDCl$_3$, δ, m.d.): 195.66, 141.81, 141.43, 140.71, 140.21, 139.29, 137.51, 135.94, 135.30, 132.82, 132.66, 131.97, 130.08, 128.50, 126.33, 126.20, 126.09, 125.75, 125.46, 124.51, 124.15, 123.42, 122.99, 120.70, 120.61, 120.43, 118.99, 118.92, 118.82, 110.08, 109.95, 109.27, 109.14, 47.57, 39.50, 31.07, 28.90, 24.46, 23.12, 14.11, 10.97. MS (APCI$^+$, 20 V): 624.44 ([M + H], 100%).

4-(9′-Octyl-[3,3′]-bicarbazol-9-yl)benzophenone (**DB40**) was synthesized by stirring 9-octyl-9′H-3,3′-bicarbazole (**3**) (0.50 g, 1.13 mmol) with 4-fluorobenzophenone (0.23 g, 1.13 mmol) in 10 mL of DMSO at 150 °C under an inert nitrogen atmosphere with potassium carbonate (1.56 g, 11.30 mmol) present. After 4 h, TLC was used to confirm the completion of the reaction, following which the reaction mixture was slowly added to ice water. Chloroform was employed to extract the organic phase, and any remaining water traces in the organic phase were removed by adding anhydrous Na_2SO_4, which was filtered off later. The desired product was purified via column chromatography using tetrahydrofuran/hexane (volume ratio 1:7) as the mobile phase and silica gel as the stationary phase, resulting in a pale-yellow amorphous material with a yield of 0.67 g (95%). T_g = 57 °C (DSC). ^{1}H NMR (400 MHz, CDCl$_3$, δ, ppm): 8.48 (dd, 2H, J_1 = 13.8 Hz, J_2 = 1.4 Hz), 8.28 (d, 1H, J = 7.6 Hz), 8.24 (d, 1H, J = 7.6 Hz), 8.14 (d, 2H, J = 8.4 Hz), 7.97–7.95 (m, 2H), 7.86–7.81 (m, 4H), 7.70–7.65 (m, 2H), 7.62–7.58 (m, 3H), 7.56–7.46 (m, 4H), 7.39 (t, 1H, J = 7.4 Hz), 7.30 (t, 1H, J = 7.6 Hz), 4.38 (t, 2H, J = 7.6 Hz), 1.95 (pent, 2H, J = 7.6 Hz), 1.48–1.29 (m, 10H), 0.91 (t, 3H, J = 7.4 Hz). ^{13}C NMR (101 MHz, CDCl$_3$, δ, m.d.): 195.66, 141.81, 140.96, 140.72, 139.72, 139.30, 137.51, 135.96, 135.33, 132.87, 132.65, 131.95, 130.07, 128.49, 126.32, 126.21, 126.10, 125.77, 125.48, 124.50, 124.14, 123.46, 123.02, 120.69, 120.60, 120.48, 119.00, 118.83,

110.06, 109.94, 108.97, 108.85, 43.26, 31.83, 29.43, 29.21, 29.06, 27.37, 22.63, 14.09. MS (APCI$^+$, 20 V): 624.44 ([M + H], 100%).

3.3. Fabrication and Characterization of Devices

A glass substrate with a pre-patterned indium tin oxide (ITO) layer, bought from Lumtec (Taiwan), was utilized in the production process of OLEDs. The mentioned substrate underwent a cleaning procedure with acetone for 30 min at 50 °C, followed by a cleaning with isopropyl alcohol for 30 min at 60 °C. Subsequently, the cleaned substrates were exposed to UV radiation for 10 min in a preheated UV chamber. The layer deposition process took place within a glove box under an inert atmosphere. For the next layer, the hole-injecting material poly(3,4-ethylene-dioxythiophene):poly(styrenesulfonate) (PEDOT:PSS) was employed. It was spin-coated onto the substrate at 4000 rpm for 20 s, followed by heating the substrates for 10 min at 130 °C. After cooling the substrates, the emissive layers, composed of host material and emitter, were formed on top of the hole injection layer. For deposition, spin-coating was also employed by spinning substrates for 20 s at 2500 rpm. Subsequently, the electron transporting layer, consisting of 1,3,5-tris(N-phenyl-benzimidazol-2-yl)benzene (TPBi), a LiF electron injecting layer, and aluminum cathode, were formed in a thermal evaporation chamber under a vacuum of 10^{-6} torr. Following this, the resulting devices, with an area of 0.09 cm², were placed in a mini chamber within the glove box under vacuum until further tests were conducted. These tests were performed under normal atmospheric conditions in complete darkness. The CS-100A luminance and color meter (Konica Minolta, Tokyo, Japan) was utilized to record voltage-current density and voltage-luminance characteristics. Additionally, the SpectraScan® spectroradiometer PR-655 (Jadak, North Syracuse, NY, USA) was used to create luminance-power efficacy and luminance-current graphs. The measurements of current-voltage characteristics were conducted using a Keithley voltmeter (Keithley Instruments, Cleveland, OH, USA). EQE was calculated using the method outlined in the literature [71].

4. Conclusions

We introduced novel emissive derivatives synthesized through a three-step process, utilizing bicarbazole and benzophenone as building blocks to achieve twisted donor-acceptor structures. The incorporation of alkyl sidechains of varying length was chosen to enhance the solubility and film-forming characteristics of the materials. Newly synthesized derivatives exhibited commendable thermal and morphological stability, as evidenced by temperatures of 5% mass loss ranging from 374 °C to 406 °C. The manipulation of alkyl sidechain length allowed control over glass-transition temperatures that spanned from 57 °C to a desirable 102 °C. Additionally, newly developed materials demonstrated short photoluminescence decay times, confirmed by time-resolved photoluminescence, and high photoluminescence quantum yields of up to 75.5%. The benzophenone-based derivatives exhibited favourable HOMO-LUMO levels as well as suitable triplet-singlet state energy values for application as potential blue TADF emitters. Upon investigation of the electroluminescent properties of the new devices, an OLED with an emissive layer comprised of 15 wt% **DB39** doped in a CBP host surpassed other devices in terms of efficiencies. The maximum current efficacy (CE$_{max}$) reaching 5.7 cd/A and 2.7% external quantum efficacy (EQE$_{max}$) were detected, followed by a maximum luminance (L$_{max}$) of 3581 cd/m^2 with a turn-on voltage of 3.9 V. This study emphasized the notable influence of energy transfer from host to guest, suitable doping concentrations, and the effect of chemical structure on solubility, thereby affecting the efficiency of wet-processed devices. It is crucial to highlight that these characteristics were observed in non-optimized OLEDs using standard laboratory conditions, suggesting potential enhancements through optimization processes. Furthermore, enhanced device efficiency could be achieved by reducing ΔE_{ST} and effectively utilizing triplet-state excitons of similar materials, making them suitable for highly efficient lighting applications. We believe that our findings suggest the potential of some materials for further exploration as promising emitters.

References

1. Hong, G.; Gan, X.; Leonhardt, C.; Zhang, Z.; Seibert, J.; Busch, J.M.; Bräse, S. A Brief History of OLEDs—Emitter Development and Industry Milestones. *Adv. Mater.* **2021**, *33*, 2005630. [CrossRef]

2. Luo, Y.-J.; Lu, Z.-Y.; Huang, Y. Triplet Fusion Delayed Fluorescence Materials for OLEDs. *Chin. Chem. Lett.* **2016**, *27*, 1223–1230. [CrossRef]

3. Zeng, H.; Huang, Q.; Liu, J.; Huang, Y.; Zhou, J.; Zhao, S.; Lu, Z. A Red-Emissive Sextuple Hydrogen-Bonding Self-Assembly Molecular Duplex Bearing Perylene Diimide Fluorophores for Warm-White Organic Light-Emitting Diode Application. *Chin. J. Chem.* **2016**, *34*, 387–396. [CrossRef]

4. Zhang, Z.; Li, W.; Ye, K.; Zhang, H. Synthesis, Structure and Properties of a Novel Benzothiazole-Based Diboron-Bridged π-Conjugated Ladder. *Acta Chim. Sin.* **2016**, *74*, 179. [CrossRef]

5. Yu, Y.; Yang, J.; Ren, Z.; Xie, G.; Li, Q.; Li, Z. Synthesis of Solution Processable Blue AIEgens and the Device Performance. *Acta Chim. Sin.* **2016**, *74*, 865. [CrossRef]

6. Im, Y.; Byun, S.Y.; Kim, J.H.; Lee, D.R.; Oh, C.S.; Yook, K.S.; Lee, J.Y. Recent Progress in High-Efficiency Blue-Light-Emitting Materials for Organic Light-Emitting Diodes. *Adv. Funct. Mater.* **2017**, *27*, 1603007. [CrossRef]

7. Root, S.E.; Savagatrup, S.; Printz, A.D.; Rodriquez, D.; Lipomi, D.J. Mechanical Properties of Organic Semiconductors for Stretchable, Highly Flexible, and Mechanically Robust Electronics. *Chem. Rev.* **2017**, *117*, 6467–6499. [CrossRef]

8. Kim, J.-J.; Han, M.-K.; Noh, Y.-Y. Flexible OLEDs and Organic Electronics. *Semicond. Sci. Technol.* **2011**, *26*, 030301. [CrossRef]

9. Jeong, E.G.; Kwon, J.H.; Kang, K.S.; Jeong, S.Y.; Choi, K.C. A Review of Highly Reliable Flexible Encapsulation Technologies towards Rollable and Foldable OLEDs. *J. Inf. Disp.* **2020**, *21*, 19–32. [CrossRef]

10. Reineke, S.; Lindner, F.; Schwartz, G.; Seidler, N.; Walzer, K.; Lüssem, B.; Leo, K. White Organic Light-Emitting Diodes with Fluorescent Tube Efficiency. *Nature* **2009**, *459*, 234–238. [CrossRef]

11. Sun, Y.; Giebink, N.C.; Kanno, H.; Ma, B.; Thompson, M.E.; Forrest, S.R. Management of Singlet and Triplet Excitons for Efficient White Organic Light-Emitting Devices. *Nature* **2006**, *440*, 908–912. [CrossRef]

12. Wang, J.; Liang, J.; Xu, Y.; Liang, B.; Wei, J.; Li, C.; Mu, X.; Ye, K.; Wang, Y. Purely Organic Phosphorescence Emitter-Based Efficient Electroluminescence Devices. *J. Phys. Chem. Lett.* **2019**, *10*, 5983–5988. [CrossRef] [PubMed]

13. Yang, X.; Yue, L.; Yu, Y.; Liu, B.; Dang, J.; Sun, Y.; Zhou, G.; Wu, Z.; Wong, W. Strategically Formulating Aggregation-Induced Emission-Active Phosphorescent Emitters by Restricting the Coordination Skeletal Deformation of Pt(II) Complexes Containing Two Independent Monodentate Ligands. *Adv. Opt. Mater.* **2020**, *8*, 2000079. [CrossRef]

14. Rajamalli, P.; Senthilkumar, N.; Huang, P.-Y.; Ren-Wu, C.-C.; Lin, H.-W.; Cheng, C.-H. New Molecular Design Concurrently Providing Superior Pure Blue, Thermally Activated Delayed Fluorescence and Optical Out-Coupling Efficiencies. *J. Am. Chem. Soc.* **2017**, *139*, 10948–10951. [CrossRef]

15. Zhu, M.; Yang, C. Blue Fluorescent Emitters: Design Tactics and Applications in Organic Light-Emitting Diodes. *Chem. Soc. Rev.* **2013**, *42*, 4963–4976. [CrossRef] [PubMed]

16. Du, C.; Lu, T.; Cheng, Z.; Chang, Y.; Liu, H.; Wang, J.; Wan, L.; Lv, Y.; Lu, P. Rational Molecular Design of Phenanthroimidazole-Based Fluorescent Materials towards High-Efficiency Non-Doped Deep Blue OLEDs. *J. Mater. Chem. C Mater.* **2022**, *10*, 14186–14193. [CrossRef]

17. Xu, H.; Chen, R.; Sun, Q.; Lai, W.; Su, Q.; Huang, W.; Liu, X. Recent Progress in Metal–Organic Complexes for Optoelectronic Applications. *Chem. Soc. Rev.* **2014**, *43*, 3259–3302. [CrossRef]

18. De Leeuw, D.M.; Simenon, M.M.J.; Brown, A.R.; Einerhand, R.E.F. Stability of N-Type Doped Conducting Polymers and Consequences for Polymeric Microelectronic Devices. *Synth. Met.* **1997**, *87*, 53–59. [CrossRef]

19. Scholz, S.; Kondakov, D.; Lüssem, B.; Leo, K. Degradation Mechanisms and Reactions in Organic Light-Emitting Devices. *Chem. Rev.* **2015**, *115*, 8449–8503. [CrossRef]

20. Lee, J.; Jeong, C.; Batagoda, T.; Coburn, C.; Thompson, M.E.; Forrest, S.R. Hot Excited State Management for Long-Lived Blue Phosphorescent Organic Light-Emitting Diodes. *Nat. Commun.* **2017**, *8*, 15566. [CrossRef]

21. Xing, L.; Zhu, Z.-L.; He, J.; Qiu, Z.; Yang, Z.; Lin, D.; Chen, W.-C.; Yang, Q.; Ji, S.; Huo, Y.; et al. Anthracene-Based Fluorescent Emitters toward Superior-Efficiency Nondoped TTA-OLEDs with Deep Blue Emission and Low Efficiency Roll-Off. *Chem. Eng. J.* **2021**, *421*, 127748. [CrossRef]

22. Chen, J.; Tao, W.; Chen, W.; Xiao, Y.; Wang, K.; Cao, C.; Yu, J.; Li, S.; Geng, F.; Adachi, C.; et al. Red/Near-Infrared Thermally Activated Delayed Fluorescence OLEDs with Near 100% Internal Quantum Efficiency. *Angew. Chem. Int. Ed.* **2019**, *58*, 14660–14665. [CrossRef]

23. Albrecht, K.; Matsuoka, K.; Fujita, K.; Yamamoto, K. Carbazole Dendrimers as Solution-Processable Thermally Activated Delayed-Fluorescence Materials. *Angew. Chem. Int. Ed.* **2015**, *54*, 5677–5682. [CrossRef]

24. Zhang, Q.; Li, J.; Shizu, K.; Huang, S.; Hirata, S.; Miyazaki, H.; Adachi, C. Design of Efficient Thermally Activated Delayed Fluorescence Materials for Pure Blue Organic Light Emitting Diodes. *J. Am. Chem. Soc.* **2012**, *134*, 14706–14709. [CrossRef] [PubMed]

25. Wu, K.; Zhang, T.; Wang, Z.; Wang, L.; Zhan, L.; Gong, S.; Zhong, C.; Lu, Z.-H.; Zhang, S.; Yang, C. De Novo Design of Excited-State Intramolecular Proton Transfer Emitters via a Thermally Activated Delayed Fluorescence Channel. *J. Am. Chem. Soc.* **2018**, *140*, 8877–8886. [CrossRef] [PubMed]

26. Goushi, K.; Yoshida, K.; Sato, K.; Adachi, C. Organic Light-Emitting Diodes Employing Efficient Reverse Intersystem Crossing for Triplet-to-Singlet State Conversion. *Nat. Photonics* **2012**, *6*, 253–258. [CrossRef]

27. Ahn, D.H.; Kim, S.W.; Lee, H.; Ko, I.J.; Karthik, D.; Lee, J.Y.; Kwon, J.H. Highly Efficient Blue Thermally Activated Delayed Fluorescence Emitters Based on Symmetrical and Rigid Oxygen-Bridged Boron Acceptors. *Nat. Photonics* **2019**, *13*, 540–546. [CrossRef]

28. Uoyama, H.; Goushi, K.; Shizu, K.; Nomura, H.; Adachi, C. Highly Efficient Organic Light-Emitting Diodes from Delayed Fluorescence. *Nature* **2012**, *492*, 234–238. [CrossRef] [PubMed]

29. Wang, Z.; Li, Y.; Cai, X.; Chen, D.; Xie, G.; Liu, K.; Wu, Y.-C.; Lo, C.-C.; Lien, A.; Cao, Y.; et al. Structure–Performance Investigation of Thioxanthone Derivatives for Developing Color Tunable Highly Efficient Thermally Activated Delayed Fluorescence Emitters. *ACS Appl. Mater. Interfaces* **2016**, *8*, 8627–8636. [CrossRef]

30. Im, Y.; Kim, M.; Cho, Y.J.; Seo, J.-A.; Yook, K.S.; Lee, J.Y. Molecular Design Strategy of Organic Thermally Activated Delayed Fluorescence Emitters. *Chem. Mater.* **2017**, *29*, 1946–1963. [CrossRef]

31. Cai, X.; Li, X.; Xie, G.; He, Z.; Gao, K.; Liu, K.; Chen, D.; Cao, Y.; Su, S.-J. "Rate-Limited Effect" of Reverse Intersystem Crossing Process: The Key for Tuning Thermally Activated Delayed Fluorescence Lifetime and Efficiency Roll-off of Organic Light Emitting Diodes. *Chem. Sci.* **2016**, *7*, 4264–4275. [CrossRef] [PubMed]

32. Hatakeyama, T.; Shiren, K.; Nakajima, K.; Nomura, S.; Nakatsuka, S.; Kinoshita, K.; Ni, J.; Ono, Y.; Ikuta, T. Ultrapure Blue Thermally Activated Delayed Fluorescence Molecules: Efficient HOMO–LUMO Separation by the Multiple Resonance Effect. *Adv. Mater.* **2016**, *28*, 2777–2781. [CrossRef] [PubMed]

33. Zheng, X.; Huang, R.; Zhong, C.; Xie, G.; Ning, W.; Huang, M.; Ni, F.; Dias, F.B.; Yang, C. Achieving 21% External Quantum Efficiency for Nondoped Solution-Processed Sky-Blue Thermally Activated Delayed Fluorescence OLEDs by Means of Multi-(Donor/Acceptor) Emitter with Through-Space/-Bond Charge Transfer. *Adv. Sci.* **2020**, *7*, 1902087. [CrossRef] [PubMed]

34. Ma, F.; Ji, H.; Zhang, D.; Xue, K.; Zhang, P.; Qi, Z.; Zhu, H. Adjusting the Photophysical Properties of AIE-Active TADF Emitters from through-Bond to through-Space Charge Transfer for High-Performance Solution-Processed OLEDs. *Dye. Pigment.* **2021**, *188*, 109208. [CrossRef]

35. Rajamalli, P.; Rota Martir, D.; Zysman-Colman, E. Pyridine-Functionalized Carbazole Donor and Benzophenone Acceptor Design for Thermally Activated Delayed Fluorescence Emitters in Blue Organic Light-Emitting Diodes. *J. Photonics Energy* **2018**, *8*, 032106. [CrossRef]

36. Ma, M.; Li, J.; Liu, D.; Li, D.; Dong, R.; Mei, Y. Low Efficiency Roll-off Thermally Activated Delayed Fluorescence Emitters for Non-Doped OLEDs: Substitution Effect of Thioether and Sulfone Groups. *Dye. Pigment.* **2021**, *194*, 109649. [CrossRef]

37. Wu, L.; Wang, K.; Wang, C.; Fan, X.-C.; Shi, Y.-Z.; Zhang, X.; Zhang, S.-L.; Ye, J.; Zheng, C.-J.; Li, Y.-Q.; et al. Using Fluorene to Lock Electronically Active Moieties in Thermally Activated Delayed Fluorescence Emitters for High-Performance Non-Doped Organic Light-Emitting Diodes with Suppressed Roll-Off. *Chem. Sci.* **2021**, *12*, 1495–1502. [CrossRef] [PubMed]

38. Aizawa, N.; Tsou, C.-J.; Park, I.S.; Yasuda, T. Aggregation-Induced Delayed Fluorescence from Phenothiazine-Containing Donor–Acceptor Molecules for High-Efficiency Non-Doped Organic Light-Emitting Diodes. *Polym. J.* **2017**, *49*, 197–202. [CrossRef]

39. Jing, Y.-Y.; Tao, X.-D.; Yang, M.-X.; Chen, X.-L.; Lu, C.-Z. Triptycene-Imbedded Thermally Activated Delayed Fluorescence Emitters with Excellent Film Morphologies for Applications in Efficient Nondoped and Doped Organic Light-Emitting Devices. *Chem. Eng. J.* **2021**, *413*, 127418. [CrossRef]

249

40. Tani, K.; Yashima, T.; Miyanaga, K.; Hori, K.; Goto, K.; Tani, F.; Habuka, Y.; Suzuki, K.; Shizu, K.; Kaji, H. Carbazole and Benzophenone Based Twisted Donor–Acceptor Systems as Solution Processable Green Thermally Activated Delayed Fluorescence Organic Light Emitters. *Chem. Lett.* **2018**, *47*, 1236–1239. [CrossRef]

41. Liu, Y.; Wu, X.; Chen, Y.; Chen, L.; Li, H.; Wang, W.; Wang, S.; Tian, H.; Tong, H.; Wang, L. Triazatruxene-Based Thermally Activated Delayed Fluorescence Small Molecules with Aggregation-Induced Emission Properties for Solution-Processable Nondoped OLEDs with Low Efficiency Roll-Off. *J. Mater. Chem. C Mater.* **2019**, *7*, 9719–9725. [CrossRef]

42. Wang, J.; Zhang, J.; Jiang, C.; Yao, C.; Xi, X. Effective Design Strategy for Aggregation-Induced Emission and Thermally Activated Delayed Fluorescence Emitters Achieving 18% External Quantum Efficiency Pure-Blue OLEDs with Extremely Low Roll-Off. *ACS Appl. Mater. Interfaces* **2021**, *13*, 57713–57724. [CrossRef] [PubMed]

43. Shizu, K.; Lee, J.; Tanaka, H.; Nomura, H.; Yasuda, T.; Kaji, H.; Adachi, C. Highly Efficient Electroluminescence from Purely Organic Donor–Acceptor Systems. *Pure Appl. Chem.* **2015**, *87*, 627–638. [CrossRef]

44. Nishimoto, T.; Yasuda, T.; Lee, S.Y.; Kondo, R.; Adachi, C. A Six-Carbazole-Decorated Cyclophosphazene as a Host with High Triplet Energy to Realize Efficient Delayed-Fluorescence OLEDs. *Mater. Horiz.* **2014**, *1*, 264–269. [CrossRef]

45. Huang, B.; Ban, X.; Sun, K.; Ma, Z.; Mei, Y.; Jiang, W.; Lin, B.; Sun, Y. Thermally Activated Delayed Fluorescence Materials Based on Benzophenone Derivative as Emitter for Efficient Solution-Processed Non-Doped Green OLED. *Dye. Pigment.* **2016**, *133*, 380–386. [CrossRef]

46. Liang, J.; Li, C.; Zhuang, X.; Ye, K.; Liu, Y.; Wang, Y. Novel Blue Bipolar Thermally Activated Delayed Fluorescence Material as Host Emitter for High-Efficiency Hybrid Warm-White OLEDs with Stable High Color-Rendering Index. *Adv. Funct. Mater.* **2018**, *28*, 1707002. [CrossRef]

47. Pocock, I.A.; Alotaibi, A.M.; Jagdev, K.; Prior, C.; Burgess, G.R.; Male, L.; Grainger, R.S. Direct Formation of 4,5-Disubstituted Carbazoles via Regioselective Dilithiation. *Chem. Commun.* **2021**, *57*, 7252–7255. [CrossRef] [PubMed]

48. Zhu, X.-D.; Tian, Q.-S.; Zheng, Q.; Tao, X.-C.; Yuan, Y.; Yu, Y.-J.; Li, Y.; Jiang, Z.-Q.; Liao, L.-S. A Sky-Blue Thermally Activated Delayed Fluorescence Emitter Based on Multimodified Carbazole Donor for Efficient Organic Light-Emitting Diodes. *Org. Electron.* **2019**, *68*, 113–120. [CrossRef]

49. Liu, F.; Zou, J.; He, Q.; Tang, C.; Xie, L.; Peng, B.; Wei, W.; Cao, Y.; Huang, W. Carbazole End-capped Pyrene Starburst with Enhanced Electrochemical Stability and Device Performance. *J. Polym. Sci. A Polym. Chem.* **2010**, *48*, 4943–4949. [CrossRef]

50. Sęk, D.; Szlapa-Kula, A.; Siwy, M.; Fabiańczyk, A.; Janeczek, H.; Szalkowski, M.; Maćkowski, S.; Schab-Balcerzak, E. Branched Azomethines Based on Tris(2-Aminoethyl)Amine: Impact of Imine Core Functionalization on Thermal, Electrochemical and Luminescence Properties. *Mater. Chem. Phys.* **2020**, *240*, 122246. [CrossRef]

51. Sebris, A.; Novosjolova, I.; Traskovskis, K.; Kokars, V.; Tetervenoka, N.; Vembris, A.; Turks, M. Photophysical and Electrical Properties of Highly Luminescent 2/6-Triazolyl-Substituted Push-Pull Purines. *ACS Omega* **2022**, *7*, 5242–5253. [CrossRef]

52. Yang, Z.; Chi, Z.; Yu, T.; Zhang, X.; Chen, M.; Xu, B.; Liu, S.; Zhang, Y.; Xu, J. Triphenylethylene Carbazole Derivatives as a New Class of AIE Materials with Strong Blue Light Emission and High Glass Transition Temperature. *J. Mater. Chem.* **2009**, *19*, 5541. [CrossRef]

53. Costa, J.C.S.; Lima, M.A.L.; Mendes, A.; Santos, L.M.N.B.F. The Impact of Phenyl–Phenyl Linkage on the Thermodynamic, Optical and Morphological Behavior of Carbazol Derivatives. *RSC Adv.* **2020**, *10*, 11766–11776. [CrossRef] [PubMed]

54. Huang, T.; Jiang, W.; Duan, L. Recent Progress in Solution Processable TADF Materials for Organic Light-Emitting Diodes. *J. Mater. Chem. C Mater.* **2018**, *6*, 5577–5596. [CrossRef]

55. Wang, J.; Liu, C.; Jiang, C.; Yao, C.; Gu, M.; Wang, W. Solution-Processed Aggregation-Induced Delayed Fluorescence (AIDF) Emitters Based on Strong π-Accepting Triazine Cores for Highly Efficient Nondoped OLEDs with Low Efficiency Roll-Off. *Org. Electron.* **2019**, *65*, 170–178. [CrossRef]

56. Li, Y.; Xie, G.; Gong, S.; Wu, K.; Yang, C. Dendronized Delayed Fluorescence Emitters for Non-Doped, Solution-Processed Organic Light-Emitting Diodes with High Efficiency and Low Efficiency Roll-off Simultaneously: Two Parallel Emissive Channels. *Chem. Sci.* **2016**, *7*, 5441–5447. [CrossRef]

57. Sun, S.; Wang, J.; Chen, L.; Chen, R.; Jin, J.; Chen, C.; Chen, S.; Xie, G.; Zheng, C.; Huang, W. Thermally Activated Delayed Fluorescence Enantiomers for Solution-Processed Circularly Polarized Electroluminescence. *J. Mater. Chem. C Mater.* **2019**, *7*, 14511–14516. [CrossRef]

58. Inoue, S.; Minemawari, H.; Tsutsumi, J.; Chikamatsu, M.; Yamada, T.; Horiuchi, S.; Tanaka, M.; Kumai, R.; Yoneya, M.; Hasegawa, T. Effects of Substituted Alkyl Chain Length on Solution-Processable Layered Organic Semiconductor Crystals. *Chem. Mater.* **2015**, *27*, 3809–3812. [CrossRef]

59. Schmaljohann, D.; Häußler, L.; Pötschke, P.; Voit, B.I.; Loontjens, T.J.A. Modification with Alkyl Chains and the Influence on Thermal and Mechanical Properties of Aromatic Hyperbranched Polyesters. *Macromol. Chem. Phys.* **2000**, *201*, 49–57. [CrossRef]

60. Makuła, P.; Pacia, M.; Macyk, W. How To Correctly Determine the Band Gap Energy of Modified Semiconductor Photocatalysts Based on UV–Vis Spectra. *J. Phys. Chem. Lett.* **2018**, *9*, 6814–6817. [CrossRef]

61. Zhao, L.; Liu, Y.; Wang, S.; Tao, Y.; Wang, F.; Zhang, X.; Huang, W. Novel Hyperbranched Polymers as Host Materials for Green Thermally Activated Delayed Fluorescence OLEDs. *Chin. J. Polym. Sci.* **2017**, *35*, 490–502. [CrossRef]

62. Sworakowski, J. How Accurate Are Energies of HOMO and LUMO Levels in Small-Molecule Organic Semiconductors Determined from Cyclic Voltammetry or Optical Spectroscopy? *Synth. Met.* **2018**, *235*, 125–130. [CrossRef]

63. Li, F.; Gillett, A.J.; Gu, Q.; Ding, J.; Chen, Z.; Hele, T.J.H.; Myers, W.K.; Friend, R.H.; Evans, E.W. Singlet and Triplet to Doublet Energy Transfer: Improving Organic Light-Emitting Diodes with Radicals. *Nat. Commun.* **2022**, *13*, 2744. [CrossRef] [PubMed]

64. Chen, C.; Huang, R.; Batsanov, A.S.; Pander, P.; Hsu, Y.; Chi, Z.; Dias, F.B.; Bryce, M.R. Intramolecular Charge Transfer Controls Switching Between Room Temperature Phosphorescence and Thermally Activated Delayed Fluorescence. *Angew. Chem. Int. Ed.* **2018**, *57*, 16407–16411. [CrossRef] [PubMed]

65. Liu, X.; Lv, D.; Wang, S.; Yu, X.; Han, Y. Improving Film Uniformity and Interface Solvent Resistance to Realize Multilayer Printing of OLED Devices. *J. Mater. Chem. C Mater.* **2024**, *12*, 4070–4084. [CrossRef]

66. Wang, G.; Chernikov, A.; Glazov, M.M.; Heinz, T.F.; Marie, X.; Amand, T.; Urbaszek, B. *Colloquium*: Excitons in Atomically Thin Transition Metal Dichalcogenides. *Rev. Mod. Phys.* **2018**, *90*, 021001. [CrossRef]

67. Trovatello, C.; Katsch, F.; Borys, N.J.; Selig, M.; Yao, K.; Borrego-Varillas, R.; Scotognella, F.; Kriegel, I.; Yan, A.; Zettl, A.; et al. The Ultrafast Onset of Exciton Formation in 2D Semiconductors. *Nat. Commun.* **2020**, *11*, 5277. [CrossRef]

68. Vaitkeviciene, V.; Grigalevicius, S.; Grazulevicius, J.V.; Jankauskas, V.; Syromyatnikov, V.G. Hole-Transporting [3,3']Bicarbazolyl-Based Polymers and Well-Defined Model Compounds. *Eur. Polym. J.* **2006**, *42*, 2254–2260. [CrossRef]

69. Gautam, P.; Shahnawaz; Siddiqui, I.; Blazevicius, D.; Krucaite, G.; Tavgeniene, D.; Jou, J.-H.; Grigalevicius, S. Bifunctional Bicarbazole-Benzophenone-Based Twisted Donor–Acceptor–Donor Derivatives for Deep-Blue and Green OLEDs. *Nanomaterials* **2023**, *13*, 1408. [CrossRef]

70. Blazevicius, D.; Siddiqui, I.; Gautam, P.; Krucaite, G.; Tavgeniene, D.; Nagar, M.R.; Kumar, K.; Banik, S.; Jou, J.-H.; Grigalevicius, S. Bicarbazole-Benzophenone-Based Twisted Donor-Acceptor-Donor Derivatives as Blue Emitters for Highly Efficient Fluorescent Organic Light-Emitting Diodes. *Nanomaterials* **2024**, *14*, 146. [CrossRef]

71. De Sa Pereira, D.; Data, P.; Monkman, A.P. Methods of Analysis of Organic Light Emitting Diodes. *Display* **2017**, *2*, 323–337.

CURRICULUM VITAE

Dovydas Blaževičius
dovydas.blazevicius@ktu.lt

Education:

2002 – 2014	Ugnės Karvelis Gymnasium, Noreikiškės, Lithuania
2014 – 2018	Kaunas University of Technology, Bachelor's degree in applied chemistry
2018 – 2020	Kaunas University of Technology, Master's degree in chemical engineering
2020 – present	Kaunas University of Technology, PhD candidate in chemistry

Work experience:

18 Sept 2018 – 03 Feb 2019	Project *New structure organic semiconductors for efficient phosphorescent light emitting diodes* engineer at Kaunas University of Technology.
02 Jan 2019 – 31 Dec 2021	Project *Novel TADF materials and device architectures to enhance the performance of OLED* engineer at Kaunas University of Technology.
02 Jan 2019 – 30 Sept 2020	Project *New Structure Electroactive Materials for Efficient Phosphorescent Organic Light Emitting Diodes* engineer at Kaunas University of Technology.
17 Aug 2020 – 31 Dec 2020	Project *New Generation Organic Semiconductors for OLED Technologies* engineer at Kaunas University of Technology.
01 Apr 2021 – 23 Dec 2021	Project *Electroactive Materials Designed by Artificial Intelligence Methods: Synthesis, Properties and Application in Optoelectronics* junior researcher at Kaunas University of Technology.
01 Apr 2022 – 29 Dec 2023	Project *Efficiency enhancement of Sn perovskite solar cells with self-assembled layer by optimizing charge injection balance* junior researcher at Kaunas University of Technology.
01 Apr 2022 – Now	Project *Long lifetime third generation organic light emitting diodes for physiologically friendly lighting* junior

researcher at Kaunas University of technology.

24 Jan 2024 – Now	Project *Making the dark lighter: infrared visualization using thermally activated delayed fluorescence* junior researcher at Kaunas University of Technology.

Scientific work:

2017 – 2020	Complected four student's scientific practices at Kaunas University of Technology, funded by the Research Council of Lithuania
2017 – Now	Research work under leadership of Prof. Dr. Saulius Grigalevičius, aiming at synthesizing novel organic semiconductors and applying them in organic light-emitting diodes

Awards and scholarships:

2018 – 2020	Four University's talent scholarships for research and study results
2019	Kazickas family scholarship
2019	Scholarship of the President of the Republic of Lithuania
2020	Award for the best Master's thesis from the Lithuanian Union of Young Scientists
2020 – 2023	Four scholarships for the most active PhD students at Kaunas University of Technology
2021	A laureate of the competition of the University students' research works organized by The Lithuanian Academy of Sciences
2023	A laureate of the competition of PhD students' and young scientists' research works organized by The Lithuanian Academy of Sciences

List of publications in peer-reviewed journals:

1. [S1; CH; OA] Siddiqui, I.; Gautam, P.; **Blazevicius, D.**; Jayakumar, J.; Lenka, S.; Tavgeniene, D.; Zaleckas, E.; Grigalevicius, S.; Jou, J.-H. Bicarbazole-benzophenone based twisted donor-acceptor derivatives as potential blue TADF emitters for OLEDs // *Molecules*. Basel: MDPI. ISSN 1420-3049. 2024, Vol. 29, iss. 7, art. No. 1672, p. 1–17. DOI:10.3390/molecules29071672. [Science Citation Index Expanded (Web of Science); Scopus; MEDLINE] [IF: 4.600; AIF: 6.400; IF/AIF: 0.718; Q2 (2022, InCites JCR SCIE)] [Field: N 003, T 004] [Contribution: 0.111]

2. [S1; CH; OA] **Blazevicius, D.**; Grigalevicius, S. A review of benzophenone-based derivatives for organic light-emitting diodes // *Nanomaterials*. Basel: MDPI. ISSN 2079-4991. 2024, Vol. 14, iss. 4, art. No. 356, p. 1–35. DOI: 10.3390/nano14040356. [Science Citation Index Expanded (Web of Science); Scopus; MEDLINE][IF: 5.300; AIF: 6.825; IF/AIF: 0.776; Q1 (2022, InCites JCR SCIE)] [Field: N 003] [Contribution: 0.500]

3. [S1; CH] **Blazevicius, D.**; Siddiqui, I.; Gautam, P.; Krucaite, G.; Tavgeniene, D.; Nagar, M. R.; Kumar, K.; Banik, S.; Jou, J.-H.; Grigalevicius, S. Bicarbazole-benzophenone-based twisted donor-acceptor-donor derivatives as blue emitters for highly efficient fluorescent organic light-emitting diodes // *Nanomaterials*. Basel: MDPI. ISSN 2079-4991. 2024, Vol. 14, iss. 2, art. No. 146, p. 1–14. DOI: 10.3390/nano14020146. [Science Citation Index Expanded (Web of Science); Scopus; MEDLINE] [IF: 5.300; AIF: 6.825; IF/AIF: 0.776; Q1 (2022, InCites JCR SCIE)] [Field: N 003] [Contribution: 0.100]

4. [S1; CH] Kotowicz, S.; Korzec, M.; Małecki, J. G.; Pająk, A. K.; Łuczak, A.; Jung, J.; Krucaite, G.; Tavgeniene, D.; Beresneviciute, R.; **Blazevicius, D.**; Zaleckas, E.; Sutkuvienė, S.; Grigalevičius, S.; Schab-Balcerzak, E. Carbazole core derivatives and their photophysical and electrochemical investigations supported by the theoretical calculations // *Synthetic Metals*. Lausanne: Elsevier. ISSN 0379-6779. 2024, Vol. 301, art. No. 117533, p. 1–13. DOI: 10.1016/j.synthmet.2023.117533. [Science Citation Index Expanded (Web of Science); Scopus] [IF: 4.400; AIF: 6.033; IF/AIF: 0.729; Q2 (2022, InCites JCR SCIE)] [Field: N 003, N 004, T 004] [Contribution: 0.071]

5. [S1; CH; OA] Gautam, P.; Shahnawaz, -.; Siddiqui, I.; **Blazevicius, D.**; Krucaite, G.; Tavgeniene, D.; Jou, J.-H.; Grigalevicius, S. Bifunctional bicarbazole-benzophenone-based twisted donor–acceptor–donor derivatives for deep-blue and green OLEDs // *Nanomaterials*. Basel: MDPI. ISSN 2079-4991. 2023, Vol. 13, iss. 8, art. No. 1408, p. 1–8. DOI: 10.3390/nano13081408. [Science Citation Index Expanded (Web of Science); Scopus; MEDLINE] [IF: 5.300; AIF: 6.825; IF/AIF: 0.776; Q1 (2022, InCites JCR SCIE)][Field: N 003] [Contribution: 0.125]

6. [S1; GB; OA] Nagar, M. R.; Kumar, K.; **Blazevicius, D.**; Beresneviciute, R.; Krucaite, G.; Tavgeniene, D.; Hao, C. T.; Banik, S.; Jou, J.-H.; Grigalevicius, S. Solution processable carbazole-benzophenone derivatives as bipolar hosts enabling high-efficiency stable green TADF organic LEDs // *Journal of Materials Chemistry C*. Cambridge: Royal Society of Chemistry. ISSN 2050-7526. eISSN 2050-7534. 2023, Vol. 11, iss. 4, p. 1579–1592. DOI: 10.1039/d2tc04820e. [Science Citation Index Expanded (Web of Science); Scopus] [IF: 6.400; AIF: 5.750; IF/AIF: 1.113; Q1 (2022, InCites JCR SCIE)][Field: N 003] [Contribution: 0.100]

7. [S1; GB] Sudheendran Swyamprabha, S.; Kishore Kesavan, K.; Siddiqui, I.; **Blazevicius, D.**; Jayachandran, J.; Eidimtas, M.; Nayak, S. R.; Nagar, M. R.; Yadav, R. A. K.; Krucaite, G.; Vaidyanathan, S.; Grigalevicius, S.; Jou, J.-H. Novel carbazole host materials for solution processed TADF organic light emitting diodes // *Dyes and Pigments*. Oxford: Elsevier. ISSN 0143-7208. eISSN 1873-3743. 2023, Vol. 208, art. No. 110821, p. 1–11. DOI: 10.1016/j.dyepig.2022.110821. [Science Citation Index

Expanded (Web of Science); Scopus] [IF: 4.500; AIF: 5.433; IF/AIF: 0.828; Q1 (2022, InCites JCR SCIE)] [Field: N 003] [Contribution: 0.076]

8. [S1; CH; OA] Tavgeniene, D.; Beresneviciute, R.; **Blazevicius, D.**; Krucaite, G.; Jacunskaite, G.; Sudheendran Swayamprabha, S.; Jou, J.-H.; Grigalevicius, S. 3-(N,N-diphenylamino)carbazole donor containing bipolar derivatives with very high glass transition temperatures as potential TADF emitters for OLEDs // *Coatings*. Basel: MDPI. ISSN 2079-6412. 2022, Vol. 12, iss. 7, art. No. 932, p. 1–10. DOI: 10.3390/coatings12070932. [Science Citation Index Expanded (Web of Science); Scopus; Dimensions] [IF: 3.400; AIF: 5.500; IF/AIF: 0.618; Q2 (2022, InCites JCR SCIE)] [Field: N 003] [Contribution: 0.125]

9. [S1; NL] Ho, C.-Y.; Krucaite, G.; Beresneviciute, R.; **Blazevicius, D.**; Lin, W. H.; Lu, J.-C.; Lin, C.-Y.; Grigalevicius, S.; Chang, C.-H. Triphenylethene-carbazole-based molecules for the realization of blue and white aggregation-induced emission OLEDs with high luminance // *Organic Electronics*. Amsterdam: Elsevier. ISSN 1566-1199. eISSN 1878-5530. 2022, Vol. 108, art. No. 106571, p. 1–10. DOI: 10.1016/j.orgel.2022.106571. [Science Citation Index Expanded (Web of Science); Scopus] [IF: 3.200; AIF: 5.750; IF/AIF: 0.556; Q2 (2022, InCites JCR SCIE)] Field: N 003] [Contribution: 0.111]

10. [S1; GB] Nagar, M. R.; Choudhury, A.; Tavgeniene, D.; Beresneviciute, R.; **Blazevicius, D.**; Jankauskas, V.; Kumar, K.; Banik, S.; Ghosh, S.; Grigalevičius, S.; Jou, J.-H. Solution-processable phenothiazine and phenoxazine substituted fluorene cored nanotextured hole transporting materials for achieving high-efficiency OLEDs // *Journal of Materials Chemistry C*. Cambridge: Royal Society of Chemistry. ISSN 2050-7526. eISSN 2050-7534. 2022, Vol. 10, iss. 9, p. 3593–3608. DOI: 10.1039/d1tc05237c. [Science Citation Index Expanded (Web of Science); Scopus] [IF: 6.400; AIF: 5.750; IF/AIF: 1.113; Q1 (2022, InCites JCR SCIE)] [Field: N 002, N 003] [Contribution: 0.090]

11. [S1; CH; OA] Shahnawaz, S.; Siddiqui, I.; Nagar, M. R.; Choudhury, A.; Lin, J.-T.; **Blazevicius, D.**; Krucaite, G.; Grigalevicius, S.; Jou, J.-H. Highly efficient candlelight organic light-emitting diode with a very low color temperature // *Molecules*. Basel : MDPI. ISSN 1420-3049. 2021, Vol. 26, iss. 24, art. No. 7558, p. 1–17. DOI: 10.3390/molecules26247558. [Science Citation Index Expanded (Web of Science); Scopus; Academic Search Ultimate] [IF: 4.927; AIF: 6.975; IF/AIF: 0.706; Q2 (2021, InCites JCR SCIE)] [Field: N 003] [Contribution: 0.111]

12. [S1; CH; OA] **Blazevicius, D.**; Tavgeniene, D.; Sutkuviene, S.; Zaleckas, E.; Jiang, M.; Swayamprabha, S.S.; Yadav, R.A.K.; Jou, J.-H.; Grigalevicius, S. Pyridinyl-carbazole fragments containing host materials for efficient green and blue phosphorescent OLEDs // *Molecules*. Basel: MDPI. ISSN 1420-3049. 2021, Vol. 26, iss. 15, art. No. 4615, p. 1–10. DOI: 10.3390/molecules26154615. [Science Citation Index Expanded (Web of Science); Scopus; MEDLINE] [IF: 4.927; AIF: 6.975; IF/AIF: 0.706; Q2 (2021, InCites JCR SCIE)] [Field: N 003, T 004] [Contribution: 0.112]

13. [S1; GB] Krucaite, G.; **Blazevicius, D.**; Beresneviciute, R.; Griniene, R. New structure hole transporting derivative for efficient organic light emitting devices // *Molecular Crystals and Liquid Crystals*. Abingdon: Taylor & Francis. ISSN 1542-

1406. eISSN 1563-5287. 2021, Vol. 716, iss. 1, p. 137–143. DOI: 10.1080/15421406.2020.1862455. [Science Citation Index Expanded (Web of Science); Scopus] [IF: 0.672; AIF: 5.524; IF/AIF: 0.121; Q4 (2021, InCites JCR SCIE)] [Field: N 003, T 008] [Contribution: 0.250]

14. [S1; GB] **Blazevicius, D**.; Krucaite, G.; Tavgeniene, D.; Griniene, R. New structure host material for phosphorescent OLED devices // *Molecular Crystals and Liquid Crystals*. Abingdon: Taylor & Francis. ISSN 1542-1406. eISSN 1563-5287. 2021, Vol. 716, iss. 1, p. 69–75. DOI: 10.1080/15421406.2020.1859697. [Science Citation Index Expanded (Web of Science); Scopus] [IF: 0.672; AIF: 5.524; IF/AIF: 0.121; Q4 (2021, InCites JCR SCIE)] [Field: N 003, T 008] [Contribution: 0.250]

15. [S1; NL] **Blazevicius, D.**; Krucaite, G.; Shahnawaz, S.; Swayamprabha, S.S.; Zaleckas, E.; Jou, J.-H.; Grigalevicius, S.. Easily synthesized and cheap carbazole- or phenoxazine-based hosts for efficient yellow phosphorescent OLEDs // *Optical Materials*. Amsterdam: Elsevier. ISSN 0925-3467. eISSN 1873-1252. 2021, vol. 118, art. no. 111251, p. 1-6. DOI: 10.1016/j.optmat.2021.111251. [Science Citation Index Expanded (Web of Science); Scopus] [IF: 3.754; AIF: 5.019; IF/AIF: 0.747; Q2 (2021, InCites JCR SCIE)] [M.kr.: N 003, T 004] [Contribution: 0.148]

16. [S1; CH; OA] Krucaite, G.; Tavgeniene, D.; **Blazevicius, D.**; Zhang, B.; Vembris, A.; Grigalevicius, Saulius. New electroactive polymers with electronically isolated 4,7-diarylfluorene chromophores as positive charge transporting layer materials for OLEDs // *Molecules*. Basel: MDPI. ISSN 1420-3049. 2021, Vol. 26, iss. 7, art. No. 1936, p. 1–11. DOI: 10.3390/molecules26071936. [Science Citation Index Expanded (Web of Science); Scopus; MEDLINE] [IF: 4.927; AIF: 6.975; IF/AIF: 0.706; Q2 (2021, InCites JCR SCIE)] [Field: N 003] [Contribution: 0.166]

List of conferences:

1. **Blaževičius, D.**; Kirstukas, M. Žvakės šviesą skleidžiantys organiniai šviestukai melatonino neslopinantiems apšvietimo prietaisams // Bioateitis: gamtos ir gyvybės mokslų perspektyvos: 16-oji Lietuvos jaunųjų mokslininkų konferencija: pranešimų tezės / leidinį sudarė J. Olechnovičienė. Vilnius: Lietuvos mokslų akademija. 2023, p. 35.

2. **Blaževičius, D**.; Beresnevičiūtė, R.; Kručaitė, G.; Tavgenienė, D.; Grigalevičius, S.; Nagar, M.R.; Hao, C.T.; Jou, J.-H.; Kumar, K. Carbazole-benzophenone derivatives as hosts for solution processable green TADF OLED devices // Baltic polymer symposium 2023, Jelgava, Latvia, September 20–22, 2023: book of abstracts. Jelgava: Latvian university of life sciences and technologies. 2023, p. 57.

3. **Blaževičius, D.**; Kručaitė, G.; Tavgenienė, D.; Grigalevičius, S.; Shahnawaz, S.; Siddiqui, I.; Jou, J.-H. Novel icarbazole-diphenylsulphone derivatives as efficient OLED hosts and emitters // Advanced materials and technologies: book of abstracts of 25th international conference-school, 21-25 August 2023, Palanga, Lithuania. Kaunas: Kaunas University of Technology. ISSN 2669-1930. 2023, P36, p. 73.

4. **Blaževičius, D.**; Kručaitė, G.; Tavgenienė, D.; Grigalevičius, S.; Gautam, P.; Shahnawaz, S.; Siddiqui, I.; Jou, J.-H. Multifuctional bicarbazole-based twisted D-A-D derivatives for blue and green OLEDS // Open readings 2023: 66th international

conference for students of physics and natural sciences, April 18-21, 2023, Vilnius, Lithuania: annual abstract book / editors: M. Keršys, Š. Mickus. Vilnius: Vilnius University Press, 2023. ISBN 9786090708835. p. 191.

5. **Blaževičius, D.**; Beresnevičiūtė, R.; Kručaitė, G.; Tavgenienė, D.; Grigalevičius, S.; Nagar, M.R.; Hao, C.T.; Jou, J.-H.; Kumar, K.; Banik, S. Central benzophenone fragment having solution processable derivatives as bipolar hosts for green TADF OLEDs // Chemistry and chemical technology: international conference CCT-2023, March 10, 2023, Vilnius: conference book. Vilnius: Vilnius University Press, 2023, P 011. ISBN 9786090708330. p. 48.

6. **Blaževičius, D.**; Beresnevičiūtė, R.; Kručaitė, G.; Tavgenienė, D.; Grigalevičius, S.; Nagar, M.R.; Jou, J.-H. 3,3'-bicarbazole derivatives for wetprocessable TADF OLEDS // Chemistry and chemical technology: proceedings of international scientific conference, Kaunas, 2022. Kaunas : Kaunas university of technology. ISSN 2538-7359. 2022, p. 77.

7. **Blaževičius, D.**; Kručaitė, G.; Grigalevicius, S.; Beresnevičiūtė, R.; Tavgenienė, D.; Shahnawaz, S.; Nagar, M.R.; Siddiqui, I.; Choudhury, A.; Jou, J-H. Bi-phenoxazine derivative as host material for efficient candlelight oled devices // Chemistry and chemical technology: proceedings of international scientific conference, Kaunas, 2022. Kaunas: Kaunas University of Technology. ISSN 2538-7359. 2022, p. 76.

8. **Blaževičius, D**.; Beresnevičiūtė, R.; Kručaitė, G.; Tavgenienė, D.; Grigalevičius, S.; Nagar, M.R.; Jou, J.-H. Bicarbazole substituted benzophenones as solution-processable TADF OLED emitters // Baltic polymer symposium 2022, Tallinn, Estonia, September 21–23, 2022: programme and abstracts. Tallinn: Tallinn University of Technology. 2022, p. 42.

9. **Blaževičius, D.**; Kručaitė, G.; Grigalevicius, S.; Samuel, N.S.; Shahnawaz, S.; Nagar, M.R.; Jou, J.-H. New host material for highly efficient candlelight OLED with a very low color temperature // Advanced materials and technologies: book of abstracts of 24th international conference-school, 22-26 August 2022, Palanga, Lithuania. Kaunas: Kaunas University of Technology. ISSN 2669-1930. 2022, B-P44, p. 81.

10. **Blaževičius, D.**; Kručaitė, G.; Grigalevicius, S.; Samuel, N.S.; Shahnawaz, S.; Nagar, M.R.; Siddiqui, I.; Choudhury, A.; Jou, J.-H. Novel host material with phenoxazine fragments for efficient omnifriendly candlelight OLED devices // IC3EM 2022: 5th international Caparica conference on chromogenic and emissive materials, Caparica, Portugal, 3-7 July 2022: book of abstracts. Caparica: BIOSCOPE research group, 2022, P.05. ISBN 9789895335039. p. 227.

11. **Blaževičius, D.**; K., Gintarė; G., Saulius; Shahnawaz, S.; Nagar, M.R.; Siddiqui, I.; Choudhury, A.; Lin, J.-T.; Jou, J.-H. Ypač žemos šviesos spalvos temperatūros organiniai šviestukai fiziologiškai draugiškiems apšvietimo prietaisams // Bioateitis: gamtos ir gyvybės mokslų perspektyvos: 14-oji Lietuvos jaunųjų mokslininkų konferencija, 2021 m. lapkričio 25 d.: pranešimų santraukos. Vilnius : Lietuvos mokslų akademija, 2021. ISBN 9789986080855. eISBN 9789986080862. p. 35.

12. **Blazevicius, D**. New diphenylsulfone-based materials as hosts for efficient third generation OLED devices // Global webinar on laser, optics and photonics, September 25-26, 2021: abstract book. Bangalore: Global scientific guild. 2021, p. 34

13. **Blazevicius, D.**; Beresneviciute, R.; Eidimtas, M.; Krucaite, G.; Grigalevicius, S.; Swyamprabha, S.S.; Kesavan, K.K.; Siddiqui, I.; Nagar, M.R.; Yadav, R.A.K.; Jou, J.-H. New carbazole based host materials for thermally activated delayed fluorescent OLEDs // Chemistry and chemical technology: 16th international conference of Lithuanian chemical society, 24 September 2021, Vilnius, Lithuania: book of abstracts. Vilnius: National center for physical sciences and technology. 2021, P081, p. 95.

14. **Blaževičius, D.**; Kručaitė, G.; Tavgenienė, D.; Grigalevicius, S.; Shahnawaz, S.; Swayamprabha, S.S.; Jou, J.-H.; Vembris, A. Vienos stadijos karbazolo ir fenoksazino darinių sintezė efektyvių oled prietaisų matricoms // Studentų mokslinės konferencijos „Chemija ir cheminė technologija 2021" pranešimų medžiaga: respublikinė studentų mokslinė konferencija, 2021 05 14 / rinkinio sudarytojai: T. Dambrauskas, G. Kručaitė, D. Sinkevičiūtė; Kauno technologijos universitetas. Cheminės technologijos fakultetas. Kaunas: Kauno technologijos universitetas. eISSN 2538-7332. 2021, p. 152.

15. **Blaževičius, D.**; Kručaitė, G.; Tavgenienė, D.; Grigalevičius, S.; Lin, C.-H.; Shao, C.-M.; Chang, C.-H. Nauji skyles pernešantys trifenilamino dariniai efektyviems raudoną šviesą skleidžiantiems organiniams šviestukams // Fizinių ir technologijos mokslų tarpdalykiniai tyrimai: 10-oji jaunųjų mokslininkų konferencija: pranešimų santraukos. [Vilnius]: [Lietuvos mokslų akademija]. 2020, p. 4-5.

ACKNOWLEDGMENTS